INDIAN AGRICULTURAL
RESEARCH INSTITUTE, NEW DELHI.

JOURNAL OF
COLLOID SCIENCE

VOLUME 3

CONTENTS OF VOLUME 3

No. 1, February, 1948

No. 2, May, 1948

No. 3, June, 1948

No. 4, August, 1948

No 5, October, 1948

No. 6, December, 1948

ASSOCIATION PHENOMENA. II. THEORIES OF CHAIN MOLECULES AND THEIR APPLICATION TO HYDROGEN BONDING IN GASEOUS HYDROGEN FLUORIDE

Rober ⁓‒‐ᵃ

From the Chemistry Department,   **V. Y.**
Received De

Intro

The phenomenon of association is well known to science, as it is only another way of describing such familiar phenomena as liquefaction and solidification. Nevertheless, it has not been emphasized as much as it deserves, especially in connection with some of its more subtle aspects. The cause of this comparative neglect may be apportioned variously but, in general, among the reasons for this neglect the following surely are important. Firstly, the interpretation of the experimental data is difficult, especially if one chooses to revert to more or less elementary concepts as a starting point. Secondly, the mathematical difficulties involved in treating a complex phenomenon of this type starting from such elementary concepts are far from simple; indeed, it is doubtful if our mathematical techniques are quite adequate to treat all the various and sundry mechanisms that have been postulated. As a result, association has been partly neglected and partly so simplified that it could be treated by the available mathematical tools.

We shall not presume here to give a solution for the whole problem, but rather shall adopt some of the mathematical tools which have been developed in the theoretical studies on the formation of high polymers (which is a type of association) and apply them to the more general problem. In particular, we shall concern ourselves with the formation of chain molecules in the gaseous phase; *i.e.*, molecules which can attach identical molecules to themselves at two positions.

In general, it is probable that a molecule is able to join another molecule at any other point of the other molecule. This tendency is, of course, opposed by the kinetic energy of the multitudinous collisions that constantly occur. However, if a bond is formed, it will usually form at that point at which the attractive force is strongest. Since both the forces of attraction and the kinetic forces of the collisions are widely distributed in

magnitude, we may safely postulate that all gases are associated into
larger aggregates, at least to a certain extent. In most gases, however, the
forces that bring about this association are rather small in magnitude,
and hence are not what we usually think of as chemical forces, that is,
primary valence forces, but are rather what we label as secondary valence
forces, the so-called van der Waals forces.

Association in the broad sense includes all chemical combinations, but
in the narrower sense which we shall use here, it is limited to that type of
association which is due to these secondary valence forces. The formation
of high polymers is a case of association according to the more general
definition but not in the restricted definition. Nevertheless, the methods
used in treating the case of association in high polymers may be adapted
to treat association due to secondary valence forces.

The methods used in the field of polymerization have been of several
types. The thermodynamic and statistical methods have been used to
describe equilibrium conditions in high polymers and the kinetic approach
has been used to describe the course of the reaction. The application of
these methods to copolymerization, which is a type of association in
which water is eliminated, has been reviewed at length by Flory (18).
It has been found that the process of vinyl polymerization involves at
least three elementary steps (1, 2). The theory of this type of behavior
has been investigated extensively by several investigators (3, 4, 5, 6).
In these treatments, however, association has been treated in a one-sided
manner. Since by far the greater part of the monomers go to form polymer
molecules, the growth aspect of association was treated but the concurrent
phenomenon of dissociation was neglected. In many cases the omission
was justifiable, since the former process was by far the more important
and the omission of the latter problem simplified the mathematics con-
siderably. However, in certain cases, as for instance when a high polymer
is subjected to thermal degradation, the dissociation aspect cannot be
neglected; here, on the other hand, the growth can be neglected. A treat-
ment of dissociation treated as a separate process has been made by
Simha and Montroll (7), Schultz (8), and Freudenberg, Kuhn and co-
workers (19, 20). In general, however, the two parts of the problem of
association (growth and dissociation) must be considered simultaneously
(9). A theory of this sort, using statistical methods, has been presented by
Tobolsky (10) and, using thermodynamic methods, by Flory (11). The
kinetic approach to this problem has been used by Blatz and Tobolsky
(12) as it regards step-wise polymerization. By making certain assump-
tions, they were able to solve the differential equations they obtained.

However, a slightly modified approach is possible. Since the equilib-
rium state is probably the most important, then, if the kinetic approach
can be modified to describe this state, the results should be important.

This can be done if we describe all the processes that occur during association. Then we can say that at the thermodynamic equilibrium point

$$\frac{dn_j}{dt} = 0, \qquad j = 1, 2, 3 \ldots,$$

where n_j is the number of molecules of polymerization degree j. By this step, the differential equations, which are often very difficult, if not impossible, to solve in an analytic manner, are converted into more or less simple sets of algebraic equations which are susceptible of solution.

MATHEMATICAL THEORY

In the Blatz and Tobolsky (12) treatment, the assumption is made that both the growth and dissociation are random processes. That is, that any molecule of polymerization degree x will combine with any other molecule of polymerization degree y with the second order rate constant k_a and that any molecule with the polymerization degree $(x + y)$ will split randomly into two fragments with the first order rate constant k_b; i.e.,

$$n_x + n_y \underset{k_b}{\overset{k_a}{\rightleftarrows}} n_{x + y}.$$
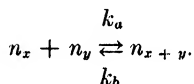
This is a possible process, but it is doubtful whether it is of general validity (13). In general, the rate at which a one-mer adds to a one-mer will probably be different than if a two-mer adds to a five-mer. Hence, in the treatment here, we shall assume that a one-mer will always add to a j-mer with a second order rate constant k_1 and that the dissociation of a one-mer from a j-mer will always proceed with a first order rate constant k_2. We shall further assume that the rate constants for the addition and splitting of one-mers is much more important than that due to the addition and splitting of fragments of higher degrees of polymerizations; and hence, that these later processes may be neglected. This seems a feasible assumption, at least as a first approximation.

TABLE OF SYMBOLS

n_1 = the number of monomer molecules

n_j = the number of polymer molecules consisting of j monomer units

k_1 = second order rate constant of growth

k_2 = first order rate constant of dissociation

$K = \dfrac{k_1}{k_2}$ = equilibrium constant for the reaction

P_N = number average degree of polymerization

The following set of kinetic equations can now be written for these mechanisms:

(1)

$$
\begin{cases}
\dfrac{dn_1}{dt} = -k_1 n_1 \sum_{j=1}^{\infty} n_j + k_2 \sum_{j=1}^{\infty} n_j + k_2 n_2 - k_2 n_1, \\[2mm]
\dfrac{dn_2}{dt} = -k_1 n_1 n_2 + \dfrac{k_1 n_1^2}{2} + k_2 n_3 - k_2 n_2, \\[2mm]
\dfrac{dn_3}{dt} = -k_1 n_1 n_3 + k_1 n_1 n_2 + k_2 n_4 - k_2 n_3, \\[2mm]
\quad \vdots \\[2mm]
\dfrac{dn_j}{dt} = -k_1 n_1 n_j + k_1 n_1 n_{j-1} + k_2 n_{j+1} - k_2 n_j,
\end{cases}
$$

also

(2) $$\frac{d}{dt} \sum_{j=1}^{\infty} n_j = -k_1 n_1 \sum_{j=1}^{\infty} n_j + \frac{k_1 n_1^2}{2} + k_2 \sum_{j=1}^{\infty} n_j - k_2 n_1.$$

At equilibrium

$$dn_j/dt = 0 \qquad j = 1, 2, 3, \ldots.$$

Hence

(3a) $$-k_1 n_1 \sum_{j=1}^{\infty} n_j + k_2 \sum_{j=1}^{\infty} n_j + k_2 n_2 - k_2 n_1 = 0,$$

(3b) $$-k_1 n_1 n_2 + \frac{k_1 n_1^2}{2} + k_2 n_3 - k_2 n_2 = 0,$$

(3c) $$-k_1 n_1 n_3 + k_1 n_1 n_2 + k_2 n_4 - k_2 n_3 = 0,$$

$$\vdots$$

(3j) $$-k_1 n_1 n_j + k_1 n_1 n_{j-1} + k_2 n_{j+1} - k_2 n_j = 0$$

and

(4) $$-k_1 n_1 \sum_{j=1}^{\infty} n_j + \frac{k_1 n_1^2}{2} + k_2 \sum_{j=1}^{\infty} n_j - k_2 n_1 = 0.$$

Solving, one obtains

(5) $$n_1 = \sum_{j=1}^{\infty} n_j + \frac{1}{K} - \left[(\sum_{j=1}^{\infty} n_j)^2 + \frac{1}{K^2} \right]^{\frac{1}{2}}$$

or

$$(6) \qquad \sum_{j=1}^{\infty} n_j = \frac{n_1\left(\dfrac{n_1}{2} - \dfrac{1}{K}\right)}{n_1 - \dfrac{1}{K}}.$$

To obtain the fraction of the molecules that are n_j, one sets $\sum_{j=1}^{\infty} n_j = 1$, then

$$(7) \qquad n_1 = \frac{1}{K}\left[K + 1 - (K^2 + 1)^{\frac{1}{2}}\right]$$

and

$$(8) \qquad n_j = \frac{K^{j-1} n_1{}^j}{2} = \frac{[K + 1 - (K^2 + 1)^{\frac{1}{2}}]^j}{2K}, \quad j = 2, 3, 4 \ldots$$

Using Eqs. (7) and (8), one can obtain the distribution spectrum once the ratio K is known. In Table I are shown some curves computed for arbitrarily chosen values of K.

TABLE I

Number Distribution Spectrum for Certain Values of K and j

j	$K = 0.01$ n_j	$K = 0.1$ n_j	$K = 0.5$ n_j	$K = 1$ n_j	$K = 2$ n_j	$K = 4$ n_j
1	0.995	0.950	0.764	0.586	0.382	0.219
2	0.495×10^{-2}	0.0451	0.146	0.172	0.146	0.0959
3	0.493×10^{-4}	0.00429	0.0557	0.101	0.111	0.0841
4	0.490×10^{-6}	0.000407	0.0213	0.0589	0.0851	0.0736
5	0.488×10^{-8}	0.0000387	0.00813	0.0345	0.0650	0.0645
6	0.485×10^{-10}		0.00310	0.0202	0.0497	0.0565
7			0.00119	0.0118	0.0390	0.0495
8			0.000453	0.00693	0.0298	0.0434
9				0.00406	0.0227	0.0380
10				0.00238	0.0174	0.0333
11						
12						0.0256

The distribution spectrum by weight can also be obtained (6, 14).

$$(9) \qquad \frac{j n_j}{\sum_{j=1}^{\infty} j n_j} = \text{weight fraction } n_j,$$

where

$$(10) \qquad \sum_{j=1}^{\infty} j n_j = n_1 + \frac{1}{2K} \frac{(K n_1)^2 (2 - K n_1)}{(1 - K n_1)^2}.$$

The distribution for various values of K are given in Table II.

TABLE II

Weight Distribution Spectrum for Certain Values of K and j

j	$K = 0.01$ jn_j	$K = 0.1$ jn_j	$K = 0.5$ jn_j	$K = 1.0$ jn_j	$K = 2.0$ jn_j	$K = 4.0$ jn_j
1	0.990	0.9005	0.5528	0.2929	0.1008	0.03023
2	0.985×10^{-2}	0.08556	0.2111	0.1716	0.0770	0.02648
3	0.147×10^{-3}	0.01219	0.1210	0.1508	0.0882	0.03480
4	0.195×10^{-5}	0.001545	0.0616	0.1178	0.0899	0.04066
5	0.243×10^{-7}	0.000183	0.0294	0.0862	0.0858	
6			0.0135	0.0606	0.0787	0.04681
7			0.0060	0.0414	0.0720	0.04785
8			·0.0026	0.0277	0.0628	0.04791
9				0.0183	0.0540	0.04722
10				0.0119	0.0458	0.04597
11						
12						0.04234

The number average degree of polymerization is usually defined as (15),

$$(11) \qquad P_N = \frac{\sum\limits_j jn_j}{\sum\limits_j n_j}.$$

Making the appropriate substitutions, this becomes:

$$(12) \qquad P_N = \frac{(Kn_1{}^2 - 2Kn_1 + 2)}{(Kn_1 - 1)(Kn_1 - 2)}.$$

In Table III is shown P_N as a function of K. It is very interesting that in

TABLE III

Number Average Degree of Polymerization for Certain Values of K

K	P_N
0.01	1.00505
0.1	1.05508
0.5	1.38186
0.8	1.72970
1.0	2.00016
1.5	2.76730
2.0	3.78931
3.0	5.44112
4.0	7.24576
5.0	9.28304
7.0	13.21853
10.0	19.20446

the case of $K = 1$; *i.e.*, $k_1 = k_2$, the number average degree of polymerization is equal almost exactly to 2!

Application to Gaseous Hydrogen Fluoride

Since these theories are all based on various assumptions, it is important that some experimental data be sought which would throw some light on the validity of the various assumptions. Unfortunately, such data is not plentiful in the literature. Some experimental work on equilibrium states in the case of high polymers has been made by Tobolsky and coworkers (16), but the data are not adequate for the application of these theories. However, a great amount of work on gaseous hydrogen fluoride is recorded in the literature. We shall use the data of Simons and Hildebrand (17). For this purpose the formulae previously derived must be recast so that the equilibrium constant can be derived from the apparent or average molecular weight. Rearranging the previous equations

$$(13) \qquad Kn_1 = \frac{(3P_N - 2) - (P_N^2 + 4P_N - 4)^{\frac{1}{2}}}{2(P_N - 1)},$$

$$(14) \qquad K = \frac{Kn_1(2 - Kn_1)}{2(1 - Kn_1)}, \, n_1 = \frac{2(1 - Kn_1)}{(2 - Kn_1)}.$$

Blatz and Tobolsky's equation can also be thus rearranged, giving

$$(15) \qquad K = 2P_N(P_N - 1).^*$$

The K in our treatment corresponds to what is usually denoted as K_x, the mole fraction equilibrium constant. To convert this to K_p we use the relationship

$$(16) \qquad K_p = K_x P^{\Delta\nu}$$

where $\Delta\nu$ = the increase in the number of molecules in the reaction. Thus

$$\Delta\nu = \sum_i jn_j - \frac{\sum_j jn_j}{P_N}.$$

Taking $\sum_i jn_j$ as 1, that is, the whole, the fractional decrease is

$$(17) \qquad \Delta\nu = 1 - \frac{1}{P_N}.$$

---

* The K in this equation is defined by our usage being $K = k_1/k_2$, not as in the paper of Blatz and Tobolsky where it is defined as $K = \frac{k_2 + k_1}{k_1}$.

We can now calculate the ΔH values for this reaction from the reaction isochore.

$$(18) \qquad \frac{d \ln K_p}{dt} = \frac{\Delta H}{RT^2}.$$

In Table IV are shown the results of this calculation.

TABLE IV

K_p and ΔH Calculated by the Theories of Blatz and Tobolsky and of This Paper from the Data of Simons and Hildebrand

T°A	V. P. Atm.	Average M. W.	P_N	K_p this paper	K_p B and T	ΔH this paper	ΔH B and T	Number of determinations of M. W.
234	.0739	87.4	4.37	.327	3.94	—	—	6
252	.1895	81.6	4.08	.645	7.165	4105	3890	3
263	.3079	74.3	3.715	.868	8.50	4115	3245	2
273	.4789	67.6	3.38	1.111	9.59	3985	2893	5
278.3	.5737	69.3	3.465	1.284	11.51	4000	3133	1
281.6	.6461	64.3	3.215	1.307	10.56	3800	2718	1
285.0	.7579	69.5	3.475	1.585	14.11	3840	2441	1
289.0	.8697	47.7	2.385	−1.589	6.09	(out of line)	(discarded)	
					Average	4009±77	3149±450	

Conclusion

From the results derived, it is impossible to obtain conclusive proof as to which theory more adequately represents the experimental data, although the ΔH values obtained by the theory in this paper scatter a little less than those derived from the Blatz and Tobolsky treatment. More experimental data are needed before the question can be decided. Work on this point is in progress.

Summary

1. A theory of association with certain limiting assumptions is derived which gives the distribution spectra by number and weight and the average molecular weight of the substance once the equilibrium constant is known.

2. This theory is compared with that of Blatz and Tobolsky and both theories are applied to data on the average molecular weight of gaseous hydrogen fluoride, the ΔH and K_p values being calculated by both theories.

References

1. See BURK, R. E., WEITH, A. J., THOMPSON, H. B., AND WILLIAMS, I., Polymerization and its Applications in the Fields of Rubber, Synthetic Resins, and Petroleum, Reinhold Publishing Co., New York, 1937.

2. See MARK, H., AND RAFF, R., High Polymeric Reactions, Interscience Publishers, Inc., New York, 1941.

3. RAKOWSKI, A., *Z. physik. Chem.* **57**, 321 (1907).

4. WEGSCHEIDER, R., *Monatsh.* **36**, 471 (1915).

5. SMOLUCHOWSKI, M.v., *Z. physik. Chem.* **92**, 129 (1917).

6. GINELL, R., AND SIMHA, R., *J. Am. Chem. Soc.* **65**, 706 (1943); **65**, 715 (1943). See also references cited therein.

7. MONTROLL, E. W., AND SIMHA, R., *J. Chem. Phys.* **8**, 721 (1940).

8. SCHULZ, G. V., HUSEMANN, E., AND LÖHMANN, H. J., *Z. physik. Chem.* **B52**, 23–49 (1942).

9. GINELL, R., Ph.D. Dissertation, Polytechnic Institute of Brooklyn, 1943.

10. TOBOLSKY, A. V., *J. Chem. Phys.* **12**, 402 (1944).

11. FLORY, P. J., *ibid.* **12**, 425 (1944).

12. BLATZ, P. J., AND TOBOLSKY, A. V., *J. Phys. Chem.* **49**, 77 (1945).

13. LASSETTRE, E. N., *Chem. Revs.* **20**, 259 (1937).

14. MAREI, F., *Acta Physicochim. U.R.S.S.* **9**, 741, 759 (1938).

15. KRAMER, E. O., AND LANSING, W. D., *J. Phys. Chem.* **39**, 153 (1935).

16. MESROBIAN, R., AND TOBOLSKY, A. V., *J. Am. Chem. Soc.* **67**, 785 (1945).

17. SIMONS, J., AND HILDEBRAND, J. H., *ibid.* **46**, 2183 (1924).

18. FLORY, P. J., *Chem. Revs.* **39**, 137 (1946).

19. FREUDENBERG, K., KUHN, W., DURR, W., BOLZ, F., AND STEINBRUNN, G., *Ber.* **63** 1510 (1930).

20. KUHN, W., *Z. physik. Chem.* **A159**, 368 (1932).

RIGIDITY OF CHAIN MOLECULES AND ITS DETERMINATION FROM VISCOSITY AND FLOW BIREFRINGENCE IN DILUTE SOLUTIONS

Werner Kuhn and Hans Kuhn

I. Qualitative Considerations Regarding Shape and Change of Shape of Chain Molecules in Solution

It is well known that a large number of substances of high molecular weight consist of chain molecules. These molecules are composed of a great number of atoms or groups of atoms which are linearly connected as a chain. Rubber, polystyrene, cellulose and its derivatives, and many protein compounds belong to this group. Dissolved in a proper medium,
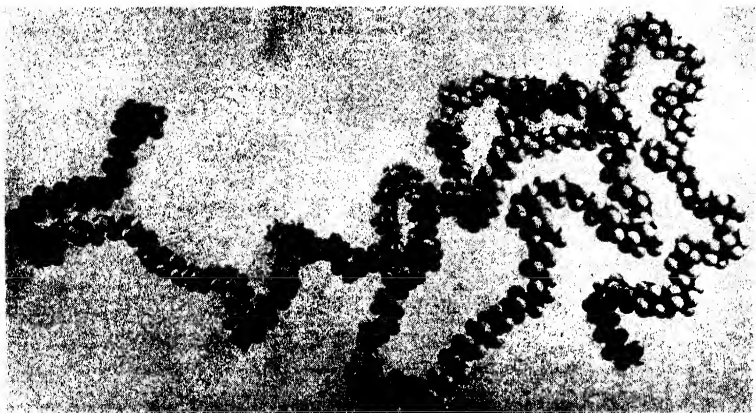
Fig. 1. Shape of a molecule of a normal paraffin hydrocarbon of high molecular weight (formula $C_{500}H_{1002}$) in benzene solution.

these molecules very often assume the shape of a so-called statistical coil (1). This is a very loose coil as shown in Fig. 1. In the following, we shall see that, apart from the total extended length of the chain, the distance between the ends, which we shall designate as h, is a very important quantity, which determines the most diverse properties of the chain, or the whole suspension, respectively.

The shape of the coil and the distance h are subject to continuous changes. The reason for these changes is given by the ability of parts of the molecule to rotate more or less freely around a given valence direction as axis relative to the rest of the molecule. These rotations around the different axes in the chain are produced by thermal agitation in the solution. *The movements occur more rapidly, the higher the temperature and the more nearly free rotation is realized.* Since the temperature is finite and rotation is restricted, and since the chain molecule is imbedded in a solvent which opposes rapid motion of the chain parts due to its viscosity, one can ask how rapidly changes of constellation [1] of a given chain molecule will occur on the average. These questions can be answered on the basis of either viscosity or flow birefringence in dilute solutions (2, 10). We shall see that, for instance, a molecule of polystyrene with a degree of polymerization of 1500 requires approximately 10^{-4} sec. in cyclohexanone to change its internal constellation completely. The time necessary to accomplish such a complete change, in the following referred to as *macroconstellation changing time*, is dependent on the so-called *shape resistance, i.e.*, on the resistance with which the chain opposes, for internal reasons, a rapid change of configuration.

For an exact definition of these parameters and their determination from viscosity and flow birefringence, it is necessary to start with some information about the characteristics of a chain molecule and its shape in a solution at rest.

II. DEGREE OF POLYMERIZATION; STATISTICAL CHAIN ELEMENT

A characteristic parameter of a high polymeric substance is represented by the degree of polymerization Z, *i.e.*, the number of monomer units which are linearly connected to a chain. It is related to the molecular weight M,

$$M = M_g \cdot Z, \tag{1}$$

where M_g is the molecular weight of the monomer unit. For rubber $M_g = 68$, so that for a molecule of degree of polymerization $Z = 1500$, $M = 100,000$. Closely connected with Z is also the maximum extent L

---

[1] We define as constellation isomers such isomers as can be produced from one another by rotation of parts of the molecule about valence directions as axis relative to the rest of the molecule. Constellation isomers are, for instance, chair and boat arrangement of cyclohexane and *cis* and *trans* isomers of ethylene derivatives.

This definition is slightly different from the definition of constellation isomerism, given some years ago by F. Ebel (Freudenberg's Stereochemie, Leipzig and Wien, 1932, pp. 535 and 825). A constellation isomerism, in this earlier definition, was limited to products produced from one another by rotation about single aliphatic C—C bonds. As the definition of a single bond has become somewhat ambiguous (*e.g.*, in benzene or other compounds containing conjugated double bonds), the more general definition including rotations about any axis seems to be appropriate.

of the zig-zag chain, *i.e.*, of the chain as obtained without distortion of valence angles or atomic distances. Because this factor is of decisive importance for the hydrodynamic behavior in solution, we call it the *"hydrodynamic length of the chain molecule."* Obviously

$$L = Z \cdot b, \tag{2}$$

where b is the *hydrodynamic length of the monomer unit, i.e.,* its length measured in the direction of the extended zig-zag chain. X-ray data show that in the monomer unit of rubber (isoprene) $b = 5.0 \times 10^{-8}$ cm., so that for a molecule of degree of polymerization $Z = 1500$, $L = 7.5 \times 10^{-5}$ cm.

We mentioned before that, apart from the hydrodynamic length L, the distance measured in a straight line, h, between the chain ends is of greatest importance for the actual behavior of a molecule. A multitude of various h values occurs simultaneously in a solution of otherwise equal chain molecules. In a given chain, h is subject to constant changes. In order to arrive at a result for the relative frequency with which the various h values occur on an average in a static solution it is necessary or at least feasible to introduce the concept of the *"statistical chain element"* (3). The chain element constitutes a part of the chain of average length A. Its definition is based on the postulate that, when proceeding along the chain, the orientation of a given statistical element will be independent of the orientation of the neighboring element in the chain. The average value of A to be assumed depends on s, the number of monomeric units joined to a statistical element. The s value is arbitrary within certain limits. There can be chosen, however, a *preferential s* value (4), *viz.* s_m, in such a way that the corresponding A value, A_m, will be equal to:

$$A_m = s_m \cdot b. \tag{3}$$

Since each preferential chain element consists of s_m, and the whole chain of Z monomer units, the total chain is divided into:

$$N_m = Z/s_m \tag{4}$$

preferential statistical elements, each of length A_m. Because of Eqs. (3), (4), and (2) we have then:

$$N_m A_m = L. \tag{5}$$

For rubber s_m is approximately 2.8 (4) and $A_m = 13 \times 10^{-8}$ cm. A rubber molecule of a degree of polymerization $Z = 1500$ (molecular weight 100,000) consists, therefore, of approximately $N_m = \dfrac{1500}{2.8} = 525$ preferential statistical elements, of length 13×10^{-8} cm.

In general A_m will be larger, the more closely the angle which is formed by two successive valence directions of the chain approaches

180°. In this case we must proceed from a given point P of the chain axis for a longer distance along the filament before the local orientation of the chain axis becomes practically independent of the orientation at point P. A_m is also larger, the bulkier the molecule. *However, there is not necessarily a connection between A_m and the shape resistance of the molecule— defined later —, i.e., no connection between length A_m and the time it takes the molecule to change its internal configuration by rotation around valence bonds.*

III. Distribution Function for Distance h in a Solution at Rest

Let us place one end of a molecule at the origin of a coordinate system and then, beginning at that end, proceed along the chain. After proceeding along each statistical element of length A_m we must determine, by playing dice for instance, the direction of the next step, *i.e.*, the orientation of the next statistical element of length A_m. This corresponds to the fact that the direction of each statistical element is independent of the direction of the preceding (and of the following) element. The position of the chain end of a molecule with N_m preferential elements can thus be determined by a number N_m of arbitrary choices of directions. *The probability $W(h)$ for the occurence of an end-to-end distance of magnitude h may therefore be obtained by purely statistical considerations.*

The result is according to Refs. (3) and (4), as follows: The probability that the value for the distance between the two ends of a molecule lies between h and $h + dh$ equals:

$$W(h)dh = Ke^{-(3h^2/2N_mA_m{}^2)}h^2dh \tag{6}$$

or the probability $\rho(x, y, z)\ dx \cdot dy \cdot dz$ that one end of the chain is located in a volume element $dx\ dy\ dz$ when the other end is placed at the origin of a coordinate system equals:

$$\rho(x, y, z)\ dx\ dy\ dz = K'e^{-[3(x^2+y^2+z^2)/2N_mA_m{}^2]}\ dx\ dy\ dz$$
$$= K'e^{-(3h^2/2N_mA_m{}^2)}\ dx\ dy\ dz. \tag{7}$$

K and K' are constants, and Eqs. (6) and (7) are approximations. More exact distribution functions can be given (4, 6), but are superfluous for the following discussion. The distribution function $\rho(x, y, z)$ of distances h is reproduced in Fig. 2 according to Eq. (7). The density has a maximum for $h = 0$. Comparing, therefore, volume elements of equal size $dx\ dy\ dz$, the probability of finding one end of the chain in a given volume element is largest at $h = 0$, *i.e.*, in the neighborhood of the other end. The mean square value of h can be computed from Eqs. (6) or (7) as:

$$\overline{h^2} = N_mA_m{}^2. \tag{7a}$$

It has been pointed out that the value for h of a random chain is continuously changing. The distribution in Fig. 2 can be considered as a measure for the relative period during which a given molecule has a
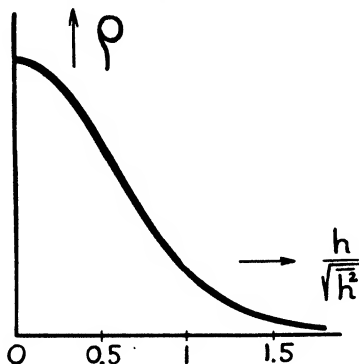
FIG. 2. Mean distribution function ρ as function of the end-to-end distance h.

distance h or as the distribution function of h among many identical chains at a given moment.

IV. KINETIC INTERPRETATION OF THE DISTRIBUTION FUNCTION IN A SOLUTION AT REST

By considering a totality of many chain molecules the distribution in h (Eqs. (6) and (7)) can be kinetically interpreted by the following picture (4, 5):

(1) the chain ends tend to assume a random distribution as a consequence of thermal motion (diffusion).

(2) a force of magnitude [2]

$$k_1 = \frac{3h}{N_m A_m{}^2} kT \tag{8}$$

[2] The assignment of a private entropy and a private free energy to a chain whose end points are fixed at distance h was introduced for the first time in 1936 by W. Kuhn (7). This has been generally accepted and used in subsequent papers by other authors (5, 12). The establishment of a stationary distribution function of the vector h in a streaming solution under the influence of the contraction force (8), the thermal motion and further forces (shape resistance and viscous resistance of the surrounding medium; for details see below) has been treated by W. Kuhn and H. Kuhn in 1943 and in subsequent papers (4, 2, 10). In these papers as well as in papers by other authors (5, 12) the hypothesis has been made that the probability force (8) can be used in a calculation of the distribution function in h in a similar way as if it were a conservative force. The validity of this procedure has consequently been proved by W. Kuhn and F. Grün (13).

is acting on the chain ends in the direction of the vector h, effecting a contraction of the chain to smaller and, according to Fig. 2, more probable values of h.

We may remark that the statistical force (8) is of importance not only for the behavior of the chains in solutions at rest or in motion, but the elastic tension in an extended piece of solid rubber can also be quantitatively explained by this type of force. To recognize this fact qualitatively, we have to consider that the vectors h corresponding to the chain parts located between vulcanization points become oriented and changed in their length during the extension of the sample.

The diffusion tendency mentioned above and the force according to Eq. (8) will be important in the streaming solution because they will determine, together with additional effects, the shape and orientation of the molecules. It can be qualitatively seen, furthermore, that the mechanical properties of the solution, especially the viscosity, depend largely on the magnitude and shape of the dissolved molecules.

V. Dependence of Optical Anisotropy of Chain Molecules on End-to-End Distance h

Since flow birefringence will be discussed later on, we wish to refer in this connection to the *optical behavior of the single chain molecule, i.e.,* to the dependence of the optical anisotropy of the molecule on its end-to-end distance h.

We first consider the individual statistical chain element as a particle which is made from optically anisotropic material, and which at the same
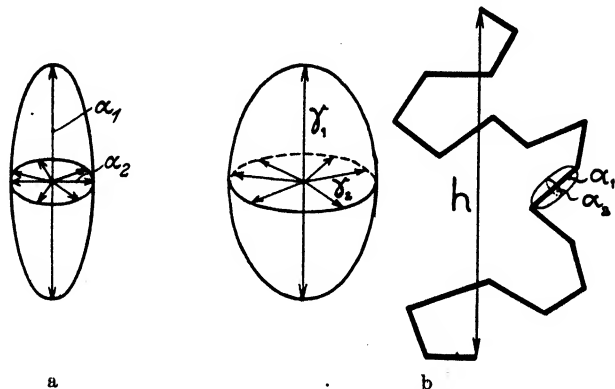
FIG. 3. (a) Optical polarizability of a statistical chain element represented as an ellipsoid of revolution with axes α_1 and α_2. (b) Chain consisting of N_m statistical elements of length A_m, the ends of the molecule being held at a fixed distance h. The optical polarizability can be described by an ellipsoid of revolution with the axes γ_1 and γ_2, $\gamma_1 - \gamma_2$ being given by Eq. (9).

time has an elongated shape. The optical polarizability of the element is determined by both of these two facts. It can be described in terms of an ellipsoid of revolution with the axes α_1 in the direction of the statistical element and α_2 perpendicular to it, respectively (6) (Fig. 3a). For rubber, for instance, $\alpha_1 - \alpha_2 = 75 \times 10^{-25}$ cm^3.

If the chain consisting of N_m statistical chain elements were completely extended, the polarizabilities of the total chain would have the magnitudes $N_m\alpha_1$, and $N_m\alpha_2$, respectively. In the case of a coiled chain the distance h will, however, be far less than L. If we then place the direction of the vector h in the z-axis, we can see that, even in this case (h much smaller than L), there must be a certain preferential orientation of the statistical elements in the h direction. W. Kuhn and F. Gruen (6) investigated the corresponding statistical problem. The result is that the polarizability of the total molecule with an end-to-end distance h can be represented by an ellipsoid of revolution with the axes γ_1 in the direction of vector h and with γ_2 normal to it.

$$\gamma_1 - \gamma_2 = \tfrac{2}{5}(\alpha_1 - \alpha_2) \frac{h^2}{N_m A_m{}^2} \tag{9}$$

(Fig. 3b). The anisotropy of the polarizability of a chain with a given h value can thus be given, and consequently also the contribution of a chain molecule with a given distance h and a definite orientation to the polarizability of the whole medium. *Therefore, the double refraction of a suspension can be given if the distribution function of the vectors h with respect to direction and amount is known.* Thus, the whole question of the flow birefringence and the viscosity of a suspension of chain molecules is *reduced to the question of the distribution functions of the various directions and values of the vectors h in the streaming solution.*

VI. Elastic Tensions and Relaxation Effects in the Motion of Solids through Viscous Media

Before proceeding to the definition of the shape resistance of long chain molecules we wish to repeat some facts about the connection between ordinary viscosity and the relaxation of mechanical stress in a viscous liquid. When moving a rod through a highly viscous liquid, such as liquid glass, we must constantly apply a force in the direction of the motion of the rod. This force causes mechanical tensions in the viscous substance, because distances between the atoms undergo small changes due to compression or shearing stresses. These tensions, nevertheless, are gradually relaxing by a reorientation of the molecules; this fact becomes especially clear when the position of the rod is supposed to be kept constant after a certain period. The force necessary for a continuous motion of the rod corresponds, therefore, to a steady state which occurs as a

consequence of relaxation of stress on one hand and simultaneous genera-
tion of new tensions through further motion of the rod on the other hand
(8). Due to the interaction of these two effects the force which we must
apply in moving the rod through the liquid is proportional to the speed
imparted to the rod. The proportionality factor depends on the size and
the geometrical shape of the rod and is essentially proportional to the
viscosity of the liquid.

VII. DEFINITION OF THE SHAPE RESISTANCE OF CHAIN MOLECULES

In the preceding section we discussed the nature of viscosity while in
earlier sections the importance of the end-to-end distance h has been
established. On this basis, there shall now be given a *definition of the shape
resistance* of a chain molecule (2). For this purpose we assume that the
end-to-end distance h of a chain molecule is abruptly changed by Δh.
At initial length h the distances between adjacent atoms, as well as the
valence angles, were distributed in such a way that the potential energy
corresponding to these distances and angles corresponded to a minimum
(disregarding some deviations through thermal agitation). Since the
change from h to $h + \Delta h$ took place fast enough, this minimum condition
no longer applies to the molecule in the extended state; interatomic dis-
tances and valence angles will be somewhat distorted. A certain potential
energy will thus be produced by the sudden distortion. To the potential
energy there corresponds a restoring force which is proportional to Δh
(and which is added to the statistical restoring force according to Eq. (8)).
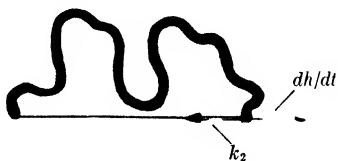
FIG. 4. Chain molecule whose ends move at speed dh/dt relative to each other opposes
this change by a force k_2 proportional to the velocity dh/dt.

When subsequently, after distortion, the distance between the ends of the
molecule is kept constant at $h + \Delta h$, the distortion of valence angles and
bond distances will disappear rapidly, and simultaneously the correspond-
ing potential energy and the restoring force due to distortion. *The elastic
tensions due to energy effects in the chain molecule disappear* (similar to the
disappearance of the mechanical tensions in a viscous liquid) *by the read-
justment of the distribution of the valence angles in the molecule by utilization
of the partial free rotation around the valence bonds.* By changing the dis-
tance h continuously at a rate of dh/dt (Fig. 4), a stationary state is
reached similar to that in the motion of the rod through a viscous liquid.
It results from an increase in the energetic elastic tension as a consequence

of continuous deformation and from a simultaneous decrease by relaxation. The force k_2 necessary to move one end of the chain with speed dh/dt relative to the other therefore becomes proportional to the speed dh/dt,

$$k_2 = - B(dh/dt). \tag{10}$$

The proportionality constant B corresponds to the viscosity in the case of a rod moving through a viscous liquid. Thus B is a *measure of the resistance of the chain molecule to rapid changes of shape, i.e.,* changes of the distance h. We shall, therefore, call B the *shape resistance* of the chain molecule. Eq. (10) gives the force which must be applied in addition to Eq. (8) to deform the chain with speed dh/dt; it is exclusively used to overcome the shape resistance of the chain. If the chain is imbedded in a highly viscous liquid, another force, namely, the force of external friction, is added to the aforementioned forces for overcoming the viscosity of the surrounding medium. All these forces will be considered during the discussion of the behavior of molecules in streaming solutions.

VIII. Orientation and Deformation of Chain Molecules in a Solution in Motion

In a previous section we have considered a solution of chain molecules in a state of rest. The distribution of magnitudes of the vectors h was given by Eq. (6), while their orientations were random in space. If such a liquid is made to move, we realize at once that only the *gradient of flow* in the solution will enable us to measure the viscosity and the flow birefringence. (A uniform translation of the liquid as a whole does not give rise to any such effects.) Let us assume a liquid with flow in the z-direction in Fig. 5a, and a velocity gradient γ in the x-direction. To simplify matters, we consider the distribution of the vectors h of our molecules in respect to magnitude and direction in the $x-z$ plane only. A molecule suspended in the solution is inclined to accommodate itself to the motion of the surrounding liquid as completely as possible. In particular, the center of gravity of the chain will assume the speed of translation of the surrounding liquid. In this way the molecule as a whole experiences a uniform translation. For the further description we introduce a coordinate system which participates in the translation of the center of gravity of the molecule, *i.e.*, a system in which the center of gravity of the molecule rests (Fig. 5b). Since a gradient of flow exists in the liquid, we can see that the parts of the molecule on the right side of its center in Fig. 5b (*e.g.*, end point 1) are surrounded by liquid moving in the upward direction, and molecule parts on the left of the origin (*e.g.*, end point 2) by parts of the liquid moving in the downward direction. Again the segments adjacent to points 1 or 2, respectively, will strive to participate as completely as possible in the motion of the surrounding liquid.
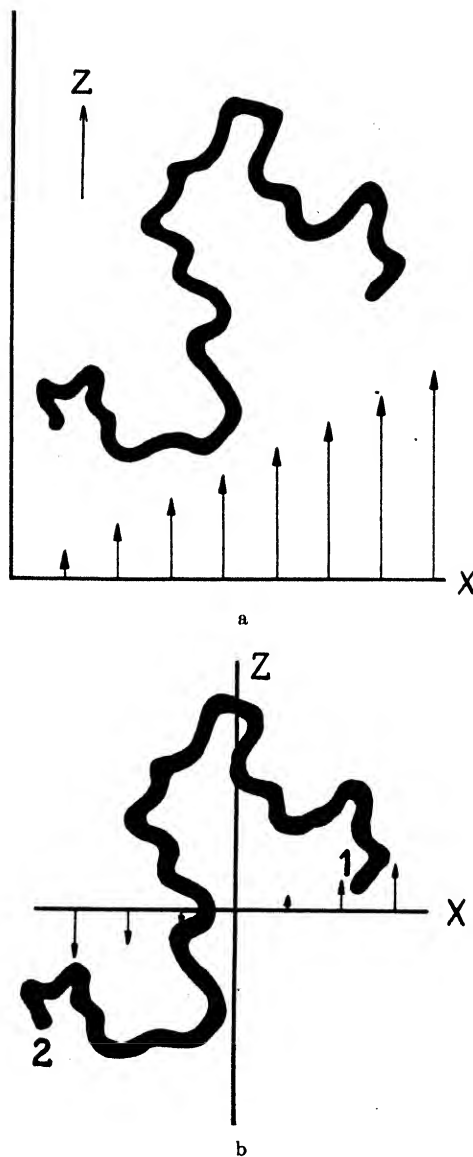
FIG. 5. (a) Chain molecule suspended in a liquid subject to a shear gradient. The center of gravity adopts the speed of the surrounding liquid volume elements. (b) Motion of the surrounding liquid as observed in a coordinate system which participates in the translation of the center of gravity.

Disregarding for the moment the shape resistance of the molecule as well as other forces, such as the force represented by Eq. (8), we see that point 1 moves in the positive and point 2 in the negative z direction. After some time, the molecule will have moved from positions 1, 2, to positions 1', 2' in Fig. 6, which means that the direction of vector h has changed. The axis of the molecule has rotated and simultaneously, the absolute value of vector h has changed, *i.e.*, increased in Fig. 6 and de-
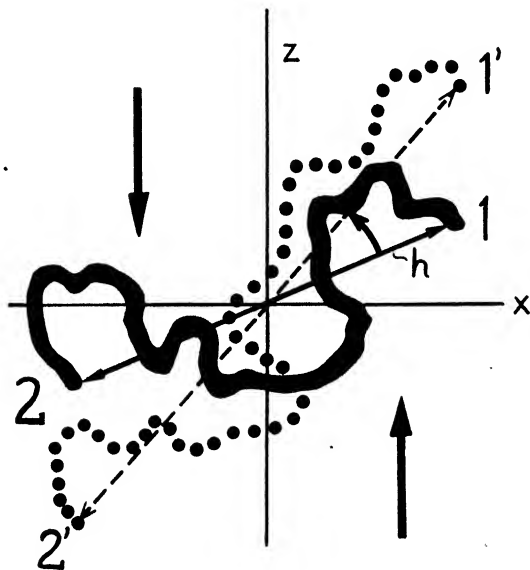
Fig. 6. Since the molecule end points have the tendency to adopt the speed of the surrounding liquid, the molecule is transferred from position 1, 2 to position 1', 2' under the influence of the gradient. Simultaneously, direction and length of vector h change (distances 1→2, 1'→2', respectively).

creased in Fig. 7. The direction of rotation of vector h is the same in both figures.

Summarizing the behavior of the chain molecule in a streaming solution, we have found that: *The molecule as a whole participates in the translation of the surrounding liquid. On this translation is superimposed a rotation of vector h occurring always in the same direction. To this motion is added a periodic dilatation and compression of the length of vector h (4).* Furthermore, the speed with which vector h rotates is large when h is perpendicular to the direction of flow (perpendicular to the z-direction of Figs. 5–7), and small when h is almost parallel to z. That means that the molecule does not spend equal periods of time in the different orientations.

Thus, a preferential orientation of the axis of the molecule is connected with the periodic dilatation and compression of the length h. This orientation of the vectors h is partly destroyed by thermal motion which tends to produce a uniform orientation of the molecule axes. The compression and dilatation of vectors h are also to some extent modified, first by the thermal motion in the direction of vector h; second, by force (Eq. 8) which causes the ends of the molecules to attract each other for statistical reasons; and third, as a consequence of the shape resistance, $i.e.$, the
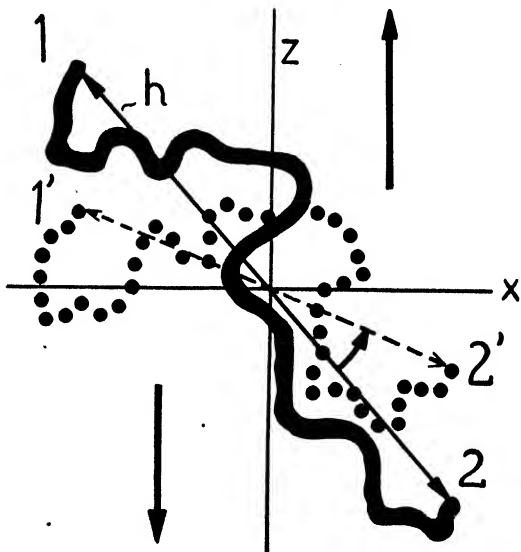
FIG. 7. During the change from position 1, 2 to 1′, 2′, a change of direction and also a contraction of vector h occur.

resistance (Eq. 10), which is proportional to the speed dh/dt of a change in distance h. It is, therefore, obvious that the speed of deformation dh/dt in the moving solution is greater, the greater the velocity gradient in the liquid surrounding the molecule. Therefore, the effect of the shape resistance of the chain molecule becomes especially evident under conditions of large shear rates.

It is easily seen that the molecule is always able to participate in the change of direction of the vectors h, but that it does not completely realize the change in length which would correspond to the change from the positions 1, 2 to 1′, 2′ in Fig. 6. This is partly prevented by forces represented in Eqs. (8) and (10). As a consequence of this only partly realized change of length, the ends of the molecules (points 1 and 2 in Fig. 6) attain, in flowing solutions, finite speeds relative to the surrounding liquid. (The

liquid moves from 1 to 1′, for instance, regardless of whether the molecule end 1 can completely follow this motion.) As a consequence of this relative velocity frictional forces appear. We can comprehend them, by assuming that there is localized one-fourth of the total chain in each of the points 1 and 2 of the molecule given in Fig. 6 while the hydrodynamic effects of intermediate chain parts are neglected. Assuming that the chain end 1 has the speed w relative to the surrounding liquid, the additional
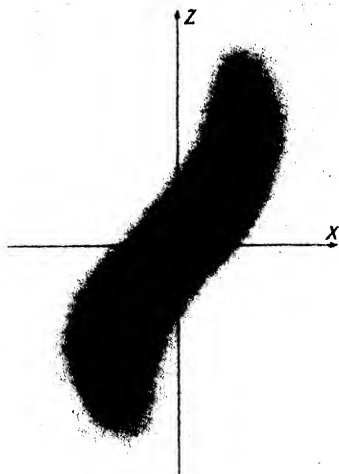
FIG. 8. Distribution of the chain end points in a streaming solution for molecules with large shape resistance. One end of all chain molecules present per unit volume is, in this representation, placed at the origin of the coordinate system. The direction of flow coincides with the z-axis; that of the gradient of flow with the x-axis. Molecules with high h values are highly oriented in the streaming solution.

force k_3 acting on this chain end as a consequence of friction with the surrounding liquid of viscosity η_0 equals

$$k_3 = w\eta_0\lambda L/4 \tag{11}$$

where λ is a frictional factor, which, for moderate values of Z as a rough approximation, is equal to $3\pi/2$ (4). According to more recent investigations (9), λ must be expressed by the equation:

$$\lambda = \frac{1}{-0.05 + 0.12 \log_{10} \dfrac{A_m}{d_h} + 0.037 \sqrt{\dfrac{b}{A_m}} \sqrt{Z}}, \tag{12}$$

where A_m represents the length and d_h the thickness of the statistical

chain element.[3] For the following it is sufficient to know that λ is a numerical constant for a given molecule.

In the solution at rest, the distribution calculated in Eq. (6) results from the interplay of the diffusion of the molecule ends and the force shown in Eq. (8). In the streaming solution a distribution function is obtained which is dependent on the gradient of flow and is based on the diffusion tendency of the molecule ends and on forces shown in Eqs. (8), (10), and (11). The detailed calculation shows, as could be expected, that we find the vectors h in certain angular positions more frequently and that their absolute values are larger in certain orientations and smaller in others (Fig. 8).

IX. DEPENDENCE OF FLOW BIREFRINGENCE AND VISCOSITY ON THE FLOW GRADIENT IN SOLUTIONS OF CHAIN MOLECULES WITH SMALL AND LARGE SHAPE RESISTANCE (2)

From the considerations just described we can not only determine the distribution function of the vectors h, but also the speed with which they rotate or change their length. Thus, again, the speed of the parts of the molecule relative to the surrounding liquid is given. These relative velocities determine essentially the rate of dissipation of energy due to the presence of a particle in the streaming solution and, therefore, the viscosity of the suspension. Thus, a knowledge of the distribution function of the vectors h makes a computation of the viscosity possible. On the other hand, the optical behavior of the solution can also be determined immediately when the distribution function is known. A chain molecule with end-to-end distance h must be considered as an ellipsoid of revolution with the polarizabilities γ_1 and γ_2 (Eq. (9)). When we know the distribution in the solution of the h values according to magnitude and orientation, we also know the polarizability of the suspension in any direction. This determines the index of refraction of the solution as a function of the direction of polarization and propagation of the light used. Consequently, the magnitude and direction of the birefringence $n_1 - n_2$ can be obtained. Parts of the results are shown in Figs. 9 and 10.

---

[3] According to Eq. (12), λ will be practically constant for low values of Z and inversely proportional to $\sqrt{Z}$ for elevated values of Z. As has already been pointed out in 1943 (4), this dependence of λ corresponds to the fact that the statistical coil consisting of a low number of chain elements is completely washed through if moved through a liquid, while an increasing amount of solvent is immobilized inside the coil if the number of statistical elements is increased. The limiting cases of complete, *viz.*, missing immobilization, has been considered in early papers by W. Kuhn (3) on one hand, and by M. L. Huggins (17) on the other. The partial immobilization of solvent inside the coil is completely neglected in some recent papers by P. Debye (16) and by H. A. Kramers (15). The concept of partial immobilization of solvent has however been adopted subsequently by P. Debye (18) and H. I. Brinkman (19).

a. Flow Birefringence

In Fig. 9, $n_1 - n_2$ is plotted against the gradient of flow γ. Curve 1 represents the case of a small shape resistance (B in Eq. (10) equals zero) and Curve 2 the opposite extreme ($B = \infty$). For small gradients of flow (γ) Curves 1 and 2 coincide, which proves that the amount of flow bire-
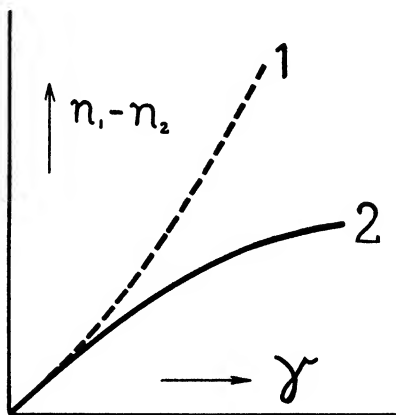
FIG. 9. Dependence of the amount ($n_1 - n_2$) of the flow birefringence on gradient of flow γ. Curve 1: Vanishing shape resistance; *i.e.*, $B = 0$; Curve 2: Large shape resistance, *i.e.*, $B \gg Zb\lambda\eta_0/8$.
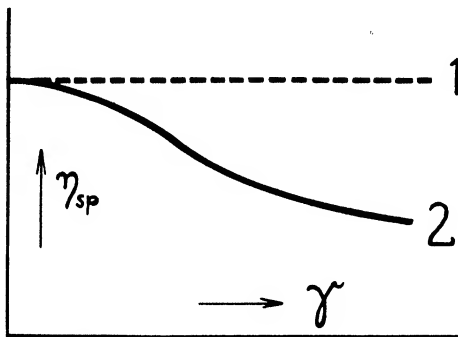
FIG. 10. Dependence of intrinsic viscosity η_{sp} on flow gradient γ. Curve 1: Vanishing shape resistance; *i.e.*, $B = 0$; Curve 2: Large shape resistance, *i.e.*, $B \gg Zb\lambda\eta_0/8$.

fringence, in this case, is independent of the magnitude of the shape resistance. We mentioned in a preceding paragraph that such behavior was to be expected, the extra force from Eq. (10) due to shape resistance becoming important only in the case of a large shear gradient, because only in this case dh/dt values of considerable magnitude will ·occur.

It therefore becomes clear that molecules with large and small shape resistance cannot be distinguished by the extent of the double refraction of flow at *small* velocity gradients. On the other hand, Fig. 9 shows that there is a very definite difference at large gradients. *In chain molecules with small shape resistance the parameter $n_1 - n_2$ increases more than proportionally to γ; for molecules with great shape resistance, that is, more nearly rigid molecules, less than proportionally to γ.* Also this behavior is easily understood from the qualitative description of the behavior in solution. In molecules with *small* shape resistance the change from positions 1, 2 in Fig. 6 to positions 1', 2', which is connected with a strong increase of vector h, can occur readily. A molecule with a great shape resistance, on the other hand, participates in the change of orientation of vector h but not in the change of length. *In molecules with great shape resistance* the distribution of length of the vectors h as it was realized in the solution at rest (Eq. (6)) is almost completely retained in the moving solution. These molecules rotate but their length changes hardly at all in the course of one rotation and only very little in the course of many. (In the solution in motion the average expanding forces somewhat exceed the average contracting forces.) In a suspension of *molecules with small shape resistance, we find, in orientation 1', 2' of Fig. 6, molecules with strongly increased h values, i.e., with very great optical anisotropy according to Eq. (9), but not in an otherwise identical solution of molecules with great shape resistance.* This explains the stronger increase in the amount of birefringence in suspensions of molecules without shape resistance than of molecules with a high shape resistance.

b. Viscosity

In Fig. 10 the dependence of the intrinsic viscosity of a solution of chain molecules of given molecular weight is plotted against the gradient γ. Here also, Curve 1 corresponds to small, and Curve 2 to large, shape resistance of the solute molecules. The intrinsic viscosity of a solution is independent of the magnitude of the shape resistance B for small gradients. The reasons for this are identical with those advocated in explaining Fig. 9. Fig. 10 also shows that the intrinsic viscosity for chain molecules with small B is independent of the gradient γ up to high γ values. On the other hand, the intrinsic viscosity for a "stiff" molecule decreases in the range of large gradients of flow. This difference can be qualitatively deduced from the fact that the molecules with a small shape resistance, but not those with a large one, are strongly expanded during the change from positions 1, 2 to 1', 2' in Fig. 6. The larger the h values, however, the larger the relative velocities between the ends of the molecule and the surrounding liquid, and the larger the dissipation of free energy in the solution and the intrinsic viscosity.

X. Comparison with Experimental Results: Dependence of Shape Resistance B on Degree of Polymerization Z

The behavior of the flow birefringence and the viscosity of solutions of chain molecules as shown in Curves 1 and 2 of Figs. 9 and 10 has also been observed in actual experiments. There are cases indicating large and others indicating small shape resistance. It is characteristic that solutions indicating small shape resistance on the basis of their birefringence show an analogous viscosity behavior and that a solution with a birefringence corresponding to Curve 1 of Fig. 9 has a viscosity curve corresponding to Curve 1 in Fig. 10 and *vice versa*. *It also appears that in a series of homologous polymers the lower members possess large B values and the higher ones small B values in Eq. (10)*. It can be shown theoretically that, with increasing degree of polymerization in a homologous series, B decreases proportionally to $1/Z$:

$$B = \beta/Z, \qquad (13)$$

where β is a constant in the series.[4]

TABLE I

Substance	Solvent	β	q cal./mole	θ sec.
Cellulose nitrate	Butylacetate	2.3×10^{-4}	11,000	1.3×10^{-3}
Cellulose nitrate	Cyclohexanone	10^{-5}	8,500	4.7×10^{-5}
Methylcellulose	Water	2×10^{-6}	7,600	6.4×10^{-6}
Polystyrene	Cyclohexanone	10^{-3}	11,400	1.6×10^{-4}

By evaluating cases where the curves for viscosity and birefringence are somewhat between those in Figs. 9 and 10, it is possible to compute the values for B in Eq. (10) or for β in Eq. (13). The β values so obtained are given in Table I, Column 3.

[4] The proportionality of B to $1/Z$, that has thus been demonstrated both experimentally and theoretically, is of interest in connection with an attempt made by Frenkel (5) to describe some relaxation phenomena in bulk rubber under a different assumption, namely, under the hypothesis that B (in the present designation) is independent of Z. It is clearly seen that Frenkel's hypothesis must be abandoned.

It must, moreover, be emphasized, that our treatment of the behavior of dissolved chain molecules should not be applied without essential changes to problems concerned with bulk rubber. Attention should be paid especially to the fact that bulk rubber exhibits, with respect to a movement of chain fragments, a viscosity which is highly dependent upon the shape and molecular weight of the diffusing parts; in the decisive region of high molecular weight M of the diffusing parts, the viscosity of bulk rubber increases exponentially with M (14).

XI. Activation Energy q for Restricted Rotation

We showed in Section VII that the shape resistance for the chain or its resistance to rapid changes in configuration are connected with the restricted rotation around the valence bonds in the chain. Actually the molecular shape resistance will be larger, the larger the activation energy q which must be applied to rotate on segment around the axis of a valency bond relative to another segment from a position of minimum potential energy into a neighboring minimum position. For ethane this energy q (necessary to rotate one CH_3 group around the C—C bond as axis by 60° from a position of minimum potential energy) is approximately 3000 cal./mole; for dichloroethane q is approximately 6000 cal./mole. Since the constant β depends on the extent of restricted rotation and, therefore, on q, it is possible to compute from the data for β (Eq. (13) and Table I, Col. 3) the activation energy q. These data are given in Table I, Col. 4. All values are slightly higher than those for ethane and dichloroethane. Taking polystyrene as an example, we find that the high values are quite reasonable because the bulky phenyl group causes steric hindrance. A comparison of the data in Table I seems to indicate that the value for q for a given substance is, within certain limits, dependent on the solvent. This also seems reasonable since the steric influences of the solvent molecules surrounding the solute molecule must become noticeable in the act of rotation.

XII. Time Requirement for Spontaneous Changes in Internal Constellation of a Chain Molecule. Diffusion Constant of the End Point of the Chain; "Macro Constellation Changing Time" (10)

At the beginning of this discussion we referred to spontaneous changes in the constellation of chain molecules in solution caused by Brownian motion. It was shown that the time the chain molecule requires for such a change depends on the freedom available for rotation. We furthermore introduced the parameter B (Eq. (10)) for characterizing the shape resistance. This parameter also depends, as we just saw, on restricted rotation. In the following we intend to indicate how to compute the time required by the molecule for changes in internal configuration once B is known. For this purpose we recall the relation between the mobility μ of a particle, *i.e.*, of the speed attained under the influence of a unit force with the diffusion constant D of the particle:

$$D = \mu kT. \tag{14}$$

This can be derived following the procedure of Einstein and Smocholuwski. Let a number of particles be brought into a potential field parallel to the z-direction such that the potential energy of an individual particle

at a point z equals $U = U(z)$. The number n of particles per unit volume in volume element at z equals, on the basis of the Maxwell-Boltzmann law:

$$n = n_0 e^{-(U(z)/kT)} \tag{14a}$$

and

$$\frac{dn}{dz} = - n_0 e^{-(U(z)/kT)} \cdot \frac{\partial U}{\partial z} \frac{1}{kT} = - n \frac{1}{kT} \frac{\partial U}{\partial z}. \tag{14b}$$

$-(\partial U/\partial z)$ is the force acting on the individual particle as a consequence of the presence of the potential field. Hence, $-(\partial U/\partial z) \cdot \mu \cdot n$ particles pass under the influence of this force per second through a cross section of unit area at z in the positive direction. If, on the other hand, D be the diffusion constant of the particles and dn/dz the gradient of concentration at point z, then the number of particles which pass as a consequence of diffusion per second through a unit cross section at z in the positive direction equals $-D(dn/dz)$. In a steady state, the sum of the two terms equals zero, thus:

$$- \frac{\partial U}{\partial z} \mu n - D \frac{dn}{dz} = 0, \tag{14c}$$

which, with the aid of Eq. (14b), gives at once relation (14).

The above proof is independent of the nature of the particles. According to Eq. (10), the mobility of the end point of the chain molecule, *i.e.*, the speed dh/dt observed when a force of one dyne reacts on the end points in the direction of the vector h, equals:

$$\mu = 1/B.$$

According to Eq. (14) we can, therefore, attribute the diffusion constant

$$D = kT/B \tag{15}$$

to the end point of the molecule for the motion in direction h. If we know, however, the diffusion constant of a particle or a point, we can find the mean square displacement of the particle or the point expected in a time interval t. For our case, the average square of distance Δh traveled by the end point of the molecule in the direction of vector h, equals:

$$\langle (\Delta h)^2 \rangle = 2D \cdot t$$

or under consideration of Eqs. (15) and (13):

$$\langle (\Delta h)^2 \rangle = \frac{2kT}{\beta} Z \cdot t. \tag{16}$$

We now replace the displacement Δh in Eq. (16) by the quantity $2\sqrt{\overline{h^2}}$ from Eq. (7a). The corresponding time θ computed from Eq. (16) is the mean period required by the chain molecule in the solution to double or

reduce by one-half, by means of thermal motion, the distance between its two end points under utilization of restricted rotation. For the sake of brevity we shall call this time the *"macro constellation changing time"* of the molecule in solution. This is the period within which the constellation of the chain molecule is spontaneously and "completely" changed. From Eqs. (3) and (4) one finds:

$$\theta = 2A_m b \frac{\beta}{kT},\tag{17}$$

which means *that the "macro constellation changing time" becomes independent of the degree of polymerization.* This is plausible. Although, with increasing degree of polymerization, the length of the path $2\sqrt{\overline{h^2}}$ the chain end travels for a complete change of constellation increases, the number of axes of rotation which cause this displacement increases simultaneously. It must be emphasized however, that this independence on Z only holds if relation (10) is valid for the force necessary to move the ends of the chain relative to each other at a rate dh/dt. We pointed out before that this force must be increased when the chain molecule is embedded in a highly viscous medium. An additional friction force is in this case due to the external resistance of the surrounding medium.

XIII. Influence of Viscous Resistance of the Surrounding Medium

Under consideration of the viscosity η_0 of the surrounding medium the "macro constellation changing time" becomes:

$$\theta = 2A_m b \frac{\beta}{kT} + L^2 \lambda \eta_0 A_m \frac{1}{4kT}\tag{18}$$

As has already been mentioned, L is the hydrodynamic length of the chain, b that of the monomer unit, A_m the length of the statistical preferential segment, η_0 the viscosity of the surrounding medium and λ a numerical factor of approximate magnitude $3\pi/2$ (see Eq. 12). It turns out that the added term which is proportional to Z^2 or L^2, respectively, can be neglected in comparison with the first one in Eq. (18) when dealing with ordinary solvents such as cyclohexanone or acetone and solutes such as polystyrene or cellulose nitrate, up to values of a few thousands for Z. The "macro constellation changing time" of the aforementioned substances is thus independent of the degree of polymerization within these limits. Data are listed in Table I, Col. 5, which show that the "macro constellation changing time" is very short, of the order of magnitude of 10^{-4} seconds, in spite of the relatively large values of the activation energies q (Table I, Col. 4). It is noteworthy that θ has small but finite values, and that, according to Eq. (18), it increases for very large Z almost proportionally

to Z^2 or L^2. Large deformations occurring in a period smaller than θ can be treated as if, during this period, the molecule did not undergo any change of internal constellation through Brownian motion. Spontaneous changes, however, will have to be considered in all processes having characteristic time constants larger than θ.

XIV. Stress Relaxation Time τ

One further characteristic quantity of long chain molecules which is intimately connected with the possibility of restricted rotation is the *stress relaxation time τ*. We may mention at once that it is related to, but at the same time distinctly different from, the macro constellation changing time θ discussed in the foregoing section. It was pointed out previously that rapid changes in the distance between the chain ends from h to $h + \Delta h$ cause changes in the interatomic distances and valence angles, that elastic tensions are thus produced in the chain and that these stresses are gradually annihilated by reorientation processes in the chain due to thermal motion. The relaxation time τ of stress is defined as the period in which the elastic tension in the chain molecule is reduced to a fraction $1/e$ of its initial value. By a consideration which can only be mentioned here (10), τ can be derived as a function of Z, q A_m, b, M_g, T and the angular distance of the minima of potential energy which occur during rotation around axes of restricted rotation. In the simple case of a hydrocarbon chain, τ equals:

$$\tau = \frac{\pi^2 kT}{864} \cdot \frac{Z}{q} \cdot \theta. \tag{19}$$

For degrees of polymerization in the neighborhood of $Z = 10^3$, τ is not very different from θ; regarding the order of magnitude of τ the same can be concluded as for the θ values in Table I. Large differences between τ and θ occur for very large values of Z, such as $Z = 10^6$.

When the chain molecule is under mechanical stress for a period longer than τ, it must be considered as completely "soft," because, in this case, there is sufficient time available for the relaxation of the stresses. But for a time scale considerably shorter than τ, there is insufficient time for the removal of the energy changes, *viz.*, of the corresponding elastic tension, by utilization of bond rotation. Under such disturbances the molecule must be considered as rigid and, therefore, brittle. By the action of a force which is applied for a very short time only, the molecule can be broken apart without the coil being able to realize any appreciable change of its shape prior to its destruction. It is probable that the depolymerization of chain molecules in solution by ultrasonics or large flow gradients is connected with the fact that under short-time stresses the chain molecule exhibits brittleness. It should also be pointed out that a

short time ago J. Ferry (11) investigated the dependence of the shearing modulus on the frequency in polystyrene solutions in toluene with the result that there is a strong increase in the shearing modulus when the period of vibration is decreased to 10^{-4} seconds. This is in accordance with the "macro constellation changing time" as determined from flow birefringence and viscosity as listed in Table I. The stress relaxation time τ will probably also be important for the behavior of rubber and similar substances under short-time stress. Under disturbances *of short duration* or high frequency the retractive force in rubber will thus not be limited to the elasticity due to entropy effects, which itself is partly dependent and partly independent of time; a component of stress due to *energy effects* will be added, which is highly dependent on time and which is caused by the incomplete relaxation of the internal stresses in the chain as discussed above. One can presume in conclusion that the idea of a shape resistance for chain molecules will be of interest for the behavior of solutions as well as that of highly elastic solids.

REFERENCES

1. KUHN, W., *Kolloid-Z.* **68**, 2 (1934); *Z. angew. Chem.* **49**, 858 (1936). Compare also GUTH, E., AND MARK, H., *Monatsh.* **65**, 93 (1934). For summary see: KUHN, W., *Experientia* **1**, 6 (1945).
2. KUHN, W., AND KUHN, H., *Helv. Chim. Acta* **28**, 1533 (1945); **29**, 71 (1946).
3. KUHN, W., *Kolloid-Z.* **68**, 2 (1934).
4. KUHN, W., AND KUHN, H., *Helv. Chim. Acta* **26**, 1394 (1943).
5. FRENKEL, T., *Acta Physicochim. U.R.S.S.* **9**, 235 (1938).
6. KUHN, W., AND GRUEN, F., *Kolloid-Z.* **101**, 248 (1942).
7. KUHN, W., *ibid.* **76**, 258 (1936); *Z. angew. Chem.* **51**, 680 (1938); *Kautschuk* **14**, 182 (1938).
8. MAXWELL, T. C., *Phil. Mag.* [4] **35**, 134 (1867); for applications to high polymers compare: KUHN, W., *Z. phys. Chem.* **42B**, 1 (1939); *Z. angew. Chem.* **52**, 289 (1939).
9. KUHN, H., *Habilititationsschrift*, Basel, 1946; KUHN, W., AND KUHN, H., *Helv. Chim. Acta* **30**, 1705 (1947); KUHN, H., AND KUHN, W., *J. Polymer Sci.* in print.
10. KUHN, W., AND KUHN, H., *Helv. Chim. Acta* **29**, 609, 830 (1946).
11. FERRY, J., *Ann. N. Y. Acad. Sci.* **44**, 313 (1943).
12. HERMANS, J. J., *Physica* **10**, 777 (1943).
13. KUHN, W., AND GRÜN, F., *J. Polymer Sci.* **1**, 183 (1946).
14. KUHN, W., KÜNZLE, O., AND PREISSMANN, A., *Helv. Chim. Acta* **30**, 307, 464 (1947).
15. KRAMERS, H. A., *J. Chem. Phys.* **14**, 415 (1946).
16. DEBYE, P., *ibid.* **14**, 636 (1946).
17. HUGGINS, M. L., *ibid.* **43**, 439 (1939).
18. P. DEBYE, *Phys. Rev.* **71**, 486 (1947).
19. H. C. BRINKMAN, *Appl. Sci. Res.* A **1**, 27 (1947); *Kon. Nederl. Akad. van Wetenschappen* **50**, No. 6 (1947).

COMPARATIVE STUDIES ON PHOTOELASTICITY
OF ELASTOMERS AND PLASTOMERS [1]

Wilfried Heller

Department of Chemistry, Wayne University, Detroit, Michigan

and

Hans Oppenheimer

Department of Chemistry, University of Chicago, Chicago, Illinois

Transparent films of elastomers and plastomers were found to differ sufficiently in their photoelastic behavior to make stress double refraction a useful criterion of the prospective mechanical properties of a given material. The stress double refraction in such films is mostly an effect of deformation, of orientation, or of both deformation and orientation of polymer chains. In such polymers, however, which crystallize under stress, a large part of the optical effect may be due to oriented crystallization. In addition to its practical value as a testing method for polymers, the photoelastic method offers, therefore, particularly in combination with simultaneous investigations of mechanical properties, the prospect of correlating mechanical properties of a polymer film with its internal structure, and of correlating changes in both qualities upon exposure of the film to different degrees of stress. Although results obtained on such films, by means of X-ray diffraction or X-ray scattering and electron-diffraction, are, in general, easier to interpret, the photoelastic method has the considerable advantage of making possible a quantitative follow-up of rapid changes in film structure, *e.g.*, of relaxations.

Fig. 1 gives a survey of the apparatus used. Its comprehensive description, and an extensive presentation and discussion of the results obtained with it, will follow in a paper to be published later. The purpose of the present preliminary account is to illustrate selected aspects of the potentialities of the method in comparative investigations, with particular reference to polythene (polyethylene).[2]

[2] The samples of polythene used were a product of the E. I. duPont Co., and were kindly given to us by Professor H. Mark of the Brooklyn Institute of Polymer Research. The samples were optically completely isotropic prior to stretching. They differed

A comparatively simple type of photoelastic investigation, by means of which characteristic differences between elastomers and plastomers and, in addition, differences between non-crystallizing and crystallizing elastomers can be detected, is the study of double refraction as a function of elongation of a film. The film, generally 180–250 μ thick, is clamped firmly in slipproof jaws of an electrically operated stretching device, and
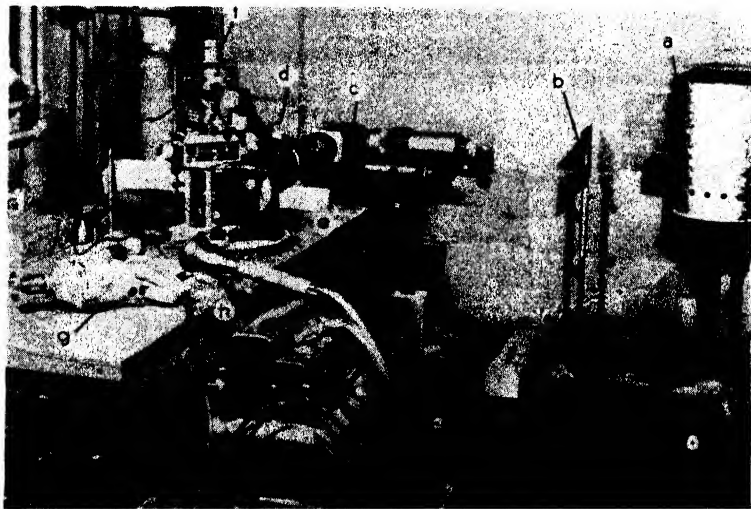
FIG. 1. Apparatus for the study of stress double refraction in films.

a, Light source (tungsten ribbon filament lamp); b, collimating lens; c, monochromator; d, heat filter; e, condensing lens; f, polarizing microscope with mounted stretching apparatus; g, drill for rapid stretching of film. (Disengages automatically at any desired elongation.) Applied at (f); h, dictaphone for the recording of rapid successive measurements.

is extended, normally to the direction of the light beam, to any elongation desired within the available range. The elongation, ΔL_s, is expressed in per cent of the original length of the sample, i.e., $\Delta L_s = \dfrac{(L_s - L_o)}{L_o} \times 100$, where L_o is the original length of the sample and L_s is its length under stress. Both lengths are known with an accuracy of better than 1%. Unless stated otherwise, the film remains under stress during the optical investigation, which is carried out with a polarizing microscope provided with a synchronous polarizer-analyzer movement and with an ellipticity

compensator (sensitivity limit of compensator: a path difference, Δ, of 30 A.). To have numbers of a convenient order of magnitude, the path difference is expressed in μ/mm. of polymer thickness. The value of $(n_s - n_o)$ is easily obtained from Δ by multiplying it by 10^{-2}. The values obtained are valid for 5461 A and for room temperature (23°–25°C.).

Fig. 2 gives the type of results obtained. They apply to the optical effect observed in the samples under stress, Δ_s, after changes with time (see below) have gone to practical completion (symbolized by the addi-
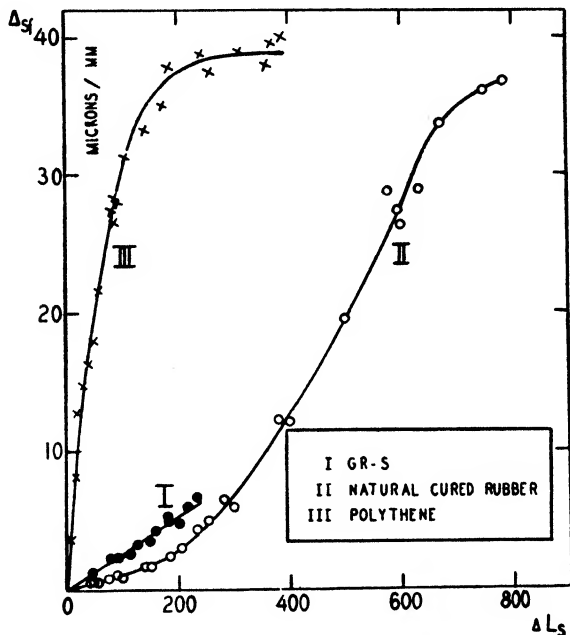
FIG. 2. Variation of final double refraction with elongation.

tional subscript: f). It may be mentioned that each experimental point, both here and in subsequent figures, excepting Fig. 4, was obtained with a different sample cut from the same film in bulk. This accounts for the scattering of the experimental points which, on the whole, is moderate. Non-crystallizing elastomers, such as GR-S rubber, show a nearly linear increase of birefringence with elongation up to the elongation where rupture of the film occurs (Curve I). Crystallizing polymers, such as cured natural rubber, show the same behavior at sufficiently small elongations. At higher elongations, however, crystallization leads to a steep increase in birefringence with elongation. The complete curve is, there-

fore, characterized by a fairly strong increase in slope at intermediate elongations (Curve II). Plastomers, such as polythene, finally, exhibit curve type III, *i.e.*, they show a very steep increase of double refraction at low elongation, followed, at moderate elongations, by an approach to saturation. At low elongations (ΔL_s of less than 150), the double refraction
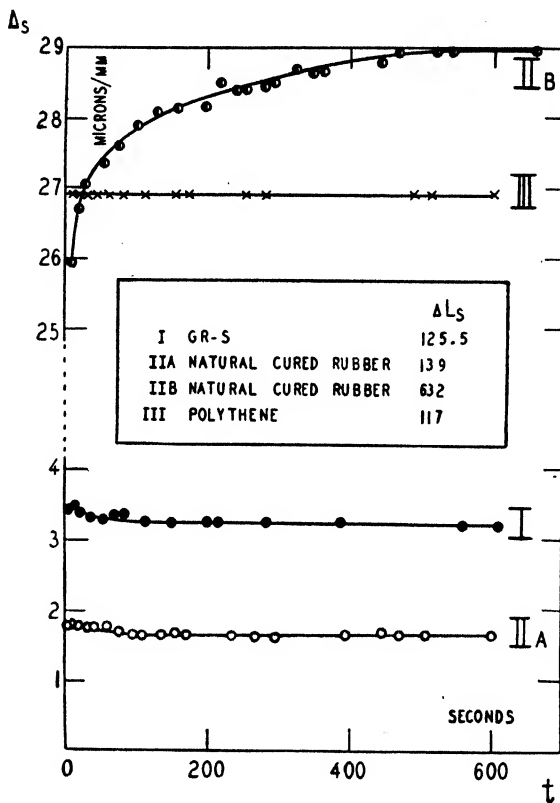
Fig. 3. Variation of double refraction with time at constant elongation.

is, at least in polythene, an order of magnitude larger than in either type of typical elastomers. This difference is far too large to be accounted for by differences in the optical anisotropy of chain elements in polythene compared to rubbers. Nor does it seem to be possible to explain this difference by a strong difference in the degree of elastic deformation of cross-linked chains. It seems to be necessary, therefore, to assume that, at
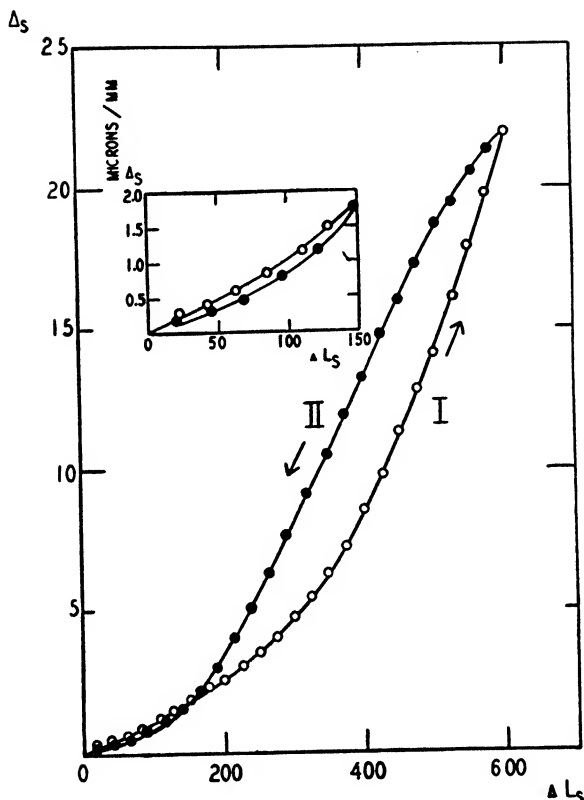
FIG. 4. Variation of double refraction with elongation, in natural cured rubber, under simultaneous variation of time.
I. Partial successive extensions; II. subsequent, partial successive retractions. (The time interval between the successive changes in elongations, and between the successive optical measurements, was 2.0 minutes throughout.)

comparable elongations, a far better orientation of polymer chains takes place in plastomers than in elastomers.[3]

Another method of differentiation between the various types of polymer films is illustrated by Fig. 3. It shows the change of double refraction with time, t, subsequent to rapid extension of a film, the latter requiring

[3] The concept of orientation in polythene under stress is supported by recent investigations of the infrared absorption of linearly polarized light by some of our stretched samples. These experiments were carried out by J. W. Ellis and L. Glatt in the Physics Department of the University of California, Los Angeles. According to a private communication by Professor Ellis, the spectrum features can be interpreted in terms of partially oriented CH_2-groups ((J. Chem. Phys., in press).

less than one second for a $\Delta L_s \leqslant 400$ and less than 2 seconds for a ΔL_s $\leqslant 800$. Curve I refers to elastomers which do not crystallize. Here, the double refraction decreases with time at constant elongation, and for all ΔL_s values, particularly during the first 20 seconds following stretching. Again, crystallizing elastomers show the same behavior provided the elongations, ΔL_s, are kept below those which cause crystallization (Curve IIa). At higher elongations, crystallization leads to an increase in double refraction with time (Curve IIb). (Special experiments seem to indicate that a decrease of double refraction with time occurs also for the higher
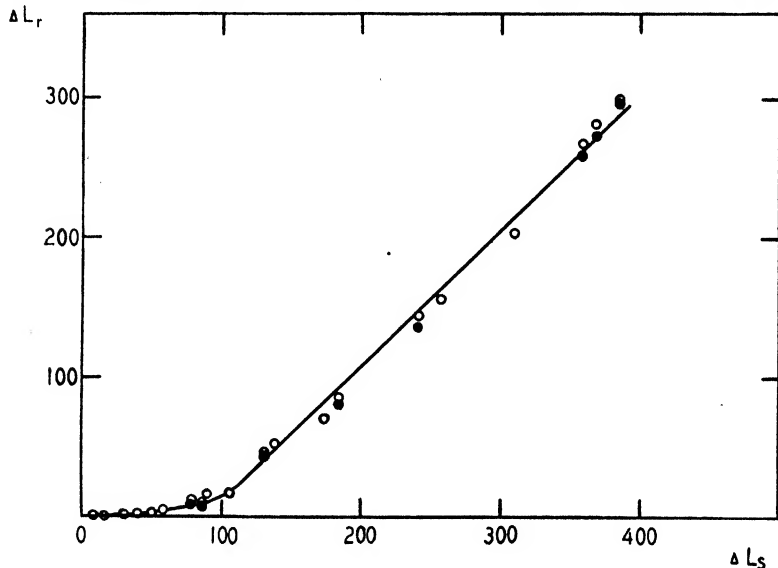
Fig. 5. Variation of mechanical retraction with the degree of preceding elongation of polythene.

○ 24 hrs. after release of stress. ● 12 days later.

elongations, but it is overshadowed by the far larger opposite effect.) Thus, quite complex curves result if the double refraction is measured in a gradually extended and subsequently gradually retracting sample. Two pointed hysteresis loops are then obtained which touch each other at a moderate elongation (Fig. 4). The existence of these two consecutive loops of which only the more pronounced one, due to crystallization, seems to have been observed previously (1), agrees with the calorimetric results obtained on crystallizing polymers by Guth and associates (2). In contradistinction to typical elastomers, polythene does not show any detectable change of double refraction with time, at least not after completion of rapid extension (Fig. 3, Curve III).

Of particular interest is the combined investigation of mechanical retraction and optical relaxation of polymer films after a complete release of stress, which leads to a length $L_r > L_o$ and to a permanent residual path difference $\Delta_r > \Delta_o$ ($\Delta_o = 0$ for the samples used.) The discussion of this point shall be limited to the special case of polythene. Fig. 5 shows the residual increment in length, $\Delta L_r = [(L_r - L_o)/L_o] 100$, as a function of ΔL_s. Fig. 6 gives Δ_r as a function of ΔL_s, and Fig. 7 illustrates the vari-
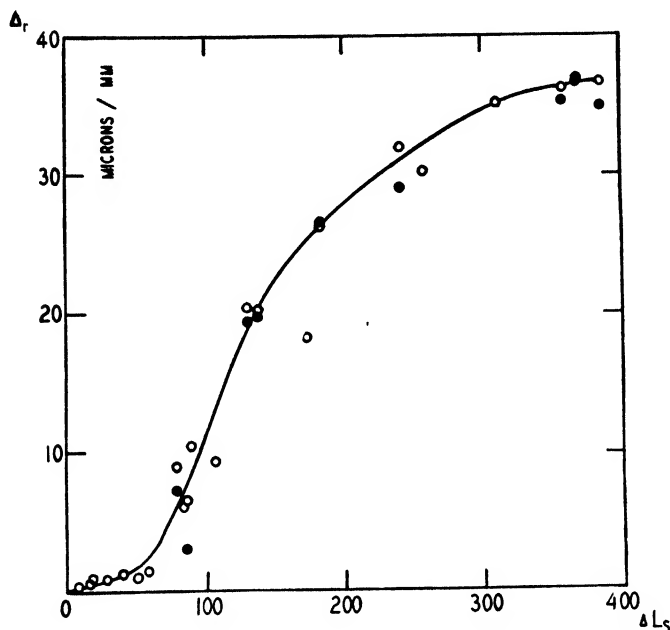
FIG. 6. Variation of residual (permanent) double refraction in retracted polythene with preceding elongation.

○ 24 hrs. after release of stress. ● 12 days later.

ation of Δ_r with Δ_{sf}. The three Figs. refer to the same series of samples. Their comparative discussion leads to the following conclusions:

(a) Polythene is predominantly elastic at low elongations.

(b) Extensive plastic flow sets in, according to Fig. 5, above a certain moderate elongation. It is accompanied by a steep increase in permanent double refraction (Figs. 6 and 7) which indicates a strong rise in irreversible orientation of polymer chains (3). Although the present data do not allow a differentiation between cause and consequence, a hypothesis seems to be inviting to the effect that a critical degree of stress-induced,

largely reversible, chain alignment is necessary and sufficient in order to start, upon further increase in stress, an extensive plastic flow and to bring about, simultaneously, an extensive, though incomplete, further and largely irreversible alignment of polymer chains.

(c) Notwithstanding the fact that plastic flow is the predominant feature if polythene is stretched beyond a "critical" range of elongations, a pronounced elastic retraction occurs also above the latter range. The
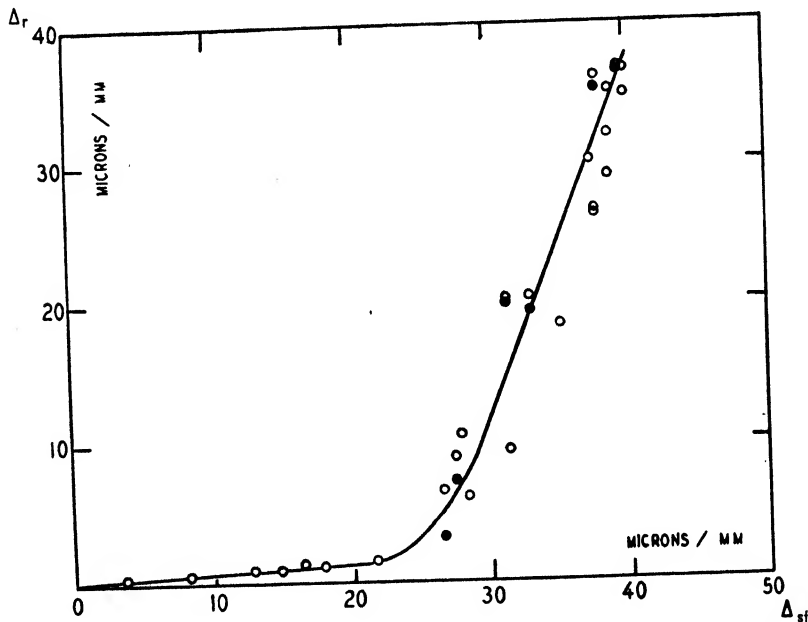
FIG. 7. Variation of residual double refraction in retracted polythene with the double refraction observed prior to retraction.

○ 24 hrs. after release of stress. ● 12 days later.

practically constant value of nearly 1 of the slope in Fig. 5 indicates that the absolute degree of elastic retraction (*i.e.*, the absolute decrement in length $(L_e - L_r)$) is then independent of elongation. The relative degree of retraction (*i.e.*, the decrement in length in per cent of the length prior to retraction), however, decreases very strongly with increasing elongation. A nearly inverse behavior is found at comparable elongations for typical elastomers, such as cured natural rubber and GR-S. Here, the relative degree of retraction is nearly independent of elongation—considering the status reached one hour after the release of stress—and the

absolute degree of retraction increases with elongation. Polythene behaves similarly at elongations below the critical range.

The absolute degree of retraction may be taken as a rough indication of the magnitude of the restoring force. It therefore appears that the restoring force in polythene changes little, if at all, with elongation, in the range where plastic flow predominates, whereas it increases with elongation below the critical range of elongations. In contradistinction, the restoring force in cured natural rubber increases with elongation throughout the range investigated (largest ΔL_s:785).

Preliminary studies on polythene suggest that there is also a correlation between the magnitude of the restoring force and the rate of optical relaxation which follows a rapid "partial" retraction. Here, the samples are allowed to retract only partially, from a length L_s to a length L_{p_1}. After a sufficiently long time, they are allowed to carry out a second partial retraction, from L_{p_1} to L_{p_2}, and so on. The relative degree of each successive partial retraction, is kept equal, *i.e.*,

$$[(L_s - L_{p_1})/L_s] \times 100$$
$$= [(L_{p(n-1)} - L_{pn})/L_{p(n-1)}] \times 100 = \Delta R = \text{constant}.$$

Such experiments show that the practically instantaneous partial mechanical retraction is not accompanied by an equally rapid adaptation of birefringence to the reduced elongation. The optical effect continues to decrease with time, particularly during the first minute after partial retraction. One may, for practical purposes, define a relaxation time, τ', which represents the time necessary to reach $1/2$ (instead of $1/e$ which would characterize τ) of the decrement $\gamma_n = (\Delta_{p(n-1)} - \Delta_{pn})$. (Thus $\gamma_1 = (\Delta_s - \Delta_{p_1})$). It is then found on polythene that τ', whenever it is large enough to be measured, increases strongly with the decrease of L_p, ΔR being constant. Table I shows a few of the results obtained considering ΔL_s values of 50 and 80, respectively. In both cases, $\Delta R = 20$. Since both ΔL_s values considered fall into the range of elongations where polythene behaves predominantly as an elastomer, it appears that τ', whenever it is measurable, decreases as the restoring force increases. It is noteworthy that τ' was immeasurably small throughout the range of elongations which lead to predominant plastic flow.

The technique of successive partial retraction makes it possible to compare, at equal elongations ΔL_p, the double refraction of samples which had previously been brought to unequal higher elongations, ΔL_s and $\Delta L_s'$, respectively. As an example, Series I and Series II of Table I yield, by interpolation, a final path difference of 13.5 and 17.9 μ/mm., respectively, on partial retraction to a ΔL_p of 40, and a final path difference of 9.5, and 13.0 μ/mm., respectively, on further partial retraction to a ΔL_p of 20. Thus, samples of comparable length have a more anisotropic structure,

TABLE I

Variation of Optical Relaxation Time, τ', with Progressive
Partial Retraction of Polythene

$\Delta R : 20.0$; Series A. $\Delta L_s : 50.0$; $\Delta_{sf} : 15.1$ μ/mm. $\Delta L_p = \left(\dfrac{L_{p_n} - L_e}{L_e}\right) \times 100$

n (successive steps)	ΔL_p	$\Delta_{p_n f}$ ($\mu/mm.$)	γ_n ($\mu/mm.$)	τ' (sec.)
1	40	13.5	1.6	<5
2	32	12.0	1.5	<5
3	25.6	10.95	1.05	<5
4	20.5	9.65	1.3	<5
5	16.4	8.6	1.05	<5
6	13.1	7.0	1.6	<5
7	10.5	5.9	1.1	<5
8	8.4	4.4	1.5	10
9	6.7	3.3	1.1	20
10	5.4	0.5	2.8	540

Series B. $\Delta L_s : 80.0$; $\Delta_{sf} : 23.8$ $\mu/mm.$

n	ΔL_p	$\Delta_{p_n f}$ ($\mu/mm.$)	γ_n ($\mu/mm.$)	τ' (sec.)
1	64	21.35	2.45	<5
2	51.2	20.0	1.35	<5
3	40.9	18.1	1.9	<5
4	32.8	16.45	1.65	<5
5	26.2	14.7	1.75	<5
6	20.95	12.7	2.0	<5
7	16.8	11.6	1.1	<5
8	13.4	9.85	1.75	~5
9	10.75	8.45	1.40	10
10	8.6	7.35	1.1	50
11	6.9	6.0	1.35	215

the larger the elongation to which they had been brought previously. In addition, it can be seen from Table I that the relaxation time, τ', is, at a given ΔL_p, larger, the larger the original elongation, ΔL_s. Finally, Figs. 5 and 6 have shown that both the permanent increase in length of a sample, ΔL_r, and its permanent birefringence, Δ_r, are larger, the larger the original elongation. Since the double refraction and, implicitly, the structural anisotropy are larger the larger the elongation (see Fig. 2), it follows that (a) the ability of a polythene film to rearrange its structure in the direction of random distribution of individual chains and in the direction of a strain-free configuration of chain elements and side chains, and (b) the rate of this structural rearrangement, are less, in comparable states of retraction, the larger the original stress-induced structural anisotropy.

The usefulness of comparative photoelastic investigations was increased considerably by including recently, in the techniques outlined, simultaneous measurements on the variation of double refraction with a numerically known stress, *i.e.*, curves of the type compiled previously by other authors, *e.g.*, by Thibodeau and McPherson (4). Results obtained on polythene by means of the latter technique will be described in the near future.

REFERENCES

1. A comprehensive review of earlier investigations has been given by Wood, L. A., *J. Applied Phys.* **12**, 123 (1941).
2. Dart, S. K., Anthony, R. L., and Guth, E., *Ind. Eng. Chem.* **34**, 1340 (1942); Dart, S. L., and Guth, E., *J. Chem. Phys.* **13**, 28 (1945).
3. Heller, W., *Phys. Rev.* **69**, 53 (1946).
4. Thibodeau, W. E., and McPherson, A. T., *J. Research Natl. Bur. Standards* **13**, 887 (1934).

CONDUCTIVITY AT THE INTERFACE BETWEEN PYREX GLASS AND SOLUTIONS OF POTASSIUM CHLORIDE

Karol J. Mysels* and J. W. McBain

From the Department of Chemistry, Stanford University, Calif.

Recieved August 22, 1947

An interface is generally the seat of electrical surface conductance, the existence of which was predicted by Smoluchowski (1) and has been confirmed qualitatively for many systems. This conductance presumably is caused by the same double layer which is the seat of electrokinetic phenomena, and its study should provide an independent approach to problems of electrocapillarity. Attempts have been made to measure quantitatively the surface conductivity between Pyrex glass and dilute solutions of potassium chloride but there is serious disagreement in the results from different laboratories (2, 3, 10).

The present work suggests that the properties of this interface may be influenced by other factors which need thorough study and require a sensitive method of determining variations of surface conductivity.

By measuring the resistence of a potassium chloride solution through a Pyrex sintered disc, with proper precautions, we obtained values of instantaneous surface conductance which were definite and reproducible to about 1%. However, the surface conductance itself was found to change slowly simply on standing, and abruptly on cleaning the glass. Simultaneously, the movement of solutions through the same disc could become impeded at least 100-fold so that a suction pump was barely able to force distilled water or potassium chloride through the disc. Yet at the same time the electrical resistance through the disc in concentrated solutions of potassium chloride remained unchanged and unaffected within 0.1%.

The latter finding is of importance in further validating the use of sintered glass in measurements of diffusion, already confirmed by measurements of free diffusion, for, if electrical conductivity is unaffected, diffusion must be equally unaffected.

Lachs and Kronman (4), to explain the erratic results of streaming potential in systems of glass and potassium chloride, assumed that glass

* Present address: Department of Chemistry, The University of Southern California, Los Angeles 7, Calif.

swells. This hypothesis was adopted by Fairbrother and Varlay (5). It was more recently shown by Hubbard, Hamilton and Finn (6) that glass does swell measurably in water. This hypothesis could account for our observation of uncharged electrical but increased hydrodynamic resistance if the swollen layer behaved like swollen gelatin or silica gel, which allow almost free passage of ions but prevent any flow of water.

Many observers (7, 8) from time to time have recorded anomalies in the flow of liquids through capillary systems, generally to the effect that the resistance to flow increases with time. Wentworth (8), for example, found this to be quite general and pronounced. In one of his experiments, in which water flowed through a 0.045 mm. brass slit, the increase in resistance was 2940-fold in 47 hours, and then remained constant for a further 91 hours. Wentworth's hypothesis is the formation of thick rigidified layers of liquid in contact with the brass or other solid. In some of his experiments he guarded against electroosmotic effects. Our observations showed no effect of conductivity of the solution (from distilled water to 0.1 N KCl) on the hydrodynamic resistance of fritted glass and thus preclude electrokinetic effects which must decrease along with the resistance.

Meyerott and Margenau (9), with discs of plate glass, confirmed some of Wentworth's results but ascribed the whole effect to obstruction by air bubbles. This explanation is excluded in our experiments by the unchanged conductance of concentrated solutions. Gas bubbles and similar mechanical obstructions would have to increase the electrical resistance at the same time as the hydrodynamic resistance. However, only the hydrodynamic resistance increased. Whenever, in preliminary experiments, air bubbles were actually found by us the results were very apparent: the conductance was erratic, depending on minute vibrations and changing suddenly when the liquid was sucked through the disc.

Many other scattered observations indicate that the liquid in the neighborhood of surfaces may be partially rigidified, yet there is no adequate explanation of this phenomenon, nor has it been known heretofore that the mobility of ions in such rigid layers may be essentially unaffected.

EXPERIMENTAL

Apparatus

A conductivity cell was designed to have a fixed and very large surface of fritted Pyrex glass between the electrodes, but otherwise following the Jones-Bollinger (11) design. The disc of fritted glass separated the cell into two electrode compartments, as in Fairbrother's device and as shown in Fig. 1.

The electrodes were of platinum and platinized *in situ*. The metal to Pyrex seal was made tight without allowing the solution to come in contact with tungsten by butt welding the stem of the electrode to tungsten wire and sealing the latter to Pyrex with a narrow lip of the glass overlapping onto the platinum. The end of tungsten in contact with mercury was thoroughly cleaned and coated with bright platinum.
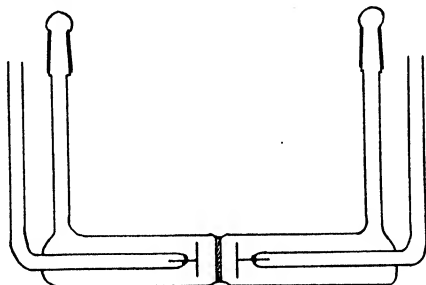
Fɪɢ. 1. Cell for measurement of surface conductance.

Measurements were made with Leeds and Northrup (12) apparatus including a Jones-Dike Bridge (13) audio-frequency oscillator and tuned amplifier.

An oil thermostat maintained a temperature of approximately 28.5°C. with a constancy of 0.002°C.

Method

Approximately 0.1 and 0.0005 N KCl stock solutions were used. The conductances were determined in a cell of conventional Jones-Bollinger design and found to be independent of frequency. If surface conductivity were absent, the ratio of conductances of these two solutions should be the same in the special cell incorporating the fritted glass disc as in the standard cell and the cell constant of the special cell independent of the concentration of the solution. In fact, however, this ratio was unmistakably different by 5–10%, the more dilute solution appearing now to conduct better; or, expressed differently, the resistance cell constant was lower by 5–10% in the dilute solution than in the more concentrated one. This difference after elimination of other causes, must be due to surface conductance of the large glass-solution interface of the fritted disc.

Observations

Using the *concentrated* solution there was no particular difficulty in obtaining constant and consistent values for the resistance of the cell throughout the period of observation. The only precaution necessary was

to avoid heating within the fritted glass by the Joule effect. Heat dissipation is, of course, slow and, due to the low resistance of the cell (67.01 ohms), a relatively high current flows even at low voltages.

The first filling of the cell with the concentrated solution, following the use of distilled water or dilute solution, despite thorough rinsing of the cell and disc with the concentrated solution, always gave a value of resistance too high by about 0.05% but subsequent fillings were constant to 0.01%.

Using the *dilute* solution, the results were perplexing until it was found that here the fritted glass does not reach an equilibrium state for
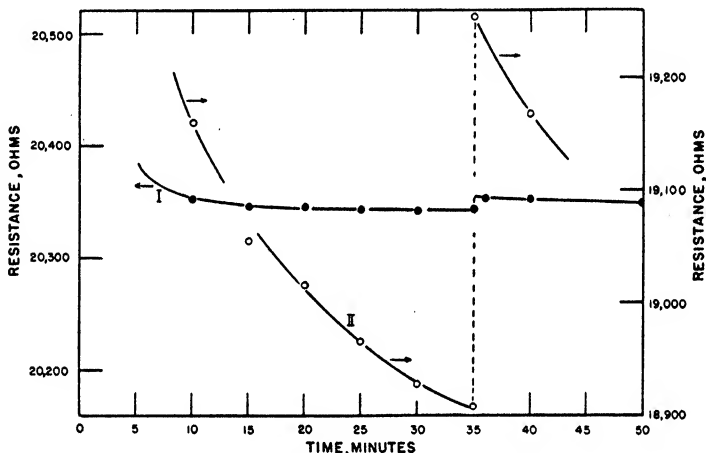
FIG. 2. Short time variation in resistance of cell when filled with dilute solution. At 35′ a small volume of the solution was sucked through the disc.

Curve I—after soaking; Curve II—before soaking.

many hours. Prior to such extended "soaking," preferably over night in the solution, the resistance decreased if the cell had been previously exposed to distilled water, and increased if it had been exposed to the concentrated solution.

Experience with the concentrated solution showed that 20 minutes was sufficient for thermal equilibrium to be reached. In the dilute solution, however, when the "soaking" was insufficient, the resistance failed to reach any definite value in hours, and sucking a small amount of solution through the fritted glass changed the resistance abruptly (as illustrated by Curve II of Fig. 2), each successive filling of the cell giving different values. These variations amounted to several per cent of the total resistance and were, therefore, of the same order of magnitude as the surface conductance.

After sufficient "soaking," however, the value of the resistance, once thermal equilibrium was established, varied little. Sucking through caused but a minor change (as illustrated by Curve I of Fig. 2) and successive fillings of the cell gave almost identical values. All these variations amounted to less than about 0.1%, *i.e.*, about 1% of the surface conductance. Consistent values thus obtained were used to measure the various factors.
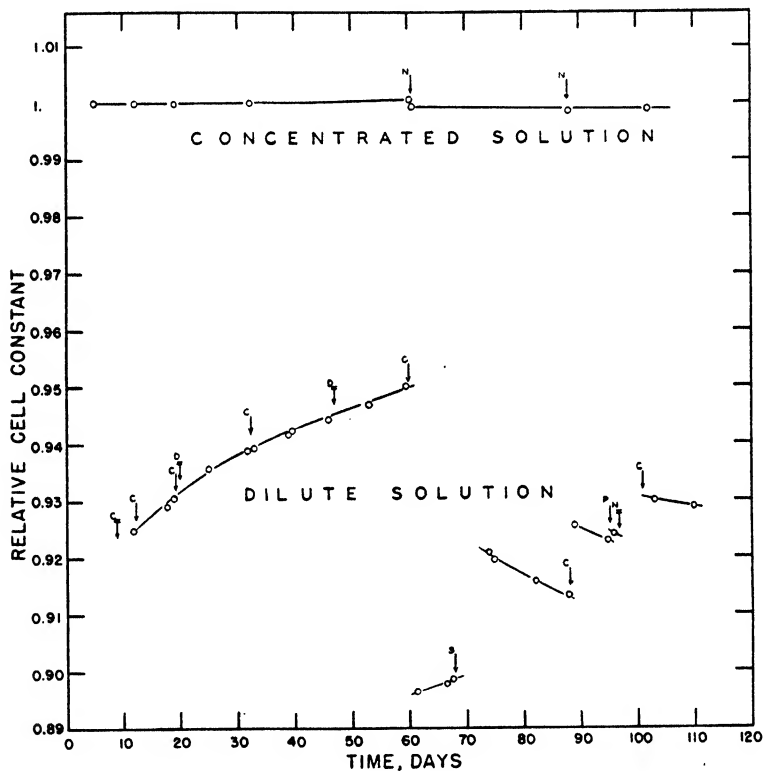
FIG. 3. Long range variations in resistance of cell and the effect of some treatments.
Simple arrows = treatment of short duration; crossed arrows = treatment over 5 days.
C = concentrated solution; D = distilled water; N = nitric acid; S = sulfochromic; P = paraffin oil.

Such resistances were unaffected by change in frequency within the available limits of 500 to 2000 cycles or by about 20-fold change in voltage if care was taken to avoid Joule heating effects by measuring the resistance immediately after applying a higher voltage.

Fig. 3 illustrates a series of experiments extending over several months. It is a plot of the variation of the apparent resistance of the two solutions expressed as relative cell constant of the cell over this period. Each point represents the mean of 3–7 measurements taken in one day and agreeing within about 0.1% in the dilute solution and 0.01% in the concentrated one. Treatments to which the fritted glass was subjected, *e.g.*, soaking in distilled water or cleaning with nitric acid, are indicated by arrows on the graph.

It may be seen that measurements using the *concentrated* solution gave results constant to 0.1%. Within this limit this constancy was unaffected by the various treatments; the only small but definite change was produced by the first cleaning with nitric acid.

Measurements made during the first 2 months using the *dilute* solution gave progressively increasing values whose smooth trend was unaffected by contact of the fritted glass with the concentrated solution or with distilled water. The glass was never allowed to dry.

During this part of the experiment a gradual increase of resistance to flow through the fritted glass occurred, of the order of 100-fold. There was no appreciable difference between the hydraulic resistance to distilled water, dilute or concentrated potassium chloride solution.

A sudden discontinuity occurred in the smooth line of surface conductivity when the cell was cleaned with nitric acid. Simultaneously the original relative ease of flow through the membrane was restored. After this cleaning the trend of resistance was upwards, as before.

Another discontinuity, but in the opposite direction, was produced by treatment of the cell with dichromate-sulfuric acid cleaning solution, and this also reversed the trend. Subsequent treatments with nitric acid produced further but smaller discontinuities and seemed to reduce the slope of the trend. No great changes of hydraulic resistance were noted during this part of the experiment.

SUMMARY

1. Surface conductances at the interface of fritted Pyrex glass-0.0005 N potassium chloride have been observed with precision of 1%.

2. This surface conductance is independent of frequency and intensity of the measuring current, but varies greatly with time over periods of months and with cleaning of the surface.

3. Hydrodynamic resistance to flow through the fritted glass may increase with time by an order of magnitude, while its resistance to movement of ions remains constant to within 0.1%.

4. This hydrodynamic resistance is not due to occlusion of air bubbles nor to electrokinetic effects.

REFERENCES

1. SMOLUCHOWSKI, M., *Physik. Z.* **6**, 529 (1905).
2. McBAIN, J. W., *et al., J. Am. Chem. Soc.* **51**, 3294 (1929); *J. Phys. Chem.* **34**, 1033 (1930); **39**, 331 (1935).
3. WHITE, H. L., URBAN F., *et al., ibid.* **36**, 120, 3152 (1932); **45**, 560 (1941).
4. LACHS, H., AND KRONMAN, J., *Roczniki Chem.* **6**, 641 (1926); *Bull. Natl. Acad. Poland* **10A**, 289 (1925).
5. FAIRBROTHER, F., AND VARLAY, H., *J. Chem. Soc.* **1927** 1584; **1931**, 1564.
6. HUBBARD, O., HAMILTON, E. H., AND FINN, A. N., *J. Research Natl. Bur. Standards* **22**, 339 (1939).
7. DUFF, A. W., *Phil. Mag.* [6] **9**, 685 (1905).
8. WENTWORTH, C. K., *Am. J. Sci.* **242**, 478 (1944).
9. MEYEROTT, R., AND MARGENAU, H., *ibid.* **243**, 192 (1945).
10. RUTGERS, A. J., *et al., Trans. Faraday Soc.* **36**, 69 (1940); **43**, 102 (1947).
11. JAMES, G., AND BOLLINGER, G. M., *J. Am. Chem. Soc.* **53**, 411 (1931).
12. Leeds and Northrup Co., Philadelphia; *Cat. No.* **4666**, **9842**, **9847**.
13. DIKE, P. H., *Rev. Sci. Instruments* **2**, 379 (1931).
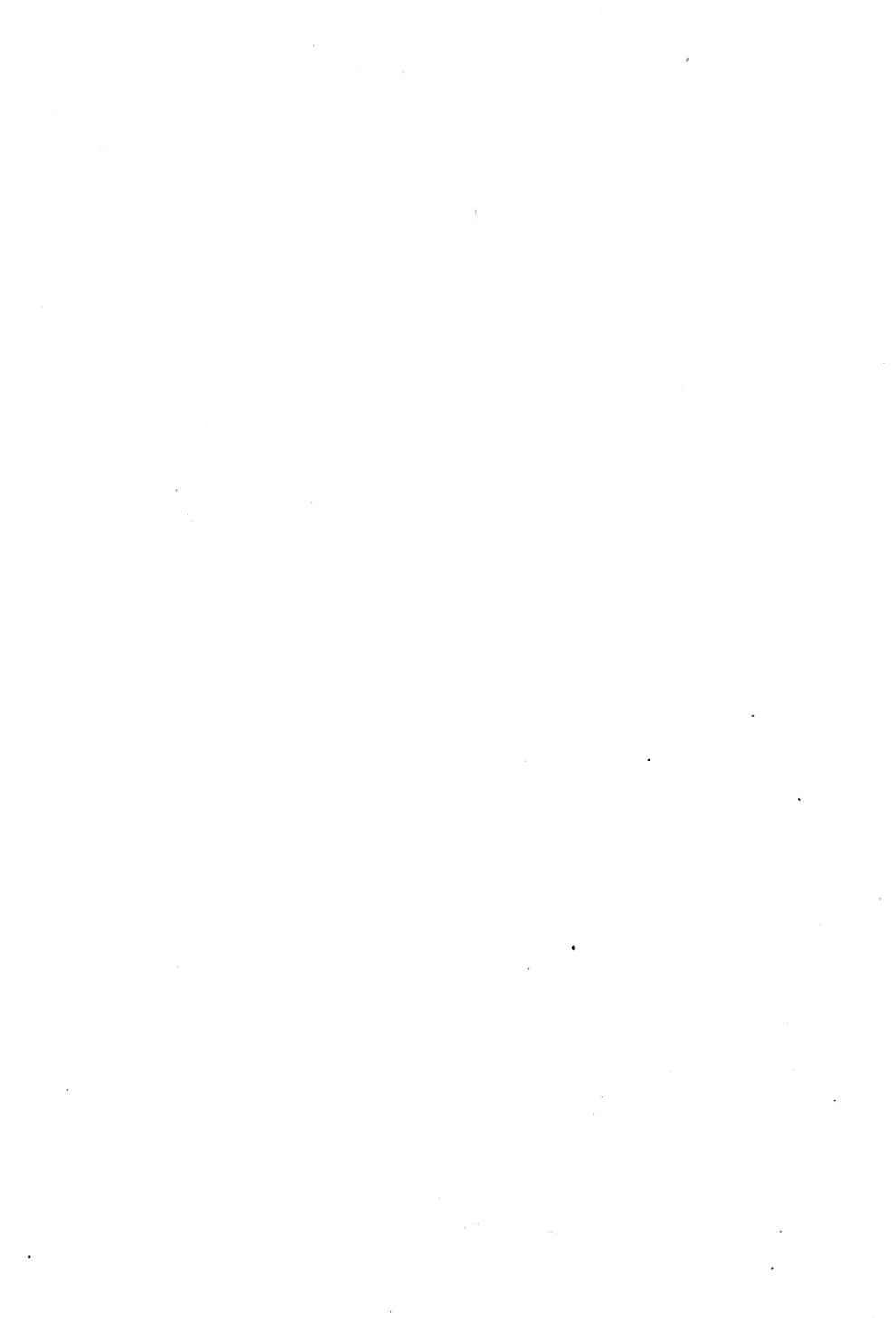
PECTINATE FILMS

T. H. Schultz, H. S. Owens and W. D. Maclay

From the Western Regional Research Laboratory,[1] *Albany, Calif.*
Received September 8, 1947; Revised October 6, 1947

INTRODUCTION

Pectinic acids are essentially long chain glycosidic polymers· of galacturonic acid esterified in the range from near zero to about 70% of theoretical with methyl alcohol. Their high molecular weight and ability to form strong cross links with polyvalent cations suggest their use for many special films and fibers, but such use has not been industrially important because of their high cost. More economical methods for the extraction and isolation of low-methoxyl pectinic acids (1, 2) (degree of esterification from 0 to 20%, or more in case of enzymatically deësterified products) have recently been devised which have overcome, to some extent, this disadvantage. It seemed advisable to reopen the investigation of properties of pectinate films and fibers. This paper offers data on strength, extensibility, plasticization, and resistance to washing, of films prepared from a variety of pectinates. Several uses are proposed, one of which has been studied. Data on yarns and filaments will be reported later.

EXPERIMENTAL METHODS

Description of Pectinic Acids Employed

The samples used in this investigation are listed in Table I with data on their properties on an ash- and moisture-free basis. The methods used for determining intrinsic viscosity (*dl./g.*) and number average molecular weight by osmotic pressure have been reported (3). All of the samples were obtained from lemon peel, and all, excepting the first three listed in Table I, were deesterified *in situ* by citrus pectinesterase (4). The second sample listed was a commercial product[2] and the third was derived from it by thermal degradation. All other samples were extracted in this laboratory and purified by precipitation with acid-alcohol and repeated washing as previously described (5).

TABLE I

Description of Pectins Used in this Investigation

Methoxyl content	Uronic anhydride	[η]	$\overline{M}_n$	Ash
Per cent	*Per cent*	*dl./g.*		*Per cent*
10.9	~80[d]	8.3	40,000	0.4
10.1	83	4.3	33,000	0.6
10.7[a]	87	1.2	18,000	0.8
7.4	82	4.4	—	0.4
4.5	~83[d]	5.2	—	0.5
4.4, No. 1	83	6.0	—	0.4
4.4, No. 2[b]	83	1.3	—	0.4
4.4, No. 3[c]	83	0.7	—	0.4
2.7	~83[d]	3.5	—	0.3

[a] Prepared by heating a solution of a pectin similar to sample 10.1 at 119°C. for 20 minutes.

[b] Prepared by heating a solution of sample 4.4, No. 1, at 120°C. for 5 minutes.

[c] Prepared by heating a solution of sample 4.4, No. 1, at 120°C. for 20 minutes.

[d] Values estimated from data on similar preparations.

Preparation of Films

Some films were prepared by extrusion of a pectinate solution through a rectangular orifice into a bath containing salts of polyvalent cations and acid. Irregularities were always present in such films. To produce uniform films, 30-ml. portions of 1% sodium hydrogen pectinate solution, adjusted to a pH near 4, and containing the plasticizer, if any, were evaporated in glass trays 5 cm. wide and 15 cm. long in a slow current of air at 25°C. for 16 hours. The dried films were removed and cut into strips 1.25 cm. wide. Sodium hydrogen pectinate was converted to polyvalent metal pectinates by gently stirring the strips in 1 N aqueous solutions of the required chloride. Five minutes of stirring permitted conversion of 90% or more of the sodium acid salt to the new one. The converted films were washed twice in distilled water, then dried between sheets of filter paper under a glass plate 5 cm. wide and 15 cm. long and a one kg. weight. To form films of pectinic acids, a bath of 0.1 N hydrochloric acid in 50% ethanol was used. Washing was done with 65 and 75% ethanol. All films were equilibrated at a relative humidity of 65% at 25°C., except those tested wet, which were soaked in water for 1 hour before testing.

The salts used were c.p. chemicals. The tetraquodichlorochromic ion largely present in the usual fresh solution of chromic chloride was converted to hexaquochromic ion before use. Glycerol, when required, was added to the tanning and the rinse solutions in 15% concentration.

Testing

Dimensions of films were determined by means of a Gaertner traveling microscope. Thickness values were in the neighborhood of 30 μ. Swelling was measured at 25°C. by the ratio of the maximum thickness when the film was wet to the thickness at 65% relative humidity.

Tensile strength and extensibility were determined in a Scott pendulum testing machine, Model J2. The clamps were separated 5 cm., and increased sensitivity was obtained by use of a wooden block on the pendulum in place of the steel one. Corrections were made for friction in the machine.

Flexibility was determined by manual folding endurance. Strips without perceptible cracks at the edges were folded and creased, then unfolded and creased in the opposite direction. Films breaking in five or less foldings were considered "poor"; those developing cracks less than 1 mm. long after 10 foldings were rated "good," while those showing intermediate behavior were rated "fair."

The resistance of polyvalent metal pectinates to washing was determined by stirring weighed strips in the following solutions: (1) Distilled water at 25°C. for 4 hours, (2) 0.1% sodium carbonate at 40–50°C. for 30 minutes, and (3) 0.1% mild soap at 40–50°C. for 30 minutes. The films were washed in distilled water, equilibrated at 65% relative humidity, and weighed. Results are expressed as per cent loss in weight.

Results

Effect of Chain Length and Methoxyl Content

Various investigations have shown that the tensile strength of fibers or films of certain high polymers varies as a direct function of the molecular weight of the polymer (6, 7, 8), at least in the lower range of molecular weights. Comparisons between fibers or films, therefore, should be based on fractionated samples; however, so many difficulties were encountered when trying to fractionate pectinic acids that this phase of the project was abandoned. The results reported were obtained on samples as extracted and purified, or on materials prepared from them by thermal degradation.

Fig. 1 illustrates the data on variation of tensile strength with intrinsic viscosity at two methoxyl contents and when diluted with glycol boriborate (9). In the absence of diluent, tensile strength appears to follow number average molecular weight more closely than weight average as estimated from intrinsic viscosity (3). As shown in Fig. 2, the per cent ultimate elongation is nearly a linear function of the intrinsic viscosity when the methoxyl content is high (10–11%, or greater than 70% of
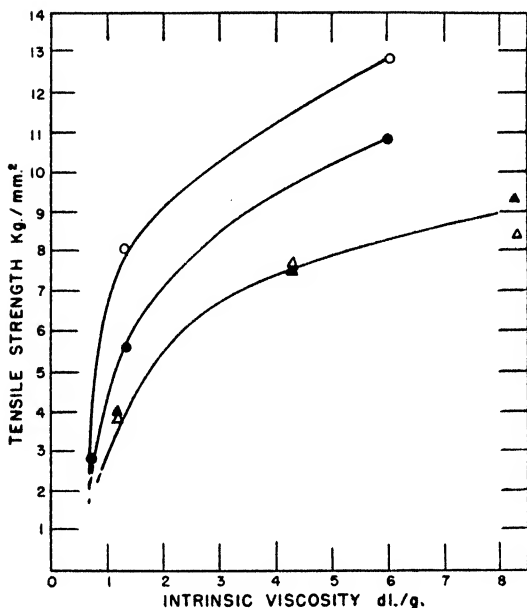
FIG. 1. Effect of intrinsic viscosity on the tensile strength
of sodium hydrogen pectinate films.

○, methoxyl content 4.4, no plasticizer; △, methoxyl content 10.1 to 10.9, no plasticizer; ●, methoxyl content 4.4, 30% glycol boriborate added; ▲, methoxyl content 10.1 to 10.9, 30% glycol boriborate added.
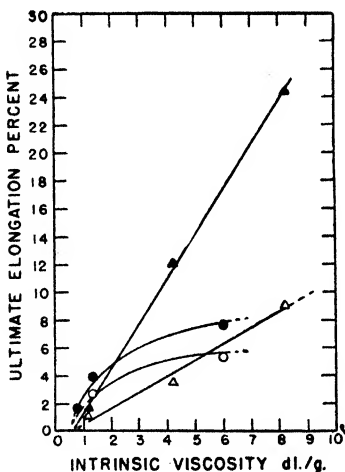
FIG. 2. Effect of intrinsic viscosity on ultimate elongation of
sodium hydrogen pectinate films.

Symbols have same meaning as in Fig. 1.

esterification) and tends to approach a constant value when the methoxyl content is low, in this case about 4%.

At a constant viscosity or weight average molecular weight, the strength of films of sodium hydrogen pectinate increases with decrease in methoxyl content, as shown in Fig. 3.
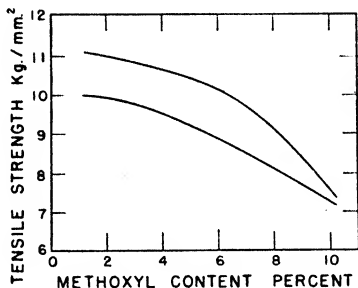
FIG. 3. Effect of methoxyl content on tensile strength of sodium hydrogen pectinate films.

Curves interpolated from experimental data to an intrinsic viscosity of 4.0. Upper curve, without plasticizer; lower curve, 30% glycol boriborate added.

Plasticization

The effect of addition of certain organic compounds on the strength of pectinate films is illustrated in Fig. 4. Organic acids and sodium
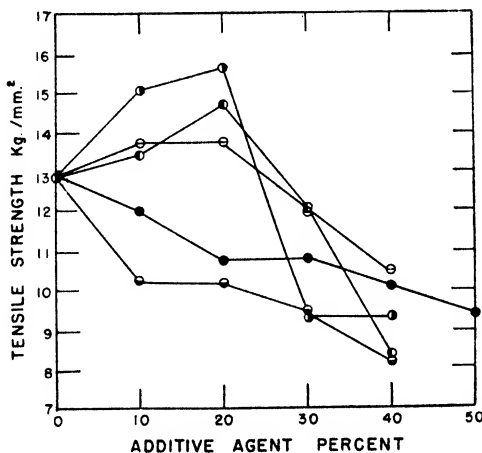
FIG. 4. Effect of additive agents on tensile strength of sodium hydrogen pectinate films; methoxyl content 4.4, intrinsic viscosity 6.0.

●, glycol boriborate; ◒, glycerol; ◐, tartaric acid; ◖, citric acid; ⊖, sodium boro-phosphate.

borophosphate increased the strength at concentrations less than 25%, and decreased it at higher concentrations. Glycerol and glycol boriborate decreased the strength at all concentrations. Glycerol, and to a much lesser extent, glycol boriborate, increased ultimate elongation. These are the only substances tried which can be considered as plasticizers, since other added agents had little influence on extensibility, as is illustrated in Fig. 5. Glycerol is much less effective when the moisture
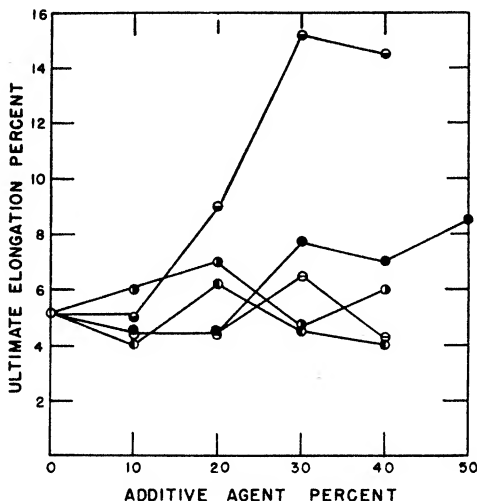
FIG. 5. Effect of additive agents on ultimate elongation of sodium hydrogen pectinate films; methoxyl content 4.4, intrinsic viscosity 6.0.
Symbols have same meaning as in Fig. 4.

content of the film is near zero, as is shown by the fact that films dried over calcium chloride had extensibilities of 4% without plasticizer, and only 6% when glycerol was present.

Polyvalent Cation Pectinates

Conversion of films to salts of polyvalent, particularly trivalent, cations decreases their flexibility but increases their resistance to water or washing agents, and also increases their wet strength, as shown in Table II. There is little effect on tensile strength.

DISCUSSION

The strength of pectinate films is close to that of films of other high polymeric saccharide materials, such as films of cellulose and its derivatives, which have strengths ranging from 4 to 12 kg./mm.^{2} (7, 8, 10).

TABLE II

Properties of Films of Polyvalent Metal Pectinates

Methoxyl content	Cation	Plasticizer	Tensile strength	Wet strength	Elongation at break	Wet elongation at break	Loss of weight in			Swelling	Folding endurance
							Water	Na$_2$CO$_3$	Soap		
Per cent			kg./mm.^{2}	Per cent of dry	Per cent	Per cent	Per cent	Per cent	Per cent		
4.5	H	None	10	0	5.5	—	—	—	—	—	—
4.4	Na-H	None	12.6	0	5.2	—	100	100	100	∞	Fair
4.5	Ca	None	11.0	21	4.0	19.5	0	8	5	2.9	Fair
4.5	Zn	None	10.7	28	3.5	29.5	0	8	9	2.5	Fair
4.5	Al	None	10.8	29	3.0	6.7	0	100	40	1.5	Poor
4.5	Cr	None	—	—	—	5.7	2	0	0	1.4	Poor
4.5	Na-H	30% Glycol boriborate	10.9	0	6.0	—	100	100	100	∞	Good
4.5	Ca	30% Glycol boriborate	14.3	20	5.5	29	1	11	8	3.6	Poor
4.5	Zn	30% Glycol boriborate	14.7	20	6.5	35	1	3	16	2.6	Fair
4.5	Al	30% Glycol boriborate	12.4	23	3.5	4.7	0	100	45	2.2	Poor
4.5	Cr	30% Glycol boriborate	11.3	28	5.2	3.5	1	0	0	1.7	Poor
4.5	Ca-Cr	30% Glycol boriborate	10.2	20	3.5	3.0	0	0	0	1.4	Poor
4.5	Zn-Cr	30% Glycol boriborate	—	—	—	7.5	2	0	0	1.7	Poor
4.5	H	30% Glycerol	6	0	6.2	—	—	—	—	—	—
4.4	Na-H	30% Glycerol	9.5	0	15.2	—	100	100	100	∞	Good
4.5	Ca	30% Glycerol	10.5	28	8.0	38	10	18	20	3.1	Good
4.5	Al	30% Glycerol	9.8	31	4.7	12	10	100	53	2.3	Poor
7.4	Na-H	None	9.8	0	4.0	—	100	100	100	∞	Fair
7.4	Ca	None	10.3	10	6.5	34	1.5	23	80	3.9	Good
7.4	Zn	None	10.1	17	8.0	41	0.5	80	46	3.0	Good

Increase in strength of pectinate films with increase in molecular weight is to be expected. Although the data are insufficient to enable one to conclude definitely whether weight or number average molecular weight is the controlling factor, the latter seems more likely. For example, low strength would be expected in a film made from a heterogeneous sample containing many short chains, due to the few cross bonds per chain and the large number of chain ends, which are considered points of weakness (8). Number average molecular weight is more sensitive than the weight average value to both of these factors.

Decrease in methoxyl content causes an increase in tensile strength of pectinic acid (or sodium hydrogen pectinate) films, because removal of ester groups enhances the probability of cross-bonding between liberated carboxyl groups. An explanation follows from consideration of the mechanisms operating during formation of the film. As the pectinate chains are brought into closer contact, collisions involving carboxyl groups are more likely to result in stable hydrogen bridges than collisions involving any combination of groups. Therefore, the chance of such hydrogen bonds occurring between pectinate chains is greater than would be expected from the ratio of free to esterified carboxyl groups. The result of this is that the chance for bridge formation is not significantly different whether all or most of the carboxyl groups are free. Consequently, little increase in tenacity would be expected when the degree of esterification is much below 50%. It should be noted also that, as carboxyl groups are liberated, a greater fraction will be in locations too far removed from other carboxyl groups to permit effective cross-bonding except in crystalline regions.

Percent elongation at the breaking point in the absence of plasticizer appears to vary little within the limits of methoxyl content examined. There is more plastic flow, that is, irreversible flow, with samples which have high methoxyl contents, and it appears that a more flexible film might be obtained if the methoxyl content were increased to higher values. The methods of esterification tried caused degradation of the pectinic acids, which prevented investigation of this hypothesis. Addition of plasticizers should also accomplish this, but only glycerol had more than a small effect, most of which was lost when the moisture content was reduced to near zero. Other agents tried, such as organic acids, apparently cross-bonded through carboxyl groups with the pectin, which caused an increase in the strength of the films but had little effect upon their flexibility. Some increase in flexibility might be obtained by the use of a small proportion of long-chain diamines, which can form cross-links through the carboxyl or ester groups, or long-chain dialdehydes, which might cross-link through alcohol groups. The amount of such material

used would have to be small so that fibrils and not a three-dimensional network would be formed. The latter would decrease the flexibility.

Exchanging polyvalent cations for hydrogen failed to increase the strength of films much more than 50%, with some of the results showing an increase of only about 10%, although the relative bond energies involved differ by about 10-fold (8). This fact might be explained in several ways. First, the carboxylic hydrogen bonds are not replaced by polyvalent cations, but this seems unlikely, since nearly an equivalent amount of cation was deposited in the films during the conversion treatment. Second, substitution of hydrogen by calcium, zinc, *etc.*, increases the cross-sectional area of the film by 10% or more. X-ray pictures of oriented pectinate fibers taken by K. J. Palmer of this laboratory also show that the equatorial distance is increased by approximately this amount. This expansion decreases the number of pectinate chains per unit area and it might decrease the magnitude of the forces that bind the chains; hence, the overall decrease in strength may be considerable. Third, electrovalent cross-bonds can be extended only a short distance before breaking, and they are less likely to reform during stretching of the film than are bonds due to van der Waals' forces. Furthermore, the distance two oppositely charged ions need be separated beyond the equilibrium point to the maximum in the force of attraction *vs.* distance curve is about 0.6 A (8), while van der Waals' forces have not reached the peak of their force of attraction until the molecules are separated by an Angstrom or more from their equilibrium distance (11). This offers the possibility that electrovalent bonds are broken first and, since the strengths of the two bonds differ by 20-fold, the electrovalent bonds must displace at least 5% of the van der Waals' bonds to keep the strength of the film constant. This explanation, accompanied by the second, accounts for the small increase in strength of the polyvalent pectinate compared to that of pectinic acid films. It also explains the brittleness of the films and of low-methoxyl pectin gels which are gelled with calcium ion (12).

USES

With the information presented it is possible to evaluate some probable uses for pectin in films. The present state of knowledge indicates that pectinate films cannot be used where a high degree of extensibility and high wet strength are necessary. There is one field, however, in which advantage might be taken of low wet strength. In meat packaging, such as casings on sausages, ham, *etc.*, pectinate films can be applied by dip coating. The process is simple, since the meat can be preformed into the desired shape and then dipped in a dispersion of calcium sodium pectinate. The temperature of the dip solution can be maintained at about 70°C., which keeps it fairly sterile yet does not change the appearance of the

meat noticeably. The gel coating is dried, and the resulting film forms an attractive casing. The casing is readily removed by boiling or is edible and tender when the meat is cooked by other methods. Tests at this laboratory have shown that pectinate films are about as permeable to water vapor as are cellulose films. Films of this type and those made with other cations offer possibilities in preservation of fish, frozen foods, cheese, *etc.*, and as an antisticking or glazing agent for dried or candied fruits.

Advantage may also be taken of the fire-retardant properties of metallic pectinates in film-coating preparations for use on flammable surfaces or as films for use as decorations or draperies.

Calcium pectinate films might be used in surgical dressings in the manner of celluronic acid gauzes.

SUMMARY

Pectinate films possess strengths between 7 and 14 kg./mm.^{2} and, are extensible to about 3–9%. They can be plasticized with glycerol, which decreases the tensile strength about 30% at effective concentrations.

Theoretical aspects of the tensile strength measurements are discussed.

Increased resistance to water and washing agents is achieved by conversion of the films to polyvalent metal pectinates.

At present, the most promising use of pectinate films is as a dip coating for food packaging.

REFERENCES

1. McCREADY, R. M., OWENS, H. S., SHEPHERD, A. D., AND MACLAY, W. D., *Ind. Eng. Chem.* **38**, 1254 (1946).
2. Unpublished work by members of Carbohydrate Section, Western Regional Research Laboratory.
3. OWENS, H. S., LOTZKAR, H., SCHULTZ, T. H., AND MACLAY, W. D., *J. Am. Chem. Soc.* **68**, 1628 (1946).
4. OWENS, H. S., McCREADY, R. M., AND MACLAY, W. D., *Ind. Eng. Chem.* **36**, 936 (1944).
5. SCHULTZ, T. H., LOTZKAR, H., OWENS, H. S., AND MACLAY, W. D., *J. Phys. Chem.* **49**, 554 (1945).
6. SULLIVAN, R. R., *J. Applied Phys.* **13**, 157 (1942).
7. SOOKNE, A. N., AND HARRIS, M., *J. Research Natl. Bur. Standards* **34**, 467 (1945).
8. MARK, H., in Cellulose and Cellulose Derivatives, by Emil Ott, pp. 990–1043. Interscience Publishers, New York, 1943.
9. BENNETT, H., *U. S. Pat.* 1,953,741 (1934).
10. GLOOR, W. H., in Cellulose and Cellulose Derivatives, by Emil Ott, p. 1071. Interscience Publishers, New York, 1943.
11. GLASSTONE, S., Theoretical Chemistry, p. 451. D. Van Nostrand Co., Inc., New York, 1944.
12. SPEISER, R., COPLEY, M. J., AND NUTTING, G. C., *J. Phys. & Colloid Chem.* **51**, 117 (1947).

NOTE ON THE MODE OF COAGULATION OF COLLOIDS—GROUP COAGULATION

Tyoku Matuhasi and Kunio Aoto

From the Institute of Physical and Chemical Research, Tokyo, Japan
Received November 7, 1947

When a sol containing two different kinds of colloid particles, say A_0 and B_0, is caused to coagulate, the particles A_0 and B_0 are usually distributed at random in the resulting precipitate. This mode of coagulation may be called *disordered coagulation* (1). In serology, however, a sol containing two kinds of antigen-antibody complex, say A and B, when coagulated (agglutinated), the resulting precipitate consists of aggregates of A and B, each having a certain number of A only and of B only. To determine whether this mode of coagulation, which might be called *group coagulation*, occurs in the coagulation of colloids commonly known, we conducted a series of experiments and obtained some examples. The experimental details are given in each case.

<p style="text-align:center">EXPERIMENTAL</p>

1. Malachite Green + Methylene Blue

Equal volumes of 0.5% malachite green and 0.5% methylene blue were mixed. No microscopic particles were observed in this mixture. The mixture was then coagulated by adding half its volume of $(NH_4)_2MoO_4$.[1] At first no precipitate was formed, but microscopically we observed green and violet aggregates having a size of about 1 μ. On standing overnight, a precipitate was formed in which green and violet aggregates were distributed at random.

The green aggregates are similar to those formed when a malachite green solution is coagulated by addition of 1 N $(NH_4)_2MoO_4$, and the violet aggregates are similar to those formed when a methylene blue solution is coagulated by addition of the same reagent. It is thought from the above observation that in the first stage of coagulation, the primary malachite green particles form green aggregates and the primary methylene blue particles form violet aggregates and these aggregates then clump together at random to form the precipitates.

[1] The preparation of 1 N $(NH_4)_2M_0O_4$: 90 g. of ammonium molybdate is dissolved in 100 cc. of 6 N ammonia solution, and 240 g. of solid ammonium nitrate is added. Water is added to the solution to make the volume 1 l.

2. *Malachite Green + Methyl Violet*

A mixture consisting of equal volumes of 0.5% malachite green and 0.5% methyl violet was used in this experiment. No microscopic particles were observed in this mixture. The mixture was coagulated by addition of one-half volume of $1\ N\ (NH_4)_2MoO_4$. At first no precipitate formed, but under the microscope we observed green and violet aggregates each having a size of about $1\ \mu$.

The aggregates are similar to those formed when malachite green or methyl violet is coagulated by addition of $1\ N\ (NH_4)_2MoO_4$. From the above observation we see that the coagulation proceeds as in case (1).

3. *Blood Charcoal Sol + Fe₂O₃ sol*

Blood charcoal was ground in an agate mortar, and to this was added human serum diluted 10-fold with water. This mixture was then diluted 20 times with water. The large particles of blood charcoal were separated by centrifugation. By this procedure we obtained a blood charcoal sol containing particles about $1\ \mu$ in size. This sol showed electrolytic migration to the anode. The Fe_2O_3 sol was prepared by Buzágh's method (2). The coarse particles of Fe_2O_3 were removed by filtration. The sol thus obtained migrated to the cathode.

On mixing these sols, mutual coagulation takes place slowly. After a few days, precipitation takes place. Under a microscope, we observed that the precipitate consisted of two kinds of aggregates containing a certain number of charcoal particles or of Fe_2O_3 particles.

ACKNOWLEDGMENT

SUMMARY

If a sol containing two different kinds of colloid particles, say A and B, is coagulated, and the resulting precipitate is composed of aggregates consisting of a certain number of A and B particles, the phenomenon may be called group coagulation. This mode of coagulation has been observed in the coagulation of the following sols:

(1) malachite green + methylene blue,
(2) malachite green + methylviolet,
(3) blood charcoal + Fe_2O_3

REFERENCES

1. FREUNDLICH, H., Kapillarchemie, II, 209, Akademische Verlagsgesellschaft, Leipzig, 1932.
2. v. BUZÁGH, A., *Kolloid-Z.* **66**, 130 (1934).

DENATURATION AND OPTICAL ROTATION OF PROTEINS

A. H. W. Aten, Jr., C. J. Dippel,
K. J. Keuning and J. van Dreven

*Natuurkundig Laboratorium der N. V. Philips' Gloeilampenfabrieken,
Eindhoven, Netherlands*

It is fairly generally admitted that denaturation consists of a loosening of the native configuration of a protein, followed by refolding according to a less regular pattern.[1]

It is a well-known fact, that in many proteins, most notably in serumalbumin, denaturation is reversible, at least as far as the bulk of the protein is concerned. However, not all characteristics of the native substance are equally well reproduced in the regenerated product. Crystallization, electrophoresis, and antigenic properties are reported to be different. As one would expect optical rotation to be rather sensitive to changes in molecular configuration, we have measured the rotation of regenerated serumalbumin. After precipitation by heating, this protein dissolves easily in 50% urea, and this solution can be dialyzed to yield a solution of protein in 5% urea. (It is quite feasible to carry dialysis even further, but this would have increased the risk of partial decomposition of the protein by prolonging the experiment.) For the sake of comparison, native serumalbumin was dissolved in 5% urea, which addition does not affect the optical rotation. No difference was observed within the accuracy

---

[1] The high energy of activation of this process has been explained by the assumption that it involves the breaking up of an appreciable number of hydrogen bonds, each requiring an energy of about 5 kcals. (NEURATH, H., GREENSTEIN, J. P., PUTNAM, F. W., and ERICKSON, J. O. *Chem. Revs.* **34**, 157 (1944); MIRSKY, A. E., and PAULING, I., *Proc. Natl. Acad. Sci. U. S.*, **22**, 439 (1936)). In this connection it must be kept in mind, however, that breaking a hydrogen bond in a substance in aqueous solution does not, in the ordinary way, involve a change in the total number of hydrogen bonds. For two broken, one between solute molecules or within a solute molecule, and one between two solvent molecules, two new hydrogen bonds arise between solute and water molecules. If, therefore, the high activation energy is to be explained by the severing of hydrogen bonds, one must postulate one of the following processes. Either a great number are broken in the activated complex, in which case small differences between individual hydrogen bonds may add up to a total of the order of 30 kcals., or some polar groups must be screened off by nonpolar parts of the molecule in the activated state, thus actually lowering the number of hydrogen bonds in the system. But it seems worth considering whether or not the main cause of the high activation energies will be found elsewhere.

TABLE I

Specific Rotation of Serumalbumin at pH 5.5

Treatment of protein	$[\alpha_D]$
Native:	
Native in water	$-65°$
Native in 5% urea .	$-61°$
Denatured:	
Native dissolved in 50% urea	$-87°$
Heat-precipitated dissolved in 50% urea	$-95°$
Regenerated:	
Native dissolved in 50% urea, dialyzed to 5% urea	$-61°$
Heat-precipitated dissolved in 50% urea, dialyzed to 5%	$-60°$
Heat-precipitated dissolved in 50% urea, diluted to 5%	$-67°$

of our experiments (about 3°) between the rotation of native and of regenerated serumalbumin.[2]

[2] PAULI, W., and WEISS, P., *Biochem. Z.* **233**, 381 (1931), have found that solutions of native and heat-precipitated serumalbumin in saturated urea solutions show the same optical rotation. In these solutions the protein is in a denatured condition, however, as is shown by the different value of $[\alpha]$.

NOTE ON EFFECT OF ULTRASONIC IRRADIATION ON THE FORMATION OF COLLOIDAL SULFUR

The production of colloidal sulfur by mixing dilute (about $0.002\ M$) solutions of sodium thiosulfate and HCl has been investigated in detail by LaMer and co-workers (1). Among other interesting results, it was found that the solution remains clear for a reproducible time, after which a Tyndall beam appears, due to a phase transition from molecularly dispersed sulfur into droplets of supercooled λ sulfur of sufficient size to exhibit light scattering. The recent work of LaMer and Yates (2) shows that ultrasonic irradiation of the distilled water used causes a 4-fold increase in the time of transition, which they tentatively attribute to the partial removal of nuclei required for growth to colloidal dimensions. They also demonstrated that the effect is not due to the production of H_2O_2 or to any detectable chemical change of the reagents.

TABLE I

Induction Period as Affected by Gases Dissolved in the Irradiated Water

Expt.	Water Treatment Before Irradiation	Time (*min.*)
1.	Untreated water, not irradiated	$13\frac{1}{2}$, $13\frac{1}{2}$
2.	Untreated water	51, 52
3.	Boiled under vacuum	$13\frac{1}{2}$, $13\frac{1}{2}$
4.	Saturated with air	51, $52\frac{1}{2}$
5.	Half-saturated with air	21, 22
6.	Saturated with nitrogen	42, 42
7.	Saturated with carbon dioxide	14, 14
8.	Saturated with oxygen	14, 15
9.	Saturated with helium	14, 14

Further study of this time delay caused by ultrasonic irradiation seemed of interest to the writer. First, the dissolved gas content of several samples of ordinary distilled water was changed in a variety of ways, as shown in Table I; then 220 ml. of each sample (except #1) was irradiated in the Ultrasonorator for 4 minutes at 1 megacycle, in a 50×400 mm. test tube at a power level of 1750 volts and 350 ma. in the plate circuit. To 100 ml. of such water, thermostated at 25°C., there

were added 2.50 ml. of 0.24 M HCl and, after thorough mixing, 2.50 ml. of 0.12 M sodium thiosulfate. The time required for the appearance of a Tyndall beam was measured in each case, using duplicate runs.

Table I lists the results obtained, for which the experimental error is about ±1 minute. Just as reported by LaMer and Yates, irradiation of ordinary water (#2) lengthens the normal transition time (#1) by a factor of 4. Also, the failure of irradiated oxygen-saturated water to delay appreciably the transition means that the effect cannot be ascribed to the well-known ultrasonic production of H_2O_2.

However, it is difficult to explain the results by a denucleation hypothesis. Boiling under vacuum should assist, rather than hinder, the subsequent ultrasonic denucleation; yet such treatment causes no delay whatever. This suggests that the retardation is due to ultrasonic action on a substance which is removed by boiling, probably a dissolved atmospheric gas. Such a view is supported by the fact that half-saturation with air gives a much smaller delay than full saturation with air. Furthermore, saturation with nitrogen causes a delay which is nearly as great as that observed with ordinary water. CO_2, O_2, and He are without appreciable effect.

Previous investigators (3) have shown that NH_3 and HNO_2 are formed in small amounts when water containing N_2 is irradiated. Apparently, then, some such reaction products as these are primarily responsible for the delay in the formation of the sulfur sol. It would be of considerable interest to elucidate the precise mechanism of this effect.

<div align="right">ALFRED WEISSLER</div>

Naval Research Laboratory,
Washington 20, D. C.,
   Dec. 5, 1947

REFERENCES

1. LaMer, V. K., and Kenyon, A. S., *J. Colloid Sci.* **2**, 257 (1947); Barnes, M. D., Kenyon, A. S., Zaiser, E. M., and LaMer, V. K., *ibid.* **2**, 349 (1947); LaMer, V. K., and Barnes, M. D., *ibid.* **1**, 76, 79 (1946); Johnson, I., and LaMer, V. K., *J. Am. Chem. Soc.* **69**, 1187 (1947).
2. LaMer, V. K., and Yates, J. W., *Science* **106**, 508 (1947).
3. Bergmann, L., Der Ultraschall, 3rd ed., p. 368. Edwards Brothers, Ann Arbor, Michigan, 1944.

BOOK REVIEWS

Colloid Chemistry, 2nd. Edit. By ROBERT J. HARTMAN, Director, Industrial Division, The Arco Company, formerly Associate Professor of Chemistry, Indiana University. 572 pp. Houghton Mifflin Co. Price $6.50.

This is a textbook in which "the author has attempted to present the fundamentals of colloidal phenomena in such a manner that they can be understood not only by students of advanced chemistry, but also by students in allied sciences. . . ." "Sufficient reference material has been included to afford at least a starting point for a comprehensive review of pertinent scientific papers" for those who expect to pursue research in this field. "The aim of this book is to present all the important phases of colloid chemistry without overemphasizing one narrow aspect of the subject at the expense of others which are, to the average student and reader, just as important." "In this second edition, a serious effort has been made to preserve the scheme of presentation and organization of the first edition, which emphasized the principles upon which the more recent advances have been based."

The table of contents indicates that the author has succeeded in one of the above objectives; namely, by including most of the important phases of colloid chemistry. However, in a text of this size, there should be at least a brief treatment of conductance of colloidal electrolytes and solubilization as developed by McBain, Tartar, Harkins and their respective collaborators. This is not mentioned. The reviewer's chief objection centers, not so much upon omissions, as upon the loose and inaccurate presentations of many of the topics. For example: Gamma, in the equation for the solubility of small particles (p. 14), is defined both as surface *tension* or *energy*. Furthermore, Gibbs did not give this equation in the form attributed to him. The Tyndall phenomenon is developed in some detail and the disturbing influence of a nonuniform particle size in nephelometry is quite properly emphasized. However, the author's understanding of the theory of light scattering is not clear (p. 191). "Thus the scattered light from particles of a magnitude approximating the *order of light waves* will show a preponderance of blue light." This impression is given repeatedly (p. 192), but on p. 291 we find "when the light scattering particles are of *large size* (italics mine), *i.e.*, in excess of 1/20 of the wave length of light, the angular distribution is not symmetrical." This is a correct statement, but then the particles are not ordinarily called large. The author also labors under the all too common, but erroneous, impression that the Mie Theory is applicable only for conducting (*i.e.*, colloidal gold) particles, whereas, he should point out that it is valid for dielectric particles (sulphur) as has been demonstrated in a series of articles in this Journal. The statement (p. 214) "the color of dielectric particles is more or less the same, regardless of the extent of subdivision" is not true in the light of results on sulphur sols, oil aerosols and the author's table (p. 317) on water aerosols in a Wilson Cloud Chamber.

Part I (pp. 1–131) is devoted to the fundamental theories and applications of surface chemistry and is based upon the classical Polanyi theromodynamic and the Langmuir kinetic approaches to adsorption and catalysis. This part is moderately satisfactory, although the colloidal bearing upon catalysis is nebulous.

The preparation, physical, optical, electrical, and filtration properties of lyophobic colloids, and their applications are stressed in Part II (pp. 132–360), followed by Chapters on aerosols and foams.

In Part III (pp. 361–452) on lyophilic colloids, the emphasis is on the electrokinetic behavior of proteins and the structure and property of gels. The works of Donnan and of Loeb are presented in good perspective, but the methods of measurement and the interpretation of viscosity are dismissed all too casually, with a drawing of an Ostwald viscometer. One looks, in vain, for any mention of the important results obtained during the past decade associated with the names of Debye, Eyring and Simha. Although the book is not up-to-date in many respects, it does contain a number of photographs and diagrammatic sketches which will be informative to the student.

In Part IV (pp. 453–564), the author really goes to town on biocolloids. Here, almost every conceivable subject is treated, ranging from the cycloid structure of proteins, saccro-colloids, lipides, cookery, the brewing of beer, biocatalysts, cell membranes, ossification (the latest reference in this active field is 1919), kidney stones, to Bancroft's famous peptization-coagulation theory of anasthesia, insanity and death. After four pages "à la Jules Verne," we are relieved to read that "his (Bancroft's) theory and the claims about sodium rhodanate have not been regarded with favor by medical men." The reviewer would add "and also the overwhelming majority of chemists." The last chapter of the textbook treats colloidal medicines, powder, creams and ointments. Here we learn (p. 552) from the "Rockefeller Centre Weekly, 1935" that "a dead orchid was brought back to life" merely by the addition of a few drops of a colloidal suspension of copper to the water to which "the dead flower" was dipped. "The experiment was so convincing that further research of a similar character is being subsidized, it is said, to the extent of $2,000,000 per year."

Such are the wonders and uncontrolled possibilities of colloid chemistry. But the reader of the 1947 edition would like to know what has been accomplished with this vast sum of money during the twelve intervening years.

<div align="right">VICTOR K. LaMer, New York, N. Y.</div>

Qualitative Analysis by Spot Tests. Inorganic and Organic Applications. By FRITZ FEIGL. 3rd, completely rev., Eng. Ed., tr. by RALPH. E. OESPER. Elsevier Pub. Co., Inc., New York-Amsterdam, 1946. xvi + 574 pp.; 37 tables, 45 figures. Price $8.00.

Dr. Feigl's standard text on spot reactions requires no further recommendation. It appears here thoroughly revised, including the newer material which has become available in recent years, with tested details of the procedures and applications. In contrast to the previous editions, this issue also presents a detailed account of the manipulations involved in spot test analysis, namely, the chapter: "Working Methods and Special Aids" from the author's "Laboratory Manual of Spot Tests." Together with the theoretical part of the original German editions, which appeared in English as "Specific and Special Reactions for Use in Qualitative Analysis," the present issue provides the best information available on the theory and practice of spot reactions.

An additional chapter on the detection of free elements, and a bibliography on application of spot reactions for special scientific and technical purposes, are included. This bibliography contains about 140 entries, in addition to those given in the 63 page chapter "Application of Spot Reactions in Tests of Purity, Examination of Technical Materials, and Studies of Minerals." A tabular summary of the limits of identification attained by the spot tests, with page references and a subject index, totaling 55 pages, complete this practical book.

The binding and printing are attractive. The paper could have been better, especially for a book which is going to be used extensively as a laboratory reference.

<div align="right">OLAV FOSS, New York, N. Y.</div>

Phenoplasts. By T. S. Carswell. 280 pp. Interscience Publishers, Inc., New York. Price $5.50.

This book is an assembly of literature references into two pictures, one picture to cover the chemical structure and the other to cover the physical structure of the phenoplasts. To these have been added sketchy chapters on the manufacture and molding of these resinous mixtures.

The chemical structure favored is largely based on a review of the publications of Zinke, Hultzsch and von Euler, which data, in turn, are based on the restricted reactions of a phenolic ring by partial substitution and then assuming that such a substituted phenol, by steps, points the way in which an unsubstituted phenol should react. In this way it was established that the simple mono addition product of phenol and formaldehyde could take any one of three paths—reversal, loss of water to give the ether, and loss of formaldehyde to give the disubstituted methane connector for two of the phenol rings. The two-formaldehyde addition to one phenol product, in addition to these reactions, seemed to give long chains or large cycles. A chain of average size of four phenyl rings was resinous but a large cycle containing four phenyl rings was still crystalline. The reasons for a fairly pure product being resinous are not attempted.

The tri addition product of formaldehyde on phenol is still more obscure. No trace of its existance has been recorded except when made by indirect methods and then stabilized for measurement as by an ether or ester.

An omission in the record (p. 31) is noted in the three dihydroxydiphenylmethanes. The diortho form (a) is known and reference should be made to Buehler, Cooper and Scrudder, *J. Org. Chem.* **8**, 316, who first published its correct properties. Corrected properties of the other isomers also would be in order. Corrections are needed to the literature, such as to Koebner's statement that "a reaction of 10 moles phenol with 6 moles formaldehyde gives a resin with a mean molecular weight of 437." In actual fact infusible resins can be so formed and their molecular weight is thus unknown (and high). The proper correction is "reaction, carried out so that the formaldehyde is evenly distributed, of 10 moles phenol and 6 moles formaldehyde give molecular weights approximating 437." Vanscheidt's formula (p. 33) requires the same safety correction. Without such a correction the statements are not true.

The section on physical structure is the stronger section of this book. There is an attempt to discover the meaning of the crack patterns of the hardened resins by causing swelling cracks to appear. The appearance of cracks are delayed by additional time-temperature cures up to a certain point. This delay coordinates to some extent with by-products evolved and with increase in per cent insolubles.

The author places emphasis in the hardening process as an aggregation to sphero-colloidal particles linked in the final step by a relatively small number of methylene bridges (pp. 72 and 69). The inference is that the swelling cracks appear along the lines of the weakness between the colloidal particles. This concept is interesting but not yet proven.

The sections on fillers, classification, properties and temperature effects are interesting for the research student but lack details needed by the commercial resin chemist. Two good short review chapters are included, one by Herr on ion exchange and the other by Whitlock on molding. The publication has been read with much interest by the reviewer and it is thought that the publication will fill a need for both college students and beginners in the commercial resin fields. Resin research chemists will find at least parts of it of value.

The book has good type but mixed paper supplies. It is suggested that it should be in every important polymer library.

<div align="right">H. L. Bender, Bloomfield, N. J.</div>

Organic Chemistry. By PAUL KARRER. *3rd English Ed., tr. from the latest German edition by* A. J. MEE. *Elsevier Publishing Co., Inc., New York, 1947. 957 pages. Price* $8.50.

As this book has become a well-established classic in the field of organic chemistry it seems unnecessary to do more than discuss the changes which have been incorporated into the latest edition. The author states in the preface that "Every chapter has been the subject of careful scrutiny and revision; where necessary, passages have been rewritten to bring them into line with the results of recent investigations. The modern literature . . . has been taken into account down to about the end of 1945." This statement is perhaps misleading. Sections have been added on Tröger's base (p. 129), biotin (p. 720), penicillin (p. 772), the synthesis of quinine (p. 850), recent work on colchicine (p. 871), and a few other minor topics. Except for these additions, however, the book remains virtually unchanged.

Almost no additional discussion of the modern theory of mechanisms of organic reactions has been introduced, and some of that which remains from the preceding edition (pp. 61–64, 377–379) seems to be of such dubious value that it might better have been omitted.

The latest edition is somewhat more attractively printed than the others. A number of misprints absent from the second edition have appeared in the third, however. While attention has been called to most of these in an Errata sheet, some are still uncorrected (for example, formula II at the top of p. 708 has an extra hydrogen and the formula for strophanthidin at the top of p. 710 is in need of a double bond).

In spite of the short-comings mentioned above the book will no doubt continue to serve as an invaluable reference work on organic chemistry, particularly in the field of natural products.

DAVID Y. CURTIN, New York, N. Y.

Röntgenographisch-Analytische Chemie. Möglichkeiten und Ergebnisse von Untersuchungen mit Röntgeninterferenzen in der Chemie. By E. BRANDENBERGER. Verlag Birkhäuser, Basel, 1945. 287 pp.; X tables, 121 figures.

This book does not present in detail the theory and practice of X-ray work, but aims to point out the manifold applicability of X-ray methods to chemical problems, and to state the possible results, as well as the limitations, obtainable in the special cases.

The first two chapters (30 pages) deal with the nature of crystals and the various experimental X-ray techniques; Chapter III (9 pages), the X-ray characteristics of crystalline and amorphous phases; Chapter IV (16 pages), methods for identification of pure and mixed crystals; Chapter V (18 pages), X-ray analysis of mixtures and evaluation of phase diagrams; Chapter VI (54 pages), the effects of crystal state on the characteristics of X-ray diagrams obtained by different experimental techniques; Chapter VII (63 pages), X-ray methods for study of rearrangements and chemical reactions in solids. The last chapter (53 pages) discusses the determination of crystal structure by X-ray methods.

The subject matter has been well covered, including topics such as molecular weight determinations by means of X-rays, small angle scattering as a means for evaluating particle dimensions, micro techniques, study of the structure of molecular films by means of X-rays and electron rays, and electron ray methods for solids.

There are no literature references in the text, but at the end of each chapter are included critical selections of pertinent literature (up to the end of 1944), with the author's commentaries. The colloid chemist will perhaps miss a reference to Weiser and Milligan's work on the structure of inorganic gels.

The book should prove of special value to research chemists, interested in the use and the aspects of X-ray methods in chemistry.

OLAV FOSS, New York, N. Y.

NOTE ON THE ORIGIN OF THE TERM "RHEOLOGY" [1]

Earl K. Fischer

From the Institute of Textile Technology, Charlottesville, Virginia
Received January 5, 1948

When, in 1929, Professor E. C. Bingham was searching for a word to cover the subjects of elasticity, viscosity, and plasticity, he considered a number of suggestions of Professor John R. Crawford of Lafayette College. The word *rheology* was selected as distinctive and explanatory. Based on the Greek roots *rheo* (to flow) and *logos* (science), it appeared adequate for the "science of the deformation and flow of matter." There can be little doubt that both Professor Bingham and Professor Crawford believed this word was new, and this description of how the word came to be "invented" has been frequently quoted (1,2,4,5).

An earlier use of rheology in the biological sciences seems to have been completely overlooked. In 1901, Forel (3) defined rheology as the study of flowing surface water as springs, brooks, streams, and rivers. ("Die Rheologie endlich studiert das flieszende Wasser der Landflächen, die Quellen, Bäche, Flüsse, und Ströme.") *Rheology* with this meaning distinguishes from the study of standing water encompassed by the term *limnology*, and Welch (6), in pointing out this distinction, deplores the physicists' definition. Presumably *rheology* was in use prior to the publication of Forel's book in 1901, but I have no citation to still earlier usage.

Rheology is not listed in the *New English Dictionary* (The Oxford Dictionary), in various encyclopedias, or in other general reference works.

Rheologists need not be disconcerted by this prior use of the term. The Bingham-Crawford definition is fairly well established in scientific and technical literature and is to be found in recent editions of the Merriam-Webster *New International Dictionary*. Scott Blair observes that the word has been translated into a "considerable number" of European languages. The biologists' definition, on the other hand, seems to have had scant use.

REFERENCES

1. British Rheologists' Club, Essays in Rheology, Pitman Publishing Corp., New York, 1947.

2. Bingham, E. C., *J. Rheology* 1, 92, 508 (1929); A. Nadai, *J. Colloid Sci.* 2, 1–5 (1947).
3. Forel, F. A., Handbuch der Seenkunde, p. 10. J. Engelhorn, Stuttgart, 1901.
4. Green, H., and Weltmann, R. W., Article on Thixotropy, Colloid Chemistry, Vol. VI, p. 329. J. Alexander, Ed., Reinhold Publishing Corp., New York, 1946.
5. Scott Blair, G. W., An Introduction to Industrial Rheology, P. Blakiston's Son & Co., Philadelphia, 1938; A Survey of General and Applied Rheology, Pitman Publishing Corp., New York, 1944.
6. Welch, P. S., Limnology, p. 10. McGraw-Hill Book Co., Inc., New York, 1935.

THE SOCIETY OF RHEOLOGY

Announcement of the establishment of a Bingham Award in Rheology was made in the February, 1947, issue of the *Journal of Colloid Science*. During the past year a number of well known scientists in the field were approached to form an award committee, contacts were made for the purpose of casting a suitable medal, and a sculptor was commissioned to design it. Announcement of the committee membership will be made in an early issue of the forthcoming A.I.P. news journal, *Physics Today*, so that nominations for the 1948 recipient may be submitted. In addition, *Physics Today* will publish, from time to time, the rehological news of general interest that has appeared previously in the *Rheology Bulletin*, which, for the time being, has been suspended in the belief that the *Journal of Colloid Science* and *Physics Today* may be of broader service to the science than was the *Bulletin*.

A PENETROVISCOMETER FOR VERY VISCOUS LIQUIDS

J. J. Bikerman [1]

INTRODUCTION

Penetrometers and viscometers are of the class of instruments most commonly used for testing adhesives. The essential part of a penetrometer (also called "gelometer" or "jelly strength tester") is a needle or cone which is pushed into the gelatinous or pasty adhesive by a given force, to a given depth, or for a given time: the "consistency" of the adhesive is a function of these 3 magnitudes. Viscometers may be of any type.

In the present work, the intention was to devise a simple apparatus which could be employed as a penetrometer, a viscometer, and also as a tackmeter, or "adhesiometer." Only a part of the program could be carried out.[2] The application of the instrument to adhesion measurements was reported briefly in an earlier paper (1). The penetrometer aspect has received little consideration thus far, but the instrument proved convenient, in some respects, for viscosity determination. It is described in the following from the point of view of viscometry.

DESCRIPTION OF THE INSTRUMENT

A vertical glass tube (see Fig. 1), about 15 cm. long and about 0.5–1.0 cm. in diameter (the middle part of a graduated 5 cc. or 10 cc. pipette), is closed at the bottom end with a rubber stopper, and partly filled with the liquid under test. On the surface of the liquid a vertical brass rod is placed, and its descent is observed with either the naked eye or by means of a low-power microscope provided with a micrometer eyepiece. (A traveling microscope magnifying about 20 times is convenient.) To facilitate observation, several scratches are made along the circumferences of the rod. To ensure the coaxial position of the rod in the tube the rod is provided with 6 "distance pins." These are pieces of copper wire, 0.16 cm. in diameter; 3 are soldered near the bottom of the rod, and the other 3 about 5–8 cm. from it. A platform to carry weights may be screwed to the top of the rod. The bottom of the rod is either flat or nearly semispherical; no other shapes were tested.

The tube is fixed between two plumb-lines in an air thermostat. The temperature of a thermometer in the thermostat varied regularly between 24.2° and 24.6°C., but the temperature of the rod-adhesive-tube system, with its larger heat capacity, deviated probably much less from the mean value of 24.4°C.
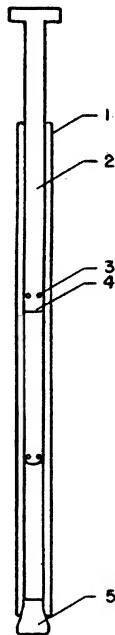
Fig. 1. The penetroviscometer. 1—graduated glass tube; 2—brass plunger; 3—distance pin; 4—upper level of the adhesive; 5—rubber stopper.

Among the viscometers described in the literature, those based on the rate of fall of a coaxial cylinder (2,3,4) or on axial translation of a cylinder (5,6,7,8,9) show the highest degree of similarity with the "penetroviscometer," but the area of contact between the cylinder and the viscous liquid does not remain constant in the "penetroviscometer"; in addition, there is no displacement of the liquid in the viscometers of the Pochettino type.

The Theory of the Instrument

$$a = \frac{gM}{4\pi\eta} f(R_0, R_1)$$

$$b = \frac{g\rho R_0^2}{4\eta} f(R_0, R_1)$$

$$c = a/b = \frac{M}{\rho \pi R_0{}^2}$$

$$f(R_0, R_1) = \frac{R_1{}^2 + R_0{}^2}{R_1{}^2 - R_0{}^2} \ln \frac{R_1}{R_0} - 1$$

g—acceleration due to gravity
h—depth of immersion
h_0—correction for the resistance to penetration
M—mass of the rod
R_0—radius of the rod
R_1—internal radius of the tube
t—time of immersion
$x = h/[c - (h + h_0)]$
η—viscosity of the liquid
ρ—density of the liquid

Other notations are explained in the text.

The weight of the brass rod forces the liquid upward through the narrow annular space between the rod and the glass tube. If the pressure gradient between both ends of the annular space is ψ, the driving force on a ring, 1 cm. thick and dR cm. wide, situated R cm. from the axis of the tube (and of the rod) is $\psi \cdot 2\pi R \cdot dR$. In the steady state it is counteracted by a numerically equal frictional force $\eta \left(\dfrac{du}{dR} + R \dfrac{d^2u}{dR^2} \right) 2\pi dR$, if the medium has Newtonian viscosity. Here u is the velocity of the liquid at the distance R from the axis. The equation thus obtained

$$\frac{d^2u}{dR^2} + \frac{1}{R}\frac{du}{dR} + \frac{\psi}{\eta} = 0 \tag{1}$$

is easily solved, and yields, since the velocity at the wall of the tube is zero,

$$u = \frac{\psi}{4\eta}(R_1{}^2 - R^2) - C \ln \frac{R_1}{R}. \tag{2}$$

Hence, the velocity U of the rod relative to the wall is

$$U = \frac{\psi}{4\eta}(R_1{}^1 - R_0{}^2) - C \ln \frac{R_1}{R_0}, \tag{3}$$

C being a constant of integration. The value of C is found from the condition that the volume of liquid displaced by the rod must be equal to that which in the same time passes through the annular slit, $i.e.$, from the equation

$$- \pi R_0{}^2 U = \int_{R_0}^{R_1} 2\pi u R\,dR, \tag{4}$$

or

$$-\frac{\psi}{4\eta} R_0{}^2(R_1{}^2 - R_0{}^2) + CR_0{}^2 \ln\frac{R_1}{R_0}$$

$$= \frac{\psi}{8\eta} (R_1{}^2 - R_0{}^2)^2 + C\left(\frac{R_0{}^2}{2} - \frac{R_1{}^2}{2} + R_0{}^2 \ln\frac{R_1}{R_0}\right). \quad (5)$$

Hence,

$$C = \frac{\psi}{4\eta} (R_0{}^2 + R_1{}^2), \quad (6)$$

and

$$U = -\frac{\psi}{4\eta}\left[(R_1{}^2 + R_0{}^2) \ln\frac{R_1}{R_0} - (R_1{}^2 - R_0{}^2) \right]. \quad (7)$$

A convincing calculation of the pressure gradient is not easy. If the column of the adhesive underneath the plunger were solid, the pressure on it would be computed by dividing the weight of the plunger by the internal cross-section of the tube. Because of the high viscosity of the liquids used, this computation seemed justified also in the present experimental set-up. Then, when the rod (plunger) is totally immersed, ψ becomes equal to $g(\rho_0 - \rho)R_0{}^2/R_1{}^2$, ρ_0 being the density of the rod material. The velocity of the rod becomes

$$U = -\frac{g(\rho_0 - \rho)}{4\eta}\frac{R_0{}^2}{R_1{}^2}\left[(R_1{}^2 + R_0{}^2) \ln\frac{R_1}{R_0} - (R_1{}^2 - R_0{}^2) \right]. \quad (8)$$

This equation governs the viscometers of Lawaczeck's type; the equation given by Lawaczeck is its first approximation for $R_1 - R_0 \ll R_0$. In the penetroviscometer the depth h of immersion continuously changes, and the pressure gradient is

$$\psi = \frac{g}{\pi R_1{}^2 h} (M - h\rho\pi R_0{}^2). \quad (9)$$

The mass M of the rod appears, because of buoyancy, reduced by the mass $h\rho\pi R_0{}^2$ of the displaced liquid. Introducing Eq. (9) and the abbreviations given in the list above into Eq. (7), the equation

$$U = -\frac{R_1{}^2 - R_0{}^2}{R_1{}^2}\left(\frac{a}{h} - b\right) \quad (10)$$

results. Since the total volume of liquid remains constant, the depth of immersion increases at the rate

$$\frac{dh}{dt} = -\frac{R_1{}^2}{R_1{}^2 - R_0{}^2} U, \quad (11)$$

i.e.,

$$\frac{dh}{dt} = \frac{a}{h} - b. \quad (12)$$

This equation can also be obtained if the velocity of the liquid is referred to that of the rod, *i.e.*, if the rod is considered stationary and the tube moving.

The rate $\dfrac{dh}{dt}$ would be given by Eq. (12), if the advancing front of the rod and the front pins met with no resistance. However, this resistance exists. The relation between this resistance and the size and shape of the rod front was intended to be, but was not investigated. The resistance appears to be equivalent to an increase of the depth h of immersion by a length h_0 which is an apparatus constant. Hence

$$\frac{dh}{dt} = \frac{a}{h + h_0} - b. \tag{13}$$

The integrated form of this equation

$$t = \frac{a}{b^2} \ln \frac{a - bh_0}{a - b(h + h_0)} - \frac{h}{b} \tag{14}$$

is not convenient for calculations, as the two terms on the right are almost equal (for the instruments used in this work). It is sufficient to expand the log term into a series and to use the first 3 terms. That gives:

$$t = \frac{1}{b} \cdot \frac{h}{c - (h + h_0)} \left[h + h_0 - \frac{c}{2} \cdot \frac{h}{c - (h + h_0)} + \frac{c}{3} \frac{h^2}{[c - (h + h_0)]^2} \right],$$

i.e.,

$$b = \frac{x}{t} \left(h + h_0 - \frac{cx}{2} - \frac{cx^2}{3} \right). \tag{15}$$

The viscosity is calculated either from the experimental value of b as found by means of Eq. (15), or from Eq. (13) rewritten as follows:

$$b = \frac{h + h_0}{c - (h + h_0)} \cdot \frac{dh}{dt}. \tag{16}$$

Evaluation of viscosity η is much simpler if the buoyancy term can be neglected; then $\dfrac{dh}{dt} = \dfrac{a}{h + h_0}$ and

$$a = \frac{h(h + 2h_0)}{2t}; \tag{17}$$

η is calculated from this value for a.

Simpler still is determination of relative viscosities for liquids having similar densities. For a given apparatus the time required to reach an immersion h is proportional to η; if the viscosity and the time of descent are, for a standard fluid, η_0 and t_0, and for the liquid under test η_1 and t_1, respectively, then $\eta_1 = \eta_0 t_1/t_0$. If c is very large, this equation is approximately valid also for liquids having different densities.

Precision of the Instrument

Among the magnitudes required for calculating viscosity the mass M of the rod, the density ρ of the liquid, and the time of immersion t can be measured very accurately, and the value of $f(R_0, R_1)$ can also be found with a satisfactory precision.[3] Practically the whole error of η values is due to those in h and h_0. It is easily shown that the relative error of η is about twice that of $(h + h_0)$.

The difficulty in measuring the depth of immersion is due to the fact that the rising meniscus of the liquid hardly ever possesses an axial symmetry and is less symmetrical the more viscous is the liquid. When the liquid is poured into the tube and warmed for a short time, the walls of the tube remain covered with a film of the liquid which is so thick that the distance pins cannot clear it. With the solutions used, longer heating, because of evaporation of the solvent, would increase the viscosity too greatly. Therefore, the film was blotted away by a plug of cotton wool. The portion of the film adjacent to the meniscus could not be removed in this way and made the position of the meniscus indefinite within, say, 0.1 cm. An error of 0.1 cm. for h of 1 cm. would cause an error of about 20% in the value of η. However, after some experience has been gained, it is possible to observe a more or less definite point of the meniscus and the determination of h can be carried out more satisfactorily; this is demonstrated in the examples of the following section.

The value of h_0 must be obtained from the experiments themselves. The values of h are substituted in Eq. (15) or (16) and that value of h_0 is found which makes b a constant for the whole experiment. It is an apparatus constant and does not depend on the liquid used; an experimental proof of this statement is given in the next section.

The instrument is capable of improvement in various respects. As it is now, it is able to measure absolute viscosities ranging from, say, 10^3 to 10^6 poises with an accuracy, in one experiment, of ± 1 or 2%.[4]

Testing the Instrument

(a) The radius, R_0, of the rod and that, R_1, of the tube are determined, respectively, by means of a micrometer gauge and by weighing with water. To check these figures the ratio of "upward movement of meniscus" to "downward movement of the rod" was determined. It was equal to the ratio $R_1^2/(R_1^2 - R_0^2)$, see Eq. (11), within the limits of accuracy of the measurement of h.

[3] It was intended to reduce the error of the value of R_1 by using precision-bore glass tubing.

[4] The admissible reproducibility of penetrometer determinations and of relative viscosity determinations of very viscous liquids is ± 2.5–$\pm 3.5\%$, see (10) and (11).

(b) For testing the applicability of Eqs. (15) and (16), measurements were carried out on solutions of rosin in wood turpentine which, according to H. Glaser (12), behave as true Newtonian liquids (*i.e.*, η is independent of the rate of shear).[5] The original solution used in the final set of experiments was rosin 80 g., wood turpentine 20 g., and had a viscosity (at 24.4°C.) of about 6×10^4 g./cm. sec. As it had to be heated (to about 105°C.) for every filling of a viscometer, it obviously was gradually losing

TABLE I

Test of Equation (15)

80% rosin in turpentine; $c = 79.28$ cm. $(\rho = 1.051)$; $h_0 = 0.10$ cm.

t min.	h cm.	$b \times 10^6$ cm./sec.
33.1	0.70	2.01
53.5	0.90	1.96
78.5	1.10	1.94
107.7	1.30	1.92
139.5	1.50	1.95
177	1.70	1.95
197	1.80	1.95
242	2.00	1.95
290	2.20	1.95
342	2.40	1.96
398	2.60	1.97

$$R_0 = 0.2100 \text{ cm.}$$
$$R_1 = 0.2825 \text{ cm.}$$
$$M = 11.55 \text{ g.}$$

With $b = 1.95 \times 10^{-6}$ that gives $\eta = 1.70 \times 10^5$ poises.

a little of the solvent, and its viscosity slowly rose to about 4×10^5 g./cm. sec. This very considerable rise in viscosity corresponds to a small increase in concentration. According to Glaser, the viscosities of 85% and 80% rosin are in the ratio 100:1, so that a concentration increase from 80% to about 81% would account for the augmented viscosity. In this way, starting from one solution, liquids of different viscosities were examined.

The increase in viscosity, evidently caused by evaporation of the solvent, can be illustrated by the following experiment. Two tubes were filled with plasticized rosin, and the time of descent of the corresponding brass rods along a stretch of 1.00 cm. was determined. It was 98 min. for one and 78 min. for the other tube. Then the filled tubes were heated, the rods taken out of the melt, the tubes with rosin left overnight in the

---

[5] Glaser's solutions flowed through capillaries in agreement with Poiseuille's law as long as the radius of the capillaries was above a limit, *e.g.*, 0.1 cm. for $\eta = 10^5$ and 0.5 cm. for $\eta = 10^7$ g./cm. sec., and ceased to move altogether at smaller radii. No such effect was observed in the present work, although the slits between rod and tube were as narrow as 0.0861 cm. and 0.0724 cm. The flow was quite regular in all tests.

thermostat, and the time of descent was measured as above. It was 138 min. and 113 min., respectively. The heating and cooling cycle was repeated again, and the time of descent rose to 240 and 160 min., respectively; all without the rosin sample leaving the tubes. A fresh filling gave then descent times equal to 43 and 42 min., respectively.

Table I shows one of the many tests of Eq. (15).

A typical test of Eq. (16) is represented in Table II. As the values of dh/dt are very small and cannot be measured with great accuracy, the spread of the individual values in Table II is large.

TABLE II

Test of Equation (16)

80% rosin in turpentine; $c = 59.93$ cm. ($\rho = 1.051$); $h_0 = 0$

t	h	$\frac{dh}{dt} \times 10^5$	$b \times 10^5$
min.	*cm.*	*cm./sec.*	*cm./sec.*
1.5	0.381	97	6.20
2.5	0.436	87	6.38
3.5	0.486	82	6.70
4.5	0.532	71	6.36
7.5	0.653	66	7.10
12.5	0.818	44	6.09
17.5	0.947	42	6.90
22.5	1.063	36	6.50
27.5	1.161	30	5.93
32.5	1.254	33	7.05
37.5	1.343	26.5	6.07
42.5	1.423	26.5	6.91
47.5	1.497	23.5	6.02
52.5	1.569	24.5	6.59
57.5	1.637	20.3	5.70
67.5	1.759	20.3	6.14
82.5	1.941	20.2	6.76
97.5	2.108	17.2	6.27

$R_0 = 0.3155$ cm.

$R_1 = 0.4016$ cm.

$M = 19.70$ g.

With $b = 6.42 \times 10^{-5}$ that gives $\eta = 7.70 \times 10^4$ poises.

To prove Eqs. (15) and (16) for a system of a very different viscosity, a solution of 70 g. rosin in 30 g. benzyl benzoate was used. Table III shows the validity of Eq. (15), and Table IV that of Eq. (16).

The experiments of Table I and Table III were made with one penetroviscometer and it is seen that the same value of h_0 makes b nearly constant in both experiments. In agreement with the assumption made, h_0 is independent of viscosity. The same observation applies to Table II and

TABLE III

Test of Equation (15)

70% rosin in benzyl benzoate; $c = 77.60$ $(\rho = 1.074)$; $h_0 = 0.10$

t min.	h cm.	$b \times 10^4$ cm./sec.
0.63	1.00	(2.05)
1.46	1.50	1.89
2.50	2.00	1.92
3.84	2.50	1.94
5.50	3.00	1.93
7.50	3.50	1.92
9.80	4.00	1.91
12.37	4.50	1.92
15.70	5.00	1.86
18.85	5.50	1.89
22.70	6.00	1.87
26.70	6.50	1.87
31.20	7.00	1.86

$$R_0 = 0.2100 \text{ cm.}$$
$$R_1 = 0.2825 \text{ cm.}$$
$$M = 11.55 \text{ g.}$$

With $b = 1.90 \times 10^{-4}$ that gives $\eta = 1.77 \times 10^3$ poises.

TABLE IV

Test of Equation (16)

70% rosin in benzyl benzoate; $c = 58.65$ $(\rho = 1.074)$; $h_0 = 0$

t	h	$\dfrac{dh}{dt} \times 10^4$	$b \times 10^4$
min.	cm.	cm./sec.	cm./sec.
1.25	1.38	93	2.25
2.25	1.86	63	2.07
3.75	2.44	60	2.60
5.5	2.93	43	2.28
7.5	3.44	42	2.60
9.5	3.90	37	2.62
11.0	4.18	29	2.23
13.0	4.53	28	2.37
15.0	4.84	22	2.02
17.0	5.14	28	2.72
19.0	5.44	22	2.22
21.0	5.72	25	2.72
23.0	5.99	22	2.47

$$R_0 = 0.3155 \text{ cm.}$$
$$R_1 = 0.4016 \text{ cm.}$$
$$M = 19.70 \text{ g.}$$

With $b = 2.40 \times 10^{-4}$ that gives $\eta = 2.16 \times 10^3$ poises.

Table IV. In these cases the depth of immersion was measured from the end of the rod to the top of the meniscus, and h_0 proved to be zero. It would have been approximately 0.15 cm. if the distance to the lower part of the meniscus were measured.

(c) A third kind of test was carried out by varying the load during the descent of the brass rod. A brass rod provided with a platform on top (see Fig. 1) was used. Its mass was 30.4 g. On the platform a 50 g. weight
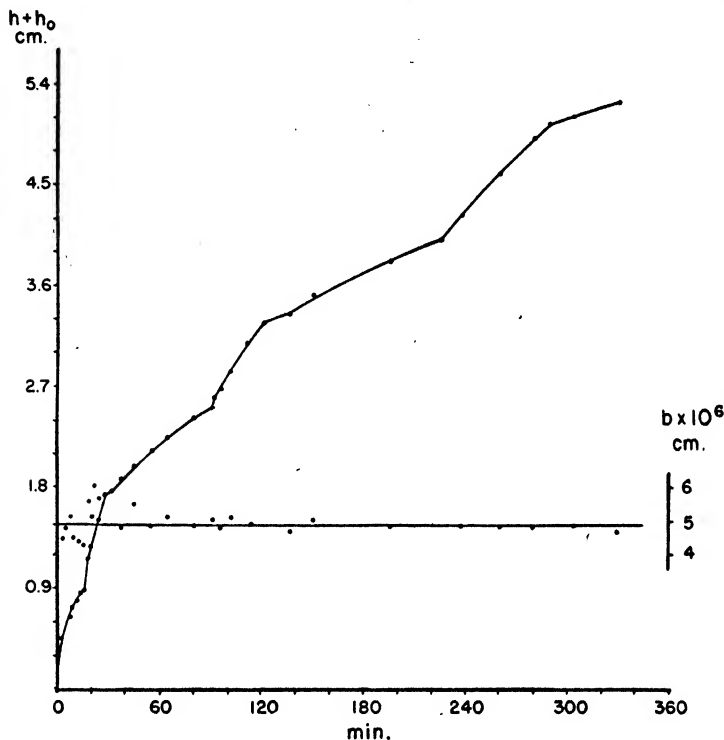
Fig. 2. Test at variable load. Abscissa—time in min. Ordinate, scale at the left— immersion depth in cm. Ordinate, scale at the right—the value of b in cm./sec. $\times 10^{-6}$. Variations of the load occurred at 15, 28, 90, 120, 225, and 290 minutes.

was placed, the rate of descent determined for a few minutes, the weight taken off, the rate of descent determined again, the weight put on again, and so on. The results obtained in the longest of these tests are shown in Fig. 2. Along its abscissa the time t of descent is plotted. Curve $(h + h_0)$ represents the depth of immersion attained at any t, and the horizontal line is b calculated from Eq. (16). Since c is proportional to the load on the plunger and, for this instrument, is much greater than $h + h_0$ the

product $(h + h_0)dh/dt$ is, at a first approximation, proportional to the load. It is seen that, as to be expected from a Newtonian liquid, b remains well constant when the load varies. The load was 80.4 g. along the steep, and 30.4 g. along the gentle slopes of the curve for $(h + h_0)$. The liquid used was rosin 80, wood turpentine 20.

The values of b are not shown for the first minute after adding or removing the additional weight. They are a little too high immediately after application of the additional load, and very small indeed (or even negative) immediately after removal of this load. That means that the brass rod penetrates into the viscous liquids too rapidly or too slowly after a sharp increase or a sharp decrease of the load. The retardation of descent after the removal of weight is especially striking and has the external aspect of elasticity. The effects are too large to be attributed to compressibility and were not due to the rubber stopper closing the tube. Similar "elastic after-effects" were discussed, *e.g.*, by F. Trouton (13), W. Braunbek (14), and J. M. Burgers (15). In the present work no attempt was made to elucidate their nature.

Summary

A new viscometer is described. The viscosity is calculated from the rate of descent of a heavy vertical rod in a coaxial tube filled with the liquid, the viscosity of which is greater than about 1000 poises.

References

1. BIKERMAN, J. J., *J. Colloid Sci.* **2**, 163 (1947).
2. LAWACZECK, F., *Z. Ver. deut. Ing.* **63**, 677 (1919).
3. BRIDGMAN, P. W., *Proc. Am. Acad. Sci.* **61**, 57 (1926).
4. WEINBERG, B., *Indian J. Phys.* **1**, 329 (1927).
5. SEGEL, M., *Physik. Z.* **4**, 493 (1903).
6. POCHETTINO, A., *Nuovo cimento* [6] **8**, 77 (1914).
7. TOLSTOI, D. M., *Kolloid-Z.* **73**, 96 (1935); *J. Phys. Chem.* (*U.S.S.R.*) **5**, 548 (1935).
8. TRAXLER, R. N., AND SCHWEYER, H. E., *Am. Soc. Testing Materials, Proc.* **36**, II, 518 (1936).
9. PUGH, H. L. D., *J. Sci. Instruments* **21**, 177 (1944).
10. Standard Methods of Test, A.S.T.M., D5–25 and D217–38T (1939 Book of A.S.T.M. Standards, Vol. III, pp. 185 and 603).
11. Standard Methods for Testing Petroleum and its Products (Inst. of Petroleum, London W.1), pp. 235, 238, and 414 (1944).
12. GLASER, H., *Ann. Physik* [4] **22**, 694 (1907).
13. TROUTON, F., *Proc. Roy. Soc.* (*London*) **77A**, 426 (1906).
14. BRAUNBEK, W., *Z. Physik* **57**, 501 (1929).
15. BURGERS, J. M., First Report on Viscosity and Plasticity. Amsterdam, pp. 41–58 (1939).
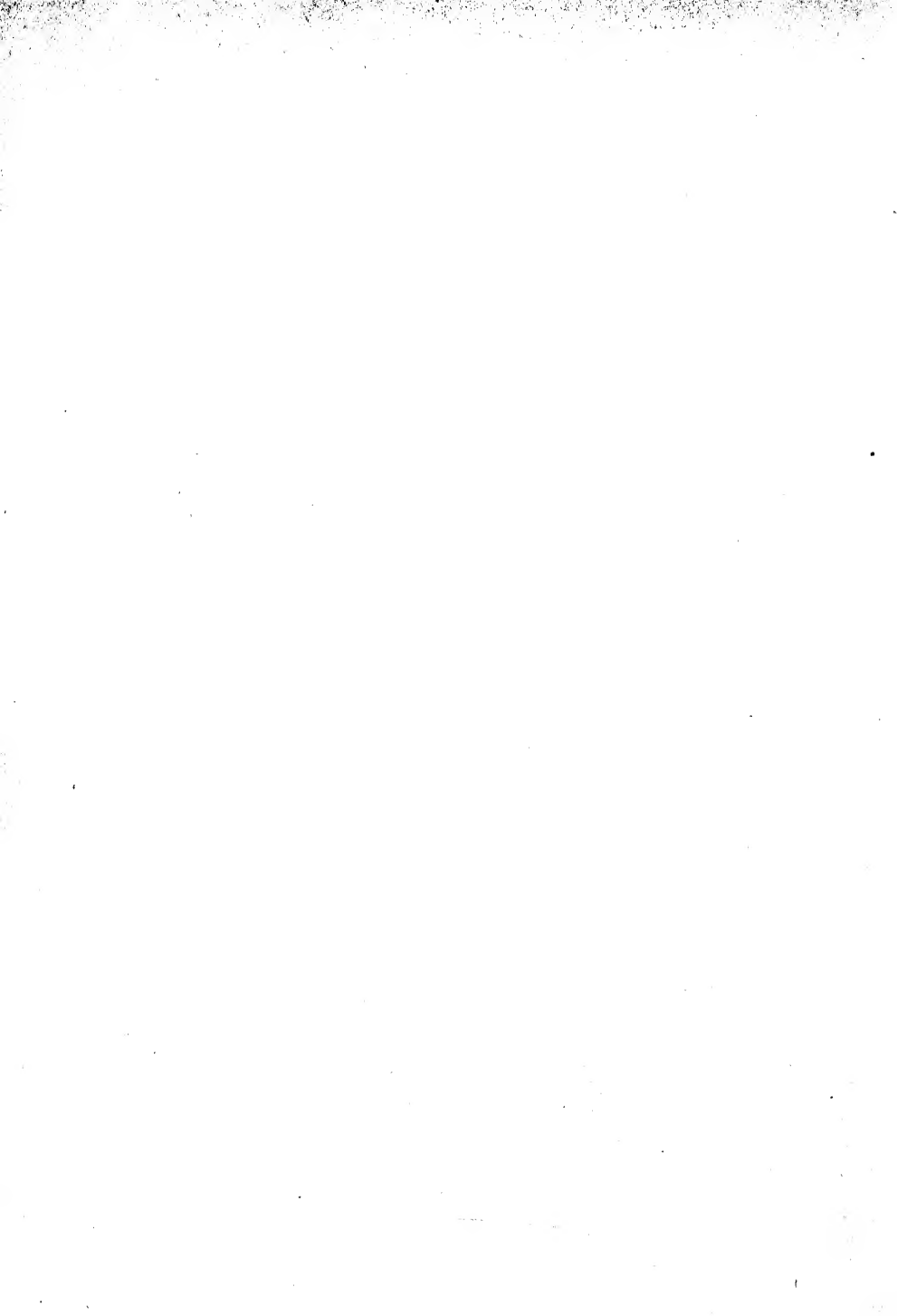
RHEOLOGY OF THERMOPLASTIC MATERIALS.
I. POLYSTYRENE [1]

Rolf Buchdahl

From the Research Department, Plastics Division, Monsanto Chemical Co, Springfield, Mass.
Received January 16, 1948

INTRODUCTION

The flow properties of polystyrene and concentrated polystyrene solutions have been the subject of several investigations during the last few years. Ferry (1) has shown that, in the case of concentrated solutions, the rheological properties are quite complex; the viscosity coefficient is not only a function of the shearing force but also depends on how long the shearing force is applied, and, upon removal of the shearing force, some solutions show a certain amount of recovery. Spencer and Williams (2) studied the solution viscosity of polystyrene over a wide concentration, temperature and molecular weight range, and obtained a general relationship between the viscosity coefficient and these variables. Because their measurements were made with a falling-ball viscometer, their results could only be given in terms of a single viscosity coefficient. In view of the results obtained by Ferry on very similar solutions, it does not seem entirely justified to characterize the flow properties of concentrated polystyrene solutions by a single constant.

Studies of the rheological properties of pure polystyrene above its second order transition point have been carried out by Wiley (3), Foote (4), Nason (5) and Flory and Fox (6). Wiley measured the rate of elongation under load at various temperatures and calculated a viscosity coefficient without attempts to obtain a relationship between the rate of shear (D) and the shearing stress (τ). Foote used both a parallel plate plastometer and capillary-type plastometer (previously described by Burns, 7). Using different pressures in the experiments with the capillary instrument, Foote found that the apparent viscosity was a function of the shearing stress, whereas the temperature coefficient of the apparent viscosity seemed to be independent of the shearing stress. Nason employed an extrusion type plastometer where the rate of extrusion at a given temperature was measured as a function of the applied pressure. His results show a non-linear relationship between extrusion rate and

applied pressure.   Although one can calculate, in principle, rate of shear
and shearing stress from these quantities, the applicability of such
equations to most extrusion-type plastometers is questionable. Finally,
Flory and Fox have measured the "melt" viscosity of different molecular
weight polystyrenes by the use of a coaxial falling cylinder viscometer
and an efflux-type viscometer; here, too, the flow properties are charac-
terized by only one viscosity coefficient.

The methods used thus far in the investigation of pure polystyrene
limit to varying degrees a complete rheological evaluation. It was, there-
fore, felt desirable to study the flow properties by the use of a rotational
viscometer, which is the most useful technique in the study of a complex
rheological system such as polystyrene.

EXPERIMENTAL METHODS

Fig. 1 shows the main parts of the instrument used in this investiga-
tion. It is a rotational viscometer of the Stormer type where the torque
and the speed of rotation are measured on the same element, usually the
inner cylinder. The outer cylinder (D) is stationary and is completely
immersed in a constant temperature bath regulated to ± 0.5°C. The
lower part of the rotating cylinder (E) is shaped into a cone and the
point of this cone rests on a conical plug (F) which closes the stationary
cylinder at the bottom. The narrow shaft of the rotating cylinder which
extends above the stationary cylinder passes through a ball bearing (C)
which is accurately centered with respect to the horizontal axis of the
instrument.   In this way the inner cylinder remains concentric with the
outer one during rotation without introducing an excessive amount of
friction. It should be emphasized that this manner of mounting the inner
cylinder by supports at the lower end is not very desirable. (An improved
rotational viscometer which eliminates this feature has been constructed.)
However, measurements with a viscous Newtonian oil (P-7 N.B.S.)
have shown that the characteristic rheological properties are not affected
by this arrangement, although the absolute viscosity value calculated from
the data without the use of end correction factors is, as would be ex-
pected, different from the value given by the Bureau of Standards. The
drum (A) and dial (B) mounted to the upper end of the rotating cylinder
are used, respectively, to apply a torque to the cylinder by means of
weights and to measure the speed of revolution. A solid preformed plug
is inserted into the inner cylinder. The material is then heated for a short
period of time to a temperature of about 230°C., and the inner cylinder
is put into position. The actual measurement consists in observing the
rotational shear at various shearing forces as a function of time. A few
measurements of the recovery after shear were made also. The material
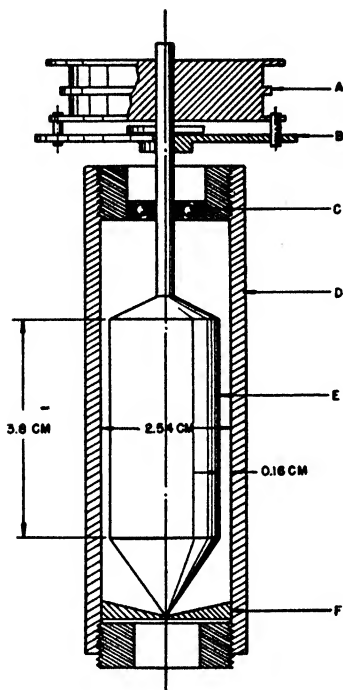
FIG. 1. Cross-section of rotational viscometer.

used in all these experiments was the standard commercial polystyrene
sold by the Monsanto Chemical Company under the trade name "Lus-
tron." This material has an intrinsic viscosity of 0.893 and an average
molecular weight (M_n) of about 113,000.

RESULTS

1. Time-Dependent Flow Properties

When a Newtonian liquid is sheared at a constant shearing stress,
the total deformation is a linear function of time and the rate of shear is,
therefore, constant. If this same experiment is performed with poly-
styrene, one obtains quite a different result as is shown in Fig. 2. The
temperature for these measurements was $150° \pm 0.5°$C. and the shearing
force was 1.15×10^5 dynes/cm². The rate of shear (which is inversely
proportional to a differential viscosity coefficient) does not remain con-
stant but changes with time in a rather complicated manner. After a
very slight increase, the rate of shear remains fairly constant for some
time and then begins to drop off. This decrease in the rate of shear is not

very pronounced but it can easily amount to a 50% change in the differential viscosity. Following this decrease the rate of shear appears to remain constant for a certain period of time, followed by a very noticeable increase in the rate of shear which might change the rate of shear by as much as a factor of 100.
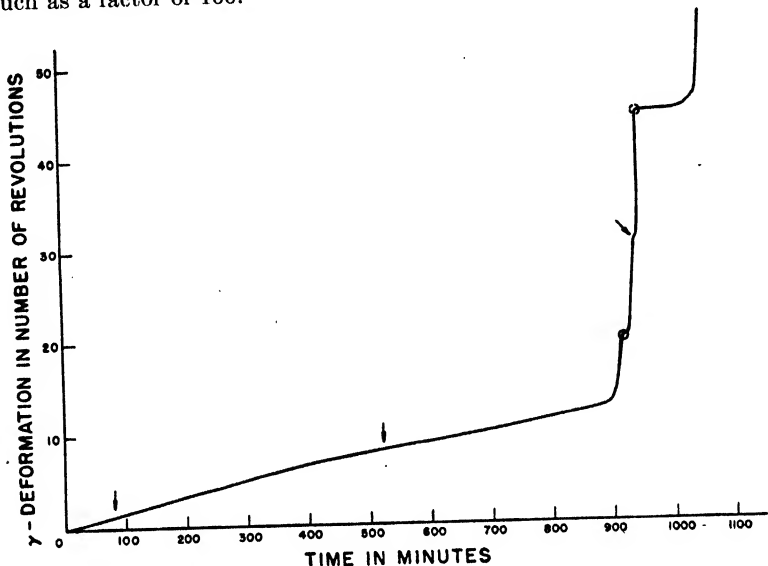
FIG. 2. Deformation-time curve. Temperature = 150°C.
Shearing force = 1.15×10^5 dynes/cm².

One of the disadvantages of a rotational viscometer of the Stormer-type is the fact that the shearing torque cannot be applied for an indefinite period of time. Every time the weights are rewound the material remains at rest for a certain period of time. It is difficult, therefore, to establish whether or not the rate of shear approaches a constant value.[2] On the other hand, it has the advantage that it demonstrates very effectively the effect of "resting" the sample—without a change in temperature on the rate of shear. The large broken circles in Fig. 2 indicate when this occurred. It will be noticed that the rate of shear decreases somewhat and the extent of the decrease is, among other things, determined by the length of the resting period; in one case the resting period was about 2

[2] Two other factors complicate the measurements at high rates of shear: (1) the precision obtainable decreases constantly as the rate of shear increases; (2) the rotating spindle has a tendency to be lifted out of the instrument. The latter phenomenon has also been observed in flow measurements of rubber by this method and is probably due to improper design of the rotating spindle.

minutes, whereas in the second case it was about 30 minutes. Because this particular experiment extended over a period of about 20 hours, the shearing was interrupted several times for a period of about 12 hours, during which time the sample was at room temperature. (The transition from the high temperature to room temperature was accomplished within a few minutes by the use of cooling coils inserted in the oil bath.) The rest periods at room temperature are indicated by arrows. It is interesting to note that the continuity of the deformation-time curve is not as much affected by this rest period in a "frozen" state as by the rest period at 150°C. The effect of rest periods on the rate of shear indicates that one is dealing, at least to some extent, with a reversible process.
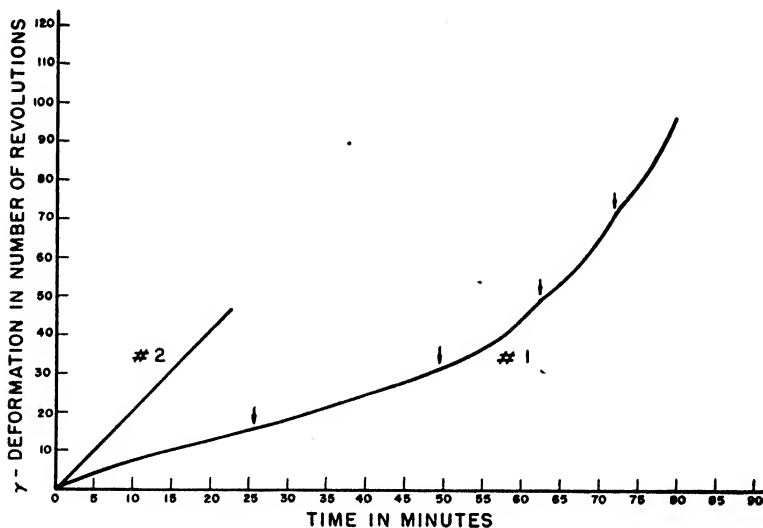
FIG. 3. Deformation-time curve. Curve 1: Temperature = 190°C. Curve 2: Temperature = 220°C.

We have further experimental evidence to substantiate this point. A sample was run at 175°C. for some time with a shearing force of about 3×10^4 dynes/cm.^{2}; the time required to complete one revolution was 270 sec. Then the temperature was raised to 235°C. for about 30 minutes without shearing the sample and then lowered again to 175°C. The time for completion of one revolution had now increased to about 340 seconds for the same shearing force. In other words, increasing the temperature during a rest period and returning to the lower temperature generally decreases the rate of shear. Finally, when the material is sheared with a higher shearing force and one then reduces the shearing force considera-

bly, the rate of shear frequently decreases slightly for a short period of time.

Raising the temperature has a marked effect on the deformation-time curve. Fig. 3 shows the results obtained at 190°C. (shearing force $= 1.15 \times 10^5$ dynes/cm.²) and at 220°C. (shearing force $= 57.5 \times 10^2$ dynes/cm.²). The deformation-time curve at 190°C. is still quite similar to the one at 150°C. However, the strong increase in the rate of shear occurs much sooner than at 150°C. and the temporary decrease in the rate of shear, although still observable, has become much less pronounced. At 220°C., the time-dependent flow properties have almost entirely disappeared, at least within the investigated range, and the rate of shear is constant.
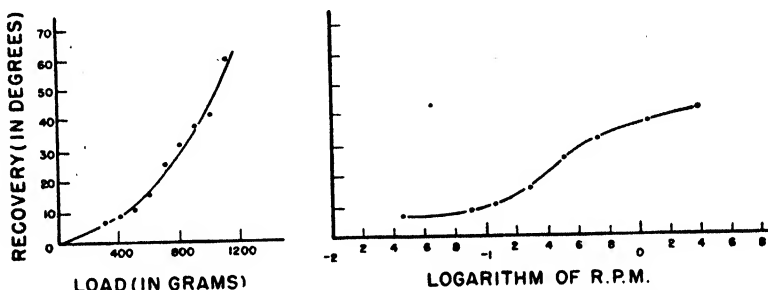
FIG. 4. Recovery of polystyrene as a function of load and r.p.m.

When polystyrene, at 175°C., is given a shear of one revolution only and the shearing force is removed immediately, a definite recovery can be observed. The amount of recovery is a function of the shearing force, or rather of the speed of deformation as is shown in Fig. 4. The recovery at this temperature is almost complete within a few minutes but no recovery-time curves have been obtained as yet. The important fact, however, is that the amount of elastic recovery increases strongly with increasing speed of deformation. After the material has been sheared for several revolutions, recovery effects disappear almost entirely.

2. Rate of Shear—Shear Stress Relationship

When the rate of shear is time-independent, the flow properties at a given temperature are completely characterized by the relationship of rate of shear to shear stress. For the particular polystyrene used, one must go to temperatures above 200°C. before these time effects become negligible. Fig. 5 shows two flow curves (D vs. τ) at 200° and 220°C. It will be noticed that at these temperatures this particular sample still
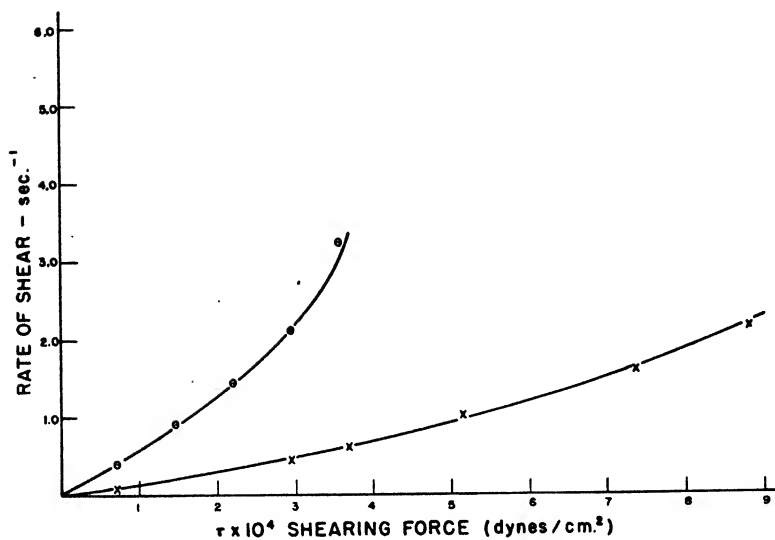
FIG. 5. Flow curves of polystyrene.

o = 220°C. $\eta_0 = 1.75 \times 10^4$ poises
x = 200°C. $\eta_0 = 7.50 \times 10^4$ poises
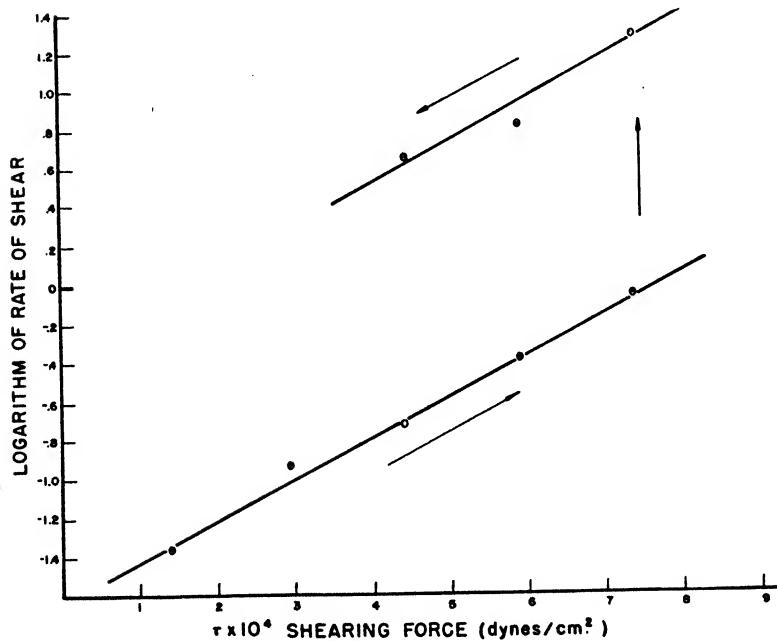
FIG. 6. Flow curves of polystyrene at 175°C.

shows non-Newtonian flow properties, the viscosity is a function of the shearing force. At lower temperatures, where the rate of shear is time-dependent, it has been difficult to establish an equilibrium value and the rheological behavior should really be expressed in three dimensions. Fig. 6 shows the relationship between τ and D at 175°C. (The log of the rate of shear is plotted as a function of τ in order to cover properly the wide range of D values.) Curve 1 gives the initial measurements going from low to high shear stresses. At $\tau = 7.35 \times 10^4$ dynes/cm.^{2} the rate of shear was allowed to increase strongly as a function of time until it reached the value given on Curve 2. The remaining points on Curve 2 were obtained by decreasing the rate of shear fairly rapidly. It will be noticed that Curves 1 and 2 have almost the same slope. This fact has been observed quite frequently in measurements of this type on polystyrene, although a change in the slope has been noticed in several experiments.

Discussion

The data obtained in this investigation show that the flow properties of polystyrene in the investigated temperature range are non-Newtonian and, therefore, the viscosity coefficient is a function of the shearing stress or rate of shear. This is in agreement with previously published data (4,5). The existence of rather marked time-dependent flow properties had not been observed so far, mainly because previous investigators employed experimental methods which made the observation of such phenomena difficult, if not impossible. Although such time-dependent, or thixotropic, flow properties have frequently been observed on other systems, particularly systems of a colloidal nature, the question arises whether or not, in the case of polystyrene, they are a property of the material itself or are due to slippage and other instrumental factors.

Before the experiments reported in this paper were undertaken, some preliminary measurements were made in a rotational viscometer (9) with an outside cylinder made of glass. No slippage could be observed when a torque was applied to the inner cylinder as the speed of rotation increased.[3] When the inner cylinder was rotated by hand at about the same speed, it was noticed that the force required decreased gradually. During the rotation of the inner cylinder the material did not tend to move out between the shearing surfaces and no voids or air bubbles were created. Furthermore, all time-dependent properties disappeared for measurements slightly above 200°C., irrespective of the rate of shear. It seems difficult to conceive of a mechanism which would explain why

[3] In some cases very small air bubbles were dispersed in the polystyrene during the application of a shear. The motion of these bubbles appeared to indicate laminar flow between the shearing surfaces.

polystyrene adheres equally well to a metal or glass surface above 200°C. but shows strong slippage a few degrees below this temperature. For these reasons we are inclined to attribute all time-dependent flow properties described in this paper to the material itself, and the following is an attempt to give at least a qualitative explanation of the observed flow properties in terms of molecular structure of an assembly of high polymer molecules. At the outset, it should be stated that more experimental data along similar lines is necessary to clear up various points which are not too well understood at the moment, and it is quite possible that further work might make it necessary to modify, or discard completely, the explanation to be given.

At the start of a deformation process, as shown for example in Fig. 2, it is reasonable to believe that the polystyrene chains are strongly entangled with each other. Such points of entanglement, or mesh points, are due to interference of two or more chain segments. We will now assume that at a given temperature mesh points are broken and reformed continuously according to certain rate processes which need not be specified at the moment. Now, as a shear is applied to an assembly of entangled polystyrene molecules and the material starts to deform, the various chain segments will be set in motion and move into new positions. However, before they have been able to move very far from their original position the stress starts to act on the mesh points and the deformation under shear is slowed down, leading to a decrease of the rate of shear. If the initial speed of deformation is fairly high, a large proportion of the mesh points retain their original configuration and the material exhibits a certain amount of elastic recovery. However, as the deformation continues, the mesh points are not sufficiently strong to support the stress indefinitely and, because the movement of the chain segments is too rapid to allow recombination of broken mesh points in new positions, the number of mesh points per unit volume will decrease, leading to a considerable increase in the rate of shear. This disentanglement of mesh points under shear might also be described as an orientation process where the chain segments are able to move without interfering too much with the movement of chain segments of neighboring chains.

Using this picutre, the effect of temperature and "resting periods" can easily be understood. Raising the temperature for a certain period of time, without shearing the material prior to the development of high rates of shear, will favor disentanglement and, therefore, the rate of deformation will be speeded up somewhat upon return to the original temperature. However, if the material has been given a considerable amount of "orientation," then the same procedure will lead to an increased entanglement and the deformation will be temporarily decreased. Lowering the temperature has the effect of "freezing" the configuration as it existed

at the moment the shear was stopped and resting the material at the same temperature will have very little effect if the chains are still strongly entangled, or it will reduce temporarily the rate of shear if "orientation" has taken place to a considerable extent. No specific statement can as yet be made with respect to the relative magnitude of the two processes because it has been difficult to obtain true equilibrium conditions.

Because of these strong time effects, it is difficult to give a proper interpretation of the rate of shear-shearing stress curves. One can obtain entirely different curves at the same temperature depending upon what region of the deformation-time curve is being used to obtain the various rate of shear values, as can be seen from the example given in Fig. 6. At higher temperatures, where the flow curves are almost independent of time effects, the relationship between τ and D is non-linear. The theory of viscous flow developed by Eyring (8) and co-workers predicts a non-linear relationship between these two quantities when the product of shear stress times flow volume is considerably larger than kT; specifically, the log of D becomes a linear function of the shear stress. If one plots the data given in Fig. 5 in this manner, one obtains a curve which appears to become linear at higher shearing forces but is non-linear at lower shearing forces. According to Eyring's theory, the slope of the log D-τ curve should be equal to the flow volume. A rough calculation of the slope gives for this particular polystyrene sample a value of about 10^6 $(A°)^3$. Such a value seems much too high[4] but more experimental work is necessary before one can reach a definite conclusion as to whether or not Eyring's theory in its present form is applicable to polystyrene at temperatures above 200°C. Below these temperatures, it seems quite certain that any theory of viscous flow[5] must first take into account time-dependent phenomena to apply to viscous flow of polystyrene and other thermoplastic high polymers.

The determination of the temperature coefficient of viscous flow is again made difficult by the existence of time-dependent flow properties. It seems possible that the energy required to move a chain segment in a disentangled structure might be quite different from the energy required to break mesh points, particularly when the polymer chain contains side groups having different interaction energies from those of the groups of the chain itself, as is the case in polystyrene. The wide discrepancies which have been reported in the literature[6] for polystyrene might, in part, be due to the fact that the viscous deformation processes are not

[4] The same has been observed when flow data on rubber obtained by Mooney (*Physics* 7, 413 (1936)) were treated in this way (SMALLWOOD, *J. Applied Phys.* 8, 3113 (1940)).

[5] See A. BONDI, *J. Applied Phys.* 16, 539 (1945) for the effect of flow orientation on the viscosity coefficient in isotropic fluids.

[6] See table in Ref. 2.

necessarily the same and depend on the particular experimental conditions. In Fig. 7 are shown the "initial" viscosity values as a function of temperature; the initial viscosity (η_0) is determined as that slope of a flow curve which passes through the origin of the D-τ diagram. The activation
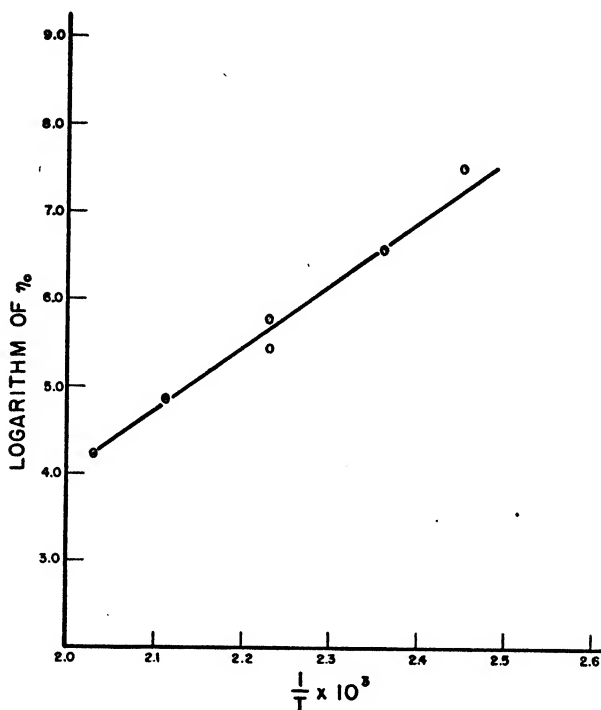
FIG. 7. Viscosity-temperature relationship for polystyrene.

Temp.	η_0 (poises)
135	3.33×10^7
150	3.78×10^6
175	$2.9 - 10^5, 6.5 - 10^5$
220	7.5×10^4
	$1.75 - 10^4$
	$E \sim 32$ Kcal.

energy of viscous flow calculated from these data is about 32 Kcal. Activation energies of this magnitude have frequently been attributed to highly elastic deformation. Although this might be the correct interpretation in some cases, it seems quite certain that the deformations from which these data were obtained were not of this nature. It is interesting to note that one can obtain a much lower activation energy from the

experimental data if one plots, for example, the viscosity obtained at 175°C. from Curve 2 in Fig. 6 and the viscosities at higher temperatures. The data of Curve 2 were obtained while the material was presumably much more oriented or disentangled than in its initial state. These findings seem to lend some support to the statement made above. However, the correct interpretation of large temperature coefficients for viscous flow is still very much in doubt.

ACKNOWLEDGMENT

REFERENCES

1. FERRY, J. D., *J. Am. Chem. Soc.* **64**, 1323, 1330 (1942).
2. SPENCER, R. S., AND WILLIAM, J. L., *J. Colloid Sci.* **2**, 117 (1947).
3. WILEY, F. E., *Ind. Eng. Chem.* **33**, 1377 (1941).
4. FOOTE, N. M., *ibid.* **36**, 244 (1944).
5. NASON, H. K., *J. Applied Phys.* **16**, 338 (1945).
6. FLORY, P. J., AND FOX, T. G., JR., Spring Meeting Am. Chem. Soc. Atlantic City, 1947.
7. BURNS, R., *Proc. Am. Soc. Testing Materials* **40**, 1283 (1940).
8. KAUZMANN, W., AND EYRING, H., *J. Am. Chem. Soc.* **62**, 3113 (1940).
9. BUCHDAHL, R., AND THIMM, J. E., *J. Applied Phys.* **16**, 344 (1945).

THE CRAGOE L FUNCTION FOR THE VISCOSITY OF OILS UNDER PRESSURE AT CERTAIN TEMPERATURES [1]

R. B. Dow

From the Bureau of Ordnance, Navy Department, Washington, D. C.

INTRODUCTION AND CONCLUSIONS

C. S. Cragoe (1), in 1933, introduced a simple function, the L function, to represent changes of viscosity of lubricating oils with change of pressure, temperature and composition. From the limited amount of data then available, he concluded that L was linearly related to temperature and its reciprocal linearly related to pressure. On examining the data of Hyde, Hersey and Shore, Kiesskalt, and Kleinschmidt, measured over a pressure range of 21,000 ψ, Cragoe found that the pressure coefficient of L, designated as β, was approximately constant for a given oil sample at a given temperature, and varied slightly with temperature over a range between 68° and 176°F.

In view of the practical value of the L function, and the fact that rather detailed viscosity data (2) are now available for a variety of oils at various pressures and several temperatures, it now becomes desirable to re-evaluate the L function for several representative petroleum oils of widely different characteristics.

The L functions of 12 representative petroleum oils have been examined over a pressure range of 28,000 ψ at temperatures of 100°, 130°, and 210°F. At constant temperature, β generally decreases with increase of pressure, although in some cases it was found to increase initially with increase of pressure. The change of β with change of pressure is most pronounced for the Pennsylvania or paraffinic type oils, the decrease being about 36% over a range of 20,000 ψ at 100°F. for oil No. 1; at 210°F., the decrease of 40% is of about the same magnitude. However, for an oil rich in naphthenic and aromatic compounds, *e.g.*, oil No. 7, β decreases only by about 4% over the same pressure range at 100°F., and 6% at 210°F. In general, the magnitude of β has been found to vary from 2.4 to 4.3×10^{-4}, depending on the pressure, temperature, and the type of oil. This is in good agreement with Cragoe (1) who reported values of β between $2.7–4.0 \times 10^{-4}$ for a number of petroleum oils from different sources. Although considerable data at atmospheric pressure are available

on the physical and chemical properties of the present oils, there appears to be no close correlation with the L function. In general, the larger values of β occur for the oils of lower viscosity index but the functional relationship is not a simple one.

The temperature coefficient of L, designated as α, for oil No. 3, a paraffinic oil, changes with pressure in such a way that a minimum value is found below 10,000 ψ, over a range of 18,000 ψ. This tendency appears to be characteristic of the paraffinic type oils which have been studied. On the other hand, α for the naphthenic and aromatic type oils, e.g., oil No. 9, slowly increases with increase of pressure. Since the temperature coefficient of viscosity increases slowly with increase of pressure, for both paraffinic and naphthenic type oils, it can be concluded that α, like β, may exhibit an interesting structural dependence which has not been fully investigated.

It is shown that the defining equation for L can be interpreted in terms of current reaction rate theory, and on this basis the pressure change of L can be related to the pressure change of the energy of vaporization, some fraction of which is taken as a measure of the activation energy for viscous flow. However, since the energy of vaporization does not appear to differ appreciably from oil to oil, regardless of type, it can be concluded that β should be about the same for all petroleum oils and should be inversely proportional to the rate of pressure change of the heat of vaporization. Since the results of the present study indicate that β is not constant, and depends not only on the pressure but on the type of the oil, it seems necessary to reject any volume theory for other than the first approximation, and to seek a more complete explanation and better quantitative agreement in terms of structural effects which are related to molecular orientation within the liquid.

METHODS

Following Cragoe (1), the absolute coefficient of viscosity of an oil can be written

$$\eta = Ae^{B/L}, \tag{1}$$

where A and B are empirically chosen constants for any oil and L is the Cragoe viscosity function. The numerical values of A and B are 5×10^{-4} and $1000 \ln 20$, respectively, as given by Cragoe.

The pressure coefficient of L is defined by

$$\beta = (L_1 - L_p)/L_p(p - 1) = - L_1 dL/L_p^2 dp. \tag{2}$$

L_1 is the value at 1 kg./cm.^{2} * and L_p is the value at pressure p.

---

* Pressure will be expressed in units of the kg./cm.^{2} in calculating β to facilitate comparison with Cragoe's values; otherwise, the pressure unit to be used will be the ψ.

Likewise, the temperature coefficient of L becomes

$$\alpha = L_t - L_0/L_0(t_t - t_0) = dL/L_0dt. \tag{3}$$

L_0 is the value at the reference temperature which will be taken to be 100°F. and L_t is the value at temperature t.

From Eqs. (1) and (2), the pressure coefficient of viscosity can be written

$$1/\eta \, d\eta/dp = -\, B/L_p^2 dL/dp = B/L_1\beta \tag{4}$$

and the temperature coefficient of viscosity can be written

$$1/\eta \, d\eta/dt = -\, B/L_t^2 dL/dt = -\frac{\alpha\beta L_0}{L_t^2}. \tag{5}$$

Twelve representative petroleum oils were chosen for the evaluation of the L function. Table I summarizes some of the physical and chemical data for these oils at atmospheric pressure. Oils No. 1, 2, and 3 were Pennsylvania type oils designated in the study of Dibert, Dow and Fink

TABLE I

Physical Data for Representative Petroleum Oils

Oil no.	Source	Ref.	Density 100°F.	Viscosity Cp 100°F.	Aniline Pt °C.	VI	Mol. wt.	Per cent Paraffins	Per cent Naph-thenes	Per cent Aromatics
1	Penn	3	0.832	14.20	101.7	127	309	78	22	0
2	Penn	3	0.841	26.20	107.1	117	370	76	24	0
3	Penn	3	0.879	406.0	122.9	102	705	77	16	7
4	Penn	4	0.863	83.00	110.3	102	550	77	13	10
5	Burma no. 1	2	0.895	17.38	73.0	79	319	67	13	20
6	Russian no. 2	5	0.887	33.30	88.0	66	364	60	30	10
7	Russian no. 1	5	0.895	88.80	94.3	49	393	59	33	8
8	Rumanian no. 1	5	0.913	21.10	60.8	35	285	54	24	22
9	U. S. Naph-thenic	Data of Fink	0.932	77.40	68.1	−4	330	48	32	20
10	Burma no. 3	2	0.938	320.3	78.9	−9	412	61	16	23
11	Rumanian no. 2	5	0.926	450.4	77.8	−36	409	51	29	20
12	U. S. Naph-thenic	Data of Fink	0.937	72.60	60.9	−38	313	47	29	24

(3), as oils No. 6, 2, and 1, respectively. The present oil No. 1 was a low boiling fraction, No. 2 a commercial "neutral," and No. 3 a commercial "bright stock." The 3 samples differed considerably in initial viscosity at 100°F. and in molecular weight. Oil No. 4 was another Pennsylvania sample studied previously by Dow (4). Oils No. 5 and 10 were from Burma

R. B. DOW

sources and have been reported by Dow and Veith (2). These two samples differed considerably in viscosity index. Typical Russian and Rumanian oils were chosen as oils No. 6, 7, 8, and 10. Their viscosity characteristics at high pressures were reported by Dow, McCartney and Fink (5). It is to be noted that the viscosity indices of these oils covered a medium to a low range, which is characteristic of the naphthenic and aromatic types. Also, other data at atmospheric pressure, e.g., viscosity at 100°F., aniline point, and molecular weight show considerable differences from one sample to another. The data on the remaining samples, oils No. 9 and 12,

TABLE II

$\beta \times 10^4$ (cm.²/kg.) at Various Temperatures and Pressures for
Representative Oils of Table I

Oil no.	10,000 ψ			20,000 ψ			28,000 ψ		
	100°F.	130°F.	210°F.	100°F.	130°F.	210°F.	100°F.	130°F.	210°F.
1	3.22	2.86	3.41	2.95	2.69	3.01	2.81	2.64	2.94
2	2.96	2.95	3.18	2.79	2.78	2.92	2.70	2.68	2.81
3	2.55	2.67	2.88	—	2.40	2.32	—	2.46	2.46
4	2.81	2.51	3.31	2.73	2.70	2.87	—	2.59	2.74
5	3.49	3.23	—	3.16	3.35^a	—	—	—	—
6	3.74	3.98	3.57	3.60	4.00	3.38	—	—	3.29
7	3.55	3.65	3.31	3.46	3.51	3.23	—	3.49	3.20
8	3.75	3.54	2.63	3.76	3.57	2.84	—	3.58	2.83
9	4.10	3.86^b	—	4.08	3.84^b	—	—	3.82^b	—
10	3.89	3.71	—	—	—	—	—	—	—
11	4.17	3.98	3.61	—	4.00	3.70	—	—	3.69
12	4.29	4.06^b	—	4.28^c	4.06^b	—	—	4.05^d	

^{a} This value at 18,000 lbs./in.².

^{b} This value at 150°F.

^{c} This value at 16,000 lbs./in.².

^{d} This value at 26,000 ψ and 150°F.

were from unpublished studies of C. E. Fink (6), and are illustrative of typical U. S. naphthenic type of oils of low viscosity index. The data of Table I were determined by conventional methods of measurement, with the exception of the structural characteristics, i.e., per cent of paraffinic compounds, etc., which were measured and computed after the method of Waterman and his associates (7).

Examples of Computations

The details of computation involved in calculating L and β are shown in Table III for the case of oil No. 3 (3), at atmospheric and 10,000 ψ (703 kg./cm.²) pressures, at the two temperatures of 100° and 210°F.

L is computed from Eq. (1) when it is put in the form of Eq. (6). The values of the constants A and B are those given above. When L is known at atmospheric pressure and 10,000 ψ, it is then possible by Eq. (2) to compute β for that pressure interval.

TABLE III

L and β for Oil No. 3 at Representative Pressures at 100° and 210°F.
100°F.

Pressure p	Coeff. visc. η	ln η/A	L_p	$L_1 - L_p$	$\beta \times 10^4$
kg./cm.²	poises				cm.²/kg.
1.06	4.15	9.026	331.9	---	-
703 (10,000 ψ)	20.90	10.641	281.5	50.4	2.55
		210°F.			
1.06	0.26	6.255	478.9	---	
703	0.92	7.519	398.4	80.5	2.88

α may be computed at 10,000 ψ between 100° and 210°F. in the following way from Eq. (3):

$$\alpha = \frac{398.4 - 281.5}{(281.5)(110)} = \frac{116.9}{30,965} = 3.78 \times 10^{-3} \; 1/°\text{F}.$$

RESULTS

Cragoe concluded from a survey of the earlier measurements of Hyde (8), Hersey and Shore (9), Kiesskalt (10), and Kleinschmidt (11), that the L function was linearly related to temperature and its reciprocal linearly related to pressure. The magnitude of β was found to range between 2.7 and 4.0 $\times 10^{-4}$ for about 12 petroleum oils at temperatures between 68° and 176°F. They were commercial products obtainable in the market from widely different sources, but little inspection data were available, and there was no evidence that the samples met any particular standards. In discussing the temperature behavior of the viscosity of those samples, Cragoe found it convenient to compute the product of some initial temperature, expressed in degrees Rankine, by the temperature coefficient of L, *i.e.*, α; the values ranged from 2.20 to 2.61 for the 12 oils at $t = 564$°R.

Eq. (1) can be put in the form

$$\ln \eta = \ln A + B/L. \tag{6}$$

Consequently, an oil obeying Eq. (1) should exhibit a linear relationship between ln η and $1/L$, the constants A and B being found as the intercept and slope, respectively, of the plotted line. An examination of this relationship at constant temperature for the oils of Table I showed that it was

not valid, since ln η departed appreciably from a linear relationship with $1/L$. Consequently, it was decided not to redetermine the numerical values of A and B from the present data, but to use the values as determined by Cragoe, and given above, in further analyzing the pressure and temperature effects on the L function.
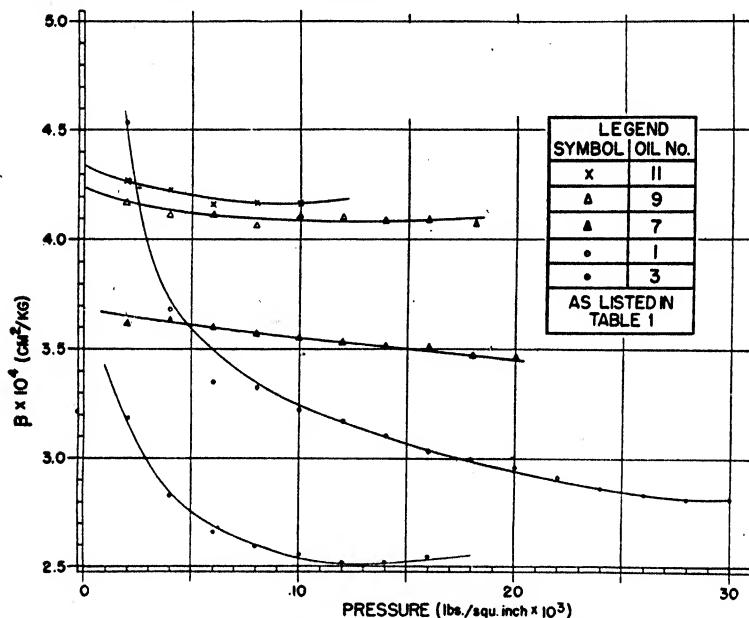
FIG. 1. Pressure coefficient at 100°F. of L vs. pressure for representative petroleum oils.

The results obtained for β at several pressures are given in Table II. Most of the values are given at 100°, 130°, and 210°F., although in some cases data were available only at 100° and 150°F. Figs. 1 and 2 illustrate

TABLE IV

$\alpha \times 10^{-3}$ $(1/F.°)$ at Various Pressures for Several Oils of Table I

Oil no.	Pressure (ψ)					
	15	4000	6000	10,000	14,000	18,000
1	3.42	3.18	3.18	3.28	3.30	3.29
3	4.03	3.31	3.72	3.78	4.04	4.39
7	4.36	4.43	4.39	4.54	4.59	4.64
9[a]	4.78	4.95	5.03	5.12	5.21	5.30

[a] Temperature interval between 100° and 150°F.

in more detail the variation of β with pressure for several of the oils at 100° and 210°F.

Some of the computations for α are given in Table IV. The temperature interval is between 100° and 210°F. The product of absolute temperature, 560°R, and α ranges from 1.82 to 2.97, not differing materially from the magnitude reported by Cragoe.
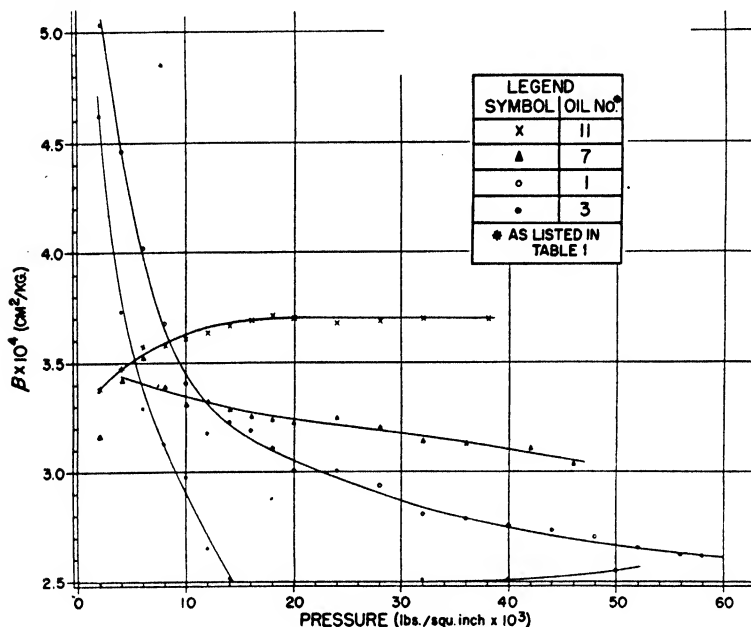
FIG. 2. Pressure coefficient at 210°F. of L vs. pressure for representative petroleum oils.

DISCUSSION

The data presented in Table II, or Figs. 1 and 2, show clearly that β is a function of pressure, rather than independent of it, as supposed hitherto over the given pressure range. The percentage change over the pressure range is considerably greater for the Pennsylvania or paraffinic type oils than for the naphthenic and aromatic types. Moreover, β does not appear to be well correlated with any of the physical and chemical data of Table I. In this respect the present study tends to confirm the opinion of the writer that it is difficult to predict accurately the pressure effects on the viscosity of oils from physical and chemical characteristics at atmospheric pressure. From a comparison of the data of Tables I and II, it is evident that there is a tendency for β to increase with decrease of

viscosity index, but the correlation is not simple. Moreover, the correlation which appears to exist between the pressure coefficient of viscosity and the aniline point (2) does not seem to be valid for β.

Likewise, α is a function of pressure, as shown by Table IV, but the temperature effects, as to be expected, are of smaller magnitude than those due to pressure. The paraffinic type oils seem to exhibit some complexity in this respect, inasmuch as there appears to be some evidence for a minimum value of α at low pressures which is not shown by the other types of oils, but the present data cannot be considered as establishing this point.

The pressure and temperature coefficients of viscosity are related to β and α, respectively, by Eqs. (4) and (5). It has been demonstrated previously (3,4,5) that paraffinic oils show the least relative change of viscosity with pressure and temperature, and it is to be expected that β and α would show a similar behavior when different types of oils are compared. Subsequently, it was found that β varies with pressure and the greater relative changes occur for the paraffinic type oils. While the temperature coefficient of viscosity increases with increase of pressure for all the oils studied, α, on the other hand, appears to increase similarly only in the case of the naphthenic and aromatic type oils. It indicates, therefore, that some structural change [2] with pressure occurs in paraffinic oils which is more noticeably [3] shown up by β and α than by the pressure and temperature coefficients of viscosity. Unfortunately, not enough viscosity data at high pressures are available at the necessary number of temperatures to permit a more detailed examination.

While Cragoe did not attach any theoretical significance to Eq. (1), its exponential form suggests comparison with the familiar equation

$$\eta = Ce^{D/T}, \tag{7}$$

which has been reviewed by Ewell (12) in regard to its interpretation by current reaction rate theory. Examination of Eqs. (1) and (7) indicates that the energy of activation for viscous flow D should vary inversely with L at constant temperature. If it is accepted that D is to be associated with some fraction of the energy of vaporization E_v, then, insofar as pressure is concerned, L should vary inversely as $E_v + pv$, where p is the applied pressure and v the specific volume.

Since dv/dp does not change appreciably with the type of oil (13), the pressure change of L should, for the most part, depend on the pressure change of E_v. It is not to be expected, however, judging from the small number of data available, that dE_v/dp would be greatly different from one type of oil to another. Trouton's constant for the simpler hydro-

---

[2] This may be associated with the wax content of the oil.

[3] Since L varies inversely as the logarithm of the viscosity.

carbons of the saturated chain type, *e.g.*, heptane, octane, *etc.*, is about 20 cal./°K. It also has about the same value for a ring type molecule like benzene. When it is recalled that no petroleum oil represents an unique molecular structure, as shown by the percentages of composition in Table I, it is difficult to conceive that E_v will be a strong function of the structural types present in the petroleum oils which have been examined during this study; in other words, in this respect ring and chain structural characteristics lose their identities in the average structural type which is common in all petroleum oils. Therefore, one would predict that β should be independent of pressure and only weakly dependent on temperature. It can then be concluded that Cragoe's method of using the L function is equivalent theoretically to applying reaction rate theory to oils, and, on the basis of the current interpretation of E_v, and the effect of pressure on it, it is to be expected that β would be approximately independent of pressure.

Reaction rate theory has been unable to quantitatively predict the change of viscosity with pressure, although as a first approximation for the simpler liquids, *e.g.*, ether, pentane, *etc.*, and as a mechanism for describing rate phenomena, it has been remarkably productive. The accuracy of the viscosity data now available for liquids under pressure has reached the point where it is useful to apply them for a critical examination of reaction rate theory. This is true especially for petroleum oils. The results of the present study, since they show that β is a function of both pressure and temperature and that β and α depend on the type of oil, demonstrate that there is no adequate explanation of the observed viscosity effects. It should be emphasized that this general conclusion is in no way limited to the L function, but depends only on the validity of the measured viscosity data which have been reviewed.

It has been stated previously (14,15) that viscosity, as a function of volume alone, cannot account for the observed pressure effects. It is extremely significant, in this respect, that a plot of viscosity against volume for an oil at 3 temperatures yields 3 distinct, widely separated curves (14). The reaction rate theory, as currently applied (16), predicts that the viscosity of a hydrocarbon should depend only on the number of "holes," and consequently, the viscosity-volume plots at different temperatures should all fall on the same line, irrespective of pressure and temperature. The principal difficulty,[4] as visualized by the writer, lies in the assumption that the breaking of molecular bonds according to the evaporation mechanism is similar for the viscous flow mechanism. Part of the energy of viscous flow should be due to the breaking of weak bonds due to preferred orientation (15) of the molecules when the liquid is under externally

[4] Another difficulty lies in the assumption that the partition function ratio is independent of the degree of orientation.

applied pressure, and it is this contribution of non-volume forces which is not accounted for or explained by the evaporation process. Evidently, this orientation effect is strongly influenced by structural characteristics of the molecules, since measurement shows that the effects of pressure on the viscosity of oils clearly depend on the type of oil, even though there is no unique type of structure associated with any one type of oil shown in Table I.

The concept of molecular orientation during flow, to describe, in part, the viscous effects observed in liquids under pressure, proposed by Dow in 1934 (17), has been further developed by Bondi (18), who has attempted to express the effects of orientation by a somewhat modified reaction rate theory. The experimental methods used in studying the chain structures of polymer molecules (19) should be applicable for further elucidation of the possible effects of orientation in oils, *e.g.*, the phenomenon of birefringence, while actively studied for some time, has not been fully correlated with viscosity effects.

Summary

The Cragoe L function for the viscosity of oils has been computed for 12 representative petroleum oils over a pressure range of $28,000\,\psi$ and a temperature range from $100°$ to $210°F$.

It has been shown that, on the basis of the viscosity measurements for these new oils, the pressure coefficient β is not approximately constant for a given oil over a low pressure range, as supposed by Cragoe, but is a function of pressure, and, to a lesser extent, a function of temperature. The magnitude of β has been found to be dependent on the type of oil, *e.g.*, whether the type is paraffinic or naphthenic and aromatic; and its pressure and temperature variation is likewise different for the different types of oils.

The defining equation for L has been interpreted in terms of current reaction rate theory, and it has been demonstrated that volume effects alone are not adequate to account for the observed viscosity effects under pressure. It has been suggested that orientation effects during viscous flow are probably responsible for the discrepancies now existing between measurement and theory.

References

1. CRAGOE, C. S., *Proc. World Petroleum Congr. (London)* **II**, 529 (1933).
2. Dow, R. B., *J. Colloid Sci.* **2**, 81 (1947).
3. DIBERT, R. M., Dow, R. B., AND FINK, C. E., *J. Applied Phys.* **10**, 113 (1939).
4. Dow, R. B., *ibid.* **8**, 367 (1937).

5. Dow, R. B., McCartney, J. S., and Fink, C. E., *J. Inst. Petroleum Technol.* **27**, 301 (1941).

6. Fink, C. E., Unpublished data from measurements at the Petroleum Refining Laboratory, The Penn State College, July, 1939.

7. Vlugter, J. C., Waterman, H. I., and Van Westen, H. A., *J. Inst. Petroleum Technol.* **21**, 661 (1935).

8. Hyde, J. H., *Proc. Roy. Soc. (London)* **97A**, 240 (1920).

9. Hersey, M. D., and Shore, H., *Mech. Eng.* **50**, 221 (1928).

10. Kiesskalt, S., *Forschungsarb.*, **291** (1927); *Petroleum Z.* **26**, 1 (1930); **27**, No. 7 (1931).

11. Kleinschmidt, R. V., *Trans. Am. Soc. Mech. Engrs.* **APM-50-4** (1928).

12. Ewell, R. H., *J. Applied Phys.* **9**, 252 (1938).

13. Dow, R. B., and Fink, C. E., *ibid.* **11**, 353 (1940).

14. Dow, R. B., *Physics* **6**, 270 (1935).

15. Dow, R. B., *Phil. Mag.* **28**, 403 (1939).

16. Glasstone, S., Laidler, K. J., and Eyring, H., The Theory of Rate Processes, Ch. IX. McGraw-Hill, 1941.

17. Dow, R. B., *Physics* **6**, 71 (1935).

18. Bondi, A., *J. Applied Phys.* **16**, 539 (1945).

19. Doty, P. M., and Mark, H., *Ind. Eng. Chem.* **38**, 682 (1946).
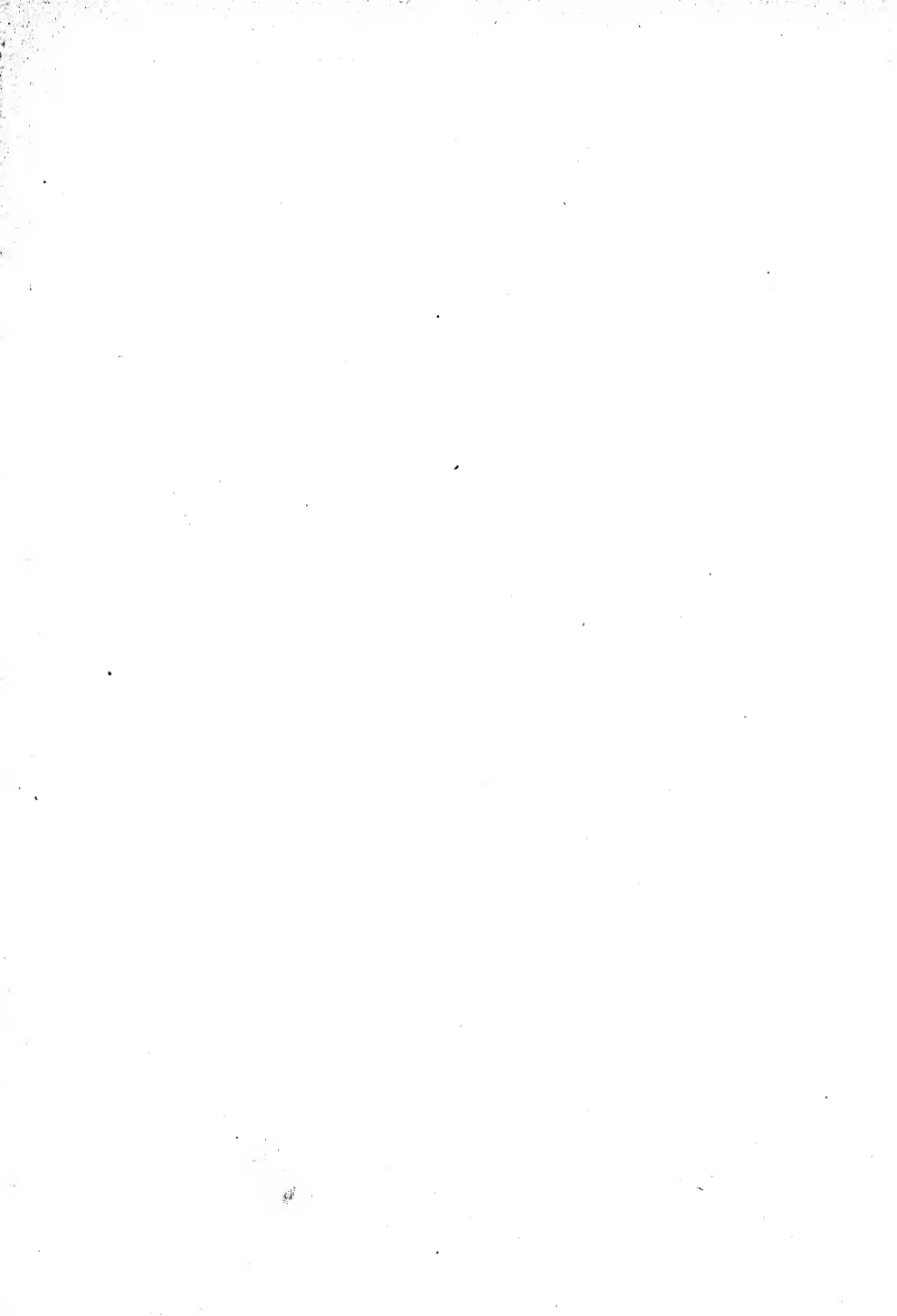
PSEUDOPLASTIC FLOW PROPERTIES OF
LYOPHILIC COLLOIDS

Earl K. Fischer and Charles H. Lindsley

From the Institute of Textile Technology, Charlottesville, Virginia
Received November 12, 1947; revision received January 5, 1948

INTRODUCTION

Colloidal solutions such as those prepared from starch, methyl cellulose, alginates, gelatin, and water-soluble gums, exhibit anomalous flow properties. Viscometric measurements on these substances give a curved line when rate of shear is plotted against shearing stress, the curvature being such that the apparent viscosity decreases as the rate of shear becomes greater. This property is connected with the solvation, aggregation, and swelling of colloidal particles.

Ostwald (15) has described numerous cases of colloids in which the dispersed material is solvated to an extent which leads to marked swelling. Such particles, because of their increased size, are considered to interact with each other to form some kind of an internal structure, and the term *structural viscosity* was adopted as descriptive of the flow properties of these systems. The use of this term has been extended to various types of non-Newtonian flow. The term *pseudoplasticity* has had fairly wide use for cases such as those we are discussing (18). One characteristic of an ideally pseudoplastic material is flow which begins at a very small shearing stress, the curve meeting the torque axis at the origin. There may, indeed, be some question about the appropriateness of the term pseudoplastic, but it is useful since it distinguishes this kind of flow from plastic, Newtonian, and dilatant flow.

Because of the frequent occurrence of pseudoplastic flow in materials used industrially, its measurement is of considerable practical importance. Fundamental difficulties in the measurement are usually resolved by standardization of a given instrument, usually in terms of process variables, and by use of a standard technique. The results of such measurements, expressed in terms of the instrument, usually serve for control purposes but the data have no general significance or validity.

The present paper is based primarily on studies of methyl cellulose solutions and starch pastes by means of the rotational viscometer. Methyl cellulose is well suited to rheological study since it is commercially avail-

111

able in a series of standardized grades, and it can be put into solution easily by soaking and stirring. Starch pastes present many more complications, both in preparation and measurement, although the flow properties of the two materials are comparable in essential respects. The data presented show that a rotational viscometer can be effectively utilized in analyzing the flow properties of pseudoplastic materials, provided certain elementary precautions in technique are observed.

EXPERIMENTAL METHODS

Five grades of methyl cellulose (Dow Chemical Co. "Methocel"), designated as 15, 100, 400, 1,500, and 4,000 centipoise, were used. Solutions were prepared by pouring hot water over the fibrous material, cooling, and then chilling in a refrigerator. The concentrations were selected on the basis of a chart of viscosity *vs.* concentration from the manufacturer's literature, in an attempt to obtain series of solutions of approximately equal viscosity from the different grades of methyl cellulose. The high-viscosity solutions entrained a considerable amount of air, and before measurements were made these solutions were centrifuged. The starches used were acid-modified corn starches. Fluidity values were supplied by the manufacturers. Pastes were prepared by heating in a covered, stainless steel double boiler; agitation was effected by a high-speed impeller agitator. Determination of the actual methyl cellulose and starch content of the solutions was made by drying in an oven at 105–110°C. to constant weight.

Rheological measurements were made on a commercial model Stormer viscometer modified in the following way. The cup and bob assembly supplied with the instrument was replaced by a cylindrical bob and two cups machined from brass, with the following dimensions:

	Cup 1	Cup 2	Bob
Radius	2.34 cm.	1.75 cm.	1.57 cm.
Height	4.9	5.2	3.53

The cups were machined to fit in the water bath supplied with the instrument. Constant temperature in this water bath was maintained by a heater of resistance wire wound around the aluminum cup. The heater was connected through a fixed-point thermoregulator immersed in the water and a relay to a Variac and source of current. With this arrangement the temperature was maintained within ±0.1° at 30°C. when the voltage applied to the heater was adjusted to provide a uniform cycle of heating and cooling. Higher temperatures, to 90°C., were obtained by changing to the appropriate thermoregulator and using a higher voltage setting. At 90°C. control was within ±1°. To reduce heat conduction from the bob to the bearing assembly at the higher temperatures, the bob was constructed of "Synthane," a laminated plastic material.

The procedure in making these measurements follows. The cup and bob were aligned carefully by means of adjusting screws on the support for the bath. The cup was filled with the material to be measured, and, to hasten the attainment of thermal equilibrium, the bob was rotated slowly for several minutes. A series of readings was taken with different loads. Most of the data were obtained at increasing loads; some readings were taken also at decreasing loads to afford an indication of any change in structure. A maximum speed of 400 r.p.m. had been established by previous tests with Newtonian oils as a practical limit below which turbulent flow was not evident.

To calculate viscosities from the experimental data, an instrument constant was computed from the dimensions of the cup and bob, using the well-known equations for the rotation of coaxial cylinders in liquids. Correction for the traction at the bottom of the bob was made by a method of multiple bobs described recently (12). Since the end-effect correction increases rapidly as the viscosity decreases below one poise, it was necessary to compute a separate constant for each 0.1 poise difference in this range.

The accuracy of the results obtainable by this procedure was found by measuring the viscosity of standard samples obtained from the National Bureau of Standards. The viscosity of these samples, with Newtonian flow properties, could be determined with an accuracy of $\pm 2\%$. The values obtained for methyl cellulose and starch are estimated to be accurate within $\pm 10\%$.

The experimental data reported in this paper have been drawn from an extensive series of rheological measurements on various types of materials of industrial importance. Most of the data were obtained with the modified Stormer viscometer. Other instruments which have been used include a specially constructed viscometer of the rotating cup type equipped with a thermostatically controlled heating element in the cup; the Brookfield viscometer; and capillary viscometers of the Ostwald-Cannon-Fenske type. In addition, experiments have been performed with the viscometer described by Kesler and Bechtel (11), which has been designed specifically for study of the starch-pasting process.

METHODS OF COMPUTATION

For both methyl cellulose and starch solutions, the curve for rate of shear (r.p.m.) as ordinate plotted against shearing stress (load in g.) as abscissa, gave a curve convex to the stress axis. Curves for solutions of low viscosity deviated only slightly from a straight line, but, as the concentration increased, the curvature became more pronounced. The viscosity of a Newtonian material, which gives a linear graph when rate of shear is plotted against stress, is the reciprocal of the slope of this line.

By analogy we may define the apparent viscosity, η_a, at rate of shear, S, as the reciprocal of the slope of the tangent to the curve of rate of shear vs. stress at S.[2]

Some discussion regarding rate of shear and its calculation for a rotational viscometer is necessary. The rate of shear (or velocity gradient) S is determined by the rate of rotation, radius of the bob, and clearance between cup and bob. For any angular velocity ω, S is not uniform throughout the annular space between the cup and bob, but depends on the distance x from the axis of rotation (see Hatschek, Ref. 6, p. 32):

$$S = \frac{2R_c^2 \times R_b^2}{R_c^2 - R_b^2} \times \frac{1}{x^2} \times \omega, \tag{1}$$

where R_c and R_b are the radii of cup and bob. The mean value of S throughout the annular space may be found as follows:

$$\bar{S} = \int_{R_b}^{R_c} S dx \bigg/ \int_{R_b}^{R_c} dx^2 = \frac{2R_c R_b}{R_c^2 - R_b^2} \times \omega. \tag{2}$$

When the clearance between cup and bob is small, the rate of shear at any point will not differ significantly from this mean value, within the limits of experimental error. It may, therefore, be calculated for any ω by multiplication by a factor involving only the radii of cup and bob. Since ω is more conveniently found in r.p.m. than in radians per second, Eq. (2) may be written:

$$\bar{S} = \frac{4\pi}{60} \times \frac{R_c R_b}{R_c^2 - R_b^2} \times \text{r.p.m.} = k_s \cdot \text{r.p.m.} \tag{3}$$

[2] It is recognized that the term *apparent viscosity* has a variable meaning. Thus, in some industrial laboratories, a single point is determined on the stress—rate of shear curve, and it is then assumed that the flow curve is a straight line extending to the origin, giving in effect a hypothetical curve for a Newtonian material. Such a curve does not, of course, coincide with the experimental curve obtained with a sequence of readings. This method of computation has, unfortunately, had wide use and leads to the definition that apparent viscosity is the quantity obtained by dividing the shearing stress by the rate of shear (5,8,19). Although the dimensions are those of viscosity (dyne-sec./cm.²), it is evident that the values so computed may be far from a correct representation of the physical properties. Apparent viscosity is defined in a different way by Williamson (18), who assumes that the curve for a pseudoplastic material becomes a straight line at high rates of shear. The slope of this linear portion is taken as the apparent fluidity and its reciprocal as the apparent viscosity. The qualification of "apparent" is intended to indicate that the measured viscosity varies with rate of shear. Further, measurements made with different instruments incapable of analysis in rational units are given as apparent viscosities. When so used, the term is considered permissible, provided, however, that it is not associated with the coefficient in the Newton equation (Ref. 1). The need for a consistent nomenclature has been frequently discussed: see, for example, the interesting discussion by Cragg (3).

To examine how closely $\bar{S}$ approximates the value of S at any point in the liquid, S was calculated for 4 values of x (Eq. 1) at equal intervals between the surface of the bob and the cup. The comparison with $\bar{S}$ for each cup is given in Table I. In the table, the constant C is $\dfrac{2R_c^2 R_b^2}{R_c^2 - R_b^2} \times \dfrac{2\pi}{60}$,

TABLE I

Rates of Shear at Different Points in a Rotational Viscometer at 10 r.p.m.

	Cup 1			Cup 2		
Radius of bob, R_b, cm.	1.565			1.565		
Radius of cup, R_c, cm.	1.746			2.342		
Clearance, d, cm.	0.181			0.777		
Constant, C, cm.²	2.61			0.932		
Mean rate of shear, $\bar{S}_{10}$, sec^{-1}	9.55			2.52		
n	$x = R_b + nd/5$	$S_{10} = 10C/x^2$	$\dfrac{\bar{S}_{10} - S_{10}}{\bar{S}_{10}}$	$x = R_b + nd/5$	$S_{10} = 10C/x^2$	$\dfrac{\bar{S}_{10} - S_{10}}{\bar{S}_{10}}$
1	1.601	10.18	−0.066	1.720	3.15	−0.250
2	1.637	9.74	−0.020	1.876	2.73	−0.083
3	1.674	9.30	+0.026	2.031	2.26	+0.103
4	1.710	8.91	+0.067	2.187	1.95	+0.226

the last factor being necessary to change ω to r.p.m., so that $S = C \times$ r.p.m./x^2. For the comparison, S and $\bar{S}$ are given at 10 r.p.m.; at any other r.p.m. the values remain in the same proportion. The third column for each cup shows the deviation of the actual rate from the mean value. As would be expected, the closer the clearance, the smaller the spread in values of S throughout the liquid. With Cup 1 the use of $\bar{S}$ as representative of the behavior at all points is justified in view of other experimental errors. With Cup 2, however, the variation is so large that no single value may be regarded as representative.

For Newtonian materials the variation in rate of shear at different rates is not important, since the viscosity is independent of this variable. For non-Newtonian materials, such as are examined here, the effect may be of considerable importance, because the apparent viscosity will not be the same throughout the liquid. If the clearance is sufficiently small, a

mean value may be found for apparent viscosity, which, as just shown, may be taken as reasonably representative of the behavior of the material being studied.

TABLE II

Composition of Methyl Cellulose Solutions

Solution no.	Methyl cellulose grade (cps.)	Concentration (weight-%)
1	1500	1.55
2	400	2.05
3	100	2.82
4	15	6.06
5	1500	2.15
6	400	2.97
7	100	4.22
8	15	9.02
9	4000	1.88
10	1500	1.91
11	400	3.92
12	100	5.36
13	15	11.2
14	4000	1.82
15	1500	2.71
16	400	3.62
17	100	5.17
18	15	11.0

There is a second effect that may become significant for materials showing highly anomalous behavior. In the derivation of Eq. (1) it is assumed that the viscosity is constant throughout the liquid being sheared. If the apparent viscosity varies rapidly with rate of shear, then the effect of variation of this last quantity from point to point may be great enough to make the above assumption invalid. Ordinarily this is a second-order effect, however, and will not introduce significant error in interpretation of experimental data.

There are two ways in which apparent viscosity may be determined. The more direct way is to draw, as accurately as possible, the tangent to the curve at the rate of shear in question and to determine its slope by actual measurement. The other way is to fit the experimental data to some empirical equation expressing stress in terms of rate of shear and then to calculate the slope at any point from the first derivative. This method does not require such accurate draftsmanship as the first and, once the empirical equation has been determined, permits immediate calculation of apparent viscosity at any rate of shear.

The form of the empirical equation chosen is rather arbitrary. All the materials studied gave nearly parabolic curves when r.p.m. was plotted against applied load (W). The most obvious form to use, therefore, is the quadratic. By the method of least squares, the experimental data are fitted to the following equation:

$$\text{r.p.m.} = a + bW + cW^2. \tag{4}$$

It is easier to fit the data obtained with the Stormer viscometer to the equation in this form; for calculation of viscosity, however, it is better to have W as a function of r.p.m. Simple algebraic solution gives Eq. (5):

$$W = [(b^2 - 4ca + 4c\cdot\text{r.p.m.})^{\frac{1}{2}} - b]/2c. \tag{5}$$

The viscosity (in poises) at any given r.p.m. is then found by multiplying the derivative by an instrument constant K_v:

$$\eta_a = K_v \frac{dW}{d\,\text{r.p.m.}} = K_v/(b^2 - 4ca + 4c\cdot\text{r.p.m.})^{\frac{1}{2}}. \tag{6}$$

The constant K_v may be found by calibration with standard samples, or calculated from the expression given in a previous paper (12):

$$K_v = \frac{60gl}{8\pi^2} \times \frac{1}{h + h_o} \times \frac{R_c^2 - R_b^2}{R_c^2 \times R_b^2}, \tag{7}$$

where g is the acceleration of gravity (980 cm./sec./sec.), l the effective lever arm of the viscometer drum, h the length of the bob, h_o the correction for end-effect of the bob, and R_c and R_b the radii of the cup and bob.

The two instrument constants k_s and K_v (from Eqs. (3) and (7)) for the cup and bob combinations used in this work are shown below:

	Cup 1	Cup 2
k_s	0.955	0.252
K_v	1.93	4.94

The experimental data may be represented by another equation of the form:

$$W = A(\text{r.p.m.})^n. \tag{8}$$

It may be noted in passing that when n is 1 in Eq. (8), the material is Newtonian in flow properties, with viscosity proportional to A; when n is between 0 and 1, the curve is concave to the rate-of-shear axis and the material is pseudoplastic; when n is greater than 1, the curve is concave to the stress axis, and the material is dilatant. Eq. (8) has only two parameters, A and n, but it assumes that there is no yield value, i.e., that the curve passes through the origin.

Equation (8) is most easily solved by changing to the logarithmic form:

$$\log W = \log A + n \log (\text{r.p.m.}). \tag{9}$$

When the experimental data are plotted on log-log paper, straight lines are obtained, as illustrated in Figs. 3 and 4. The reciprocal of the slope of any line gives the value for n, and substitution of this value in Eq. (9) gives A. To find the apparent viscosity the same procedure as before is followed:

$$\eta_a = K_v \cdot \frac{dW}{d \text{ r.p.m.}} = K_v A n \ (\text{r.p.m.})^{n-1}. \tag{10}$$

EXPERIMENTAL RESULTS AND DISCUSSION

Apparent viscosities for the methyl cellulose solutions were determined by the three ways just described: (a) determining graphically the slope of the curve r.p.m. *vs.* load at any rate of shear and multiplying its reciprocal by the instrument constant K_v; (b) finding the constants a, b, and c in Eq. (4) and solving for η_a by substitution in Eq. (6); or (c) finding n and A in Eq. (8) or (9) and substituting in Eq. (10). All three methods yield substantially the same results.

Methyl Cellulose Solutions

Experimental data for solutions of methyl cellulose are presented in Figs. 1–5 and Tables III–V. Composition of the solutions is given in Table II; numerals on the curves refer to these solutions.
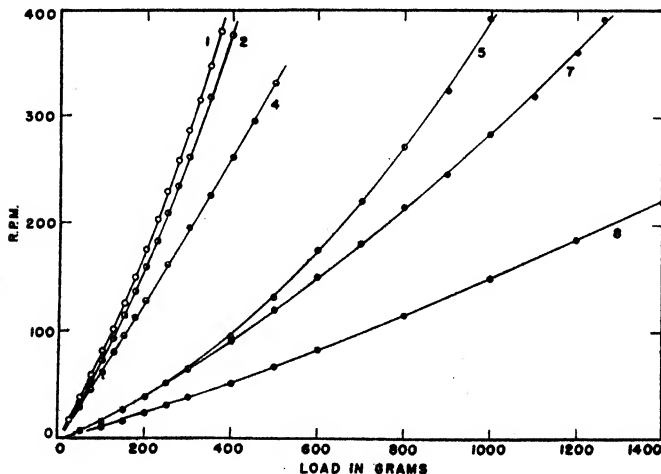

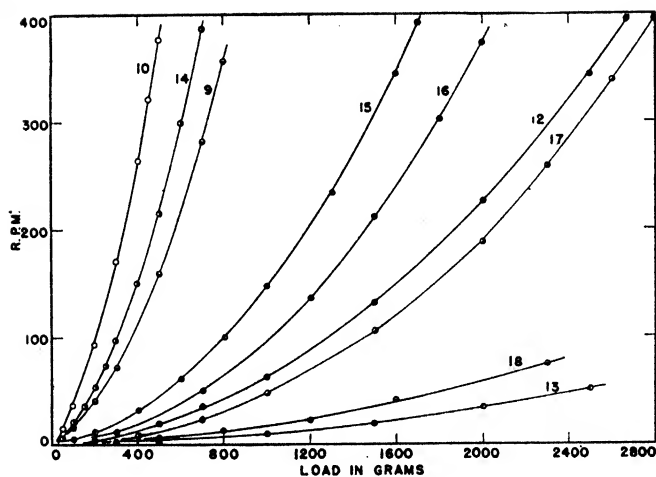FIG. 1. Viscosity curves of methyl cellulose solutions at 30°C. (low range).

FIG. 2. Viscosity curves of methyl cellulose solutions at 30°C. (high range).
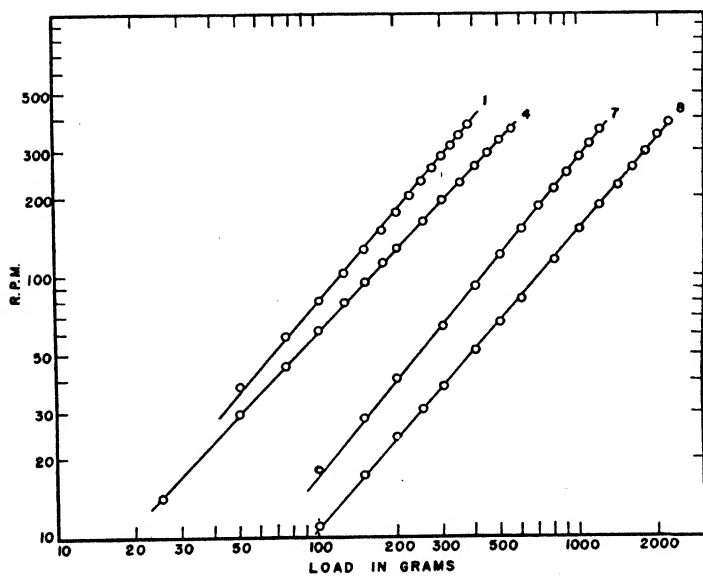

FIG. 3. Log-log plots of load-r.p.m. data for methyl cellulose
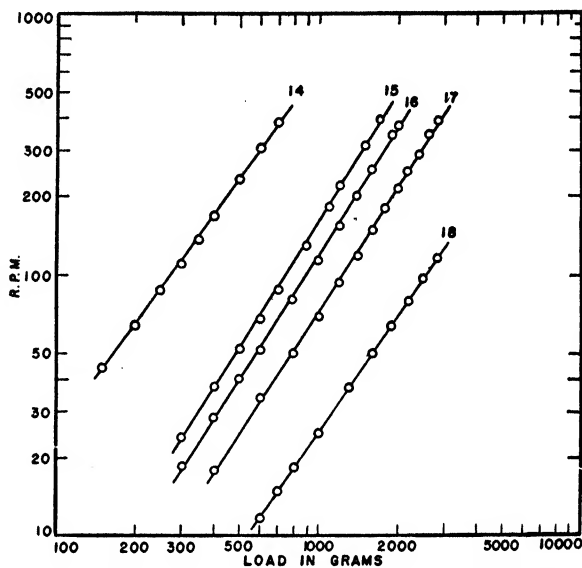solutions at 30°C. (low range).

FIG. 4. Log-log plots of load-r.p.m. data for methyl cellulose solutions at 30°C. (high range).
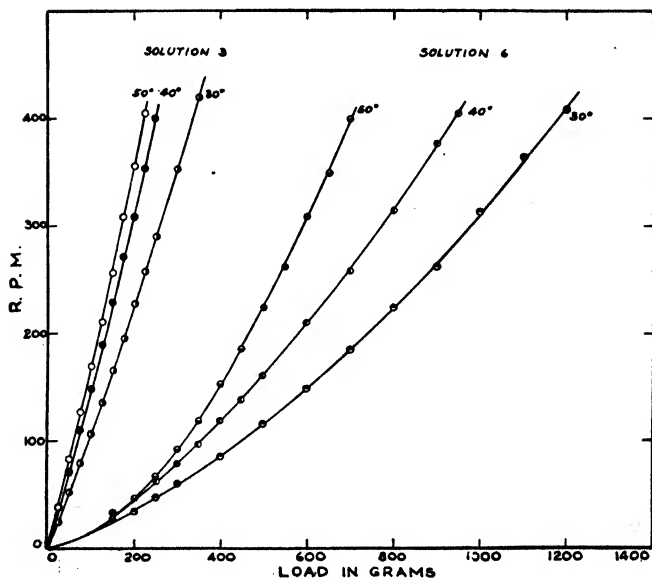

FIG. 5. Viscosity curves of methyl cellulose solutions at different temperatures.

TABLE III

Apparent Viscosities of Methyl Cellulose Solutions at Different Rates of Shear for Two Clearances (30°C.)

Rate of shear, sec⁻¹	Apparent viscosity (poises)					
	10		50		100	
Cup no.	1	2	1	2	1	2
Clearance, cm	0.18	0.78	0.18	0.78	0.18	0.78
Solution no.						
1	2.6	3.2	2.3	2.5	2.1	2.1
2	2.8	2.7	2.5	2.5	2.2	2.3
3	1.8	2.2	1.8	2.2	1.7	2.1
4	3.0	3.1	2.9	3.0	2.9	2.9
5	11.0	11.0	7.1	6.4	5.4	4.7
6	10.5	10.8	7.8	7.7	6.3	6.0
7	9.0	11.4	7.8	8.1	6.9	6.4
8	13.9	17.2	12.9	13.8	11.9	11.5

TABLE IV

Apparent Viscosities of Methyl Cellulose Solutions at Different Temperatures
(Rate of shear = 50 sec⁻¹)

Solution no.	Apparent viscosity (poises)		
	Temperature, °C.		
	30	40	50
1	2.3	1.9	1.2
14	5.1	3.6	1.8
5	7.1	5.0	3.2
11	21.	16.	10.
13	59.	44.	34.

It is of some theoretical interest that, even at the highest rates of shear used (400 r.p.m. with Cup 1 corresponds to 380 reciprocal seconds), the data still follow the curves very closely. This has bearing on the nature of pseudoplastic flow. Some investigators have contended that, in the plots of shear *vs.* stress, after an initial curved portion the graph is linear, and that the slope of this linear part gives the viscosity and its intercept on the stress axis the yield value. There is no evidence for any linearity in the curves for the materials studied; nor is there any indication of an intercept corresponding to a yield value. This is most clearly shown in

the log-log plots, where any linear portion of the normal curves would appear as deviations toward the log-stress axis.

In all cases, values for η_a decreased as the rate of shear became greater (Table III), as is evident from the shape of the curves. Table III also shows the effect of increased clearance between cup and bob on the values of η_a. As was shown in Table I, at the lower clearance (0.18 cm.) conditions of uniform rate of shear and laminar flow would be rather closely approached, and the values of η_a are regarded as reasonably accurate, probably to within $\pm 10\%$ (the precision of course being much better). It was not expected, however, that these conditions would be even approximately realized at the greater clearance (0.78 cm.), in view of the wide spread in rate of shear (again Table I). It was, therefore, surprising that the agreement found at each rate of shear with the two cups was as close as Table III shows. (It should be noted that with Cup 2 the angular velocity is nearly 4 times greater than with Cup 1 to give the same mean rate of shear.) It must be that the effects of high and low shearing rates, even over a wide range, average out, so that a mean value of apparent viscosity may be found that is approximately valid. It would appear safer, however, to use as small a clearance as other circumstances permit.

The decrease in apparent viscosity with rise of temperature is shown in Table IV. Some of the solutions exhibited visible gelation at 50°C. When gelling occurred the measurements were of no significance, for only a portion of the material in the cup was sheared.

Capillary and Brookfield Viscometers

The kinematic viscosities of solutions 1–4 were determined with capillary viscometers of the Ostwald type. These had been calibrated previously with Bureau of Standards samples. The specific gravity of these methyl cellulose solutions was found to be close to 1.00, so that the absolute viscosity could be taken as equal, within experimental error, to the kinematic viscosity. In a capillary viscometer, the mean rate of shear can be taken to be $8V/3\pi r^3 t$, where V is the volume of liquid flowing through a capillary of radius r in time t. In the Ostwald type, the rate of outflow decreases with time, because the head of liquid is constantly decreasing; hence, the formula holds only approximately. Table V shows the viscosity values found at approximate rates of shear in comparison with comparable data for the modified Stormer viscometer. The agreement between corresponding values is fair when the difference in measuring methods is considered.

When measurements were made with capillary viscometers at temperatures higher than 30°C., and on solutions of greater apparent viscosity, the time of outflow changed during testing. In one case a two-fold increase in time was observed. This is evidence of change in structure of

the solution. In view of this behavior, the agreement between the two sets of data may be considered satisfactory.

The necessity for consideration of the rate of shear in measurements with capillary viscometers has been shown by Conrad (2) and Lyons (13). These investigators point out that failure to take this factor into account has been a serious defect in numerous measurements on cuprammonium solutions of cellulose. They observe, further, that the assumption of Newtonian flow at low concentrations is untenable. Farrow, Lowe and Neal (4) also pointed out the necessity for measurements at known rates of shear in working with dilute starch solutions.

Measurements were also made with the Brookfield viscometer; data are given in Table V. With standard oils showing Newtonian flow, fairly

TABLE V

Apparent Viscosity of Methyl Cellulose Solutions at 30°C. Measured by Different Instruments

Solution no.	Ostwald capillary	Modified Stormer		Brookfield		
	Rate of shear	Rate of shear: 15 sec⁻¹ radial clearance:		Rate of spindle rotation (r.p.m.)		
	10–20 sec⁻¹	0.18 cm.	0.78 cm.	12	30	60
	Poises	Poises	Poises		Poises	
1	1.75	2.6	3.0	——	0.4	0.4
2	2.61	2.7	2.6	2.1	1.9	1.8
3	1.37	1.8	2.2	1.2	1.1	1.0
4	2.76	3.0	3.0	4.0	3.4	3.1

satisfactory measurements were obtained, but the data for methyl cellulose solutions show considerable divergence from those obtained with other viscometers. The source of this divergence may lie in lack of knowledge regarding rate of shear in the instrument, since the bob (spindle) rotates in a rather large volume of solution.

Starch Pastes

When a water suspension of starch is heated, no change is observed in the appearance of the granules until a definite temperature is reached. At temperatures which are characteristic of starch varieties and the extent of chemical modification, the granules begin to swell, the suspension becomes translucent, and the viscosity increases rapidly. This process, termed gelatinization, is irreversible. On further cooking, the starch paste passes through a region of maximum viscosity, after which the viscosity diminishes. The viscometer designed by Kesler and Bechtel (11) is particularly useful for studying this behavior. The lowering of viscosity on

continued cooking is due to the gradual leaching of soluble matter from the starch, together with shrinkage, deformation, and finally disintegration of the granules.

The manner in which the breakdown of the starch can be followed rheologically is shown in Figs. 6 and 7 and Tables VI and VII. As cooking
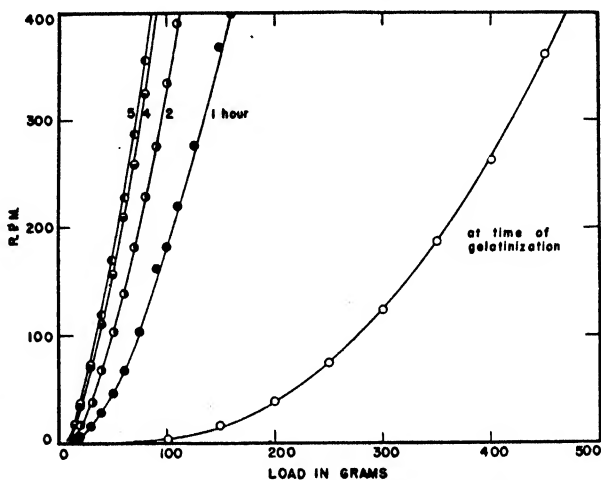

FIG. 6. Flow curves obtained after different periods of cooking starch paste. (Low-modification, gum-type starch; concentration 9%, dry basis; 90°C.).
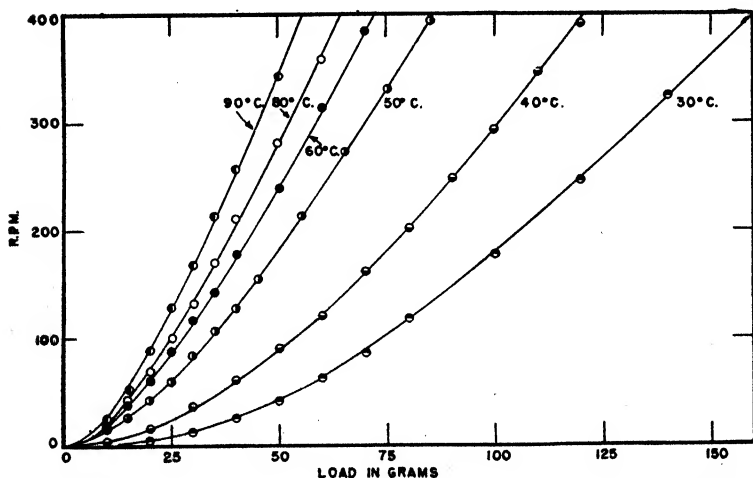

FIG. 7. Flow curves of a starch paste at different temperatures. (Low-modification, gum-type starch; concentration 6.4%, dry basis).

continued cooking is due to the gradual leaching of soluble matter from
the starch, together with shrinkage, deformation, and finally disintegration
of the granules.

The manner in which the breakdown of the starch can be followed
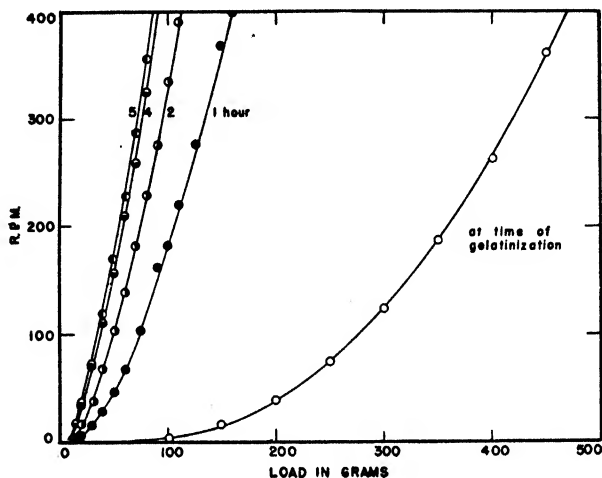rheologically is shown in Figs. 6 and 7 and Tables VI and VII. As cooking

FIG. 6. Flow curves obtained after different periods of cooking starch paste.
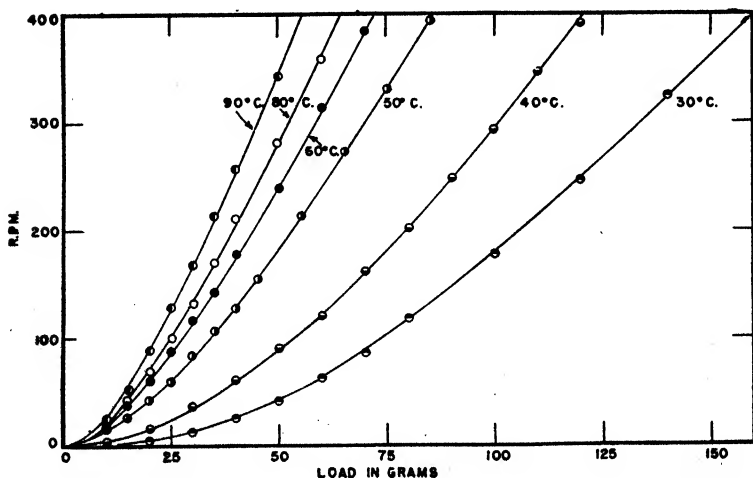(Low-modification, gum-type starch; concentration 9%, dry basis; 90°C.).

FIG. 7. Flow curves of a starch paste at different temperatures. (Low-modification,
gum-type starch; concentration 6.4%, dry basis).

TABLE VI

Change in Apparent Viscosities of Starch Pastes on Cooking

($T = 90°C.$; rate of shear $= 100$ sec^{-1}; Starch content: 10% dry basis)

Starch sample no.	Fluidity rating	Apparent viscosity (poises)		
		Time of cooking (hours)		
		1	2	3
6	60	0.27	0.25	0.23
5	40	0.44	0.38	0.34
3	80	0.73	0.57	0.59
10A	20	1.9	1.5	1.3

TABLE VII

Apparent Viscosities of Starch Pastes at Different Rates of Shear

($T = 90°C.$; starch content: 10% dry basis)

Description	Fluidity rating	Apparent viscosity (poises)		
		Rate of shear, sec^{-1}		
		3.6	1.	300
Starch 1, ½ hr. cook	—	—	1.7	0.65
Starch 5, ½ hr. cook	40	9.5	3.7	1.0
Starch 9D, 1 hr. cook	20	9.7	4.2	1.2
Starch 10A, 1 hr. cook	20	22.0	9.7	1.4

proceeds, the curves show a progressive change; after several hours, little further change occurs (Fig. 6). As the temperature of the cooked paste is reduced, there is a progressive increase in apparent viscosity, as shown by the curves in Fig. 7. The manner in which the rate of shear affects the computed viscosity values is shown in Table VII.

The progress of pasting, shown by viscometric changes, can also be followed microscopically. At the start, the granules are only slightly swollen, but, as the viscosity increases, a corresponding increase in the granule size becomes apparent. With continued heating, the granules begin to disintegrate until finally (after 3–4 hours under the conditions of these experiments) the granular structure is no longer present. At this stage the hot starch paste has its lowest viscosity. Starch paste viscosity is due to the presence of swollen granules, fragments, and colloidal material dissolved from the granules.

It may be noted in passing that the fluidity rating supplied by the manufacturers gives no reliable information with regard to the apparent

viscosity that is obtained on pasting. It should be added, however, that the ratings by any particular manufacturer of his products do have relative significance. Evaluation by subjective means or by use of simple efflux-type instruments (as is commonly practiced) has led to completely false ratings. This situation emphasizes the need for dependable methods to obtain data expressible in absolute units.

The range of apparent viscosities is of interest in studying the industrial use of pseudoplastic materials, as in the preparation and application of warp-yarn sizes and finishing compositions, to draw examples from textile processing. Apparent viscosities of 10% starch covered a range from about 0.1 poise to more than 25 poises when measured at low rates of shear (5 sec⁻¹). At higher rates of shear (in excess of 300 sec⁻¹) this range is diminished. Still higher rates of shear seem to be of minor importance, however, for both preparation and application are made at rates of shear of low magnitude, certainly less than 50 sec⁻¹.

General Considerations

In the most common cases of pseudoplasticity, the dispersed phase is lyophilic, *i.e.*, capable of absorbing and swelling in the liquid phase. The particles thus are appreciably solvated and may be pictured as surrounded by an envelope of the colloid-liquid complex. In a material which is capable of forming a gel, the boundaries of one particle merge with those of adjacent particles. As the mixture is sheared, the particles are disturbed from an equilibrium condition, and are deformed and oriented to some extent in the direction of flow. Some of the liquid associated with the particles may be separated, with the result that the particles themselves are effectively smaller; consequently, interaction during shearing is reduced and hence there is a decrease in resistance to shear. As the rate of shear increases, the extent of such change in effective particle size becomes greater, and, as a consequence, the apparent viscosity falls off. If a point were reached at which no further change in particle size occurred, then the relationship between stress and rate of shear would become linear. It is doubtful, however, if this condition could be met experimentally without the complicating effects of turbulence. This explanation appears to account adequately for the experimental observations. The subject has received considerable attention from colloid chemists, and reference may be made to Freundlich (6), Hatschek (9), and McBain (14) for a more extended discussion.

The suspension of a lyophobic solid (one in which solvation does not occur) presents a different case, although there is, in some respects, a superficial resemblance to certain features of pseudoplasticity. In a suspension of a finely divided solid in a liquid, the particles may be associated in the form of clusters or floccules. The floccules form a continuous net-

work and on stirring the network is broken into fragments. As the rate of shear increases, the floccules continue to break down, but if the rate of shear is held constant, the floccules no longer change in grouping and achieve a stable state during shear. As a limiting case, the dispersed particles may be present in a completely deflocculated condition. When a suspension of this kind is allowed to remain at rest, the network may be formed again by flocculation of the particles. When the structure is broken down and rebuilt reversibly, the material is thixotropic. If the period required to reform the structure is sufficiently long to allow measurement on a rotational viscometer, the curve for increasing rates of shear is similar in shape to that of the lyophilic colloid discussed above. After a steady state of breakdown is reached (at a given rate of shear), the curve obtained at decreasing rates of shear is usually a straight line. The loop formed by the two curves is taken as a measure of thixotropic breakdown by Green and Weltmann (7). An essential condition is the reversible nature of the process.

The question of whether thixotropy occurs in pseudoplastic materials is sometimes raised, but difficulties in the measurement and analysis of the flow properties have prevented a definite answer. De Waele (17) has discussed the possibility. Heymann (10) in his study of the sol-gel transformation of methyl cellulose solutions found evidence for thixotropy in the transition region. Starch pastes are sometimes described as thixotropic. If a loop in the flow curve is taken as the criterion of thixotropy, the materials examined in the present experiments cannot be regarded as showing this behavior when measured at temperatures where gelation does not occur. (Starch pastes gel on cooling, and methyl cellulose solutions gel when heated above the gelation temperature.) Near the gel point, a structure is formed which is broken down on shearing, and the curves obtained at increasing and decreasing rates of shear do not then coincide. At present, however, there is no evidence that the essential conditions for thixotropy (an isothermal, reversible transition) are met.

Summary

Rheological measurements on two typical pseudoplastic materials, methyl cellulose and starch, are presented. Data were obtained on a rotational (modified Stormer) viscometer. Methods of computation are presented which provide values in absolute units. Since the viscosity of pseudoplastic materials is dependent on the rate of shear, this factor must be specified to have data which are significant and independent of a given instrument. When data obtained on the rotational viscometer were compared with data from capillary viscometers, the agreement was fair, in view of the rough approximation to rate of shear in the latter instrument.

In the cases studied, there was no evidence for linearity in the curves of torque *vs.* rate of shear, nor was there any indication of an intercept on the torque axis corresponding to a yield value.

The method for rheological study of pseudoplastic materials described is relatively simple and can replace, in many instances, the erroneous techniques currently employed in certain industries.

REFERENCES

1. British Rheologists' Club, *Rheology Bull.* **18**, 8–13 (1947).
2. CONRAD, C. M., *Ind. Eng. Chem., Anal. Ed.* **13**, 526–33 (1941); CONRAD, C. M., AND TRIPP, V. W., *Textile Research J.* **16**, 275–83 (1946).
3. CRAGG, L. H., *J. Colloid Sci.* **1**, 261–69 (1946).
4. FARROW, D. K., LOWE, G. M., AND NEALE, S. M., *J. Textile Inst.* **19**, T18–T31 (1928).
5. FISCHER, E. K., GREEN, H., AND WELTMANN, R. N., *Interchem. Rev.* **2**, 9–15 (1943).
6. FREUNDLICH, H., Colloid and Capillary Chemistry, tr. from the 3rd German ed. by H. S. HATFIELD. Methuen & Co., Ltd., London, 1926.
7. GREEN, H., AND WELTMANN, R. W., Chapter 15, pp. 327–47 in Colloid Chemistry. Vol. VI, J. Alexander, Ed. Reinhold Publishing Corp., New York, 1946; *J. Applied Phys.* **15**, 414–20 (1944).
8. GREEN, H., AND WELTMANN, R. W., *Ind. Eng. Chem., Anal. Ed.* **15**, 201–6 (1943).
9. HATSCHEK, E., The Viscosity of Liquids. G. Bell & Sons, Ltd., London, 1928.
10. HEYMANN, E., *Trans. Faraday Soc.* **31**, 846–64 (1935).
11. KESLER, C. C., AND BECHTEL, W. G., *Ind. Eng. Chem., Anal. Ed.* **19**, 16–21 (1947).
12. LINDSLEY, C. H., AND FISCHER, E. K., *J. Applied Phys.* **18**, 988–996 (1947).
13. LYONS, W. J., *ibid.* **13**, 43–52 (1945).
14. McBAIN, J. W., *J. Phys. Chem.* **30**, 239–47 (1926).
15. OSTWALD, WO., *Kolloid-Z.* **36**, 99–117; 157–67; 248–59 (1925).
16. SCOTT BLAIR, G. W., An Introduction to Industrial Rheology. P. Blakiston, Philadelphia, 1938.
17. WAELE, DE, A., *J. Am. Chem. Soc.* **48**, 2760 (1926); *J. Rheol.* **1**, 139–148 (1930); *ibid.* **2**, 141–62 (1931).
18. WILLIAMSON, R. V., *Ind. Eng. Chem.* **21**, 1108–1111 (1929).
19. WINDING, C. C., BAUMAN, G. P., AND KRANICH, W. L., *Chem. Eng. Progress* **43**, 527–36 (1947).

THE EFFECT THE CONSISTENCY CURVE HAS HAD ON THE DEVELOPMENT OF MODERN VISCOMETERS

Henry Green *

From the Interchemical Corporation, New York
Received February 2, 1948

When Bingham (1) in 1916 emphasized the advantage of using the consistency curve in place of the single point measurement in viscometry, he unconsciously instigated a trend in the development and manufacture of commercial viscometers. Consistency curves (stress *vs.* rate of shear) had been in use for many years prior to Bingham's employment of them, but they were employed more with the idea of increasing the precision of viscosity measurements than as a means of recording, in a more logical manner, the rheological factors of the material under test.

Bingham's prime achievement was to show that plastic materials, in distinction to purely viscous materials, cannot be analyzed by a single point method, but actually demand the recording of a complete consistency curve before anything comparable to a coefficient of viscosity can be deduced. His pioneering work in the study of plasticity of clay-water suspensions was made with a capillary tube viscometer where the shearing stress could be varied quickly over a wide range. This method of using a viscometer, while not new, actually constituted the first step in the trend of viscometer development as discussed in this paper.

Two assumptions about the capillary tube consistency curves, Fig. 1, were made in 1916 that subsequently were found to be incorrect. These were (a) that the upper part of the curve is linear, and the other (b) was that the non-linear part at the lower end of the curve was the result of either slippage or seepage flow. As a consequence, Bingham felt justified in writing the equation of plastic flow as follows:

$$\frac{V}{t} = \frac{\pi R^4 (P - p)}{8l\eta}.$$

It is apparent that this is the Poisseuille equation modified by the introduction of the pressure factor p. This pressure p arises from the force required to start flow and was obtained from the intercept on the pressure axis made by extrapolating the "straight" part of the curve to that axis.

---

* Dr. Green died just prior to the publication of this article.

A few years later it became well established that no straight part of the curve existed for plastic suspensions of materials such as Bingham and his collaborators used. Microscopic examination of flow in capillary tubes revealed a cause for the curvature at the lower end of the curve. It could be seen that this condition was brought about by the gradual change from plug to laminar flow as the pressure was increased. Nothing could be discovered, however, about the method of flow taking place in the remainder of the curve.
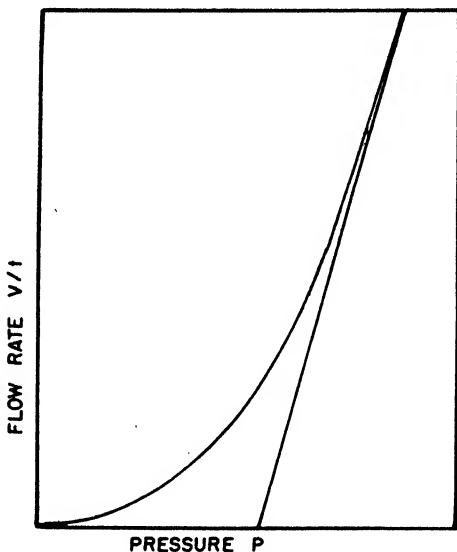

FIG. 1. Consistency curve of a Bingham body in a capillary tube.

In 1921, Buckingham undertook a mathematical analysis of this problem (2). He derived an equation of capillary flow for plastic materials on the assumption that the yield value (a function of p) is a material constant, *i.e.*, it does not change its value with a change in the rate of flow. Buckingham's work showed clearly that if a constant yield value exists, the consistency curve must be a hyperbola and so has no straight part. In addition, his equation contains 4 variables, which make it exceedingly difficult to solve.

The above conclusions indicated that some radical change would have to be made in the construction of the viscometer if it were to be used for the measurement of Bingham bodies, *i.e.*, where a true yield value exists.

In 1927, Reiner and Riwlin (5) showed rheologists how this difficulty could be overcome. The solution, they pointed out, was to give up the capillary tube viscometer, except in the case of Newtonian liquids, and

employ in its place the rotational viscometer. While either type of rotational viscometer can be used, for certain reasons the type in which the cup rotates is the one that is preferable.

Reiner and Riwlin pointed out, after the development of their equation of flow, that the consistency curve of a Bingham body on the rotational viscometer, Fig. 2, contains a straight part which can be solved very simply for yield value and plastic viscosity. This part of the curve theoretically starts at the point A where the flow has completely changed
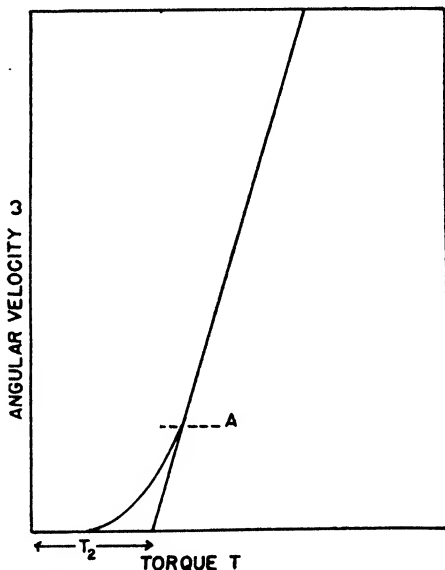

FIG. 2. Consistency curve of a Bingham body on a rotational viscometer.

from plug to laminar and from there on continues to be linear indefinitely. Their equation can be reduced to the following form:

$$U = \frac{(T - T_2)S}{\omega},$$

where U is the plastic viscosity, T_2 is the yield value intercept on the torque axis, and T and ω are the torque and angular velocity of any point on the straight section of the curve. It can also be shown from the Reiner and Riwlin equation that the yield value, f, is obtained from the equation

$$f = T_2 C.$$

S and C are instrumental constants. $S = \left(\dfrac{1}{R_b{}^2} - \dfrac{1}{R_c{}^2} \right) \Big/ 4\pi h,$ and

$C = S/\ln(R_c/R_b)$, where R_b is the radius of the bob, R_c the radius of the cup, and h is the depth of immersion of the bob.

There is another reason why the trend in viscometer construction will be in the direction of the rotational viscometer. This reason appears in the study of thixotropic systems. Pryce-Jones (4) has pointed out that the logical method for studying such systems is by the use of two consistency curves, one showing the material before extensive breakdown has taken place, and the other, after the material has been subjected to stirring and a much greater breakdown has been induced.
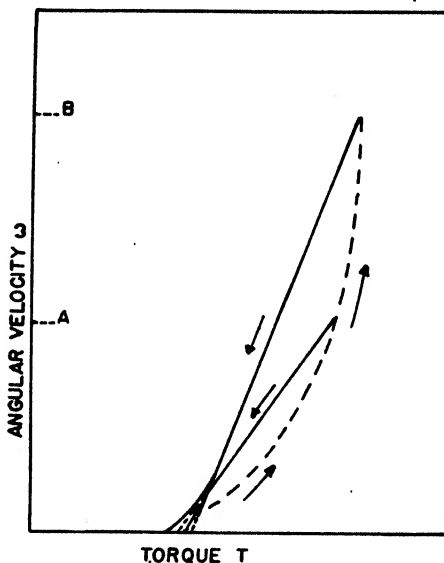

FIG. 3. Consistency curve of a thixotropic material on a rotational viscometer.

Curves at different thixotropic levels are easily obtained by means of a rotational viscometer, for the material is not extruded, but remains in the cup, where it is subjected to continuous breakdown during the operation of the instrument. It has been shown (3) that the so-called hysteresis loop, Fig. 3, obtained by plotting up-and-down curves of a thixotropic material in the rotational viscometer gives in reality two thixotropic levels, at $\omega = A$ and at $\omega = B$, from which the thixotropic breakdown can be calculated. The up-curve, which is run first, is bowed indicating continuous breakdown. The down-curve is linear (except at the extreme lower end) showing that a level has been reached where further breakdown ceases to occur as long as the rate of shear is being rapidly decreased by the operator. From the up-and-down curves, the amount of thixotropic

breakdown measured in viscosity decrease per unit increase of shearing rate can be determined (3).

The result of the Reiner and Riwlin work made it clear that the construction of the usual rotational viscometer must be changed in such a way that a large series of different rates of shear can be had easily and quickly. This means that a device must be attached to the viscometer that will enable the operator to change the speed of the rotating cup. When this is done, a consistency curve can be obtained which, in the case of Newtonian liquids and Bingham bodies, can be solved for η, U, and f by the equations previously given. Briefly, reviewing the trend so far described, it can be stated that the construction of the viscometer for such materials as Bingham bodies has passed through the stages exemplified by the single point capillary viscometer, the multiple point viscometer, and the multiple point rotational viscometer. There is one step indicated which has not yet been accomplished and that is a viscometer employing rates of shear so high that they compare in magnitude with the rate of shear employed by roller coating machines and high speed printing presses. The difficulty here will be to obtain those high rates of shear without creating objectionable increases in temperature. Rheologists are now working on this problem, but very little has yet appeared in print in regard to this matter.

References

1. BINGHAM, E. C., *Natl. Bur. Standards (U. S.), Sci. Paper* **278** (1916).
2. BUCKINGHAM, E., *Am. Soc. Testing Materials, Proc.* **21**, 1154 (1921).
3. GREEN, H., AND WELTMANN, R. N., *Ind. Eng. Chem., Anal. Ed.* **15**, 201 (1943).
4. PRYCE-JONES, J., *J. Oil & Colour Chemists' Assoc.* **19**, 293 (1926).
5. REINER, M., AND RIWLIN, R., *Kolloid-Z.* **43**, 1 (1927).

AN INSTRUMENT FOR MEASURING STRESS RELAXATION
OF HIGH POLYMER MATERIALS *

W. S. Macdonald and A. Ushakoff

W. S. Macdonald & Co., Cambridge, Mass.

INTRODUCTION

Standard test methods in the field of stress relaxation of high polymer materials have been neglected partly because satisfactory instrumentation has not been available. One method of measurement recommended by the A.S.T.M. (1) has been described as a "Compression Set Test," under which a sample of standard size and shape is distorted by clamping between metal plates, heated for a prescribed time in an oven, then unclamped and allowed to resume its shape for a period of one hour. The ratio of the thickness of the sample before clamping to that after release is used as a figure of merit of the material tested.

This A.S.T.M. method does not, of course, give a dynamic measurement of stress relaxation under strain, and, although the measurements provide an index by which materials may be graded, it is often desirable to obtain more accurate and detailed information, and be able to predict by extrapolation the expected future behavior of the material. Furthermore, as the sample is clamped before being heated, it is difficult to separate the effects of temperature change from those caused by the fundamental decay of the material.

The authors were desirous of making rapid measurements which would allow the classification of materials to a higher degree of accuracy than could be obtained through the use of the compression set method. In addition, it was hoped that enough information would be obtained to enable predictions to be made of relaxation values as a function of time following the application of a given load to the material. It was expected that this might be accomplished by extrapolation of data taken in a short period of time with a suitable instrument. The possibilities of extrapolating by use of mathematical equations involving molecular theory and the chemical approach have been investigated by others (2). However, results have not thus far been reduced to an equation involving but one proportionality constant. The apparatus developed by the author to

---

[1] This paper was presented at the annual meeting of the Society of Rheology, New York City, Oct. 31st–Nov. 1st, 1947.

solve this problem applies a predetermined initial stress to the sample; the strain built up in the sample is then maintained essentially constant and the stress is allowed to relax. The stress as a function of time is recorded automatically for the entire period of the test.

Through experimentation with this instrument it was found that the data obtained by plotting stress relaxation *vs.* time at constant temperature yield logarithmic curves. Therefore, by plotting on semilog paper, straight lines result, the slopes of which can be used as indices of the stress relaxation characteristic of the materials. This is in agreement with work done on creep tests of textiles (3). The straight lines obtained in tests of a few hours duration apparently may be extrapolated to periods of a month or more; actual tests carried to over 1800 hours have indicated very close adherence to the straight line plot. Tests are currently being extended to a period of several months to provide additional experimental verification of the logarithmic stress relaxation behavior.

REQUIREMENTS

The requirements for a suitable measuring jig were as follows:

(a) It should be able to apply, in less than a second, a predetermined initial stress of several hundred pounds per square inch to a sample one square inch in cross section and one-half inch thick.

(b) The measuring spring deflection should be small (less than 5% of the sample compression under load) so that the spring may be affected only by relaxation, and that the sample may remain under nearly constant strain.

(c) The anvil upon which the sample to be measured is clamped should deflect less than 1% of the spring deflection under load.

(d) The measuring element should be temperature-compensated so that measurements can be taken at any desired temperature without the instrument sensitivity or zero point shifting.

(e) It should be possible to measure samples in compression, tension, and shear.

(f) Provision should be made to keep the surfaces of the samples from slipping in the clamps.

(g) The recorder should be able to make a record of the output of the measuring jig over periods of several days with an error of less than 0.2% of full instrument scale.

APPARATUS

The unit to be described meets the above stated requirements. It consists of two components, the first a measuring jig which is used to apply a desired initial stress to the sample and to measure its relaxation on a continuous basis after the test starts. The second part of the system is a suitable recorder.

In accordance with the requirements that the allowable spring travel be small, a flat leaf spring is used as the measuring element. The stress in the sample causes a proportional deflection of the leaf spring, which is measured by means of an electrical resistance strain gage bridge cemented to the spring. This bridge can be accurately balanced and calibrated; and since all 4 arms are cemented directly to the spring's surface, the bridge can easily be temperature-compensated.

An early model jig is shown in Fig. 1. It was made to check the method and to obtain information for further development. The base or anvil
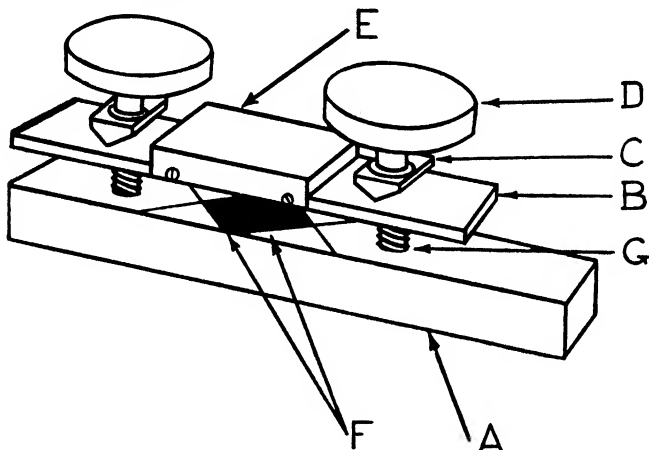

Fig. 1

plate (A) was made of 1″ cold rolled steel, the spring (B) of 0.25″ cold rolled steel 2″ wide and 5″ between knife edges. The knife edges (C) were driven by clamping bolts (D). The strain gage bridge was cemented to the upper surface of spring (B) at (E), and the two clamping surfaces (F) were knurled to prevent sample slippage. Springs (G) held the measuring spring plate (B) from contact with base plate (A) before the clamping bolts were tightened. This jig proved the usefulness of the instrument but a means of quickly applying a known load to the test sample was lacking. This made it difficult to duplicate readings for a given material.

To overcome this, the jig illustrated in Fig. 2 was designed. In this jig the fixed anvil of the previous model is replaced by a movable, variable-length plunger driven by a lever-operated cam (A). The spring plate (B) is the anvil upon which the sample under test is clamped. The adjustable plunger allows for the use of test samples of varying thicknesses, and for predetermining the strain (and initial stress) to be applied to the sample. The cam drive always moves the plunger through a fixed distance, and

assures positive clamping in a minimum amount of time. The strain gage bridge, after being cemented to the lower spring surface (B), is balanced and temperature-corrected so that it holds its zero reading within 0.2% over the controllable temperature range of from 70° to 180°F. under no-load conditions. Subsequently, a calibration curve of load in pounds *vs.* millivolts/volt applied to the bridge is run.

A modified Foxboro Dynalog (c) is used for recording the output of the electrical strain gage bridge. This recorder was designed specifically for use with strain gages and incorporates the voltage supply for the
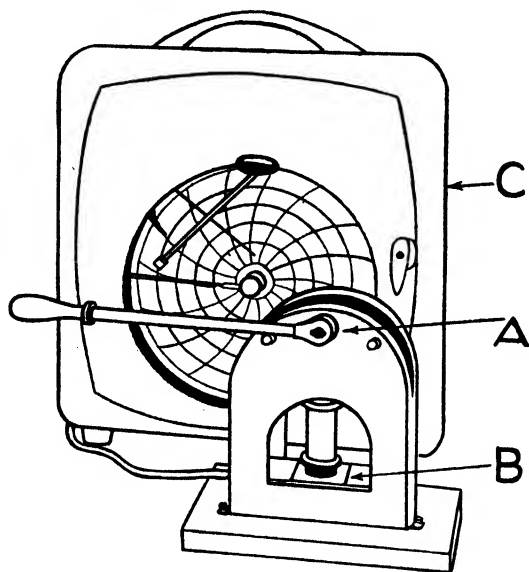

FIG. 2

bridge in addition to performing its main function of recording output voltage. The modification consists of adding a range-extending switch to suppress the zero of the instrument in three steps, thus changing the normal 4″ deflection range of the instrument to 12″.

In the final version of the apparatus—the measuring jig, Fig. 2—a temperature-regulated oven and a Foxboro recorder have been integrated into a compact unit.

PROCEDURE

The specimen size selected for tests is the standard pellet of the A.S.T.M. normally used for measuring rubber compression set. This pellet measures 0.5″ thick by 1.129″ in diameter (1 sq. in. in area). The standard 2″ high plastic sample, however, may be used.

The testing procedure consists of subjecting the specimen to a predetermined initial stress and recording the decay continuously as ordinate against time as abscissa. A pellet is centered on the spring and the plunger adjusted by trial until the pressure exerted by the spring on the specimen reaches the desired value. The expended specimen is then removed in each case and a new one of the same material substituted before the recorder is started.

It has been found desirable to hold the temperature of the testing jig constant during tests; otherwise the volume expansion of the material produces an error in reading. While the expansion error might be corrected, it is more straightforward to control the measuring jig temperature. Individual tests have covered periods ranging from one hour to three months. At the end of each test a check reading of the instrument zero is made to make certain that no drifts have occurred during the analysis.

The test data are analyzed by plotting, as ordinate, the ratio between the stress at each point on the record curve and that at a common reference point, against a logarithmic time scale as abscissa.

Since the rate of decay of stress is at first, in all instances, very rapid, it has been found impractical to use the peak recorded stress as the common denominator for the interpretation of results. Accordingly, there is selected the earliest point for which accurate measurements can be made after the relaxation of the specimen has stabilized. In the work covered by this report, this time was established as 0.01 hours after the stress had been applied to the specimen.

After the above-defined stress ratios have been plotted against a logarithmic time scale for each test run, the negative slopes of the curves are determined graphically. Figs. 3, 4, 5, and 6 are characteristic of the
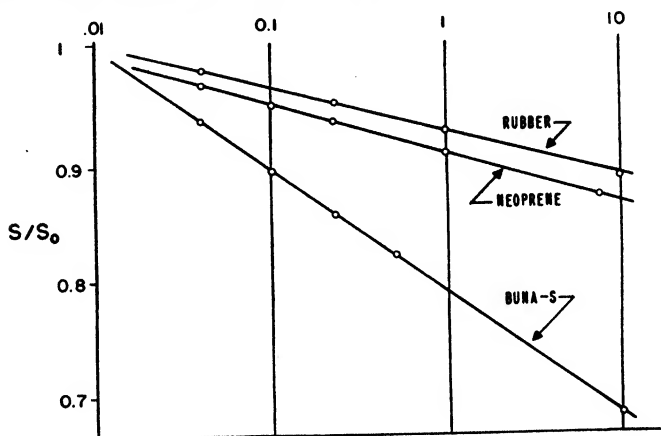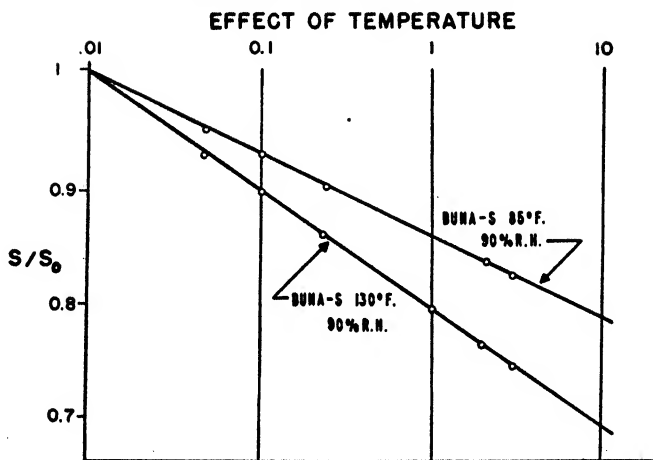

Fig. 3

EFFECT OF TEMPERATURE
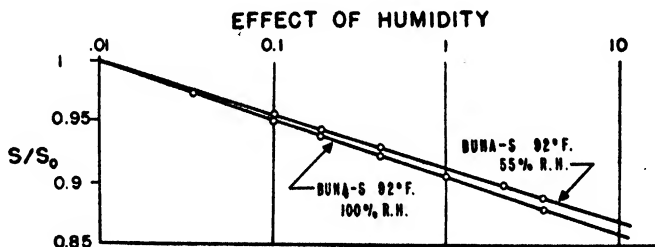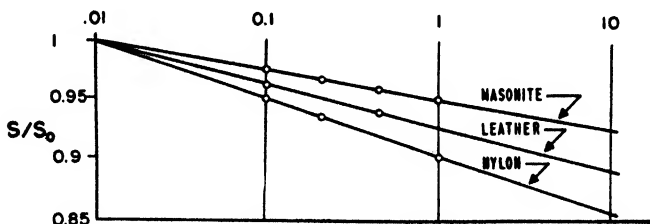

FIG. 4

EFFECT OF HUMIDITY

FIG. 5

FIG. 6

plots obtained. Fig. 3 shows a comparison between the curves for certain
samples of natural rubber, Neoprene, and Buna-S. Fig. 4 shows the effect
of ambient temperature on specimens of Buna-S. Fig. 5 shows the effect
of humidity variation at constant temperature. Fig. 6 shows a group of
curves taken on other materials and suggests that the method of test is
useful for a wide variety of plastics.

All these measurements were made with an initial stress of approximately 300 pounds per square inch. Additional measurements with initial stress up to 600 p.s.i. indicated variations in slopes smaller than inherent variations among individual sample pellets of any one material.

Although cylindrical samples were used, the shape factor is not important as long as comparisons are made between specimens of identical geometry.

The nature of the stress-time decay curves as illustrated in Figs. 3–7 is apparently that of a logarithmic relaxation in stress with respect to time. Fig. 7 shows an extended period test with measurements up to 1600
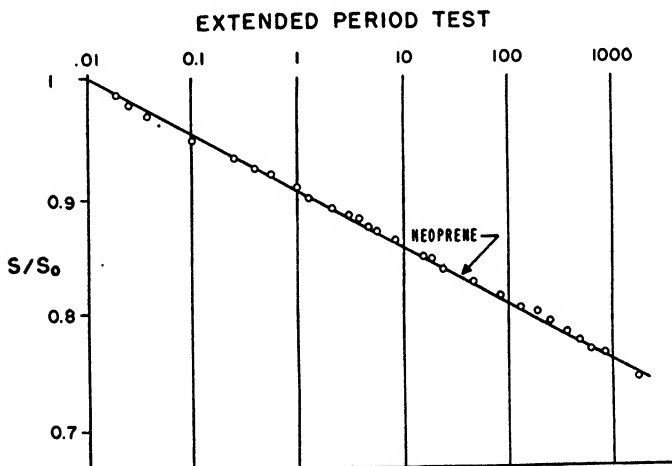
EXTENDED PERIOD TEST

FIG. 7

hours, in which the logarithmic stress relaxation is very closely maintained. On the basis of these data the pressure exerted on relatively stiff clamping members by a plastic sample at times greater than 0.01 hours may be calculated from the equation:

$$(S/S_0) = 1 - K(\log t/t_0),$$

where

S = the clamping pressure at time t

S_0 = the clamping pressure at time t_0

t_0 = 0.01 hours

K = slope of the time decay curves.

The case for which t_0 is less than 0.01 hour is excluded since the instrument does not lend itself to analysis over such short periods.

At the start of each test a slight slippage of the material along the surface of the clamping plates is apparent. This effect lasts for varying lengths of time depending on the material under test. Since it is also logarithmic in character, it appears in the final plot of the test data as an increase in the slope of the curve. The slippage, when it is noticeable, seldom lasts for more than 0.1 hour and is easily separated from the stress relaxation of the specimen, by the appearance of a discontinuity in the slope of the curve. This may be seen clearly in Fig. 8. As has been stated,
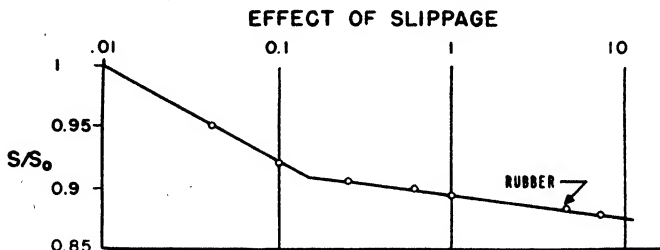

FIG. 8

the clamping plates are roughened to reduce the slippage effect and avoid the necessity of cementing or vulcanizing the specimen to them.

To give further experimental support to the method of extrapolating the data, several long-term tests were conducted on Buna-S and Neoprene covering periods in excess of 60 days. These showed satisfactory linearity when plotted on semilog paper, and, therefore, agreed closely with extrapolation from the early data of the respective tests. In connection with these and all other tests it was also found that the linearity of the data improved with the care taken in performing the experiment. Such items as stabilizing the oven and sample temperatures before test have relatively large influence upon the appearance of the resulting data.

Specimens have also been tested in tension and shear by simple adaptation of the clamping device. The resulting curves have been indistinguishable from the ones taken in compression.

APPLICATIONS

A stress relaxation measurement, making possible the extrapolation to a period of months of a curve requiring but a short test to establish, lends itself admirably to industrial problems involving gaskets, shock mounts, retaining bands, supports, *etc.* In an effectively rigid system the high polymer member may be adjusted to insure proper pressures or positions in the future. Since the shape factor presents no limitations, jigs can be adapted to an unlimited number of articles to be tested. Thus, the

uncertainty of choosing a material best suited to a given set of conditions is reduced once a set of these tests has been performed.

Curves may be run on materials which are in process of curing, aging, dehydrating, *etc.* Extrapolations of purely theoretical interest may also be carried out on samples whose properties are not stable enough to permit long-term testing. Successive curves taken on a series of supposedly identical samples will indicate the effects resulting from a process, whether it be natural or the result of a predetermined set of imposed conditions. Controlled atmospheres containing moisture, ozone or solvents, may be introduced.

The instrument can be used for quality control. Samples from production lines may be tested to be sure that the effects of plasticizer, accelerator, or solvent remain constant. Variations in performance beyond those permissible for the process would be quickly recognized and call for corrective action.

EXAMPLE

A problem of the stress relaxation of a gasket will serve as an example of the use of information obtained in the above-described manner. Assume that a Neoprene gasket must be compressed to 500 p.s.i. to prevent leak-
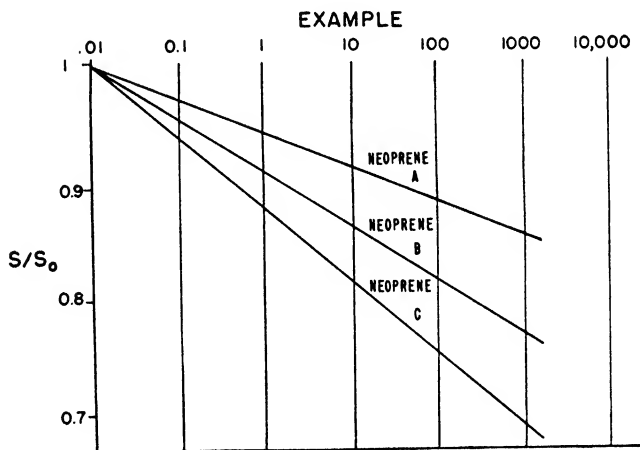

Fig. 9

age in a pipe joint. Three arbitrary formulations are available: A, B, and C (Fig. 9). The mechanics of the system (Fig. 10) limit the maximum gasket stress to 700 p.s.i. Which composition may be used to prevent leakage over a period of 1000 hours?

If all 3 gaskets are originally tightened to 700 p.s.i., gaskets A, B, and C will, in 10 hours, relax to 640, 610, and 570 p.s.i., respectively. At the end of 100 hours they will have relaxed to 625, 580, and 525 p.s.i., respectively. Gasket C will fail at 400 hours, but at 1000 hours, gaskets A and B will still be exerting safe loads of 600 and 545 p.s.i.
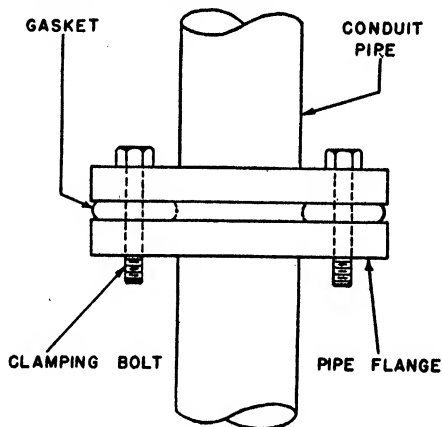

Fig. 10

CONCLUSIONS

Up to now, little use has been made of the strain gage as a means of measuring stress, although the idea is not original and has been used recently in textile and building materials laboratories. Chain balances (4), sliding balance weights actuated by wires (5), and servo mechanisms (6) have been incorporated in most constant strain tests which have necessitated cumbersome equipment.

The instrument used in the above-described experiments is a compact unit, measuring $2'8'' \times 1'4.5'' \times 1'$, containing a minimum of moving parts, essentially free from draft and vibration effects, and with the advantage that it measures the relaxation characteristics of a substance under constant strain (constant sample deflection).

Since identical curves have resulted from samples in tension and from those under compression, the compression test is generally used because of its relative simplicity.

The relaxation characteristics of a number of materials may be specified by one constant when tested under given temperature and humidity conditions and for a specified sample shape. Since all characteristic curves are straight lines on semilog paper, the suggested ideal parameter is the slope K of the characteristic curve as indicated by the equation:

$$(S/S_0) = 1 - K(\log t/t_0).$$

The unit requires a 110 volt A.C. supply, but is voltage-stabilized to withstand normal industrial line voltage variations. The temperature range of the oven extends to 180°F. and is controlled to within ±1°F.

The materials reported on in this paper were furnished through the courtesy of the General Tire and Rubber Company and E. I. du Pont de Nemours, Inc.

The authors wish to acknowledge the help and encouragement of Mr. W. E. C. Eustis of the Naval Ordnance Laboratory who first presented the problem, and to Mr. M. J. Sanger of the General Tire and Rubber Company and Mr. W. N. Keen of E. I. du Pont de Nemours, Inc., for furnishing samples for this work.

A commercial model of the apparatus described has recently been made available by Baird Associates, Inc., Cambridge, Mass., under the commercial name "Hi-Po-Log."

APPENDIX

The following is a tabulation of the material stock numbers and code letters for the samples illustrated in Figs. 4 through 8:

Figure	Material	Code	duPont Stock No.
4	Rubber	UE	846–14
4	Neoprene	UH	846–N–1592
4	Buna S	UG	846B–27
5	Buna S	CB	1333B–2A
6	Buna S	CB	1333B–2A
7	Buna S	UG	846B–27
8	Rubber	UE	846–14

REFERENCES

1. A.S.T.M. Standards, p. 1770, 1944.
2. GUTH, E., AND JAMES, H. M., *Ind. Eng. Chem., Ind. Ed.* **33**, 624 (1941).
3. FRIED, R. P., Load Relaxation and Recovery in Certain Textile Yarns. M.S. Thesis, Textile Eng. Dept., Mass. Inst. Tech., 1947.
4. MOONEY, M., WOLSTENHOLM, W. E., AND VILLARS, D. S., *J. Applied Phys.* **15**, 324 (1944).
5. TOBOLSKY, A. V., PRETTYMAN, D. B., AND DILLON, J. H., *ibid.* **15**, 380 (1944).
6. CAYCE, K., Mech. Eng. Thesis, Mass. Inst. Tech., 1944.

VISCOSITY AND SHEAR ELASTICITY MEASUREMENTS OF LIQUIDS BY MEANS OF SHEAR VIBRATING CRYSTALS

W. P. Mason [1]

From the Bell Telephone Laboratories, Murray Hill, N. J.
Received November 29, 1947

ABSTRACT AND CONCLUSIONS

By employing torsional and shear vibrating crystals, viscous and shear waves can be set up in liquids. As discussed in a former paper (1), the loading such waves apply to the crystals provides a measurement of the viscosity and shear elasticity in liquids. Methods for cutting torsional crystals of ammonium dihydrogen phosphate (ADP) and quartz are discussed. Calculations indicate that such crystals can generate high shearing rates in light liquids, and this technique may be of interest in determining the effects of high rates of shear on viscosity. Frequencies in the megacycle range can be covered by using thickness shear crystals covered with thin films of the liquid.

The technique has been employed in measuring the properties of three liquids in detail. These are polyisobutylene, arochlor and silicone putty. The last two show shear elasticities in the crystalline range while the first one has a much lower shearing modulus than is obtained in crystalline materials. It is suggested that this low shearing modulus is connected with a combination rotation and translation which occur with different activation energies.

I. METHOD OF MEASUREMENT

If we set a crystal vibrating in a purely torsional mode, all the motion is tangential to the surface, and, as discussed first by Stokes, highly attenuated viscous waves can be set up in a medium. The equations of propagation can be derived from the definition of viscosity and the equation of motion

$$T = \eta \dot{S} = \eta \left[\frac{\partial \dot{\zeta}}{\partial x} + \frac{\partial \dot{\xi}}{\partial z} \right] ; \quad \rho \frac{\partial \dot{\xi}}{\partial t} = \frac{\partial T}{\partial z} , \tag{1}$$

where T and S are the shearing stress and strain, $\dot{S}$ the time rate of

---

[1] This paper was presented at the Annual Meeting of the Society of Rheology, New York City, October 31st–November 1st, 1947.

change of strain, η the coefficient of viscosity, $\dot{\zeta}$ the displacement velocity along the Z axis, $\dot{\xi}$ the displacement velocity along the X axis, and ρ the density. For a plane wave propagating along Z, all the motion is tangential to the direction of propagation and $\dot{\zeta} = 0$. Inserting the first equation of (1) (the definition of viscosity) in the second equation, the differential equation becomes

$$\rho \left(\frac{\partial \dot{\xi}}{\partial t} \right) = \eta \frac{\partial^2 \xi}{\partial z^2}. \tag{2}$$

For simple harmonic motion, the plane viscous wave has the solution

$$T = T_o \cosh \Gamma z + \dot{\xi}_o Z_o \sinh \Gamma z,$$

$$\xi = \dot{\xi}_o \cosh \Gamma z + \frac{T_o}{Z_o} \sinh \Gamma z, \tag{3}$$

where Γ, the propagation constant, and Z_o, the image impedance, have the values

$$\Gamma = \sqrt{\frac{j\omega\rho}{\eta}} = \sqrt{\frac{\pi f \rho}{\eta}} (1 + j), \quad Z_o = \sqrt{j\omega\rho\eta} = \sqrt{\pi f \rho \eta}(1 + j), \tag{4}$$

where $\omega = 2\pi f$ where f is the frequency. For carbon tetrachloride, with a density $\rho = 1.595$ and a viscosity of 0.0098 poises, the attenuation is 2660 nepers/cm. at 14 kilocycles, so that the shearing stress is appreciable for only a few thousandths of a centimeter from the crystal surface. Although the attenuation for such waves is too high to permit their wave propagation properties to be investigated, they do introduce a loading effect on the crystal which can be measured by the increase in the resonant resistance and the decrease of the resonant frequency of the crystal as it is changed from a vacuum to the medium under investigation.

The use of such a crystal for measuring viscosities was discussed in a former paper (1), and it was there shown that the change in the measured electrical resistance ΔR_E and the lowering in frequency Δf determined the mechanical resistance R_M/cm.^{2} and the mechanical reactance X_M/cm.^{2} according to the formulae

$$R_M = \frac{\Delta R_E}{K_1} ; \quad X_M = - \frac{\Delta f}{K_2}$$

where

$$K_1 = \frac{r}{2\pi f_R{}^2 C_o I} \left[\frac{R^3 + R_o{}^3 + (R^4 - R_o{}^4)}{l} \right],$$

$$K_2 = \frac{R^3 + R_o{}^3 + (R^4 - R_o{}^4)/l}{2I}, \tag{5}$$

where r is the ratio of capacities of the crystal determined by measuring the resonance frequency f_R, the antiresonance frequency f_A, and setting

$r = f_R/2(f_R - f_A)$; C_o is the static capacity of the crystal in farads; R the outside diameter and R_o the inside diameter of the torsional crystal; l its length and I the moment of inertia, per unit length, given by the formula

$$I = \frac{\pi}{2} \rho_c(R^4 - R_o^4), \tag{6}$$

where ρ_o is the density of the crystal.

The method for making a torsional crystal from ammonium dihydrogen phosphate (ADP) is shown by Fig. 1. Here a crystal is cut with its length along the X crystallographic axis, and a hole is bored along this
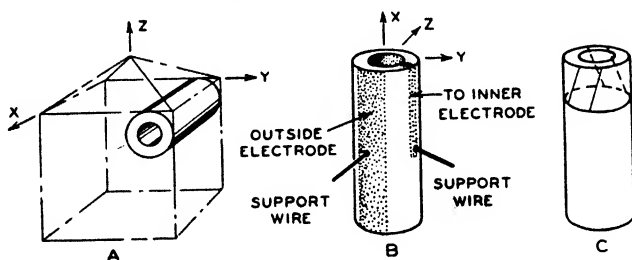

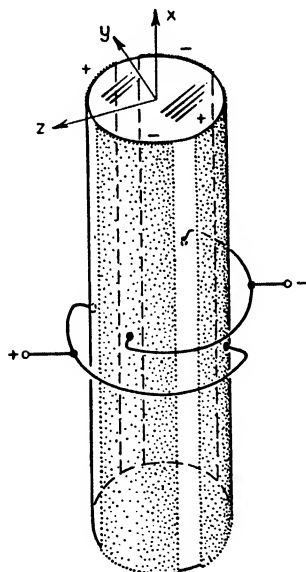Fig. 1. Method for obtaining torsional crystal of ADP.

Fig. 2. Method for obtaining torsional crystal of quartz.

axis. A cylinder is then turned as shown in Fig. 1B. Since the mode of motion generated is a face shear mode when the field is impressed along the Z crystallographic axis, a plating is made continuous on the inside cylindrical surface and is divided into two 90° segments on the outside surface, which are connected together electrically. The center lines of these two surfaces lie along the Z axis. As shown by Fig. 1C the field in one segment produces a face shear in one direction, while the field in the other segment produces a face shear in the other direction. The result is a torsional motion of the crystal as a whole. As shown by Fig. 2, a torsional vibration can also be produced in a quartz crystal, and such crystals may be of use, especially if wide temperature ranges are to be covered. This crystal uses a thickness shear and requires 4 evenly spaced electrodes to generate the motion.

As discussed in the former paper (1), the viscosity of a number of light liquids was measured by using the experimental arrangement shown by Fig. 3. This consisted of an ADP crystal, suspended from the 3 wires at
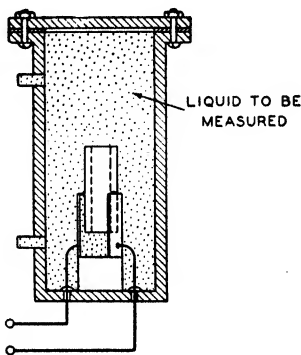

LIQUID TO BE MEASURED

FIG. 3. Experimental arrangement for measuring viscosities.

its nodal points, mounted inside a container of small diameter. This container acts as a wave guide tube and tends to attenuate highly any complicated vibrations of the longitudinal type which can be set up in the tube. The result is that, if any such vibrations are set up by the fact that the motion of the crystal surface is not exactly tangential to the surface, the only effect that such waves have is to change the reactance loading on the crystal, and this is usually small. Measurements made of the loading due to nitrogen as a function of pressure, with the crystal inside and outside of wave guide tubes, have shown that the longitudinal loading is negligible, provided the diameter of the crystal is a tenth or less of the length.

The outside container of Fig. 3 has two copper to glass seals for the electrical wires to connect to the crystal. The chamber can be evacuated and filled with liquid through the two stop cocks. If desired, pressure can be put on the liquid by means of external gas pressure. The process of measurement consists in determining the resonant frequency f_{R_0} and the resistance at resonance R_0 in a vacuum. Then, introducing the liquid, the new resonant frequency f_{R_1} and the new resistance at resonance R_1 are determined. For liquids having a small viscosity, these values can be
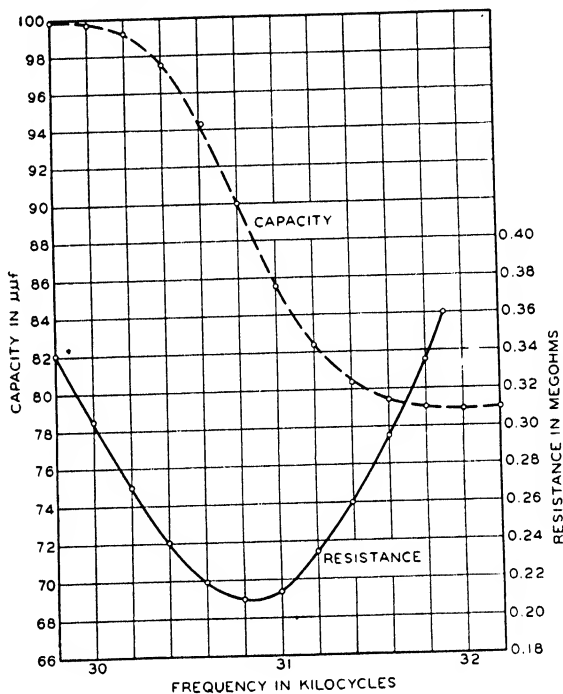

Fig. 4. Curve of resistance and reactance of castor oil.

determined accurately by measuring the current through the crystal when a low impedance was connected on either side. The resonant frequency occurred at the frequency for which the current was a maximum, and the resonant resistance was measured by a substitution method. However, for very viscous liquids, this procedure does not accurately locate the resonant frequency, and measurements of resistance and reactance were made with a bridge circuit. A curve of the resistance for polymerized castor oil is shown by Fig. 4. The resonant frequency is determined as the lowest point of the resistance curve, or more accurately, by taking the

average of two frequencies of equal resistance greater than the minimum, while the resistance used is the lowest value on the curve.

As an example, an ADP crystal, vibrating at nearly 14,000 cycles, and having the dimensions

$$L = 6.9 \text{ cm.;} \quad OD = 0.93 \text{ cm.;} \quad ID = 0.64 \text{ cm.,} \quad (7)$$

had a resonant frequency of 13,948 cycles, an antiresonant frequency of 14,098.5, and a resistance at resonance of 1300 ohms, all measured in a vacuum. The capacity of the crystal was $C_o = 140 \ \mu\mu f$. The density of ADP is 1.804. From these values the constants K_1 and K_2 can be calculated as

$$K_1 = 366; \quad K_2 = 0.673. \quad (8)$$

At 24°C., measurements were made of the viscosity of a number of light liquids. For dimethyl phthalate, for example, the resonant resistance was 36,500 ohms. Hence, the viscosity, with the density $\rho = 1.186$, is

$$\eta = \left(\frac{\Delta R_E}{K_1} \right)^2 \times \frac{1}{\pi f_R \rho} = 0.178 \text{ poises.} \quad (9)$$

This compares with 0.170 measured by flow methods, which agrees within 5%. This appears to be about the accuracy obtained, due principally to the lack of a better temperature control. Measurements were made over a range of viscosities from 0.01 to 6 poises and these agreed with those measured by flow methods within a few per cent.

However, measurements made with very viscous liquids, such as polymerized castor oil, indicate that these liquids do not behave as simple viscous liquids since the reactance and resistance components are not equal, the resistance becoming progressively larger than the reactance at high frequencies. This is illustrated by Fig. 5, the points of which represent the resistance and reactance values measured for polymerized castor oil as a function of frequency. The dot-dash line shows the resistance and reactance terms that would be obtained if the liquid were a viscous medium having a density of 0.967 and the viscosity of 18 poises measured by flow methods. The resistance is above this line and the reactance below.

This divergence and the shape of the curve are accounted for if the liquid is assumed to have a shear elasticity as well as a shear viscosity. The impedance of such a wave is most easily calculated by means of an equivalent circuit in which the stress corresponds to the voltage and the particle velocity to the current. For a purely viscous medium, the equivalent circuit is shown by the left side of Fig. 5. The series arm is an inductance equal to the density times the length dx, where dx is a length in the order of the mean free path. The shunt arm is a resistance equal

to the viscosity η divided by the length dx. The equivalent circuit is valid for a cross-section of 1 cm.[2] This circuit is repeated indefinitely for an infinite medium, or it may be terminated after a finite number of repetitions if it represents a finite path length. The characteristic im-

MEASURED RESISTANCE AND REACTANCE FOR A SHEAR VIBRATION OF POLYMERIZED CASTOR OIL

EQUIVALENT CIRCUIT FOR A VISCOUS MEDIUM

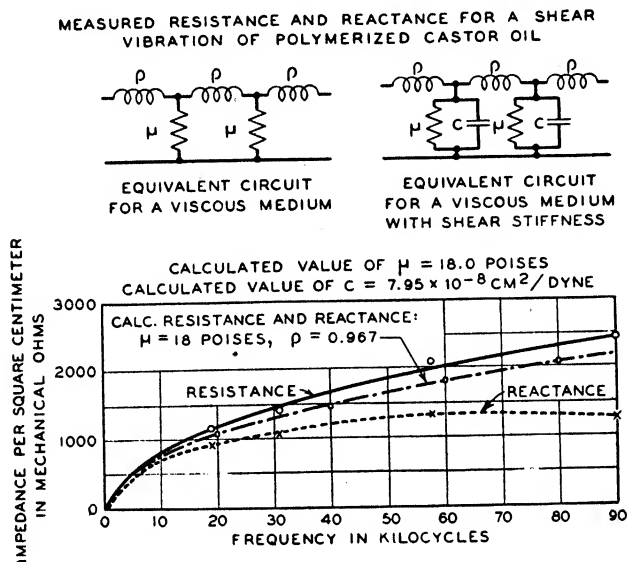EQUIVALENT CIRCUIT FOR A VISCOUS MEDIUM WITH SHEAR STIFFNESS

Fig. 5. Mechanical resistive and reactive loading of castor oil as functions of frequency.

pedance (impedance of an infinite line) and the propagation constant are given by the equations (2)

$$Z_o = \sqrt{Z_1 Z_2} = \sqrt{j\omega\rho dx \frac{\eta}{dx}} = \sqrt{j\omega\rho\eta} = \sqrt{\frac{\omega\rho\eta}{2}}\,(1+j),$$

$$\Gamma = \sqrt{\frac{Z_1}{Z}} = \sqrt{\frac{j\omega\rho dx}{2\eta/dx}} = \sqrt{\frac{j\omega\rho}{\eta}}\,dx = \sqrt{\frac{\pi f\rho}{\eta}}\,(1+j)dx,$$

$$(10)$$

where Z_1 is the series impedance and Z_2 the shunt impedance of the network. These equations agree with the same equations calculated from hydrodynamics, as shown by Eq. (4).

The effect of a shear elasticity can be represented by shunting the viscous resistance η/dx by a compliance (inverse of a stiffness) equal to $C_s dx$ where C_s is the modulus of compliance of the liquid. This network is the one shown by the right side of Fig. 5. Hence, at low frequencies, where the value of the resistance is much less than the reactance of the shunt compliance, the liquid behaves as a viscous liquid. On the other hand,

when the frequency is high enough, so that the reactance of the compliance C_s equals the viscosity, a different reaction occurs. For very high frequencies it should be possible to transmit a shear wave in such a medium. The propagation constant Γ and the characteristic impedance Z_o can be calculated by using the series and shunt impedances

$$Z_1 = j\omega\rho dx, \qquad Z_2 = \left(\frac{(-j/\omega C_s)\eta}{\eta - j/\omega C_s}\right)\frac{1}{dx}. \tag{11}$$

From these we find $Z_o = R_m + jX_m$, where

$$R_M = \sqrt{\frac{\omega^2\eta^2\rho C_s + \sqrt{\omega^4\eta^4\rho^2C_s{}^2 + \omega^2\eta^2\rho^2}}{2[1 + \omega^2\eta^2C_s{}^2]}},$$

$$X_M = \sqrt{\frac{-\omega^2\eta^2\rho C_s + \sqrt{\omega^4\eta^4\rho^2C_s{}^2 + \omega^2\eta^2\rho^2}}{2[1 + \omega^2\eta^2C_s{}^2]}}, \tag{12}$$

$$A = \sqrt{\frac{-\omega^2\rho C_s + \sqrt{\omega^4\rho^2C_s{}^2 + \omega^2\rho^2/\eta^2}}{2}},$$

$$B = \sqrt{\frac{\omega^2\rho C_s + \sqrt{\omega^4\rho^2C_s{}^2 + \omega^2\rho^2/\eta^2}}{2}}, \tag{13}$$

where R_M is the resistance/cm.², X_M the reactance/cm.², A the attenuation of the wave in nepers/cm., and B the phase shift in radians/cm.
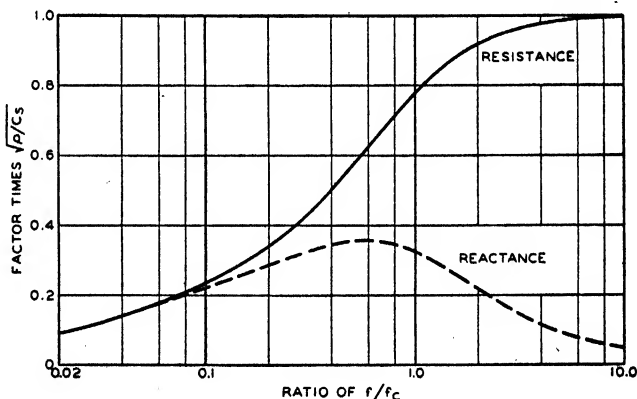

Fig. 6. Mechanical resistance and reactance of liquid having shear elasticity.

Fig. 6 shows a plot of the resistance and reactance terms plotted as a function of the ratio of the frequency to the relaxation frequency f_c. The resistance at low frequencies behaves like that for a viscous fluid, but at high frequencies it becomes asymptotic to the value $\sqrt{\rho/C_s}$. The reactance

equals the resistance for low frequencies. For high frequencies it approaches zero.

Solving Eq. (13) for the viscosity and the compliance, we find

$$\eta = \frac{(R_M{}^2 + X_M{}^2)^2}{2 R_M X_M \omega \rho}, \qquad C_s = \frac{(R_M{}^2 - X_M{}^2) R}{(R_M{}^2 + X_M{}^2)^2}. \qquad (14)$$

Taking the value of R_M and X_M at 30,840 cycles, the value of η and C_s for polymerized castor oil becomes

$$\eta = 18 \text{ poises}, \qquad C_s = 7.95 \times 10^{-8} \text{ cm.}^2/\text{dyne.} \qquad (15)$$

Assuming these values, the calculated values of resistance and reactance are given by the full and dotted lines of Fig. 5. These agree well with the experimental values.

Since a viscous wave penetrates only a small fraction of a centimeter before it is attenuated by many nepers, a thin film will produce saturation effects. Hence, this technique can be applied to measuring the viscosity of very small samples. The device might also be made into a continuous reading viscosimeter, since the crystal resistance and resonant frequency can be continuously measured and recorded.

The question arises as to whether this type of device can be used to study viscosity and shear elasticity of liquids at very high rates of shear. In the discussion of the previous paper (1) it was shown that the shearing strain generated in a liquid S_L adjacent to the torsional crystal was equal to the product of the maximum tangential displacement d_o times the attenuation factor A, or

$$S_L = d_o A = d_o \sqrt{\frac{\pi f \rho}{\eta}}. \qquad (16)$$

In terms of the crystal strain S_C, the maximum displacement (which occurs on the two ends of the crystal) is

$$d_o = \frac{l}{2} S_C, \qquad (17)$$

where l is the total length of the crystal and S_C the maximum shearing strain. For crystalline material the maximum strain is around 10^{-4}, although heavily etched crystals, for which surface cracks are removed, may be strained as high as 10^{-3}. This is multiplied by a factor A which may amount to 500 nepers/cm. for light liquids, so that very high strains are possible in the liquid adjacent to the surface. However, it would require a very complicated differential equation solution to evaluate the effect of the strain, since it is going to vary along the length of the crystal and very rapidly for positions in the liquid some distance from the crystal. Also, heating effects may be important. So far, no attempt has been made to evaluate these features, and no experimental results have been obtained.

The frequency limit for torsionally vibrating crystals is probably around 500 kilocycles because of the small sizes of the cylinders that are required. The question arises as to whether thickness shear vibrating crystals of the AT and BT type can be used to produce viscous and shear elastic waves in liquids. When the crystal is entirely surrounded by liquid it was found that the shear coupling to flexural modes produced so high a loading due to longitudinal waves set up in the liquid that the shear loading could not be determined with certainty. However, by using the thin film technique it has been found possible to at least roughly measure the shear viscosity and elasticity of liquids that will wet the surface of the crystal. The film is so thin that it is only a small fraction of a wave length for longitudinal waves and hence acts as a mass loading without appreciable resistance. For a viscous wave, however, the wave length is so short that nearly complete saturation of the damping is obtained in less than 0.0001 cm.

A few measurements have been made with a well dimensioned BT quartz crystal vibrating at 3527 kilocycles. The constants K_1 and K_2 relating the resistance loading/cm.^{2} to the change ΔR_E in electrical resistance, and the reactance loading to the change in frequency can be derived from Eq. (5) by letting $R = R_o + t$ where t is the crystal thickness and letting R_o approach infinity. This would result in a shearing crystal of infinite radius (a flat crystal), and gives the formula

$$K_1 = \frac{r\left[1 + \frac{2t}{l}\right]}{2\pi^2 f_A{}^2 C_o \rho_c t}, \qquad K_2 = \frac{-\left[1 + \frac{2t}{l}\right]}{2\pi \rho_c t}. \qquad (18)$$

However, it is known from the study of crystal surface motions that contoured crystals of these types do not have a uniform motion over the whole crystal surface, and hence one would expect these formulae to be only approximate. The BT crystal used had the constants $l = W = 12$ mm.; $t = 0.7$ mm.; $f_r = 3,527,000$ cycles; $\Delta f = 3,450$; $r = 510$; $C_o = 5\mu\mu f$; resistance at resonance = 180 ohms; $\rho_o = 2.65$. Inserting these values in Eq. (18) we find $K_1 = 2.2$; $K_2 = -0.85$. Measurements with a number of light liquids into which the crystal had been dipped and the excess liquid had been shaken off agreed within 20% of their low frequency values if K_1 was taken as 0.83. The decrease in frequency was several times larger than could be accounted for by the viscous reactance, indicating that the mass loading of the flexure modes was also lowering the frequency. When a film of polymer B polyisobutylene (as discussed in the next section) was tried, the loading at 28°C. was 3200 mechanical ohms, indicating that the shear stiffness of about 12×10^6 dynes/cm.^{2} still persisted up to 3×10^6 cycles. It appears that this method shows promise for extending the frequency range to higher frequencies than can be reached by torsional crystals.

II. Measurement of Shear Stiffness and Viscosity of Three Liquids

As examples of the use of such methods in studying the properties of liquids, measurements have been made for 3 viscous liquids, all of which show shear elastic properties. These liquids are polyisobutylene, arochlor and silicone (bouncing) putty. The results for polyisobutylene for both shear and longitudinal waves are incorporated in another paper (2), and the results for shear waves are summarized here. Ordinarily, if a liquid behaved as a solid for high frequencies or low temperatures, one would expect to find stiffnesses in the order of 10^8–10^{10} dynes/cm.^{2}, and indeed it is found that the liquids silicone putty and arochlor (pentachloro-diphenyl) do have stiffnesses in this region. However, polymerized castor oil and polyisobutylene (vistanex) described in this section have much lower shear stiffnesses in the order of 5×10^6–5×10^7 dynes/cm.^{2}, and this behavior is characteristic of such complex molecules as the polymers.

Polyisobutylene is a polymer molecule that occurs in a long chain. It has the formula shown by Fig. 7A and the zigzag form shown by Fig. 7B.
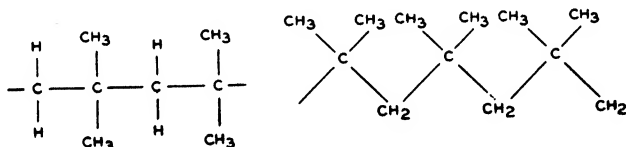

Fig. 7. Structure of polyisobutylene.

This chain, in an ordered, stretched state, appears to rotate about the direction of its length once in every 9 pairs of CH_3 groups. Accordingly, nonplanar zigzag segments can be expected in the liquid state. The specimens used were designated A, B, C, and D which had, respectively, average molecular weights of 903, 3520, 4550, and 5590.

Measurements of the viscosity of these 4 samples were made by both the falling ball method and by the crystal method over a temperature range and are shown plotted as the log of the viscosity *vs.* the inverse temperature by Fig. 8. The two methods check within about 5%, which is probably the experimental error of the crystal method for a liquid with elasticity. All of these liquids have the same slope, which indicates, according to Eyring's (3) theory, that the element which moves from one potential well to an adjacent one is a segment of the chain, 20 molecules or so, whose length is essentially independent of the total chain length. The densities of these liquids are shown by Fig. 9.

Since both shear viscosity and stiffness are present, the method used for evaluating them is to determine the shape of the resistance curve as a function of frequency. The experimental arrangement is that shown by
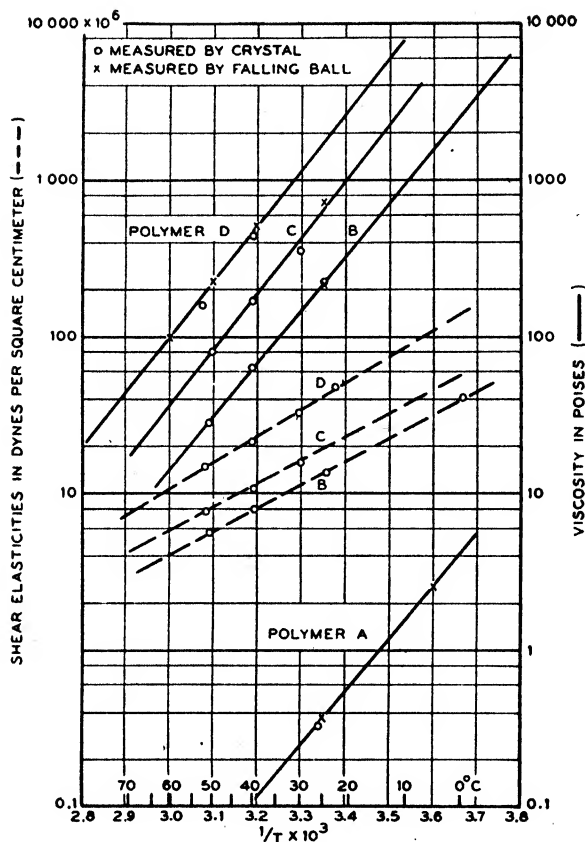
FIG. 8. Viscosity and shear elasticity of polyisobutylene as
function of temperature.

Fig. 3. The measurements were made with a balanced electrical bridge,
and data similar to those of Fig. 4 were used to evaluate the resistance
loading. Measurements were made at the first, third, and fifth harmonics
of the crystal. For the harmonics, the same values of K_1 hold as for the
fundamental. Typical data for the resistance loading per square centi-
meter in terms of the frequency and temperature are shown for the poly-
mer "B" liquid of Fig. 10. To interpret these data in terms of shear vis-
cosity and stiffness, use is made of the calculation of the resistance and
reactance loading for a liquid having shear stiffness and viscosity given
by Fig. 6. Comparing this with the data of Fig. 10, we see, for example,
that at 0°C. the loading is nearly independent of frequency, which means

that the relaxation frequency is considerably below the lowest measuring frequency of 17.5 kilocycles. The curves of 24°, 40°, and 50°C., however, show enough bending with frequency to allow one to fit them to the
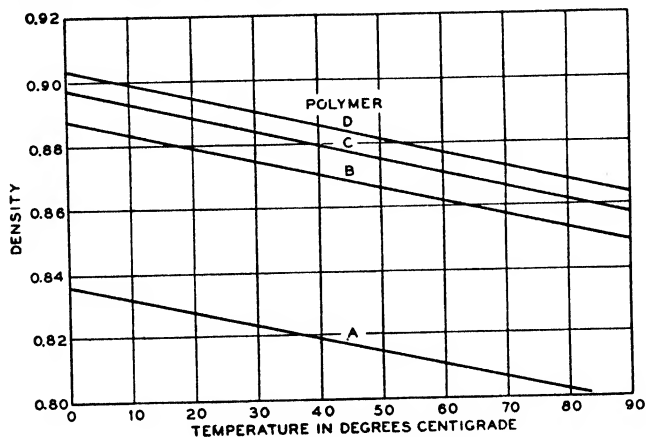

FIG. 9. Density of polyisobutylene.
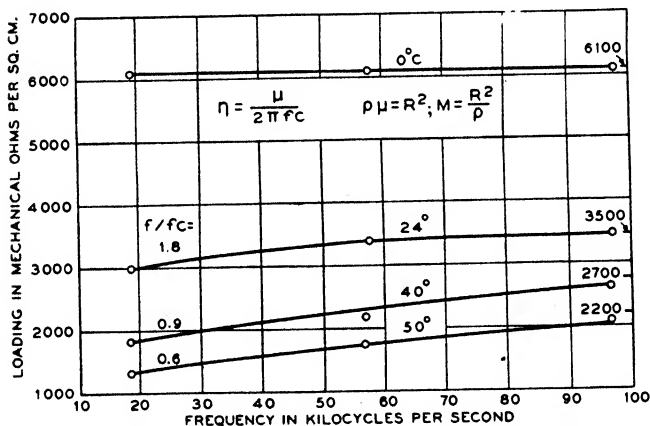
FIG. 10. Resistance loading of polyisobutylene as function of temperature and frequency.

theoretical curve. From these data, one can find that the ratio of the lowest frequency (about 17.5 KC) to the relaxation frequency is given by the second column of Table I, while the asymptotic value of the loading resistance at very high frequencies is given by the third column. Since the shear stiffness is related to the resistance loading at high frequencies

TABLE I

Polyisobutylene "B"

Temperature	f/f_c	R at high frequencies	μ dynes cm.^{2}	Relaxation frequency, f_c	Value of shear viscosity
°C.		mechanical ohms		cycles	poises
0	—	6100	42×10^6	—	—
24	1.8	3500	14×10^6	9700	230.0
40	.9	2650	8×10^6	19400	68.8
50	.6	2200	5.6×10^6	29200	30.5

by the formula

$$\sqrt{\rho\mu} = R \qquad \text{or} \qquad \mu = R^2/\rho, \tag{19}$$

the shear stiffness is shown by the fourth column. The fifth column shows the calculated relaxation frequency, while the sixth column shows the shear viscosity η which can be calculated from the formula

$$\eta = \frac{\mu}{2\pi f_c}. \tag{20}$$

The values of viscosity measured by the crystal are shown plotted by the circles of Fig. 8 for all liquids and, as is evident, they agree with the values measured by the falling ball method within 5%, which is probably the accuracy of measurement by the present method.
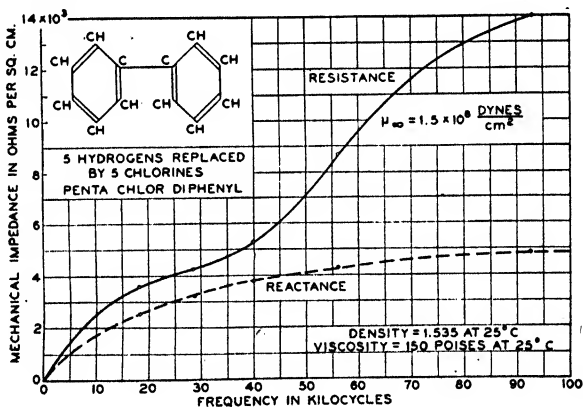

FIG. 11. Resistance and reactance loading of arochlor.

The values of shear stiffness measured for the 3 polymer liquids, B, C, and D, are shown plotted by the dashed lines of Fig. 8. They lie nearly on straight lines of uniform slope when plotted as $\log \mu$ *vs.* $1/T$, at least within the temperature range shown.

Two other measurements made on other liquids appear to be significant. Measurements were made for arochlor, which is a pentachlorodiphenyl having the structure shown by Fig. 11. At 24°C. it has a density of 1.535 and a viscosity of 150 poises. Over a frequency range the resistance and reactance values are shown by Fig. 11. The values cannot be fitted by a single relaxation time and indicate the presence of at least two relaxation times and a much lower compliance (high stiffness) of about 6×10^{-9} cm.²/dyne. This stiffness approaches that of a crystal. In the former paper (1) by shear wave methods, the compliance of silicone putty was measured at 50,000 cycles and a room temperature of 25°C. This had a compliance of 1.35×10^{-9} cm.²/dyne, which is a stiffness of nearly 10^9 dynes/cm.² and approaches that of a crystalline material.

III. DISCUSSION OF THE ORIGIN OF SHEAR ELASTICITY IN LIQUIDS

The present study shows two different types of behavior in the shear stiffnesses of liquids. Polymer type liquids show a shear stiffness in the order of 10^6–10^7 dynes/cm.² which persists up to frequencies in the megacycle range. Short chain liquids of high viscosity show a much higher stiffness in the order of 10^8–10^9 dynes/cm.². The stiffness of both types decreases as the temperature is raised, contrary to what occurs in the "kinetic theory," for which an increase of stiffness occurs with an increase in temperature.
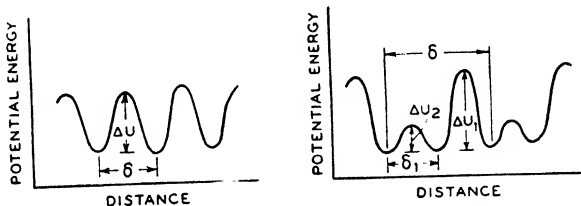

FIG. 12. Potential well distribution of ordinary liquid and for polymer.

The conclusion is drawn in the paper on polymer stiffness (2) that the low stiffness was due to a composite motion of the chain, including translation and hindered rotation within chains. Such a motion would be affected by chain length, through a chain articulation effect. If sufficient time is given to establish equilibrium, the "kinetic theory" type of stiffness prevails for the polymer. For short times, equilibrium is not established, and the reaction depends on nearest neighbors and is of the type treated by free energy wells. Under these conditions the stiffness decreases as the temperature increases.

From a free energy point of view, the action of the rotation and translation corresponds to the free energy well distribution shown by Fig. 12B. Most light liquids probably have a free energy well distribution shown by Fig. 12A. When a shearing stress is put on the liquid, one well is lowered compared to the other, and at low frequencies sufficient time is available so that heat energy causes a viscous flow in the direction of the stress. At very high frequencies there is not time for the direction of flow to be perturbed by the applied stress, and the only effect is a displacement of the equilibrium position, which results in a high shear stiffness of the crystalline type. For a polymer type, however, a combined rotation and translation is required for a viscous flow and hence the viscosity is controlled by the high free energy peak ΔU_1. At frequencies high enough so that the combined motion cannot occur, a reversible rotation across the lower free energy peak ΔU_2 is still possible. Since the displacement δ_1 is much larger than that occurring in a single well, the stiffness is much lower, and shear stiffnesses in the order of 10^6 dynes/cm.^{2} are obtainable. This stiffness will continue with increasing frequency until sufficient time is not available to perturb the rate of crossing ΔU_2, after which the single well type of stiffness will occur. From measurements of polyisobutylene, the low shear stiffness must hold up to at least 3×10^6 cycles, and ΔU_2 must be less than half ΔU_1. For arochlor, shown by Fig. 11, however, since both relaxation frequencies are not separated much in frequency ΔU_1 cannot be much larger than ΔU_2.

REFERENCES

1. MASON, W. P., *Trans. Am. Soc. Mech. Eng.* **69**, 359–370 (1947).
2. A discussion of the equations of transmission lines and their application in describing the mechanical properties of matter will be found in the following publications.
   JOHNSON, K. S., Transmission Circuits for Telephonic Communication, Chapters XI and XII. D. Van Nostrand, 1925.
   MASON, W. P., Electromechanical Transducers and Wave Filters, Chapter I and Appendix B. D. Van Nostrand, 1942.
   BRILLOUIN, L., Wave Propagation in Periodic Structures, Chapters I, II, and III. McGraw-Hill, 1946.
   FRENKEL, J., Kinetic Theory of Liquids, Chapter IV. Oxford University Press, 1946.
3. MASON, W. P., BAKER, W. O., McSKIMIN, H. J., AND HEISS, J. H., *Phys. Rev.* April 15 (1948).
4. KAUZMANN, W., AND EYRING, H., *J. Am. Chem. Soc.* **62**, 3113–3125 (1940).

THE VISCOUS FLOW OF MOLTEN POLYSTYRENE [1]

R. S. Spencer and R. E. Dillon

From the Dow Chemical Company, Midland, Michigan
Received November 12, 1947

INTRODUCTION

The flow characteristics of high polymers subjected to shearing stresses are of considerable practical significance. Such properties are among the major factors determining optimum fabrication conditions and the time-temperature-load limits of applicability of fabricated objects. Recognition of the need for such information is evidenced by the multiplicity of "softening point tests," "flow tests," "heat distortion tests," *et al.*, which have been proposed from time to time. The usefulness of these tests in industry is determined by how well they correlate with working experience, and it must be admitted that few of them are suited to the obtaining of fundamental rheological data on polymers.

The deformation-time behavior of a polymer is, in general, complex, and account of this fact must be taken in designing experiments. Aside from ordinary elasticity, which we shall not consider, two principal modes of behavior are apparent. In the first, viscous flow, the deformation increases linearly with time under the action of a uniform shearing stress and is nonrecoverable, that is, the deformation is permanent when the stress is removed. In the second type of behavior, the deformation approaches a constant value as time increases under constant stress, and the deformation is completely recoverable in the sense of the limiting value of deformation as the time of recovery increases. This second mode of behavior has been termed variously *rubberlike elasticity, high elasticity,* and *retarded elasticity.* Under many conditions of temperature and stress, both mechanisms will contribute somewhat to the observed deformation, and it is customary, therefore, to classify high polymers generally as *viscoelastic* materials. Ideally, one would like to carry out experiments which isolate the two types of deformation, or which permit separation of the contributions of the two mechanisms. Failing this, or as a useful adjunct to the more direct approach, recourse may be had to various rheological models, or other methods of specifying viscoelastic behavior, as aids in analyzing observed deformation-load-time relationships (1,3,5).

Let us consider viscous flow in a little more detail. In carrying out a hypothetical experiment we shall subject the test material to various shearing stresses (τ), maintaining other conditions constant, and observe the corresponding rates of shear (D). The relationship

$$D = F(\tau), \tag{1}$$

together with its dependence upon such parameters as temperature, defines the viscous behavior of the material. For many simple liquids the rate of shear is directly proportional to the shearing stress, *i.e.*,

$$D = \frac{\tau}{\eta}. \tag{2}$$

Such liquids are termed *Newtonian* and the proportionality constant, η, is known as the *viscosity*. It has been shown by Fox and Flory (10) that polystyrene is a Newtonian liquid within the temperature interval between 125°C. and 217°C., at shearing stresses below 3×10^3 dynes/cm.².

In addition to the shearing stress, several other factors have been found to influence markedly the rate of shear of polystyrene. Temperature has been mentioned, its role has been reported by Weith, Turkington and Allen (24), Fox and Flory (10), Foote (9), Wiley (25), Nason (18), Scheele, Alfeis and Friedrich (19), and Jenckel and Ueberreiter (15). The molecular weight of the polymer is another important parameter whose effect has been observed by several of the above workers (10,15,18). Lastly, the rate of shear is dependent upon the amount of low molecular weight materials present (solvents or plasticizers), as was shown by Jenckel and Ueberreiter (15), Ferry (8), Scheele, Alfeis and Friedrich (19), and Spencer and Williams (21). Most of the work just cited was carried out under conditions in which Newtonian behavior was obtained. The influence of the variables listed was observed through the behavior of the viscosity, which (1) decreased with rising temperature, (2) increased with increasing molecular weight, and (3) decreased with increasing solvent concentration.

Of the above factors the present paper is concerned principally with the effects of temperature and shearing stress. Foote (9) and Nason (18) have observed that, under high shearing stresses, molten polystyrene is non-Newtonian, that is, it does not obey the simple relationship of equation (2). Rather, the rate of shear increases with shearing stress more rapidly than would be expected from the direct proportionality. Both of these workers used capillary viscometers, which type of instrument is particularly suitable when high shearing stresses are desired. For the same reason a capillary viscometer was employed in the present work.

For the case of capillary flow, Tobolsky, Powell and Eyring (22) have derived an expression analogous to Poiseuille's law, based upon the rate

of shear-shearing stress relationship of Eyring (7). Their equation may be rewritten as

$$Q = \frac{\pi R^4 P}{8 L \eta_0} \cdot F\left(\frac{\beta R P}{2L}\right), \tag{3}$$

where

$$F(x) = \frac{4}{x^3}\left[\left(x + \frac{2}{x}\right)\cosh x - 2\sinh x - \frac{2}{x}\right]$$

and Q is the volume velocity through any cross-section, R is the radius of the capillary, L its length, P the difference in pressure between ends of the capillary, η_0 is the limiting viscosity as the shearing stress approaches zero, and β is a lumped constant expressing the extent of deviation from Newtonian behavior and containing the "viscous volume" and the abso-lute temperature. This equation was applied by its originators to the data of Dillon and Johnston (6) on the capillary flow of rubber, and it has been applied recently by Greenblatt and Fensom (12) to a variety of hetero-geneous systems. One of the purposes of the present paper is to discuss the adequacy of this relationship in describing the capillary flow of molten polystyrene.

EXPERIMENTAL METHODS

The apparatus used was a duplicate of that described by Nason (18). The polymer sample was placed in a vertical chamber (1 in. internal diam.) immersed in an oil bath, and sufficient time allowed for it to come to the temperature of the bath. Then a nitrogen cylinder was connected to the top of the sample chamber and pressure applied, forcing the polymer through a vertical capillary coupled to the bottom of the chamber. A steel ball-bearing just fitting into the chamber rested on the polymer and prevented channeling by the nitrogen. The pressure was controlled by a Victor Gas-O-Dome Regulator and was measured by one of two calibrated gauges reading from 0 to 300 and 0 to 1500 lbs./in.^{2}. The temperature was controlled to about 0.3°C.

TABLE I
Capillary Dimensions

Identification no.	Radius (cm.)	Length (cm.)
1	0.0541	2.062
4	0.1616	5.086
7	0.0498	0.706
8	0.0529	3.211

Four capillaries were used in the measurements, with dimensions as set forth in Table I. The only difficulty encountered in this regard was with capillary No. 4, the longest of the four, which protruded below the lower level of the oil bath. This permitted air cooling of the lower end

of the capillary with the result that viscosities determined with capillary
No. 4 were appreciably higher than those obtained with the other three.
For this reason the data corresponding to this capillary were not included
in the discussion following. The same range of variables was covered with
each capillary, within the limits imposed by the apparatus and practical
extrusion rates. The temperature was varied from 165°C. to 253°C., and
the shearing stress at the capillary wall from 0.2×10^5 to 36.5×10^5
dyne/cm^{-2}.

The flow rates were determined by cutting off the section of filament
extruded during a measured time interval, cooling, and weighing. This
weight was then converted into a volume rate, using the specific volume
data of Spencer and Boyer (20). Several determinations of the extrusion
rate were made at each set of conditions and the results averaged.

The flow orientation data were obtained by measuring the diameter
of the filaments at room temperature and correcting to the extrusion
temperature, using the expansion coefficients reported by Spencer and
Boyer (20). The effective average relative length during flow through the
capillary was computed from the formula

$$\bar{\alpha} = \left(\frac{d}{d_0} \right)^2, \tag{4}$$

where d is the diameter of the extruded filament and d_0 is the diameter
of the capillary. This procedure was based on the assumption that the
volume was constant during orientation, *i.e.*, that Poisson's ratio has a
value of 0.5 for polystyrene. As long as measurements are restricted to
the region of rubberlike behavior this assumption is probably a fair one,
inasmuch as measurements on rubbers (14,23) have indicated a Poisson's
ratio of very nearly 0.5. In addition, Boyer and Spencer (2) have reported
that the volume change of polystyrene upon stretching is very small.

Several difficulties limit the range of conditions suitable to flow orien-
tation measurements. At lower temperatures the longer relaxation time
may not permit essentially complete recovery of the orientation during
the brief period when the filament is still hot. Higher temperatures and/or
low extrusion rates allow the filament to stretch under its own weight.
These factors, plus uncertainties in the temperature correction, and the
presence of surface roughness in some instances, render the flow orienta-
tion measurements less reliable than the extrusion rate data.

The polystyrene used in most of this work was the same polymer used
in the volume-temperature-time studies reported by Spencer and Boyer
(20). It was an unfractionated material having a weight-average (light
scattering) molecular weight of 360,000. A few measurements were made
also using another unfractionated polystyrene of weight-average molecu-
lar weight 162,000.

THEORETICAL CONSIDERATIONS

It is assumed that in simple shear the material being investigated is characterized by a relationship

$$D = F(\tau), \tag{1}$$

where D is the rate of shear and τ is the shearing stress. In the case of capillary flow the additional assumptions are made that (1) the flow is laminar, and (2) the pressure is uniform over a cross-section normal to the axis of the capillary. These lead to the relationships

$$D = - dv/dr, \tag{5}$$

$$(\tau) = \tfrac{1}{2}gr, \tag{6}$$

where v is the velocity of flow at a distance r from the axis and g is the pressure gradient along the axis. From this it may be shown (4) that the volume velocity of flow through a cross-section is given by

$$Q = \int_0^R \pi r^2 F(\tfrac{1}{2}gr)dr, \tag{7}$$

where R is the radius of the capillary.

Having made observations of the dependence of the volume velocity Q on the pressure gradient g it is possible to determine the function of Eq. (1) from the relationship

$$F(\tfrac{1}{2}gR) = \frac{1}{\pi R^3} \left(g \frac{dQ}{dg} + 3Q \right). \tag{8}$$

For our purposes this is more conveniently written in the form

$$\eta_0 F(\tau_\omega) = \tau_\omega \frac{d}{d\tau_\omega} \left(\frac{\eta_0 Q}{\pi R^3} \right) + 3 \left(\frac{\eta_0 Q}{\pi R^3} \right), \tag{9}$$

where η_0 is the limiting viscosity at zero shearing stress and τ_ω is the shearing stress at the wall of the capillary.

An analogous expression has been developed by the authors for the case of flow orientation. The variable considered is the relative length, $\alpha = L/L_0$, where L is the stretched, and L_0 the unstretched, length in the direction of the shearing stress. A function relating the relative length and the shearing stress is now assumed as

$$\alpha = E(\tau). \tag{10}$$

Inasmuch as the shearing stress varies over the cross-section in capillary flow, some sort of average relative length is determined by our measure-

ments. It is assumed that this is a volume average, thus

$$\bar{\alpha} = \frac{1}{Q} \int_0^R 2\pi r v E(\tfrac{1}{2}gr) dr. \tag{11}$$

Having determined the dependence of both $\bar{\alpha}$ and Q upon the pressure gradient, the elasticity function of Eq. (10) may be obtained from the relationship

$$E(\tfrac{1}{2}gR) = \omega + \tfrac{1}{2} \cdot \frac{d\omega}{dx}, \tag{12}$$

where

$$\omega = \bar{\alpha} + 1/[3 + (dy/dx)] \frac{d\bar{\alpha}}{dx}$$

and

$$y = \log_e Q,$$
$$x = \log_e g.$$

Combining these, the following equation is obtained:

$$E(\tau_\omega) = \bar{\alpha} + \frac{1}{2}\left[\frac{\left(5 + \dfrac{dy}{dx}\right)}{\left(3 + \dfrac{dy}{dx}\right)} - \frac{\dfrac{d^2y}{dx^2}}{\left(3 + \dfrac{dy}{dx}\right)^2} \right] \frac{d\bar{\alpha}}{dx}$$
$$+ \frac{1}{2\left(3 + \dfrac{dy}{dx}\right)} \cdot \frac{d^2\bar{\alpha}}{dx^2}. \tag{13}$$

Details of the derivation will be found in the appendix at the end of this paper.

Discussion

1. Flow

The raw data are obtained in the form of corresponding values of the mass rate of extrusion and the applied pressure, at each temperature and for each capillary employed. These are readily converted into values of the volume velocity (cm.³-sec.⁻¹) and the shearing stress at the capillary wall (dyne-cm.⁻²). Inasmuch as polystyrene is a Newtonian liquid under low shearing stresses, a region of some practical interest, it is desirable to be able to compute the Newtonian viscosity (limiting viscosity at zero shearing stress) from these data. In the region of Newtonian behavior Poiseuille's law will be obeyed, from whence we can write

$$\frac{1}{4\eta_0} = \frac{Q}{\pi R^3 \tau_\omega}. \tag{14}$$

The problem is now that of computing values of the right-hand quantity and extrapolating to obtain the value at zero shearing stress. It was found empirically that this extrapolation was facilitated by plotting $\log \dfrac{Q}{\pi R^3 \tau_\omega}$ against τ_ω, in which manner straight lines were obtained, in most cases, up to about $\tau_\omega = 9 \times 10^5$ dyne-cm^{-2}. The linearity of the plot made it an easy matter to determine the intercept at zero shearing stress, from whence the Newtonian viscosity could be calculated by Eq. (14). This type of plot is illustrated in Fig. 1, the data having been obtained at 225°C., using capillary No. 8.
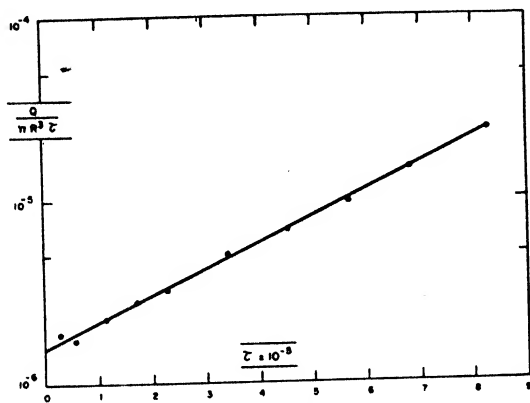

FIG. 1. Method of plotting capillary flow rate data for extrapolation to zero shearing stress.

All of the flow data were handled in this way and Newtonian viscosities computed at each temperature, with results as listed in Table II. In Fig. 2 this information is presented in the usual fashion, with $\log \eta_0$ as ordinate and the reciprocal of the absolute temperature as abscissa. Fig. 2 also shows the Newtonian viscosities at 175°, 200° and 225°C. of a polystyrene of molecular weight 162,000, determined using capillary No. 8. It will be noted that neither curve is linear, both being convex toward the reciprocal temperature axis. This is in agreement with the observations of Fox and Flory (10), who reported a similar type of behavior. They gave a value of the apparent activation energy at 217°C. of 22 kcal., which may be compared with a value of 22.9 kcal. at the same temperature, calculated from the upper curve of Fig. 2. However, their curve rises a little more rapidly than that of Fig. 2 as the temperature is lowered.

Some interesting speculations as to the reasons for this curvature may be made on the basis of Eyring's theory of the viscosity of liquids (11).

TABLE II

Newtonian Viscosities of Polystyrene
(Mol. wt. = 360,000)

Temperature	η_0 Poises		
	Capillary No. 1	7	8
°C.			
165.0	9.26×10^6	—	—
175.0	2.78×10^6	—	2.98×10^6
180.5	—	3.84×10^6	—
200.0	4.39×10^5	—	6.41×10^5
202.4	—	7.95×10^5	—
219.7	—	3.38×10^5	—
225.0	1.85×10^5	—	1.62×10^5
250.0	—	6.25×10^4	5.21×10^4
253.0	—	7.14×10^4	—

Eyring has found that, in the case of small molecules, the activation energy of viscous flow is a certain fraction of the energy of vaporization. He has further suggested that, for polymers, the activation energy of viscous flow is the same fraction of the energy of vaporization per mole
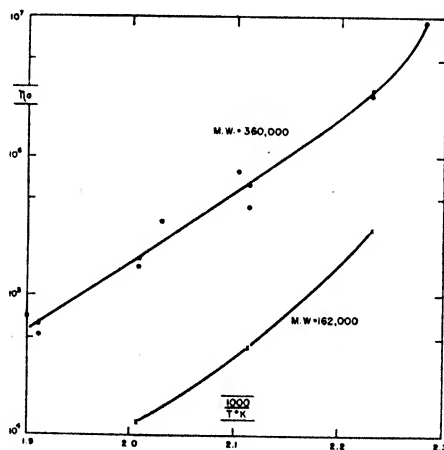

FIG. 2. Dependence of Newtonian viscosity (limiting viscosity as shearing stress approaches zero) of polystyrene upon temperature.

of the kinetic segments which act as units in the flow process. It is well known that the energy of vaporization varies with temperature, and this effect is in the right direction to account for at least part of the curvature noted in Fig. 2 and in the work of Fox and Flory. However, preliminary

calculations would seem to indicate that this variation of the energy of vaporization cannot possibly give rise to the amount of curvature actually observed. This leads to the conclusion, if the Eyring picture of viscosity is maintained, that the segment length must be increasing as the temperature is lowered. Detailed analysis of this effect, however, must await publication of more extensive viscosity-temperature data.

The Newtonian viscosities having been determined, the data were reduced to a common basis by plotting $\log \frac{\eta_0 Q}{\pi R^3 \tau}$ against τ. This procedure revealed the unexpected fact that very nearly all of the effect of temperature upon flow rate was due to the temperature-dependence of the Newtonian viscosity. Thus, within the limits of experimental error, it was not possible to distinguish between curves obtained at 165°C. and at 250°C. All of the flow rate data obtained on the 360,000 mol. wt. polystyrene, using capillaries 1, 7 and 8, are plotted in this manner in Fig. 3. It may be seen that the points are fitted reasonably well
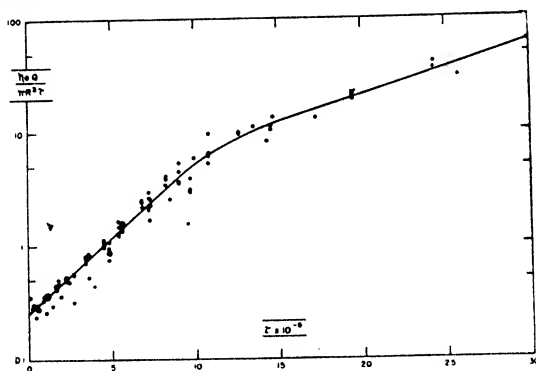

FIG. 3. Dependence of the capillary flow rate of 360,000 molecular weight polystyrene upon the shearing stress at the capillary wall. This mode of representation essentially eliminates the effect of temperature.

at the extremes by straight lines, with perhaps an intermediate curved region. The linearity of the upper portion of the curve is not as well defined as the lower, there being fewer data in this region. A certain amount of scatter is present, but no systematic trend away from the curve was noted, either with variations in temperature or capillary dimensions. The equation of the straight line in the lower shearing stress region is

$$\frac{\eta_0 Q}{\pi R^3 \tau} = 0.25 e^{3.08 \tau \times 10^{-4}} \qquad (15)$$

and that in the higher shearing stress region is

$$\frac{\eta_0 Q}{\pi R^3 \tau} = 2.5 e^{1.07\tau \times 10^{-4}}.\qquad(16)$$

The question naturally arises at this point as to the effect of other variables known to influence the viscosity. That is, will changes in molecular weight or solvent concentration alter only the Newtonian viscosity, or will they also change the curve of Fig. 3? The authors have as yet only a few data on the influence of solvent concentration, but a little can be said as to the effect of molecular weight. The flow data obtained with the 162,000 mol. wt. polystyrene are plotted in Fig. 4 in terms of
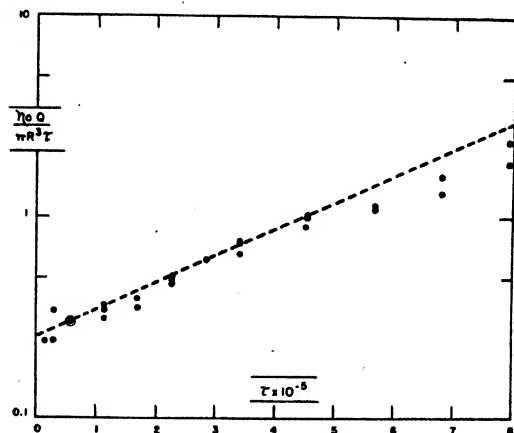

FIG. 4. Dependence of the capillary flow rate of 162,000 molecular weight polystyrene upon the shearing stress at the capillary wall (circled points). The dotted line represents the curve of Fig. 3 (360,000 molecular weight polystyrene) for comparison.

the same variables as Fig. 3, the curve of Fig. 3 being shown for comparison. The agreement between the two polymers is good at low shearing stresses, with an indication that the point of departure from the straight line may have been shifted to a lower value of shearing stress by the decrease in molecular weight. A few other data were obtained on polystyrene fractions covering a wide range of molecular weights, but the only conclusion that can safely be reached at present is that, while molecular weight may possibly influence the curve of Fig. 3, the effect is probably not too large.

Eq. (9) of the previous section was applied to the curve of Fig. 3 to give the relationship between rate of shear and shearing stress. This is shown in Fig. 5 as the solid curve. The circled points, which fit the curve

fairly well, were calculated from the following empirical equation,

$$\eta_0 D = \tau + 7.404 \times 10^{-13} \tau^{3.268}. \tag{17}$$

This function is suggested as a reasonably good approximation to the experimentally determined relationship.
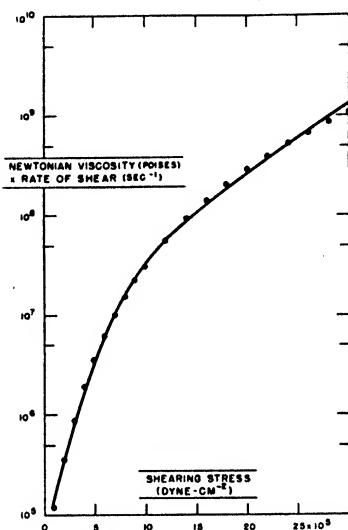

Fig. 5. Relationship between rate of shear and shearing stress for polystyrene in simple shear (solid line). The circled points correspond to values calculated from Eq. (17).

2. *Flow Orientation*

In capillary flow there is a gradient of shearing stress from zero at the axis to a maximum at the wall of the capillary. This gives rise to a force couple acting on each polymer molecule, tending to stretch it out and orient its long axis in the direction of flow. When the material emerges from the capillary the couple no longer acts and the elongated molecules contract to their normal configurations, resulting in a radial expansion of the filament. Thus the diameter of the extruded filament is greater than the diameter of the capillary, and this is taken as a measure of the average amount of orientation during flow, as indicated by Eq. (4). It is realized that this really only measures the elongation of the molecules and provides no information on their rotation during flow.

The theory of rubber elasticity (13) predicts that Hooke's law will be obeyed in shear, leading to the relationship

$$\tau = G(\alpha - 1/\alpha), \tag{18}$$

where $\alpha - 1/\alpha$ is the shearing strain and G is the shearing modulus. This relationship was tested on our data, substituting the shearing stress at the capillary wall for τ and the average relative length $\bar{\alpha}$ for α, and was found to describe the experimental relationship quite well. Rubber elasticity theory predicts, and experiments have confirmed, that the modulus is proportional to the absolute temperature. Our measurements showed no significant variation of the average shearing modulus with temperature, but this is perhaps not too surprising when it is remembered that the temperature range covered extended over only 50°C., and that the experimental uncertainties are relatively large. For these reasons all of the flow orientation data were lumped together and a single line drawn in to represent the average behavior over the interval between 175°C. and 225°C. This is shown in Fig. 6.
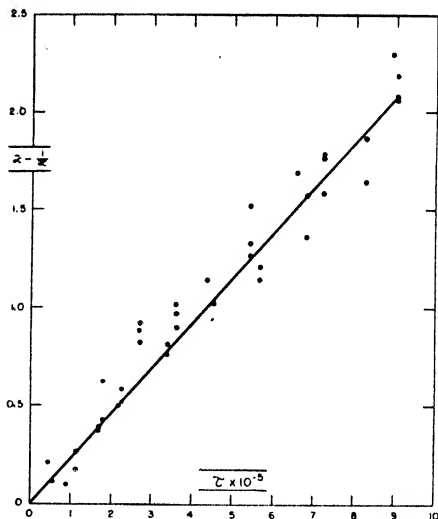

Fig. 6. Relationship between average relative length, due to capillary flow orientation, and shearing stress at the capillary wall (360,000 molecular weight polystyrene).

The curves of Figs. 3 and 6 were combined with Eq. (13) to give the elasticity function of Eq. (10). The shearing stress range covered was from 10^5 to 10^6 dyne-cm.$^{-2}$, and the values obtained were in almost perfect agreement with Eq. (18), the theoretical relationship. The shearing modulus, G, was found to be 3.31×10^5 dyne-cm.$^{-2}$. If Poisson's ratio is 0.5, Young's modulus is 3 times the shearing modulus, giving a value of 9.93×10^5 dyne-cm.$^{-2}$. Mark and Kuhn (17) have derived an expression for the modulus of the uncoiling of an isolated polymer molecule which would give a value of 7.65×10^5 dyne-cm.$^{-2}$ at 200°C. for our material.

It is interesting to note the rough agreement between this value and the experimentally determined one.

In concluding, we wish to consider briefly the application of Eyring's rate of shear-shearing stress relationship to our results. This may be written in the form

$$\eta_0 D = \frac{1}{\beta} \sinh (\beta\tau), \tag{19}$$

where $\beta = \dfrac{\lambda A}{2kT}$, λ is the distance traveled by the flow unit in one "jump," and A is the effective cross-sectional area of the flow unit normal to the direction of flow. Since the right-hand side of this equation contains only a single constant, β, its value may be computed at each point of the curve of Fig. 5. A few values are shown in Table III, where we see that β decreases markedly as the shearing stress increases.

TABLE III

Application of Eyring's Equation to the Experimental Shearing Function

τ (dyne-cm.$^{-2}$)	β (cm.^{2}-dyne^{-1})	$\beta \cdot \bar{\alpha}$
1×10^5	15.5×10^{-6}	17.4×10^{-6}
2	11.4	14.3
3	9.60	13.5
4	8.60	13.4
5	7.84	13.6
10	6.01	16.1
15	4.57	17.0
30	3.00	21.1

Kauzmann and Eyring (16) have stated that even in cases in which flow orientation is an important factor the Eyring relationship should hold, except that the "constants" will be dependent upon the shearing stress. A qualitative picture of the reason for this behavior may be arrived at by considering the nature of the constant β. It is not unreasonable to imagine that, as the polymer molecules become elongated and oriented in the direction of flow, the cross-sectional area of the flow unit, perpendicular to the direction of flow, will decrease. If it were assumed that this area would decrease, on the average, proportionately with the cross-sectional area of the filament, then $\beta \cdot \bar{\alpha}$ should be a constant. This quantity is shown in the last column of Table III, where it may be noted that it is, at least, more nearly constant than β. The tendency seems to be for $\beta \cdot \bar{\alpha}$ to remain relatively constant at low shearing stresses and to increase somewhat as the shearing stress is raised. This subsequent rise in the value of $\beta \cdot \bar{\alpha}$ might be attributed to an increase in λ, the distance between equilibrium positions, as the molecules become relatively extended. That is, as the flow units become elongated the distance between

jumps may also increase. This suggestion must be considered as highly speculative, however. To a rough approximation, the assumption of a decrease in the effective area of the flow units is sufficient to explain the facts.

From this it might be concluded that the observed flow phenomena are in accord with the Eyring theory of viscosity, with the complication that the effective area of the flow units depends upon the amount of flow orientation present. However, this is perhaps not too useful a conclusion from the practical viewpoint. The introduction of flow orientation into the Eyring theory leads to equations for capillary flow which are exceedingly cumbersome, and the authors feel that the approach outlined in the present paper is more straightforward.

ACKNOWLEDGMENTS

SUMMARY

The non-Newtonian capillary flow of a polystyrene of molecular weight 360,000 has been studied over a temperature range of from 165°C. to 250°C. and over a shearing stress range of from 0.2×10^5 to 30×10^5 dyne-cm^{-2}. The relationship between rate of shear and shearing stress was determined and an empirical equation suggested for it. The limiting value of the viscosity as the shearing stress approached zero was calculated and its dependence upon temperature noted. It was observed that essentially all of the temperature dependence of the rate of shear-shearing stress relationship was due to the variation of the zero-shear viscosity with temperature. Molecular orientation during capillary flow was observed and a method was developed for determining the relationship between highly elastic shearing strain and shearing stress from measurements of flow orientation and flow rates. By this method the average value of the shearing modulus over the temperature interval between 175°C. and 225°C. was found to be 3.31×10^5 dyne-cm^{-2}. The application of the Eyring theory of viscosity to the experimental observations was discussed.

APPENDIX

Derivation of Eq. (13)

Two assumptions are made initially: *first,* the existence of a function relating the relative length and the shearing stress,

$$\alpha \equiv \frac{L}{L_0} = E(\tau) = E(\tfrac{1}{2}gr), \tag{A1}$$

and *second*, that the relative length calculated from measurements of the "ballooning" of an extruded filament is the volume average. Thus

$$\bar{\alpha} = \frac{1}{Q} \int_0^R 2\pi r v E(\tfrac{1}{2}gr) dr, \qquad (A2)$$

where Q is the volume velocity through a cross-section of the capillary, R is the radius of the capillary, v is the velocity at a distance r from the central axis of the capillary, and g is the pressure gradient along the axis.

Eq. (A2) is multiplied by Q and differentiated with respect to g, giving

$$\bar{\alpha} \frac{dQ}{dg} + Q \frac{d\bar{\alpha}}{dg} = 2\pi \int_0^R r \left(E \frac{\partial v}{\partial g} + v \frac{\partial E}{\partial g} \right) dr. \qquad (A3)$$

Eq. (A2) is also integrated by parts to give

$$\bar{\alpha} Q = \pi [v E r^2]_0^R - \pi \int_0^R r^2 \left(E \frac{\partial v}{\partial r} + v \frac{\partial E}{\partial r} \right) dr. \qquad (A4)$$

Under the assumption that there is no slipping at the wall of the capillary the first term on the right-hand side of Eq. (A4) vanishes, leaving

$$\bar{\alpha} Q = - \pi \int_0^R r \left(E r \frac{\partial v}{\partial r} + v r \frac{\partial E}{\partial r} \right) dr. \qquad (A5)$$

Multiplying Eq. (A3) by g and Eq. (A5) by 2 and adding gives, as a result,

$$\bar{\alpha} g \frac{dQ}{dg} + Q g \frac{d\bar{\alpha}}{dg} + 2 \bar{\alpha} Q$$
$$= 2\pi \int_0^R r \left[E \left(g \frac{\partial v}{\partial g} - r \frac{\partial v}{\partial r} \right) + v \left(g \frac{\partial E}{\partial g} - r \frac{\partial E}{\partial r} \right) \right] dr. \qquad (A6)$$

Differentiation of Eq. (A1) shows that

$$g \frac{\partial E}{\partial g} = r \frac{\partial E}{\partial r} = \tfrac{1}{2} g r \frac{dE}{d\tau}, \qquad (A7)$$

which reduces (A6) to

$$\bar{\alpha} g \frac{dQ}{dg} + Q g \frac{d\bar{\alpha}}{dg} + 2 \bar{\alpha} Q = 2\pi \int_0^R r E \left(g \frac{\partial v}{\partial g} - r \frac{\partial v}{\partial r} \right) dr. \qquad (A8)$$

If the relationship between rate of shear and shearing stress is defined as

$$D = F(\tau) = F(\tfrac{1}{2} g r), \qquad (A9)$$

then

$$v = \int_r^R F(\tfrac{1}{2} g r) dr. \qquad (A10)$$

From this

$$g \frac{\partial v}{\partial g} = \int_r^R g \frac{\partial F}{\partial g}\, dr \left.\right\}$$
$$r \frac{\partial v}{\partial r} = - rF(\tfrac{1}{2}gr) \quad\left.\right. \tag{A11}$$

giving

$$g \frac{\partial v}{\partial g} - r \frac{\partial v}{\partial r} = rF(\tfrac{1}{2}gr) + \int_r^R g \frac{\partial F}{\partial g}\, dr. \tag{A12}$$

It may be shown from (A9) that

$$g \frac{\partial F}{\partial g} = r \frac{\partial F}{\partial r}, \tag{A13}$$

which converts Eq. (A12) to

$$g \frac{\partial v}{\partial g} - r \frac{\partial v}{\partial r} = rF(\tfrac{1}{2}gr) + \int_r^R r \frac{\partial F}{\partial r}\, dr. \tag{A14}$$

Integrating the last term by parts reduces this to

$$g \frac{\partial v}{\partial g} - r \frac{\partial v}{\partial r} = RF(\tfrac{1}{2}gR) - v. \tag{A15}$$

Eq. (A8) now becomes

$$\bar{\alpha}g \frac{dQ}{dg} + Qg \frac{d\bar{\alpha}}{dg} + 2\bar{\alpha}Q = 2\pi RF(\tfrac{1}{2}gR) \int_0^R rE\,dr - 2\pi \int_0^R rEv\,dr. \tag{A16}$$

The last term is $\bar{\alpha}Q$, by Eq. (A2), thus

$$\bar{\alpha}\left(g \frac{dQ}{dg} + 3Q \right) + Qg \frac{d\bar{\alpha}}{dg} = 2\pi RF(\tfrac{1}{2}gR) \int_0^R rE\,dr. \tag{A17}$$

Substituting Eq. (8) of the main body of the paper, this reduces to

$$\bar{\alpha} + \frac{Qg \dfrac{d\bar{\alpha}}{dg}}{g \dfrac{dQ}{dg} + 3Q} = \frac{2}{R^2} \int_0^R rE\,dr. \tag{A18}$$

Defining the left-hand expression as ω, differentiating with respect to g, and multiplying by g, gives

$$g \frac{d\omega}{dg} = \frac{2}{R^2} \int_0^R rg \frac{\partial E}{\partial g}\, dr. \tag{A19}$$

Integration of the right-hand side of (A18) by parts leads to

$$\omega = E(\tfrac{1}{2}gR) - \frac{1}{R^2} \int_0^R r^2 \frac{\partial E}{\partial r}\, dr. \tag{A20}$$

The sum of (A20) and one-half of (A19) is

$$\omega + \tfrac{1}{2}g\,\frac{d\omega}{dy} = E(\tfrac{1}{2}gR) + \frac{1}{R^2}\int_0^R r\left(g\,\frac{\partial E}{\partial g} - r\,\frac{\partial E}{\partial r}\right)dr \qquad (A21)$$

and with Eq. (A7) this reduces to

$$E(\tfrac{1}{2}gR) = \omega + \tfrac{1}{2}g\,\frac{d\omega}{dg}. \qquad (A22)$$

Substitution of the full expression for ω, together with the substitution $y = \log Q$, $x = \log g$, gives as the final result

$$E(\tfrac{1}{2}gR) = \bar{\alpha} + \frac{1}{2}\left[\frac{\left(5 + \dfrac{dy}{dx}\right)}{\left(3 + \dfrac{dy}{dx}\right)} - \frac{\dfrac{d^2y}{dx^2}}{\left(3 + \dfrac{dy}{dx}\right)^2}\right]\frac{d\bar{\alpha}}{dx}$$
$$+ \frac{1}{2\left(3 + \dfrac{dy}{dx}\right)}\cdot\frac{d^2\bar{\alpha}}{dx^2}. \qquad (A23)$$

Note added Feb. 11, 1948: Dr. Spencer writes that, in connection with the following note of Dienes and Dexter, through oversight the point for 180°C. in Table II was not included in Fig. 2.

References

1. ALFREY, T., AND DOTY, P., *J. Applied Phys.* **16**, 700 (1945).
2. BOYER, R. F., AND SPENCER, R. S., *ibid.* **16**, 594 (1945).
3. BURGERS, J. M., First Report on Viscosity and Plasticity, pp. 5-72. Nordemann, New York, 1939.
4. *Ibid.*, p. 90.
5. DIENES, G. J., *J. Colloid Sci.* **2**, 131 (1947).
6. DILLON, J. H., AND JOHNSTON, N., *J. Applied Phys.* **4**, 225 (1933).
7. EYRING, H., *J. Chem. Phys.* **4**, 283 (1936).
8. FERRY, J. D., *J. Am. Chem. Soc.* **64**, 1330 (1942).
9. FOOTE, N. M., *Ind. Eng. Chem.* **36**, 244 (1944).
10. FOX, T. G., JR., AND FLORY, P. J., Paper presented before the Am. Chem. Soc., Atlantic City, April 15, 1947.
11. GLASSTONE, S., LAIDLER, K. J., AND EYRING, H., Theory of Rate Processes, p. 477, McGraw-Hill, New York, 1941.
12. GREENBLATT, J. H., AND FENSOM, D., *Ind. Eng. Chem.* **39**, 1037 (1947).
13. GUTH, E., JAMES, H. M., AND MARK, H., *Advances in Colloid Sci.* **2**, 253 (1946).
14. HOLT, W. L., AND MCPHERSON, A. T., *J. Research Natl. Bur. Standards* **17**, 657 (1936).
15. JENCKEL, E., AND UEBERREITER, K., *Z. physik. Chem.* **182A**, 361 (1938).
16. KAUZMANN, W., AND EYRING, H., *J. Am. Chem. Soc.* **62**, 3113 (1940).
17. MARK, H., Physical Chemistry of High Polymeric Systems, p. 69. Interscience, New York, 1941.
18. NASON, H. K., *J. Applied Phys.* **16**, 338 (1945).
19. SCHEELE, W., ALFEIS, M., AND FRIEDRICH, I., *Kolloid-Z.* **108**, 44 (1944).

20. SPENCER, R. S., AND BOYER, R. F., *J. Applied Phys.* **17**, 398 (1946).
21. SPENCER, R. S., AND WILLIAMS, J. L., *J. Colloid Sci.* **2**, 117 (1947).
22. TOBOLSKY, A. V., POWELL, R. E., AND EYRING, H., The Chemistry of Large Molecules, Frontiers of Science, Vol. **1**, pp. 125–90, Interscience, New York, 1943.
23. VOGHT, W. W., AND EVANS, R. D., *Ind. Eng. Chem.* **15**, 1015 (1923).
24. WEITH, A. J., TURKINGTON, V. H., AND ALLEN, I., *ibid.* **32**, 1301 (1940).
25. WILEY, F. E., *ibid.* **33**, 1377 (1941).

NOTES ON

"THE VISCOUS FLOW OF MOLTEN POLYSTYRENE"

BY

SPENCER AND DILLON [1]

G. J. Dienes and F. D. Dexter

*From the Development Laboratories of the Bakelite Corporation,
Bound Brook, N. J.*

Received November 12, 1947

Much of the published rheological data on polystyrene is characterized by the large deviation between results from different types of tests. It is, therefore, of interest to consider, in connection with Spencer's and Dillon's paper on the extrusion properties of polystyrene, the correlation between two rheological measurements which are quite different in nature. We had the welcome opportunity of carrying out parallel plate plastometer measurements on the same sample of polystyrene (M.W. by light scattering = 360,000) that Spencer and Dillon studied in detail. It is the purpose of this note to compare extrusion plastometer results with parallel plate plastometer viscosities.

Parallel plate plastometer measurements were carried out according to the techniques and equations described in previous publications (1,2). Polystyrene was found to be a typical viscoelastic material and the absolute viscosity was calculated from the straight line portion of the normalized deformation—time curve. Most measurements were run for about an hour in order to ascertain that the linear portion had been reached. The absolute viscosities are to be compared with the values obtained by Spencer and Dillon by extrapolating to zero stress, *i.e.*, η_0. This comparison is made in Fig. 1, where the viscosities are plotted in the usual $\log \eta$ *vs.* $1/T$ fashion.

Fig. 1 shows that, over the common temperature region, agreement is obtained between the two methods. The $\log \eta$ *vs.* $1/T$ curve is definitely non-linear over the wide temperature range covered. Accordingly, the magnitude of the activation energy for viscous flow depends on the temperature region being considered. Spencer's and Dillon's data give 23

---

[1] Note given in connection with Spencer-Dillon paper, which was presented at the annual meeting of the Society of Rheology, New York City, October 31st–November 1st, 1947.
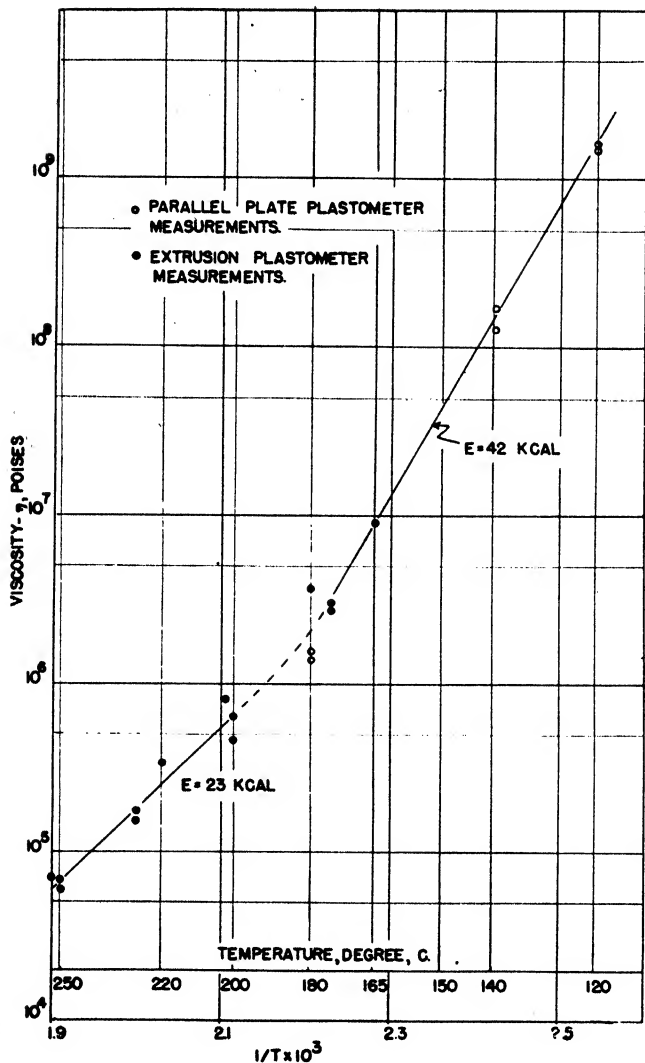
Fig. 1. Correlation of viscosity measurements by extrusion plastometer (extrapolated to zero stress) and parallel plate plastometer.

Kcal. over the temperature range covered by their measurements, while the value computed from parallel plate plastometer results, covering a lower temperature region, is 42 Kcal. The excellent agreement shown over the common temperature region is gratifying for rheological measurements on such a complex viscoelastic material.

REFERENCES

1. DIENES, G. J., AND KLEMM, H. F., *J. Applied Phys.* **17**, 458 (1946).
2. DIENES, G. J., *J. Colloid Sci.* **2**, 131 (1947).
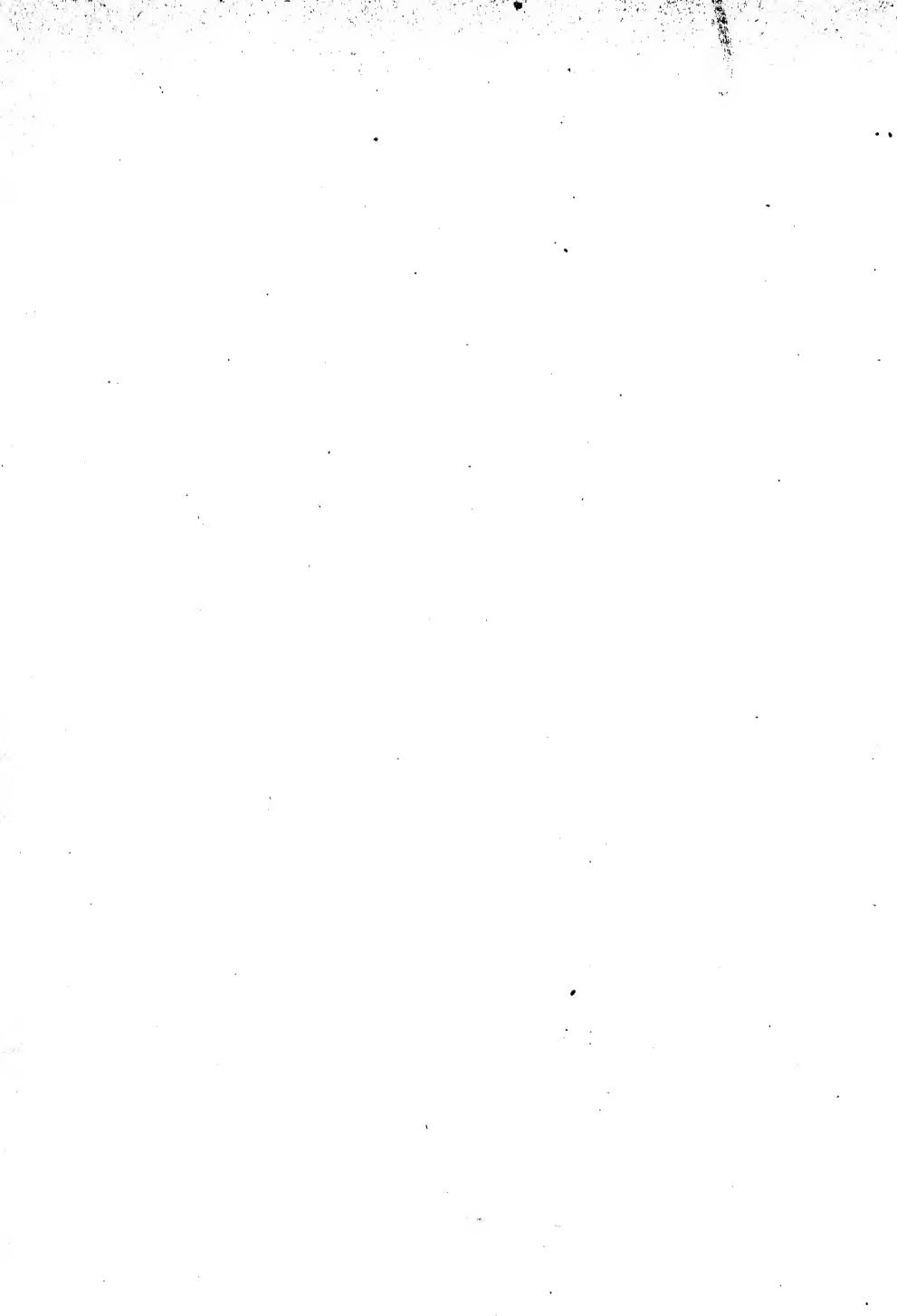
A DIFFUSION ANALYSIS OF REFINED
LIGNIN SULFONIC ACID

E. D. Olleman, D. E. Pennington and D. M. Ritter

From the Pulp Mills Research Project, University of Washington, Seattle, Washington
Received January 16, 1948

INTRODUCTION

The conclusion reached from diffusion analysis of a fermented sulfite waste liquor was that the impurity found in largest amount consists of low molecular weight non-methoxyl-bearing sulfur compounds and some carbohydrate material (1). In this communication are given the results of diffusion analyses on lignin sulfonic acids obtained by a procedure designed to eliminate the non-ligneous material.

The fractionation process shown in Fig. 1 and described in greater detail in the experimental part is a combination of the well-known mixed solvent-precipitation method and a liquid phase extraction process based upon the quinolinium salt precipitation methods of Freudenberg and Sohns (2) and of King, Brauns and Hibbert (3).

EXPERIMENTAL

Acetone Fractionation of Barium Lignin Sulfonate

Crude ammonium lignin sulfonate (1), 90 g., in one liter of solution was concentrated to 300 ml. and de-ashed with a cation exchange resin. The acid of the solution was neutralized with approximately 0.4 equivalent of barium hydroxide in a hot carbonate-free solution. The resulting solution, containing colloidally dispersed barium sulfate, was concentrated to 450 ml. and 10 ml. was removed for analysis. The solution was found to contain 103.1 g. total solids. The barium salt solution was made 30% in acetone by the addition of 200 ml. of acetone, which coagulated the suspended barium sulfate and precipitated a small portion of barium lignin sulfonate. The precipitate was removed by centrifuging, and the cake, after washing with 100 ml. of 30% aqueous acetone, was dried to give fraction Ba-I.

The solution now had a volume of 572 ml. with a solvent consisting of 23 parts of water and 10 parts of acetone. It was diluted with 758 ml. of acetone to give a solution containing 70% of the organic solvent. The
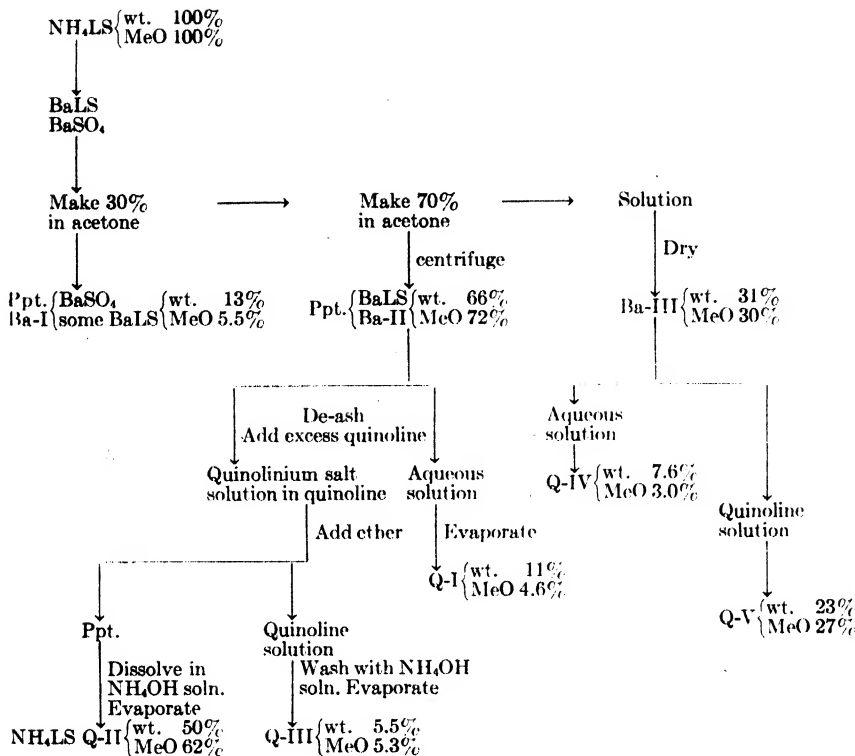
NH₄LS {wt. 100% / MeO 100%}

↓

BaLS
BaSO₄

↓

Make 30% in acetone → Make 70% in acetone → Solution

Ppt. {BaSO₄ / Ba-I some BaLS} {wt. 13% / MeO 5.5%}

centrifuge

Ppt. {BaLS / Ba-II} {wt. 66% / MeO 72%}

Dry → Ba-III {wt. 31% / MeO 30%}

De-ash / Add excess quinoline

Quinolinium salt solution in quinoline   Aqueous solution

Aqueous solution

Q-IV {wt. 7.6% / MeO 3.0%}

Add ether   Evaporate

Q-I {wt. 11% / MeO 4.6%}

Quinoline solution

Q-V {wt. 23% / MeO 27%}

Ppt.   Quinoline solution

Dissolve in NH₄OH soln. Evaporate

NH₄LS Q-II {wt. 50% / MeO 62%}

Wash with NH₄OH soln. Evaporate

Q-III {wt. 5.5% / MeO 5.3%}

Fig. 1.

precipitate formed was separated by centrifuging and dried in the air to give fraction Ba-II. This is the principal barium lignin sulfonate fraction. The material remaining in the aqueous acetone solution, fraction Ba-III. was processed as described later. The material balance is given in Table I,

Fractionation of Lignin Sulfonic Acid by Solvent Extraction of the Quinolinium Salt

Barium lignin sulfonate (Ba-II), 65.2 g., was dissolved in the minimum quantity of water, about 200 ml., de-ashed with a cation exchange column and treated with 250 ml. of quinoline. The precipitate formed dissolved in the excess quinoline and a phase separation occurred on standing. The two layers were separated and the aqueous layer was made alkaline with 250 ml. of concentrated ammonia. The solution was extracted 3 times with 300 ml. portions of ether to remove the quinoline. The aqueous

TABLE I

Material Balance for Acetone Fractionation of Barium Lignin Sulfonate

Fraction	Weight	MeO content	Total MeO
	g.	*Per cent*	*g.*
BaLS starting matl.	103.1	7.47	7.70
Ba-I	13.4	3.25	0.43
Ba-II	68.0	8.18	5.56
Ba-III	30.1	7.11	2.14
Aliquot	2.3	7.11	0.16
	—		—
Total	113.8		8.30
	111%		108%

ammonia solution was evaporated to dryness at 45°C. to give the solid fraction Q-I.

The quinoline solution of the quinolinium lignin sulfonate, which had a volume of 305 ml., was diluted by the addition of 295 ml. of quinoline followed by 257 ml. of diethyl ether. A viscous precipitate was formed which was allowed to settle over night. The supernatant quinoline solution was decanted; the precipitate was washed with 100 ml. of a 30:70 ether-quinoline solution, and the washings added to the mother liquor. The precipitate was extracted with aqueous ammonia to give a milky solution which was washed 3 times with ether to remove the quinoline. The ammoniacal solution was evaporated at 45°C. and dried to constant weight *in vacuo* to give the principal fraction Q-II. The ether-quinoline solution was extracted with concentrated aqueous ammonia until no more amber colored solute was removed from the ether-quinoline solution. This required nearly 3 liters of aqueous solution. After evaporation to dryness at 45°C. a solid was obtained, fraction Q-III. The material balances for the quinoline extraction step are given in Table II.

TABLE II

Material Balance for Quinolinium Salt Fractionation of Acids from Barium Lignin Sulfonate Insoluble in Aqueous Acetone

Fraction	Weight	MeO content	Total MeO
	g.		*g.*
Ba-II	57.0	9.4	5.35
Q-I	8.1	4.0	0.32
Q-II	37.2	11.7	4.35
Q-III	4.1	8.9	0.37
	—		—
Total	49.4		5.04
	87%		94%

Fraction Ba-III, containing those barium salts and other substances soluble in 70% acetone, was carried through the quinolinium salt fractionation outlined above. The barium salt (Ba-III), 82 g., was dissolved in approximately 400 ml. of water and de-ashed with a cation exchange column. Quinoline, 350 ml., was added to the aqueous solution. The quinolinium salt solution in quinoline was separated from the aqueous phase and extracted with ammonia to give the ammonium lignin sulfonate, fraction Q-V. The water-soluble fraction Q-IV was recovered by treatment with aqueous ammonia and removal of quinoline with ether. The material balances for this step are given in Table III. The discrepancies in the methoxyl balance are considered to arise from the difficulty of completely drying the large amounts of hygroscopic material.

TABLE III

Material Balance for Quinolinium Salt Fractionation of Acids from Aqueous Acetone-Soluble Barium Lignin Sulfonate

Fraction	Weight	MeO content	Total MeO
	g.		*g.*
Ba-III	82	7.11	5.8
Q-IV	19.7	3.34	0.66
Q-V	60.7	9.75	5.9
	80.4		6.56

Determination of Diffusion Coefficients

Diffusion coefficients were determined in sintered glass diffusion cells as described in detail in the previous communication (1). As before, the diffusion coefficients were calculated from the integrated form of Fick's law:

$$D = \frac{2.303\,V}{2K\,t} \log \frac{C_o}{C_o - 2C_2}.$$

Potassium chloride, 0.10 N, was used as the reference salt with an assumed integral diffusion coefficient of 1.631 cm.^{2}/day as determined by McBain and Liu (4).

The procedure used for determining the total solids diffused by simple solids determination as described in the previous paper was found to be in error, owing to the accumulation of an ash content during the course of the diffusion. The ash was identified as silica and a correction made for its presence in the solids determination. The ash contents were determined from the residues obtained after analysis for sulfur by dry combustion. The necessity of correcting for the ash content introduces an additional

source of error into the determination of diffusion coefficients based on the diffusion of total solids. The methoxyl determinations were made by the micro Zeisel method and the absorption coefficients were obtained by spectrophotometric measurements on the lignin sulfonic acid absorption band at 2800 Å using a Beckmann quartz spectrophotometer.

Viscosity measurements, upon which calculations of the shape factor are based, were made on fraction Q-II in a precision Ostwald viscometer. This Pyrex glass apparatus had a flow time of 486.5 seconds with 1 N ammonium acetate solution at 25°C., and during its construction and operation the precautions observed were some of those described by Jones and coworkers (5).

Results and Discussion

In Tables IV and V are given the diffusion coefficients obtained for the 2 portions of lignin sulfonic acid obtained by acetone precipitation of the barium salts. It is apparent that the ammonium lignin sulfonate derived from the barium salt insoluble in acetone and representing the bulk of the ligneous material is the higher molecular weight fraction.

Considering the high molecular weight fraction, a comparison of the diffusion coefficients[1] for the transport of total solids, methoxyl, and substances absorbing light at 2800 Å shows an agreement well within the experimental error. A higher diffusion coefficient for the transfer of sulfur indicates the presence of some faster diffusing sulfur-containing material differing from the bulk of the lignin sulfonic acid. The fractional change in methoxyl content in the process of diffusion analysis indicates the residual material to have a slightly higher methoxyl content than the starting material. The converse is true in the case of the sulfur content, and the final material is found to contain less sulfur than was the case in the beginning. Of the multitude of explanations, one which appears logical is that the low molecular weight lignin sulfonic acids, some of which are probably present in this mixture, have higher sulfur contents and lower methoxyl contents than is the case with the high molecular weight acids.

The diffusion coefficients for the low molecular weight material derived from the barium lignin sulfonate soluble in 70% aqueous acetone are given in Table V. The higher diffusion coefficients for sulfur-bearing components indicate that a substantial proportion of sulfur-containing substances has an average weight lower than the ligneous material. In

[1] Comparisons should be made between values for a given interval in each cell. It is not to be expected that average integral diffusion coefficients obtained on a highly polydispersed solute should agree when the determinations are made in cells with different cell constants and therefore at different rates of fractionation. In a given cell, and within a particular interval, diffusion coefficients for a series of parameters should agree if the diffusate is chemically homogeneous in respect to those parameters.

respect to methoxyl content and substances absorbing light at 2800 Å, the diffusion coefficients are very nearly the same and there exists no basis for distinguishing any separate components. The diffusion coefficients based on the transfer of total solids have values between those

TABLE IV

Diffusion Analysis of High Molecular Weight Fraction Q-II

Diffusion Coefficients Based on Total Solids Diffusing
Cell 3: Vol. 185 ml.; $K = 0.775$

Time	Cumulative percentage of solids diffused	C_o	C_2	D
hours		*mg./ml.*	*mg./ml.*	*cm.²/day*
0– 338	13.0	3.743	0.488	0.107
338– 770	26.4	3.255	0.503	0.102
770–1178	36.2	2.752	0.365	0.090
1178–1802	47.0	2.387	0.405	0.079
1802–2713	58.8	1.982	0.445	0.078

Cell 4: Vol. 174 ml.; $K = 0.623$

0– 338	11.3	4.065	0.465	0.108
338– 770	24.0	3.600	0.514	0.109
770–1178	33.3	3.086	0.375	0.096
1178–1802	43.8	2.711	0.433	0.086
1802–2713	56.5	2.278	0.514	0.092

Diffusion Coefficients Based on Transfer of Material
Absorbing Light at 280 mμ
Cell 3: Vol. 185 ml.; $K = 0.775$

Time	k Spect. ext.	Cumulative percentage E diffused	C_o	C_2	D
hours			E	E	*cm.²/day*
0– 338	14.5	13.2	53.2	7.05	0.108
338– 770	13.9	26.4	46.2	7.00	0.100
770–1178	14.7	36.4	39.2	5.36	0.093
1178–1802	15.4	48.2	33.8	6.23	0.088
1802–2713	14.0	59.8	27.6	6.23	0.079

Cell 4: Vol. 174 ml.; $K = 0.623$

0– 338	14.8	11.3	60.3	6.87	0.107
338– 770	13.7	23.1	53.4	7.04	0.099
770–1178	15.5	32.8	46.4	5.83	0.090
1178–1802	15.9	44.2	40.5	6.87	0.093
1802–2713	13.7	55.8	33.7	7.04	0.083

TABLE IV—*Continued*

Diffusion Coefficients of Methoxyl-Bearing Components
Cell 3: Vol. 185 ml.; $K = 0.775$

Time	Methoxyl in diffusate	Cumulative percentage methoxyl diffused	C_o	C_2	D
hours	*Per cent*		*mg./ml.*	*mg./ml.*	*cm.²/day*
0– 338	11.8	12.9	0.448	0.058	0.105
338– 770	11.9	26.3	0.391	0.060	0.101
770–1178	12.1	36.1	0.331	0.044	0.092
1178–1802	12.1	47.0	0.286	0.049	0.080
1802–2713	12.1	59.0	0.237	0.054	0.079
Final	12.1				

Cell 4: Vol. 174. ml; $K = 0.623$

0– 338	11.8	11.2	0.492	0.055	0.105
338– 770	11.9	23.8	0.437	0.062	0.107
770–1178	12.0	33.0	0.375	0.045	0.094
1178–1802	12.5	43.8	0.331	0.054	0.089
1802–2713	11.9	56.3	0.276	0.061	0.090
Final	12.2				

Diffusion Coefficients of Sulfur-Bearing Components
Cell 3: Vol. 185 ml.; $K = 0.775$

Time	Sulfur in diffusate	Cumulative percentage sulfur diffused	C_o	C_2	D
hours	*Per cent*		*mg./ml.*	*mg./ml.*	*cm.²/day*
0– 338	8.3	15.2	0.264	0.040	0.129
338– 770	7.25	29.2	0.223	0.037	0.109
770–1178	7.95	40.2	0.187	0.029	0.109
1178–1802	7.26	51.2	0.158	0.029	0.089
1802–2713	6.6, 6.9	62.2	0.128	0.029	0.080
Final	6.5, 6.8				

for methoxyl transfer and those for sulfur diffusion, as might be expected in a chemically inhomogeneous system.

The average integral diffusion coefficients offer no basis for estimating a true molecular weight distribution. From an examination of the values obtained, however, certain qualitative conclusions can be drawn. For the low molecular weight fraction, the assumption that the molecules are spherical will introduce no error any greater than that already caused by the use of an average integral diffusion coefficient for calculating a molecular weight. The Stokes-Sutherland-Einstein (6) equation can therefore be applied directly to the calculation of molecular weight. Using

TABLE V

Diffusion Analysis of Low Molecular Weight Fraction Q-V

Diffusion Coefficients of Total Solids Diffusing
Cell 3: Vol. 185 ml.; $K = 0.775$

Time	Cumulative percentage solids diffusing	C_o	C_2	D
hours		*mg./ml.*	*mg./ml.*	*cm.²/day*
166.3	15.9	5.676	0.900	0.27
289.5	36.0	4.776	1.142	0.27
305	50.4	3.634	0.818	0.23
Final		2.816		

Diffusion Coefficients of Methoxyl-Bearing Components
Cell 3: Vol. 185 ml.; $K = 0.775$

Time	MeO in diffusate	Cumulative percentage MeO	C_o	C_2	D
hours	*Per cent*		*mg./ml.*	*mg./ml.*	*cm.²/day*
166.3	8.7	14.2	0.5905	0.0840	0.23
289.5	9.0	33.2	0.5065	0.1122	0.24
305	9.5	47.8	0.3943	0.0862	0.23
Final	10.5		0.3081		

Cell 4: Vol. 174 ml.; $K = 0.623$

Time	MeO in diffusate	Cumulative percentage MeO	C_o	C_2	D
166.3	8.5	12.9	0.5927	0.0761	0.25
289.5	9.2	31.4	0.5166	0.1096	0.27
305	9.4	45.4	0.4070	0.0836	0.24
Final	10.4		0.3234		

Diffusion Coefficients of Substances Absorbing at 2800 Å
Cell 3: Vol. 185 ml.; $K = 0.775$

Time	k Spect. ext. C_2	Cumulative percentage E diffused	C_o	D
hours			E	*cm.²/day*
166.3	10.28	14.9	68.98	0.25
289.5	13.00	33.8	58.70	0.24
305	9.65	47.7	45.70	0.21
Final	36.05			

Cell 4: Vol. 174 ml.; $K = 0.623$

Time	k Spect. ext. C_2	Cumulative percentage E diffused	C_o	D
166.3	9.53	13.6	70.07	0.27
289.5	12.26	31.2	60.54	0.25
305	9.53	44.6	48.28	0.23
Final	11.11		38.75	

TABLE V—*Continued*

Diffusion Coefficients of Sulfur-Bearing Components

Cell 3: Vol. 185 ml.; $K = 0.775$

Time	Sulfur in diffusate	Cumulative percentage sulfur diffused	C_o	C_2	D
hours	*Per cent*		*mg./ml.*	*mg./ml.*	*cm.²/day*
166.3 ·	8.08	18.2	0.4273	0.0778	0.30
289.5	7.70	40.6	0.3495	0.0956	0.33
305	7.44	56.5	0.2539	0.0674	0.30
Final	6.36		0.1865		

the value taken from Table V for the diffusion of methoxyl-bearing components in the third interval, 0.24 cm.²/day, a molecular weight of 1500 is obtained. The small degree of fractionation which appears to occur during successive intervals of diffusion with this low molecular weight material indicates that this ligneous material is rather uniform in molecular size. Therefore, the molecular weight value calculated here is probably a satisfactory average value. Using an average integral diffusion coefficient for the last interval for the diffusion of the higher molecular weight substances ($D_{av.} = 0.080$ cm.²/day), the molecular weight calculated by assuming a spherical particle is found to be very high, and some knowledge of the shape factor is necessary before even these little-applicable data can be used for calculation of apparent average molecular weights.

Of the many methods proposed for estimating the shape factor for dissymmetric macromolecules, that developed by Polson from the Kuhn equation appears most suitable for use with the lignin sulfonic acids (7). The equation based upon relative viscosity measurements is:

$$\eta/\eta_o = 1 + 4.0G + 0.098G \ (b/a)^2$$

where G is the partial specific volume divided by 100; b and a are the major and minor axes, respectively, of the prolate spheroid assumed as the molecule. In Table VI are given the viscosity and density data upon which are based the use of the Polson equation for ammonium lignin sulfonate. Ammonium acetate solution was used as the solvent instead of ammonium carbonate because the ionic strengths of the two solutions were thought to be similar and ammonium acetate is much more stable. Because the viscosity data deviated from the Arrhenius equation it was necessary to determine the quantity ln α at infinite dilution. This was done by transforming the Arrhenius equation to the form:

$$\ln \alpha = \frac{\ln \eta/\eta_o}{c}$$

TABLE VI

Viscosity and Density Data on Ammonium Lignin Sulfonate in
1 N Ammonium Acetate Solution

Vol.-%[a] NH₄LS	n/n_o[b]	$\ln \alpha$[c]	$V_s - V_o$[d]
6.73	1.420	0.0521	0.0462
4.16	1.220	0.0475	0.0280
3.32	1.166	0.0462	0.0218
1.66	1.075	0.0435	
1.04	1.045	0.0423	

$\ln \alpha_{c=0} = 0.0405$; partial specific volume, $V_1 = 0.67$.

[a] Weight of solute in 100 ml. of solution $= C$.

[b] Relative viscosity.

[c] $\ln \alpha = \dfrac{\ln \eta - \ln \eta_o}{c}$.

[d] Volume of solute in 1 ml. solution = volume of solution − volume of solvent.

The linear relation between $\ln \alpha$ and the concentration was extrapolated to infinite dilution to obtain the value used for the application of the Polson equation. The shape factor calculated from these data is 4.6, and the frictional coefficient calculated by the use of this value in the Perrin equation (8), gives $\dfrac{f}{f_o} = 1.22$. The form of the Stokes-Sutherland-Einstein equation for a prolate spheroid (9) is:

$$M = \frac{K(f_o/f)^3}{D^3 V} \text{ where } K = \frac{(RT)^3}{162\pi^2\eta^3 N^2}.$$

D = the diffusion coefficient, V = the partial specific volume, η = the viscosity of the solvent, N = Avogadro's number, f_o/f = the frictional coefficient ratio. When D is in cm.²/day, $K = 13.5$. Using this equation, there is calculated for the last diffusion interval an apparent average molecular weight of 21,000. Considering that one-half the material has already diffused and that the diffusion coefficients are beginning to level off, this value is perhaps a reasonable average for the high molecular weight fraction.

Apparent molecular weights calculated in this way certainly offer no basis for estimating a true molecular weight distribution. An apparent integral distribution curve and the differential distribution derived from it are artifacts produced by averaging the simultaneous diffusion of all the molecular species present. For that reason those curves are not reproduced here. It is obvious, however, that the distribution of molecular weights is very broad and that the lignin sulfonic acids used in this study consist of 2 fractions, each present in rather large amount, and widely

different in molecular weight. The apparent molecular weight distribution for the high molecular weight fraction and the course of the diffusion indicate that this fraction contains a rather large proportion of the low molecular weight material. This result is predicted by the thermodynamic theory of high polymer solutions for solvent fractionation of molecular species in a single step from a concentrated solution (10). It can be taken as evidence that separation by solvent precipitation should be applied with caution to molecular fractionation of lignin sulfonic acids.

SUMMARY

The ligneous material present in sulfite waste liquor is estimated to be composed of lignin sulfonic acids with rather uniform chemical composition of which about 30–40% have molecular weights averaging 1,500–2,000, and 50–60% have an average molecular weight in the neighborhood of 20,000.

REFERENCES

1. PENNINGTON AND RITTER, *J. Am. Chem. Soc.* **69**, 665 (1947).
2. FREUDENBERG AND SOHNS, *Ber.* **66**, 262 (1947).
3. KING, BRAUNS AND HIBBERT, *Can. J. Research* **13B**, 88 (1935).
4. McBAIN AND LIU, *J. Am. Chem. Soc.* **53**, 59 (1931). This value based on the data of Cohen and Bruins differs from the value 1.58 cm.^{2}/day based on calculations from the differential diffusion coefficients of Harned and French, *Ann. N.Y. Acad. Sci.* [5] **46**, 280 (1945) as shown by Gordon, *ibid.* [5] **46**, 285 (1945).
5. JONES AND DOLE, *J. Am. Chem. Soc.* **51**, 2950 (1929).
   JONES AND TALLEY, *ibid.* **55**, 624 (1933).
6. SUTHERLAND, *Phil. Mag.* [6] **9**, 781 (1905).
   EINSTEIN, *Z. Elektrochem.* **14**, 235 (1908).
7. POLSON, *Kolloid-Z.* **88**, 51 (1939).
8. PERRIN, *J. phys. radium* **7**, 1 (1936).
9. SVEDBERG, *Proc. Roy. Soc. (London)* **B127**, 1 (1939).
10. SCOTT, *J. Chem. Phys.* **13**, 172, 188 (1945).

PORE VOLUME OF ELECTROLYTICALLY PRODUCED
PROTECTIVE COATINGS ON ALUMINUM [1]

K. Huber

(Experimental Collaboration of A. Gaugler; Translation by J. J. Bikerman)

From the Institute of Inorganic Chemistry, The University, Berne, Switzerland

Received January 19, 1948

It is well known that aluminum electrodes become coated with a protective film, consisting mainly of alumina, when placed in suitable baths and treated with alternating current or anodically with direct current. In the industry these films are produced on a large scale to prevent corrosion and seizing (Alumilite and Eloxal processes). Sulfuric acid is the chief electrolyte used, oxalic acid being a second choice.

I

The pore structure of these films is of great scientific and industrial interest. In isolated films the pore structure can be recognized with the unaided eye by looking through them at a suitable source of illumination. It appears more clearly as a fine silky shimmer on cross-sections of the film. Careful microscopic investigations were carried out by Rummel (1) and Baumann (2). Cross-sections of the film show that the pores run parallel to one another and normally to the plane of the film. The pores of coatings produced in oxalic acid are larger than those from sulfuric acid. Direct current produces larger pores than alternating current. Finally, the pore structure becomes coarser with increasing voltage, current density, and bath concentration. The diameter of even the largest pores reaches only a fraction of a micron. Thus, it is impossible to determine the dimensions of a pore using a light microscope as they are below the limit of resolution. However, Rummel succeeded in estimating the pore diameter. The distance between two pores in a definite film was approximately 0.5 μ. From this he calculated the number of pores to be $4 \times 10^6/\text{mm}^2$. From the water adsorption of the film, which corresponded to a total pore volume of 4%, from the number of pores, and from the thickness of the layer, he computed the diameter of a single pore, assumed to be a cylinder with circular cross-section, to be about 0.1 μ. A protective film was sepa-

---

[1] Sixth paper of the series On Chemistry and Structure of Anodically Produced Precipitates and Protective Coatings. For 5th paper see (8).

rated from the metal, soaked in electrolyte, and an electric current sent through it normally to the plane of the film. From the resistance offered to this current, the number of pores, and the conductivity of the electrolyte, he calculated the pore diameter to be 0.075 μ.

II

The resolving power of the electron microscope would have been sufficient for a more exact analysis of the pore structure but another difficulty is encountered here. The electron beam is only able to penetrate films 100–1000 times as thin as the films used in industry.
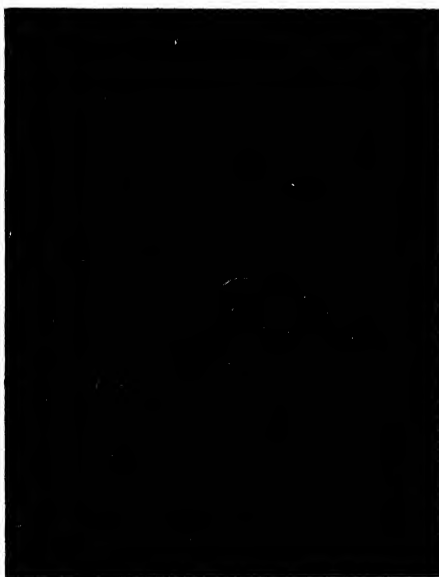
FIG. 1. Magnification 28,000 ×. Thin coating viewed normally to the plane of the coating. Preparation—Al 99.99%, single crystal, ground along 110, electrolytically polished; M H$_3$PO$_4$, 72 volts direct current, 2 min., room temperature. Loosening of the coating in perchloric acid bath for electrolytic polishing.

Fischer and Kurz (3) avoided this difficulty by using sufficiently *thin and transparent layers* obtained by a very short electrolytic oxidation (for a fraction of a minute to a few minutes). They concluded from the variation of the voltage with time, at a constant current density, that films prepared in this manner have structural features essentially identical with those of thicker films. The excellent electron photomicrographs show, in agreement with the results obtained with a light microscope,

that oxalic acid baths give rise to larger pores than sulfuric acid baths but, contrary to the microscopic evidence, that alternating current produces larger pores than direct current. The diameter of the pores varies according to the conditions of formation of the layer from about 0.1 to 0.02 μ. From the photographs the volume of the pores can be calculated to be about 8% but the authors estimate it to be about 12%, as some pores may be tilted from the normal to the plane of the film.

Our own experiments, conducted according to Fischer and Kurz, confirmed the result that neighboring pores have similar dimensions. Fig. 1 illustrates this. The coating was produced in phosphorous acid, which
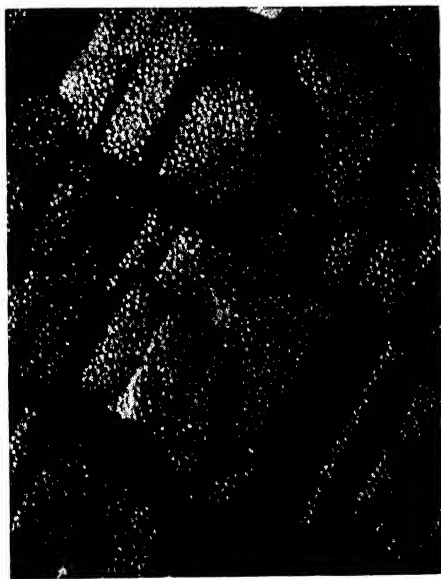
FIG. 2. Magnification 21,000 ×. Thin coating viewed normally to the plane of the coating. Preparation—Al 99.99%, single crystal, ground along 100, etched with HF 40%/HCl conc. (1:2); M H_3PO_3, 72 volts direct current, 2 min., room temperature. Loosening of the coating in a bath for electrolytic polishing.

yielded especially regular pore structures. The experiments confirmed also that the pores, as a rule, are spread at random and appear more crowded and lined up only along flaws of the metal support, such as scratches. The distribution of pores is affected also by the waviness which appears following an unsuccessful electrolytic polishing.

Experiments using single crystals of aluminum ground in definite directions proved that the crystallographic orientation of the metal support does not affect either the distribution or the dimensions of the

pores. This is clearly seen in Fig. 2 which represents a coating produced on an etched crystal and reveals the cubic etch pattern in addition to the pores.

The coatings described thus far had a thickness roughly corresponding to the pore diameter. They may be compared to a sieve. They give no information on the character of pores in thicker coatings. *Thicker coatings* can be prepared for study by comminution, elimination of coarse particles by gravity separation, and spreading on foils. It is always possible to find fragments suitable for observation. Thicker coatings are relatively soft
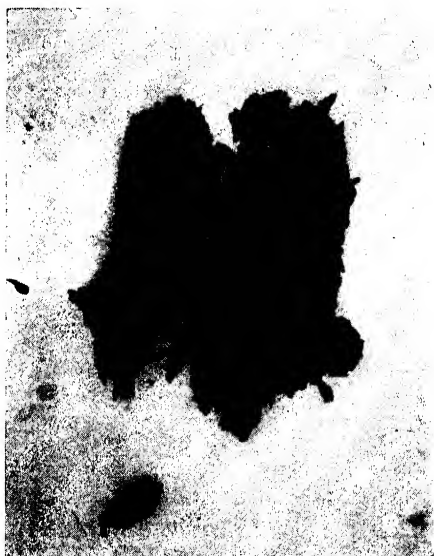
Fig. 3. Magnification 14,000 ×. Fragment of a thicker film. Preparation—Al 99.99%, rolled plate, electrolytically polished; M H_2SO_4, 16 volts direct current, 8 hours, room temperature.

at the outside (*i.e.*, near the electrolyte) and harder at the inside (*i.e.*, near the metal). This may be due to an attack by the electrolyte on the outer layers *via* the pores. Electron microscope pictures reveal this in the following manner. When the outer, then the middle, and finally the inner layers of a coating are scraped off and separately collected and set up, the fragments of the outer layer show a definite structure of pores and fibers (see Fig. 3), whereas the middle layer has only a trace of structure and the inner layer yields dense smithers having no visible structure.

The fibers are bent as a result of the mechanical stress during the rupture of the coating. Pictures which are better in this respect are

obtained by making a polystyrene replica of a rupture surface normal to the plane of the coating, evaporating silica onto this replica, and casting a gold shadow on it. Fig. 4 shows the separated replica. The strictly straight and parallel direction of the pores is striking. It corresponds to the schematic outline given by Rummel (1).

Summarizing, it may be stated that observations made with the light microscope and electron microscope yielded some information on the dimensions and the distribution of pores. However, the magnitude of the

Fig. 4. Magnification 14,000 ×. Replica of a rupture surface across a thicker film. Preparation—Al 99.99%, rolled plate, electrolytically polished; saturated oxalic acid, 72 volts direct current, 8 days, room temperature. Film thickness 0.8 mm.!

total pore volume remains uncertain. In addition to the values given by Rummel (4%) and by Fischer and Kurz (8 or 12%), Baumann's determination should be mentioned. Baumann's value, obtained from weight, thickness and chemical composition, was about 30%. Above all, the *relation between the degree of porosity and the thickness of the coating* remains unknown. It is attempted in the following to reach a solution of this problem by a study of the coatings in *polarized light.*

III

Several earlier investigators proved that these coatings are doubly refracting. More detailed and more recent studies are those by Lacombe

(4). However, X-ray and electron diffraction photographs of the coatings reveal only weak lines of a highly dispersed cubic γ-aluminum oxide (or γ'-aluminum oxide). Chemical analysis shows that amorphous hydroxide and a hydroxy salt containing the anion of the electrolyte are present in the oxide (5). At any rate, the coating certainly consists of a material which is not doubly refracting.

According to Wiener (6), a "mixed body," consisting of parallel cylinders of an isotropic material penetrating through the whole thickness of another isotropic material, behaves optically as a uniaxial positive crystal if the structure elements are smaller than the wave length of light used. In particular,

$$n_\epsilon{}^2 - n_\omega{}^2 = \frac{\delta_1 \delta_2 (n_1{}^2 - n_2{}^2)^2}{(\delta_1 + 1)n_2{}^2 + \delta_2 n_1{}^2}; \; \delta_1 + \delta_2 = 1.$$

The double refraction of the body, $n_\epsilon - n_\omega$, depends on the volume fractions δ_1 and δ_2 of the components, and on their refractive indices n_1 and n_2. The equation shows, moreover, that the double refraction of the body is smaller the smaller the absolute value of the difference $n_1 - n_2$, and becomes zero when $n_1 = n_2$.

When a coating is embedded successively in liquids having different refractive indices and the value of the double refraction observed is plotted against the refractive index of the liquid, a curve is obtained which agrees with Wiener's equation. This proves that the double refraction of the coating is due to the latter's disperse structure, *i.e.*, is an instance of *"form double refraction"* (7).

Electron photomicrographs, especially Figs. 1 and 4, show that the structure of the coatings corresponds pretty well with that of an ideal "columnar mixed body," the pores representing the cylinders (the "columns"). (The coatings simulate the ideal behavior also in that they do not swell and are not affected by the imbibed liquid, at least as long as the experiment lasts. However, this is of no importance for the following because the coatings were studied dry, "embedded in air," except when n_1 was determined.) Therefore, an attempted *application of Wiener's theory to the structure of the coatings* appeared promising.

The n values of the above equation must be determined by experiment to make the calculation of the volume fractions δ_1 and δ_2 possible. The refractive index, n_1, of the solid substance of the coating is given by the minimum of the above-mentioned curve for double refraction. It is about 1.65. Since the double refraction becomes zero simultaneously for the outer and the inner layers of the coatings, the value of n_1 cannot vary much with the thickness of the coatings. The index n_2 for the dry coating is that of air, *i.e.*, 1.00. The determination of the main refractive indices, n_ϵ and n_ω, of the mixture is less easy. The optics of the coatings must be

looked into more carefully. Coatings from oxalic acid baths may serve as an example.

When observed normally to the plane of the layer, the double refraction varies between zero and about 0.0025 according to the crystallographic orientation of the grains of the underlying metal.[2] When observed parallel to the plane of the layer, the double refraction is considerably greater, and the variations of the wave having the higher refractive index occur normally to the plane of the layer. These observations can be expressed in the language of crystal optics as follows. The indicatrix is an elongated ellipsoid of rotation or a triaxial ellipsoid which differs but little from an elongated ellipsoid of rotation. The long axis of the indicatrix (n_ϵ or n_ω) is always perpendicular to the plane of the coating. When the direction of observation is parallel to this plane, the double refraction is not constant in a definite coating. It increases with the distance from the metal boundary; see the example shown in Fig. 5.
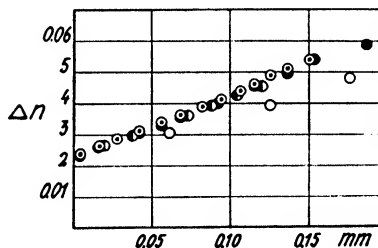
FIG. 5. Dependence of the double refraction observed parallel to the plane of the film on the distance from the metal support. Sodium light. Preparation of the film—Al 99.99%, rolled plate, recrystallized, electrolytically polished; 0.8 M oxalic acid, 48 volts direct current, 15.5 hours, room temperature.

Note on the Determination of the Values Plotted in Fig. 5

Isolated coatings usually break under mechanical stress almost exactly normally to the plane of the coating, that is, along the pores. Therefore, it is possible to prepare prismatic fragments whose "refracting edge" is perpendicular to this plane. The quality of the shape can readily be judged, using a binocular microscope. Fig. 6 represents such a fragment from above, i.e., viewed normally to the plane of the coating. Fig. 7 shows the side view of the same fragment at the same magnification in the dry state. The photograph was made in sodium light between crossed nicols, and the photographs in polarized light were combined with one made in natural light to render the outline of the fragment visible.

The upper part of Fig. 8 is an enlarged schematic copy of Fig. 7. It allows computation of the path differences at different spots of the fragments by counting the interference fringes. It was proved by means of white light and Red I that the first visible fringe cor-

---

[2] The coating is uniaxial on cube and octahedron faces of aluminum crystals and biaxial on all other faces. For details see (8).

responded to the first order. The lower part of Fig. 8 is a similar copy of Fig. 6. It allows measurement of the corresponding paths of light. The 4 series of points seen in Fig. 5 belong to the 4 cross-sections marked on Fig. 8.

Wiener's equation contains the difference between the squares of the main refractive indices, as distinct from the difference between the indices which can be determined in the manner specified above. Therefore, the values of the main refractive indices must be known.
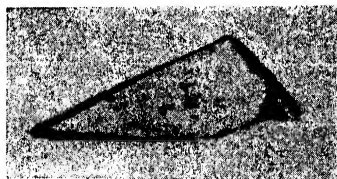
Fig. 6. Prismatic fragment of a coating viewed normally to the plane of the film. For preparation of the coating see legend to Fig. 5.

Fig. 7. Same fragment viewed from the side. "Embedding medium"—air. Sodium light, crossed nicols. For preparation of the coating see legend to Fig. 5.

The customary methods for determining the refractive index of a solid (use of refractometers, immersion method, and the Becke line test) are out of the question because they necessitate a contact between the sample and a liquid. This contact would affect the optical properties of the sample. The coatings are not uniform enough for an interferometric measurement.

A crude determination was achieved by a simple procedure. A beam of light was narrowed by a diaphragm and directed against the surface of a cross-section in such a manner that it was parallel to the plane of the coating but formed a definite angle with the normal to the cross-section. Since the coatings are somewhat turbid, the refracted ray could be followed for some length in the coating by means of a microscope. The angle of incidence and the angle of refraction yielded a medium value for the refractive index. Use of polarized light was deemed unnecessary since the error of these measurements is of the same order of magnitude as the double refraction. The measurement yielded values between 1.4 and 1.5. The correct value presumably is nearer 1.5. This value was used for constructing the paths shown in Fig. 8 but, in this instance, even a considerable error would not be important.

To take account of the uncertainty of the absolute value of the main refractive indices of the mixture, the pore volume was computed for both
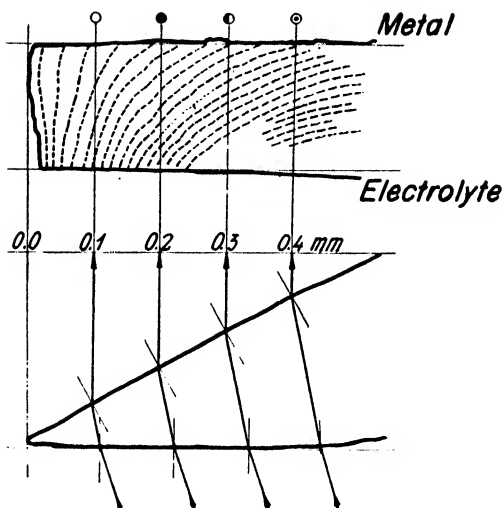
FIG. 8. Enlarged copy of Figs. 6 and 7 for determining the
path difference and direction of the ray.

$n_\omega = 1.4$ and $n_\omega = 1.5$. Consequently, the following values were used for calculation:

n_1 (refractive index of the solid part of the coating)....................1.65

n_2 (refractive index of the "embedding medium," *i.e.*, air)..............1.00

n_ω (refractive index of the sample for the ordinary ray).................1.40 or 1.50

$n_\epsilon - n_\omega$ (double refraction of the sample) near the metal side 0.02

$n_\epsilon - n_\omega$ (double refraction of the sample) near the electrolyte side 0.06

The calculation yields *4.3% or 4.4% for the pore volume of the coating near the metal side* and *15.5% or 16.9% near the electrolyte side.* Clearly, these figures are confined within the range of the expected values.

Note on the Calculation

Solution of Wiener's equation yields two roots. One is meaningful from the physico-chemical viewpoint, as the other would make the pore volume considerably larger than that of the solid.

The results show that the uncertainty of the main refractive indices does not make the calculation procedure fruitless.

Actually the computation is valid only for a uniaxial coating. However, it may also be a good approximation otherwise since electron microscope study shows that the number and the diameter of pores depend but little on the crystallographic orientation of the underlying metal.

ACKNOWLEDGMENT

SUMMARY

Earlier microscope studies and electron photomicrograms taken by the author and other investigators show that protective oxide coatings produced electrolytically on aluminum have a structure closely similar to that of an ideal "columnar mixture" of Wiener. Therefore, an attempt is made to compute the pore volume, basing the computation on Wiener's theory. Determinations of the necessary optical properties of the coatings have been reported.

The calculation shows that the pore volume increases from the inner toward the outer layers of the coatings. In one case investigated, it was about 4% near the metal, and about 16% near the electrolyte side.

REFERENCES

1. RUMMEL, TH., *Z. Physik* **99**, 518 (1936).
2. BAUMANN, W., *Z. Physik* **111**, 708 (1939).
3. FISCHER, H., AND KURZ, F., *Korrosion u. Metallschutz* **18**, 42 (1942); see also KELLER F., AND GEISLER, A., *J. Applied Phys.* **15**, 696 (1944).
4. LACOMBE, P., *Chimie & industrie* **53**, 222 (1945).
5. *Cf.* recently F. LIECHTI AND W. D. TREADWELL, *Helv. Chim. Acta* **30**, 1204 (1947).
6. WIENER, O., *Abhandl. math. phys. Klasse sächs. Akad. Wiss. (Leipzig)* **32**, 507 (1912); AMBRONN-FREY, Das Polarisationsmikroscop, Leipzig, 1926.
7. HUBER, K., *Helv. Chim. Acta* **28**, 1416 (1945).
8. HUBER, K., AND GAUGLER, A., *Experientia* **3**, 277 (1947).

THE EFFECT OF CONCENTRATION AND TEMPERATURE
ON GELATION TIME

Gopal S. Hattiangdi

From the Chemistry Department, University of Southern California, Los Angeles
Received January 21, 1948

Empirical and semi-empirical equations expressing the setting time of
a gel as functions of concentration or temperature have been presented by
various investigators. The present paper presents an equation in which
the variation of setting time with both concentration and temperature is
represented in a single simple equation. The accuracy with which this
relation fits the data for two widely differing types of gels suggests that
the equation itself may be of some significance.

Prakash and Dube (4) suggested the relation

$$t = ac^{-b}, \tag{1}$$

where t is the setting time, c the concentration of the disperse phase, and
a and b are empirical constants. This equation is manifestly closely re-
lated to the suggestion of Hurd and Letteron (2) that the gelation of gels
(of silicic acid in water) behaves kinetically like a chemical reaction of
high order. The constant b is the effective order of the reaction.

The effect of temperature on setting time is generally represented by
an equation of the Arrhenius type:

$$t = Ae^{-Q/RT}, \tag{2}$$

where t is the setting time, T the absolute temperature, and A and Q are
constants. Q is the activation energy of the process being described while
A is related to the entropy difference between the activated and unacti-
vated states. The precise significance of these quantities for a gelating
system is somewhat obscure.

The single equation

$$t = ac^{-Q/RT}, \tag{3}$$

is seen at once to have all the properties of (1) at constant temperature
and of (2) at constant composition. The constant b of (1) has been re-
placed by Q/RT; because in (3) the concentration c replaces the pure
number e of relation (2), a cannot be simply related to A.

For test, it is convenient to write Eq. (3) in logarithmic form:

$$\log t = \log a - \frac{Q}{RT} \log c, \tag{4}$$

$$\log c = \frac{RT}{Q} (\log a - \log t). \tag{4a}$$

From (4a) it is apparent that a plot of $\log c$ against T for equal time of set should give a straight line whose slope is $R/Q(\log a - \log t)$. Figs. 1 and 2 show such plots for the data of Prasad, Hattiangdi and Vishvanath (5)
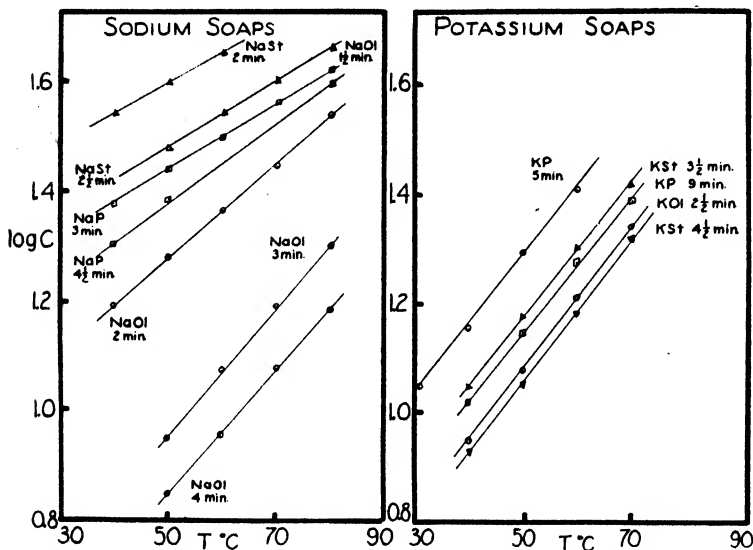
FIG. 1. Concentration-temperature relations for equal setting times for soap gels in pinene (Prasad, Hattiangdi and Vishvanath's data (5)).

on gelation of alkali soaps in pinene and of Hurd and Letteron (2) on silicic acid in water.

Direct combination of Eqs. (1) and (2) leads to the relation

$$t = (aA)^{\frac{1}{2}} c^{-b/2} e^{-Q/2RT}, \tag{5}$$

$$\log t = \tfrac{1}{2}\log aA - \frac{b}{2} \log c - Q/2RT, \tag{5a}$$

$$\log c = -Q/RTb + \frac{1}{b} \log aA - \frac{2}{b} \log t. \tag{5b}$$

According to this relation, log c should give a straight line when plotted against $1/T$. The same data as above were replotted to test Eq. (5b), and the non-linearity obtained shows that Eq. (3) is much the more accurate representation.

The data on gelation of sodium oleate in pinene are sufficiently numerous to apply a more rigorous test of Eq. (3) based on form (4) by plotting log t against $(\log c)/T$, which should yield a straight line of slope Q/R and intercept (at c = unity) equal to log a. The result is shown in Fig. 3, and is seen to be reasonably satisfactory.
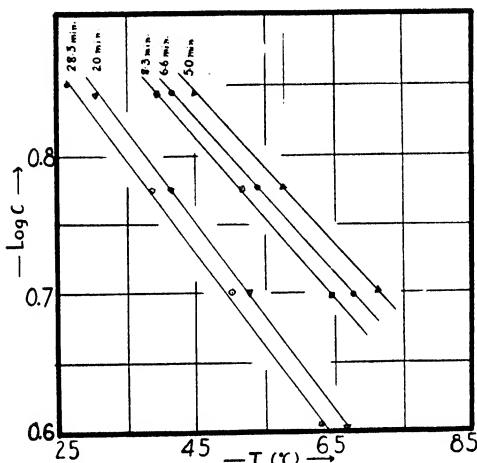
Fig. 2. Concentration-temperature relations for equal setting times for silicic acid gels (Hurd and Letteron's data (2)).

Eq. (3) constitutes a departure from the attempt to consider the gelation process as a simple agglomeration reaction of high order. For if Eq. (3) is interpreted in this fashion, the "order" of the reaction becomes a function of temperature (Q/RT) and the "activation energy" (from a plot of log t vs. $1/T$) becomes a function of concentration $Q \log c$. (Note that since the setting time of soap gels increases with rising temperature, the activation energy is opposite in sign to that of a normal chemical reaction. This has the possible interpretation that only molecules or physical aggregates having less than the average thermal energy are capable of adhering to each other to form a gel structure.)

The sol-gel transformation is believed to involve numerous intermediate states, the most significant of which are (i) the production of a sufficient number of colloidal particles of an adequate size, shape and degree of solvation by gradual growth of the particles initially present in the fresh

sol, and (ii) the knitting up of these colloidal entities into a more or less fibrous structure which envelops the entire dispersion medium.

It is reasonable to suppose that the tendency to form secondary aggregates would decrease with increasing temperature, at least in systems (such as those, for example, discussed by Krishnamurthi (3)) where increasing temperature increases the solubility of the disperse phase, so that a high-temperature gel might be expected to have a less extended bridgework of aggregates holding it together. This picture constitutes a rationalization of the apparent decrease of reaction order with rising temperature, on the assumption that the rate-determining step in gelation is the rate of formation of secondary aggregates.
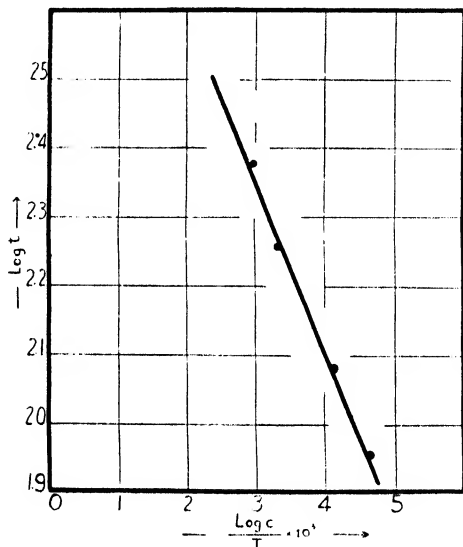
FIG. 3. Relation between setting time (t), concentration (c), and temperature (T) for sodium oleate gels in pinene (Prasad, Hattiangdi and Vishvanath's data (5)).

It has been pointed out elsewhere (1) by the author that, when a hot solution of a soap in an organic solvent is cooled gradually, saturation of the system is caused by the reduction in solubility of the solute. From this stage onward, the saturated solution of the soap, and not the pure solvent, acts as the dispersion medium, and the soap micelles remain suspended in the system. For the formation of a true jelly or gel, it is necessary that these micelles should aggregate to form some sort of meshwork which may be determined, in part, by packing considerations. As temperature drops, the size of the primary particles remains somewhat

constant at first whereas the number increases, and further cooling results in the formation of larger secondary particles due to aggregation without substantial change in the number of primary particles. On these grounds it seems as though an increase in the magnitude of the apparent negative activation energy with increasing concentration is due to the fact that, with dropping temperature, a greater proportion of the particles fall below the critical velocity, essential for the formation of larger aggregates, in the concentrated systems than in the dilute ones.

The fact that reaction order varies with temperature, and activation energy with concentration, leads to the suggestion that gels of equal time of set do not, in consequence, contain equal numbers of particles of equal degree of solvation, *etc.*, but rather that the condition of equal setting time is a point of balance between the two factors, (i) concentration of primary colloidal particles, and (ii) extent of secondary aggregation. At low concentrations and temperatures, the second factor is dominant, while for the same setting time at high temperatures, decline of the secondary aggregation is compensated for by the increased concentration of primary particles at the higher concentrations.

SUMMARY

An empirical equation of the form $t = ac^{-Q/RT}$ has been presented which represents the variation of the setting time (t) of a gel with both concentration (c) and temperature (T). This functions as a modified type of Arrhenius' equation at constant concentration, and expresses the kinetics of gelation at constant temperature.

Plots of $\log t$ vs. $(\log c)/T$ yield a straight line, suggesting that reaction order varies with temperature, and activation energy with concentration.

The condition of equal setting time, achieved with increasing concentrations at elevated temperatures, is possibly the point of balance between (a) the concentration of primary colloidal particles, and (b) the extent of secondary aggregation, the latter factor being dominant at low concentrations and temperatures, and the former at higher ones.

REFERENCES

1. HATTIANGDI, G. S., *J. Sci. Ind. Research (India)* **4**, 489 (1946).
2. HURD, C. B., AND LETTERON, H. A., *J. Phys. Chem.* **36**, 606 (1932).
3. KRISHNAMURTHI, K., *Proc. Roy. Soc. (London)* **122A**, 76 (1929).
4. PRAKASH, S., AND DUBE, H. L., *Z. anorg. Chem.* **208**, 163 (1932).
5. PRASAD, M., HATTIANGDI, G. S., AND VISHVANATH, C. V., *Proc. Indian Acad. Sci.* **21**, 56 (1945).
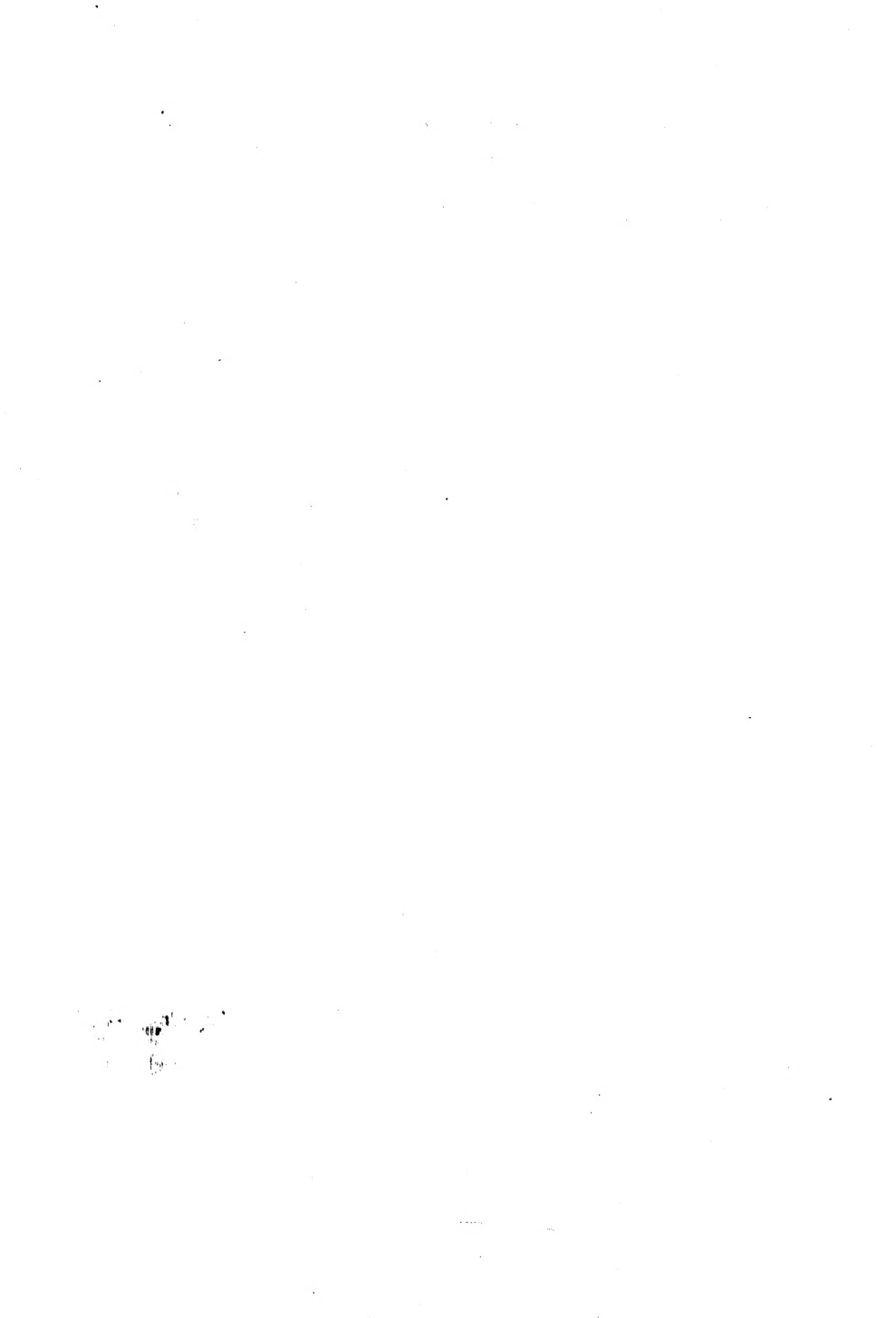
THE SORPTION OF VAPORS BY SUGAR CHARCOAL OVER A PERIOD OF TWENTY YEARS

James W. McBain and R. F. Sessions [1]

From the Department of Chemistry, Stanford Univ., Stanford, Calif.
Received January 22, 1948

INTRODUCTION

The sorption isotherm for water on charcoal does not remain constant over long periods of time (1), but changes through chemical interaction which forms water gas. Isotherms for organic substances show very slight change after standing for periods up to 4 years (2). The previously reported experiments have now been standing in sealed systems for 19.5 years. It seemed desirable to determine whether or not further shifting of the isotherm for water occurs; also to extend the observations on the equilibrium conditions of the organic vapors.

Silica springs undergo stretching, or relaxation, in a heated atmosphere of water vapor at relatively high humidity (3,4,5,6,7,8). It therefore seemed desirable to determine whether or not the "apparent" equilibrium for organic substances was real or due to a coincidental equilibrium conditioned by spring slippage. This could be determined by a recalibration of the silica springs used in preparation of the original McBain-Bakr sorption balances. The springs now have been exposed to their respective vapors for 19.5 years.

EXPERIMENTAL

Details of preparation of the sorption balances and the purity of the materials used are given in previous communications (1,2). During the interim, since last measurements were made, the balances have been standing at room temperature. Temperature variations may have been as much as 20° during a single day with maximum extremes being between 10 and 35°C. Before readings were made, the charcoal was allowed 'to stand at the temperature of the isotherm for 48 hours, or longer, for equilibrium to be reestablished.

The usual method of plotting x/m against relative humidities is followed. The curves represent values previously reported (1,2). The plotted points represent the values after the 19.5 year period. Sorption values are given in open circles, desorption values in solid circles. The particular
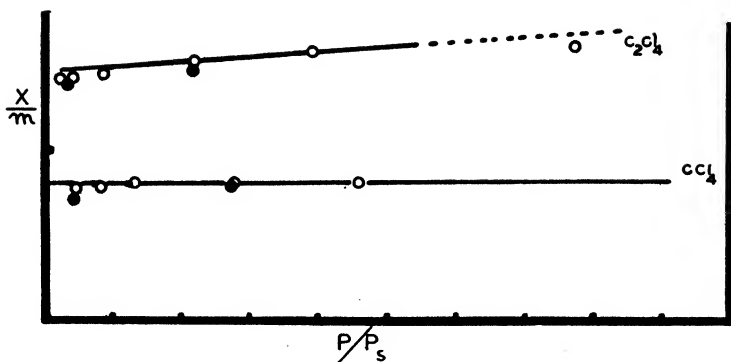
FIG. 1. Carbon dichloride and carbon tetrachloride sorption isotherms. $\bigcirc$ = sorption, 120°C.: $\bullet$ = desorption, 120°C. Plotted values are measurements after 19.5 years compared with previously established isotherm [curves as drawn] (2).
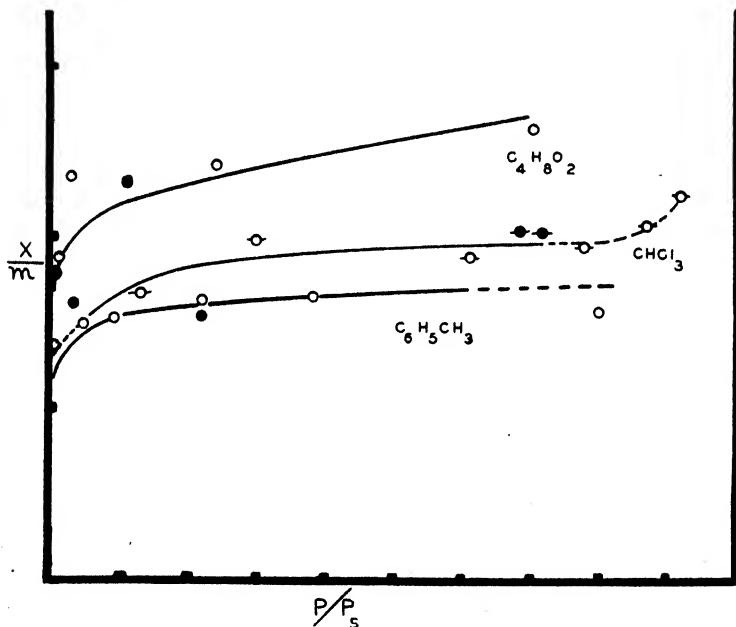
FIG. 2. Butyric acid, chloroform, and toluene sorption isotherms. $\bigcirc$ = sorption, 120°C.; $\bullet$ = desorption, 120°C. Plotted values are measurements made after 19.5 years. Curves drawn are values previously reported (2).

experiment in the case of diethylamine has not previously been reported. Therefore, all the points are plotted (the 3 year values are plotted as parallelograms). All values reported represent equilibrium of at least 24 hours duration except point No. 4, Fig. 3, which had been at the temperature of the reading for 4.5 hours, readings constant over a 2 hour interval.

DISCUSSION

Figs. 1 and 2 show that certain organic compounds are strongly sorbed by charcoal and establish equilibrium rapidly. After sorption takes place, it is extremely difficult to completely remove last traces except with
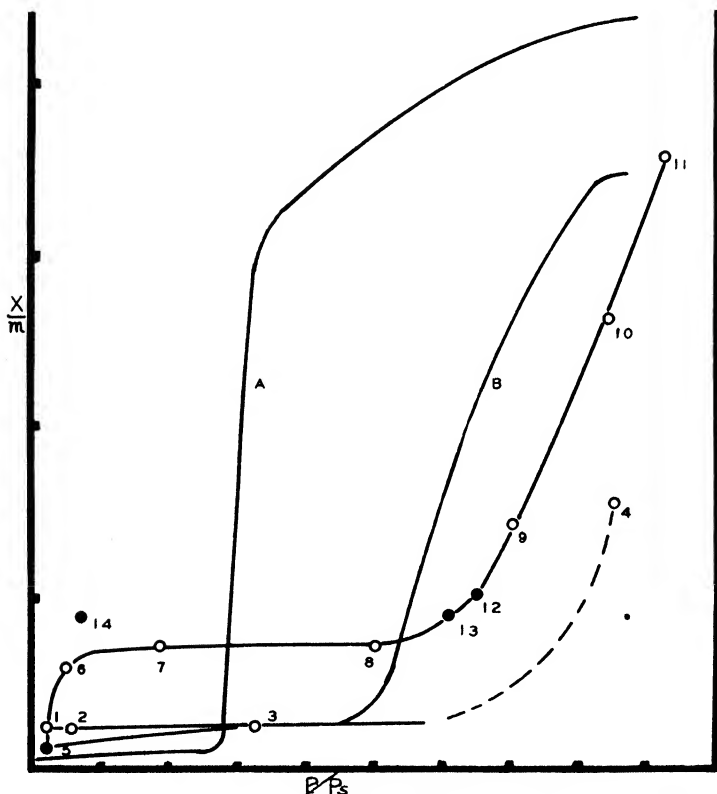
FIG. 3. Sorption of water. $\bigcirc$ = sorption, 120°C.; $\bullet$ = desorption, 120°C. "A" values obtained within 15 days after start of the experiment (1). "B" values obtained after a period of 15 months. Numbers adjacent to plotted values indicate the successive order of the determinations after 19.5 years. Seven readings were taken between No. 3 and No. 4 over a period of 8 hours. No appreciable uptake of water was noted until a relative pressure of 0.85 was reached.

drastic evacuation. Upon clean surfaces, and in the absence of impurities, the isotherms do not show hysteresis. Neither the relative magnitude nor the form of the isotherm change over a period of 19.5 years. The activity of the charcoal has not been changed by the sorbed gases or vapors. The probability of reaction between that charcoal and the vapors is small. The sorption is reversible, the greater portion of the sorption taking place at low relative pressure.

Fig. 3 indicates that the sorption of water by charcoal completely breaks down in the course of time. This probably is due to interaction of the water with the charcoal according to the water gas reaction (1). Thus, the introduction of competing impurities would tend to alter the
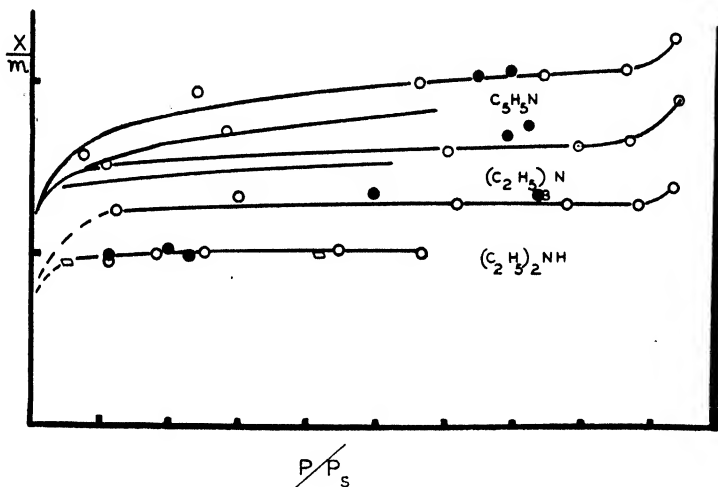
Fig. 4. Diethylamine, triethylamine and pyridine sorption isotherms. $\bigcirc$ = sorption 120°C.; $\bullet$ = desorption 120°C. Solid line curves represent previously reported values. The lower curve for diethylamine represents the short time experiment [not previously reported]. $\square$ $\triangleq$ 3 year values.

form of the isotherm. The general shape of the final isotherm does indicate the presence of impurities. These could only have been introduced as a result of reaction between sorbent and sorbate since the system has been sealed in glass tubes. The values have not been corrected for spring slippage which probably has occurred.

Diethylamine, triethylamine, and pyridine, over the 19 year period, show a slight increase in x/m values. In all of the experiments these substances are the only ones that show a clear cut case of increase in sorption. At high relative pressures condensation seems to be taking place, as shown by the rise in the sorption curve at p/p_s above 0.9.

TABLE I

Comparison of Original Length of Silica Springs and Length
After 20 Years Exposure to Vapors

Spring no.	Balance no.	Exposed to vapors of	Original zero length	Zero length after 20 yrs.	Stretch[a]
			mm.	*mm.*	*mm.*
18	CCl_4-2	CCl_4	64.10	64.43	0.24[b]
19	CCl_4-1	CCl_4	63.28	63.52	0.33
23	$C_4H_8O_2$-3	$C_4H_8O_2$	71.06	70.98	−0.08
32	C_2Cl_4-1	C_2Cl_4	89.84	90.50	0.66[c]
76	H_2O-2	H_2O	55.08	55.99	0.91

[a] These values were established before it was realized that exposure to air after standing in other vapors might cause any change in the length of the silica springs.

[b] Four days after this measurement was made the spring was again measured, having stood at room temperature and exposed to air, and the spring had stretched an additional 0.42 mm. making a total stretch of 0.66 mm.

[c] See Table II.

Table I gives a comparison of the stretching of the silica springs over the 19 year period. It will be noted that, in the case of the water balances, a small but positive slippage is indicated. In the case of the organic vapors, however, no appreciable stretching has occurred. Table II shows that, in the case of springs standing in tetrachloroethylene, no stretching has occurred. However, when the spring was removed for recalibration, it was exposed to moisture in the air, and stretching occurred so rapidly that calibration was difficult. This observation adds further evidence for

TABLE II

Stretch of Silica Spring No. 32 After Removal From Atmosphere
of Carbon Dichloride and Exposure to Air

Date	Time	Time exposed to air	Length of spring	Stretch
		hrs.	*mm.*	*mm.*
3/22/28	—	—	89.84	—
7/15/47	—	0	89.84[a]	0
8/7/47	1600	1.5[b]	90.50	0.66
8/7/47	1630	2	90.58	0.74
8/8/47	0900	18.5	90.90	1.06
8/8/47	2140	31	91.09	1.25
8/10/47	?	72±	91.09	1.25

[a] Value assumed since points on the isotherm at the temperature of calibration have not changed during the past 19.5 years.

[b] An estimated value from time and dates in notebook. At the time it was not realized that anything peculiar was taking place and no exact record of the time was made.

the fact that charcoal, chabasite, and now silica, expand on adsorption. It might be postulated that the silica is rejecting the organic vapors and taking up water in a manner similar to that of silica gel (9,10).

CONCLUSIONS

1. Over a period of nearly 20 years, sorption increases slightly in the case of triethylamine, diethylamine, and pyridine.

2. Carbon tetrachloride, carbon dichloride, toluene, butyric acid, and chloroform sorb on charcoal, reaching a saturation value within a short time which has not varied over the 20 year period.

3. The sorption of water on charcoal completely breaks down due to reaction between adsorbent and adsorbate. The isotherm finally represents sorption of a mixture.

4. Stretching of silica springs in a closed system exposed to organic vapors takes place to a negligible extent, if at all. Springs exposed to water vapor stretch appreciably only when exposed at high relative pressure, and usually at somewhat elevated temperature.

5. Silica springs, constant in length when exposed only to vapors of carbon tetrachloride and carbon dichloride, stretched rapidly when removed and exposed to air.

6. At high values of p/p_s, condensation takes place within the capillaries. This causes a sudden rise in "sorption" values at p/p_s above 0.95.

REFERENCES

1. McBain, J. W., Porter, J. L., and Sessions, R. F., *J. Am. Chem. Soc.* **55**, 2294 (1933).
2. McBain, J. W., and Sessions, R. F., *ibid.* **56**, 1 (1934).
3. Lee, W. W., Thesis, Stanford University.
4. Stamm, A. J., and Woodruff, S. H., *Ind. Eng. Chem., Anal. Ed.* **13**, 836 (1941).
5. Rao, K. S., *Current Sci. (India)* **8**, 546 (1939).
6. Seburg, C. O., Simmonds, F. A., and Baird, P. K., *Paper Trade J.* **107**, 223 (1938).
7. Shreve, G. W., Thesis, Stanford University, 1946.
8. Sosman, P. B., The Properties of Silica. Chemical Catalog Co., New York.
9. Chaney, N. K., Ray, A. B., and St. John, A., *Ind. Eng. Chem.* **15**, 1250 (1923).
10. Hoffert, W. H., *J. Soc. Chem. Ind. (London)* **44**, 357 (1925).

FILMS AT OIL-WATER INTERFACES. I

Eric Hutchinson [1]

From the Department of Chemistry, Stanford University, Palo Alto, Calif.
Received January 21, 1948

INTRODUCTION

In a recent investigation (17) into the effects of boundary films on the rate of diffusion of alcohols across a benzene-water interface, experiments were carried out using films *adsorbed* from aqueous solutions of surface active materials such as sodium cetyl sulfate. For that particular purpose the slow aging of films of sodium cetyl sulfate at the interface proved undesirable, and a search was made for materials which would reach equilibrium more rapidly. Films adsorbed from solutions of aliphatic alcohols and acids in the benzene phase proved more satisfactory. Search in the literature provided very little information (3, 6, 14, 18, 23) on adsorbed films at benzene-water interfaces, so the scope of the investigation was widened and the results of these experiments are presented in this paper. Here the distinction is drawn between films formed by adsorption and by spreading.

A very large body of work has been accumulated on the behavior of soluble and insoluble monomolecular films at air-water interfaces (1). For many years it has been recognized that orientation, reactions, and interactions occurring in films on water, may have an important bearing on phenomena in biological systems. Nevertheless, brief consideration shows that, of the various types of interfaces encountered in biological systems, air-water interfaces are relatively uncommon, and it appears much more probable that film behavior at oil-water and solid (protein)-water interfaces is of much more general importance. Yet this field is comparatively unexplored. It will be shown in this paper that too close analogies between behavior at air-water and oil-water interfaces are not necessarily valid; hence, there is considerable need for a more detailed study of oil-water systems. The techniques of investigating films in these systems present some difficulties, the chief being that most of the materials which form *insoluble* films on water are oil-soluble. Danielli (9) found that films of fatty acid derivatives prepared by *spreading* dissolved rapidly at a chlorobenzene-water interface. Alexander (4) spread films of sodium cetyl sulfate at a benzene-water interface and obtained a

---

[1] Bristol-Meyers Company Postdoctorate Fellow in Chemistry.

force-area curve for the film, but makes no mention of the instability of
the system. The author was unable to maintain constant pressure for this
film for periods greater than 1–2 min. owing to the solubility of the sodium
cetyl sulfate in the water. Some materials, such as lecithin and cephalin
(4, 8), are more stable but, in general, it is much more difficult to prepare
and maintain films at an oil-water interface, and long term stability is
essential in the study of film interactions (16). This imposes formidable
difficulties, since, with insoluble films, the number of molecules n_f in-
jected into the film is known and any subsequent change in film properties
may be interpreted in terms of changes in these n_f molecules. If stable
insoluble films cannot be prepared, and attention is restricted to *adsorbed*
films, then the number of molecules in the film may only be determined
indirectly by application of the Gibbs theorem. Since any accurate ap-
plication of the theorem requires information on the osmotic properties of
the solutions, the number of measurements required is greater and the
calculated values of the number of molecules in the adsorbed film are
likely to be much less precise. Further, to study *interactions* in adsorbed
monolayers, it would be necessary to apply the Gibbs theorem to a sys-
tem with more than 2 components, and the number of measurements
required for a complete solution of the problem would be very large un-
less some assumptions could be made to limit the number of variables.
Experiments are planned to test the applicability of approximate equa-
tions, but the results below are restricted to one solute species only.

EXPERIMENTAL

A number of methods were tested in studying the interfacial tensions
of the systems benzene (aliphatic alcohol)-water (17) and difficulty was
encountered in reconciling the results of the various methods.

The ring method (15) was of little use in systems containing methyl,
ethyl, and propyl alcohols, as it was found that, on moving the ring
through the interface, the "skin" of liquid attached to the ring peeled
off in an irreproducible manner instead of rupturing in the usual way.
For alcohols with longer chain lengths this phenomenon was less marked,
but frequent irreproducibility attested to the lability of the contact
angle and the method was discontinued.

The drop-volume method (13) gave reproducible values for these
systems when due attention was paid to the time of formation of the drop.
Using Gaddum's (1) modification of the method, involving a micrometer
syringe, and forming the last 5% of the drop during periods greater than
2 minutes, reproducible values in agreement (± 0.2 dyne/cm.) with the
sessile drop method (below) were obtained. However, in those cases in
which aging occurred, notably when water-soluble detergents such as
sodium cetyl sulfate were used, irreproducible results were obtained.

The pendant-drop method (5) yielded results which were reproducible for each tip used, but the results for various sizes of tip were inconsistent with one another. For example, using tips of diameter 2 mm. and 5 mm., values for the interfacial tension of benzene–water of 34.5 dynes/cm. and 32.3 dynes/cm., respectively, were obtained. Such variations with pure liquids were not obtained using any of the other methods and it is difficult to understand why they should occur here since no such variations are explicit in the accounts of the method. Aging of drops was a serious problem with this method. It is difficult to estimate the amount of liquid which can be expressed into the drop so that a drop of suitable shape shall remain *after aging*. In many cases it was found that, after standing for 3 or 4 hours, the interfacial tension had decreased so much that the original volume of liquid could no longer be supported and the drop fell off.

The sessile bubble method (2, 7, 11) has proved by far the most convenient and reliable method whether aging occurred or not. The method has been fully described in the literature, but there are a few points worthy of mention. The measurements involved are (1) the maximum diameter $2r$ of the "bubble" and (2) the height h from the maximum diameter to the tip of the "bubble." In general we have

$$\gamma = f(h \cdot r \cdot \rho_1 \rho_2,)$$

where ρ_1 and ρ_2 are the densities of the two phases. For the so-called large bubble the approximate theory gives (24)

$$\gamma = \tfrac{1}{2} h^2 g \cdot (\rho_1 - \rho_2)/(1 + 0.609\, h/r).$$

In measuring the *surface* tension of common liquids $(\rho_1 - \rho_2) \sim 1.0$ and a large bubble is one with a diamter $> ca.$ 5 cm. In measuring interfacial tensions $(\rho_1 - \rho_2) \sim 0.1$ to 0.3 and a large bubble to which the above equation applies has a diameter greater than 10–15 cm. Hence, for practical purposes it is preferable to use a small bubble with diameter 2–3 cm.
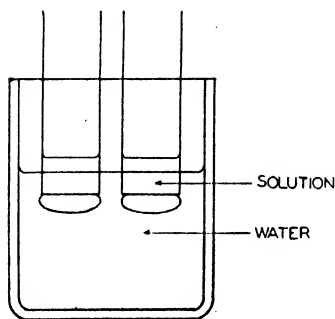
Fig. 1. Apparatus for forming sessile bubbles (schematic).

and to apply the correction terms of Porter (19) founded on Bashforth and Adam's tables. By choosing bubbles of such a size that $h/r \sim 0.5$ it is possible to work in the region where the correction terms are known very accurately. The advantage of the method over the pendant drop is that, if aging occurs, portions of the bubble, formed from the less dense liquid, break away from the bubble in such a way that the bubble remaining still has a shape suitable for measurement. By the use of flanged tubes
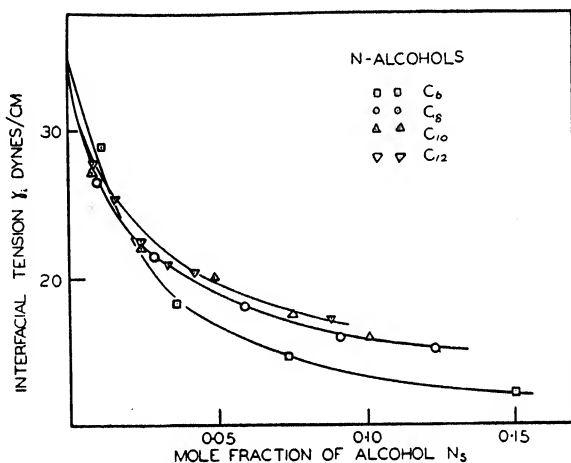
FIG. 2. Interfacial tension of solutions of primary alcohols as a function of the mole fraction.
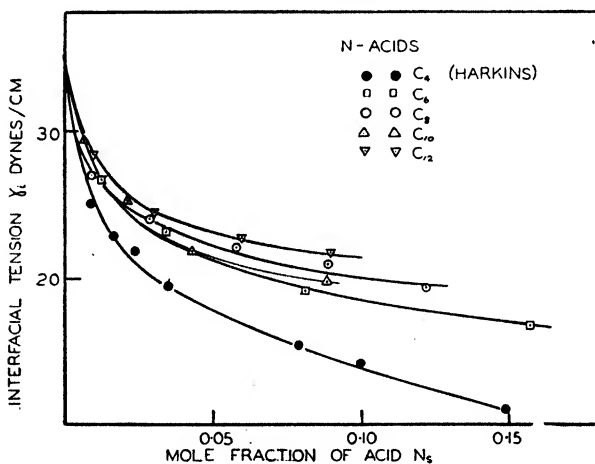
FIG. 3. Interfacial tension of solutions of fatty acids as a function of the mole fraction.
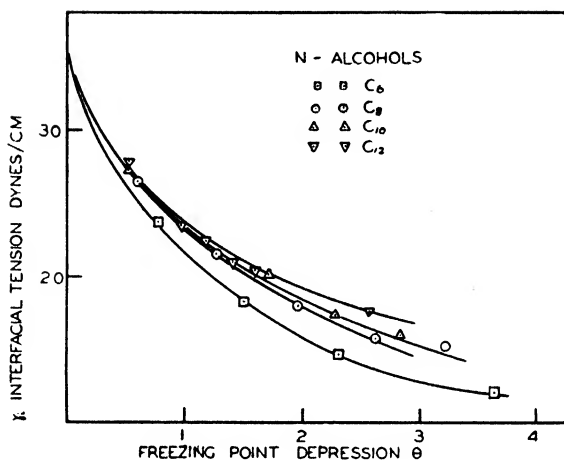
FIG. 4. Interfacial tension of solutions of primary alcohols as a function of the freezing point depression.
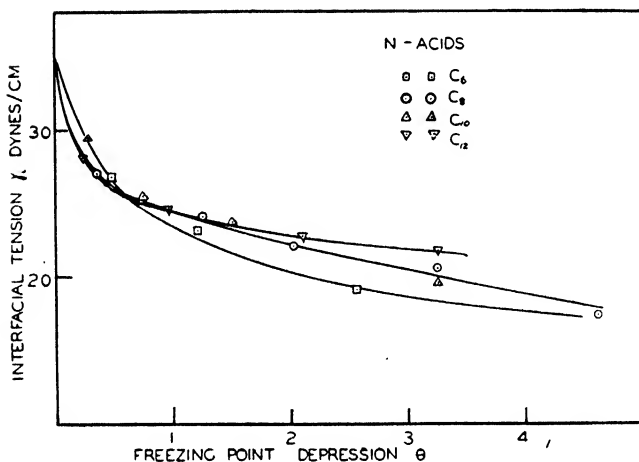
FIG. 5. Interfacial tension of solutions of fatty acids as a function of freezing point depression.

on which to form the bubbles this rupture of the bubble could readily be overcome.

The apparatus used is shown in Fig. 1. It consisted of an optical cell $8 \times 6 \times 4$ cm. with fused Pyrex walls, various Pyrex tubes with ground ends, and a traveling microscope reading to 0.001 cm. The position of the tip of the bubble was readily observed by viewing against a light back-

ground and the position of the maximum diameter located by means of the astigmatic image formed by reflection in the bubble of a small lamp at a distance of about 2 feet (7). At this stage no attempt was made to thermostat the apparatus as the room temperature remained at $23 \pm 1°C$. during the course of the experiments. However, as will appear later, to carry out detailed analysis of the results, greater precision is required and this will necessitate thermostating in future work.

Results were calculated as follows:

$$\gamma = \beta^2 g(\rho_1 - \rho_2),$$

where

$$\frac{\beta^2}{r^2} = \frac{1}{2}\frac{h^2}{r^2} + \text{(correction factor)}$$

and values of β^2/r^2 corresponding to the measured quantities h^2/r^2 are obtained from Porter's (19) tables. ρ_2 the density of the solution of alcohol or acid in benzene was measured at the temperature of each experiment by means of a pycnometer of $ca.$ 25 ml. capacity. Using materials of chain lengths of 6 carbons or more, the solubility of the surface active material in water was assumed to be zero and the density taken as that
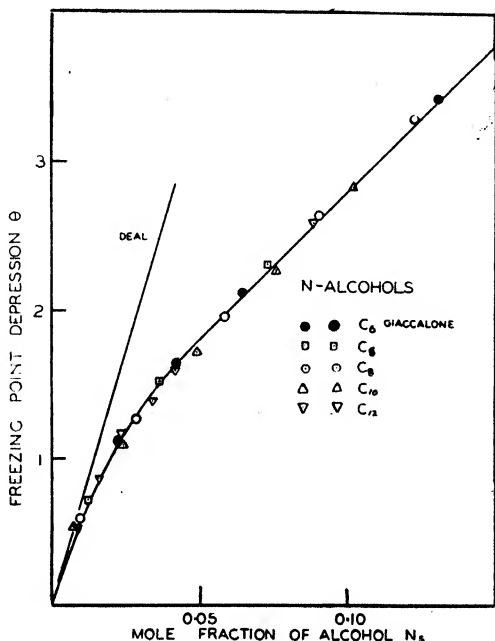
Fig. 6. Freezing point curve for solutions of primary alcohols in benzene.
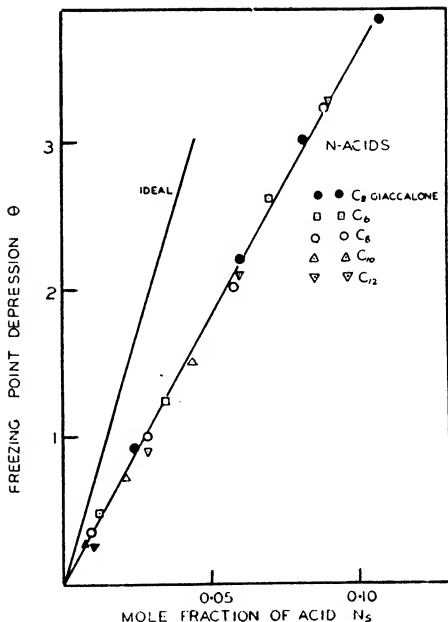
FIG. 7. Freezing point curve for solutions of fatty acids in benzene.

of pure water at the appropriate temperature. Harkins' (14) data on the density of solutions of butyric acid in water indicate that the error involved thereby is small.

For benzene-conductivity water a value of 35.1 ± 0.1 dyne/cm. was obtained. This order of accuracy is as good as may be expected in the absence of careful temperature control. With the solutions of alcohols and acids the reproducibility was of the order ± 0.2 dyne/cm. It was at first thought that such variations might be due to faulty cleaning, but, as the variations were regularly encountered, it is more likely that they were due to adventitious changes in contact angle, for, although the method is theoretically independent of contact angle, this is only true when variations from point to point are insufficient to distort the bubble from a figure of revolution about the vertical axis.

The solutions of alcohols and acids used were of such concentrations that the approximate form of the Gibbs equation

$$\Gamma = \frac{1}{RT} \frac{\partial \gamma}{\partial \log C}$$

could not be used, and data on the activity coefficient of the solute were required. Freezing point data for the solutions were obtained by the standard Beckmann method using 25 ml. of solution.

TABLE I

Interfacial Tension of Butyric Acid Solutions Against Water (Harkins)

Mole fraction of acid N_s	Freezing pt. depression θ	Interfacial tension γ	$\frac{\partial \gamma}{\partial \theta}$	$\Gamma_s^{(1)}$	$\Gamma_s^{(N)}$	$\Gamma_s^{(u)}$	Area/mole. A	Surface pressure
		dynes/cm.					in Å²	*dynes/cm.*
0.218		7.4	0.529	3.87	3.03	5.26	31.4	27.7
0.148	5.43	11.0	0.813	3.72	3.17	4.28	38.5	24.1
0.100	3.73	14.2	1.19	3.47	3.13	3.90	42.3	20.9
0.0791	2.87	15.4	1.54	3.50	3.21	3.80	43.5	19.7
0.0354	1.23	19.4	3.59	3.48	3.36	3.63	45.4	15.7
0.0233	0.83	21.8	5.31	3.36	3.28	3.44	48.0	13.3
0.0164	0.59	22.95	7.41	3.23	3.17	3.28	50.3	12.1
0.0088	0.33	25.0	13.51	3.13	3.10	3.16	52.2	10.1
0.0045	0.20	28.0	22.22	2.63	2.62	2.71	62.2	7.1

TABLE II

Interfacial Tension of n-Caproic Acid Solutions Against Water

Mole fraction of acid N_s	Freezing pt. depression θ	Interfacial tension γ	$\frac{\partial \gamma}{\partial \theta}$	$\Gamma_s^{(1)}$	$\Gamma_s^{(N)}$	$\Gamma_s^{(u)}$	Area/mole. A	Surface pressure
		dynes/cm.					in Å²	*dynes/cm.*
0.157	5.74	16.7	0.558	2.49	2.11	3.33	49.6	18.4
0.126	3.98	17.8	0.806	2.45	2.20	2.97	55.5	17.3
0.0701	2.62	19.1	1.22	2.43	2.26	2.77	59.6	16.0
0.0344	1.24	23.1	2.59	2.43	2.34	2.60	63.5	12.0
0.0123	0.49	26.7	6.58	2.15	2.13	2.23	74.0	8.4

TABLE III

Interfacial Tension of n-Caprylic Acid Solutions Against Water

Mole fraction of acid N_s	Freezing pt. depression θ	Interfacial tension γ	$\frac{\partial \gamma}{\partial \theta}$	$\Gamma_s^{(1)}$	$\Gamma_s^{(N)}$	$\Gamma_s^{(u)}$	Area/molc. A	Surface pressure
		dynes/cm.					in Å²	*dynes/cm.*
0.358	17.05[a]	14.9	0.169	2.49	1.60	4.37	37.9	20.2
0.228	10.73[a]	17.2	0.272	2.10	1.62	3.34	49.4	17.9
0.122	4.71	19.3	0.609	2.23	1.96	2.87	57.6	15.8
0.0893	3.23	20.9	0.885	2.28	2.07	2.67	61.9	14.2
0.0584	2.040	22.0	1.389	2.27	2.14	2.48	66.4	13.1
0.0285	1.002	24.0	2.832	2.18	2.12	2.32	70.7	11.1
0.0094	0.353	27.0	8.196	2.04	1.86	1.92	85.8	8.1

[a] Taken from Giaccalone.

TABLE IV

Interfacial Tension of n-Capric Acid Solutions Against Water

Mole fraction of acid N_s	Freezing pt. depression θ	Interfacial tension γ	$\dfrac{\partial\gamma}{\partial\theta}$	$\Gamma_s^{(1)}$	$\Gamma_s^{(N)}$	$\Gamma_s^{(u)}$	Area/mole. A	Surface pressure
		dynes/cm.					in Å²	dynes/cm.
0.104	3.61	18.4	0.909	2.72	2.51	3.47	47.5	16.7
0.088	3.23	19.7	1.101	2.78	2.55	3.23	51.0	15.4
0.0435	1.51	21.8	2.352	2.82	2.69	3.02	54.5	13.3
0.0412	1.44	22.8	2.469	2.77	2.67	2.97	55.5	12.3
0.0211	0.72	25.3	4.926	2.77	2.73	2.89	57.0	9.8
0.00697	0.27	29.5	14.18	2.62	2.60	2.61	63.2	5.6

TABLE V

Interfacial Tension of Lauric Acid Solutions Against Water

Mole fraction of acid N_s	Freezing pt. depression θ	Interfacial tension γ	$\dfrac{\partial\gamma}{\partial\theta}$	$\Gamma_s^{(1)}$	$\Gamma_s^{(N)}$	$\Gamma_s^{(u)}$	Area/mole. A	Surface pressure
		dynes/cm.					in Å²	dynes/cm.
0.0906	3.27	21.7	0.794	2.08	1.89	2.58	64.0	13.4
0.0600	2.09	22.7	1.242	2.09	1.96	2.39	69.1	12.4
0.0287	0.98	24.4	2.659	2.07	2.01	2.23	74.0	10.7
0.0104	0.25	28.3	5.681	1.57	1.56	1.64	101.0	6.8

TABLE VI

Interfacial Tension of n-Hexanol Solutions Against Water

Mole fraction of alc. N_s	Freezing pt. depression θ	Interfacial tension γ	$\dfrac{\partial\gamma}{\partial\theta}$	$\Gamma_s^{(1)}$	$\Gamma_s^{(N)}$	$\Gamma_s^{(u)}$	Area/mole. A	Surface pressure
		dynes/cm.					in Å²	dynes/cm.
0.151	3.76	12.0	1.499	7.00	5.95	7.19	22.9	23.1
0.0733	2.31	14.6	3.194	6.65	6.16	6.71	24.4	20.5
0.0364	1.52	18.2	5.617	5.48	5.39	5.76	28.7	16.9
0.0119	0.73	23.6	8.928	2.83	2.79	2.89	57.0	6.1

TABLE VII

Interfacial Tension of n-Octanol Solutions Against Water

Mole fraction of alc. N_s	Freezing pt. depression θ	Interfacial tension γ	$\dfrac{\partial\gamma}{\partial\theta}$	$\Gamma_s^{(1)}$	$\Gamma_s^{(N)}$	$\Gamma_s^{(u)}$	Area/mole. A	Surface pressure
		dynes/cm.					in Å²	dynes/cm.
0.123	3.281	15.1	2.032	7.48	6.56	7.52	21.5	20.0
0.0904	2.628	15.7	2.610	6.83	6.22	6.93	23.8	19.4
0.0589	1.946	18.0	3.521	5.78	5.44	6.24	26.4	17.1
0.0282	1.261	21.1	5.434	5.07	4.90	5.30	31.1	14.0
0.00968	0.597	26.5	11.49	2.95	2.92	3.04	55.0	8.6

TABLE VIII

Interfacial Tension of n-Decanol Solutions Against Water

Mole fraction of alc. N_s	Freezing pt. depression θ	Interfacial tension γ	$\frac{\partial\gamma}{\partial\theta}$	$\Gamma_s^{(1)}$	$\Gamma_s^{(N)}$	$\Gamma_s^{(u)}$	Area/ mole. A	Surface pressure
		dynes/cm.					in Å²	dynes/cm.
0.102	2.823	16.0	2.427	7.25	6.50	7.37	22.4	19.1
0.0756	2.255	17.4	3.048	6.56	6.06	6.78	24.3	17.7
0.0491	1.710	20.2	4.010	5.45	5.18	5.57	29.7	14.9
0.0238	1.096	22.0	6.289	4.03	3.94	4.12	40.1	13.1
0.00764	0.54	27.2	12.66	2.56	2.54	2.59	63.7	7.9

TABLE IX

Interfacial Tension of Laurol Solutions Against Water

Mole fraction of alc. N_s	Freezing pt. depression θ	Interfacial tension γ	$\frac{\partial\gamma}{\partial\theta}$	$\Gamma_s^{(1)}$	$\Gamma_s^{(N)}$	$\Gamma_s^{(u)}$	Area/ mole. A	Surface pressure
		dynes/cm.					in Å²	dynes/cm.
0.0899	2.58	17.5	2.380	6.19	5.63	6.34	25.8	18.6
0.0421	1.600	20.3	4.291	4.96	4.75	5.08	32.5	14.8
0.0332	1.400	20.9	4.545	4.11	3.97	4.20	39.3	14.2
0.0245	1.178	22.4	5.376	3.55	3.47	3.67	44.9	12.7
0.0162	0.996	25.5	6.944	3.01	2.96	3.09	53.4	9.6
0.00802	0.520	27.8	13.15	2.79	2.77	2.86	57.8	7.3

Peters (18) records that the interfacial tensions of benzene solutions of fatty acids against water are markedly affected by pH in the range pH 6–10. Acidification of the conductivity water by means of hydrochloric acid produced no measurable change in interfacial tension, and it is felt that the free fatty acid is the true molecular species to which the calculations below apply.

In general, the values quoted in Tables I–IX are those obtained after the system had been standing for about 12 hours. With the exception of *n*-capric acid solutions, no change in interfacial tension greater than 0.1–0.2 dyne/cm. was observed after some 3 minutes from the formation of the bubble. This no doubt explains why the drop-volume method gave agreement with these results. However, in the case of *n*-capric acid decreases of 3–4 dynes/cm. in interfacial tension were observed. The source of the capric acid was unknown and it is felt that this aging was due to impurities. That the problem of purity of samples is acute, is shown by the fact that the molecular weight of the material in question was within 1% of the theoretical value as determined by titration.

The alcohols used were obtained from the Connecticut Hard Rubber

Co., and the acids, with the exception of n-capric acid, were obtained from Eastman Kodak Company.

Freezing point data for a number of acids and alcohols dissolved in benzene were obtained by Giaccalone (10). His values for n-hexanol and n-caprylic acid are shown for comparison in Figs. 6 and 7. Agreement is considerably better than 1%.

The only comparable data on interfacial tensions available are those of Harkins (14) for solutions of butyric and acetic acids. The data are given in Fig. 3 for comparison, and calculations on these data taken with Giaccalone's freezing point data are given in Table I.

DISCUSSION

In calculating adsorption data the methods of Guggenheim and Adam (12) have been followed throughout.

The only reported data for the areas of fatty acids at a benzene-water interface are those of Harkins (14). These are calculated on the assumption that the quantity

$$\Gamma_s = -\frac{2.303}{RT}\frac{\partial\gamma}{\partial \log_{10} C_s},$$

where C_s = concentration of solute in moles/1000 g. solvent, may be equated to the actual number of molecules of fatty acid in the monomolecular interfacial film, and Harkins arrives at a figure of $ca.$ 30 Å^2 for the area of butyric acid in the close packed film. The calculations contain a number of errors. At the concentrations used, $viz.$, $ca.$ 1 g.-mole/l. in the aqueous phase, and the corresponding value of $ca.$ 5 g.-moles/l. in the benzene phase, the concentration term C_s can no longer be even approximately equated to the thermodynamic terms $(f_s N_s)$. Further, through an arithmetic slip Harkins inverted the logarithmic conversion factor 2.303 so that his values are too small by a factor of $(2.303)^2$. Schofield and Rideal (21) in deriving a force-area curve from Harkins' data avoid this error and obtain an area of $ca.$ 100 Å^2 in the close packed film, but neglect to account for changes in the activity coefficient f_s.

The need for this is readily shown by the marked deviations from ideality demonstrated in the freezing point curves and noted by numerous authors (20).

The Gibbs equation may be written:

$$-\partial\gamma = \sum_i \Gamma_i \partial\mu_i. \tag{1}$$

In the present systems there are three components, solute, benzene and water. To make calculations possible, we make the reasonable assumption that the chemical potential of the water in the benzene phase

is invariant; hence we may write:

$$- \partial\gamma = \Gamma_s \partial\mu_s + \Gamma_o \partial\mu_o, \tag{2}$$

where,

Γ_s = surface excess of solute S,
Γ_o = surface excess of solvent, benzene,
μ_x = chemical potential of solute S,
μ_o = chemical potential of solvent, benzene.

Following Guggenheim and Adam we may write

$$- \partial\gamma = \Gamma_s^{(1)} d\mu_s. \tag{3}$$

This is the so-called "Gibbs" convention which postulates that $\Gamma_o^{(1)} = 0$.

Alternatively, we may adopt a more useful convention by defining a quantity $\Gamma_i^{(N)}$ such that a portion of the liquid embracing unit area of surface contains $\Gamma_i^{(N)}$ moles of each species i more than an equal volume in the bulk phase containing exactly the same total number of moles of all species. Then by definition

$$\sum_i \Gamma_i^{(N)} = 0. \tag{4}$$

Lastly one may place the "Gibbs" geometrical surface so as to separate the bulk homogeneous phase from the assumed *monomolecular* surface layer above it. On this u convention $\Gamma_s^{(u)}$ and $\Gamma_o^{(u)}$ are the actual number of solute and solvent molecules in the film.

We have (12) the following relations:

$$\Gamma_x^{(1)} = - \frac{\partial\gamma}{\partial\mu_s}, \tag{5}$$

$$\Gamma_s^{(N)} = \Gamma_s^{(1)} \Big/ \left(1 + \frac{N_s}{N_o} \right), \tag{6}$$

$$\Gamma_s^{(N)} = N_s \Gamma_s^{(u)} - N_s \Gamma_o^{(u)}, \tag{7}$$

where N_s and N_o are the mole fractions of solute and solvent, respectively.

Now

$$\mu_o = \mu_0^0 + g \cdot RT \log N_o, \tag{8}$$

where g = the osmotic coefficient of the solvent.

$$\therefore \quad \partial\mu_s = RT\partial(g \log N_o) \tag{9}$$

and by the Gibbs Duhem equation

$$N_o \cdot \partial\mu_o = - N_s \partial\mu_s. \tag{10}$$

$$\therefore \quad \partial\mu_s = - \frac{N_o}{N_s} \cdot RT \cdot \partial(g \log N_o). \tag{11}$$

But

$$- g \log N_o = \frac{L}{R T_o^2} \cdot \theta, \tag{12}$$

where

θ = the freezing point depression of the solution,
T_o = the freezing point of the benzene,
L = the latent heat of fusion of benzene.

$$\therefore \quad \partial(g \log N_o) = - \frac{L}{R T_o^2} \cdot \partial\theta, \tag{13}$$

$$i.e. \quad \Gamma_s^{(1)} = - \frac{N_s}{N_o} \cdot \frac{T_o^2}{L \cdot T} \cdot \frac{\partial\gamma}{\partial\theta}. \tag{14}$$

In order to calculate N_s to substitute in Eq. 14 it is necessary to postulate some molecular model for the system. Since in very dilute solution, i.e., $< 0.01 \ M$, the solutions of both alcohols and acids yield freezing point depressions in accordance with ideal behavior, the model adopted is that of single molecules of alcohol or acid in benzene. The manifest deviations from this behavior at higher concentrations are then taken into account by the θ term. Secondly, Eq. 7 for obtaining $\Gamma_s^{(u)}$ contains 2 unknowns $\Gamma_s^{(u)}$ and $\Gamma_o^{(u)}$; to solve the equation we may employ the additional equation:

$$A_s\Gamma_s^{(u)} + A_o\Gamma_o^{(u)} = 1, \tag{15}$$

where

A_s = the area/g.-mole of solute, and
A_o = the area/g.-mole of solvent benzene.

The choice of values for A_s and A_o is somewhat arbitrary but may be determined approximately. Since, from C_4 to C_{12} derivatives, there is no sign of behavior analogous to that occurring at the air-water interface, and designated as Traube's (22) rule, it is highly probable that the film molecules are *not* oriented parallel to the interface as postulated for the low pressure gaseous films at air-water interface, but are simply anchored to the interface by means of the polar group, the hydrocarbon chain remaining entirely in the benzene phase. This hypothesis is supported by energetic considerations of the competing effects of the interactions, benzene $\leftrightarrow$ hydrocarbon chain and water $\leftrightarrow$ hydrocarbon chain. Hence the values selected for A_s are those commonly accepted as the areas of the polar heads derived from insoluble films (1). The value for A_o, the area of the benzene, has been taken as 24 Å^2 per molecule, a value common to most simple p-substituted benzene derivatives in insoluble films. From Eqs. 7 and 15 we have:

$$\Gamma_s^{(u)} = \frac{\Gamma_s^{(N)} \cdot A_o + N_s}{N_o A_o + N_s A_s}. \tag{16}$$

From 16 we see that, even for values of N_s as large as 0.15, a change in A_o by a factor of 2 results in a change of $\Gamma_s^{(u)}$ less than 10%. Variations at values of $N_s < 0.05$ are less than 3% and variations due to changes in the value of A_s are practically negligible. Thus, the arbitrary choice of values for A_o and A_s results in no serious error.

From Eqs. 16 and 14 we can calculate the number of molecules of solute in the film. Values of $\partial\gamma/\partial\theta$ were obtained as follows: a plot of γ against $\log\theta$ gives a straight line from which an equation of the form

$$\gamma = A + B \log \theta \tag{17}$$

may be obtained, where A and B are constants. From this it follows that

$$\left(\frac{\partial\gamma}{\partial\theta}\right)_{\theta=\theta_0} = \frac{B}{\theta_0}. \tag{18}$$

The areas per molecule in the film, $A = 1/\Gamma_s^{(u)}$ together with values of $\Gamma_s^{(1)}$, $\Gamma_s^{(N)}$ and $\Gamma_s^{(u)}$ are given in Tables I–IX.

It is immediately apparent that errors involved in using the approximate form of Gibbs equation are large. Using Harkins' results for butyric acid, a close packed area of $ca.$ 100 Å² is obtained by neglecting changes in activity coefficient whereas the $\Gamma_s^{(u)}$ value gives an area of $ca.$ 40 Å². Again the errors involved in neglecting changes in Γ_o may be as large as 40% in concentrations where $N_s > 0.1$.

The force-area curves for the adsorbed films are plotted in Fig. 8. The curves for the fatty acids all show a point of transition from expanded films to more highly condensed films. The transition pressures form a uniform series,

Butyric................19.5 dynes/cm.
Caproic................16.4 dynes/cm.
Caprylic...............15.5 dynes/cm.
Capric.................14.6 dynes/cm.
Lauric.................13.2 dynes/cm.,

the transition pressure decreasing steadily with increasing chain length. With the exception of capric acid, the transition areas form a similar series. Capric acid was the only compound with which aging effects were experienced, and, due to the likelihood of impurity in the specimen, the results for this compound may be erroneous.

Data for the alcohol films are not so complete over the whole pressure range, but the alcohol films appear to be more highly condensed than the corresponding acids, as is the case at air-water interfaces (1), in all cases being above the transition pressure. The close packed areas approximate to 20Å² in agreement with data obtained with insoluble films at air-water surfaces.

To work out the details of the force-area curves, more extended and more precise data need to be accumulated, but the results show that film behavior at a benzene-water interface is essentially similar to that at an air-water interface.
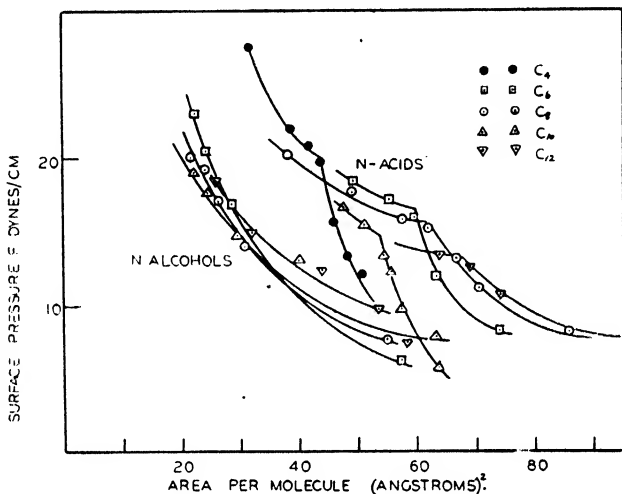
Fɪɢ. 8. Force-area curves for films adsorbed at the benzene-water interface.

SUMMARY

A number of methods of measuring interfacial tensions between two liquids are compared, and it is concluded that the "sessile bubble" is most convenient and trustworthy. For systems where the interface does not age appreciably the drop-volume method gives results in agreement to within ±0.2 dyne/cm. with the sessile bubble method.

The interfacial tension of benzene solutions of a number of alcohols and acids against conductivity water at 23° C. have been determined, together with the freezing points of the solutions.

The Traube rule does not apply at the benzene-water interface, from which it is concluded that the molecules in an expanded film are not oriented parallel to the interface.

From calculations of the adsorption at the interface, force-area curves are deduced for the adsorbed film. The fatty acids give curves with a transition point similar to those obtained with myristic acid on water at

25°C. and, at the highest pressure used, occupy an area of about 40 Å². The alcohols appear to be more condensed in the surface film than the corresponding acids, and close pack to an area of about 20 Å².

REFERENCES

1. ADAM, The Physics and Chemistry of Surfaces. Oxford, 1943.
2. ADAM AND SHUTE, *Trans. Faraday Soc.* **34**, 1 (1938).
3. ADDISON, *ibid.* **34**, 628 (1938); *Nature* **144**, 249, 783 (1939).
4. ALEXANDER AND TEORELL, *Trans. Faraday Soc.* **35**, 727 (1939).
5. ANDREAS, HAUSER AND TUCKER, *J. Phys. Chem.* **42**, 1001 (1938).
6. BARTELL AND DAVIES, *ibid.* **45**, 1321 (1941).
7. BURDON, *Trans. Faraday Soc.* **28**, 866 (1932).
8. CHEESEMAN, *Arkiv Kemi Mineral. Geol.* **22**B, No. 1 (1946).
9. DANIELLI AND AITKEN, *Proc. Roy. Soc. (London)* **155**A, 695 (1935).
10. GIACCALONE, *Gazz. chim. ital.* **72**, 348, 429 (1942).
11. GOUY, *Ann. phys.* **6**, 5 (1916).
12. GUGGENHEIM AND ADAM, *Proc. Roy. Soc. (London)* **139**A, 218 (1933).
13. HARKINS AND BROWN, *J. Am. Chem. Soc.* **41**, 499 (1919).
14. HARKINS AND KING, *ibid.* **41**, 985 (1919).
15. HARKINS AND JORDAN, *ibid.* **52**, 1751 (1930).
16. HARKINS, Colloid Chemistry, edited by J. Alexander, p. 68. Reinhold, New York, 1944.
17. HUTCHINSON, *J. Phys. & Colloid Chem.* in press.
18. PETERS, *Proc. Roy. Soc. (London)* **133**A, 140 (1931).
19. PORTER, *Phil. Mag.* **16**, 163 (1933); **34**, 823 (1937).
20. RALSTON AND HOERR, *J. Org. Chem.* **7**, 546 (1944).
21. SCHOFIELD AND RIDEAL, *Proc. Roy. Soc. (London)* **109**A, 67 (1925).
22. TRAUBE, *Ber.* **17**, 2294 (1884); *Ann.* **265**, 27 (1891).
23. TRAUBE et al., *Biochem. Z.* **217**, 400 (1930); *Z. phys. Chem.* **178**, 323 (1937).
24. WORTHINGTON, *Phil. Mag.* **20**, 51 (1885).

FILMS AT OIL-WATER INTERFACES. II

Eric Hutchinson [1]

From the Department of Chemistry, Stanford University, Palo Alto, Calif.
Received March 12, 1948

INTRODUCTION

In a previous communication (8), data were presented for the interfacial tensions against water of a series of solutions of fatty acids and alcohols. This work has been extended to higher homologues of the acids and alcohols, and variations in temperature and the nature of the solvent have been studied.

EXPERIMENTAL

In the previous paper the interfacial tension data were obtained by means of the sessile bubble method (4) but it was found that the drop-volume method (6) yielded results in good agreement with these (±0.2 dynes/cm.) provided the systems which were studied showed no marked aging. One difficulty with the sessile bubble method, however, lay in the poor thermal control which was achieved. Hence, in the present work the results have, in general, been obtained by the drop-volume method because of the great ease of thermostating; the results being checked where possible, *viz.*, at 25°C., against the sessile bubble method. The agreement was good, and confidence is felt in those results obtained at 10°C. and 40°C. which could not be checked against the sessile bubble method. Previous work indicated that, with solutions of the lower members of the fatty acids and alcohols, the ring method (7) occasionally gave erroneous results due to variations in the contact angle on the ring. For higher members, notably cetyl alcohol and myristic acid, the ring method gave results in good agreement with the drop-volume and sessile bubble methods.

As the details of the methods of measuring interfacial tension were given in the previous paper, no further description will be given here.

Freezing point data necessary to the calculation of the Γ's were obtained, as before, by a standard Beckmann method using 25 ml. of solution.

The caprylic and myristic acids, cetyl alcohol, benzene, cyclohexane, and nitrobenzene were supplied by Eastman Kodak Company. The *n*-octyl alcohol and *n*-tetradecane were supplied by the Connecticut Hard

Rubber Company. The myristic acid required 3 recrystallizations from acetone solutions before "aging," due to impurities, became negligible.

RESULTS

Values for the interfacial tensions against water for n-octyl alcohol and n-caprylic acid in benzene at 10°C. and 40°C. are given in Tables I–IV, values for n-octyl alcohol and n-caprylic acid in a number of solvents in Tables V–IX, and values for cetyl alcohol in benzene, and myristic acid in benzene and cyclohexane in Tables X–XII.

Calculations of the surface excesses Γ require a knowledge of the freezing point depression θ of the solution under investigation. In the case of cetyl alcohol and myristic acid the low solubilities at ~ 5°C. preclude the possibility of measuring θ for all the solutions which were used. Since such data for dilute solutions as could be obtained fell on the general $\theta - N_s$ curves for homologues given in the last paper, the *assumption* has been

TABLE I

Caprylic Acid in Benzene at 10°C.

N_s	θ	γ	$\dfrac{N_s}{N_o}$	$\dfrac{\partial \gamma}{\partial \theta}$	$\Gamma^{(1)}$	$\Gamma^{(N)}$	$\Gamma^{(u)}$	A	F
	°C.	dynes/cm.			g.-moles/cm². $\times 10^{-10}$			Å²	dynes/cm.
0.358	17.05	13.6	0.588	0.210	3.14	1.97	4.74	34.8	21.4
0.218	7.99	16.3	0.279	0.445	3.16	2.47	4.13	40.0	18.7
0.122	4.71	18.6	0.139	0.750	2.65	2.31	4.09	50.9	16.4
0.0584	2.040	22.1	0.0621	1.75	2.76	2.60	2.80	58.8	12.9
0.0285	1.002	25.1	0.0293	3.60	2.65	2.57	2.63	62.7	9.9
0.0094	0.353	27.8	0.00948	10.0	2.41	2.39	2.47	66.9	5.2
0.000	0	35.0							

TABLE II

Caprylic Acid in Benzene at 40°C.

N_s	θ	γ	$\dfrac{N_s}{N_o}$	$\dfrac{\partial \gamma}{\partial \theta}$	$\Gamma^{(1)}$	$\Gamma^{(N)}$	$\Gamma^{(u)}$	A	F
	°C.	dynes/cm.			g.-moles/cm². $\times 10^{-10}$			Å²	dynes/cm.
0.358	17.05	12.9	0.588	0.210	3.14	1.98	4.74	34.8	20.9
0.218	7.99	15.3	0.279	0.450	3.18	2.50	4.18	39.5	18.5
0.122	4.71	17.6	0.139	0.752	2.66	2.33	4.09	50.9	16.2
0.0893	3.23	18.7	0.098	1.10	2.74	2.50	3.13	52.7	15.1
0.0584	2.04	20.7	0.0621	1.74	2.74	2.59	2.80	58.8	13.1
0.0285	1.002	23.1	0.0291	3.55	2.63	2.55	2.63	62.7	10.7
0.0094	0.353	26.7	0.00948	10.3	2.44	2.39	2.51	66.3	7.1
0.0047	0.180	27.7	0.00473	19.7	2.37	2.35	2.40	68.8	6.1
0	0	33.8							

TABLE III

n-Octyl Alcohol in Benzene at 10°C.

N_s	θ	γ	$\dfrac{N_s}{N_o}$	$\dfrac{\partial \gamma}{\partial \theta}$	$\Gamma^{(1)}$	$\Gamma^{(N)}$	$\Gamma^{(u)}$	A	F
	°C.	dynes/cm.			g.-moles/cm². $\times 10^{-10}$			Å²	dynes/cm.
0.123	3.281	14.4	0.140	1.73	6.05	5.30	6.29	26.3	20.6
0.0904	2.628	16.1	0.0995	2.16	5.37	4.88	5.59	29.5	18.9
0.0589	1.946	17.3	0.0625	2.92	4.56	4.29	4.71	35.0	17.7
0.0282	1.261	19.9	0.0290	4.50	3.26	3.17	3.39	48.8	15.1
0.0230	1.070	20.8	0.0235	5.30	3.11	3.04	3.22	51.3	14.2
0.0162	0.825	22.3	0.0165	6.90	2.84	2.80	2.92	56.4	12.7
0.00968	0.597	24.5	0.00975	9.52	2.32	2.30	2.39	69.1	10.5
0.00541	0.350	28.2	0.00544	16.25	2.21	2.20	2.25	73.6	6.8
0	0	35.0	0						

TABLE IV

n-Octyl Alcohol in Benzene at 40°C.

N_s	θ	γ	$\dfrac{N_s}{N_o}$	$\dfrac{\partial \gamma}{\partial \theta}$	$\Gamma^{(1)}$	$\Gamma^{(N)}$	$\Gamma^{(u)}$	A	F
	°C.	dynes/cm.			g.-moles/cm². $\times 10^{-10}$			Å²	dynes/cm.
0.123	3.281	16.2	0.140	1.73	6.05	5.30	6.29	26.3	16.6
0.0904	2.628	17.2	0.0995	2.16	5.37	4.88	5.59	29.5	15.8
0.0589	1.946	18.7	0.0625	2.92	4.56	4.29	4.71	35.0	14.1
0.0282	1.261	22.3	0.0290	4.50	3.26	3.17	3.39	48.8	10.5
0.0230	1.070	22.8	0.0235	5.30	3.11	3.04	3.22	51.3	10.0
0.0162	0.825	24.8	0.0165	6.90	2.84	2.80	2.92	56.4	8.0
0.00968	0.597	25.8	0.00975	9.52	2.32	2.30	2.39	69.1	7.0
0.00541	0.350	29.1	0.00544	16.25	2.21	2.20	2.25	73.6	3.7
0	0	33.8							

TABLE V

n-Octanol in Cyclohexane at 25°C.

N_s	θ	γ	$\dfrac{N_s}{N_o}$	$\dfrac{\partial \gamma}{\partial \theta}$	$\Gamma^{(1)}$	$\Gamma^{(N)}$	$\Gamma^{(u)}$	A	F
	°C.	dynes/cm.			g.-moles/cm². $\times 10^{-10}$			Å²	dynes/cm.
0	0	49.6							
0.147	7.35	16.1	0.172	0.4	7.0	5.97	7.38	22.4	33.5
0.0708	4.62	18.1	0.0762	1.0	7.75	7.21	7.82	21.1	31.5
0.0348	2.77	20.0	0.0361	1.7	6.24	6.03	6.32	26.1	29.6
0.0125	1.484	23.4	0.0127	4.7	6.07	6.01	6.14	26.9	26.2
0.00655	0.949	26.6	0.00660	8.8	5.91	5.90	6.01	27.5	23.0
0.00342	0.693	31.0	0.00345	16.6	5.65	5.65	5.72	28.9	18.6
0.00224	0.494	34.3	0.00226	24.5	5.63	5.63	5.63	29.3	15.3
0.00156	0.363	37.0	0.00158	31.2	5.02	5.02	5.02	32.9	12.6
0.000816	0.190	41.3	0.00082	31.2	2.60	2.60	2.60	63.4	8.3
0.000423	0.100	44.2	0.00042	31.2	1.33	1.33	1.33	124.0	5.4

TABLE VI

n-Caprylic in Cyclohexane at 25°C.

N_s	θ	γ	$\frac{N_s}{N_o}$	$\frac{\partial\gamma}{\partial\theta}$	$\Gamma^{(1)}$	$\Gamma^{(N)}$	$\Gamma^{(u)}$	A	F
	°C.	dynes/cm.			\multicolumn{3}{c}{g.-moles/cm². × 10⁻¹⁰}	Å²	dynes/cm.
0	0	48.2							
0.0785	9.45	20.7	0.0852	0.487	4.12	3.79	4.43	37.3	27.5
0.0486	5.85	22.9	0.0511	0.788	3.99	3.80	4.22	39.1	25.3
0.0330	4.01	24.9	0.0342	1.145	3.88	3.75	4.00	41.2	23.3
0.0168	2.126	27.8	0.0171	2.17	3.68	3.61	3.77	43.8	20.4
0.00852	1.070	30.9	0.00860	4.30	3.66	3.64	3.71	44.4	17.3
0.00426	0.525	33.6	0.0043	8.77	3.74	3.73	3.69	44.7	14.6
0.00155	0.194	37.2	0.00156	15.9	2.46	2.46	2.46	67.2	11.0
0.00040	0.040	41.1	0.00040	58.2	2.31	2.31	2.31	71.5	7.1

TABLE VII

n-Octyl Alcohol in Nitrobenzene at 25°C.

N_s	θ	γ	$\frac{N_s}{N_o}$	$\frac{\partial\gamma}{\partial\theta}$	$\Gamma^{(1)}$	$\Gamma^{(N)}$	$\Gamma^{(u)}$	A	F
	°C.	dynes/cm.			\multicolumn{3}{c}{g.-moles/cm². × 10⁻¹⁰}	Å²	dynes/cm.
0	0	24.7							
0.0159	0.795	21.0	0.0162	4.10	1.50	1.48	1.58	104.0	3.7
0.0314	1.415	18.8	0.0324	3.60	2.65	2.57	2.76	59.8	5.9
0.0609	2.254	16.0	0.0648	2.90	4.27	4.00	4.46	37.1	8.7
0.0888	2.792	14.8	0.0975	2.50	5.54	5.04	5.70	29.0	9.9
0.115	3.168	13.6	0.130	2.20	6.50	5.75	6.64	24.8	11.1
0.139	3.440	13.1	0.162	1.90	6.97	6.00	7.01	23.6	11.6
0.245	4.450	11.1	0.324	1.50	12.6				

TABLE VIII

n-Caprylic Acid in Nitrobenzene at 25°C.

N_s	θ	γ	$\frac{N_s}{N_o}$	$\frac{\partial\gamma}{\partial\theta}$	$\Gamma^{(1)}$	$\Gamma^{(N)}$	$\Gamma^{(u)}$	A	F
	°C.	dynes/cm.			\multicolumn{3}{c}{g.-moles/cm². × 10⁻¹⁰}	Å²	dynes/cm.
0	0	24.9							
0.0154	0.56	20.6	0.0157	4.75	1.67	1.64	1.76	97.7	4.3
0.0312	0.951	19.7	0.0322	2.95	2.13	2.06	2.28	72.2	5.8
0.0605	1.746	17.1	0.0644	1.82	2.62	2.46	2.89	57.2	7.8
0.0860	2.432	15.4	0.0941	1.47	3.09	2.83	3.44	48.0	9.5
0.114	3.079	15.1	0.126	1.23	3.46	3.08	3.89	42.5	9.8
0.138	3.73	14.4	0.160	0.98	3.50	3.02	4.06	40.6	10.5
0.244	6.42	12.5	0.323	0.57	4.11	3.11	4.86	34.0	12.4

TABLE IX

Caprylic Acid in Tetradecane at 25°C.

N_s	θ	γ	$\dfrac{N_s}{N_o}$	$\dfrac{\partial\gamma}{\partial\theta}$	$\Gamma^{(1)}$	$\Gamma^{(N)}$	$\Gamma^{(u)}$	A	F
	°C.	dynes/cm.			g.-moles/cm². $\times 10^{-10}$			Å²	dynes/cm.
0.290	2.47	15.2	0.409	2.30	4.40	3.11	5.39	30.6	33.2
0.154	1.310	18.9	0.182	4.50	3.83	3.23	4.46	37.1	29.5
0.0793	0.670	22.4	0.0861	7.60	3.06	2.82	3.43	48.1	26.0
0.0291	0.245	27.2	0.0300	18.1	2.54	2.46	2.68	61.6	21.2
0.0133	0.115	30.3	0.0135	29.6	1.86	1.84	1.95	84.9	18.1
0.00665	0.060	33.4	0.0067	32.4	1.01	1.00	1.01	(165)	15.0
0.00332	0.030	36.2	0.0034	68.4	1.08	1.07	1.10	150	12.2
0	0	48.4							

TABLE X

Cetyl Alcohol in Benzene at 25°C.

N_s	θ	γ	$\dfrac{N_s}{N_o}$	$\dfrac{\partial\gamma}{\partial\theta}$	$\Gamma^{(1)}$	$\Gamma^{(N)}$	$\Gamma^{(u)}$	A	F
	°C.	dynes/cm.			g.-moles/cm². $\times 10^{-10}$			Å²	dynes/cm.
0.0595	1.99	18.3	0.0633	3.82	6.36	5.98	6.54	25.3	16.3
0.0313	1.308	21.4	0.0323	5.78	4.91	4.76	5.04	32.7	13.4
0.0214	1.01	23.8	0.0219	7.50	4.32	4.23	4.44	37.2	11.1
0.0144	0.750	25.6	0.0146	8.4	3.22	3.18	3.30	50.0	9.3
0.00772	0.470	28.2	0.00775	10.4	2.12	2.11	2.17	76.1	6.7
0.00404	0.300	30.8	0.00407	13.2	1.42	1.42	1.44	115	4.1
0.00148	0.100	33.3	0.00149	16.8	0.654	0.654	0.654	252	1.6
0	0	34.9							

TABLE XI

Myristic Acid in Benzene at 25°C.

N_s	θ	γ	$\dfrac{N_s}{N_o}$	$\dfrac{\partial\gamma}{\partial\theta}$	$\Gamma^{(1)}$	$\Gamma^{(N)}$	$\Gamma^{(u)}$	A	F
	°C.	dynes/cm.			g.-moles/cm². $\times 10^{-10}$			Å²	dynes/cm.
0.0435	1.114	23.4	0.0455	3.20	3.83	3.65	3.98	41.4	11.7
0.0292	0.78	24.8	0.0301	4.68	3.70	3.60	3.83	43.1	10.3
0.0197	0.54	26.7	0.0201	6.76	3.57	3.50	3.59	44.9	8.4
0.00994	0.305	28.3	0.0101	10.3	2.74	2.71	2.80	59.0	6.8
0.00664	0.215	29.5	0.0067	14.05	2.49	2.48	2.49	66.7	5.6
0.00363	0.100	30.8	0.00363	18.1	1.72	1.71	1.75	94.0	4.3
0.00182	0.050	31.8	0.00182	25.0	1.19	1.18	1.20	138	3.3
0		35.1							

TABLE XII

Myristic Acid in Cyclohexane at 25°C.

N_s	θ	γ	$\dfrac{N_s}{N_0}$	$\dfrac{\partial \gamma}{\partial \theta}$	$\Gamma^{(1)}$	$\Gamma^{(N)}$	$\Gamma^{(u)}$	A	F
	°C.	dynes/cm.			\multicolumn{3}{c}{g.-moles/cm². × 10^{-10}}		Å²	dynes/cm.
0.0366	4.42	28.7	0.0380	(0.6)	(2.26)				
0.0270	3.27	29.5	0.0277	1.2	3.29	3.21	3.49	47.3	20.3
0.0179	2.77	31.0	0.0181	1.85	3.24	3.19	3.35	49.3	18.8
0.00862	1.07	33.8	0.00867	3.80	3.26	3.24	3.32	49.8	16.0
0.0058	0.73	35.4	0.00582	5.20	3.00	2.99	3.06	53.9	14.8
0.00316	0.39	37.0	0.00317	7.00	2.20	2.19	2.23	74.0	12.8
0.00085	0.10	40.7	0.00085	21.65	1.83	1.82	1.83	90.2	9.1
0		49.8							

made that θ for more concentrated solutions can be read from the general curves.

In Figs. 1–10 are plotted interfacial tensions against freezing point depression θ and mole fraction of surface active material N_s. Due to the close linearity between θ and N_s in the case of the fatty acids the $\gamma \sim \theta$ and $\gamma \sim N_s$ curves are practically indistinguishable but this is not so for the alcohols.
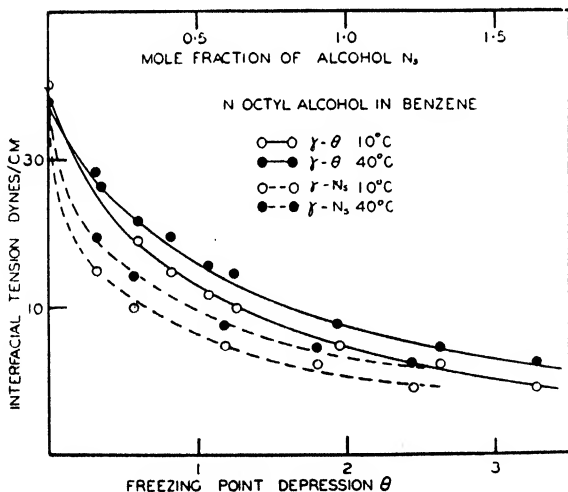
FIG. 1. Interfacial tension *vs.* freezing point depression for solutions of *n*-octyl alcohol in benzene.
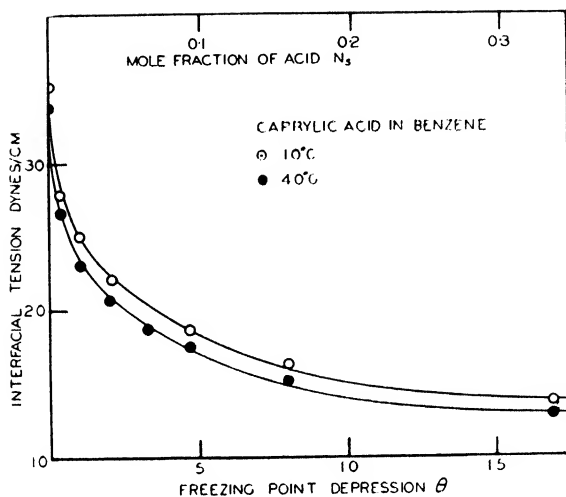
Fig. 2. Interfacial tension *vs.* freezing point depression for solutions of
n-caprylic acid in benzene.
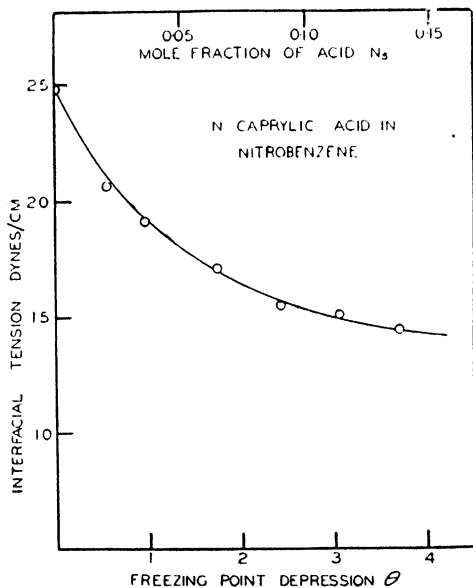
Fig. 3. Interfacial tension *vs.* freezing point depression for solutions of
n-caprylic acid in nitrobenzene.
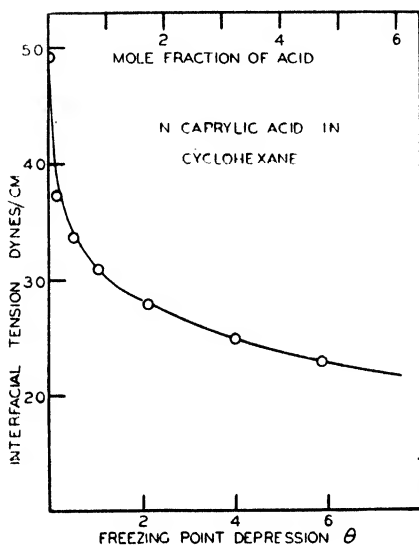
FIG. 4. Interfacial tension *vs.* freezing point depression for solutions of
n-caprylic acid in cyclohexane.
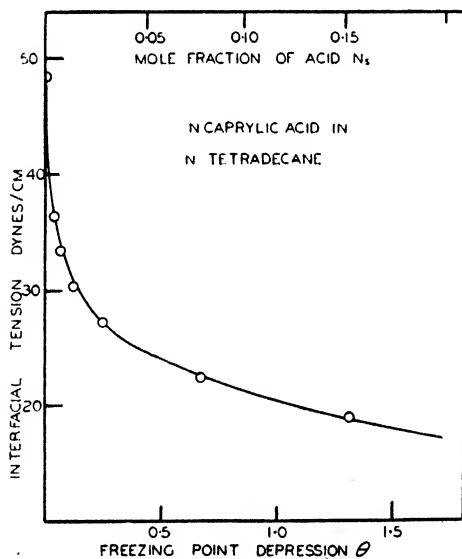
FIG. 5. Interfacial tension *vs.* freezing point depression for solutions of
n-caprylic in *n*-tetradecane.
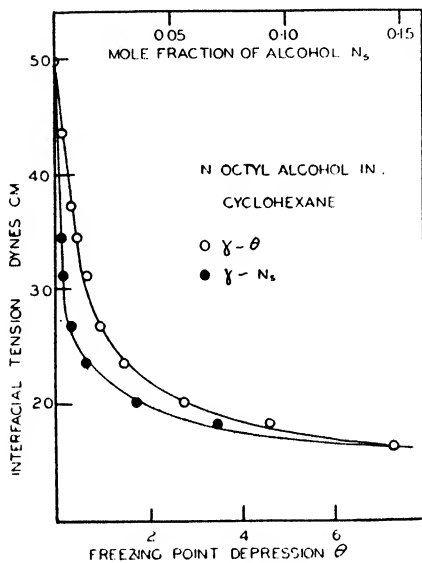
FIG. 6. Interfacial tension *vs.* freezing point depression for solutions of
n-octyl alcohol in cyclohexane.
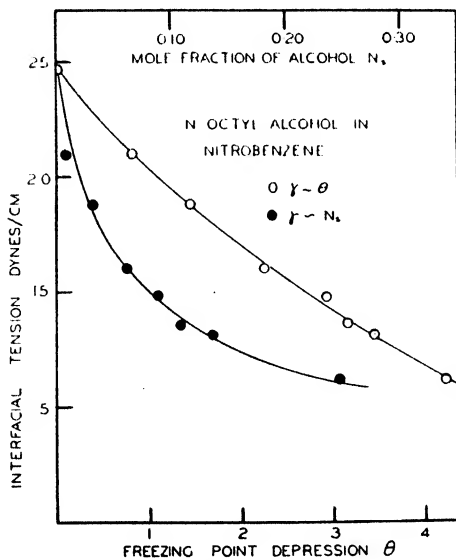
FIG. 7. Interfacial tension *vs.* freezing point depression for solutions of
n-octyl alcohol in nitrobenzene.
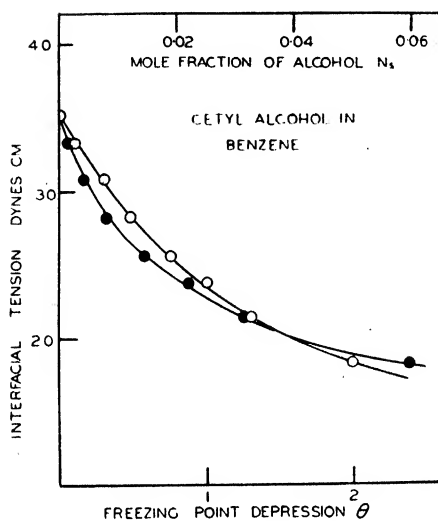
FIG. 8. Interfacial tension *vs.* freezing point depression for solutions of cetyl alcohol in benzene.
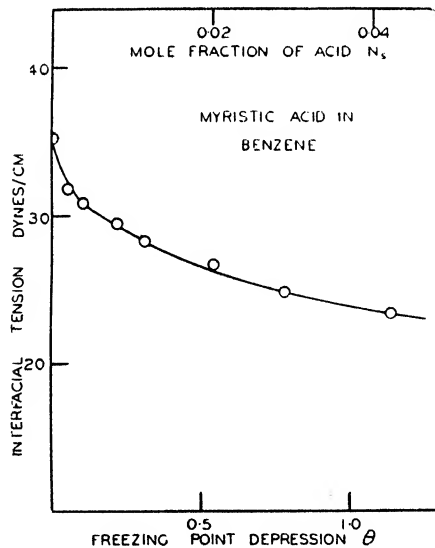
FIG. 9. Interfacial tension *vs.* freezing point depression for solutions of myristic acid in benzene.
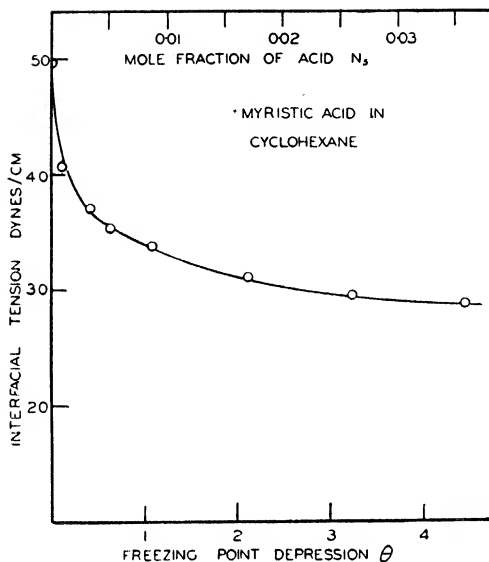
FIG. 10. Interfacial tension *vs.* freezing point depression for solutions of myristic acid in cyclohexane.

Finally in Figs. 11–13 are drawn force-area curves for the adsorbed films, the area per molecule being calculated as shown below.
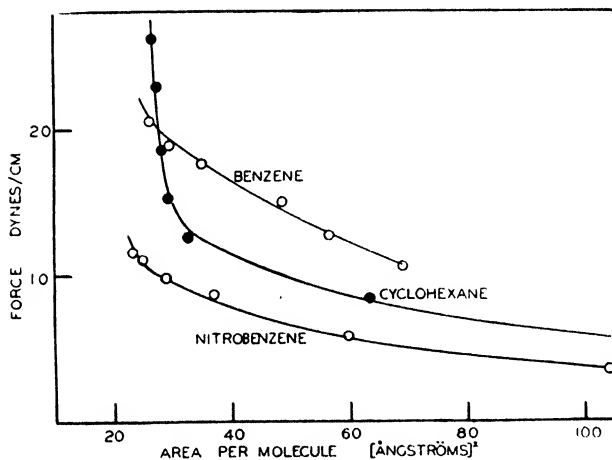
FIG. 11. Force-area curves for *n*-octyl alcohol in various solvents.
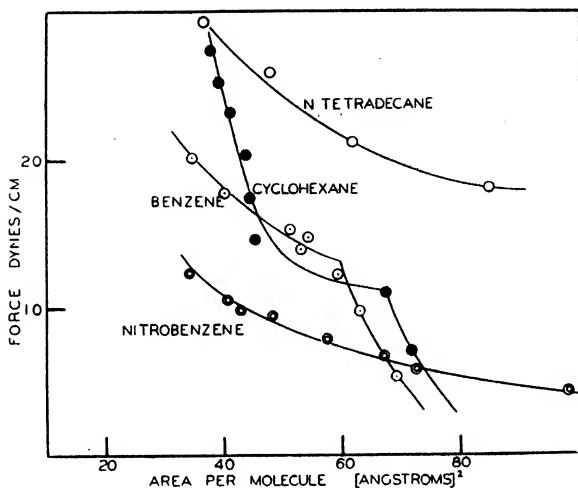
Fig. 12. Force-area curves for *n*-caprylic acid in various solvents.
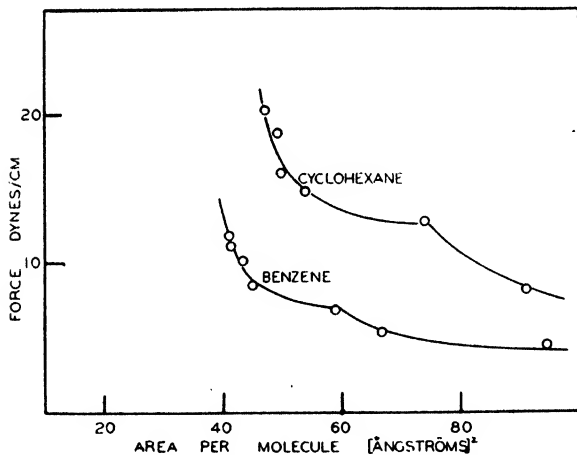
Fig. 13. Force-area curves for myristic acid in benzene and cyclohexane.

Discussion

The calculation of the surface excess of the film-forming compound, $\Gamma^{(1)}$, $\Gamma^{(N)}$, $\Gamma^{(u)}$, as defined by Guggenheim and Adam (5), follows exactly the treatment given in the previous paper, *viz.*

$$\Gamma^{(1)} = \frac{N_s}{N_o} \cdot \frac{T_o^2}{L \cdot T} \cdot \frac{\partial \gamma}{\partial \theta} \qquad (1)$$

and

$$\Gamma^{(N)} = \frac{\Gamma^{(1)}}{1 + \dfrac{N_s}{N_o}}, \tag{2}$$

$$\Gamma^{(a)} = \frac{A_o\Gamma^{(N)} + N_s}{A_oN_o + A_sN_s}, \tag{3}$$

where

A_s = cross-sectional area of solute molecule,
A_o = cross-sectional area of solvent molecule.

The area, A, per solute molecule in the adsorbed film is given by $A = 1/\Gamma^{(a)}$ and the force $F = \gamma - \gamma_o$ where γ_o is the interfacial tension of the pure solvent against water.

It was suggested in the previous paper that oil-soluble compounds adsorbed at the oil-water interface are oriented with the polar group in the interface and the hydrocarbon chain *entirely* in the oil phase. This conclusion was based on consideration of the energetics and on the remarkably small effect of increased chain length compared to corresponding effects at air-water surfaces. The force-area curves for n-caprylic acid and myristic acid, and for n-octyl alcohol and cetyl alcohol, show that doubling the chain length has very little effect on the properties of the film

Adam (1) makes the general statement that, at oil-water interfaces, the lateral adhesion between the hydrocarbon chains is so reduced that a material which forms a "liquid-expanded" film on water forms a "gaseous" or highly expanded film at an oil-water interface. This does not appear to be borne out by the present data, for while it is true that, at a given surface pressure, myristic acid occupies a larger area in the film at an oil-water interface than at an air-water surface, yet, nevertheless, the force-area curve contains a transition point characteristic of "liquid-expanded" films. Further, although the area per molecule is about 100% greater under a given pressure, at an oil-water interface, still the "transition pressure" is actually lower by *ca.* 10 dynes/cm. Similarly, the lower homologues occupy an area in the film at oil-water interfaces approximately twice that at an air-water surface, at a given pressure. This may be described as an "expansion" in going from an air-water to an oil-water interface. On the other hand, however, the fatty acids $C_4 - C_{14}$ yield force-area curves with a transition point and a shape characteristic of "liquid-expanded" films on water. This is in sharp contrast to their behavior at an air-water surface, where the fatty acids $C_4 - C_{12}$ form imperfect "gaseous" films (at *ca.* 20°C.) in which lateral adhesion between neighboring film molecules is small. Hence, if the particular shape of force-area curve is truly indicative of a "liquid-expanded" film at an

oil-water interface, then the fatty acids would appear to form films at an oil-water interface in which lateral adhesion is greater than at air-water surfaces. In this event the area per molecule in the film at a given surface pressure would not be the sole criterion for determining whether the film is more "expanded" at an oil-water interface. The whole force-area curve would need to be considered.

There is, moreover, some basis for reasoning that, although the area per molecule in the film may be greater at an oil-water interface, lateral adhesion in the film may be greater.

The films discussed here resemble expanded films, as discussed by Langmuir (9), in that the polar groups are relatively far apart except under high compression. However, Langmuir considers that, at an air-water surface, the hydrocarbon chains form what might loosely be termed a liquid, in which the forces operating between the chains are the cohesive forces of pure paraffin liquids. Increased temperature causes the film molecules to "evaporate" from an environment which is essentially a liquid to one in which the molecules are relatively far apart and the forces between neighboring molecules are small. Thus, the latent heat of "evaporation" is considerable, ca. 2 kcals./mole, and the effect of temperature on the film properties is quite marked.

Now, in the suggested model for a film at an oil-water interface, solvent molecules are present in addition to the film molecules and the closeness of approach between hydrocarbon chains will be governed by the balance of cohesive forces between the chains themselves, and between the chains and the solvent molecules. A separation of hydrocarbon chains from a state in which they are close neighbors to one in which they are relatively far apart would merely remove the film molecule from an environment of its fellows to one in which solvent molecules are still close neighbors. Thus, the change in force field, and hence the latent heat, corresponding to such a separation or "expansion" would be much less than for the similar change at an air-water surface.

Experiments using n-octyl alcohol and n-caprylic acid at 10°C. and 40°C. show clearly the small effect of temperature changes, in accordance with this hypothesis.

Such effects of temperature, moreover, would be greatest for systems in which the cohesion between the hydrocarbon chains and the solvent molecules is small, so that under high compression the film molecules can squeeze out solvent molecules and approach one another closely.

In fact, however, general observations on the relative solubility of paraffin derivatives in paraffins and other solvents suggest that interactions between hydrocarbon chains and many solvent molecules, $e.g.$, benzene, are considerably stronger than between the chains themselves. Thus, there is a strong likelihood that, even at high surface pressures, the

film molecule will be preferentially surrounded by solvent molecules rather than by its fellows.

Variations in the cohesive forces between solvent molecules and hydrocarbon chains should be reflected in the properties of the films adsorbed from various solvents. The greater the interaction the less will the film approximate to the "gaseous" type encountered at air-water surfaces. Thus, due to this lateral adhesion, we should expect films adsorbed from benzene solutions to be less "gaseous" or more "condensed" than those adsorbed from paraffin solutions. Experiment shows that this is indeed so; in the case of tetradecane the film molecules of n-caprylic occupy a much greater area, at a given surface pressure, than they do when benzene is the solvent. Cyclohexane solutions behave in much the same way as benzene solutions, as might be expected from a comparison of their respective solvent properties as regards fatty acids, alcohols, *etc.* Films of n-caprylic acid occupy even less area, at a given pressure, when adsorbed from nitrobenzene solutions. At first sight this would appear to be anomalous, in that nitrobenzene exhibits an inferior solvent power compared to benzene for fatty acids. However, it is probable that at the oil-water interface the $-NO_2$ group is oriented toward the water so that polar-head interaction occurs in addition to the interactions between the benzene ring and the hydrocarbon chain.

However, although in general the results are in agreement with the proposed model for the film at an oil-water interface, much work remains to be done before any general quantitative conclusions may be reached. Many of the solvents which would be of interest in this investigation have freezing points inconveniently low for osmotic determinations and recourse to boiling point measurements will be necessary in future work.

Summary

Experiments on the properties of films adsorbed at oil-water interfaces have been extended to include variation of the chain length of the adsorbed molecules, temperature, and the nature of the oil. In general, the evidence supports the hypothesis of an interfacial film in which the polar group is anchored at the interface and the hydrocarbon chain is entirely within the oil phase.

Changes in the degree of "condensation" or "expansion" of the films adsorbed from a number of solvents support the hypothesis that the cohesion between the solvent molecules and the hydrocarbon chain of the film molecule is an important factor, and reasons are adduced to show

that lateral adhesion in films adsorbed at oil-water interfaces may be greater, rather than less, than at air-water surfaces.

REFERENCES

1. ADAM, The Physics and Chemistry of Surfaces. Oxford, 1941.
2. ALEXANDER AND TEORELL, *Trans. Faraday Soc.* **35**, 733 (1939).
3. ASKEW AND DANIELLI, *Proc. Roy. Soc. (London)* **155**A, 695 (1935).
4. GOUY, *Ann. phys.* **6**, 5 (1916).
5. GUGGENHEIM AND ADAM, *Proc. Roy. Soc. (London)* **139**A, 218 (1933).
6. HARKINS AND BROWN, *J. Am. Chem. Soc.* **41**, 499 (1919).
7. HARKINS AND JORDAN, *ibid.*, **52**, 1751 (1930).
8. HUTCHINSON, *J. Colloid Sci.* **3**, 219 (1948).
9. LANGMUIR, *J. Chem. Phys.* **1**, 756 (1933).

THE DETERMINATION OF THE PARTICLE SIZE OF AEROSOLS BY SCATTERED LIGHT [1]

Locke White, Jr.[2] and Douglas G. Hill

From the Departments of Chemistry of The University of North Carolina, Chapel Hill, and Duke University, Durham, North Carolina

Received January 27, 1948

There is currently much interest in the determination of the state of aggregation of polymers in solution by means of their light-scattering properties. During World War II similar methods were used to determine the particle size of aerosols. According to a procedure devised by La Mer and Sinclair (1), there are two size ranges easily characterized by somewhat different properties: for aerosols with particles of uniform radii between 0.3 and 1 μ, the size is indicated by the number of so-called "spectral orders"; for radii from 0.3 μ down to about 0.05 μ, the degree of polarization of light scattered perpendicularly is the most convenient measure of size. La Mer and Sinclair showed that the appearance of "spectral orders" followed from the theoretical work of Mie (2), upon which the determination of size from polarization measurements was also based. This paper reports a brief experimental confirmation of the predictions of the theory in the polarization range.

The method of Wells and Gerke (3) was chosen for an independent determination of particle size. In this method, the motion of charged spherical smoke particles under an alternating electric field is photographed in an ultramicroscope. The amplitude of the vibratory motion is proportional to the velocity of the particle, from which the diameter may be calculated by Cunningham's (4) corrected form of Stokes' law. When, as is usual in this procedure, the particles are artificially charged after formation of the smoke, an error is introduced because of the large number of multiply charged particles, while the calculations assume single charges. Since our smokes were formed by condensation of a non-volatile liquid on ionic nuclei (by a procedure also due to La Mer and his co-workers), it was considered that the particles would be predominantly singly charged. This supposition was directly confirmed by a crude modi-

fication of Millikan's procedure for determining the electronic charge. The cell designed for the Wells and Gerke procedure was used for the measurements of charge. Brownian movement was so strong as to cause diffusion of many of these small particles out of focus before the measurements could be completed, so that the procedure was very tedious. Nevertheless, the charges of 31 particles from three smokes were measured, and only one of these was multiply charged. Furthermore, it was the strong impression of the observers that the fraction of multiply charged particles was almost certainly less than 1/31. It was not possible in the cell of the Wells and Gerke apparatus to isolate only a single particle in the field; instead, many particles were visible. Although only one of these was specifically timed in each individual measurement, most of the visible particles affected by the field (certainly 20–30) seemed to move up and down in unison with the application and removal of the electrical field, without seriously changing their relative positions. It was very unusual to find a charged particle with inconsistent behavior, although such behavior was immediately obvious. Since these aerosols were of very uniform particle size, it was evident that the overwhelming majority of the particles were charged singly or not at all.

In the Wells and Gerke procedure we used a cell with electrodes 1 cm. square, separated by 4 mm. The field of the ultramicroscope limited the observations to a small, undistorted region of the electrical field. A high-pressure mercury arc (General Electric H-6) was used as light source in conjunction with a Bausch and Lomb ultramicroscope, and photography was on Agfa Superpan Supreme 35 mm. film with a Micro-Ibso attachment for a Leica camera. Rather than making enlargements of the negatives, we found it more convenient, and at least as accurate, simply to draw the zigzag paths on paper placed in the enlarger. Particles were considered only if at least two amplitudes of oscillation could be measured.

Size distribution histograms of 5 smokes were determined with the following results:

Smoke	A	B	C	D	E
Optical radius, μ	0.155	0.25	0.32	0.46	0.48
Radius at maximum of distribution histogram	0.15–0.17	0.225–0.275	0.31–0.35	0.45–0.51	0.41–0.47
Average radius from histogram	0.18	0.26	0.37	0.46	0.42
Range of radii including middle 50% of observed particles	0.14–0.200	.23–0.29	0.31–0.40	0.40–0.51	0.37–0.49

By optical radius is meant the radius determined by the light-scattering method appropriate to the size. For A and B, the polarization method was used; for C, D, and E, the method of spectral orders.

We consider the agreement of the Wells and Gerke method with the method of spectral orders, which has had experimental corroboration by other methods, as further justification of the use of the Wells and Gerke method to confirm the polarization measurements. The agreement in the polarization range (smokes A and B) is well within experimental error.

In the course of this investigation, the following general observations concerning the Wells and Gerke method were made:

(1) An attempt to charge any large fraction of the particles after the smoke is formed will result in excessive multiple charging.

(2) Even if singly charged particles are used, noticeable discrimination against the smaller particles will result if the fields are too strong. In general, confidence should be placed only in distribution curves which are not significantly changed if the concentrations and the field strengths are reduced.

Our apparatus was not sufficiently sensitive to record the oscillations of particles much smaller than 0.15 μ radius.

REFERENCES

1. LA MER, V. K., AND SINCLAIR, D., *OSRD Rept. No.* **1857** (1943). Available as OPB No. 944. Also see SINCLAIR, D., *J. Opt. Soc. Am.* **27**, 475 (1947), and LA MER, V. K., AND BARNES, M. D., *J. Colloid Sci.* **1**, 71, 79 (1946).
2. MIE, G., *Ann. Phys.* **25**, 377 (1908).
3. WELLS, P. V., AND GERKE, R. H., *J. Am. Chem. Soc.* **41**, 312 (1919).
4. CUNNINGHAM, *Proc. Roy. Soc. London* **83A**, 357 (1910).

ON THE TEMPERATURE DEPENDENCE OF THE INTENSITY OF ELECTRON DIFFRACTION OF THE AGGREGATE OF MINUTE CRYSTALS—A POSSIBLE MEANS TO DETERMINE THE CLEAVAGE SURFACE OF MINUTE CRYSTALS

Shigeto Yamaguchi and Tominosuke Katsurai

From the Institute of Physical and Chemical Research,
Komagome, Bunkyo-ku, Tokyo, Japan
Received February 2, 1948

This brief account shows the intensity change of electron diffraction occurring in some inorganic substances with rising temperature. A high temperature camera, especially designed, was used to study iron oxide, thorium oxide, nickel, and magnesium oxide powder crystals. As shown in Fig. 1, the filament of nickel, platinum or tungsten was used as both
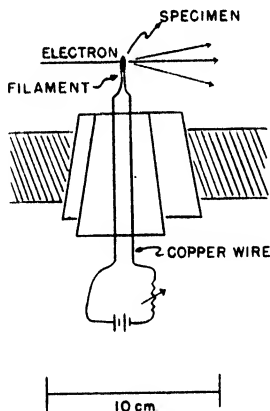
FIG. 1.

an electric furnace and specimen holder, the filament being heated to high temperature by means of direct current. Alternating current should not be used, as oscillation of the electron beam takes place in the magnetic field. The preparation of the sample was carried out by immersing the hot filament in a concentrated aqueous solution of salt (1), the crystalline sample thus obtained being suitable for the electron diffraction.

The electron beam grazes along the sample in the filament. The diffraction patterns were studied at room temperature and at the temperature range 500°–6000°C., the temperature being estimated by observing the sample's color. The results are given in each case.

1. Iron Oxide

The crystalline sample was prepared by bringing the tungsten filament, heated to 500–600°C. by a current of about 2 A, into contact with a concentrated aqueous solution of ferric nitrate. The Debye-Scherrer diffraction patterns observed at room temperature (15°C.) and 500°C. showed formation of ferroso-ferric oxide (Fe_3O_4) crystals. Temperature elevation from 15°C. to 500°C., considerably weakened the (111) and (333) diffractions, while the others remained approximately constant. (*cf.* Table I).

TABLE 1

Fe_3O_4

d_{obs}	d_x	$h_1 h_2 h_3$	$I_{obs}(15°C.)$	$I_{obs}(500°C.)$
4.8 A	4.85	*111*	w	f
3.0	2.97	220	w	w
2.53	2.53	311	v.s	v.s
2.10	2.10	400	w	w
1.63	1.61	*333*	s	m
1.48	1.48	440	m	m
1.28	1.28	533	w	w
1.10	1.09	553	m	m
0.970	0.970	751	w	w
0.858	0.859	844	w	w

d_{obs}: spacings observed in the present study.

d_x: spacings observed by X-ray diffraction (2, 3).

$h_1 h_2 h_3$: Miller indices.

$I_{obs}(15°C.)$: diffraction intensities observed at 15°C.

$I_{obs}(500°C.)$: diffraction intensities observed at 500°C.

w: weak; v.s.: very strong; s: strong;

m: moderate; f: faint.

2. Thorium Oxide

The sample was prepared from an aqueous solution of thorium nitrate by a similar procedure. Again the diffraction patterns revealed crystals of thorium oxide (ThO_2) (*cf.* Table II). Heating from 15°C. to 500°C., decreased the intensity of (311) diffraction, while the others remained constant.

TABLE II

ThO₂

d_{obs}	d_x (4, 5)	$h_1h_2h_3$	$I_{obs}(15°C.)$	$I(50_{obs}0°C.)$
3.2 A	3.22	111	s	s
2.83	2.80	200	w	w
1.98	1.97	220	s	s
1.68	1.68	*311*	*s*	*m*
1.28	1.280	331	w	w
1.14	1.140	422	w	w
1.07	1.074	333	w	w

3. Nickel

The specimen was prepared from an aqueous solution of nickel nitrate or sulphate, and diffraction studied at 15°C. and 500°C., the patterns showing formation of nickel crystals with random orientation (*cf.* Table III). The intensity of diffraction from (200) and (220) at 500°C. was

TABLE III

Ni

d_{obs}	d_x (6, 7)	$h_1h_2h_3$	$I_{obs}(15°C.)$	$I_{obs}(500°C.)$
2.0 A	2.03	111	m	m
1.76	1.76	*200*	s	*m*
1.25	1.244	*220*	*v.s*	s
1.08	1.061	311	m	m
1.02	1.017	*222*	w	w
0.803	0.808	331	s	s
0.788	0.788	420	m	m
0.719	0.719	422	w	w
0.678	0.678	333	w	w

distinctly less than that observed at 15°C., while that of other diffraction patterns remained approximately constant.

4. Magnesium Oxide

Crystals were prepared by sputtering magnesium oxide smoke on the cleavage surface of galena and the diffraction studied at 15°C. and 300°C. Here, only the (200) diffraction intensity diminished abnormally. The electron microscopic image shows the MgO crystals to have an exact cubic form, *i.e.*, the (100) cleavage. As in the case of Fe_3O_4, the cleavage face of MgO is identical with that of the same substance seen under the electron microscope.

5. Interpretation

We understand from the theory of X-ray diffraction in crystals, that the diffraction intensity decreases with the elevation of temperature, the decrease being attributed to the atomic vibration in the crystal lattice. At a given temperature, the atoms in the cleavage surface vibrate more violently than those in the interior of the crystal. Thus, it is expected that the intensity of electron diffraction from the Bragg surface layers begins to decrease at a comparatively lower temperature as compared with the case of the electron diffractions from the inner Bragg layers.

It has been confirmed in the present study that there are two kinds of d'ffraction: (1) abnormal intensity decrease with rising temperature, (2) intensity remaining constant, independent of temperature. The corresponding Bragg layers therefore appear to (2) exist in the interior of the crystals. Table I shows only the intensity of the (111) and (333) diffractions from the Fe_3O_4 powder crystals decreases with the elevation of the temperature. The cleavage faces of a single crystal are (111) planes. As the single crystal of natural magnetite (Fe_3O_4) has the octahedral form with cleavage surfaces of the (111) planes and their equivalent [1], the surface of the Fe_3O_4 powder crystals is identical with the cleavage faces of a single crystal of natural magnetite.

Similarly, the cleavage surfaces of ThO_2 crystals are the (311) planes (cf. Table II) while the nickel crystals are (100) and (110) (cf. Table III). A similar relation likewise holds for MgO. By observation of intensity changes of electron diffraction at various temperatures, determination can, therefore, be carried out as to which planes are the cleavage faces in the dust crystals.

SUMMARY

A special camera was constructed for the study of electron diffraction at high temperature, Fe_3O_4, ThO_2, Ni, and MgO powder crystals being used. From the change of the intensity of diffraction from various planes taking place at various temperatures, the cleavage faces of the powder crystals can be determined.

REFERENCES

1. YAMAGUCHI, S., *Nature* **146**, 333 (1940); **147**, 296 (1941).
2. HANAWALT, J. D., RINN, H. W., AND FREVEL, L. K., *Ind. Eng. Chem.* **30**, 488 (1938).
3. WYCKOFF, R. W. G., The Structure of Crystals, 291. Chemical Catalog Co., New York, 1931.
4. HANAWALT, J. D., RINN, H. W., AND FREVEL, L. K., *loc. cit.* 509.
5. WYCKOFF, R. W. G., *loc. cit.* 239.
6. HANAWALT, J. D., RINN, H. W., AND FREVEL, L. K., *loc. cit.* 496.
7. WYCKOFF, R. W. G., *loc. cit.* 206.

[1] A single crystal of magnetite of octahedral form, one edge having a length of about 1 cm., was kindly supplied by Prof. J. Suzuki of Hokkaido Imperial University.

SORPTION OF CYCLOHEXANE VAPOR BY
ALUMINUM DILAURATE [1]

George W. Shreve [2]

From the Department of Chemistry, Stanford University, Calif.
Received March 17, 1948

Aluminum dilaurate, $AlOHL_2$, shows a marked affinity for hydrocarbons. At high temperature and high dilution the soap may dissolve as very small micelles (5), forming sols. At low temperature, and at higher concentration, it forms swollen gels consisting of discrete lumps (1) in which the original soap crystallites are moistened and distended; and under intermediate conditions transparent, elastic jellies are formed which differentiate sharply from the gel but pass imperceptibly into the sol (4).

The study of the sorption of cyclohexane vapor by aluminum dilaurate in a McBain-Bakr sorption balance (2) provides information at high soap concentrations, a range not easily accessible to other methods. Two consecutive isotherms were obtained with a sample of soap exposed at 50°C. to varying pressures of cyclohexane vapor. The curves are shown in Fig. 1. The vapor pressure was increased from 9% to saturation, then reduced and again increased to saturation, and reduced again. The soap returned to its initial dry weight after both runs but showed marked differences during the course of the two isotherms.

During the first isotherm the soap remained as a white powder throughout, but during the second run it became clear and transparent. This indicates that the soap formed a gel and remained as such throughout the first isotherm, but changed to a jelly during the second sorption, probably at a pressure equal to about 85% relative pressure.

As is shown by the isotherms, the jelly not only sorbed a great deal more vapor at a given cyclohexane pressure than did the gel, but also exhibited marked hysteresis. The cycle for the gel form was perfectly reversible. The markedly lower vapor pressure of the jelly at the same composition shows that the gel was metastable up to at least 85% of soap at 50°C.

Whether gel or jelly, the soap sorbs a large amount of the solvent and the isotherm presents no flat portions. This may be contrasted with the very low sorption of water by the same soap (7). On the other hand, the behavior of the jelly form of the present soap is similar, for example, to that of rubber, which sorbs hydrocarbon avidly and gives a smooth isotherm which is, however, always completely reversible (6). Many other jelly-forming colloids show a similar behavior.
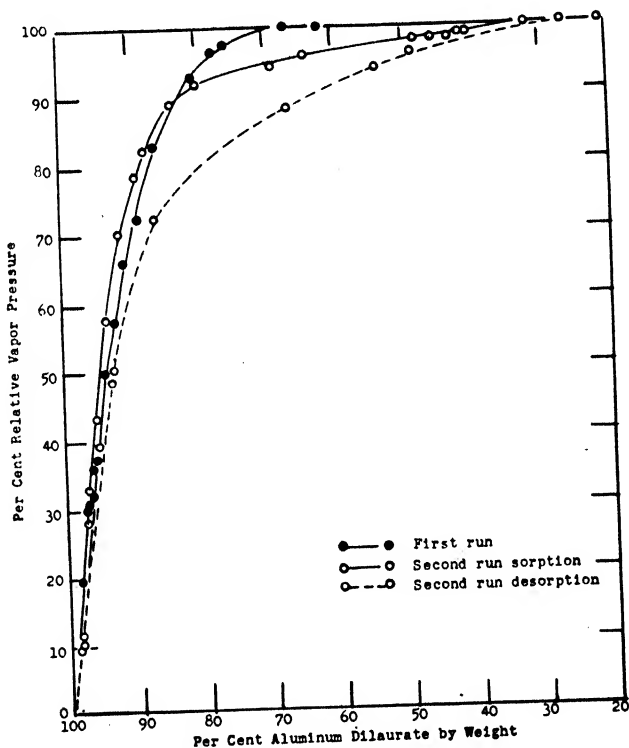
FIG. 1. Sorption of cyclohexane by aluminum dilaurate at 50°C.

The aluminum dilaurate employed in this study was the same material as that used in a previous study (7) of its water sorption. It was dried by evacuation for 5 hours within the sorption balance just prior to sealing. Cyclohexane was a middle cut, redistilled from Eastman Kodak Company No. 702 reagent grade material, m.p. 3–5°C.

The silica spring technique will be described in detail elsewhere and was adapted from that already described (2, 3, 7). The time allowed for equilibrium at each set of conditions was at least 24 hours.

Summary

Two sorption-desorption isotherms were determined at 50°C. for the system aluminum dilaurate-cyclohexane. During the first run the aluminum soap remained in the gel form, but a transition from the gel to jelly form occurred during the second sorption at 85% relative pressure. The jelly sorbed a great deal more cyclohexane at given vapor pressures than had the gel, indicating that the gel is metastable at least in the range 85–100% vapor pressure. Further, the jelly showed marked hysteresis during the desorption. In general, the form of the isotherms is similar to that observed for other jelly-forming colloids.

References

1. Marsden, S. S., Mysels, K. J., and Smith, G. H., *J. Colloid Sci.* **2**, 265 (1947).
2. McBain, J. W., and Bakr, A. M., *J. Am. Chem. Soc.* **48**, 690 (1926).
3. McBain, J. W., and Lee, W. W., *Oil & Soap* **20**, 17 (1943).
4. McBain, J. W., Mysels, K. J., and Smith, G. H., *Trans. Faraday Soc.* in press.
5. McBain, J. W., and Working, E. B., *J. Phys. & Colloid Chem.* **51**, 974 (1947).
6. Shreve, G. W., unpublished data.
7. Shreve, G. W., Pomeroy, H. H., and Mysels, K. J., *J. Phys. & Colloid Chem.* **51**, 963 (1947).

ELASTICITY, PLASTICITY, AND COMPRESSION FOR CYLINDRICAL PLANT TISSUES, AND FINE STRUCTURE OF THEIR CELL WALLS

Otto Treitel [1]

From the Botanical Laboratory, University of Pennsylvania, Philadelphia, Pa.

Received March 22, 1948

I. INTRODUCTION

The longitudinal Young's modulus E for cylindrical tissues of higher plants was measured by using the equation $E = \dfrac{\text{stress}}{\text{strain}}$ (3). This equation is only valid in the elastic range. The transverse modulus of elasticity μ, with respect to bending, was found by using the equation in the elastic range

$$\mu = \frac{\dfrac{F}{\text{cross sect.}}}{\dfrac{d}{2l}} \text{ g/cm.}^2$$

In this equation Fg is the force which produces the deflection d cm. for the cylindrical plant tissue of length $2l$ cm.

It would be a difficult problem to find the transverse Young's modulus by using lateral extension, but there is a relatively simple method to find the transverse modulus of compression by measuring lateral compression of cylindrical plant tissues.

II. METHOD AND RESULTS

The apparatus used for obtaining the transverse modulus of compression was composed of a transparent lucite prism with rectangular cross section and a metal piston (Fig. 1). The piston loosely fits in the lucite prism. This piston has a platform at the top and a cm. scale in the lengthwise direction. At the bottom of the prism, a pile of cylindrical pieces of the plant tissue to be investigated is placed. The rectangular bottom of the piston has the sides a cm. and b cm. (Fig. 2). In each layer

FIG. 1. p = platform
m = metal piston
lu = lucite prism
t = pile of pieces of the cylindrical plant tissue.
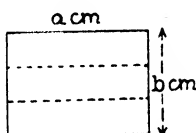
FIG. 2.

of the pile there may be 3 pieces of the plant material. The pieces touch each other. Such a pile was observed in the case of petioles of *Nymphaea*. The transverse modulus of compression in the elastic range is

$$\nu = \frac{\text{stress}}{\text{numerical compression}}.$$

The stress was found by using weight Fg on the platform. Then there is stress $= \dfrac{F}{kab}$, where k must be determined for each plant tissue. It is

$$\nu = \frac{\dfrac{F}{kab}}{\dfrac{c}{l}} \text{ g/cm.}^2,$$

where numerical compression $= \dfrac{c}{l}$. l cm. is length of the plant pile (Fig. 1) without force Fg applied, c cm. is the linear compression for the force Fg applied.

An average value for the width in the circular cross section (radius r) of the cylindrical plant tissue is $\frac{2}{3} \cdot 2r$. By taking into account air cham-

bers, in the case of *Nymphaea*, it was found necessary to substitute $2r$ by $\frac{1}{2} \cdot \frac{1}{3}b$. Generally $2r$ is substituted by the length of the solid diameter. Hence, for a cylindrical piece of plant tissue the average width $= \frac{2}{3} \cdot \frac{1}{2} \cdot \frac{1}{3}b = \frac{1}{3} \cdot \frac{1}{3}b$. The average width in a layer of the pile is $\frac{1}{3} \cdot b$. Therefore, the transverse modulus of compression for petioles of *Nymphaea* is

$$\nu = \frac{\dfrac{F}{\frac{1}{3}ab}}{\dfrac{c}{l}} \text{ g/cm}^2.$$

Generally, the transverse modulus of compression of cylindrical plant tissues is

$$\nu = \frac{\dfrac{F}{kab}}{\dfrac{c}{l}} \text{ g/cm.}^2$$

In the special case of *Nymphaea*, $k = \frac{1}{3}$.

Now, the elastic and plastic properties in the transverse direction of plant tissues investigated are determined by constructing force-compression curves. These curves were constructed for young stipes of *Laminaria agardhii*, petioles of *Nymphaea gladstonia*, stems of *Brasenia schreberi*, and branches of *Salix babylonica*. To obtain the curves we must measure force Fg and linear compression c cm. (Fig. 1). For small forces Fg we get compressions c cm. $= e$ cm., which completely disappear when the force is removed. For greater forces Fg we obtain compressions which do not completely disappear when the force is removed. This compression c cm. is composed of two parts, an elastic compression e cm. and a plastic compression p cm.; therefore, $c = e + p$. c cm. and p cm. are easily measured, and then e cm. is easily computed. If we plot a curve with Fg values as abscissas and c cm. as corresponding ordinates, we obtain the elasticity curve for the transverse direction. The elasticity curves for transverse direction of all tissues investigated are ascending curves, whose initial parts are straight lines. Fig. 3 shows the transverse elasticity curve in the case of stipes of *Laminaria agardhii*. If we plot a curve with Fg as abscissas and p cm. as corresponding ordinates, we get the plasticity curve for the transverse direction. In the case of stipes of *Laminaria agardhii* the straight line for this curve is obvious (Fig. 3). In the other cases, the straight line is more or less probable. The plasticity curve always intersects the F-axis at a point to the right of the origin. The ordinate of this point intersects the elasticity curve at the elastic limit.

In transverse direction for all tissues investigated we find ascending elasticity curves and straight plasticity curves.
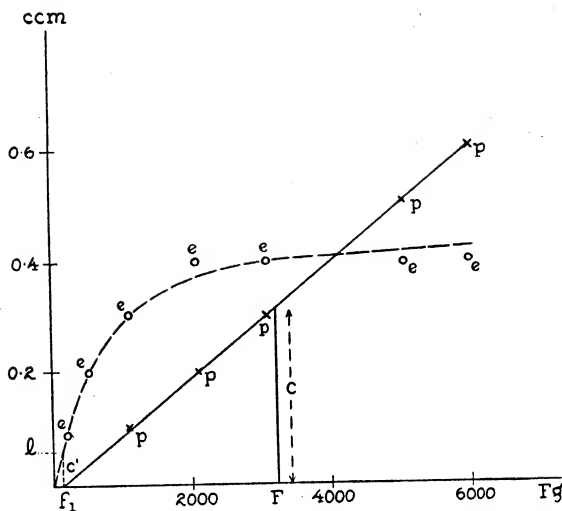
F$_{IG}$. 3.   Elasticity curve—dashes
Plasticity curve—solid line
1 = elastic limit
O = e are experimental points of the elasticity curve.
$\times$ = p are experimental points of the plasticity curve.
(F, c) is a point of the plasticity curve. In this case c is plastic compression.

Now it is possible to compute the transverse modulus of compression

$$\nu = \frac{\dfrac{F}{kab}}{\dfrac{c}{l}} \text{ g/cm.}^2$$

In the case of stipes of *Laminaria agardhii*, $k = \frac{2}{3}$, because the whole cross section is solid. At the elastic limit, Fig. 3 shows that $F = f_1 = 50$ g., and $c = 0.015$ cm. Besides, there is $l = 3.0$ cm., $a = 1.90$ cm., and $b = 0.78$ cm. Hence, for young stipes of *Laminaria agardhii* the transverse modulus of compression is

$$\nu = \frac{\dfrac{50}{\frac{2}{3} \cdot 1.90 \times 0.78}}{\dfrac{0.015}{3.0}} \text{ g/cm.}^2 = 0.1 \times 10^5 \text{ g/cm.}^2$$

This value is also obtained as average value of several measurements.

If compression is replaced by deflection with respect to bending, force-deflection curves of cylindrical plant tissues are obtained (3).

By using these force-deflection curves it was possible to compute the transverse modulus of elasticity, the transverse yield value with respect to bending, and the transverse coefficient of plasticity with respect to bending. In a similar way, by using force-compression curves (Fig. 3), it is possible to compute the transverse modulus of compression, the transverse yield value with respect to compression, and the transverse coefficient of plasticity with respect to compression.

From Fig. 3 it is found transverse yield value with respect to compression

$$f_1' = \frac{f_1}{kab} \text{ g/cm.}^2,$$

where f_1 is the distance between the origin and the beginning of the plasticity curve.

From Fig. 3 there is obtained the transverse modulus of compression

$$\nu = \frac{\dfrac{f_1}{kab}}{\dfrac{c'}{l}} \text{ g/cm.}^2 = \frac{f_1'}{\dfrac{c'}{l}} \text{ g/cm.}^2,$$

where c' cm. is the linear compression at the elastic limit of the elasticity curve.

Finally, from Fig. 3 the equation of the plasticity curve (straight line) is found to be

$$c = \phi_1(F - f_1),$$

where c cm. is compression with respect to the plasticity curve.

$$\frac{c}{l} = \phi_1' \cdot \frac{F - f_1}{kab}.$$

ϕ_1' cm.^{2}/g. is defined as transverse coefficient of plasticity with respect to compression. It is

$$\phi_1' = \frac{\dfrac{c}{l}}{\dfrac{F - f_1}{kab}} \text{ cm.}^2/\text{g.}$$

(c cm. is related to the plasticity curve).

In the case of stipes of *Laminaria agardhii*, $k = \frac{2}{3}$ (previous derivation). In the case of petioles of *Nymphaea gladstonia*, $k = \frac{1}{3}$ (previous derivation). Because of a circular cross section and air chambers in the case of stems of *Brasenia schreberi*, k is found to be 0.38. Because of a circular cross section and observation of the xylem in the case of branches of *Salix babylonica*, $k = 0.151$.

The results of measurement and computation for cylindrical plant tissues are given in the following table. In this table

ν g/cm.^{2} = transverse modulus of compression;
f_1' g/cm.^{2} = transverse yield value with respect to compression;
ϕ_1' cm.^{2}/g = transverse coefficient of plasticity with respect to compression.

TABLE I

Cyl. pl. tiss.	ν g/cm.^{2}	f_1' g/cm.^{2}	ϕ_1' cm.^{2}/g
Young stipes of *Lam. ag.*	0.11×10^5	1467.7	0.00003175
Pet. of *Nymph. gladstonia*	0.12×10^5	1524	0.00004603
Stems of *Brasenia schreberi*	0.07×10^5	732	0.00002825
Branches of *Salix babylonica*	$1.2 \ \times 10^5$	6165	0.000007808

III. Discussion

There are two systems of elastic and plastic values which have a bearing on results about the submicroscopic structure of cylindrical tissues of higher plants.

In the first system the structure is related to the longitudinal Young's modulus E, to the transverse modulus of elasticity with respect to bending μ, and to the transverse coefficient of plasticity with respect to bending ϕ (3).

In the second system the structure is related to the longitudinal Young's modulus E, to the transverse modulus of compression ν, and to the transverse coefficient of plasticity with respect to compression ϕ_1'. The elastic and plastic values of the second system are defined for a pile of cylindrical plant tissues.

According to Treitel (4) the submicroscopic structure in secondary cell walls of higher plants is determinable by the percentage of cellulose and the ratio of crystalline and amorphous cellulose. The result was found by using the elastic and plastic values of the first system.

For the second system, Table I shows that stipes of *Laminaria agardhii*, petioles of *Nymphaea gladstonia*, and stems of *Brasenia schreberi* have the same small transverse modulus of compression 0.1×10^5 g/cm.^{2} This supports the theory that for rubber-like elastic cylindrical plant tissues there is weakness in transverse direction. Between the chains of cellulose weak van der Waals forces are acting. The van der Waals forces are distance forces, *i.e.*, they are not produced by chemical bonds. Hence, it is to be understood that for different rubber-like elastic cylindrical plant tissues there is the same value 0.1×10^5 *g*/cm.^{2} of the transverse modulus of compression.

By using the first system values of the longitudinal Young's modulus E, of the transverse modulus of elasticity with respect to bending μ, and of the transverse coefficient of plasticity with respect to bending ϕ, other structural results are found.

For cylindrical plant tissues it is reasonable that the higher the value E of Young's modulus in length direction, the higher is the modulus of elasticity μ in transverse direction and the smaller is the coefficient of plasticity ϕ. Hence there is the equation

$$E = m \cdot \frac{\mu}{\phi},$$

where m is a constant, or

$$\frac{E}{\mu} \cdot \phi = m.$$

For proving this equation the following table is used (3). Petioles of

TABLE II

Cyl. pl. tiss.	$\frac{E}{\mu}$	ϕ cm.²/g	$\frac{E}{\mu} \cdot \phi$ cm.²/g
Petioles of *Nymphaea*	3	0.0000067.5	0.00002
Rhiz. of *Equisetum fluviatile*	4	0.000002016	0.00001
Stems of *Brasenia schreberi*	8	0.000003196	0.00002
Roots of *Rhus glabra*	14	0.000001293	0.00002
Branches of *Salix*	33	0.00000319	0.0001

Nymphaea, rhizomes of *Equisetum fluviatile*, stems of *Brasenia schreberi* and roots of *Rhus glabra* are rubber-like elastic cylindrical plant tissues. For these tissues $m = 0.00002$ cm.²/g,

$$E = 0.00002 \frac{\mu}{\phi} \text{ cm.}^2/\text{g}.$$

The elementary process of elastic and plastic expansion takes place in molecular or micellar dimensions. There is a relation between the equation $\frac{E}{\mu} \cdot \phi = m$ for rubber-like elastic cylindrical plant tissues and submicroscopic structure of cell walls. The ratio of moduli of elasticity $\frac{E}{\mu}$ is probably related to the crystalline domain of the submicroscopic structure, the coefficient of plasticity ϕ is probably related to the amorphous domain of the submicroscopic structure.

The equation $\frac{E}{\mu} \cdot \phi = m$ suggests that there is a similar submicroscopic structure in cell walls of rubber-like elastic cylindrical plant tissues.

According to Kubo (1), for rubber-like substances, elastic modulus
and double refraction depend upon characteristic properties of polymers
and network structure. This conclusion supports our result that elasticity
and plasticity of plant tissues are closely related to the submicroscopic
structure.

There is a distinction between the stress-strain curves of living cylin-
drical tissues of higher plants and the stress-strain curves of dead metallic
rods. This distinction is related to a distinction of structure in both cases.

(a) Rubber-like elasticity in cylindrical tissues of higher plants occurs
if the stress-strain curve is S-shaped. A small stress produces a large
strain. The average secondary cell wall contains more amorphous than
crystalline cellulose (3). There is a molecular network structure and
some micelles of cellulose in the average secondary cell wall.

(b) Metal-like elasticity in cylindrical tissues of higher plants occurs
if the stress-strain curve is a straight line with a tail. A rather large stress
produces a rather small strain. The average secondary cell wall contains
more crystalline than amorphous cellulose. There is a molecular network
structure of cellulose and many micelles in the average secondary cell wall.

(c) Elasticity in metal rods occurs if the stress-strain curve is a
straight line with a more complicated tail than in case (b). In case (c)
a large stress produces a small strain. If the metal is crystalline, the
material contains a crystalline lattice.

By using equations we get a better understanding of the cases (a),
(b), and (c).

The equation of the S-curve in (a) or, more accurately, of the elastic
part of the curve is stress $\sigma = G\left(\alpha - \dfrac{1}{\alpha^2}\right)$, where $\alpha = 1 + \text{strain } \epsilon$ (3),
σ is small, and ϵ is large.

The equation of the straight line in (b) is $\sigma = G\left(1 + \epsilon - \dfrac{1}{(1 + \epsilon)^2}\right)$,
where σ is rather large and ϵ is rather small.

$$\sigma = G\left(1 + \epsilon - \frac{1}{1 + 2\epsilon + \epsilon^2}\right) = G\left(1 + \epsilon - \frac{1}{1 + 2\epsilon}\right) = G(1 + \epsilon - 1 + 2\epsilon).$$

$\sigma = 3G\epsilon$ is the equation for the straight line in the elastic range. The
equation of the straight line in the elastic range of (c) is $\sigma = E\epsilon$, where
E is Young's modulus, σ is large, and ϵ is small. This equation represents
Hooke's law for the elasticity of solids.

Living cylindrical tissues of higher plants have the elastic behavior
represented in cases (a) and (b), dead metallic rods have the elastic
behavior represented in case (c). According to Luyet (2) solidification
of protoplasm in the amorphous state does not kill protoplasm whereas
crystallization is lethal. In the average secondary cell wall of cylindrical

plant tissues layers of crystalline and of amorphous cellulose alternate (4). Hence, it may be assumed that life for cylindrical plant tissues is only possible if the ratio of crystalline and amorphous cellulose in the average secondary cell wall is small enough. According to as yet unpublished results, this ratio increases with age. Death in plants occurs if the ratio becomes too great, or if the ratio of the longitudinal modulus of elasticity and the transverse modulus of elasticity becomes too great. In the case of *Equisetum fluviatile* rhizomes death may occur if the elastic ratio becomes greater than 6.2. Then the submicroscopic structure of this dead rhizome contains a great deal of crystalline cellulose.

IV. Summary

1. The transverse modulus of compression for rubber-like elastic cylindrical plant tissues has the small value 0.1×10^5 g/cm.^{2}

2. Van der Waals forces between the chains of cellulose in the secondary cell walls of rubber-like elastic cylindrical plant tissues are small and are only dependent on distance.

3. Elasticity, plasticity, and submicroscopic structure of average secondary cell walls in rubber-like elastic cylindrical plant tissues are closely related to each other because of the same elasticity-plasticity equation for these tissues $\frac{E}{\mu} \cdot \phi = m$. In this equation is $m = 0.00002$ cm.^{2}/g, $\frac{E}{\mu}$ is the elastic ratio, ϕ is the transverse coefficient of plasticity with respect to bending.

4. Living cylindrical tissues of higher plants have stress-strain curves which are S-shaped, or straight lines with a simple tail. In the secondary cell walls of these tissues crystalline and amorphous layers of cellulose alternate. Death occurs if the amount of the crystalline layers is too great. Dead metallic rods have stress-strain curves which are straight lines with a complicated tail. These metals may have a crystalline lattice structure. Hence, it may be assumed that a large amount of crystallization in cylindrical plant tissues means death. The life conditions are related to the amorphous layers of cellulose in cell walls which have a molecular network structure.

References

1. Kubo, R., *J. Colloid Sci.* **2**, 527–535 (1947).
2. Luyet, B. J., The Physical States of Protoplasm Compatible with Life, in Alexander, J., Colloid Chemistry, pp. 859–863, Reinhold, New York, 1944.
3. Treitel, O., *J. Colloid Sci.* **1**, 327–370 (1946).
4. Treitel, O., *ibid.* **2**, 237–246 (1947).

HIGHER ORDER TYNDALL SPECTRA
WITH BACTERIAL SUSPENSIONS [1]

Recently it was reported (1) that when supernatants obtained in serological precipitation experiments involving SI, the type-specific capsular polysaccharide of Type I pneumococcus, and a polyvalent antipneumococcus I and II horse serum were allowed to stand in the refrigerator for several days there gradually developed an additional turbidity; at the same time it became possible to demonstrate with the turbid supernatants the optical effects which have been called "higher order Tyndall spectra" (2). Since controls, consisting of antiserum devoid of antigen and antigen devoid of antiserum, remained clear and spectrally negative during the experimental period, the spectral scattering of the turbid supernatants was attributed to the presence of a relatively monodisperse immunochemical precipitate which had formed slowly at low temperature. At approximately 1000 magnifications the suspended substance of the supernatants appeared to consist predominantly of apparently spherical particles with a diameter of approximately 1 μ.

There was possible, however, an alternative interpretation, namely, that the suspended material consisted of bacteria which succeeded in growing in the antiserum when the two serological reagents were mixed. To test this possibility we inoculated fresh samples of the spectrally negative antiserum with small portions of the serological supernatants and observed that appreciable bacterial growth occurred within 1 day at 37°C.; moreover, the bacterial suspensions obtained in this way were spectrally positive. On the other hand, control samples of antiserum, which were not inoculated, remained clear and spectrally negative during this period, as did inoculated samples which were covered with toluene and kept at 37°C., and inoculated samples, with or without toluene, which were kept in the refrigerator. In addition, we found that samples of proteose-peptone nutrient solution which were inoculated with the spectrally negative stock antigen solution became turbid and spectrally positive in 2 days at 25°C. and in 3 days at 37°C. With respect to intensity of spectra and number of spectral orders, some of these bacterial suspensions resembled the serological supernatants, while others dis-

played spectra which were considerably weaker and less abundant; no precise quantitative comparisons were carried out.

Extending these observations, we found that the spectral scattering was not unique to the bacterial contaminants of our serological reagents, but that every one of approximately a dozen different kinds of bacteria which we examined possessed this remarkable property. Of these bacteria, which included *E. coli*, *B. subtilis*, Type I pneumococcus, *S. lutea*, a bacterium resembling *P. lepiseptica*, and several unidentified forms, mostly bacilli, the most satisfactory were *E. coli* and *B. subtilis*, with each of which it was possible to observe 3 or 4 spectral orders, and the least satisfactory was *S. lutea*, with which only a faint first order could be discerned. With *E. coli* and *B. subtilis* it was possible to demonstrate a beautiful spectral phenomenon within 4–5 hours after inoculation of a relatively colorless proteose-peptone medium. Later, as the bacterial growth became massive, the intensity of the spectra was diminished and could be improved by dilution of the dense bacterial suspensions with saline.

In addition, we were able to observe a striking spectral phenomenon with thin colonies of several of the bacteria on agar, as well as with bacterial sediment deposited along the wall of a centrifuge tube and with bacterial films which formed at the surface of inoculated nutrient medium.

We have decided to report these qualitative observations since it appears unlikely that we shall be able to continue this investigation in the immediate future.

REFERENCES

1. LANNI, F., *J. Colloid Sci.* 2, 463 (1947).
2. LA MER, V. K., AND BARNES, M. D., *J. Colloid Sci.* 1, 71, 79 (1946); JOHNSON, I., AND LA MER, V. K., *J. Am. Chem. Soc.* 69, 1184 (1947); KEYNON, A. S., *Trans. N. Y. Acad. Sci.* 9, 234 (1947).

FRANK LANNI [2]
DAN H. CAMPBELL

Gates and Crellin Laboratories of Chemistry,
California Institute of Technology,
Pasadena 4, Calif.
    December 17, 1947

[2] National Institute of Health Research Fellow. Present address: Department of Experimental Surgery, Duke Hospital, Durham, N. C.

COLLOID SCIENCE AND RHEOLOGY

Ernst A. Hauser

Massachusetts Institute of Technology, Cambridge, Mass.

Professor Hauser's discussion of the dependence of interpretation of certain rheological phenomena upon an understanding of the colloidal structure of many materials provoked interesting response from the audience. He pointed out that a tendency toward description of rheological processes by mathematical functions alone would not necessarily solve the flow characteristics of all systems. It is his belief that many of the properties of colloids that contribute to anomalous flow behavior cannot be described by mathematical functions but are dependent on the individual nature, size and surface charges of the particles involved. As he stated in part "Thixotropy, rheopexy and dilatancy also depend on the morphology of the colloidal micelle or (in other words) on the composition of their surfaces and the properties based thereupon. This cannot be expressed in mathematical terms." Furthermore, "How can a purely mathematical concept explain that a gelatin gel is elastic if one only takes the configuration of the gelatin molecule into consideration, or that the low molecular weight fraction of natural rubber is not elastic but is a very viscous fluid and its high molecular weight fraction, in contrast thereto, hard and brittle?" He is convinced that "---colloidal phenomena cannot be harnessed by rigid mathematics."

THEORY OF PLASTIC FLOW VERSUS THEORY OF PLASTIC DEFORMATION

W. Prager

Brown University, Providence, Rhode Island

Plasticity theories for metals in the strain hardening range can be divided into two groups: plastic deformation and plastic flow (1). Theories of the first group assume that, during continual loading, the state of strain is uniquely determined by the state of stress, whereas theories of the second group assume the increment of strain is uniquely determined by the existing stress and the increment of stress.

Under the circumstances of the customary methods of testing, it should be pointed out that, for so-called neutral changes of stress, the former leads to difficulties which do not arise with the latter. A neutral change of stress occurs when the stress components are varied so that the principal stresses preserve their values while the principal stress directions rotate with respect to the stressed material. A neutral change of stress can be considered as a limiting case of either loading or unloading.

It seems reasonable to demand that the stress-strain relations for both loading and unloading should predict the same change when applied to a neutral state of stress.

In this paper Professor Prager's clear and concise theoretical deductions show that the stress-strain relations of the plastic flow concept fulfill this condition whereas the deformation theory does not, despite Ilyushin's argument.

This complete paper will appear in an early issue of *The Journal of Applied Physics*.

REFERENCE

1. Terminology introduced by Ilyushin; *Prikladnaia Matematika i Mekhanika*, **9**, 207 (1946).

BOOK REVIEWS

Surface Chemistry for Industrial Research. By J. J. BIKERMAN, Merck Research Laboratories, Rahway, N. J. 464 pages and 153 figures. Academic Press, Inc., New York, N. Y., 1947. Price $8.00.

Dr. Bikerman has prepared a book which will be found very useful for physicists, chemists, and biologists in the field of pure science as well as by those engaged in industrial research. While the book contains in principle much that is familiar to students of Freundlich's Kapillarchemie, it goes into greater detail of exemplification which many readers will welcome, and includes discussions of results very recently published. The reviewer is impressed by the many references to the literature of the present decade.

Those who are interested in problems involving interfacial phenomena will find this book enjoyable and stimulating to read, as well as a valuable reference shelf volume. Dr. Bikerman has, through his labors, rendered a valuable service to colloid science.

ARTHUR W. THOMAS, New York, N. Y.

Modern Colloids. By R. B. DEAN, Assistant Professor, University of Oregon. 303 pp. D. Van Nostrand, New York, 1948. Price $3.75.

"This book is designed to serve as an introduction to the behavior of colloidal materials. It is based on a course for undergraduate students who intend to specialize in chemistry, biology, medicine, or agriculture. In many schools colloid chemistry, if it is given at all, is reserved for graduate students, and the average undergraduate may justly complain that chemistry does not tell very much about the things he sees outside the classroom."

"Colloid chemistry has made great strides in the past ten or fifteen years, which may be said to mark the coming of age of the science. It has also given rise to at least one lusty offshoot, polymer science, which is already a respectable science in its own right: so respectable in fact that some polymer chemists refuse to admit that they deal with colloids. This attitude undoubtedly reflects the bad repute into which colloid chemistry had fallen. Colloids was once a synonym for complex terminology and unpredictable behavior. Although it is still necessarily complex we are beginning to see our way clearly and much of the dead wood is being cleared away."

This quotation from the author's preface states his viewpoint. The matter is elementary and the treatment does not require more than introductory short courses in physics and organic chemistry as prerequisites. The book is copiously illustrated with diagrams and photographs, with only one table of data. The author recognizes that his book may not represent an adequate survey of colloid chemistry, but the readers to which it is addressed are hardly mature enough for a comprehensive survey. The student whose interest has been aroused will find ample references to monographs at the end of each chapter to satisfy his needs. He will then perceive the need of securing a thorough foundation in the quantitative aspects of physical chemistry and physics if he intends to proceed in colloid science.

It would be very helpful if the references in basic physical chemistry had not been restricted to one text but had directed the student to examine several of the other well-known texts. A set of elementary questions and problems on each chapter and a good index are included.

VICTOR K. LaMER, New York, N.Y.

DISTRIBUTION OF MOLECULAR WEIGHTS
OF PECTIN PROPIONATES

Harry S. Owens, Jackson C. Miers and W. Dayton Maclay

From the Western Regional Research Laboratory,[1] Albany, Calif.

Received March 30, 1948

INTRODUCTION

Knowledge of the average molecular weight and its distribution in pectin is of considerable importance to both theoretical and practical aspects of pectin chemistry. Such knowledge can be applied as a test of validity to many of the equations and theories currently being developed for high polymers and can be used as a point of attack in the study of the nature of "protopectin." Practical importance lies in the fact that weight average molecular weight ($\bar{M}_w$) controls the viscosity of pectin solutions, thereby affecting processing characteristics, while number average molecular weight ($\bar{M}_n$) may control its gel properties and largely determine its economic value. It is hoped that this type of study will permit fundamental examination of raw materials in an effort to find sources of less heterodisperse pectin of good gelling qualities; further, it may be useful in the modification of processing conditions to produce less heterodisperse material.

There are advantages in fractionating the original material, but the electrolytic properties of pectin necessitate working with buffered solutions (1) when determining molecular weights. With low-methoxyl pectin products, these charge effects cannot be counterbalanced, except by a large excess of salts, when the pectin becomes only slightly soluble. In the course of this investigation many fractionations were attempted by solvent precipitation or extraction, but in each case degradation of pectin occurred. Because of these difficulties, investigators have preferred to fractionate derivatives of pectin, and the most extensive work has been done on the nitrate. The nitrate has two drawbacks: (a) the nitration technique must be carefully controlled to prevent nitration from proceeding to differing degrees, causing marked changes in the physical properties of the product (2) as has been noted with other polysaccharide nitrates (3), and (b) nitration is so drastic that some degradation is certain to occur.

Schneider and Fritschi (4) fractionated pectin nitrate prepared from sugar beet pectin. Speiser and Eddy (5) have done similar work with apple pectin nitrates and have shown that careful treatment reduces degradation.

The propionates were used in the present study because acylation can be performed under very mild conditions. Their molecular weights at various methoxyl contents were measured, they were fractionated according to molecular weight, the gel grades of the original pectins were determined and compared to molecular weights averaged in different ways, and the applicability of several equations to the data was examined.

EXPERIMENTAL

The pectins used were prepared by methods previously described (6, 7, 8) and, in most cases, are the same samples used to study mobilities (9) and film properties (10). Their source, method of de-esterification, and analytical properties are given in Table I. They were converted to the

TABLE I

Description of Pectins Used in This Investigation

Sample no.[a]	Source	Uronic anhydride	Intrinsic viscosity
		per cent	*dl./g.*
11.3	Lemon	84	9.6
10.1	Lemon (comm.)	85	4.0
9.8	Apple	84	3.9
7.2E	Lemon	80	5.3
5.4E	Lemon	80	5.2
4.5E	Lemon	80	4.3
3.5B	Lemon	87	3.2

[a] The number represents methoxyl content and the letter designates the method of de-esterification: B = base (7), E = enzyme (6).

propionates by the method of Carson and Maclay (11). Since it has been shown that the methoxyl content does not change during acylation (12), the decrease in methoxyl was considered a measure of degree of propionylation, and modified Zeisel determinations (13) were used to measure the extent of acylation. The propionyl content averaged about 90–95% of theoretical, based on methoxyl content, and recovery was about 90% of theoretical.

The samples were fractionated by adding petroleum ether (b.p. 63.3–70°C.) to 2% solutions of the propionate in dioxane until a cloud point was obtained at the initial temperature. This temperature was maintained for at least 1 hr. after the last addition of precipitant or solvent to insure a close approach to equilibrium for the faint cloud point. The temperature

of the system was then lowered in a water or air bath and maintained at the lower temperature for at least 18 hrs. The precipitate was centrifuged at that temperature in a constant-temperature centrifuge, the supernatant liquid was decanted, and the process repeated. The last fraction of each series was obtained by evaporation of the liquid. Fraction II of sample P.11.3-3X was so large that it required refractionation to obtain more homogeneous material. These fractions are designated II_1, II_2, and II_3 in Table IV. The combined fractions of each sample weighed about 5%
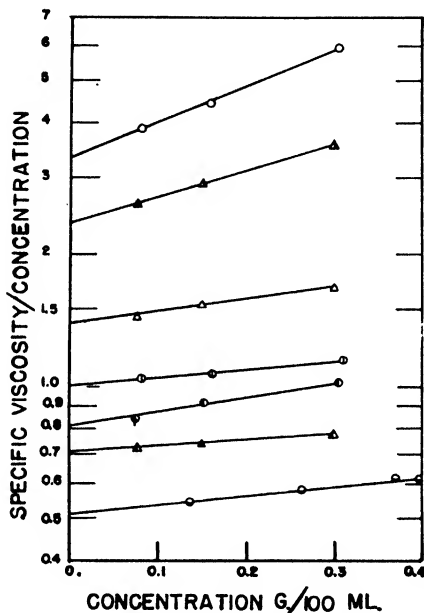
FIG. 1. Log of the ratio of specific viscosity to concentration plotted against concentration in g. of pectin propionate/100 ml. of acetone solutions. ○ represents P11.3-3X-II_1; ⦶,-IV; ▲, P9.8-1X-II; △,-IV; ▲,-VI; ⦿, P3.5-1X-III; ⦵,-XI. Fraction numbers are the same as those used in Table IV.

less than the initial weight, and a proportional correction has been applied to increase the combined weight to 100% of the total.

Viscosities of acetone solutions were measured in Ostwald-Cannon-Fenske pipets which were used and calibrated previously (1), and the intrinsic viscosity was obtained from the intercept of the log (η_{sp}/c) vs. c plot in which the concentration (c) is expressed in g. of solute/100 ml. of solution. Typical curves obtained with various fractions of pectin propionates described in Table IV are shown in Fig. 1. The temperature at which measurements were taken was $25° \pm 0.03°$C.

Osmotic pressures of the acetone solutions were measured in stainless-steel cells slightly modified from the previous description (14). These modifications consisted of sealing of glass parts to metal through Kovar alloy and sealing of 2-mm. capillary filling arms by means of drill rod and pools of mercury as recommended by Zimm and Myerson (15) for another type of osmometer. Some difficulty had been encountered in obtaining tight seals around the membrane and the latest version of the cell, illustrated in Fig. 2, has eight sealing bolts, since it was found that a

FIG. 2. Unassembled osmometer. Drill rods fit tubes with funnels.

slight amount of buckling resulted with fewer bolts, as was noted also by Goldblum (16). To reduce the flow of solvent through the membrane gasket, the cells were placed in a container of xylene in a water bath. Membranes were prepared from No. 600 PT Cellophane swelled in 3% sodium hydroxide at 15°C. for 30 mins. The alkali was removed by continuous washing with distilled water for at least 1 hr., followed by soaking in 50% acetone-water for at least 1 hr. and then soaking in pure acetone 1 hr. or longer. The porosity of cellulose membranes is readily controlled by regulation of the concentration of the sodium hydroxide, since increase in alkali concentration increases the porosity. Molecular weights

were calculated from the intercepts of the pressure/concentration *vs.* concentration curves. Typical curves obtained with various fractions described in Table IV are given in Fig. 3.

Preparation of pectin gels at pH 2.5, the measurements of shear moduli by means of a rigidometer, and conversion to gel grades, have been described completely elsewhere (17).
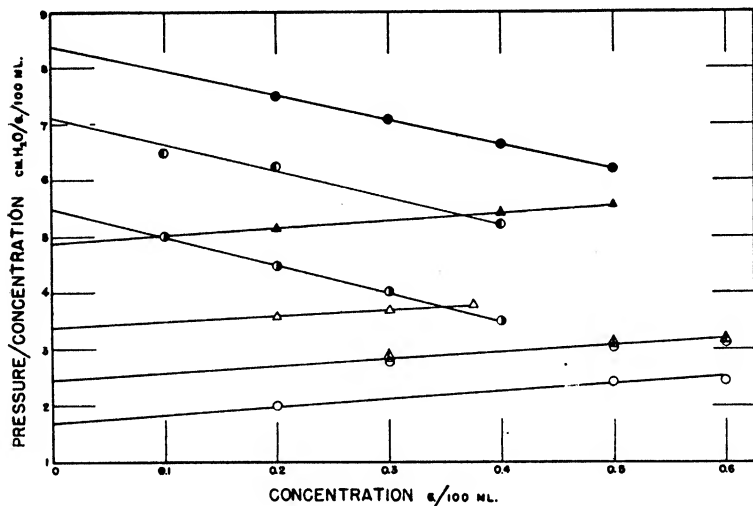
FIG. 3. Change in ratio of osmotic pressure in cm. of water to concentration with change in concentration expressed in g. of pectin propionate/100 ml. of acetone solution. ○ represents P11.3-3X-II₁; ◑,-III; △, P9.8-1X-III; ▵,-IV; ▲,-V; ◑,P3.5-1X-I; ◐,-III; ●, whole sample. Fraction numbers are the same as those used in Table IV.

RESULTS

Propionylation is very mild and it was assumed that pectin, like other polysaccharides, would not be degraded by the treatment. Two experiments (Table II) indicated that this assumption is unwarranted. The extent of degradation during the first acylation was measured as shown in Table III. Later work has shown that part of the degradation occurs during isolation, when acid, which prevents formation of pyridinium pectinate, is used. A small amount (2%) of low-molecular-weight material was lost in the alcohol washes.

To establish molecular-weight heterogeneity, but not the form of the distribution curve in linear polymers, it is unnecessary to fractionate the samples if the relationship between intrinsic viscosity and molecular weight is known. Measurements of viscosity and osmotic pressure can

TABLE II

Effect of Repeated Propionylations on the Viscosity
of Acetone Solutions of Pectin Propionate

Preparation		$[\eta]$ $dl/g.$
P11.3	1X[a]	2.87
	2X	2.51
	3X	2.26
P9.8	1X	1.33
	2X	1.08

[a] P refers to the propionate; 1X, *etc.*, to the number of acylations.

TABLE III

Effect of Time of Propionylation on the Viscosity and Methoxyl
Content of Pectin Propionates (Sample Number P10.1)

Hours of acylation	MeO *per cent*	$[\eta]$ $dl/g.$
2	6.90	1.73
4	6.52	1.71
8	6.64	1.62
Theoretical	6.1	2.00[a]

[a] Table VI gives the calculated molecular weight of the pectin propionate derived from sample 10.1. From the $[\eta]$ *vs.* $\bar{M}$ curve, a value for $[\eta]$ was obtained.

be used to calculate values for viscosity average molecular weight (which in many cases is identical to weight average molecular weight) and number average molecular weight. These two together are measures of the heterogeneity of the sample. One requirement that must be fulfilled with pectin propionates is that the degree of esterification of both the alcohol and carboxyl groups is consistent. To refer results to the original pectin, it is necessary that an undegraded propionate be studied. The results of 3 fractionations are shown in Table IV. The methoxyl content of the fractions of each sample showed no significant trend; therefore, it has been assumed that no fractionation according to degree of esterification has been obtained and that esterification is completely random. The first and last fractions of P11.3-3X and P9.8-1X had lower methoxyl contents than those of the other fractions. These were the only exceptions.

If it is assumed that the individual fractions are sufficiently homogeneous that the molecular weights averaged differently are the same, it is possible to calculate molecular weights for the original samples and to compare them with observed values. The results of such calculations are given in Table V. The small differences between the observed and calculated values indicate that the methods used are fairly reliable and that viscosity average and weight average molecular weights are identical.

Table VI compares gel grades with molecular weights (1, 14) of 3 high-methoxyl pectins. (Molecular weights of the corresponding propi-

TABLE IV

Yields, Intrinsic Viscosities, and Number Average Molecular Weights
of Fractions of Various Pectin Propionates

Fraction no.	Temp. interval	Yield	$[\eta]$	M_n
	°C.	per cent	dl/g.	
P11.3-3X				
I	Incompletely soluble	2.62	2.78 (soluble portion)	160,000 (soluble portion)
II$_1$	25–15	38.0	3.27	158,000
II$_2$	15–1	3.95	2.94	155,000
II$_3$	Residue of fraction II	19.0	2.20	115,000[a]
III	25–1	17.8	2.14	103,000
IV	25–1	1.8	1.00	55,000
V	Residue	16.8	1.01	39,000
P9.8-1X				
I	Incompletely soluble	0.3	—	—
II	30–15	23.	2.35	122,000
III	30–15	22.	1.90	102,000
IV	30–15	20.	1.38	75,000
V	30–15	11.5	1.03	56,000
VI	30–1	12.	0.71	39,000
VII	Residue	11.5	0.31	21,000
P3.5-1X				
I	30–18	12.8	1.02	47,000
II	25–18	15.5	0.91	40,000
III	25–18	9.1	0.81	36,000
IV	25–18	3.8	0.81	36,000[a]
V	35–19	8.5	0.81	36,000[a]
VI	35–19	4.8	0.73	33,000[a]
VII	40–19	4.8	0.66	31,000[a]
VIII	45–19	4.4	0.66	33,000
IX	35–6	5.0	0.55	25,000[a]
X	35–6	4.0	0.55	25,000[a]
XI	35–2	4.2	0.51	24,000[a]
XII	40–2	2.3	0.45	21,000[a]
XIII	40–2	3.5	0.40	18,000[a]
XIV	Residue	17.4	0.30	14,000[a]

[a] From interpolation of curve of $[\eta]$ vs. $\bar{M}_n$ values.

onates are given in Table VIII.) Although samples 10.1 and 9.8 were reported previously (13), there has been a decrease in weight average molecular weight (and methoxyl content), while the gel grade has remained nearly constant. This is further evidence that number average molecular weight is controlling gelation characteristics. A definite conclusion will be held in abeyance until more samples have been examined.

TABLE V

*Comparison of Number and Weight Average Molecular Weights of Pectin
Propionates Observed and Calculated from the Distribution Curves*

Sample	$\bar{M}$ viscosity	$\bar{M}_w$ calc'd	$\bar{M}_n$	
			Calc'd	Observed
P11.3-3X	120,000	118,000	91,000	95,000
P9.8-1X	70,000	79,000	58,000	55,000
P3.5-1X	33,000	31,000	27,000	30,000

TABLE VI

Variation of Gel Grade with Molecular Weight Averaged in Different Ways

Sample no.	Gel grade[a]	Pectin	
		$\bar{M}_n$	$\bar{M}_w$
11.3	260	40,000	115,000
10.1[b]	200	33,000	64,000
9.8[b]	170	27,000	61,000

[a] Gel grade is defined, in this case, as the amount of sugar gelled by a unit weight of pectin to form a 65% solids gel with a shear modulus of 3 g./cm².

[b] Sample 10.1 is the same as appears in Ref. 10 and in Ref. 18 as No. 10.7; while 9.8 is the same sample reported as 10.9 in previous publications including Refs. 1 and 10. The change in viscosity and methoxyl content is due to degradation occurring during storage and redrying.

Lansing and Kraemer (19) derived an equation to describe the distribution of molecular weights in heterogeneous polymers based on the assumption that small molecular weight fractions are absent. The distribution curve satisfying this condition is logarithmic and the equation is:

$$\Delta w / W = \frac{1}{M_n \, \beta \sqrt{\pi}} . e^{-((1/\beta) \ln M/M_o)^2} \, \Delta M,$$

where Δw is the weight of the fraction which has a molecular weight in the range ΔM, β is a constant defined by any pair of molecular weight averages, e.g., $M_w/M_n = e^{0.5\beta^2}$, M is the mean molecular weight in the range defined by ΔM, and M_o is the molecular weight at the maximum of the molecular weight-distribution curve and may be defined by the equation $M_w/M_o = e^{0.75\beta^2}$.

Application of the equation to one of our samples is shown in Fig. 4, which also includes a histogram constructed from the observed fractionation. The lack of agreement is apparent, indicating that the molecular

weights of pectin are not distributed logarithmically about the mean value, which is not surprising since the equation is restricted to a particular form of distribution curve. Similar calculations based on the work of Speiser and Eddy (5) show similar deviations between observed and calculated values. A plot of our data on probability paper indicated that the distribution is Gaussian. The integral curves drawn on that assump-
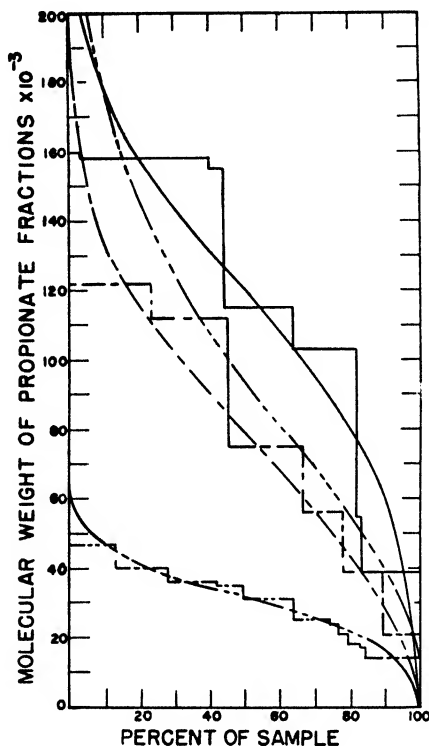
FIG. 4. Histograms constructed from the data on fractionation of various pectin propionates. — is P11.3-3X; — — —, P9.8-1X; — — — — — —, P3.5-1X; — — — — — — — —, curve representing P11.3-3X constructed from distribution equation of Lansing and Kraemer (19).

tion are shown in Fig. 4 for each of the samples, and correspond well with the histograms. The values for the dispersion of the probability curves (root mean square of the deviation from the arithmetic mean, which is the weight average molecular weight in this case) is 45,000, 43,000, and 11,000 for samples P11.3-3X, P9.8-1X, and P3.5-1X respectively. The ratios of $\bar{M}_w$ to $\bar{M}_n$ are 1.26, 1.29, and 1.07 for the corresponding samples,

showing that the dispersion is controlled by that ratio, but the data are insufficient to derive a general equation from that assumption.

The extraction and isolation of pectin apparently involve some degradation, which decreases the molecular weight heterogeneity as compared to that obtained during synthetic reactions (20).

If $\bar{M}_n$ for the various fractions, which are assumed to be homogenous, is plotted against $[\eta]$ it is found that a straight-line relationship is obtained showing that a in the equation, $[\eta] = KM^a$ is 1 and permits direct calculation of K. If the reciprocal of K is used, the equation for propionates prepared from high-methoxyl pectins examined is: $\bar{M}_w = 5.3 \times 10^4 [\eta]$ and for the low-methoxyl it is $\bar{M}_w = 4.6 \times 10^4 [\eta]$. The decrease in the slope of the line with decrease in methyl ester content is apparently due to a change in solute-solvent interaction effects, discussion of which may be published later. The values for the slopes appear to be close to those calculated for the nitrates (5).

These propionates are one of the few polymeric systems which follow the simplest form of Staudinger's equation over a range from 20,000 to 150,000. The linearity of the curves suggests that Simha's equation for the viscosity of solutions of elongated ellipsoids might apply in this case as well as to pectin in aqueous buffered solution (14).

This equation (21) yields values for the ratio of length to diameter of the solute molecules directly from the intrinsic viscosity expressed in ml./ml. The diameter of the molecule can be calculated from the partial specific volume (0.81 ml./g. for pectin propionate in acetone), the weight of the repeating unit (300), its length (4.3×10^{-8} cm.) and Avogadro's number. A cylindrical shape for the molecule has been assumed. In Table VII are assembled some data for various polysaccharides. These indicate that there is some flexibility in the galacturonide chain, and that the measured length of the extended chain is longer than the average effective length as the molecule exists in solution. The increase in the ratio of the measured molecular weight to that calculated from the above equation is indicative of the increased tendency of the longer chains to coil (21).

From the equation (21)

$$L/D = CZ^p,$$

where Z is the degree of polymerization, p is a flexibility parameter, and L/D is the ratio of length to diameter calculated from Simha's equation for viscosity of solutions of elongated ellipsoids, values for p have been calculated and are included in Table VII. Only the value for pectin is different to a marked degree, but even so, the exponent, "a" in the $[\eta]$ vs. $\bar{M}$ curve, is 1.7 times "p" as empirically determined by Simha for a variety of compounds (21). It is assumed that relatively rigid chains cause these high values for p, although they are apparently influenced

TABLE VII

Observed Molecular Weights Compared to Values
Calculated from Simha's Equation

Values for the flexibility parameter (p) (21) and the exponential (a) (21) in $[\eta]$ vs. $\bar{M}$ curve are included.

Substance	$\bar{M}_w$	$\bar{M}_s$	a	p
Pectin propionate	155,000	50,000	1	0.61
Pectin propionate	55,000	27,000		
Pectin propionate (low methoxyl)	47,000	27,000	1	0.56
Pectin propionate	36,000	23,000		
Pectin (13)	115,000	56,000	1.34	0.79
Pectin (13)	27,000	17,500		
Galactomannan acetate (22)	290,000	51,000	—	—
Cellulose nitrate (3)	231,000	51,000	1	0.60
Corn amylose nitrate (23)	64,000(M_n)	16,000	—	—
Corn amylose acetate (24)	108,000	17,000	0.97	—

by solute-solvent interaction effects. The values calculated for the flexibility parameter agree with the postulation that there is restricted rotation around glycosidic bonds in pectin, so that the chain is less flexible than chains of hydrocarbon units. If a value of 1.7 for "C" is used, reasonable values for the molecular weights of pectin and cellulose derivatives can be calculated directly from intrinsic viscosity measurements.

Amylose, amylopectin, and galactomannan derivatives yield data which do not conform to this equation. This lack of agreement has been interpreted as further evidence of helical structure for amylose and branching in amylopectin. Evidence is not yet complete for galactomannan, but it apparently does not have a simple linear structure like cellulose or pectin, and probably has short branches along the chain, as indicated by methylation studies by Swanson (25), periodic acid oxidation by Carson and Maclay (26), and X-ray studies by Palmer (27).

The average molecular weights of the original pectins measured in buffered solutions converted to the value for the ester is compared in Table VIII with the measured values. There apparently is a tendency to lose smaller molecules during the preparation and isolation of the propionates. A loss of less than 5% of material with molecular weight of 10,000 or less accounts for the discrepancies in the number average molecular weights noted in Table VIII. Unavoidable degradation during the acylation causes decrease in weight average molecular weight and appears especially noticeable in the samples having a lower methoxyl content. In each case, however, the degradation represents less than 0.5% of the bonds broken, provided it is assumed that all bonds in pectin are the same (29). Apparently osmotic pressure and intrinsic viscosity

TABLE VIII

Comparison of Observed and Calculated Molecular Weights of Pectin Propionates

Sample no.	Pectin		Pectin propionate			
			$\bar{M}_n$		$\bar{M}_w$	
	$\bar{M}_n$	$\bar{M}_w{}^a$	Calc'd	Obs.	Calc'd	Obs.
11.3[b]	40,000	115,000	66,000	100,000	189,000	157,000
10.1	33,000	64,000	54,000	76,000	105,000	92,000
9.8	27,000	61,000	44,000	55,000	100,000	70,000
3.5B	—	42,000	—	—	70,000	33,000
7.2E	—	80,000	—	—	130,000	60,000
5.4E	—	80,000	—	—	130,000	60,000

[a] Values calculated from a combination of data by Säverborn (28) and those previously published (1).

[b] Propionate was acylated only one time and has a higher molecular weight than the sample reported in Table V.

measurements on pectin in aqueous buffered solutions yield values for molecular weights satisfactory for comparative purposes.

The pectin used as a starting material for de-esterification has a degree of polymerization of about 300, while that for the alkali-de-esterified sample is about 230. This reduction corresponds to the breaking of about 0.5% of the bonds in the chain, provided all the bonds in the chain are the same (29). Ordinarily the glycosidic bond is considered stable to alkali (barring oxidation); thus the presence of a second linkage in pectin is indicated. There are indications that the Arrhenius energy of activation for the alkaline hydrolysis of the linkage involved is around 25–30 kcal. (7), which is much higher than expected for the obvious possibility of an ester bond as the second linkage in the main chain. X-ray pictures of sodium pectate (27) indicate that the crystallites contain 200 or more units in the chain direction. This evidence practically eliminates a second linkage unless it has bond distances approximating those of a glycoside bond. Also, the energy of activation for acidic degradation is about 30 kcal. (30), which is the same as that for glycosidic bond hydrolysis. The presence of a hemiacetal postulated by Pacsu (31) is unlikely, since pectin shows its greatest stability in the region near pH 4. On the other hand, calculations based on Montroll and Simha's equations (29) for the depolymerization of long-chain molecules show that the alkali-hydrolyzed product is far more homogeneous with respect to molecular weights than would be predicted. While greater losses of low-molecular-weight material would be encountered with degraded pectin, such a degree of homogeneity could be achieved only if a second linkage, much less stable

than the predominating glycoside bond, were present at the end of uniform repeating units along the chain.

Jansen and MacDonnell (32) have examined the course of the methanolysis reaction on pectin and have concluded that a second linkage must be present. This conclusion is different from that of Mark (33), who has assumed that the carboxyl group in the sixth position decreases the stability of the glycuronide group. In this connection, it should be mentioned that partially methanolyzed pectin can be methylated in alkaline solution (34), and work at this laboratory shows that methyl galacturonide has no reducing power toward alkaline oxidizing agents. The possibility of oxidation, or of progressive decomposition from the reducing end of the chain, has not been eliminated, so that no definite conclusion can be drawn at this time.

Alkali-de-esterified citrus pectin as typified by the sample acylated in this work is apparently less heterogeneous than samples of apple pectin de-esterified by either acid or enzyme *in vitro* (5). Inasmuch as gel grade seems to follow number average molecular weight, it is suggested that, at a given gel grade, the alkali-prepared samples would offer two advantages: (a) increased dispersibility, and (b) decrease in processing difficulties due to the lower viscosity.

In view of the uncertain state of knowledge of the structure of pectin, the reliability of extrapolation of the molecular weight of pectin to that of protopectin is highly doubtful. It is quite unlikely that the number average molecular weight of protopectin in lemon is much above 100,000; thus, it seems improbable that high molecular weight alone causes the slight solubility of protopectin. In fact, the solubility of protopectin in solutions of sodium polymetaphosphates, even in the cold as found in this laboratory, supports Henglein's (35) contention that protopectin is bonded to celluronic acid groups, pectic acid, and similar constituents of the intercellular layers in plants, by means of polyvalent cations such as calcium. These electrovalent bonds are probably aided by hydrogen bonding between pectin molecules and between pectin and cellulose, so that heat plus a calcium sequestering agent or acid, which reduces the ionization of pectinic acids, increases the efficiency of extraction of pectin. This hypothesis agrees generally with that of Pallmann and Deuel (36).

SUMMARY

A number of pectins have been esterified to form the corresponding propionates. These compounds are readily fractionated according to molecular weights by formation of a saturated solution in a suitable solvent system at a high temperature followed by reduction of the temperature and repetition of the operation several times. The molecular weight ·of

the individual fractions has been measured and it was found that viscosity- and weight-average molecular weights of pectin propionates are identical. This means that a measure of molecular weight distribution can be obtained directly from osmotic pressure and viscosity measurements of solutions of unfractionated samples. For this purpose it is recommended that the acylation proceed only two or three hours in order to reduce degradation, so that the ester will have a molecular weight distribution near that of the unchanged pectin.

The distribution of molecular weights in the samples examined follows a Gaussian distribution and not the logarithmic one of Lansing and Kraemer. The peak of the distribution curve is controlled by the weight average molecular weight and the dispersion is controlled by the ratio of weight to number average molecular weight.

Application of the viscosity equations of Simha shows that the propionylated galacturonide chain in acetone solutions is relatively rigid, although not so rigid as pectin in aqeuous solutions.

REFERENCES

1. Owens, H. S., Lotzkar, H., Merrill, R. C., and Peterson, M., *J. Am. Chem. Soc.* **66**, 1178 (1944).
2. Henglein, F. A., and Schneider, G., *Ber.* **69B**, 309 (1936).
3. Jullander, I., *Arkiv Kemi, Mineral. Geol.* **21A**, (8), 100 (1945); Blaker, R. H., Badger, R. M., and Noyes, R. M., *J. Phys. Colloid Chem.* **51**, 574 (1947).
4. Schneider, G., and Fritschi, U., *Ber.* **69B**, 2537 (1936).
5. Speiser, R., and Eddy, C. R., *J. Am. Chem. Soc.* **68**, 287 (1946).
6. Owens, H. S., McCready, R. M., and Maclay, W. D., *Ind. Eng. Chem.* **36**, 936 (1944).
7. McCready, R. M., Owens, H. S., and Maclay, W. D., *Food Inds.* **16**, 794 (1944).
8. Schultz, T. H., Lotzkar, H., Owens, H. S., and Maclay, W. D., *J. Phys. Chem.* **49**, 554 (1945).
9. Ward, W. H., Swenson, H. A., and Owens, H. S., *J. Phys. Colloid Chem.* **51**, 1137 (1947).
10. Schultz, T. H., Owens, H. S., and Maclay, W. D., *J. Colloid Sci.* **3**, 53 (1948).
11. Carson, J. F., and Maclay, W. D., *J. Am. Chem. Soc.* **68**, 1015 (1946).
12. Carson, J. F., and Maclay, W. D., *ibid.* **67**, 787 (1945).
13. Clark, E. P., *J. Assoc. Offic. Agr. Chemists* **15**, 136 (1932); **22**, 100, 622 (1939).
14. Owens, H. S., Lotzkar, H., Schultz, T. H., and Maclay, W. D., *J. Am. Chem. Soc.* **68**, 1628 (1946).
15. Zimm, B. H., and Myerson, I., *ibid.* **68**, 911 (1946).
16. Goldblum, K. B., *J. Phys. Colloid Chem.* **51**, 474 (1947).
17. Owens, H. S., and Maclay, W. D., *Food Inds.* **19**, 606 (1947).
18. Owens, H. S., and Maclay, W. D., *J. Colloid Sci.* **1**, 313 (1946).
19. Lansing, W. D., and Kraemer, E. O., *J. Am. Chem. Soc.* **57**, 1369 (1935).
20. Taylor, G. B., *ibid.* **69**, 638 (1947).
21. Simha, R., *J. Chem. Phys.* **13**, 188 (1945).
22. From unpublished data by Carson, J. F., and Owens, H. S.

23. CAESER, G. V., GRUENHUT, N. S., AND CUSHING, M. L., *J. Am. Chem. Soc.* **69**, 617 (1947).

24. DOMBROW, B. A., Ultracentrifugal and Viscometric Studies of Amylose Acetates, Dissertation, Columbia Univ., 1944.

25. SWANSON, J. W., Abstracts Am. Chem. Soc. Meeting, Sept., 1947.

26. CARSON, J. C., AND MACLAY, W. D., Results to be published.

27. PALMER, K. J., private communication.

28. SÄVERBORN, S., A Contribution to the Knowledge of the Acid Polyuronides, Uppsala, 1945.

29. MONTROLL, E. W., AND SIMHA, R., *J. Chem. Phys.* **8**, 721 (1940).

30. MERRILL, R. C., AND WEEKS, M., *J. Am. Chem. Soc.* **67**, 2244 (1945).

31. PACSU, E., AND HILLER, JR., L. A., *Textile Research J.* **16**, 243 (1946).

32. JANSEN, E. F., MACDONNELL, L. R., AND WARD, W. H., Results to be published. *J. Biol. Chem.*

33. MARK, H., presented at meeting Technical Association of Pulp and Paper Industry, Portland, Oregon, 1947.

34. BEAVAN, G. H., AND JONES, J. K. N., *J. Chem. Soc.* **1947**, 1218.

35. HENGLEIN, F. A., *J. makromol. Chem.* **1**, 121 (1943).

36. PALLMANN, H., AND DEUEL, H., *Chimia* **1**, 27, 51 (1947).

BOUND AND FREE ACID IN ALUMINUM SOAP
PREPARED BY PRECIPITATION [1]

Richard H. Coe [2], Karol J. Mysels [3] and Gerould H. Smith [4]

From the Department of Chemistry, Stanford University, Palo Alto, Calif.

Received February 2, 1948

The object of this work was to differentiate experimentally between the ways in which fatty acid is held in unextracted aluminum soaps as precipitated in aqueous solution, and to report and discuss some results which were obtained by varying the extraction of these mixtures.

Free Acid. The term "free acid" is frequently [5] applied to any acid which may be extracted from a soap under a given set of conditions. Such methods, in general, actually determine the acid which is freed during the experiment; this is much more than the "free acid" present as such in the soap, and is often greater than the sorbed acid. The strict use of the term "free acid" is to denote only that acid present in the soap which has an activity substantially equal to that of pure acid.

Bound "Molecular Acid." Some excess acid is not free but is bound to, or sorbed by, the soap in molecular form, and its activity and solubility may be reduced to 1% or less of that of the pure acid. This decrease in activity may be brought about by formation of an acid soap, or "acid of solvation," or a solid solution, or by sorption. Because of the physical heterogeneity of the aluminum soaps (1) we have been unable to distinguish definitely between these possibilities by extraction measurements, but these and X-ray data (2) favor sorption of fatty acid or solvation rather than a solid solution or formation of an acid soap.

Experimental

Measurement of the Amounts of Combined, Sorbed, and Free Acids

Probably the simplest experimental criterion for determining the form in which the acid is held is based on the solubility of the acid in a solvent

[2] Present address: Wesleyan University, Middletown, Conn.

[3] Present address: University of Southern California, Los Angeles.

[4] Present address: Union Oil Company of California, Oleum, Calif.

[5] For example, Frank's Chemical Company catalog.

inert with respect to the aluminum soap but capable of dissolving appreciable amounts of the acid. Under these conditions free acid would have the same solubility as the pure acid. The bound acid would have a lower solubility than the pure acid, and the manner in which the extraction proceeds might distinguish between the presence of a chemical compound, a solid solution, or a compound resulting from sorption of the uncombined molecular acid. The practical application of this criterion presents difficulties mainly because it is difficult to find a solvent which is inert to the aluminum soap and removes none of the combined acid. After extraction of the excess acid, aluminum soaps prepared in the usual way by precipitation have substantially the composition of a di-soap such as aluminum dilaurate, $Al(OH)L_2$ (3).

There are two important sources of error to be avoided. When any decomposition of the soap occurs, high results are obtained for the amount of uncombined acid. Low results are obtained by incomplete separation of the uncombined acid. Hence, to distinguish between free and loosely bound fatty acid one should employ solvents which do not decompose the soap and, furthermore, do not appreciably liberate sorbed acid.

Even traces of moisture in the solvent can cause some hydrolysis of the soap. However, when the extraction is carried out with acetone dried over Drierite with successive amounts of acetone, each exposed to the aluminum soap until the concentration of fatty acid in the acetone ceased to change, it was possible to separate nearly all of the uncombined acid without appreciably decomposing the soap. For each batch, treatment at 30°C. for one day was usually sufficient. Errors from the second source were eliminated by repeated extraction of the soap.

If it were possible to treat a large amount of soap with a very small amount of some dry solvent, isooctane, for example, and then determine the extent to which it becomes saturated, the problem would be simplified. The soaps, however, imbibe such large quantities of solvent that this method is not directly applicable.[6] The method used is treatment of the soap with an almost saturated solution of the fatty acid in acetone and observation of the *direction* of the change in concentration of the acid.

Quantitative comparisons of the effective solubility of the sorbed acid with that of the pure acid in the same solvent give an indication of the strength with which the acid is held.

This method may be contrasted with exhaustive Soxhlet extraction (3) which constantly exposes the sample to pure fresh solvent and may use many liters of acetone for only 1 g. of soap, the residue being substantially pure di-soap.

A preceding paper (3) deals with aluminum distearate, dilaurate,

[6] C. G. McGee in this laboratory has suggested that use of a film balance would render the analysis possible.

dicyclohexane carboxylate, and moderately pure dioleate prepared by aqueous precipitation followed by thorough extraction with dry isooctane or acetone. The present study is directed toward the examination of the precipitated aluminum stearate. The stearic acid was obtained from the Eastman Kodak Company and had a neutralization number of 198; theory 197.3.

Apparatus and Procedure

Soap and solvent were placed in screw-cap vials (Braun-Knecht-Heimann No. 63481) of 2 or 8 dr. capacity. The vials were selected with care for smooth lips and for mechanical strength to stand subsequent centrifugation. Samples of soap weighing from 0.05 to 0.1 g. were used in the small vials with about 6 g. of solvent, and in the large vials, samples of about 1 g. of soap were used with about 16 g. of solvent. To avoid contamination or loss of solvent, the inside of the cap was lined first with a thin layer of rubber, then with two layers of lead foil, and finally with two layers of pinhole-free pure tin foil. When the containers were closed with this gasket, they usually lost less than 5 mg. of solvent in 18 hours at 30°C. A blank containing acetone alone showed no increase in acidity on thermostating and mixing.

The filled vials were placed in the head of an angle centrifuge which was stored on its side in a small air thermostat maintained at 30° ± 0.05° C. and was connected to a geared-down motor placed outside the thermostat. The head of the centrifuge could thus be turned at the rate of one complete revolution per min., insuring continuous *mixing*, but slow enough to avoid heating by friction. Variation in time, from 12 hrs. up to 4 days, had no appreciable effect on the final concentration obtained.

After about 18–24 hrs., the thermostat was opened for a moment, the vials tapped to remove aluminum soap adhering to the cap, the centrifuge placed upright for *centrifuging* and spun (still within the thermostat) for 5 mins. at about 4000 r.p.m. This yielded a clear supernatant layer of solvent when acetone was used as a solvent. When isooctane was used, the supernatant liquid was slightly opalescent because small slightly-swollen aluminum soap particles have a tendency to remain suspended. This caused the values for the concentration of acid to be slightly high but did not cause significant errors.

Once the phases were segregated, the vials were removed from the thermostat and a portion of the supernatant solvent was rapidly withdrawn. The amount of liquid was determined either volumetrically, using a syringe pipette, or by weighing the vial before and after removal of the aliquot portion. Occasional checks on the supernatant liquid showed that it contained only from 0 to 1% of the total aluminum soap present.

The concentration of fatty acid in the solvent is determined either by

titrating in an alcoholic solution or by weighing the residue after evaporation. From this result and the total volume of acetone present, the amount of acid extracted from the soap can be found and the ash content of the undissolved residue can then be computed.

The residue itself was either dried and ashed, and its composition thus determined, or a weighed amount of solvent was added to the vial and the experiment continued.

The precision and accuracy of the final composition of the extracted soap after 10 successive exposures to acetone was about 1%. When isooctane was used, the results were only slightly less precise.

The absolute values of the solubilities of the stearic acid in acetone and in isooctane at 30°C. were determined separately and found to be 34 g./l. in acetone and 90 g./l. in isooctane. The values for the solubilities are reported as per cent relative saturation. The effect of moisture content of the dried acetone on the solubility of acid was not taken into account, but it is not believed to be appreciable.

RESULTS

On the diagrams in which the composition of the soap (in terms of per cent ash, or moles acid/g.-at. of aluminum) is plotted against the concentration of fatty acid in the solvent, the solubility of stearic acid in a saturated solution of stearic acid being taken as 100%, each solubility experiment is described by 2 points: one corresponds to the initial state of the soap and solvent, and the other corresponds to the final state. Each experiment is represented by an arrow connecting these two points. These arrows show what happens when soap and solvent of given compositions are placed in contact. This method of representation is shown in Figs. 1–5, incl.

When the composition of the soap was obtained by calculation, it is shown by an open circle, and when it was determined by ashing, it is shown by a dark circle.   The solubility was almost always determined by titration, although weighing was occasionally used. When acetone was the solvent, the arrows are drawn as full lines, and when isooctane was used, they are dotted.

The points of similar arrows are connected by a heavy line which delineates a curve that shows the essentially constant composition of the soaps which were in contact with the solutions of given final compositions.

Three samples of aluminum stearate were used. All were prepared at 60°C. and examined at 30°C. We know of no significant difference in the history of the samples that would account for the differences in behavior of the third sample from the other two.

Sample "a" had an empirical composition of $Al(OH)Str_2O.82HStr$, corresponding to its ash value of 6.07%. When acetone, which was

63–75% saturated with stearic acid, was used, only about 0.24 moles of stearic acid was extracted, leaving $2.82 - 0.24 = 2.58$ moles, as may be seen in Fig. 1; the concentration of fatty acid in the acetone was still far below that which would have been given by free stearic acid. That is, the sample lost only 6.7% of its original weight to acetone which was still capable of dissolving more stearic acid. This was only 0.24/0.82 or
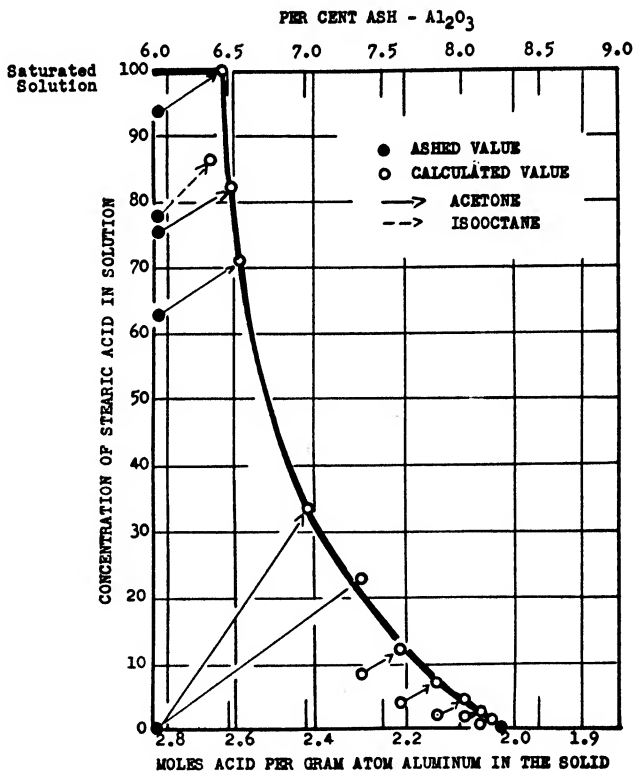
FIG. 1. Distribution of stearic acid between solvent and aluminum stearate, sample "a," in acetone and in isooctane at 30°C.

less than one-third of the stearic acid in excess of that combined as the distearate. Most of the stearic acid in excess of that required for the distearate is therefore not free, but must be bound.

On the other hand, the initial flat portion of the curve in the upper left hand corner of Fig. 1, at 100% saturation of the acetone with stearic acid, shows that 5.7% of the original unextracted aluminum soap, or 25% of the molecular acid, is completely *free*, mechanically admixed stearic acid,

since the horizontal section represents an isothermally invariant solution saturated with two solid phases. The excess free stearic acid was capable of dissolving in 93% saturated acetone and bringing it to 100% saturation.

The successive extractions indicated by the arrows in Fig. 1 show that, as the extraction proceeds, the acid becomes less and less available, as if the acid were being progressively desorbed. To obtain a crucial test for the presence of $Al(OH)Str_2.HStr$ by this method the specimen would have to be fully homogeneous. Comparison of the X-ray diffraction patterns of extracted and unextracted aluminum soaps suggests that part of the molecular acid may be dissolved in the soap causing a distortion of the crystal lattice of the soap (2).
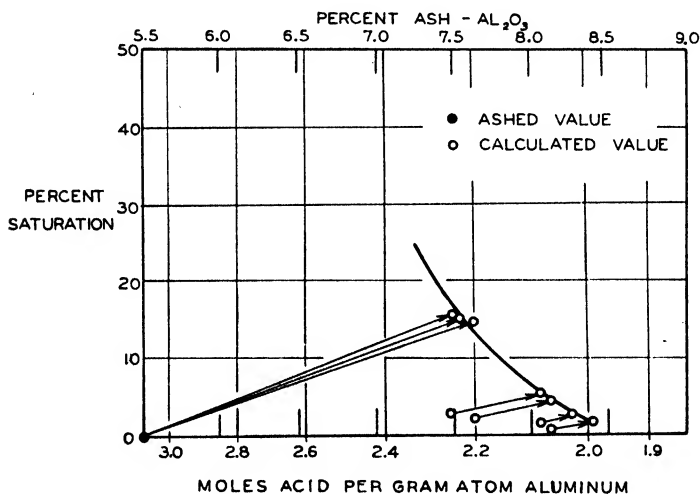
FIG. 2. Distribution of stearic acid between solvent and aluminum stearate, sample 'b," in acetone at 30°C.

As the composition of the extracted aluminum soap approaches that of pure distearate the effective solubility of any stearic acid (Fig. 1) is reduced to a vanishing point, and the conclusion that the original soap was composed of pure di-soap and free and sorbed stearic acid appears justified. This confirms the conclusion reached by extrapolation of results obtained by exhaustive extractions under various conditions (3).

The possibility that there was too little solid in proportion to liquid to produce a greater degree of saturation was removed in many of our experiments by exposing an extracted residue again to a lower concentration of fatty acid in the same solvent. This is shown in Figs. 1, 2, 3, and 4 by a series of successive arrows. The calculated beginning of each arrow

lies vertically under the end of the preceding arrow. Further fatty acid always dissolved, which showed that the acid was there but that it was bound.

Only one extraction with isooctane was performed with this soap and the result was qualitatively the same as when acetone was used (Fig. 1).
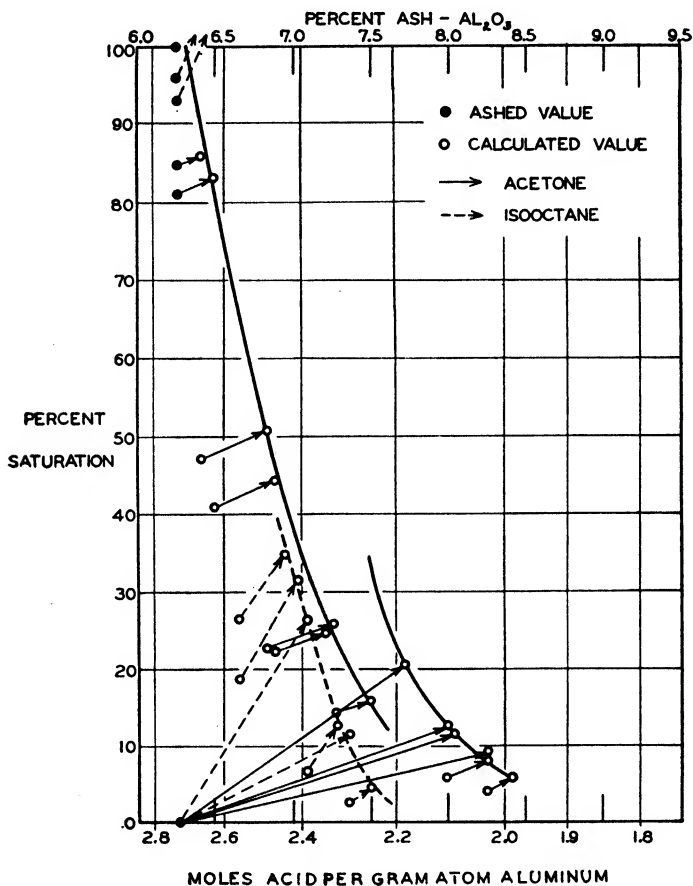
Fig. 3. Distribution of stearic acid between solvent and aluminum stearate, sample "c," in acetone and in isooctane at 30°C.

Results obtained with sample "b" are reported in Fig. 2. They show essentially the same behavior, but it appeared that the acid would be all extracted at a composition corresponding to about 90% of distearate and 10% of the monostearate.

Sample "c" gave the results shown in Fig. 3. This soap was tested with both acetone and isooctane. Values for the solubility of the acid in these 2 solvents were quite different, suggesting that, when acetone was used, some acid was freed. In addition, the values obtained with acetone, instead of falling upon a single line, seem to lie on two lines, one of which points toward the composition of the distearate and the other toward a
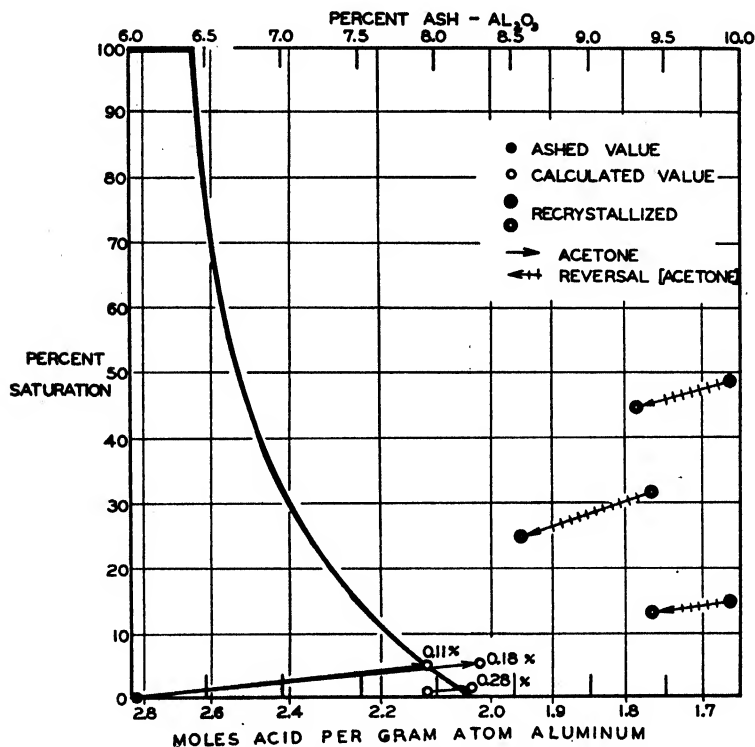
FIG. 4. Distribution of stearic acid between solvent and aluminum stearate, sample "a," in acetone at 30°C., illustrating reversal and the effect of moisture. (Figures indicate added percentage of moisture in solvent.)

composition of a mixture of mono- and distearate. The former curve was obtained when the soap was treated initially with a solution of stearic acid, the latter when treated with acetone alone. This discrepancy of solubilities from sample "c" is beyond experimental error and shows that some change occurred in the soap.

The effect of the presence of moisture in the acetone which is so marked in exhaustive extraction (3) was investigated, and was unex-

pectedly found to be negligible as is shown by the upward pointing arrows in Figs. 4 and 5 for samples "a" and "c," respectively. The numbers next to each arrow show the percentage of water added to acetone. The plotted line is that obtained when dried solvent was used, Figs. 1 and 3, re-
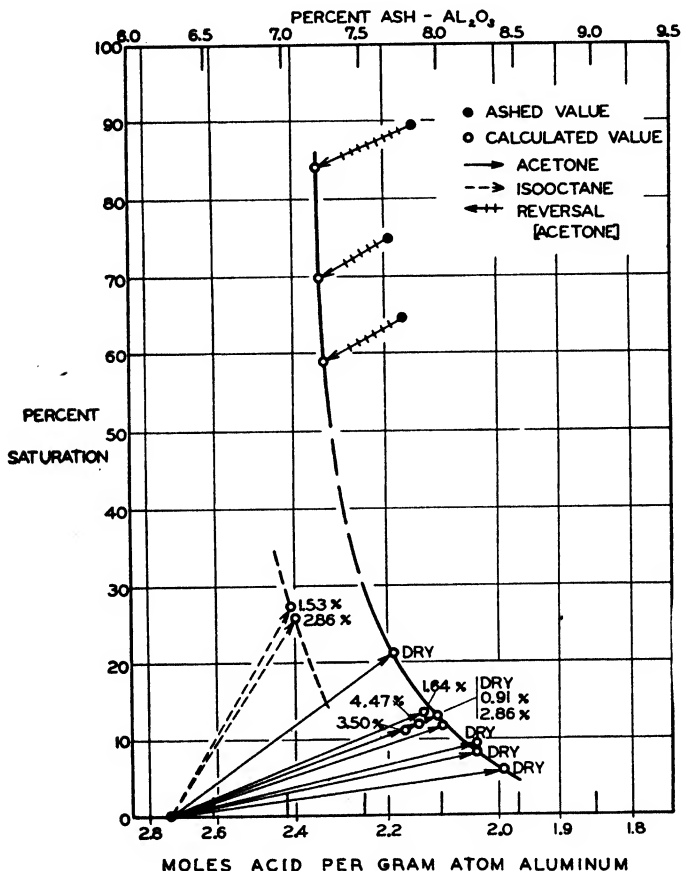
Fig. 5. Distribution of stearic acid between solvent and aluminum stearate, sample "c," in acetone and in isooctane at 30°C., illustrating reversal and the effect of moisture. (Figures indicate added percentage of moisture in solvent.)

spectively. The results, while somewhat less precise, show little effect of the moisture present. This indicates that the reaction of the distearate with water to form fatty acid and other soaps [probably the monostearate, $(Al(OH)_2Str)_x$ or $Al_2(OH)_2OStr_2$] (4) is repressed by the presence of fatty

acid, which was present at a concentration of only a few per cent of saturation.

The converse process, removal of acid from acetone by an extracted soap, is shown by arrows pointing downward in Figs. 4 and 5. The over-extracted "a" sample was prepared by exhaustive extraction with boiling acetone. In the presence of a solution of stearic acid in acetone this soap removed some of the acid from solution but not nearly as much as was retained by the unextracted "a" soap in a solution of the same composition.

The sample of "c" soap was obtained by extraction with isooctane at room temperature. This sample sorbed acid from acetone solution, and concentrations were reached which may be considered as lying on the extension of that solubility line for this soap which is farthest to the right. As a result of the peculiar behavior of this particular soap in these experiments it is again impossible to decide definitely whether or not true equilibrium was attained.

The experiments definitely show that a partially extracted soap may again take up dissolved stearic acid.

Summary

In aluminum stearate precipitated from aqueous solution there are present:

(1) Free fatty acid, readily dissolved to form solutions of concentration up to that of the saturated solution of the fatty acid itself.

(2) Loosely bound or sorbed fatty acid, amounting to about 0.6 mole/g.-at. of aluminum which may without difficulty be dissolved out of the soap to form solutions of concentration below that of the fully saturated solution of the fatty acid.

(3) Firmly bound fatty acid, resistant to solvent, amounting to approximately 2 moles/g.-at. of aluminum, leaving the composition of the distearate $Al(OH)Str_2$.

Hydrolysis of aluminum soap by moist acetone may be repressed by the presence of dissolved fatty acid.

References

1. Mysels, K. J., and McBain, J. W., "Variability and Inhomogeneity of Pure Aluminum Dilaurate," a paper presented at the April, 1948, meeting of the American Chemical Society.

2. Marsden, S. S., Jr., Mysels, K. J., Smith, G. H., and Ross, S., *J. Colloid Sci.* In press.

3. Smith, G. H., Pomeroy, H. H., McGee, C. G., and Mysels, K. J., *J. Am. Chem. Soc.* **70**, 1053 (1948).

4. McGee, C. G., Master's Thesis, Stanford University, 1947.

SORPTION FROM SOLUTION BY
ACTIVE MAGNESIUM OXIDE

James W. McBain and Robert C. Dunn

From the Department of Chemistry, Stanford University, Palo Alto, Calif.

Received February 2, 1948

INTRODUCTION

Most studies of sorption from solution neglect or ignore the effect of the solvent on rate of sorption and on the equilibrium between solvent, sorbate and sorbent. The fact that these effects are significant forms the basis for chromatographic adsorption analysis, in which activated magnesium oxide is frequently employed.

In the production of commercial active magnesium oxide, an empirical "Iodine Number" is used to indicate the activity of the material. As this type of a determination is a laboratory control procedure, it must be accomplished as quickly as possible. A typical industrial procedure is described by Zettlemoyer and Walker (1) and, in their particular case, the iodine-carbon tetrachloride solution is in contact with the magnesia for 30 mins. Where results are relative only to some predetermined standard, they may form an excellent control procedure. The principal practical shortcoming of the method is that the time must be accurately controlled, as the rate of sorption is still quite appreciable after 30 minutes of contact; and, of course, strict precautions must be taken against introduction of moisture.

It is the purpose of this paper to point out the effects of time and solvent on sorption by active magnesium oxide, and to show that great caution is to be exercised in deducing surface areas from measurements of sorption from solution if gross errors are to be avoided.

EXPERIMENTAL

Materials

The magnesium oxide used for the experimental work was furnished by Permanente Metals Corporation of Los Altos, Calif. It was -200 mesh. The electron micrograph of a previous similar sample, taken by Dr. L. Marton, is here reproduced (Fig. 1). The lightburned sample was specially prepared from magnesium hydroxide by calcining. Minor con-

stituents amounted to:

Cl⁻, 0.19; CaO, 1.40; SiO_2, 0.50; R_2O_3, 0.34; SO_3, 0.36; Mn, 0.03; B_2O_3, 0.2.

Other materials were of reagent grade. All solvents were redistilled under such conditions as to insure that they were water free.

FIG. 1. MgO extra light. × 17,000 diameters.

The main specimen, whose ignition loss was 11.1%, was divided among a number of sealed glass bottles. Samples were withdrawn from these and quickly weighed in presence of Drierite. Concurrently, other samples were taken and checked to see that the ignition loss had remained between 11.0 and 11.2%.

I. The Sorption of Iodine

The effect of time on sorption of iodine from solution was determined experimentally as follows: Exactly 0.500 g. of active magnesia was weighed into a vial of 15 ml. capacity. To this was added 10 ml. of 0.1 N, iodine in carbon tetrachloride, using a calibrated pipette. The bottle was then stoppered with its plastic cap (protected by lead foil) and placed in a 25°C. shaker for the required time. Toward the end of the contact time the sample was removed from the shaker and placed on the centrifuge for 15 minutes to insure that all suspended magnesium oxide was down. A 5 ml. aliquot was then pipetted from the supernatant liquid and transferred to a beaker containing 10 ml. of a saturated aqueous potassium iodide solution. The sample was then titrated with 0.05 N sodium thiosulfate from a 10 ml. calibrated burette. Blank determinations were run with each series to insure an accurate initial concentration. Contact time was measured from the introduction of the initial iodine solution until the withdrawal of the 5 ml. aliquot of terminal solution.

Terminal concentration was calculated as follows:

$$\text{Titer } \frac{Na_2S_2O_3 \times N\ Na_2S_2O_3}{5.00 \text{ ml.}} = \begin{array}{c} \text{Concentration of } I_2 \text{ at equilibrium} \\ \text{in equivalents.} \end{array}$$

The results are tabulated in Table I.

TABLE I

Effect of Contact Time on Sorption

Time hrs.	I_2 sorbed/100 g. MgO millimoles
0.5	49.8
1	51.7, 51.4
3	53.3, 53.2
18	56.4, 56.2
24	56.4
46	56.9, 56.9

The 25°C. isotherm for 24 hrs. of contact in each case was determined by a procedure similar to that just outlined, the exception being that the quantities of magnesia used were varied between 0.200 and 0.700 g. These results are shown in Table II.

Sorption studies of iodine vapor (2) on magnesium oxide showed a very rapid sorption at 82°C.; the further rate is barely appreciable after one hr. Sorption from solution shows an appreciable rate even after 24 hrs. This must be attributed principally to the effect of the solvent in displacement and competition.

A saturated solution of iodine and carbon tetrachloride would contain 0.237 moles/l., and the amount of sorption shown in Table II is still

TABLE II

Sorption after 24-Hour Contact

Concentrations $M/l.$	x/m in millimoles I_2 sorbed/100 g. MgO
0.0046	47
0.0064	50
0.0101	55
0.0140	58
0.0190	64
0.0205	65
0.0304	70
0.0318	70
0.0404	76

increasing with concentration, and could reach the value 130 millimoles iodine/100 g. magnesium oxide, which is the saturation value for the sorption of iodine vapor at 82°C. However, sorption of iodine from vapor is a more direct, definitive and significant method than sorption from solution.

II. Sorption of Cetyl Alcohol from Solutions in Various Solvents

Oleic acid (3) and methyl stearate (4) have been used by other investigators to determine the area of finely divided solids. Oleic acid reacts chemically with magnesium oxide. Methyl stearate proved unsatisfactory because equilibrium was not obtained even in a day. Cetyl alcohol gives more definite results. When sorbed from 0.1 M solution in carbon tetrachloride, the sorption of cetyl alcohol amounted to 24.0 millimoles/100 g. magnesium oxide at 15 mins., 24.1 at one hr., and 24.7 at 24 hrs. In contrast, under the same conditions, sorption of methyl stearate was 6.9 at one hr., which increased to 14.2 in 24 hrs. Cetyl alcohol, therefore, offers the advantage over iodine that the sorption is very rapid and leads soon to a value that is constant over a range of concentration which might have been interpreted as a monomolecular layer.

The experimental procedure used was as follows: Exactly 0.500 g. of magnesia was placed in a 15 ml. vial, to which was added 10 ml. of cetyl alcohol solution (initial concentration from 0.05 M to 0.2 M). The sample was then placed in a 25°C. shaker and agitated for 24 hours. After centrifuging, a 5 ml. aliquot was pipetted from the supernatant liquid and transferred to a tared crystallizing dish, and the solvent was allowed to evaporate. Duplicate and blank determinations were accorded identical treatment. The samples were heated *just* to fusion twice and allowed to cool, to insure complete removal of the solvent. The blanks act as a control and check the initial concentration. The effect of the various solvents on rate of sorption was determined by sorption-time experiments. The results are tabulated in Table III, and shown in Fig. 2.

TABLE III

*Rates of Adsorption of Cetyl Alcohol from Various Solvents
at 25°C. (0.2 M Cetyl Alcohol)*

(Expressed in millimoles/100 g. MgO)

Time	$CHCl_3$	C_6H_6	C_6H_{12}
hrs.			
2	—	—	27.2
3	—	46.4	—
6	11.15	—	—
24	16.19	—	27.2
25	—	46.4	—
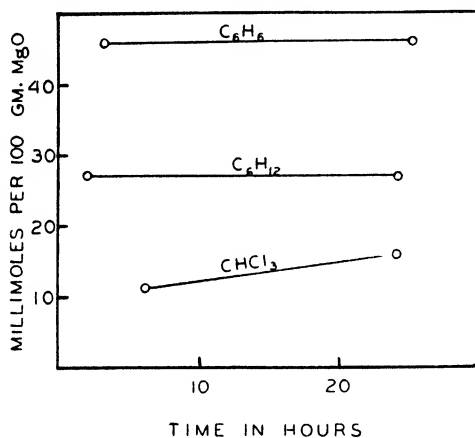
FIG. 2. Rate of adsorption of cetyl alcohol from various solvents, at 25°C.

Applying Ewing's method (4), if one were to assume that the flat portion of the curve with carbon tetrachloride indicated the completion of the monomolecular layer, and ascribe to each cetyl alcohol an area of 21.6 square Å, since 0.0255 moles of cetyl alcohol covers 100 g. of magnesium oxide, the area would be calculated as 33.2 m.²/g. of magnesium oxide. However, we have previously shown (2) that the area is many times greater, being 122 m.²/g. by direct sorption of iodine vapor, or 126 ± 10 m.² by low temperature nitrogen adsorption using the B.E.T. method, both methods involving strong degassing. Hence, the sorption of cetyl alcohol from carbon tetrachloride indicates only a small fraction of the actual area.

Paneth (5) studied the sorption of dyes, brucine, and acetone by surfaces whose areas were already known from his radioelement meas-

urements, and found that in only one case, Methylene Blue HB, the horizontal portion of the sorption isotherm corresponded to a complete monomolecular layer. Other values ranged from 10% to 95% of a monomolecular layer.

Brunauer (6) noted that methyl stearate values obtained by Ewing for zinc oxide "indicate roughly half as large surface areas as the nitrogen adsorption does." He also found that silicic acid adsorption obtained by G. Boyd "gives a smaller value in every case. The discrepancy for titanium oxide is less than two-fold, for graphite more than eight-fold."

If sorption from solution were a trustworthy method of determining surface area, the results would have been independent of the solvent. However, this is not the case, as is seen for cetyl alcohol in several solvents, as given in Fig. 2, which includes the following measurements:

From benzene solution:

Equilibrium conc.	0.0338	0.0704	0.108	0.149	0.186
mM/100 g. MgO	12.2	18.7	21.3	24.1	46.4

From cyclohexane solution:

Equilibrium conc.	0.0427	0.071	0.150	0.187
mM/100 g. MgO	14.7	15.8	16.0	27.2

It is seen that sorption from cyclohexane on the horizontal portion of the isotherm amounts to 16 millimoles as compared with 26 millimoles from carbon tetrachloride, with an intermediate value for benzene; all these increasing to only a small fraction of the true area of magnesium oxide.

Sorption was rapid from benzene and cyclohexane solutions, being the same at 24 hrs. as at 2 hrs. However, sorption from chloroform is much slower, being 11.1 millimoles at 6 hrs., rising to 16.2 at 24 hrs., from an initial concentration of 0.2 N cetyl alcohol. Hence the chloroform isotherm was not studied.

The most striking results were obtained when cetyl alcohol was dissolved in lower alcohols. Both with ethyl alcohol and n-butyl alcohol, originally 0.2 N with respect to cetyl alcohol, there was no apparent adsorption, evidently because the solvents were being adsorbed in proportion to the cetyl alcohol present. When *tert.*-butyl alcohol was used as a solvent with the cetyl alcohol, the magnesium oxide actually caused an increase in concentration, that is, negative adsorption.

III. Sorption of Orange OT and of Naphthacene

Paneth and Vorwerk (7) used a dye to measure surface areas. We have, therefore, chosen Orange OT (1-*o*-tolylazo-2-naphthol) from carbon tetrachloride solution, and naphthacene ($C_{18}H_{12}$) from benzene solution, since both are colored. Concentrations were determined by

means of a Lumetron photoelectric colorimeter using a blue 420 filter. The naphthacene solution was protected from light throughout the experiment to avoid the colorless peroxide.

Orange OT is rapidly sorbed, being the same at one hour as at 28 hours, whereas the naphthacene is more slowly sorbed, being 3 times greater at 24 hours than at one hour, but then approaching constancy. The sorption isotherms are given in Fig. 3. It will be noted that the measurements with Orange OT were carried out at 0°C. as well as at 25°C. and that, although for very dilute solutions the results were the same, they diverged greatly with increase of concentration.
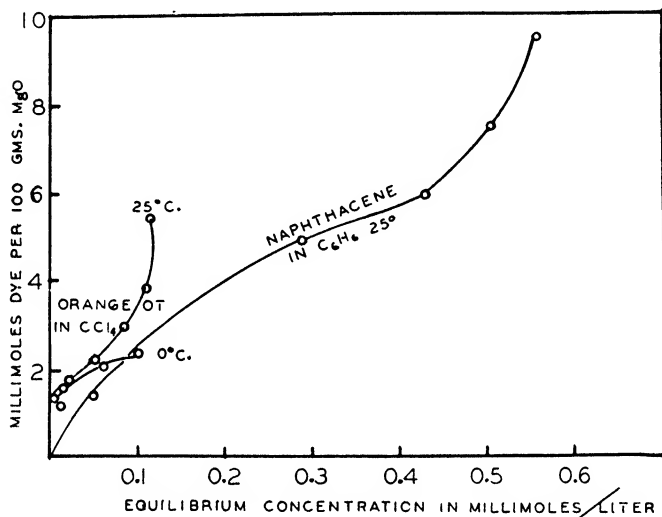
FIG. 3. Sorption isotherms of Orange OT at 0° and 25°C., and of naphthacene at 25°C., from solutions of carbon tetrachloride and benzene, respectively.

Finally, for comparison, sorption of Orange OT was measured with sludge magnesium oxide, which proved only 40% as active as the light-burned magnesium oxide, and with deadburned magnesium oxide, and with magnesium smoke, both of which showed no sorption of the dye. These latter two are nonporous crystals, whereas the lightburned magnesia is highly porous.

The sorption of naphthacene from benzene solution is due to its higher molecular weight in comparison with that of the aromatic solvent. Maier and Forziati (8) concluded from the sorption of toluene from solution in n-heptane that aromatic compounds are sorbed by magnesium

oxide preferentially to aliphatic. However, our result shows that cetyl alcohol was sorbed more from benzene than from cyclohexane.

DISCUSSION

The foregoing observations show that it is extremely hazardous to employ sorption from solution as a measure of surface area of finely porous materials such as magnesium oxide. In no case was the sorption anywhere near the known true area accessible to iodine or nitrogen molecules.

In addition to the competition between solute and solvent for the available surface, there enters the question of pore size and also the affinity of the surface groups of the solid for the specific solute. For equally accessible surfaces the more aromatic substances, or those of higher molecular weight, would be preferentially sorbed, but the experiments with cetyl alcohol dissolved in lower alcohols show that the finer pores are accessible only to the smaller molecules.

It has already been shown that iodine is chemisorbed (2). The surface of lightburned magnesium oxide, which exposes magnesium atoms, hydroxyl groups, and oxygen atoms, differs from that of ordinary finely crystallized magnesium oxide, which does not sorb Orange OT.

SUMMARY

1. The sorption of iodine, cetyl alcohol, Orange OT and naphthacene by highly porous active lightburned magnesium oxide has been studied in various solutions, and compared with the surface area determined with iodine vapor and nitrogen. In no case was the surface indicated by the sorption from solution more than a small fraction of that measured with nitrogen and iodine vapor.

2. Cetyl alcohol gives quite different results with the same specimen of magnesium oxide using different solvents, and with the lower alcohols it may show no apparent sorption or may even show negative sorption.

3. Use of sorption from *solution* for measurements of the area of highly porous materials involves arbitrary assumptions and can lead to highly erroneous results.

REFERENCES

1. ZETTLEMOYER, A. C., AND WALKER, W. C., *Ind. Eng. Chem.* **39**, 70 (1947).
2. DUNN, R. C., AND POMEROY, H. H., *J. Phys. Colloid Chem.* **51**, 981 (1947).
3. HARKINS, W. D., AND GANS, D. M., *J. Am. Chem. Soc.* **53**, 2804 (1931).
4. EWING, W. W., *ibid.* **61**, 1317 (1939).
5. PANETH, F., Radio Elements as Indicators, p. 71, Table XVII. McGraw-Hill, New York, 1928.
6. BRUNAUER, S., Adsorption of Gases and Vapors, Vol. I, p. 296. Princeton Univ. Press, 1943.
7. PANETH, V. P., AND VORWERK, W. V., *Z. physik. Chem.* **100**, 445, 480 (1922).
8. MAIER, B. J. M., AND FORZIATI, A. F. F., *J. Research Natl. Bur. Standards* **32**, 165 (1944).

THE DISTRIBUTION OF IONS AT INTERFACES

The Concept of a Surface Phase

J. T. Davies and E. K. Rideal, F. R. S.

From the Davy Faraday Laboratory, The Royal Institution

Received March 22, 1948

INTRODUCTION

In recent years various views have been advanced to express the ionic distribution "at" or near a charged interface in contact with a solution of electrolyte. The assumptions on which these theories are based are by no means verified experimentally. It seemed desirable at the present time that the theories should be examined and compared, and the postulates stated clearly.

Gouy (1910) was the first to evolve a satisfactory expression for the number of ions at or near a charged surface by equating electrical and diffusion forces on an ion situated near the surface. In his derivation any interionic force is neglected, *i.e.*, the solution must be dilute, and the surface charge not too great. An expression for the number of ions per unit volume at any definite distance from the surface can be obtained in terms of known quantities, assuming no adsorption on definite sites, nor any specific forces of adsorption, such as might set up a fixed double layer.

Wilson (1916) advanced the view that "the distribution of ions in the layer of solution surrounding the particle will be different from that in the bulk of the dispersion medium, a condition to which Donnan's work on membrane equilibria can be applied." It is to be noted that the condition of non-diffusibility of some of the ions at the surface of a colloid particle has been established by Donnan and his co-workers and by Bjerrum (1924) and other investigators. Wilson thus extended the concept of Donnan (1911) to the case where no actual membrane is present.

Danielli (1941) assumes a thickness of $\frac{1}{\kappa}$, the effective radius of Debye and Hückel, for the "surface phase," the volume of which thus depends on the ionic strength of the bulk solution.

Hartley and Roe (1940) considered that the electrokinetic potential could be employed in conjunction with a Boltzmann distribution law to

determine the concentration of hydrogen or other soluble ions at the surface of shear of a colloidal particle.

Steinhardt and Harris (1940), titrating wool fibers with hydrochloric acid, found equal amounts of hydrogen and chloride ions were taken up by the fiber. They interpreted this in terms of partially dissociated complexes being formed between groups in the protein and hydrogen and chloride ions, respectively. They suggested that this complex would greatly reduce the differences in ionic concentrations predicted by the Donnan equations (applied to the actual volume of keratin) for the case of combination with hydrogen ions alone, so that no account need be taken of differences of pH inside and outside the fiber.

More recently, Gilbert and Rideal (1944) assumed that on the keratin fiber there are two separate sorts of "sites," one for protons and the other for anions. They consider the complex formed on the addition of acid to be an ideal localized monolayer, which implies, *inter alia*, strong forces preventing a chloride ion, for example, from moving in the plane of the surface when it is attached to one of the sites. They point out that, in the case of a fibrous protein, only a few cations or anions can be adsorbed independently, since this process produces a large charge on the fiber, necessitating a further adsorption of anions and cations together. They treat their ideal localized monolayer by the method of Fowler and Guggenheim (1939), which considers the number of ways in which the adsorbed molecules or ions can be arranged at the surface on the different sites.

In general, when we are dealing with a system in which the hydrogen ion adsorption is involved, the Donnan equations, in which activities are employed, must hold, but as the anion interaction increases, either through accumulation of charge, or through specific adsorption, the theory of Gilbert and Rideal is applicable.

These various theories will now be considered in relation to the assumption of a definite surface phase, treated using the Donnan equations.

(1) The Theories of Gouy (1910) and of Donnan (1911)

Gouy's equations for the distribution of ions at an interface, for the case of a uni-univalent electrolyte, may be summarized as

$$\rho = F(C \cdot {}_xU_c - C \cdot {}_xU_a) \times 10^{-3}, \tag{1}$$

$$\Gamma \times 10^{-3} \times F = q = \int_x^\infty \rho \, dx, \tag{2}$$

$${}_oU_c + \frac{1}{{}_oU_c} - 2 = \left(\frac{\kappa \Gamma}{2C} \right)^2, \tag{3}$$

$${}_oU_c = \frac{1}{{}_oU_a} = \coth^2 \frac{\kappa}{2}(x_o), \tag{4}$$

$$_zU_c = \frac{1}{_zU_a} = \coth^2\frac{\kappa}{2}(x + x_o),$$ (5)

where ρ is the excess charge/unit area of surface, F is the Faraday, C is the number of gram ions/l. in the bulk solution, Γ is the surface density of charge in milli-equivalents/cm.², x is the distance from the surface, q is defined by (2), $_oU_c$ is the ratio of cation concentrations at the surface and in the bulk phase at very large values of x, $_zU_c$ is this ratio at a distance x from the surface, $_oU_a$ and $_zU_a$ are the ratios for the anions, $\frac{1}{\kappa}$ is the Debye-Hückel "effective ionic atmosphere radius" expressed in cms., and x_o is defined by (4).

If the surface charge be considered now to be uniformly distributed in a "surface phase," and $_dU_a$ and $_dU_c$ refer to the ratios of concentrations of anions and cations in the surface and bulk phases, application of the Donnan equations gives

$$(C \cdot _dU_a)(C \cdot _dU_c) = C^2$$

or

$$_dU_a \cdot _dU_c = 1,$$ (6)

where activity coefficients have been omitted, and the electrolyte is uni-univalent.

The assumption of Danielli (1941) that the surface phase is of thickness $\frac{1}{\kappa}$ means that the concentration of non-diffusible ions in the surface is $\kappa\Gamma$, so that, if the surface be negatively charged and the surface phase electrically neutral,

$$\kappa\Gamma + C \cdot _dU_a = C \cdot _dU_c.$$ (7)

Eliminating $_dU_a$ between (6) and (7), we obtain

$$_dU_c - \frac{1}{_dU_c} = \frac{\kappa\Gamma}{C}.$$ (8)

But, from the Gouy equation (3),

$$2\left(\sqrt{_oU_c} - \frac{1}{\sqrt{_oU_c}}\right) = \frac{\kappa\Gamma}{C}.$$ (9)

At first sight (8) and (9) appear fundamentally different, but in fact $_oU_c$ and $_dU_c$ are distinct ratios, $_dU_c$ being the average value of $_zU_c$ between $x = 0$ and $x = \frac{1}{\kappa}$.

It will now be shown that, under certain conditions, the assumption of a "surface phase" of uniform concentration and of thickness $\frac{1}{\kappa}$, and

through which the surface charge is diffused, is justifiable from the Gouy equations. Further, equations (8) and (9) above, derived respectively from the "surface phase" theory, using the distance $\dfrac{1}{\kappa}$ for the thickness, and from Gouy's equations, will be shown to be almost identical.
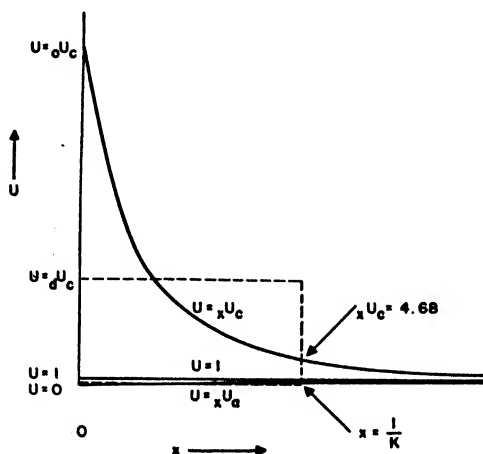
FIG. 1. $_xU_c$ and $_xU_a$ against x for a dilute solution of a uni-univalent salt at a negative surface. Broken lines enclose the "surface phase."

Fig. 1 shows a plot of $_xU_c$ for the case of a negatively charged surface. The abscissa is the distance from surface, and $\dfrac{1}{\kappa}$ is great in comparison with x_o.

Writing $\phi = \dfrac{\kappa}{2}(x + x_o)$,

$$_dU_c = \frac{1}{\phi_2 - \phi_1}\int_{\phi_1}^{\phi_2} \coth^2 \phi\, d\phi = 1 - \left(\frac{\coth \phi_2 - \coth \phi_1}{\phi_2 - \phi_1}\right). \quad (10)$$

Since, by (5), $\tanh \phi = \dfrac{1}{\sqrt{_xU_c}}$, and if ϕ is small, $\tanh \phi \to \phi$,

$$_dU_c \doteq 1 - \left(\frac{\sqrt{_2U_c} - \sqrt{_1U_c}}{\dfrac{1}{\sqrt{_2U_c}} - \dfrac{1}{\sqrt{_1U_c}}}\right);$$

$$\therefore \quad _dU_c \doteq 1 + \sqrt{_2U_c \cdot _1U_c}. \quad (11)$$

Putting $_1U_c = {}_oU_c$, and $_2U_c$ being the value of $_xU_c$ at $x = \dfrac{1}{\kappa}$,

$$_dU_c \doteq 1 + 2.16\sqrt{_oU_c} \quad (12)$$

if the solution is dilute and Γ is not too low, since under these circumstances x_o is small compared with $\frac{1}{\kappa}$, and so

$$_2U_c = \coth^2\left(\tfrac{1}{2}\right) = 4.68. \tag{13}$$

Under the same circumstances $_oU_c$ will be large, so that as a first approximation

$$_dU_c \doteq 2.16\sqrt{_oU_c}. \tag{14}$$

Substituting this value of $\sqrt{_oU_c}$ into (9),

$$2\left(\frac{_dU_c}{2.16} - \frac{2.16}{_dU_c}\right) \doteq \frac{\kappa\Gamma}{C}, \tag{15}$$

which is very close to

$$_dU_c - \frac{4}{_dU_c} = \frac{\kappa\Gamma}{C}. \tag{16}$$

The validity of (7) in actual cases will now be considered. The excess of anions per unit area of surface, α, is given by

$$\alpha = \frac{2C}{\kappa}\int_1^{\phi_2}\coth^2\phi\cdot d\phi - C(x_2 - x_1 =)\frac{2C}{\kappa}\left(\sqrt{_1U_c} - \sqrt{_2U_c}\right). \tag{17}$$

The fraction of this lying outside a distance $\frac{1}{\kappa}$ from the surface is given by

$$\frac{\sqrt{_2U_c} - \sqrt{_\infty U_c}}{\sqrt{_oU_c} - \sqrt{_\infty U_c}} = \frac{1.16}{\sqrt{_oU_c} - 1}. \tag{18}$$

In dilute solutions $\sqrt{_oU_c}$ is large, and this fraction becomes negligible. The excess of cations per unit area, β, is given by

$$\beta = C(x_2 - x_1) - \frac{2C}{\kappa}\int_{\phi_1}^{\phi_2}\tanh^2\phi\cdot d\phi,$$

i.e.,

$$\beta = \frac{2C}{\kappa}\left(\frac{1}{\sqrt{_2U_c}} - \frac{1}{\sqrt{_1U_c}}\right). \tag{19}$$

The fraction outside the distance $\frac{1}{\kappa}$ is thus

$$\left(\frac{\dfrac{1}{\sqrt{_\infty U_c}} - \dfrac{1}{\sqrt{_2U_c}}}{\dfrac{1}{\sqrt{_\infty U_c}} - \dfrac{1}{\sqrt{_oU_c}}}\right), \tag{20}$$

where $\sqrt{_2 U_c}$ now refers to $\sqrt{_x U_c}$ at $x = \dfrac{1}{\kappa}$, and is equal to 0.54 if $\sqrt{_o U_c}$ is large.

Hence (7) should strictly be written

$$\kappa\Gamma + \frac{C \cdot _d U_a}{0.46} = C \cdot _d U_c \qquad (21)$$

and the "surface phase" equation (8) becomes

$$_d U_c - \frac{2}{_d U_c} \doteq \frac{\kappa\Gamma}{C}, \qquad (22)$$

which is to be contrasted with

$$_d U_c - \frac{4}{_d U_c} \doteq \frac{\kappa\Gamma}{C} \qquad (16)$$

derived from Gouy's equations. The difference between (22) and (16) is in fact very small, since $\dfrac{1}{_d U_c}$ is small in comparison with $_d U_c$ if C is small and Γ not too small. For example, with one fixed negative ion per 55A^2, $\Gamma = 3 \times 10^{-7}$ milliequivalents/cm.^{2}, and, if $C = \dfrac{1}{100}$, $_d U_c = 100$, so the difference between (22) and (16) is only 0.02%. The actual discrepancy between (22) and (16) evidently arises from the assumptions of uniformity and electrical neutrality of the surface phase when the Donnan equations are applied.

A more fundamental connection between the treatments using the Gouy and Donnan equations may be seen from (2). If all the ionic atmosphere is assumed to lie in the surface phase, of thickness x_1,

$$q = \int_o^{x_1} \rho dx = 10^{-3} FC \int_o^{x_1} {_x U_c} \cdot dx - 10^{-3} FC \int_o^{x_1} {_x U_a} \cdot dx. \qquad (23)$$

But $q = \Gamma \times 10^{-3} \times F$;

$$\therefore \quad \frac{\Gamma}{x_1} = \frac{1}{x_1} \int_o^{x_1} C \cdot {_x U_c} dx - \frac{1}{x_1} \int_o^{x_1} C \cdot {_x U_a} dx;$$

$$\therefore \quad \kappa\Gamma = C \cdot {_d U_c} - C \cdot {_d U_a} \qquad (24)$$

since $x_1 = \dfrac{1}{\kappa}$.

Equation (24) is equivalent to the electrical neutrality equation (7) of the surface phase treatment.

The two derivations use the same principles of opposing electrical and diffusion forces, the Donnan equation depending on the ions behaving according to the ideal gas law, as does the diffusion term in Gouy's deri-

vation. In actual systems activity coefficients must be taken into account, except when both the bulk and surface phases are very dilute. The Donnan equations may easily be corrected if appropriate values are known, but for salts such as dyes the activity coefficients may be unknown and far from unity. In this case the Gouy and Donnan equations cannot be applied, and recourse must be had to the Gilbert-Rideal theory, where an empirical $\Delta\mu$ term takes account of deviations from ideal behavior, and the ions may be considered to adhere to definite "sites" in the surface instead of forming a diffuse cloud, as in the Gouy treatment.

(2) The Theory of Hartley and Roe (1940)

The fundamental equation may be written

$$\bar{C}_{H^+} = C_{H^+} \left(e^{-\frac{\zeta F}{RT}} \right), \tag{25}$$

where $\bar{C}$ refers to concentrations in the surface, C to those in the bulk, subscripts refer to the ion considered, ζ is the electrokinetic potential, F the Faraday, and R and T have their usual significance.

Since, however, ζ is the electrostatic potential between the surface of shear of the double layer and a point at infinity in the bulk solution, the pH at the surface, pH_s, is defined in terms of concentrations and refers to conditions at the surface of shear. If the Donnan equations be applied, as suggested by Wilson (1916), the Donnan potential between the surface and the bulk is given by

$$\psi = \frac{RT}{F} \ln \left(\frac{C_{H^+}}{\bar{C}_{H^+}} \right). \tag{26}$$

For the case of ovalbumin, Danielli (1941) found that $\bar{C}_{H^+}$ calculated from (25) and from (8) were practically identical for equal values of C_{H^+}, which means that under these conditions $\psi = \zeta$. Since ψ is an average value over a distance $\frac{1}{\kappa}$ from the surface, and ζ refers to the surface of shear, there must be, in the case of ovalbumin, a number of ions taken into account in the Donnan treatment (using titration valencies for the protein) which move with the molecule in an electric field. It is doubtful, however, whether the experimental accuracy justifies any definite conclusions on this point.

(3) The Theory of Steinhardt and Harris (1940)

This theory has been correlated with that of Gilbert and Rideal (1944) by these latter authors, and since the dissociation constants K of Stein-

hardt and Harris may be written

$$K = e^{-\mu}/RT, \tag{27}$$

the only difference in the results of the two theories arises from fundamental assumptions about the nature of the sites. Since in the following section the Gilbert and Rideal theory has been shown to be related to that of a definite "surface phase," the Steinhardt and Harris theory must be similarly related.

(4) The Theory of Gilbert and Rideal (1944)

These authors use the equation of Fowler and Guggenheim (1939),

$$\frac{\mu_A}{RT} = \ln\left(\frac{\theta_A}{1 - \epsilon_A \theta_A}\right) - \ln a_A(T), \tag{28}$$

where μ_A is the partial chemical potential of species A, and $\theta_A, \theta_B, \cdots$ are the fractions of sites occupied by molecules of types $A, B, \cdots$. $a_A(T)$ is the partition function for the internal degrees of freedom of the adsorbed molecules or ions, including vibrations relative to their mean positions in the sites. No translational movement of the ions is considered in the equation. Gilbert and Rideal introduce an electrical potential correction, ψF, into (28), where ψ is the potential difference between the surface and the bulk.

The equations developed by these authors lead to

$$2\psi F = \Delta\mu_A{}^0 - \Delta\mu_C{}^0, \tag{29}$$

using their nomenclature.

Thus ψ is constant at constant temperature and pressure, since $\Delta\mu_A{}^0$ and $\Delta\mu_C{}^0$ are constant under these conditions. Further, from the equations of Gilbert and Rideal

$$RT \ln\left(\frac{\theta_C}{1 - \theta_C}\right) = -\Delta\mu_C{}^0 - \psi F + RT \ln C$$

or

$$\theta_C = \frac{C}{C + B}, \tag{30}$$

where

$$B = \exp\left(\frac{(\Delta\mu_C{}^0 + \Delta\mu_A{}^0)}{2RT}\right),$$

so that (30) indicates a Langmuir type of adsorption between bulk and surface for cations, and a similar expression may be derived for anions. Thus, the magnitude of ψ makes no fundamental difference to the relation between the fraction of surface covered and the bulk concentration of the ion concerned.

It is important to note that $a(T)$ will depend to some extent on the environment of the adsorbed ion, *i.e.*, on the composition and ionic strength of the "surface phase," which, however, will be of small thickness in the present theory.

If a "surface phase" is postulated, in which are the adsorbed hydrogen and chloride ions, it is possible to omit the electrostatic term and write

$$\mu_A = \mu_A{}^0(T, P)_{\text{fiber}} + RT \ln \left(\frac{\theta_A}{1 - \theta_A} \right) = \mu_A{}^0(T, P)_{\text{bulk}} + RT \ln \bar{a}_A,$$

where $\bar{a}$ refers to activity in the surface, and μ represents chemical potentials.

$$\therefore \quad - RT \ln a_A(T) + RT \ln \left(\frac{\theta_A}{1 - \theta_A} \right)$$
$$= RT \ln \left(\frac{\bar{f}_A \bar{C}_A N}{1,000} \cdot \frac{h^3}{(2\pi m k T)^{3/2}} \right), \quad (31)$$

using the partition function form of the chemical potential, where N is Avogadro's number, h is Planck's constant, k the Boltzmann constant, and m the mass of the ion A. $\bar{f}_A$ refers to the activity coefficient in the surface.

Hence

$$\bar{C}_A \cdot \bar{f}_A \left(\frac{Nh^3}{1000(2\pi m k T)^{3/2}} \right) = \frac{1}{a_A(T)} \left(\frac{\theta_A}{1 - \theta_A} \right). \quad (32)$$

This equation gives the fundamental connection between this theory and that of a "surface phase." If hydrogen ion is considered, (32) shows that, as θ increases, the pH in this "surface phase" will fall, if $a_A(T)$ is appreciably constant. The "thickness" of the surface phase corresponds to the amplitude of vibration of the adsorbed ion perpendicular to the plane of the surface. The small variation of $a(T)$ with concentration shows that $a(T)$ is a function of $\bar{C}_A$, *i.e.*, the concentration of the "surface phase" depends upon its volume, just as in the case of the treatment in terms of the Donnan equations.

A further connection between the two theories is that ψ is equal to the electrochemical potential given by

$$\psi = \frac{RT}{F} \ln \left(\frac{\bar{C}_A}{C_A} \right)$$

in the "surface phase" treatment.

The advantage of the Gilbert and Rideal theory for systems where a large molecule such as a dye is involved, is that activity coefficients in the "wool phase" do not have to be evaluated. The system involved would doubtless be far from ideal.

The authors are indebted to Dr. R. K. Schofield for stimulating discussion about the Gouy treatment.

Summary

Recent theories of the distribution of ions at a charged surface have been examined, and have been compared with the practically convenient treatment based on the idea of a definite "surface phase." In particular, the equations of the Gouy theory have been shown to be compatible with those for a "surface phase" of thickness $\dfrac{1}{\kappa}$ to which the Donnan equations have been applied.

References

Bjerrum, *Z. physik. Chem.* **110**, 656 (1924).

Danielli, *Biochem. J.* **35**, 470 (1941).

Donnan, *Z. Electrochem.* **17**, 572 (1911).

Fowler and Guggenheim, Statistical Thermodynamics, p. 426. Cambridge Univ. Press, 1939.

Gilbert and Rideal, *Proc. Roy. Soc. (London)* **182A**, 335 (1944).

Gouy, *J. phys. radium* [4] **9**, 457 (1910).

Hartley and Roe, *Trans. Faraday Soc.* **36**, 101 (1940).

Steinhardt and Harris, *J. Research Natl. Bur. Standards* **24**, 335 (1940).

Wilson, *J. Am. Chem. Soc.* **38**, 1982 (1916).

SURFACE PRESSURE–AREA MEASUREMENTS FOR FILMS OF POLYVINYL ACETATE POLYMERS SPREAD ON WATER [1]

G. C. Benson and R. L. McIntosh

From the Division of Chemistry, National Research Council, Ottawa, Canada

Received April 26, 1948

INTRODUCTION

The possibility of determining molecular weights from surface pressure-area measurements on monomolecularly spread films has been indicated by the work of a number of investigators, in particular Adam (1) and his collaborators. However, there is some doubt about the practicability of such a procedure for molecules of relatively high molecular weight. Apparently Guastalla (2) was the first to use the method for certain large protein molecules such as gliadin, egg albumin, and hemoglobin. Bull (3, 4, 5) has carried out similar determinations for films of egg albumin and β-lactoglobulin spread on ammonium sulphate solutions and has obtained linear plots of "surface-pressure $\times$ area" against "surface pressure" for a range of surface pressure from about 1.0 down to 0.10 dynes/cm. The values obtained by these two authors for the molecular weights of several proteins are in good agreement with each other and with those obtained from osmotic pressure and ultracentrifuge measurements.

The success of this method depends on the ability of the film, at low surface pressures, to exhibit a gaseous region where its behavior is analogous to that of a perfect gas in two dimensions. In regard to protein films Adam (6) has stated "their molecules are much too large for gaseous films to be detectable." The existence of such a gaseous region for gliadin at measurable surface pressure has been questioned by Hughes and Rideal (7), who found that, at large film areas per molecule, the film pressure became constant. Similar results were obtained by Philippi (8) for β-lactoglobulin and serum albumin. Bull (9) has attributed these discrepancies to differences in spreading techniques.

A similar lack of agreement exists in the literature concerning the determination of the molecular weights of synthetic high polymers. Thus, Guastalla (10) has reported film molecular weights of about 40,000 and 150,000 for two fractions of polyvinyl chloride, while Crisp (11) calcu-

lated that, for a fraction of polyvinyl acetate of molecular weight as small as 4000, the film is not in a gaseous state until the film pressure is less than 0.02 dynes/cm. The work of Crisp showed that the area occupied per unit of polymer is independent of its molecular weight. Similar results have been obtained by Moss (12) for polyethylene succinates and by Harkins, Carman and Ries (13) for polymers of ω-hydroxydecanoic acid.

These discordant results and statements have led the present authors to study in some detail the surface pressure-area curves for a number of different fractions of polyvinyl acetate polymers. These polymers were chosen because of their good spreading characteristics (11, 14) and low solubilities in water.

Apparatus and Materials

Determinations of the surface pressures were made by the Wilhelmy method as developed by Harkins (15, 16) and his coworkers. A good analytical chainomatic balance was used as a semi-null instrument. Balance was obtained to the nearest mg. by means of the chain, and deviations from zero of a glass fiber attached to the end of the pointer were read with a microscope having an eyepiece scale. Using a thin microscope cover glass, 5 cm. wide and 0.02 cm. thick, suspended from one arm of the balance, one division of the eyepiece corresponded to a change in weight of about 0.02 mg. In this way changes in pressure of the order of 0.002 dynes/cm. could be observed. The balance was so arranged that, when the beam was brought to rest, off the knife edge, the slide was immersed a millimeter or two more than when the beam was on the knife edge and the pointer at zero. This procedure facilitated good wetting of the slide. The beam was brought to rest after each pressure reading, before the film was compressed for the next.

The tray, with inside dimensions $115 \times 20 \times 1$ cm. and an edge 1 cm. wide, was made of brass. The interior and top edge of the tray were gold plated. Strips of plate-glass 1.8 cm. wide and 0.6 cm. thick were used as barriers. These could be moved along the tray by forks carried by a cross-piece which, in turn, was driven by a threaded rod having 10 threads/in. and mounted in the supporting framework beneath the tray. The tray and supporting framework were enclosed in a glass case standing on two massive concrete piers. Provision was made for maintaining a high relative humidity within the case. During a "run" the barrier could be controlled from outside the case, and its position relative to the threaded rod was recorded by a counter and circular scale divided into 200 parts. Back lash in the coupling between the threaded rod and the cross bar carrying the forks was greatly reduced by use of a specially designed spring nut. The accuracy of the threaded rod was checked with a

cathetometer. The dimensions of the tray and glass slide were carefully calibrated.

The paraffin used to coat the barriers and edges of the trough was suitably purified and leached with hot water. The distilled water employed throughout the research was redistilled from alkaline permanganate in an all Pyrex still, according to the recommendations of Bauer (17). The solvents, benzene and petroleum ether, were also redistilled in a Pyrex still. In the case of the latter, a fraction boiling between 60° and 65°C. was collected. Both solvents were tested for surface active material by spreading them on a water surface, waiting for them to evaporate, and finally measuring the change in surface pressure on compression.

The polyvinyl acetate polymers were commercial "Gelvas" manufactured by Shawinigan Chemicals, Ltd. The method adopted for purifying them has been outlined by Robertson, McIntosh and Grummitt (18). Eastman Kodak reagent stearic acid was used to check the performance of the surface balance.

EXPERIMENTAL PROCEDURE AND RESULTS

The general techniques of monomolecular film work have been well described in the literature. No attempt will be made to repeat the details here.

The water surface was cleaned by repeated sweeping with the barriers. This process was continued until a 90% decrease of surface area resulted in an increase of surface pressure of less than 0.05 dynes/cm.

All solutions were prepared gravimetrically, but the final amount spread on the surface was measured volumetrically with a Blodgett (15) pipette. Several pipettes with volumes of about 0.1 ml. were used. The deliveries of these were calibrated and were reproducible to a few tenths of 1%. Good agreement was obtained between films spread with different pipettes. In calculating the amount of material spread on the surface, allowance was made for the change in density of the solution with temperature. The solution was spread dropwise from the Blodgett pipette, keeping the additions near the center of the tray and touching each drop to the surface. The film was allowed to stand for 10 mins. to permit evaporation of the solvent before compression of the film was started.

When stating surface areas, the increase in area due to curvature of the surface at the glass slide and the edges of the trough was taken into account. In this connection, images of the water surface near the edge of the tray suitably illuminated by an arc lamp, were projected on a screen by a lens system. These magnified images were traced and measured, thus making possible the calculation of correction factors.

As mentioned previously, the apparatus and technique was checked by measurements on stearic acid. Films of this material were spread from

petroleum ether solution on a substrate of 0.01 N sulphuric acid. The
"surface pressure-area" or "F-A" curve obtained was similar to that given
by Nutting and Harkins (19). The average value of the limiting area at
zero film pressure obtained from seven individual determinations was
24.33 Å^2/molecule with a deviation from the mean of ±0.37%. If this
error is expressed as a percentage probable error of the mean, the final
result may be stated as 24.33 ± 0.12% Å^2, which compares favorably
with the 24.41 ± 0.18% Å^2 given by Nutting and Harkins.

Films of the polyvinyl acetates were spread from benzene solution on
water substrate. In studying the F-A curves of these polymers it was
convenient to divide them into two ranges, a dilute range where the
surface pressures were less than 2 or 3 dynes/cm. and a more concentrated
range from 1 dyne/cm. to collapse pressures. The solutions spread to
obtain these two ranges were, respectively:

(a) about 2.5 × 10^{-4} g. of polymer/g. of solution; and
(b) about 6.5 × 10^{-4} g. of polymer/g. of solution.

The overlap of the two ranges between 1 and 3 dynes/cm. was used as a
check on the consistency of the measurements. In general, this matching
was not perfect; the upper part of the curve from an (a) solution lay
slightly above the low pressure end of the curve from a (b) solution, and
deviations became more noticeable upon further compression of the film
from the less concentrated solution. Thus, at an area of 3100 m.^{2}/g.
(surface pressure about 1.5 dynes/cm.) the curve for an (a) solution was
roughly 0.05 dynes/cm. higher than that for a (b) solution, while at
2600 m.^{2}/g. (surface pressure about 2.5 dynes/cm.) the difference was
approximately twice as large. This effect was apparently due to contamin-
ation of the surface, which became more noticeable as the originally more
dilute film was compressed. If an (a) solution was spread at a smaller
initial area, such that the initial surface pressure reading was 1–2 dynes/
cm., the curve obtained on compression checked the lower end of the
curve from a (b) solution.

The preceding remarks apply to films of all the polyvinyl acetate
polymers studied, except the highest molecular weight fraction. The be-
behavior of films of Gelva V 1700 was somewhat anomalous. For this
polymer, curves from (a) solutions lay slightly below those from (b)
solutions in the overlap region. The surface pressure-area plots for films
spread from solutions of an intermediate concentration

(c) about 3.8 × 10^{-4} g. of polymers/g. of solution

lay between the previous two. On the other hand, further dilution of an
(a) solution did not change the F-A plot. At present no adequate explana-
tion can be given for this effect.

The polymer films in most cases appeared quite stable except when the rate of compression was too great. For the low pressure range, the compression could be quite rapid and steady values of the surface pressure result. However, for pressures greater than a few dynes/cm., too rapid a compression led to falling values of the surface pressure. These drifts if followed did not end in a reproducible value. Often the final value obtained in such a case was lower than the equilibrium value observed by slower compression of the film. Steady readings were obtained when the increase of surface pressure did not exceed 0.5 dynes/cm. every 6 mins. Under these conditions, the surface pressures were reversible within a few hundredths of a dyne/cm. for small expansions and compressions.

For films of Gelva V $1\frac{1}{2}$ steady surface pressures above 2 dynes/cm. were unobtainable. Higher pressures fell off noticeably, and steady readings could not be obtained by any reasonable decrease in the rate of compression of the film. In this case, an approximate idea of the F-A curve was obtained by compressing the film at about the same rate as for the other polymers and disregarding the drift observed in the readings. This observed instability of films of Gelva V $1\frac{1}{2}$ is probably attributable to the higher solubility of the lower molecular weight components of the fraction as the surface pressure is increased. Crisp (11) has made a similar suggestion to explain the lower value of the limiting surface area obtained for polyvinyl acetate polymers of small chain length.

The surface pressure-area measurements for each polymer were checked for reproducibility by doing 3 or 4 runs on films spread from at least two completely independent solutions. These results were plotted on large scale graphs, smooth curves were drawn and the values of the surface pressure were read off at rounded values of the surface area/g. Corresponding numbers from different runs on the same polymer were averaged. Except in the case of Gelva V 1700, the overlap between curves from (a) solutions and (b) solutions was adjusted by empirically lowering, on a percentage basis, the averaged results from (a) solutions over a pressure range from about 0.8 to 1.5 dynes/cm. In this way a continuous curve was obtained.

A typical F-A plot is illustrated by curve (A) of Fig. 1. Curve (B) shows results for Gelva V $1\frac{1}{2}$. The dotted upper portion of the latter curve represents non-equilibrium readings as mentioned previously. Since it is impossible to indicate the separate curves for the other polymers on a small scale graph, a few of the final smoothed values are given for comparison in Table I. The anomalous behavior of Gelva V 1700 has been illustrated by indicating in separate columns the values obtained for films spread from the 3 different solution concentrations. Small changes in temperature from one run to another were found to have no noticeable

effect on the curves. The average temperature within the case containing the trough was about $25 \pm 1°C$. during the course of this work.

DISCUSSION

The general characteristics of the polyvinyl acetate films studied in this research may be summed up as follows. The surface pressure-area curves for these polymers are almost identical, showing only a slight dependence on the average molecular weight of the fraction. Thus, surface
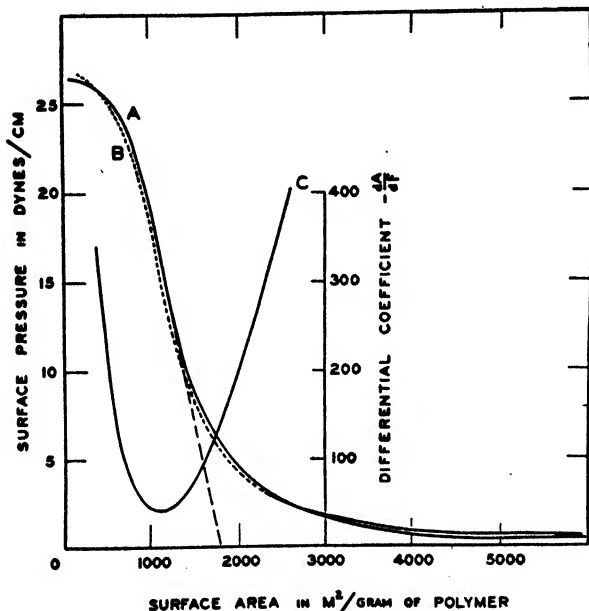
FIG. 1. A, Typical surface pressure-area curve for polyvinyl acetate polymers; B, Surface pressure-area curve for Gelva V 1½; C, Differential coefficient $\frac{-dA}{dF}$ plotted against surface area.

pressure must be associated more closely with the polymer unit than with the molecule. Above 23 dynes/cm., films of Gelva V 1700 appear to exert slightly greater surface pressures than the lower polymers at comparable surface concentrations. This may indicate a second order dependence on molecular weight. In this same region of pressure, Crisp (11) has noted that "the molecular weight has a small but definite effect on the mechanical properties of the film, the higher fractions gelating at slightly larger areas and lower surface pressures." Certainly the restraint imposed by the bonds between the polymer units might be expected to

TABLE I

| Area | Average surface pressures for polymers (in dynes/cm.) | | | | | Gelva V 1700 | | |
	Gelva V 1½	Gelva V 7	Gelva V 15	Gelva V 45	Gelva V 360	Spread from an (a) solution	Spread from a (c) solution	Spread from a (b) solution
$m.^2/g.$								
9800	0.128	0.067	0.072	0.058		0.044		
9400	0.135	0.071	0.077	0.064	0.072	0.046		
9000	0.145	0.076	0.082	0.072	0.078	0.052		
8600	0.158	0.081	0.092	0.083	0.086	0.055		
8200	0.171	0.089	0.104	0.092	0.096	0.061		
7800	0.189	0.101	0.118	0.106	0.107	0.071		
7400	0.208	0.118	0.135	0.122	0.122	0.086		
7000	0.232	0.140	0.157	0.140	0.142	0.103		
6600	0.263	0.166	0.188	0.167	0.165	0.124		
6200	0.298	0.203	0.223	0.199	0.195	0.152		
5600	0.366	0.277	0.291	0.266	0.257	0.212	0.226	
4800	0.519	0.435	0.442	0.422	0.410	0.344	0.392	
4000	0.798	0.748	0.749	0.732	0.702	0.609	0.681	
3600	1.016	1.003	0.999	0.991	0.948	0.830	0.926	
3100	1.442	1.502	1.467	1.511	1.445	1.285	1.400	1.44
2900	1.74	1.80	1.81	1.81	1.76	1.55	1.67	1.73
2700	2.10	2.18	2.19	2.16	2.13	1.88	2.04	2.12
2500	(2.52)	2.64	2.65	2.62	2.60	2.30	2.50	2.61
2300	(3.04)	3.22	3.23	3.22	3.20	2.83	3.07	3.21
2100	(3.72)	3.96	4.01	3.98	3.97	3.46	3.73	3.98
1900	(4.64)	4.96	5.05	5.00	4.98			4.99
1700	(5.92)	6.35	6.47	6.40	6.39			6.41
1500	(7.74)	8.47	8.62	8.45	8.55			8.50
1300	(10.52)	11.70	11.93	11.74	11.88			11.86
1100	(14.71)	16.29	16.50	16.37	16.54			16.50
900	(19.31)	20.90	20.99	20.89	20.95			21.03
800	(21.27)	22.60	22.72	22.59	22.68			22.74
700	(23.06)	23.92	23.95	23.93	24.00			24.07
600	(24.42)	24.90	24.90	24.86	24.94			25.04
500	(25.40)	25.59	25.56	25.52	25.56			25.70
400	(26.06)	25.98	25.96	25.92	25.94			26.12
300	(26.42)	26.21	26.18	26.12	26.16			26.39

exert some influence on the way in which the units can be crowded together on the surface. The higher surface pressures observed for Gelva V 1700 probably indicate that the larger molecules cannot be packed together as closely as the smaller ones when orientated in the surface.

It is customary to estimate the "limiting area" by extrapolation of the linear region of the F-A curve to zero surface pressure. Characterization of proteins by this procedure has been criticized by Bull (9), who

pointed out that the curves are only approximately linear. The same statement appears valid for polyvinyl acetate films. The *F-A* curves for these polymers show no extensive linear portion. This can be seen clearly from curve (C) of Fig. 1, where the differential coefficient $(-dA/dF)$ is plotted against A. The areas at the point of inflection of each *F-A* curve, obtained from the minimum in plots of this type for the various polymers are shown in Table II along with the limiting areas obtained by drawing

TABLE II

Polymer	Approximate molecular weight (number average)	Area at point of inflection Å²/polymer unit	Limiting area at zero surface pressure Å²/ polymer unit
Gelva V 1½	2×10^3	(15.0)	(24.9)
Gelva V 7		15.9	25.6
Gelva V 15	6.1×10^4	15.7	26.0
Gelva V 45	1.5×10^5	16.0	25.4
Gelva V 360	4.1×10^5	15.9	25.2
Gelva V 1700	8.5×10^5	15.6	26.0
		Av. 15.8	Av. 25.6

tangents to the *F-A* curves at the points of inflection and extrapolating to zero value of the surface pressure. Omitting the results for Gelva V 1½, which are undoubtably low due to solubility in the substrate, the average values for these two areas are 15.8 and 25.6 Å²/polymer unit, respectively.

It is rather difficult to compare the results of the present research quantitatively with the data of Crisp which are presented chiefly in graphical form. Also, a strict comparison of results for quite different preparations of polymers is open to question. In general, it would appear that, in the region above 2 or 3 dynes/cm. for the same value of the surface pressure, our values for the areas are about 1–2 Å²/unit larger than those of Crisp. Thus, a limiting area of 24 Å² was obtained by the latter.

At small surface concentrations, films of Gelva V 1½ exert noticeably higher surface pressures than those of the other polymers. On the other hand, films of Gelva V 1700 exert the smallest surface pressures. This may be taken as an indication of a trend toward "ideal gas" behavior. However, even at pressures below 0.1 dynes/cm., the films are not in a gaseous state. Plots of $F \times A$ against F for the low pressure region from 0.3 dynes/cm. down to 0.05 dynes/cm. are not linear but rather are concave towards the *F*-axis. Extrapolation of these curves to zero value of the surface pressure involves quite large uncertainties, and values of the molecular weights calculated from these intercepts are meaningless, although that for Gelva V 1½ does seem to be of the right order of magni-

tude. Approximate molecular weights estimated from some unpublished osmotic data and the work of Robertson, McIntosh and Grummitt (18) have been indicated in the second column of Table II. In comparison, the molecular weight calculated from extrapolation of the $F \times A$-F curve for Gelva V $1\frac{1}{2}$ is 3.1×10^3, while that for Gelva V 1700, 9.9×10^3, is probably low by a factor of 100.

ACKNOWLEDGMENTS

SUMMARY

Except for solubility of low molecular weight fractions and anomalous spreading of the very high molecular weight fraction Gelva V 1700, the films of the polyvinyl acetate polymers studied were stable and well behaved. Extrapolation of the $F \times A$-F plots for these films to obtain molecular weights does not appear feasible, as it would necessitate the accurate measurement of extremely small surface pressures in a region of low surface concentration, where unavoidable contamination introduces an increasing uncertainty in such measurements.

REFERENCES

1. ADAM, N. K., The Physics and Chemistry of Surfaces, 3rd ed. Oxford University Press, London, 1941.
2. GUASTALLA, J., *Compt. rend.* **208**, 1078 (1939).
3. BULL, H. B., *J. Am. Chem. Soc.* **67**, 4 (1945).
4. BULL, H. B., *ibid.* **67**, 8 (1945).
5. BULL, H. B., *ibid.* **68**, 745 (1946).
6. ADAM, N. K., Ref. (1), see p., 87.
7. HUGHES, A. H., AND RIDEAL, E. K., *Proc. Roy. Soc. London* **137A**, 62 (1932).
8. PHILLIPPI, G. Th., Thesis, Univ. Leiden, 1936.
9. BULL, H. B., *Advances in Protein Chem.* **3**, 95 (1947).
10. GUASTALLA, J., Soc. Chim. Phys., Section de Physique des Surfaces, Extrait du Procès-Verbal de la séance du 2 Mai, 1946.
11. CRISP, D. J., *J. Colloid Sci.* **1**, 49 (1946).
12. Moss, S. A., *J. Am. Chem. Soc.* **56**, 41 (1934).
13. HARKINS, W. D., CARMAN, F. E., AND RIES, H. E., *J. Chem. Phys.* **3**, 692 (1935).
14. KATZ, J. R., AND SAMWEL, P. J. P., *Naturwissenschaften* **16**, 592 (1928).
15. HARKINS, W. D., AND ANDERSON, T. F., *J. Am. Chem. Soc.* **59**, 2189 (1937).
16. BOYD, G. E., AND HARKINS, W. D., *Ind. Eng. Chem., Anal. Ed.* **14**, 496 (1942).
17. BAUER, N., Chap. III, p. 72 in Physical Methods of Organic Chemistry, Vol. I. Ed. A. Weissberger, Interscience Publishers, Inc., New York, 1945.
18. ROBERTSON, R. E., McINTOSH R., AND GRUMMITT, W. E., *Can. J. Research* **24B**, 150 (1946).
19. NUTTING, G. C., AND HARKINS W. D., *J. Am. Chem. Soc.* **61**, 1180 (1939).

THE EFFECT OF SALTS AND CHAIN LENGTH ON THE CRITICAL CONCENTRATIONS OF COLLOIDAL ELECTROLYTES

M. L. Corrin[1]

From the Department of Chemistry, University of California, Berkeley
Received January 9, 1948

INTRODUCTION

The abrupt change with concentration in many physical properties of aqueous solutions of long-chain paraffin salts has been attributed to the formation of colloidal aggregates (1), and the concentration at which this change occurs has been termed "the critical concentration for the formation of micelles." It has been concluded, on the basis of the experimental observations, that the concentration of the aggregate, or micelles, must increase rapidly with overall concentration of the salt at concentrations exceeding the critical concentration. According to Grindley and Bury (2) this aggregation may be considered as a reversible process in which many paraffin chain ions coalesce to form a micelle. The rapid increase in aggregate concentration with overall concentration is then due to the large exponent with which the ion activities enter into the mass law expression governing the equilibrium. Similar views have been advanced by Murray and Hartley (3) in discussing the solubility-temperature relationships in solutions of long-chain salts.

An extension of this mass law treatment to other phenomena encountered in the study of colloidal electrolytes is of considerable interest. In the present paper it is shown that such considerations lead to equations describing the effect of added salts on the critical concentration and to the variation of critical concentration with paraffin chain length for homologous series of long-chain salts. In a future paper, it is proposed to extend this treatment to the problem of adsorption of long-chain salts from aqueous solution.

THE EFFECT OF SALTS UPON CRITICAL CONCENTRATION

The effect of salts upon the critical concentration for the formation of micelles in solutions of colloidal electrolytes has been treated from the experimental standpoint in a previous paper (4). It was there shown that

---

[1] Present address: Dept. of Chemistry, University of Chicago.

the effect could be represented by an equation of the form

$$\log \text{cmc.} = -k_1 \log C_s + k_2, \tag{1}$$

in which cmc. represents the critical concentration of the colloidal electrolyte; C_s, the total concentration of the counter-ion; and k_1 and k_2 are constants. This relation was observed for potassium laurate, sodium dodecyl sulfate, dodecyl ammonium chloride and decyl trimethylammonium bromide. It was also reported that the nature and concentration of that ion of the added salt which bore a charge of the same sign as that of the existing colloidal aggregate had no measurable effect on the critical concentration.

Cassie and Palmer (5) have derived an equation of the above general form for the salt effect by an extension of the theory developed for the interfacial energy of colloidal electrolytes; they consider the charge density upon the micelle-solution interface as a function of the concentration of long-chain ions and ions of added salt. This treatment leads to the conclusion that the only ions which are effective in lowering the critical concentration are those possessing a charge opposite in sign to that on the aggregate. In their equation, however, k_1 has the value unity while experimentally it varies from 0.570 to 0.343 in those instances investigated. No possible reason for this discrepancy will be considered here.

This problem can, however, be approached from the standpoint of the law of mass action governing the equilibrium between the unassociated long-chain ions and the aggregate. This equation takes the form

$$\frac{(\gamma_a C_a)}{(\gamma_d C_d)^m (\gamma_s C_s)^n} = K, \tag{2}$$

where γ_d, γ_s, and γ_a are the activity coefficients of the long-chain ion, the counter-ion and the aggregate, respectively; C_d, C_s, and C_a are the corresponding concentrations; m and n are the number of paraffin ions and counter-ions, respectively, entering into one micelle; and K is the equilibrium constant. The phenomenon of micellization is thus considered represented by the following process:

$$mD^{\mp} + nS^{\pm} \rightleftarrows (D_m S_n)^{\mp(m-n)},$$
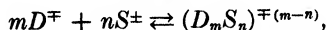
in which D represents the long-chain ion and S the counter-ion. It is, of course, necessary that the sign of charge on D be opposite to that on S.

A theory concerning activity coefficients in solutions of such highly assymmetrical, high-valent electrolytes is lacking; this problem has been discussed by Hartley (6). It is therefore assumed in the following discussion that, in accord with both experimental (7, 8, 9, 4) and theoretical (6) conclusions, the ionic strength principle is herein valid. For want of

further information the activity coefficient ratio, $(\gamma_d)^m(\gamma_s)^n/(\gamma_a)$, is assumed independent of the various concentrations at the critical concentration; this ratio will be designated as R. Actually, the concept of activity coefficients in systems similar to those under consideration is not particularly helpful due to the difficulties encountered in the choice of standard states.

Eq. (2) may be written in the form (3)

$$R(C_d')^m(1-x)^m(C_s')^n(1-xn/m)^n = C_d'x/Km, \qquad (3)$$

in which x represents the fraction of long-chain ions in aggregated form and the primed, C's stoichiometrical concentrations. It will be further assumed that m and n are essentially indepenent of salt concentration at the critical concentration; this is equivalent to the constant surface-charge-density assumption of Cassie and Palmer. Then, making the approximation that, at the critical concentration, x is negligibly small compared to unity,

$$\log C_d' = (-n/m) \log C_s' + (1/m)\log C_d'x - (1/m)\log KRm. \qquad (4)$$

It is necessary at this stage to define the term "critical concentration" in terms of the reversible aggregation process (10). A convenient and satisfactory definition is that the critical concentration represents the total concentration of long-chain electrolyte at which, for compounds possessing the same polar head-group, a small and constant number of long-chain ions are in aggregated form. The number of aggregated ions at the critical concentration for a homologous series of paraffin chain salts is thus independent of the hydrocarbon chain length. This definition is in accord with the nature of the end-point in the determination of critical concentrations by the dye spectral method (11). If, as is likely, the dye is adsorbed at the interface micelle-solution, the onset of measurable adsorption and consequently the end-point would occur at the same total micellar area for long-chain electrolytes with the same polar head-group. It has been shown that for a given head-group the area occupied by each long-chain molecule on the surface of the micelle is, regardless of chain length or total concentration, a constant (12). Consequently, the concentration at which a constant micellar area is attained is dependent only upon the number of ions in aggregated form.

Since the number of such aggregated ions is $C_d'x$, Eq. (4) becomes

$$\log \text{cmc.} = -(n/m) \log C_s' + \text{const.} \qquad (5)$$

since at the critical concentration $C_d' = \text{cmc.}$ within the approximation that x is small.

The constant k_1 in the experimental Eq. (1) thus represents the ratio of the number of counter-ions to long-chain ions entering into the micelle.

The values of this ratio, as expected, are less than unity and vary for different polar head-groups. It has been shown by S. H. Herzfeld (13) that the value of k_1 for potassium caprate is equal, within experimental error, to that for potassium laurate. Values of the ratio given below are reproduced from an earlier paper (4).

Long-chain electrolyte	$-k_1 = n/m$
Potassium laurate	0.570
Potassium caprate (13)	0.562
Sodium dodecyl sulfate	0.458
Dodecyl ammonium chloride	0.562
Decyl trimethylammonium bromide	0.343

The values of this ratio as determined by the salt effect on critical concentrations are in fairly good agreement with those calculated by Hartley (14) on the basis of freezing point, electromotive force and mobility measurements.

The Effect of Hydrocarbon Chain Length upon Critical Concentration

It has been reported by Hess, Philippoff and Kiessig (15), by Scott and Tartar (16), by Hartley (14), by Stauff (17), and quoted by Harkins (18) that the relationship between critical concentration and hydrocarbon chain length for a homologous series of long-chain electrolytes is given by

$$\log \text{cmc.} = k_3 N + k_4 \tag{6}$$

or, in the equivalent form used by Harkins,

$$(\text{cmc.})_N / (\text{cmc.})_{N'} = B^{(N'-N)}, \tag{7}$$

where N is equal to the number of carbon atoms in the paraffin chain and k_3, k_4 and B are constants. These equations are valid only over a limited range of hydrocarbon chain lengths.

From Eq. (2) and the assumption that the activity coefficient ratio, R, is constant at the critical concentration

$$(N_o^{(m+n-1)}/Rm)\,(n_a/n_d^{(m+n)}) = \exp\,(-\Delta F^0/N_o kT), \tag{8}$$

where ΔF^0 is the standard free energy of micellization; n_a and n_d are the number of long-chain ions in aggregated and unaggregated forms respectively; N_o, Avogadro's number; k, Boltzmann's constant and T, the absolute temperature. The absence of an n_s term is due to the fact that, at the critical concentration, n_s is approximately equal to n_d in the absence of added salt.

Micellization occurs due to the reduction in free energy brought about by removal of the hydrophobic carbon chains from solution in an aqueous

environment to the nonpolar interior of the micelle. The free energy of micellization may be considered as a sum of terms including that described above, a term involving the repulsion of the head-groups in the micelle and others of lesser importance. Only the first term would be expected to depend on the length of the hydrocarbon chain if the same head-group were involved. Designating this environmental term as ΔF_I^0 and placing all terms independent of chain length in ΔF_R^0,

$$\Delta F^0 = \Delta F_I^0 + \Delta F_R^0 = k_I N + \Delta F_R^0, \tag{9}$$

where N is the number of carbon atoms in the chain and k_I is a constant. This is true only for chains of such length that a change in length does not affect the head-group repulsion.

Eq. (8) then becomes

$$\psi \ (n_a/n_d^{(m+n)}) = \phi \exp \ (-k_I N/N_o k T), \tag{10}$$

where ψ is equal to $N_o^{(m+n-1)}/mR$ and ϕ is equal to $\exp \ (-\Delta F_R^0/N_o k T)$. This may be written in logarithmic form as

$$\log_{10} n_d = [0.434 k_I/N_o k T(m+n)] \ N + (1/m+n) \log_{10}(\phi \ n_a/\psi). \tag{11}$$

It was assumed previously that m and n are independent of concentration at the critical concentration which, in turn, was defined as that concentration at which n_a is constant for long-chain electrolytes with the same head-group. Since n_d is proportional to the critical concentration

$$\log_{10} \text{cmc.} = k_3 N + k_4 \tag{12}$$

at constant temperature. In this expression

$k_3 = 0.434 \ k_I/N_o k T(m+n)$ and
$$k_4 = (1/m+n)\log_{10}(\phi \ n_a/\psi) + \log_{10} N_o.$$

Since k_I, m, n, ψ, and ϕ are temperature dependent, k_3 and k_4 should vary with temperature.

SUMMARY

It is shown that the effect of salts upon the critical concentration for the formation of micelles in solutions of long-chain electrolytes can be treated by considering the mass law as applied to the equilibrium between the unassociated long-chain ions, counter-ions and the aggregate. From the experimental observations, it is possible in this manner to calculate the ratio of long-chain ions and counter-ions which enter into the micelle.

Similar considerations lead to the development of an equation which describes the variation in critical concentration with paraffin chain length for long-chain paraffin salts possessing the same polar head-group.

REFERENCES

1. McBain, J. W., *Trans. Faraday Soc.* **9**, 99 (1913). For references regarding the physical properties involved in the aggregation see Corrin, M. L., Klevens, H. B., and Harkins, W. D., *J. Chem. Phys.* **14**, 480 (1946).

2. Grindley, J., and Bury, C. R., *J. Chem. Soc.* **1929** 679; see also Hartley, G. S., Aqueous Solutions of Paraffin Chain Salts, Hermann et Cie, Paris, 1936.

3. Murray, R. C., and Hartley, G. S., *Trans. Faraday Soc.* **31**, 183 (1935).

4. Corrin, M. L., and Harkins, W. D., *J. Am. Chem. Soc.* **69**, 683 (1947).

5. Cassie, A. B. D., and Palmer, R. R., *Trans. Faraday Soc.* **37**, 156 (1941).

6. Hartley, G. S., *ibid.* **31**, 31 (1935).

7. McBain, J. W., *J. Am. Chem. Soc.* **50**, 1639 (1928).

8. McBain, J. W., and Betz, M. D., *ibid.* **57**, 1912 (1935).

9. McBain, J. W., and Searles, J., *J. Phys. Chem.* **40**, 493 (1936). References (7), (8), and (9) were unfortunately omitted in (4).

10. For a discussion of this point see Lamm, O., *Arkiv Kemi, Mineral. Geol.* **18A**, No. 9, (1944).

11. Corrin, M. L., and Harkins, W. D., *J. Am. Chem. Soc.* **69**, 679 (1947).

12. Harkins, W. D., Mattoon, R. W., and Corrin, M. L., *ibid.* **68**, 220 (1946).

13. Herzfeld, S. H., unpublished work.

14. Hartley, G. S., *Kolloid-Z.* **88**, 22 (1939).

15. Hess, K., Philippoff, W., and Kiessig, H., *ibid.* **88**, 40 (1939).

16. Scott, A. B., and Tartar, H. V., *J. Am. Chem. Soc.* **65**, 692 (1943).

17. Stauff, J., *Z. physik. Chem.* **183A**, 55 (1938).

18. Harkins, W. D., *J. Am. Chem. Soc.* **69**, 1428 (1947).

POLYMORPHIC TRANSFORMATIONS OF CALCIUM STEARATE AND CALCIUM STEARATE MONOHYDRATE [1]

Robert D. Vold, Joseph D. Grandine, 2nd, and Marjorie J. Vold

Contribution from the Chemistry Department, University of Southern California, Los Angeles, Calif.

Received January 12, 1948

INTRODUCTION

This paper describes the results of an investigation of the polymorphism of anhydrous calcium stearate, using differential thermal analysis and X-ray diffraction methods, undertaken as a part of a study of the phase behavior of calcium stearate in hydrocarbon solvents. It was further established that calcium stearate, like calcium palmitate (8), forms a monohydrate whose stability and polymorphism likewise were examined.

The manufacture of calcium-base greases has long been rather more of an art than a science; the practical properties of the grease are known empirically to depend on the exact manner of incorporation of the soap in the oil, as well as on the gross chemical composition, and the presence · of additives such as water, esters, free fatty acids, *etc.* Regarding grease as a gel of fine soap crystallites possibly dissolving some oil and enmeshing the rest, it is apparent that processing conditions affecting the rate of crystallization will affect the texture and stability of the resulting grease. However, it seems likely that the crystal form itself may be dependent on the processing conditions, particularly in view of recent developments in the technology of aqueous sodium soap systems (1, 5, 20, 21). Thus, the possible crystal forms of calcium stearate and their rates of interconversion under different conditions become of interest.

In addition to several different crystal forms, some of which may be hydrates of low water content, the sodium soaps exhibit a sequence of transformations to mesomorphic states intermediate between crystal and true liquid (22). Some light may be thrown on the nature of this stepwise melting by comparing the behavior of soaps of different cations, in addition to that supplied by comparisons between the sodium soaps of homologous fatty acids (17, 18).

EXPERIMENTAL

The calcium stearate used for this work, except for samples reported in the section on technical calcium stearate, was prepared by P. J. Arnis[2] by metathesis in alcohol solution between calcium chloride and potassium stearate. Dr. G. S. Hattiangdi of this laboratory has established, by determining the calcium content, that the formula of the calcium stearate so prepared is $Ca(C_{18}H_{35}O_2)_2$. The stearic acid was obtained from the Eastman Kodak Co. and was further purified by fractional crystallization and recrystallization of its lead salt from alcohol, followed by recrystallization of the recovered acid from acetone.[3] The acid had a m.p. of 68.8–69.5°C., an iodine number of 0.05, and an equivalent weight of 284.0. The prepared soap was free of excess stearic acid and potassium and chloride ions. It was air dried at room temperature after washing with successively increasing concentrations of alcohol in water, and finally with ethyl ether. Comparative experiments were carried out on 2 samples of technical calcium stearate obtained from the Metasap Chem. Co., and on one prepared from Neo-fat 1-65 (Armour Chem. Div.). Constants for these are given in Table I.

TABLE I

Analytical Data for Technical Stearic Acids

Source of acid	Iodine no.	Equiv. wt.	M.P. °C. (corr.)
Armour Co. Neofat No. 1–65	4.5	287	65–66
Recovered from Metasap Ca(Str)₂,			
1941 sample	6.9	273	48–49
1947 sample	3.6	282	56–57
Recovered from Dr. G. S. Hattiangdi's Ca(Str)₂	3.0	267	54–56

X-ray diffraction patterns were obtained using the North American Philips Co. X-ray spectrometer (7) with Cu Kα radiation, and automatic recording (by a Brown Electronik Strip Chart Recording Potentionmeter, model 153XlaV-X-30), of the intensity of the scattered radiation as a function of the diffraction angle between 2° and 50°. A systematic investigation of the dependence of the results upon instrumental variables and manner of sample preparation led to adoption of the following invariable routine: The X-ray tube, Geiger tube, and recording circuit were allowed to warm up for 30 minutes before each run. The slit widths defining the X-ray beam, and the angular width of the diffracted beam entering the Geiger tube, were held constant throughout, as were the controls of the amplifying circuit, the "amplitude," and "damping." The routine settings were: medium X-ray slit (width 1.5 mm.), angular divergence (horizontal) of beam 0° 47'; medium Geiger slit (width 0.50 mm.), angular coverage, $2\theta = 0° 13' 30''$.

Samples for X-ray examination were packed into a circular hole 5/8" in diameter cut in a 1 × 3" microscope slide, and smoothed off with a glass plate. This procedure does not eliminate the possibility, inherent in the design of the spectrometer, that anisometric crystallites may pack in an oriented rather than a random manner, thus vitiating con-

---

[2] Deceased.

[3] The purification was carried out by Dr. L. L. Lyon, present address, Institute of Industrial Research, University of Wichita, Wichita, Kansas.

clusions based on the relative intensity of bands in the resulting pattern. No definite procedure has yet been devised for detecting or controlling this factor. All that can be said is that no differences in pattern were found to result from further grinding of crystalline calcium stearate or from attempts to induce orientation by repeated unidirectional stroking of the sample.

Measurements were made to 0.01° in the value of the diffraction angle (2θ, where θ is the Bragg angle). The position measured usually was the center of the band at half maximum intensity. Values of the spacings calculated from the measurements were reproducible to 0.02 Å at large angles and 0.2 Å even at angles as small as $2\theta = 5°$, corresponding to the "long" or "c" spacing of the soap. X-ray patterns given in this paper are pantograph reductions of the original curves.

Differential thermal analysis was carried out in the calorimeter furnace described by Vold and Griffiths (20), but with completely revised controls and sample cells. One of the twin cells is shown in Fig. 1. The sample is seen to be essentially a cored cylinder,
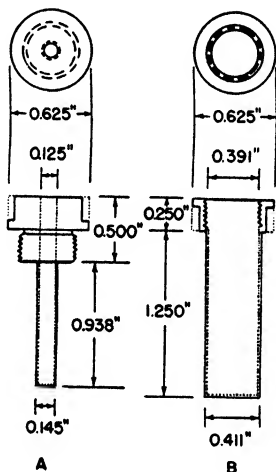
Fig. 1. Cross-sectional view of calorimeter cell.
A—cap with thermocouple well. B—cell.

with the thermocouples for temperature and temperature difference measurements located in the center of the core in a thin-walled (0.005") stainless steel well.

For measurement of temperature difference a triple-junction iron-constantan thermopile was used. The junctions are insulated from each other by glass fiber woven sleeving further impregnated with silicone varnish (Dow Corning No. 996). The temperature difference between the sample cell and reference cell is recorded continuously by means of a Brown strip chart potentiometer, model 153X11V-X-Y-12. As supplied, this instrument has a range of 0–5 millivolts, with a pen travel of 12". By replacing one of the internal resistances with a Leeds and Northrup variable resistance box it was found convenient to increase the sensitivity of the potentiometer by as much as a factor of 5. At maximum sensitivity, and using the 3-junction thermopile, one scale division (the position of the pen can be estimated to 0.1 division) corresponds approximately to $\Delta T = 0.08°$. By adding a second variable resistance in parallel with another of the

internal resistances, it was possible to adjust the zero position so that both positive and negative values of ΔT could be recorded. The wiring diagram of the potentiometer circuit showing these changes is given in Fig. 2.[4]

The temperature of the reference cell was recorded as a function of time by a single junction iron-constantan thermocouple attached to a Brown circular chart recording pyrometer, model 152P131P-68-15. This instrument is also a time-temperature pattern controller operating by transmitting a variable air pressure to a Conoflow air motor which controls the heat input to the calorimeter by turning the control dial of a 0–130 volt "Variac" (General Radio Co., model VMT5).

The operation of the entire calorimeter assembly is thus fully automatic. A given time-temperature pattern (in this case a linear rise of 1.5°/min.) can be imposed on the system. However, to eliminate fluctuations of the heating rate about the imposed value as a mean, careful adjustment of the controls of the instrument to the heat requirements of the particular calorimeter is necessary. The steady state temperature difference be-
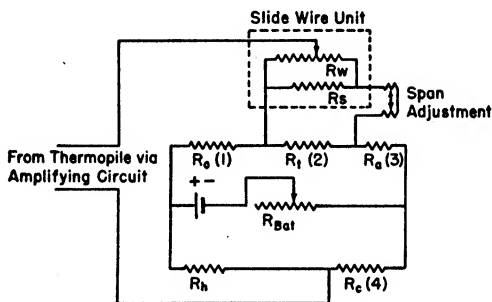
FIG. 2. Wiring diagram of strip chart potentiometer. R_a (3), 253.4 ohms; R_c (4), 509.5 ohms; R_h, 5.00 ohms; slide wire unit, 20 ohms. R_o (1) was originally 2.474 ohms but was made variable by placing a 20–150 ohm resistance in parallel with it. R_t (2) was originally 1.474 ohms but was made variable at from 0.3–1.5 ohms, the lower figure giving maximum sensitivity.

tween sample and reference cells is proportional to the heating rate (15), and consequently fluctuations in heating rate must be avoided if a smooth base line is to be obtained. The two controls are "throttle range," governing the per cent of available air pressure supplied for a given deviation between the actual and control temperature, and "automatic reset." The former adjustment applies full air pressure for a temperature deviation equal to a given per cent of the full range (400°C.). Thus, 20% throttling means that 100% of the controlling air pressure is applied for an 80° deviation, 10% for 8°, etc. The "automatic reset" controls a gradual continuous increase in applied air pressure which is superimposed on the partial "high-low" control of the throttling range adjustment. Its principles are fully discussed by the suppliers (23). The type of base line obtained in the present instance is given in Curve I of Fig. 3. The choice of control settings for best results with the given furnace (20% throttling, reset dial 9, 30–120 volts applied for 0–100% air pressure) was determined by trial and error.

Procedures

Samples for X-ray analysis of dry calcium stearate were prepared by sealing about 0.6 g. of dry soap in an evacuated pyrex tube, and then heating the soap to the desired temperature for 1 hr. The tube was then quenched in a dry ice-alcohol bath, allowed to warm to room temperature, and opened. The treated soap was powdered with a minimum of grinding and loaded into an X-ray slide. Many modifications of this thermal treatment were carried out, as shown in the tables of data and description of the results.

Samples for calorimetric study were packed into the calorimeter cell and given the desired thermal pre-treatment directly in the cell, before running.

EXPERIMENTAL RESULTS

Visual Observations during Heating and Cooling Anhydrous Calcium Stearate

Bulk samples (1–2 g.) were placed in sealed pyrex glass tubes and observed in an air oven provided with glass windows as it was heated at the rate of 1–2°/min. No change was detected below 123°,[5] although during drying at 110°, P. J. Arnis observed that the powder seemed more coherent beginning at about 100°. At 125° the loose particles coalesce and the whole mass becomes somewhat translucent. At 150–155° it becomes nearly transparent. At about 200°, a slight loss in transparency and increase in fluidity is discernible. The phases present between 125 and 150° and 150 and 200° and above, though faintly orange in color between crossed polaroids, do not have the conspicuous brilliant anisotropy characteristic of the liquid crystalline forms of anhydrous sodium soaps.

A small sample was placed in a sealed flat capillary and observed during heating and cooling in a small furnace (16) mounted on the stage of a Bausch and Lomb polarizing microscope under 50× and 100× magnification. Again no change was observed below 123°. At this temperature a marked increase in translucency occurs. At 150°, the whole sample becomes very nearly transparent and flows together. Trapped bubbles, however, do not assume a spherical shape and there is a pebbly structure visible. At 195° minute bright hair-like spots appear and the sample simultaneously becomes brighter. The same characteristic changes are observed on cooling.

The Hydration of Calcium Stearate

The Arnis preparation of calcium stearate, air-dried at room temperature, loses 2.73% water at 110°C., close to the 2.88% calculated for the stoichiometric monohydrate $Ca(Str)_2 \cdot H_2O$. The per cent water lost by the hydrous material as a function of drying temperature in air under otherwise constant conditions (sample weight and area of exposure, time,

---

[5] All temperatures are expressed in °C.

relative humidity, drafts, *etc.*), shown in Fig. 3, is strong presumptive evidence that the material is a stoichiometric hydrate with a decomposition temperature near 110°C. at 1 atm. total pressure. A similar hydrate has been reported by Buerger for calcium palmitate (8). Höppler (9) reports the existence of a dihydrate of calcium oleate.
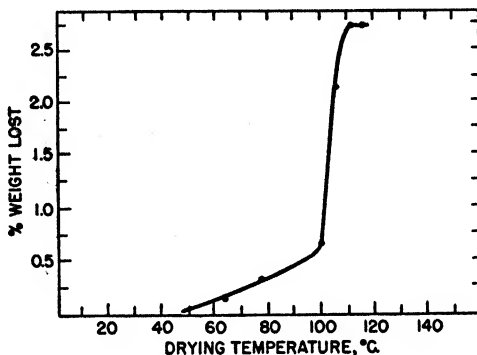
FIG. 3. Loss of weight of Ca(Str)₂ on drying. Obtained by heating sample for 2 hours at each temperature.
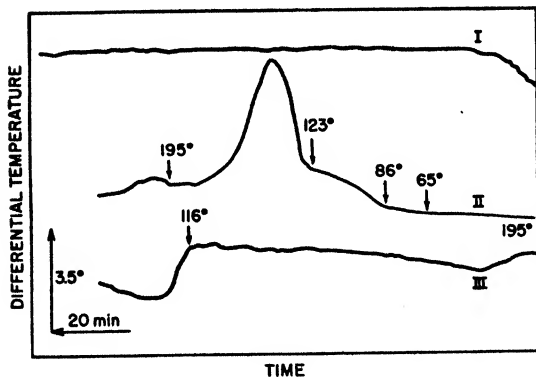
FIG. 4. Differential thermal analysis of anhydrous crystalline calcium stearate. Curve I, base line obtained with Nujol in both sample and reference cells. Curve II, heating Ca(Str)₂ at 1.5°/min. Curve III, cooling Ca(Str)₂ at from 2.5°/min. at 200° to 0.5°/min. at 100°. Temperatures of increase or decrease of ΔT, as marked, indicate transitions.

That the hydrated material is a true compound is further demonstrated by the results of X-ray diffraction. Fig. 5 shows the patterns obtained for the hydrous and anhydrous material, for a mechanical mixture of the two in equal weights, and for samples of intermediate water contents prepared

by partial drying of the hydrous material. The positions of the centers of the most prominent bands in the diffraction patterns are given in Table II. These were calculated from the Bragg equation using $\lambda = 1.542$ Å (2). It is apparent that the hydrate and the anhydrous material give qualitatively different patterns, and that partially dehydrated samples give patterns substantially identical with those of mechanical mixtures of the hydrate and the anhydrous soap. The pattern published by Smith and Ross (13) for "normal" calcium stearate appears to be that of the monohydrate, although it might possibly be the result of use of a less pure stearic acid (*cf.* section on technical calcium stearate).
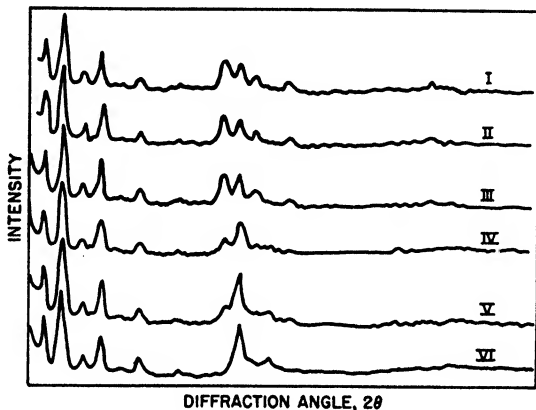
FIG. 5. X-ray diffraction patterns for partially dehydrated $Ca(Str)_2 \cdot H_2O$. Water content: I, 2.73%; II, 2.60%; III, 1.82%; IV, 1.36%; V, 0.85% VI, 0.00%.
Curve IV was obtained on a mechanical mixture of equal weights of the materials used for curves I and VI.

Anhydrous calcium stearate adsorbs 0.2% moisture on exposure to laboratory air at room temperature for one hour, 0.1% in the next hour, and very little thereafter. However, it does not recrystallize to the hydrate appreciably (as judged by the absence of any change in the diffraction pattern) when suspended in liquid water at room temperature or at 60°C. for as long as 36 hours. At 100°C., however, reformation of the hydrate is substantially complete after the anhydrous material has stood for one hour in contact with liquid water.

Calorimetric Results on Anhydrous Crystalline Calcium Stearate

Curve II of Fig. 4 is typical of the several differential thermal curves for anhydrous crystalline calcium stearate (obtained by drying the prepared hydrate to constant weight at 110°C.). Detectable increases in

TABLE II

X-Ray Diffraction Pattern for Partially Dehydrated Ca(Str)$_2 \cdot$H$_2$O
Amplitude Values (Height of Diffraction Maximum)
Arbitrary units

Per cent H$_2$O	2.73	2.60	1.82	1.36[b]	0.85	0.00
Per cent hydrate	98.3	90.2	64.2	49.2	29.5	0.00
d/n[a]						
4.82	2	2	2	—[c]	2	—
4.40	28	24	25	13	12	2
4.13	23	22	25	27	42	43
3.87	14	11	12	4	11	7
3.67	—	—	—	4	10	13
3.41	9	6	6	3	5	—
2.50	2	2+	3−	2	2	2
2.38	2	4	4−	2−	2−	3
2.28	5	5+	5	2−	2	—
2.21	—	—	—	—	3	4
2.18	2−	2	3−	2+	3	3
Long Spacing Å	49.70	49.78	49.83	50.54	50.38	50.34

[a] These are mean values. Fluctuations and shifts not greater than 0.02 Å were found in the different samples.

[b] This sample is a mechanical mixture of equal weights of hydrate and anhydrous material.

[c] A dash indicates absence of a noticeable diffraction maximum corresponding to this spacing.

the rate of heat absorption by the soap occur at 65°, 86°, 123°, and 195°C. No further evidence of transitions was found up to 280°C. Calcium stearate is reported to decompose with melting at about 350°C. (10). The behavior at 123° and 195° is typical of that expected for a true polymorphic inversion. The temperature difference continues to rise as the transformation proceeds until a maximum is reached, at a position dependent on the rate of the transformation, the magnitude of its heat effect, and the rates of heat transfer between cells, and from furnace to cell. Thereafter, the temperature difference again declines to its steady state value. After the initial increases in ΔT beginning at 65° and 86°, no such decline is observed. It may be that the rates of these transformations are so slow that the expected maximum in ΔT is masked by the onset of the next succeeding transformation at the rate of heating employed (1.5°/min.), or it may be that the transformations are of the "second order," *i.e.*, involve only a discontinuous change in heat capacity rather than in heat content.

Curve III of Fig. 4 is typical of those obtained on cooling calcium

stearate from above 200°C. The cooling rate is uncontrolled, though reproducible from run to run, being about 2.5°/min. at 200°C., and 0.5°/min. at 100°C. The transformation at 195° is readily reversible at the same temperature on heating or cooling. That at 123° is also readily reversible, usually with a few degrees of undercooling at this cooling rate. No evidence of transformations at 86° or 65° is obtained on cooling. This result is capable of 3 interpretations among which no choice can be made: (a) the heats of the transformations at 65° and 86° are too small to detect at the very slow cooling rate imposed by the design of the furnace, (b) the rates of these transformations are too slow, or (c) the transformations are second order, in which case they would be very difficult to detect with slow cooling. A fourth possibility, that the soap undercools through these changes, is ruled out by the finding that transformations occur again at 65° and 86° on heating the cooled soap, provided it had not been heated originally above 145°C.

X-ray Diffraction Data for Anhydrous Calcium Stearate

In the absence of a satisfactory cell for obtaining diffraction patterns at controlled elevated temperatures, samples which had been quenched from various higher temperatures were examined at room temperature in the hope that the molecules would be frozen in the relative orientations characteristic of each of the high temperature forms. Fig. 6 shows the results obtained for samples quenched from 105°, 115°, 135°, 145°, 155°, 170°, 225°, 267°, 280°, and 320°C. It is at once apparent that there is a difference at room temperature between samples quenched from 145°

DIFFRACTION ANGLE, 2θ
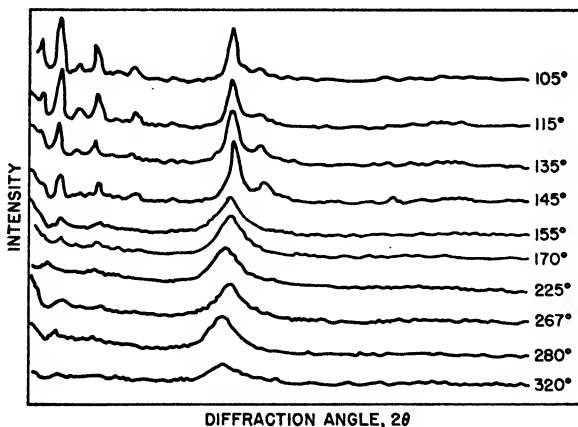
FIG. 6. X-ray diffraction patterns of anhydrous Ca(Str)$_2$ run immediately after quenching from various temperatures.

and 155°C. It was observed visually that calcium stearate becomes quite translucent at 150°C., and this temperature has been taken by some observers as the "melting point" of the soap.[6] This transition at 150°C., despite the accompanying gross change in X-ray diffraction pattern, apparently does not have a significant heat effect (a suggestion of a heat effect at this temperature has been found in a few runs made with the differential calorimeter, while in others no indication of this transition was to be found).

Table III gives values of d/n calculated from the observed diffraction bands, measured at the center of the band at half maximum amplitude or (for poorly resolved bands) at the top of the corresponding peak. For the smaller angles these values are readily identifiable as successive orders of a crystal spacing corresponding to the double length of the $Ca(Str)_2$ molecule (i.e., this spacing is $c \cdot \sin \beta$, where β = angle between the axis of the molecule and the plane containing the polar $(COO)_2Ca$ groups, and c = perpendicular separation of these basal planes). For larger diffraction angles, each of the bands is undoubtedly a composite of many reflections, to which little interpretation can be given until the lattice type and space group of the crystal is determined. However, these data are still of considerable value for purposes of identification and for studying the effect of various processing treatments on the sample.

Samples quenched from above 150°C. are characterized by a progressively decreasing intensity of the diffraction maxima arising from the long spacing, and loss of resolution among the short spacings, the two principal peaks at 4.12 Å and 3.67 Å being replaced by a broad halo whose center is about 4.18 Å. The value of the long spacing also decreases significantly. Samples quenched from between 125° and 150° can be distinguished from those quenched from lower or higher temperatures by the intermediate intensity of the long spacings, coupled with the continued sharpness of the short spacings, in agreement with the calorimeter finding of a major heat absorption at 123°C.

Calcium Stearate Pseudo-Glass

The translucent calcium stearate phase existing between 150° and 195°C. is an anisotropic liquid or liquid crystal, since it exhibits spontaneous double refraction of light, appearing bright when viewed between crossed polaroids. The quenched material at room temperature displays many of the properties associated with glasses, but since a glass is by definition an undercooled liquid, it is preferred to refer to the quenched liquid cyrstal as a pseudo-glass.

The calorimetric behavior of calcium stearate pseudo-glass is shown

TABLE III

X-Ray Diffraction Bands from Anhydrous Ca(Str)$_2$ No. 1[a]

Quenching Temp. °C.	[b]	105[f]	[c]	115[f]	[d]	135	135[e]	145[f]	155[f]	170[f]	225[f]	267[f]	280[f]	320	320[g]
Orders of Long Spacing (n, d Å)															d
3	49.55	49.74	50.11	49.29	49.92	51.39	50.40	49.20	49.65	50.01	50.49	48.48	48.48	48.2	
4	49.18	49.72	50.22	50.04	49.88	51.24				50.00					
5	49.68	50.07	50.40	49.56	50.05	51.15	50.40	49.56	49.73	49.96	50.25	48.75	49.70		
6	49.56	49.84	50.22	49.74											
7	49.98	50.20	50.33	49.89	50.13	50.95	50.49	50.33			50.21				
9	50.35	50.48	50.77	50.31	50.48	50.89	50.80	50.48							
Ave. Value	49.7 (47)	50.0 (50)	50.3 (64)	49.8 (44)	50.1 (47)	51.1 (27)	50.5 (13)	49.9 (22)	49.7 (9)	50.0 (7)	50.3 (7)	48.6 (6)	48.8 (5)	48.2 (3H)	
Short Spacings	4.57 (3)					4.42 (5)									
	4.11 (40)	4.14 (47)	4.14 (43)	4.13 (43)	4.12 (45)	4.14 (48)	4.12 (55)	4.10 (55)	4.18 (31H)	4.18 (32H)	4.19 (34H)	4.20 (29H)	4.15 (29H)	4.16 (13H)	4.28 (9H)
	3.92 (7)	3.96 (5)	3.95 (6)	3.90 (6)	3.96 (4)	3.93 (6)									
	3.67 (11)	3.70 (12)	3.70 (11)	3.69 (10)	3.68 (12)	3.69 (15)	3.67 (18)	3.67 (17)							
	3.52 (3)	3.58 (4)	3.52 (3)	3.54 (5)	3.51 (4)	3.53 (3)	3.47 (6)	3.49 (4)							
					2.49 (3)	2.49 (3)	2.48 (4)	2.48 (4)							
	2.36 (3)		2.36 (3)		2.36 (3)	2.37 (3)	2.37 (2)								
	2.20 (5)	2.22 (3)	2.22 (3)	2.20 (3)	2.20 (4)	2.22 (2)	2.15 (3H)	2.20 (3)							
						2.14 (2)		2.13 (3)							

[a] The numbers in parentheses are the heights of the diffraction peaks (arbitrary units, but comparable from run to run). For the long spacing, this is the amplitude of the third order. The symbol H refers to a band so wide as to be designated as a "halo."

[b] Dried at 105°C.

[c] Dried at 110°C.

[d] Dried at 115°C.

[e] Heated to 280°, cooled slowly to 135° and then quenched.

[f] Runs plotted in Fig. 6.

[g] Unground glassy surface.

by the curves of Fig. 7. Heat is absorbed continuously on heating, beginning about 72°C. and becoming more rapid at 108–117°C. The temperature of more rapid heat absorption decreases as the quenching temperature increases. The fact that the pseudo-glass shows the same transition at 195° as the crystalline material, indicates that above 150°C. both have reverted to the same state again. The same conclusion çan be reached by comparing the differential cooling curves obtained for initially crystalline and initially glassy material (Curve III of Fig. 2 and Curve II of Fig. 7).

There is some evidence that a partial devitrification of the pseudo-glass occurs as it is heated in the vicinity of 48°C. This is accompanied by heat evolution, since the temperature difference between the cells decreases instead of increasing. Fig. 3 shows the X-ray diffraction patterns of a
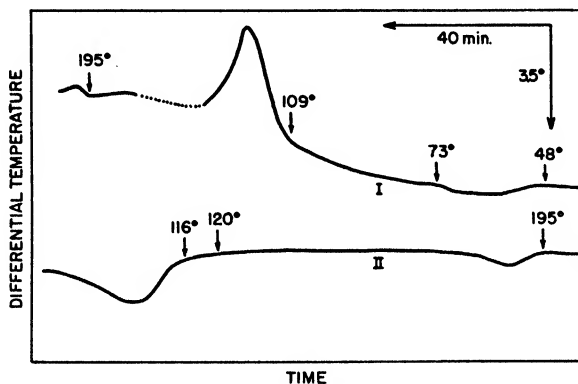
Fig. 7. Differential heating and cooling curves for calcium stearate "pseudo-glass." Curve I, heating. The dotted line represents a short interruption in measurements for instrument adjustment. Curve II, cooling.

sample quenched from 320° before and after reheating to 60°C. Three orders of the long spacing appear after reheating to 60° in place of the one detectable immediately after quenching, and the value of the long spacing has increased from 48.2 Å to 49.3 Å. The original halo, centered at 4.15 Å, has been shifted to 4.08 Å, and also shows evidence of having several partially resolved crystalline reflections superposed on it.

The third curve of Fig. 8 was obtained on a sample of pseudo-glass formed by quenching from 320°C., and mounted directly in the X-ray beam without previous powdering. The long spacings are completely absent and the halo rather broader and centered at 4.27 Å. This indicates that the small amount of grinding associated with preparation of the other samples in powder form probably produces some devitrification.

The pseudo-glass, in contrast with the dry crystalline material,

readily reforms the crystalline hydrate in contact with either liquid water or water vapor at room temperature, as is demonstrated by the diffraction method. Curve IV of Fig. 8 is that of a glassy sample after exposure to liquid water for 45 mins. at room temperature.
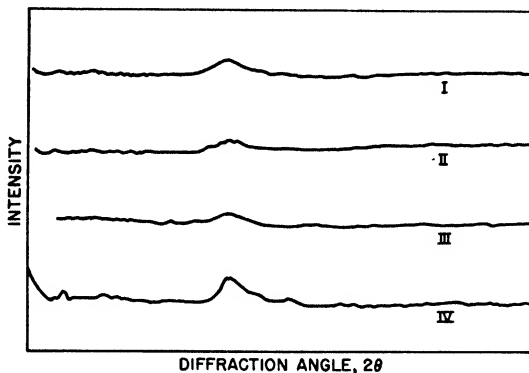
FIG. 8. X-ray diffraction patterns of Ca(Str)₂ pseudo-glass. I, quenched from 320°; II, same material after reheating to 60°; III, same as I, but unground sample; IV, same material as I after exposure to H₂O for 45 min. at room temperatures.

Reversibility of the Transformations of Anhydrous Calcium Stearate

The transformation at 195°C. is rapidly reversible and is always found on the curve of temperature difference *vs.* time for samples cooled in the calorimeter (cooling rate of about 2.5°/min. at this temperature). At 150° or above, rapid cooling (quenching, 100°/min.) produces the pseudo-glassy form discussed above. The differential heating curve and X-ray diffraction pattern of a sample which had been cooled slowly (1.5°/min.) from 280° to 135° and then quenched are given in Fig. 9. The heating curve is intermediate between those for pseudo-glassy and crystalline calcium stearate, favoring the latter; the diffraction curve is also intermediate, but resembles that of the glassy material more closely in the weakness of the reflections due to the long spacing. The transformation at 123° appears to be completely reversible on cooling at 1.5°/min., although there is a tendency for undercooling of a few degrees, as already pointed out. A sample quenched from 138°C. showed, on reheating, transformations at 88°, 112°, and 152°, indicating that a metastable state resulted which did not revert to the normal form on reheating at 1.5°/min. until the "parent" form of the pseudo-glassy state was reached. Although no direct evidence for the reversibility of the transition at 86° has been obtained, it is always present on reheating samples either quenched or

slow-cooled from above this temperature. The same is true for the change at 63°, insofar as slow-cooled samples are concerned, but not for quenched samples.
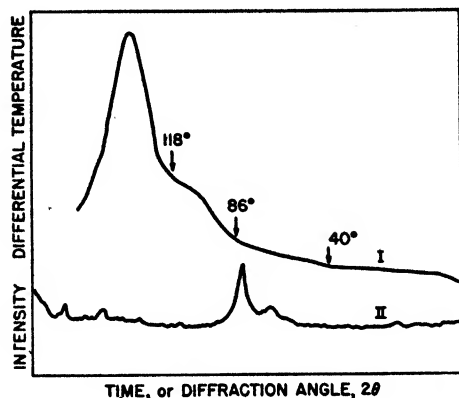
FIG. 9. I, differential heating curve, and II, X-ray diffraction pattern of anhydrous Ca(Str)₂ cooled slowly from 280° to 135° and then quenched. This material is sufficiently different from cystalline Ca(Str)₂ (form VI) and also from the pseudo-glassy form (VI″) to suggest the existence of a metastable form (VI′).

Aging Experiments on Quenched Samples

Some of the samples whose diffraction curves are given in Fig. 5 were allowed to age at room temperature and reexamined after 9 days and
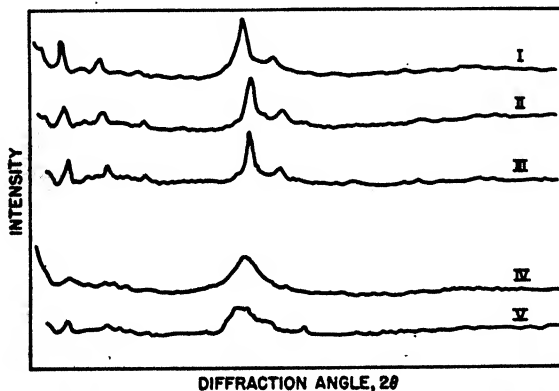
FIG. 10. X-ray diffraction patterns obtained after different aging periods with quenched samples. Upper curves for sample quenched from 135° run immediately (I), and aged for 9 days (II), and 11 weeks (III). Lower curves for samples quenched from 267° run immediately (IV), and aged for 9 days (V).

again after approximately 10 weeks. Typical time sequences for a pseudo-glassy sample (quenched from above 150°) and for a crystalline sample (quenched from below 150°) are shown in Fig. 10. The glassy sample (VI″ of Fig. 14) apparently reverts slowly to the crystalline form (VI of Fig. 14) on standing. Even though the samples were covered (with scotch tape over glass on the X-ray slides), the developing crystal pattern is that of the monohydrate. The crystalline sample also reverts slowly from the metastable form (VI′), presumed on the basis of calorimetric data, to the stable form (VI). After 9 days, both patterns are present, superposed on each other.

Results on Technical Calcium Stearate[7]

Figs. 11 and 12 contain the X-ray diffraction patterns of dry and hydrated calcium stearates of various origins. Analytical data for these are given in Table I. Transition temperatures of these samples, as determined from differential heating curves, are given in Table IV. The 3 distinct transformations of the pure crystal at 65°, 86°, and 123° are but poorly resolved from each other, if at all, in the less pure preparations. The X-ray diffraction patterns of the hydrates do not differ appreciably from that of the pure soap except in relative intensity of the different lines. However, as is clear from Fig. 11, the patterns of several of the anhydrous calcium stearates prepared from these acids resemble that for the pure hydrate rather than that of the pure anhydrous soap. It seems that the oleate or
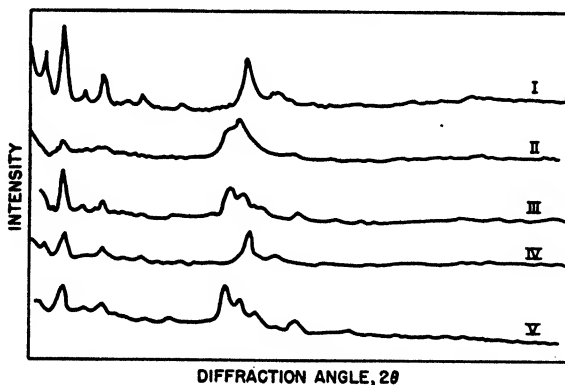
FIG. 11. X-ray diffraction patterns of anhydrous Ca(Str)₂ from different sources. The numbers on these curves refer to the corresponding samples in Table IV.

[7] Included with these is a calcium stearate prepared and studied by Dr. G. S. Hatti-angdi of this laboratory in connection with an examination of a series of metal stearates.
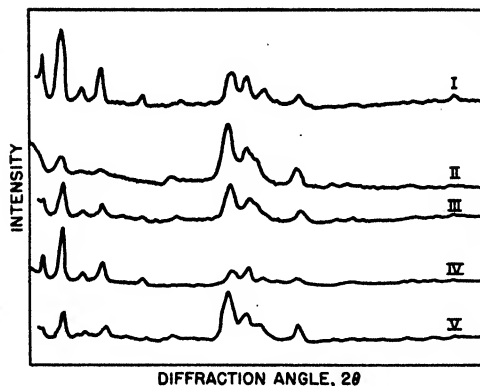
Fig. 12. X-ray diffraction patterns of hydrous Ca(Str)₂ from different sources. The numbers on these curves refer to the corresponding samples in Table IV.

TABLE IV

Calorimetric Transition Temperatures of Calcium Stearates

Sample no.	Source of Ca(Str)₂	Transition temperatures °C.			
I	Arnis Preparation	65	86	123	195
II	Metasap Chemical Company[b]	—[a]	86	*ca.* 109	not studied
III		—	—	*ca.* 108	187
IV	From Armour Acid No. 1–65	—	73	114	184
V	G. S. Hattiangdi[c]	—	89	107	190

[a] Dash indicates transition was absent.

[b] II is a sample supplied in 1941 and III a sample supplied in 1947. Sample III showed continuous heat absorption throughout the region of the 65° and 86° transitions and earlier, but only the two recorded definite peaks.

[c] This sample also exhibited a detectable thermal effect corresponding to the transition at 150° found only by X-ray methods with the other samples.

other impurity present in the technical acids prevents the recrystallization which otherwise occurs on dehydration.

Polymorphism of Calcium Stearate Monohydrate

Differential heating curves for calcium stearate monohydrate between room temperature and 150° are given in Fig. 13. The sample was held in a sealed container which substantially prevented the escape of water. The hydrate shows absorption of heat over a range of temperature between 48°

and 73°, and a further transformation at 123° under these conditions. Successive runs on the same sample yield identical results, indicating that, if water is expelled on heating, it is retained in the cell and recombines with the soap on cooling. Under these circumstances it is likely that the observed transformation at 123° actually pertains to the anhydrous soap.
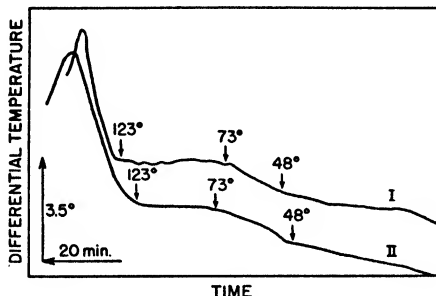
FIG. 13. Differential heating curves for $Ca(Str)_2 \cdot H_2O$ (in a closed container). Curves I and II are successive runs on the same sample.

Heats of Transition

The size of a peak in the curve of temperature difference *vs.* time is a measure of the magnitude of the heat of the transformation. In the past, one of us (R. D. V.) (18) has attempted to make quantitative estimates of heats of transformation by empirical comparison of the peaks with those obtained by melting materials of similar chemical nature and known heats of fusion in the same calorimeter. This procedure could be applied to the present data. However, another of us (M. J. V.) has been developing a theory of the method from which quantitative values may be obtained without empirical comparisons of this type. Preliminary values calculated for anhydrous crystalline calcium stearate by this procedure are 63°, 600 cal./mole; 86°, 4,500 cal./mole; 123°, 11,000 cal./mole; 150°, not detectable, probably less than 250 cal./mole; 195°, 500 cal./mole.

Transformation Scheme for Calcium Stearate

The experimental results can be combined to yield the transformation scheme for calcium stearate given in Fig. 14. In this scheme the sequence of phases occurring as the stable anhydrous crystalline form is heated from room temperature to 350° appears at the left, with the transition temperatures and reversibility indicated. The forms are numbered conventionally with Roman numerals beginning with I just below the true melting point. The metastable anhydrous forms can be realized at room

temperature by quenching the hot soap as indicated by arrows. These are given the same numeral as the stable form (VI) but with primes for distinguishing marks. The behavior of the metastable forms on heating is indicated by arrows. The monohydrate is placed in the right hand column, and the conditions under which it forms or decomposes are indicated by arrows. The existence of forms VI (crystal), VI″ (pseudo-glassy) and VIH (monohydrate) is firmly established. Whether the slight differences in X-ray diffraction pattern and thermal behavior obtained for samples quenched from form III justify designation of the material as being in a different phase state at room tmeperature (VI′), and after the first transformation (IV′), has not been definitively determined.

FIG. 14. Transformation scheme for Ca(Str)₂.

DISCUSSION

The experimental data obtained in this investigation serve two purposes. The facts obtained are expected to prove useful in interpreting the behavior of systems of calcium stearate and hydrocarbon solvents. In addition, interpretation of the data in terms of the structural changes occurring at the several transitions may lead to an increased understanding of the mechanism of melting of this type of compound.

It is reasonable to suppose that a gel of calcium stearate with hydrocarbon solvents will depend in consistency and stability on which phase or mixture of phases is present, as well as on the size and manner of aggregation of the colloidal particles or crystallites. For example, a gel in-

volving the anhydrous pseudo-glassy state (VI'') would be expected to be sensitive to water, since even water vapor is effective in converting this form into the crystalline hydrate (VIH). On the other hand, a gel involving the hydrate would be expected to be stable toward water at room temperature but unstable above 110°C., the decomposition temperature of the hydrate under ordinary atmospheric conditions. As another example, the less regular arrangement of molecules in the pseudo-glassy state and its "parent phase" (II), stable between 150° and 195°C., would be expected to result in a greater tendency for the soap to swell and incorporate the hydrocarbon molecules within the soap lattice or within colloidally dispersed soap aggregates or micelles; this may account for the great increase in viscosity displayed by a dispersion of soap in oil when it is heated to about 150°C.

Structural Changes Produced by Heating

Calcium stearate exists at room temperature in crystals which, like those of the fatty acid and alkali soap crystals, display a regular Bragg spacing corresponding approximately to double the length of the stearate chain. This "long spacing" is the perpendicular separation of the basal planes containng the cations of the soap lattice. Using Pauling's values (12) for atomic dimensions[8] the dimensions of the stearate ion can be calculated to be 4.03 Å × 4.10 Å × 26.14 Å. In a careful study of single crystals of sodium stearate hemihydrate, in which the molecular axis is nearly perpendicular to the planes containing the terminal group, Buerger finds a "c" spacing of 103.96 Å, or 26.0 Å per sodium stearate molecule, in good agreement with this calculated value (4). The calcium ion, with a radius of 0.99 Å is small enough to fit into spaces similar in size to those between oxygens when the hydrocarbon chains exist in a close packed arrangement.

The value of 49.7 Å for the long spacing of calcium stearate corresponds to an angle of inclination of the chains to the basal planes of 71°. This value is markedly larger than that for anhydrous sodium stearate, whose reported long spacing, 44.7 Å (3, 11) corresponds to an angle of tilt of only 64°. The principal short spacing of anhydrous calcium stearate is 4.1 Å, which is the value to be expected from hexagonally close packed chains whose interchain distance is 4.7 Å, and has been found with many long chain paraffin hydrocrabons (6). Sodium stearate, on the other hand, has two principal short spacings (3) at 4.05 and 4.68 Å. It is evident that

[8] Carbon, covalent radius 0.771 Å; hydrogen, covalent radius 0.66 Å, van der Waals radius 1.29 Å; oxygen, ionic radius 1.40 Å; calcium, ionic radius 0.99 Å. In carboxylate ion, O—C—O bond angle 124°, C—O distance 1.27 Å. In hydrocarbon chain, C—C—C bond angle 111°30'.

the manner of packing of the hydrocarbon chains is different in the room temperature crystal forms of the two soaps.

The amphipathic nature of soap molecules (*i.e.*, containing both strongly polar and nonpolar portions) has led naturally to an attempt to correlate each observed phase transformation with a change in packing of the hydrocarbon or polar portions of the lattice, or both. This point of view was originally justified by the observation (18) that, in the homologous series of sodium soaps from laurate to stearate, some heats of transition varied regularly with increasing molecular weight while others were independent of the length of the hydrocarbon chain. If this view is correct, those transformations which involve primarily changes in the packing of the hydrocarbon chains should be analogous for sodium and calcium soaps, while transformations involving primarily a change in the polar portion of the lattice should reflect the difference in cation.

In drawing conclusions from the X-ray diffraction data obtained on samples quenched from high temperatures, it is necessary to remember that the structure of the quenched material is not necessarily identical with or very similar to the structure stable at the higher temperature. A sample which has been heated through a number of thermal transitions may, on quenching, (1) pass back reversibly through all the intermediate forms to the structure which is thermodynamically stable at room temperature; (2) go back through one or more, but not all, of these transitions, the room temperature product being an undercooled form of a phase stable at some intermediate temperature; or (3) loose thermal energy so rapidly that the arrangement at room temperature is that of the phase stable at the temperature from which the sample was quenched. Nevertheless, even though the room temperature pattern may not correspond to that of the high temperature phase, differences in the X-ray spacings of samples quenched from two different temperatures can be taken as evidence that a phase transition has occurred between those temperatures.

In general those phase transitions involving a reorganization of both the polar and the hydrocarbon portions of the lattice would be expected to be least likely to undergo reversal upon quenching. Transitions involving changes in the manner of packing of the hydrocarbon chains of such a nature that no fundamental rearrangement is involved should be reversed on quenching, except for any disaggregation. Samples quenched from above such transitions would, therefore, be expected to have the pattern characteristic of the low temperature form except for possible changes corresponding to a decrease in the spatial extent of regularly ordered regions within the crystallite, such as decrease in intensity and increase in width of line.

The fact that the calorimetric study revealed transitions at 65° and 86° after the sample had been dried at 110° indicates that these two

transitions must be reversed on cooling, and the absence of any X-ray evidence for the occurrence of these transitions indicates that this reversal also occurs on quenching. The transition at 65° for calcium stearate is probably of the second order and may be analogous to the 70° transition for sodium stearate (19). This change is believed to be the "genotypic" effect described by Thiessen and Ehrlich (14). For both soaps it is absent in samples which have been heated through the succeeding two transformations, and is usually absent in samples which have been heated through only the first of these. The heat effect of the 86° transition for calcium stearate is similar to that of the 89° transition of sodium stearate.

The transformation of calcium stearate at 123° has a large heat effect, but there is little difference in the X-ray diffraction patterns of samples quenched from above and below that temperature. The lower intensity of the long spacing in the case of samples quenched from above this transition probably corresponds to a smaller average extent of crystallinity above this transition. This disaggregation is the expected characteristic of a transformation in which only the hydrocarbon chains are involved. The magnitude of the heat effect accompanying this transition can be explained by assuming that the hydrocarbon chains acquire considerable freedom of motion at this transition temperature. Calorimetrically the 123° transition of calcium stearate resembles in heat effect the 117° and 132° transitions of sodium stearate. That sodium stearate has two successive transformations (at 117° and 132°) of similar character to the single transformation at 123° for calcium stearate may be associated with the difference observed in initial crystal form for the two soaps.

The change in X-ray diffraction pattern observed with samples of calcium stearate quenched from above and below 123° resembles that reported for sodium stearate at 125° by de Bretteville and McBain (3), where the chief difference in the higher temperature form was a decrease in the intensity of the long spacing. (A slight increase in the value of the interchain short spacings of sodium stearate reported by these authors probably reflects expansion due to increased thermal motion in the sub-waxy phase.)

The 150° transition of calcium stearate gives rise to a pronounced change in the X-ray pattern of the quenched samples. The single short spacing halo present in samples quenched from above 150° (the parent state of the pseudo-glassy material) corresponds very well with the 4.1 Å separation calculated for hexagonally close-packed hydrocarbon chains. The heat effect accompanying this transformation is so small that it is not observed in our present calorimeter. A visible change also occurs at this temperature, the calcium stearate becoming translucent and only faintly anisotropic above 150°. The 167° change of sodium stearate (waxy to super-waxy) likewise has a very slight heat effect, and very similar

changes in X-ray pattern. However, the long spacing of the sodium stearate pattern decreases in going from 145° to 170° (3) while the calcium stearate spacing remains unchanged until a temperature of 225° (prior to quenching) is reached.

The transition at 195° for calcium stearate resembles the 205° transition for sodium stearate (super-waxy to sub-neat) in having a minor heat effect and no great change in the X-ray pattern. Again, the calcium stearate long spacing, unlike the sodium stearate long spacing, shows no decrease at this transition. Above this temperature the parallelism of the two soaps ceases. The decrease in the long spacing of calcium stearate, which is first noticeable in samples quenched from above 225°, indicates that another calorimetrically undetectable transition may exist. Proof for the existence of such a transition cannot be obtained with quenched samples only. Sodium stearate is known to undergo a further transition to neat soap at 257°C., followed by melting to isotropic liquid at 288°. Calcium stearate remains very viscous and does not melt below 350°. This dissimilarity is probably a direct result of the difference in cations between the two soaps.

It is curious that the transformations at lower temperatures involve at once both the higher heats of transformation and the less drastic changes in diffraction pattern. It is possible that a complete structure determination, based on diffraction studies of single crystals (not yet successfully prepared for calcium soaps) would show greater differences between the low temperature forms than is suggested by the powder type patterns of quenched samples. However, a comparison of heats of transformation per carbon atom at the lower temperatures (where the transformations are presumed to involve the chains) with heats per mole of soap at higher temperatures (where the transformations are presumed to involve the polar heads) brings the heat effects into correspondence qualitatively with the apparent extent of the corresponding structural rearrangements. Thus, at 86° and 123° the heats of transformation per carbon atom are 125 and 305 calories, respectively, while the heat per mole of calcium stearate at 195° is 500 calories per mole.

SUMMARY

Anhydrous calcium stearate undergoes transformations at 65°, 86°, 123°, 150°, and 195°C. It melts with decomposition at 350°C. The substance can be obtained at room temperature either as a stable crystal, an unstable crystal (by quenching from between 123° and 150°), or a vitreous form (by quenching from above 150°). Differential heating and cooling curves and X-ray diffraction patterns of quenched samples at room temperature are presented.

The set of transformations is partially analogous to that for sodium stearate, the resemblance being greater at low temperatures and less marked at high temperatures where, with the hydrocarbon chains irregularly packed and relatively mobile, the difference in binding power between sodium and calcium ions becomes important.

Calcium stearate forms a monohydrate whose decomposition temperature at atmospheric pressure is about 110°C.

Calcium stearates of technical quality resemble the pure material but tend to assume the vitreous form more readily and to crystallize completely only with difficulty.

REFERENCES

1. BODMAN, J. W., *U. S. Patent* 2,215,539, September 24, 1940.
2. BRAGG, W. S., *J. Sci. Instruments* **24**, 27 (1947).
3. DE BRETTEVILLE, A., AND MCBAIN, J. W., *J. Chem. Phys.* **11**, 426 (1943).
4. BUERGER, M. J., *Am. Mineral.* **30**, 551 (1945).
5. BUERGER, M. J., SMITH, L. B., BYER, F. V., AND SPIKE, J. E., *Proc. Natl. Acad. Sci. U. S.* **31**, 226 (1945).
6. BUNN, C. W., *Trans. Faraday Soc.* **35**, 482 (1939).
7. FIRTH, F. G., The Geiger-Muller X-Ray Spectrometer, in J. ALEXANDER's *Colloid Chemistry*, Vol. VI, 108. Reinhold, New York, 1946.
8. GARDINER, K. W., BUERGER, M. J., AND SMITH, L. B., *J. Phys. Chem.* **49**, 417 (1945).
9. HOPPLER, F., *Fette u. Seifen* **49**, 700 (1942).
10. LAWRENCE, A. S. C., *Trans. Faraday Soc.* **34**, 660 (1938).
11. MCBAIN, J. W., DE BRETTEVILLE, A., AND ROSS, S., *J. Chem. Phys.* **11**, 179 (1943).
12. PAULING, L., The Nature of the Chemical Bond, 2nd ed. Cornell Univ. Press, Ithaca, N. Y., 1944.
13. SMITH, G. H., AND ROSS, S., *Oil & Soap* **23**, 77 (1946).
14. THIESSEN, P. A., AND EHRLICH, E., *Z. physik. Chem.* **165A**, 453 (1933).
15. VOLD, M. J., to be communicated shortly for publication.
16. VOLD, M. J., AND DOSCHER, T. M., *Ind. Eng. Chem., Anal. Ed.* **18**, 154 (1946).
17. VOLD, M. J., MACOMBER, M., AND VOLD, R. D., *J. Am. Chem. Soc.* **63**, 168 (1941).
18. VOLD, R. D., *ibid.* **63**, 2915 (1941).
19. VOLD, R. D., *J. Phys. Chem.* **49**, 315 (1945).
20. VOLD, R. D., GRIFFITHS, B., AND VOLD, M. J., to be submitted to *Ind. Eng. Chem*
21. VOLD, R. D., KONECNY, C., AND LYON, L. L., to be submitted to *Ind. Eng. Chem.*
22. VOLD, R. D., AND VOLD, M. J., *J. Am. Chem. Soc.* **61**, 808 (1939).
23. WEREY, R. B., Instrumentation and Automatic Control in the Oil Refining Industry, 61. The Brown Instrument Co., Phila., 1941.

INTERPRETATION OF THE MECHANISM OF CATALYTIC REDUCTIONS WITH COLLOIDAL RHODIUM IN THE LIQUID PHASE

L. Hernandez and F. F. Nord

From the Department of Organic Chemistry,[1] Fordham University, New York 58, N. Y.

Received May 25, 1948

I. INTRODUCTION

The present trend to explain a number of reactions on the basis of electron transfer has, no doubt, thrown light on the mechanism of some reactions otherwise difficult to understand. Various types of reactions, especially in organic chemistry, have been extensively studied; to cite but a few instances: the wide field of acid-base catalysis by Brønsted *et al.* (1), the hydrolysis of methyl bromide (2), and the catalytic autoxidation of benzaldehyde in the presence of the ferrous ion (3).

However, not too much is known in this respect (4) regarding catalytic hydrogenation of organic substances with noble metals, a fact which is even more true in the case of catalysis in the liquid phase. In particular, the literature available with regard to the catalytic action of Rh is very scarce. Perhaps this is due to its high cost and to the traditional belief that Rh possesses but slight catalytic activity when compared with other metals in its group (5).

However, recent reports on metal films (6) disclosed that Rh in the proper physical state can be far more active than the other metals.

It has been known that the particle size of the catalyst is of the utmost importance for its catalytic activity (7). Colloidal size has proven excellent for maximum performance, and various supporting colloids have been employed for this purpose. Synthetic high polymers have been used recently (8) in the preparation of highly active and stable colloidal Pd and Pt catalysts, with practical application to a number of organic substrates (9a). These encouraging results led to investigation of a colloidal *rhodium* catalyst. Remarkable discrepancies between the behavior of Pd and Rh were noticed immediately (10), suggesting a fundamental difference in the mechanism of catalytic hydrogenation by the two metals.

To ascertain these findings, a rhodium-polyvinyl alcohol (Rh-PVA)

catalyst was prepared as in the method adopted previously for Pd-PVA (8). Under identical experimental conditions, several series of compounds, involving the nitro group and the double bond, were hydrogenated separately with Rh-PVA and Pd-PVA. The most salient differences consist in the fact that the rate of hydrogenation with Rh is greatly influenced by changes in pH and by the presence of adjacent functional groups in the substrate molecule, whereas hydrogenation with Pd is affected but little, or not at all, by the factors mentioned. The experimental results furnished a basis for an electronic interpretation that seems to explain the reduction with Rh of the compounds studied through the formation of an intermediate complex involving "ionized" hydrogen.

II. Experimental

Preparation of the Rh-PVA Catalyst

A 2% aqueous solution of polyvinyl alcohol is prepared by dissolving 2 g. of polyvinyl alcohol of medium viscosity (DuPont Type B) in 100 ml. water. A solution is promptly formed on warming gently and shaking vigorously. To this colloidal dispersion, 5 ml. of an aqueous solution of $RhCl_3.3H_2O$ containing 10 mg. Rh/cc. are added. Then, with shaking, enough NaOH is added drop by drop until the turbidity first formed disappears. This transforms the chloride to the hydroxide, an indispensable prerequisite for subsequent reduction to metallic rhodium. The clear yellow solution is then heated on the water bath for 15 mins., the color changing to a dark brown. After this, the solution is allowed to cool and reduced by shaking for 15 mins. with commercial hydrogen at room temperature and atmospheric pressure. The resulting black liquid is carefully neutralized with acetic acid and stored for use; 20 ml. of this solution contain 10 mg. of Rh metal. The colloidal dispersion thus prepared is very stable and will retain its catalytic activity for months.

Hydrogenation of Organic Substrates

A given amount of the substance—calculated to take up 500–700 cc. of hydrogen—is dissolved in ethyl alcohol, its concentration and volume depending upon the solubility of the substrate under investigation. The propylene derivatives—such as allyl alcohol, allylamine, *etc.*—were dissolved in 50 cc. of 50% ethanol, while some of the substituted nitrobenzenes required 100 cc. of 75% alcohol for solution. As a rule, the amount and concentration of the solvent does not influence the rate of hydrogenation, provided it is kept within certain limits, since a very small amount will not favor effective shaking, and too large a quantity causes extreme dilution. Fifty to one hundred cc. were found best. To insure identical experimental conditions, all the compounds belonging to

the same series were dissolved in the same amount of solvent. The desired amount of catalyst—generally 20 cc. of Rh-PVA, equivalent to 10 mg. Rh—was then added to the ethanol substrate solution and the mixture placed in a shaking vessel. The apparatus (11) consists of a 1000 cc. burette connected with a shaking vessel—shaking at a speed of 258 strokes/min. Commercial hydrogen is supplied from the burette, water replacing the gas consumed; by equalizing the external and internal pressures with a leveling bulb, the volume of hydrogen utilized can be measured at any interval of time. All hydrogenations were invariably conducted at atmospheric pressure and room temperature (21–23° C.).

III. Discussion and Results

The simplest mechanism of hydrogenation is expected to be that of the C=C double bond. As this structure has the further advantage of being readily reduced, we chose it as the first group for our theoretical study. Compounds possessing various functional groups, such as NH_2, OC_2H_5, COOH, were hydrogenated in order to study the influence of the said groups on the velocity of hydrogenation of the adjacent double bond. The experimental results are recorded in Fig. 1, where the volume of hydrogen taken up is plotted against time, k being given by the slope.

In all cases, the rate of reaction was proportional to the amount of catalyst used and of zero order with respect to substrate, within the usual limits. These statements were confirmed by systematic kinetic studies in which the amounts of catalyst and substrate were gradually and independently increased. These results are recorded in Figs. 2 and 3.

An attempt was made to correlate the k values for the hydrogenation of the propylene derivatives with Rh with some property of the adjacent functional groups. Although the electrolytic dissociation of the allyl derivatives is not recorded in the literature, we thought it justifiable to compare k with the dissociation constants of the analogous ethyl series. This justification is based on the fact that the diversity of values of the dissociation of the ethyl compounds—ethanol, ethylamine, acetic acid, etc.—is exclusively due to the functional group, since the remainder of the molecule is identical in all cases. If we have a series of compounds such as $CH_2=CH-CH_2OH$, $CH_2=CH-CH_2NH_2$, $CH_2=CH-COOH$, etc., the variations in dissociation will also be due solely to the functional group, and they must be in the same sequence and approximate relationship as those of CH_3-CH_2OH, $CH_3CH_2NH_2$, CH_3COOH, etc. In Table I the observed k values are recorded in decreasing order. A comparable gradation is noticed in the dissociation constants of the ethyl derivatives:

Acrolein shows a large deviation, but the low rate can be explained by the stabilizing conjugated system $H_2C=CH-HC=O$, which renders the hydrogenation of both C=C and C=O more difficult.
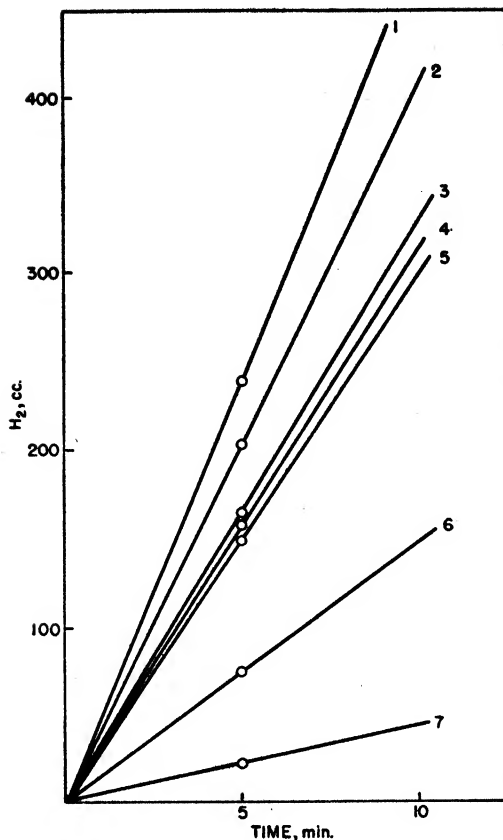
FIG. 1. Hydrogenation of propylene derivatives with Rh-PVA. 1, Allylamine; 2, Acrylic acid; 3, Acrylonitrile; 4, Allyl alcohol; 5, Allyl acetate; 6, Allyl ethyl ether; 7, Acrolein.

TABLE I

Substrate	$10^4 k$ mol. sec.$^{-1}$	Diss. constant of ethyl analogue[a]
Allylamine	3.12	4.6×10^{-4}
Acrylic acid	2.63	1.8×10^{-5}
Acrylonitrile	2.12	1.9×10^{-7}
Allyl alcohol	2.08	1.35×10^{-9}
Allyl acetate	1.94	1×10^{-9}
Allyl ethyl ether	0.97	4×10^{-18}
Acrolein	0.28	5.5×10^{-6}

[a] These values are taken from International Critical Tables.

It is observed that, in general, the greater the dissociation of the functional group the higher the rate of hydrogenation.

Two other significant series of organic compounds were hydrogenated to understand better the factors influencing reduction with Rh. These compounds were nitrobenzenes with various substituents in the *p*- and *m*-positions.
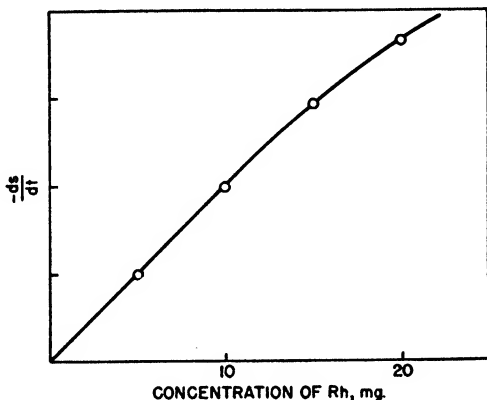
FIG. 2. Rate of reduction of 1 cc. nitrobenzene with increasing amounts of Rh. Ordinate units are arbitrary.
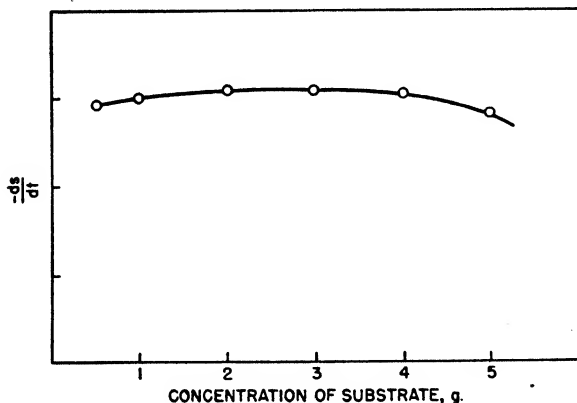
FIG. 3. Rate of reduction of varying amounts of nitrobenzene with 10 mg. Rh as Rh-PVA. Ordinate units are arbitrary.

Equimolecular amounts of substituted nitrobenzenes (equivalent to 1.19 g. $C_6H_5NO_2$) were reduced to the corresponding aniline with 10 mg. of Rh (as Rh-PVA) and 10 mg. of Pd (as Pd-PVA). The results for the *p*- and *m*-substituted compounds are represented in Figs. 4 and 5, respectively:
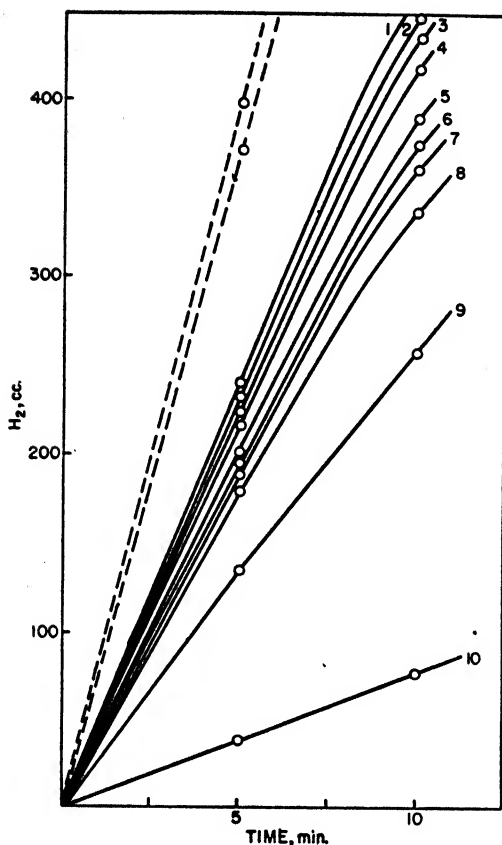
FIG. 4. Reduction of p-substituted nitrobenzene with Rh-PVA and Pd-PVA. Pd curves are indicated by dotted lines. 1, p-CN; 2, p-CHO; 3, p-NO$_2$; 4, p-COOH; 5, p-I; 6, p-Cl; 7, p-Br; 8, nitrobenzene; 9, p-OCH$_3$; 10, p-NH$_2$.

The divergence between Rh and Pd is most remarkable. While the rate of reduction with Pd-PVA was not affected by any of the p-substituents (except for a small deviation in the cases of p-CN and p-CHO—both reducible themselves) the activity of Rh-PVA was highly influenced. With the m-substituents, palladium showed only slight variations.

Two factors could be considered responsible for the difference in rate of hydrogenation of the p-substituted nitrobenzenes in the case of Rh: (1) the polarity of the substituent, (2) its ability to effect electron shiftings. Of these two factors, the first cannot be the determining one, since groups with such different dipoles as p-NO$_2$ ($\mu = -3.93$) and p-COOH ($\mu = -0.8$) affected the rate to almost the same extent.
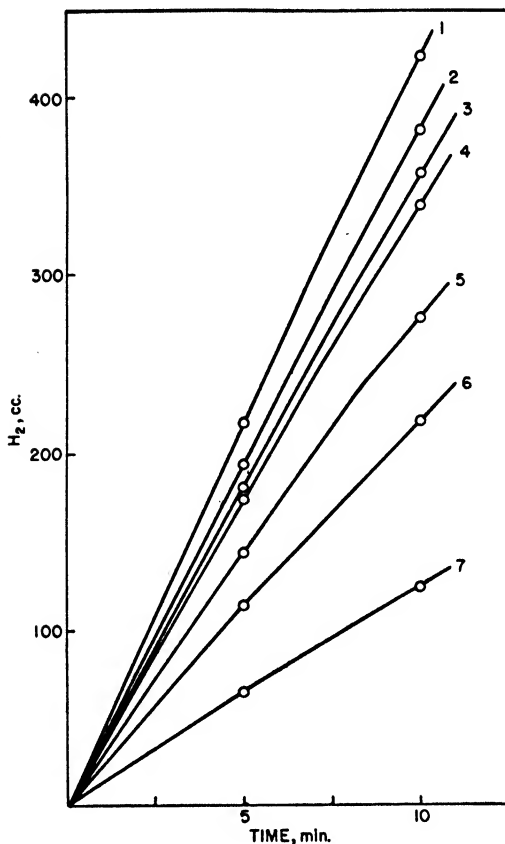
FIG. 5. Reduction of *m*-substituted nitrobenzene with Rh-PVA. 1, *m*-Cl and *m*-Br; 2, *m*-CHO; 3, nitrobenzene; 4, *m*-OH; 5, *m*-OCH₃; 6, *m*-COOH; 7, *m*-NH₂.

The second factor mentioned, *i.e.*, the electron-shifting capacity of the substituent, seems to be the decisive factor. There is a linear relationship between the log of the rate of the reaction of substituted aromatic compounds and a value σ characteristic for each substituent (σ = substituent constant). This value is chiefly dependent upon the electron-shifting ability of the substituent. The following equation correlates these values:

$$\log k - \log k^0 = \rho\sigma,$$

where k is the velocity constant of reaction for substituted compound, k^0 is the velocity constant of reaction for the unsubstituted compound, and ρ is a reaction constant, characteristic for each type of reaction.

If these σ values of the group under consideration are compared with k, a close relationship is noticed. In Table II are recorded the σ and k values. Fig. 6 further shows the linear relationship between log k and σ.

TABLE II

Compound	$k \times 10^6$	σ[a]
p-NO$_2$C$_6$H$_4$CN	11.1	1.000
p-NO$_2$C$_6$H$_4$CHO	10.8	1.126
p-di NO$_2$C$_6$H$_4$	10.4	0.778
p-NO$_2$C$_6$H$_4$COOH	10.1	0.728
p-IC$_6$H$_4$NO$_2$	9.25	0.276
p-ClC$_6$H$_4$NO$_2$	9.02	0.218
p-BrC$_6$H$_4$NO$_2$	8.79	0.232
Nitrobenzene	8.33	0.000
p-OCH$_3$C$_6$H$_4$NO$_2$	6.25	−0.262
p-NH$_2$C$_6$H$_4$NO$_2$	1.85	−0.660

[a] σ values are taken from the compilation made by L. P. Hammett, Physical Organic Chemistry, p. 188. McGraw-Hill, New York, 1940.
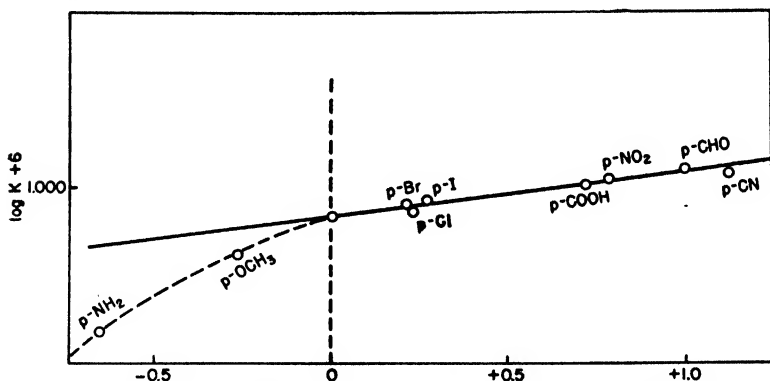
FIG. 6. Relationship between the log of rate of reduction of p-substituted nitrobenzenes and the substituent constant σ.

The discrepancies shown by the p-NH$_2$ and p-OCH$_3$ groups are explained if it is assumed that hydrogenation with Rh is affected more by polar fields than most other types of reactions for which the values of σ were calculated. Since, in the NH$_2$ group (with a high positive dipole), the inductive effect is in the same direction as the mesomeric effect, and, on the other hand, ρ for hydrogenation with R his positive, the value of k must be abnormally low.

This interference of forces is eliminated in the m-substituted compounds, since, in these, the mesomeric effect is practically negligible.

The results are represented in Fig. 5.

Here, the most favorable influence is exerted by the halogens, because

their great inductive polar force on the adjacent carbon atom is not counteracted by their heavy electronic density which renders them electron-repelling when in p- or o-position. Likewise, the amino group does not retard the reduction of the NO_2 group as much because only the inductive effect is of significance. How these forces retard or favor reduction of the NO_2 group will be explained in subsequent paragraphs.

In view of all these experimental results, we assume that hydrogenation with Rh involves ionization of hydrogen. The Rh atom has one electron in the outermost orbit, enabling hydrogen to form the unstable hydride $Rh:H$; this is confirmed by the fact that 100% of the hydrogen adsorbed by Rh is chemically bound (12). The $C\!=\!C$ bond, especially under the influence of polar fields, tends to assume the following electronic configuration:

$$-\overset{}{\underset{+}{C}} : \overset{..}{\underset{-}{C}} -$$
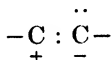
which attaches itself to the hydride because of the strong nucleophilic tendency of the $\overset{..}{C}{}^-$. Thus, the formation of an unstable intermediate complex can be conceived:

$$\begin{array}{cc} \text{Rh} & \text{Rh} \\ \overset{..}{H} & \overset{...}{H} \\ \searrow & \swarrow \\ -\underset{+}{C} : & \underset{-}{C} - \end{array}$$
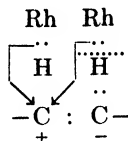
Another hydride molecule supplies the $\overset{..-}{H}$, but the attack seems to be originated by the H^+.

This also applies to the $-C\!=\!O$ group; but in this case oxygen is the negative member of the dipole $\overset{+}{C}:\overset{..-}{O}:. :\overset{..-}{O}:$ is stable and less nucleophilic than $\overset{..}{C}{}^{..}$, and, since the attack must start on this side (the negative side), a very slow reaction is to be expected. This concept agrees perfectly with the difficult reduction of C_6H_5CHO with Rh-PVA (see Table III).

The reduction of $-C\!\equiv\!N$ to $-CH_2NH_2$ is more complex, since two steps are involved:

$$-C\!\equiv\!N \overset{1}{\rightarrow} -CH\!=\!NH \overset{2}{\rightarrow} -CH_2NH_2$$

The observations regarding the polarization of the $C\!=\!C$ are still truer in the case of the triple bond $-C\!\equiv\!N$, and, as expected, Rh is a fair catalyst for the first step. But the second step involves disadvantages similar to those mentioned for the $-C\!=\!O$, although to a lesser degree, as nitrogen is less electronegative than oxygen. Palladium, however,

TABLE III

Rate of Hydrogenation of Various Groups with Rh and Pd

Substrate	Amount	k Rh	k Pd
	g.		
Nitrobenzene	1.2	1.38×10^{-5}	1.62×10^{-5}
Maleic acid	3.4	1.15×10^{-5}	4.60×10^{-6}
Benzaldehyde	3.1	1.18×10^{-6}	5.90×10^{-6}
Benzonitrile	1.6	9.72×10^{-7}	No reduction

which does not seem to act through an ionic mechanism, catalyzes this second step well, as confirmed experimentally by hydrogenation of the aldimine prepared by Steven's method. Hence, a mixture of Rh and Pd should be ideal for complete reduction of the nitrile to the amine. This was confirmed experimentally.

Reduction of the NO_2 group takes place in several steps: $NO_2 \xrightarrow{1} NO \xrightarrow{2} NHOH \xrightarrow{3} NH_2$. Step (1) is essentially an electrophilic attack on oxygen:

$$
\begin{array}{c}
O \\
:: \\
-N \\
\overset{+}{}\diagdown \\
OH^- \diagup \quad :O:H^+ \\
\underset{-..}{} \\
H^+
\end{array}
$$
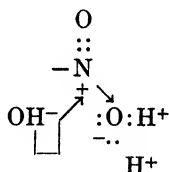
The semipolar $N^+ \rightarrow O^-$ bond is necessarily weakened by the presence of OH^-, thus accounting for the rate increase in alkaline medium as shown in Fig. 7.

In contrast to this behavior, the hydrogenation of the double bond is favored by acid medium (see Fig. 8) since the concentration of the H^+, necessary to start the attack, is thus increased. Step (2) in the reduction of the NO_2 group is similar to the reduction of the $C=O$, and consequently is expected to proceed slowly with Rh. Such is the case. The rate of the reaction $NO \rightarrow [NHOH] \rightarrow NH_2$ is about 3 times slower with Rh-PVA than with Pd-PVA, despite the fact that, for the reaction $NHOH \rightarrow NH_2$, Rh was found to be 3 times more active than Pd. Step (3) may start with an electrophilic attack on nitrogen:

$$
\begin{array}{c}
Rh \\
.. \\
H \\
.. \\
-N:OH \\
.. \\
H
\end{array}
$$
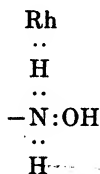
This agrees with the increased rate of this reaction when catalyzed by Rh.

Also in support of this hypothesis are the results of the hydrogenation of substituted nitrobenzenes. It was seen that the electron-attracting groups (such as NO_2, CHO, COOH) facilitated the reduction of the NO_2 group when in p-position. The electron-repelling groups (NH_2, OCH_3) produced the opposite effect.
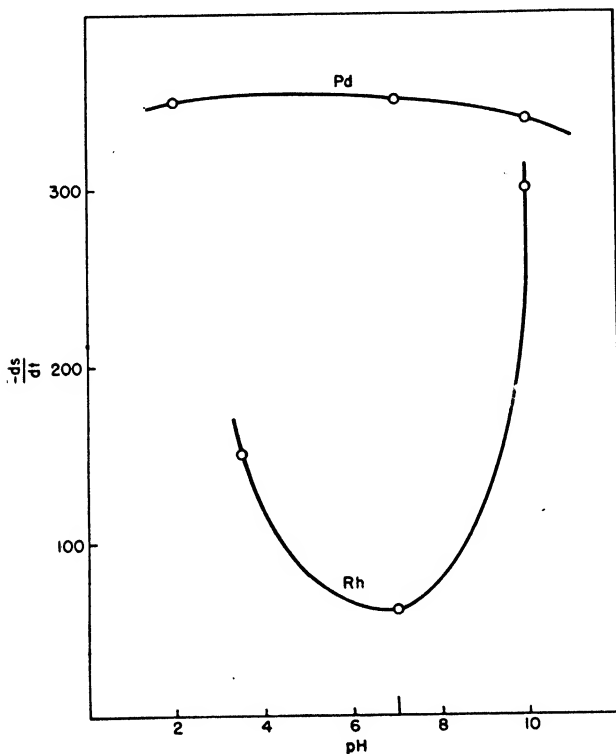
Fig. 7. Rate of reduction of nitrobenzene with Rh-PVA and Pd-PVA at different pH's. Ordinate units are arbitrary.

Probably the 2nd step (the rate-determining step) (9b) $NO \rightarrow NHOH$ is the one affected by the p-substituent. Since hydrogenation with Rh requires the structure

$$-\overset{+}{N}\overset{..-}{:}\overset{..}{O}:$$

a heavy electron density near the nitrogen atom should be prejudicia

as in the case of *p*-aminonitrobenzene

$$:O:-$$
$$:N^+$$
$$:NH_2$$
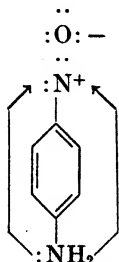
whereas a low density should increase the polarization of the NO group.

In the case of the *m*-substituents, only the inductive effect is significant. Thus, chlorine tends to induce a strong dipole $\overset{+}{C}\!-\!\overset{-}{Cl}$ pulling
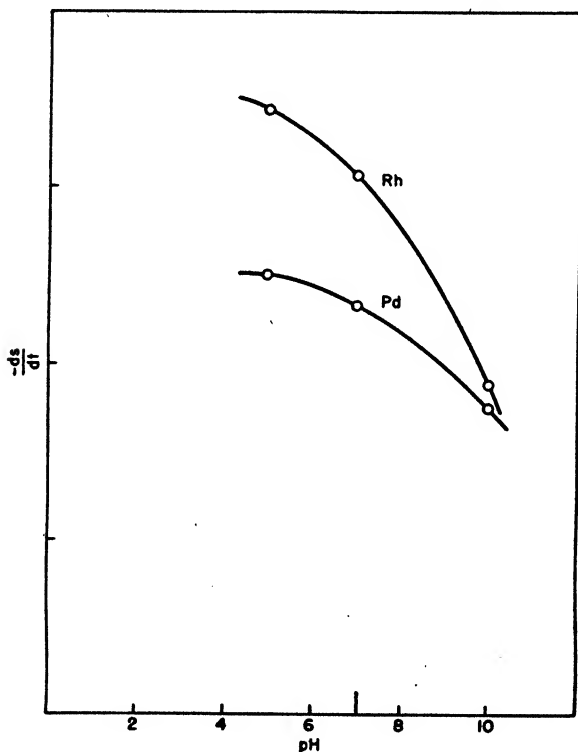
FIG. 8. Rate of hydrogenation of 2-pentene with Rh-PVA and Pd-PVA at different pH's. Ordinate units are arbitrary.

electrons toward the carbon atom and consequently intensifying the dipole of the nitroso group.

Since the facts supporting the 'ionization' theory are absent in hydrogenation with *palladium*, it might be possible to conclude that the latter is not accomplished by means of an ionic mechanism. Rather, the available evidence would point to a mechanism in which Pd converts molecular hydrogen to the atomic form.

IV. Summary

1. A method is given for the preparation of a stable, highly active rhodium-polyvinyl alcohol catalyst.

2. The application of this catalyst to the hydrogenation of organic substrates containing the carbon-carbon double bond or the nitro, carbonyl, and nitrile groups, is described.

3. Rhodium and palladium are compared with regard to their behavior in the hydrogenation of the above-mentioned substrates and their sensitivity to changes in pH.

4. A systematic kinetic study is instituted on the reduction of a series of propylene derivatives and of *p*- and *m*-substituted nitrobenzenes.

5. The experimental results are interpreted electronically and the hypothesis is proposed that rhodium acts through the formation of an intermediate complex involving "ionic" hydrogen.

References

1. Brønsted, J. N., and Pedersen, K., *Z. physik. Chem.* **108**, 185 (1924).
   Brønsted, J. N., and Wynne-Jones, W. F. K., *Trans. Faraday Soc.* **25**, 59 (1929).
   Brønsted, J. N., Nicholson, A. L., and Delbanco, A., *Z. physik. Chem.* **169A**, 379 (1934).
2. Moelwyn-Hughes, E. A., *J. Chem. Soc.* **1938**, 779.
3. Wieland, H., and Richter, D., *Ann.* **486**, 226 (1931).
4. Wagner, C., and Hauffe, K., *Z. Elektrochem.* **45**, 409 (1939).
5. Phillips, F. C., *Am. Chem. J.* **16**, 163, 255 (1894).
6. Emmett, P. H., *Record Chem. Progress (Kresge-Hooker Sci. Lib.)* **7**, 41 (1946).
7. Rampino, L. D., Kavanagh, K. E., and Nord, F. F., *Proc. Natl. Acad. Sci. U. S.* **29**, 246 (1943).
8. Rampino, L. D., and Nord, F. F., *J. Am. Chem. Soc.* **63**, 2745 (1941).
   Kavanagh, K. E., and Nord, F. F., *ibid.* **65**, 2121 (1943).
9a. Rampino, L. D., and Nord, F. F., *ibid.* **63**, 3268 (1941).
 b. Nord, F. F., *Ber.* **52**, 1705 (1919).
10. Hernandez, L., and Nord, F. F., *Experientia* **3**, 489 (1947).
11. Franck, H. H., *Chem. Ztg.* **37**, 958 (1913).
12. Mueller, E., and Schwabe, K., *Z. physik. Chem.* **154**, 143 (1930).

THE INFLUENCE OF SULFUR ON CATALYTIC
DEHYDROGENATIONS WITH RHODIUM

L. Hernandez and F. F. Nord

From the Department of Organic Chemistry,[1] Fordham University, New York 58, N. Y.

Received May 25, 1948

INTRODUCTION

According to the current concept of catalysis, whereby a catalyst should promote reverse as well as direct reaction, we thought it appropriate to undertake a kinetic study of catalytic dehydrogenation with Rh dispersed in polyvinyl alcohol in order to better understand the concepts reported (1) on the mechanism of catalytic hydrogenation with Rh in a microheterogeneous system.

Rhodium black has been utilized in the catalytic decomposition of formic acid (2) at the temperature of boiling water, and similar experiments have been carried out with the help of other noble metal catalysts (3).

Under more drastic conditions, *i.e.*, at higher temperatures ranging from 200° to 800°C. in the gas phase, it has been possible to dehydrogenate *n*-propyl and isopropyl alcohol, for instance, with Re and Cu (4), and alloys of the platinum metals.

Insofar as the dehydrogenation of formic acid: $(HCOOH \rightarrow CO_2 + H_2)$ with rhodium is concerned, it has been reported (2) that the catalytic activity of this metal is negligible unless it is 'activated' with oxygen, or, still better, with sulfur. We have verified this latter statement in the case of the Rh-PVA catalyst also, and by means of a quantitative systematic study we have tried to approach the problem of the mechanism of dehydrogenation and, in particular, the puzzling beneficial influence of sulfur.

Moreover, due to the fine state of subdivision of our colloidal Rh catalyst we succeeded in dehydrogenating isopropyl alcohol under the much milder conditions of the water bath. The rate of dehydrogenation is, however, so slow that quantitative measurements were not feasible, but the nitroprusside test for acetone (5) was given after 5 or 10 mins. This decomposition did not take place in the absence of sulfur, nor when catalyzed by palladium with or without sulfur.

For a quantitative kinetic study formic acid was invariably used as the substrate.

A given amount of the Rh-PVA catalyst, prepared according to the description given in detail elsewhere (1), is brought to constant temperature in the thermostat at 95°C. Formic acid is added from a small separatory funnel and the volume of gas evolved is read in a burette from which saturated KCl solution is being displaced into a leveling bulb.

For comparative purposes, experiments were always conducted separately with Rh-PVA and Pd-PVA prepared according to previous instructions (6). Sulfur was introduced in the elementary form dissolved in ethyl alcohol in which it is soluble to the extent of 0.50–0.66 g./l. at 25°C.

The rate of decomposition of formic acid increased with increasing amounts of sulfur up to a maximum attained when the amount of sulfur was 5 mg. Five mg. of Rh in 10 cc. of 2% PVA were invariably employed. In accordance with the difference in the behavior of Rh and Pd reported earlier (1), it was also found here that the decomposition of formic acid by Pd, far from being favored by sulfur, is thoroughly inhibited by its presence.

II. Experimental

Dehydrogenation of Isopropyl Alcohol

To 10 cc. of an alkaline aqueous solution of 2% polyvinyl alcohol, 0.5 cc. of a solution of $RhCl_3.3H_2O$ containing 10 mg. Rh metal/cc. is added. Two cc. of a saturated aqueous H_2S solution are then added and the mixture placed on the water bath for 10 mins., when the dispersion becomes brown. One cc. of isopropyl alcohol is then added, the whole mixture heated at 95°C., and the vapors collected in a test tube. After about 10 mins., the Na nitroprusside test for acetone is positive on the liquid condensate.

Decomposition of Formic Acid

The Rh-PVA was prepared as mentioned previously. For the introduction of sulfur, 500 mg. of elementary sulfur are dissolved in 1 l. of 95% ethanol. Ten ml. of this solution will contain 5 mg. sulfur. Ten ml. of Rh-PVA containing 5 mg. metallic Rh are placed in each of 7 small flasks with a ground glass neck. 0, 1, 2, 4, 5, 10, and 15 ml. of the alcoholic sulfur solution are added to each flask and then pure alcohol to equalize the volumes in the 7 flasks. These are then placed on the water bath for 15 minutes and allowed to cool. Each flask is then closed with a ground glass device provided with a small separatory funnel and an outlet tube. The latter is connected with a small oblique condenser so that the ethanol vapors may return to the flask. The other end of the condenser is attached to the upper end of a burette, the lower tip of which is connected to a glass bulb by rubber tubing. Both burette and bulb are filled

with a saturated solution of KCl. The flask is placed on the thermostat at 95°C. and the liquid begins to fall in the burette due to the pressure exerted inside the flask. By opening the stopcock in the separatory funnel the liquid will rise again to the zero mark of the burette. When the inside temperature is constant, so that no more air is displaced, 1 ml. of formic acid is poured into the flask from the separatory funnel. The volume of gas evolved is measured from time to time after lowering the bulb so that the liquid in this and in the burette are at the same level.

III. DISCUSSION

The experimental results of the decomposition of formic acid by Rh-PVA at 95°C. in the absence and in the presence of increasing amounts of sulfur are represented in Fig. I.
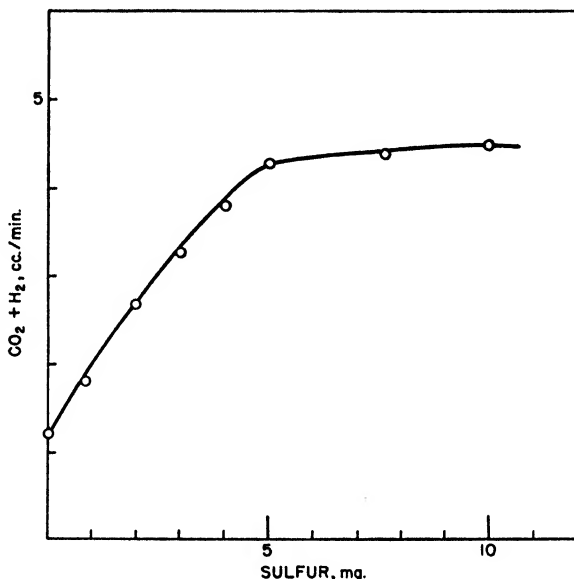
FIG. 1. Relationship between the rate of dehydrogenation of formic acid with Rh-PVA and the amount of sulfur.

As shown in the graph, the rate of decomposition increases with the quantity of sulfur present. But the sudden bend of the curve at a maximum suggests that there is a stoichiometric relationship between rhodium and sulfur. Since this maximum occurs for 5 mg. Rh and 5 mg. S, the approximate value of this ratio should be $Rh/S = 1/3$ corresponding to the formula $Rh(SH)_3$ or $Rh_2S_3 \cdot 3H_2S$ which had the brown color described in the literature (7). This interpretation is supported by the observations of Maxted and Marsden (8), who found that the toxicity of H_2S, H_3P,

H₃As, H₃Sb, and H₃Bi is proportional to their equivalents and inde-
pendent of the atomic radii or other properties.

The concept of the formation of a true chemical combination between
Rh and S is confirmed by a study of the toxicity of sulfur in the catalytic
hydrogenation of maleic acid. A quantitative investigation showed that
there is also a relationship between the rate of reaction and the amount
of sulfur (Fig. 2).
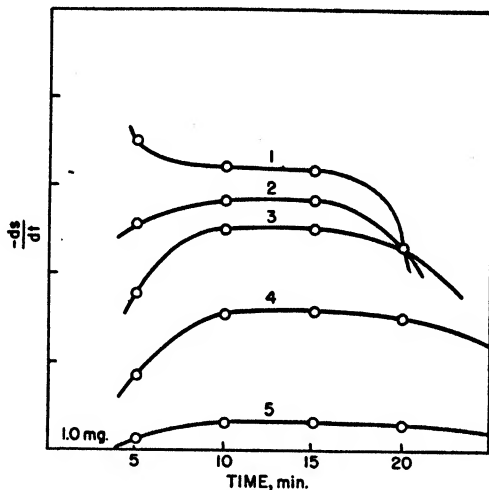
Fig. 2. Hydrogenation of maleic acid with Rh-PVA in the presence of elementary
sulfur. 1, no sulfur; 2, 0.250 mg. sulfur; 3, 0.500 mg. sulfur; 4, 0.750 mg. sulfur; 5, 1.000
mg. sulfur. 10 mg. Rh used in all cases. The units in the ordinates are arbitrary.

The amount of sulfur required to completely inhibit the reaction has
the ratio Rh/S = 8/3, but it is striking that, after a lapse of time, the
catalyst recovers part of its activity as shown by the curves. In the
compound Rh₂S₃, the S atoms have two free electron pairs. It is conceiv-
able, then, that Rh atoms are attached to them according to the following
scheme:

$$Rh \qquad Rh \qquad Rh$$

$$S::Rh:S:Rh::S$$

$$Rh \qquad Rh \qquad Rh$$
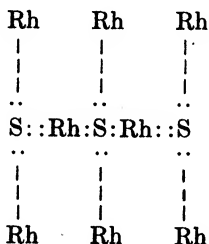
giving the 8:3 ratio.

The secondary Rh....S linkages (represented by dotted lines) would be easily broken in the presence of hydrogen, thus accounting for the rise in rate after a period of time. This interpretation through secondary valences is possible since it was proven (9) that sulfur compounds are toxic as long as there are unshared pairs in the sulfur atom (elementary sulfur, sulfides, and sulfites, but not sulfates).

All the above considerations prompt us to assign a 2-fold role to sulfur: (1) Sulfur acts as a hydrogen acceptor; thus, the catalytic decomposition of HCOOH by S-Rh-PVA resembles the enzymatic dehydrogenation of isopropyl alcohol when conducted in the presence of sulfur (10).

We postulate the following sequence of reactions:

$$\text{(a) } 2RH + 3S \rightarrow Rh_2S_3$$
$$\text{(b) } Rh_2S_3 + 3S + 3HCOOH \rightarrow 2Rh(SH)_3 + CO_2$$
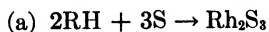
where $Rh(SH)_3$ or $Rh_2S_3.3H_2S$ is the unstable intermediate complex.

$$\text{(c) } Rh(SH)_3 \xrightarrow{95°} Rh_2S_3 + 3S + H_2$$
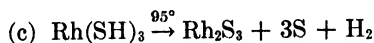
Rh_2S_3 and S are regenerated for further action on HCOOH. Since some H_2S is evolved during the reaction, some $Rh(SH)_3$ might decompose thus:

$$\text{(d) } Rh(SH)_3 \xrightarrow{95°} \tfrac{1}{2}Rh_2S_3 + 1\tfrac{1}{2}H_2S.$$
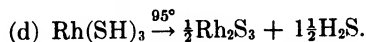
When all the sulfur is consumed as H_2S, the rate of decomposition of HCOOH falls to the low values obtained with Rh-PVA alone.

(2) Since Rh alone, without sulfur, catalyzes the decomposition of formic acid, although slowly, it is necessary to assume that at least some hydrogen is removed from HCOOH by direct attachment to the Rh surface. The electronic interpretation (1) of catalytic hydrogenation through an intermediate complex involving ionic hydrogen agrees with the formation of the following complex:
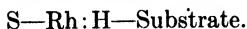
$$S—Rh:H—Substrate.$$

The density of negative charges afforded by sulfur to the Rh atom strengthens the Rh:H bond and consequently weakens the H-substrate linkage, thus facilitating *de*hydrogenation. In the light of this interpretation, the poisonous character of sulfur in catalytic *hydrogenation* is clearly understood, since, in the latter case, weakening of the Rh:H and strengthening of the H-substrate bond is required.

IV. SUMMARY

1. Rhodium dispersed in polyvinyl alcohol has the ability to dehydrogenate isopropyl alcohol and formic acid at moderately high temperature.

2. Elementary sulfur increases the dehydrogenating efficiency of Rh but not that of palladium.

3. A true chemical binding is postulated between rhodium and sulfur, forming a compound with the formula $Rh_2S_3 \cdot 3H_2S$ or $Rh(SH)_3$.

4. The favorable influence of sulfur on catalytic *dehydrogenation* with Rh-PVA is contrasted with its poisonous effect on catalytic *hydrogenation*.

5. Two roles are assigned to sulfur, the first being that of a hydrogen acceptor, and the second consisting in the strengthening of the Rh:H linkage.

REFERENCES

1. HERNANDEZ, L., AND NORD, F. F., *J. Colloid Sci.* **3**, 363 (1948).
2. BREDIG, G., AND BLACKADDER, TH., *Z. physik. Chem.* **81**, 385 (1913).
3. MUELLER, E., AND LOERPABEL, W., *Monatsh. 53/54*, 825 (1929).
4. PLATONOW, M. S., AND ANISSIMOV, S. B., *Ber.* **69**, 1050 (1936).
   COHN, G., AND HEDVALL, J. A., *J. Phys. Chem.* **46**, 844 (1942).
5. FEIGL, F., Laboratory Manual of Spot Tests, p. 179, Academic Press, Inc., New York.
6. RAMPINO, L. D., AND NORD, F. F., *J. Am. Chem. Soc.* **63**, 2745 (1941).
7. LEIDIÉ, E., *Compt. rend.* **106**, 1533 (1888).
8. MAXTED, E. B., AND MARSDEN, A., *J. Chem. Soc.* **1938**, 839.
9. MAXTED, E. B., AND MORRISH, R. W. D., *ibid.* **1940**, 252.
10. SCIARINI, L. J., AND NORD, F. F., *Arch. Biochem.* **3**, 261 (1943).

X-RAY INVESTIGATION OF THE STRUCTURE OF TRANSPARENT OIL-WATER DISPERSE SYSTEMS. I

J. H. Schulman

Department of Colloid Science

and

D. P. Riley

Department of Mineralogy and Petrology and Crystallographic Laboratory,
Cavendish Laboratory, University of Cambridge, England

I. Introduction

X-ray diffraction bands of aqueous soap solutions of concentrations varying between 5% and 25% have been measured by a number of authors (see (1) for references). They considered that the large dimensions (40–100 Å) given by the diffraction bands were those between the polar groups of layers of orientated soap molecules. These layers were close packed owing to the high concentration of orientated micelles consisting of approximately 80–180 vertically orientated soap molecules in the form of bimolecular leaflets with the polar groups pointing towards the water. The smaller X-ray spacings of *ca.* 4.5 Å were considered to relate to the distance between the neighboring molecules in the monolayers.

It was thought significant by Schulman and McRoberts (1) that these systems could absorb only a small quantity of a nonpolar oil with a consequent small increase of the large X-ray dimensions and sharpening of the X-ray band, whereas by the addition of a polar oil (*e.g.*, long chain alcohol), together with a nonpolar oil, to the aqueous soap solutions, the oil/water ratio could be varied within very wide limits and still give equilibrium conditions. These transparent oil/water disperse systems of comparatively low viscosity could be either nonconducting or conducting, depending on whether oil or water was the disperse phase. This was shown to be related to the constitution of the interfacial mixed monolayer and its wettability to either oil or water.

These facts suggested that the systems were obtained by the combined action of the polar and nonpolar oils. The swollen lamellar structure of the soap micelle is broken down by the penetration of the monolayer of soap molecules, by the polar oil and by the swelling of the bimolecular leaflets by the absorption of the nonpolar oil between the layers of the methyl groups. This results in a liquid or disordered system instead of an

ordered system such as a swollen crystallite, thus enabling droplets of spherical shape to be formed, consisting of water dispersed in oil if non-conducting, or oil dispersed in water if conducting. These systems were then considered to consist of uniform spheres, in closest packing or nearly so, each droplet being covered by a mixed monolayer of the polar oil molecule and the soap molecule.

If this concept is correct, low-angle X-ray diffraction bands should be given by such systems, and their spacings should be related to the mean distance between the centers of neighboring spheres. Knowing the ratio of the oil and water phases, the electrical conductivity of the system, and the interfacial area of the mixed monolayer, calculations can be made regarding the diameters of these spheres, the distance between them, and
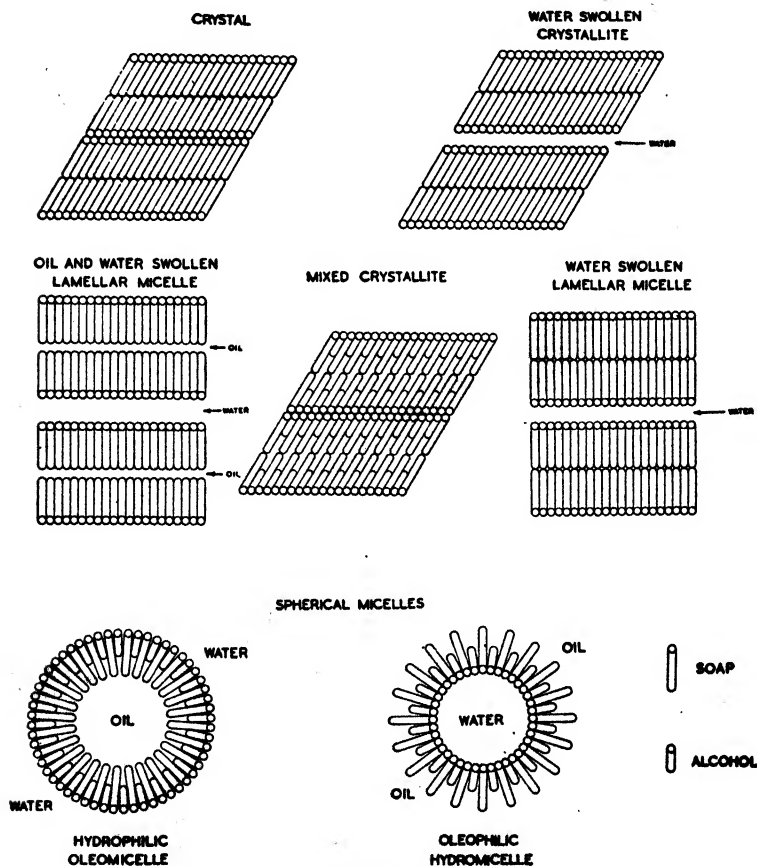
FIG. 1. Drawings illustrating formation of various types of micelle.

the nature of their packing from the geometry of the system. The work reported here uses the low-angle X-ray scattering technique as a means of testing the above concepts.

II. Structural Hypotheses

In Fig. 1 are portrayed the various possible forms of associations of soap molecules in combination with nonpolar oil, polar oil and water, compatible with the physicochemical and X-ray evidence.

The double molecular unit of potassium oleate is 48.5 Å long; consequently the molecules are arranged in the crystal in an inclined fashion.
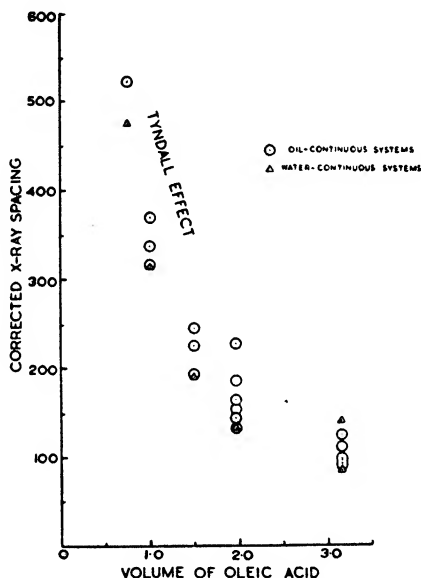
Fig. 2. Corrected X-ray spacings in Å plotted against volume of oleic acid to show general trend of results.

The vertical spacing of the double layer in the crystal lattice is known from X-ray photographs to be 38 Å (2), although evidence for various other forms has been given which suggests different angles for the tilt (40.8, 41.9, 44.5 Å) (2,3). Further, the lattice may be swollen with the water of crystallization contained in various solid soap phases (soap curds or neat soap, etc.). These latter systems dissolve or become transparent in water at a well defined temperature (Krafft point). It is presumed that the molecules in this system are vertically orientated, since the dimensions obtained are always greater than that of the double molecular unit. It is also considered that they are free to rotate about

their long axis, since the side spacing has increased from 4.2 Å in the crystal, to 4.5 Å in the lamellar micelle, corresponding to columnar hexagonal packing.

The long spacing obtained by the highest concentration of potassium oleate in water, in this work 38%, was 54 Å, and it is known from the results of other workers that this dimension can expand on dilution, in the case of sodium oleate, to values as great as 90 Å. Evidence for the existence of a dimension due to an unchanging vertically orientated bimolecular leaflet during this dilution, has been given by Harkins (4). The fact that these lamellar micelle units are not liquid in all directions is shown by the manner in which they swell only within certain limits with nonpolar oils, and by the observation that this swelling increases on raising the temperature above 50°C. (5). These systems become saturated with nonpolar oil, giving an increase in the long spacing with no change in the side spacing, at a concentration equal to 50% by weight of the soap. Thus, a 16% soap solution will take up a maximum of 7% nonpolar oil. It has been shown in the present work that, if a polar oil, such as amyl alcohol or p-methylcyclohexanol, be added to the lamellar micelle unit giving a long spacing of 54 Å, the unit is shrunk, possibly by ejection of water between the polar ends of the leaflet, to an inclined mixed crystallite giving a long spacing of 42 Å. It is significant that the addition of the polar oil shrinks the main lattice dimension by ejection of the water. The reverse is observed by the addition of a nonpolar oil. The main lattice dimension in this case increases by approximately 2.5 times the actual increase to be expected from the volume of oil divided by the area of the interfacial monolayer (6). This has been previously thought to be due to a change in tilt of the molecules in the laminar lattice. This is difficult to imagine as they are considered to be vertically aligned under these conditions. These systems are still transparent greases rather similar to swollen concentrated soap micelle systems with water alone.

There is considerable evidence from the monolayer penetration work of Schulman and collaborators (see 7) on the Langmuir trough, and recently from the X-ray work of Harkins and his colleagues (8), that the polar oils will penetrate into the monolayer forming the leaflets to form equimolecular mixed films, and do not penetrate between the monolayers, as with the nonpolar oils.

It has been shown by Schulman and McRoberts (1) that the combination of the polar oil and the soap solution enables the nonpolar oil to be absorbed within very wide limits to give nonconducting or conducting systems, which are in equilibrium and transparent. This suggested that in the nonconducting system the water swells the lamellar leaflet, which now being liquid in all directions and being more wettable by oil than by water, can enclose the water in the form of a sphere with the nonpolar

portions of the mixed monolayer (see Fig. 1) orientated toward the non-polar oil. This is now the continuous phase between the water droplets (spheres) surrounded by the mixed monolayer. Likewise, in the conducting systems, the nonpolar oil swells the mixed monolayer which is more wettable by water than by oil, to enclose the nonpolar oil, leaving the molecules in the monolayer to orientate their polar groups on the surface of the oil droplet toward the continuous water phase (Fig. 1). The oil droplets, since they can be of molecular dimensions, have been named hydrophilic oleomicelles, and the water droplets, oleophilic hydromicelles. A similar mechanism could give rise to the formation of cylindrically shaped micelles of both types. It is significant that the soap-water and soap-water-alcohol solutions are strongly streaming-birefringent and viscous, whereas the transparent systems containing the soap-water-alcohol-oil are thin fluids of low viscosity and show no signs of streaming-birefringence when strongly agitated or flowed between glass slides. This suggests that, where cylinders exist, they must be of very short length.

III. Physicochemical Preparation

Transparent oil/water systems with varying concentrations of soap and alcohol, but with constant and equal amounts of oil and water, were made as described by Schulman and McRoberts (1). Two systems were chosen for detailed investigation, one of which gave the electrical conductivity of the oil phase, and the other of which gave the electrical conductivity of the aqueous phase.

The first system consisted of benzene, water, potassium oleate, and p-methylcyclohexanol, which was benzene continuous; the second consisted of C_{18} paraffin (Thin Nujol), water, potassium oleate, and p-methylcyclohexanol, which was water continuous (see Table I).

Systems were further chosen in which the relative volume of the continuous phase was increased. Thus, in cases where, owing to the high concentration of the soap-alcohol complex, a possible distorted close packing of the spherical droplets of the dispersed phase would take place, (see Section VI) an expansion of the disperse phase would allow room for a separation of the droplets.

The conductivities of the benzene, the alcohol solution, and the aqueous soap solutions, were measured independently with an Avometer, and these values were compared with the conductivity of a given transparent oil/water system to determine the constitution of the disperse phase. As is indicated in Table I, certain oil-continuous systems containing much soap possessed an intermediate conductivity and are classed as anomalous.

Potassium oleate was chosen as the soap, since it possesses several advantages. First, the potassium ion has a comparatively high X-ray scattering power, and secondly, the potassium soap is well above the

TABLE I

Spec-imen	Volume (cc.) of									Extra salts
	Oleic acid	2 N KOH	Water	Ben-zene	Oc-tane C_8	Thin nujol C_{18}	p-Methyl cyclo-hexanol	1-Hexa-nol	1-Pent-anol	
1				5.00				4.25		
2					4.80				3.15	
3[a]	3.16	5.00		5.00			6.32			
4[a]				5.00			3.70			
5[a]					5.00		6.55			
6[a]					5.00		4.63			
7[a]	2.46	3.90	1.10		5.00		3.80			
8					5.00		2.55			
9				5.00			2.22			
10				5.00			2.82			
11	1.97	3.54	1.46	5.00			2.00			0.25 g. K_2SO_4
12				10.00			3.15			
13				15.00			2.55			0.25 g. K_2SO_4
14[a]				1.67			2.47			0.25 g. K_2SO_4
15				5.00			2.15			0.25 g. CsI
16					5.00		1.65			
17	1.50	2.37	2.63	5.00			2.00			
18				5.00			2.33			
19					5.00		1.38			
20	1.00	1.58	3.42	5.00			1.80			
21				5.00			1.85			
22	0.75	1.18	3.82	5.00			1.68			
23				5.00					3.85	
24						5.00		7.50		
25	3.16	5.00				5.00	5.07			
26			3.80			5.00	4.82			
27	1.97	3.54	1.46			5.00	3.28			
28	1.50	2.37	2.63			5.00	2.77			
29	1.00	1.58	3.42			5.00	1.80			
30	0.75	1.18	3.82			5.00	2.08			

(Left margin group labels: "Oil continuous" spans specimens 1–22; "Water continuous" spans specimens 23–30.)

[a] Anomalous, slightly conducting.

Krafft point at room temperature. This enables solutions of the soap to be made at concentrations considerably higher than with the sodium soaps. In this work results were obtained with 40% potassium oleate as solutions or as clear aqueous dispersions. Redistilled colorless oleic acid was used, to which was added the correct quantity of KOH (in 5 cc. of solution) necessary to neutralize the acid. To the 5 cc. of water and potassium oleate in appropriate concentration was added 5 cc. (usually) of the non-polar oil [benzene, C_8 paraffin, C_{18} paraffin (Thin Nujol)], and the whole titrated to transparency by the addition of the polar oil (amyl alcohol, hexyl alcohol or p-methylcyclohexanol) under vigorous stirring. p-Methylcyclohexanol gave stable systems with the soap in much lower concentrations than could be obtained with the other alcohols. It has not thus far been found possible to make transparent oil-water dispersions with the chlorinated hydrocarbons, using them either as the polar oil in the presence of benzene or as the nonpolar oil in the presence of alcohols.

The composition of the systems studied is given in detail in Table I.

IV. X-Ray Photography

The X-ray photographs were taken with $CuK\alpha$ radiation (nickel-filtered) of wavelength $\lambda = 1.54$ Å. The specimen-to-film distance for the high spacings was 50 cm. in most cases, although 30 cm. and 40 cm. were used at the beginning of the work. All photographs were taken *in vacuo* to eliminate air-scattering and exposures of *ca.* 24 hrs. were necessary with the gas-tube used. A few photographs were also taken with crystal-reflected monochromatic X-rays, but the exposure times were too lengthy for an initial survey.

The essential feature of the instrument was that the two final slits defining the X-ray beam could be adjusted reproducibly with micrometer precision. Similarly, the lateral movements of the specimen-holder and of the film-holder were precisely controllable. To avoid any trace of "parasite" scattering, the final slit was faced with carefully selected cleavage slips of calcite, and its adjustment needed to be performed with great delicacy. A nickel backstop was used of thickness sufficient to absorb most, but not all, of the energy in the direct beam.

The liquid specimens were enclosed in small vacuum-tight Hysil glass tubes, 1 mm. in diameter and 0.02–0.03 mm. wall thickness. The sealing of these tubes was done in an oxygen-gas flame in such manner as not to affect the liquid contents.

The low spacing photographs were taken at 4, 5, and 6 cm. using a small cell made of Tufnell with 2 beryllium plates 1 mm. apart. Baked shellac was used as the adhesive.

TABLE II

Oil-Continuous Systems

Specimen	Volume of oleic acid (cc.)	Phase ratio φ	Calculated spacings (Å)				Observed X-ray spacings (Å)			Remarks
			Spheres (diameters and gap)	Cylinders (diameters)	Lamellae Unswollen by oil	Lamellae Completely swollen by oil	d (Bragg)	d (Corrected)	Probable error in d (corrected)	
(1)	(2)	(3)	(4)	(5)	(6)	(7)	(8)	(9)	(10)	
1	3.16	1.60	(−1)	96	73	106	80	98	± 3	
2		1.38	(−2)				78	96	± 3	Broad band
3ᵃ		2.01	120 (1)				73	90	± 4	Outer band
4ᵃ		1.48	(−2)				90	111	±12	
5ᵃ		2.04	(2)				84	103	± 5	Broad band
6ᵃ		1.67	(−1)				75	92	± 6	
							102	125	±12	
7ᵃ	2.46	1.57	141 (2)	110	80	123				Blank photograph
8	1.97	1.35	(6)	126	88	141	108	133	± 5	
9		1.28	(5)			(182)	125	154	± 7	
10		1.40	(6)			(216)	117	144	± 5	
11		1.24	164 (4)				133	164	± 5	
12		2.47	(20)				151	186	± 5	
13		3.35	(40)				185	228	±10	
14ᵃ		0.67	(−4)							
15		1.27	(5)				118	145	± 7	Very broad band

TABLE II—*Continued*

Specimen	Volume of oleic acid (cc.)	Phase ratio g	Calculated spacings (Å)					Observed X-ray spacings (Å)		Probable error in d (corrected)	Remarks
			Spheres (diameters and gap)	Cylinders (diameters)	Lamellae		d (Bragg)	d (Corrected)		
					Unswollen by oil	Completely swollen by oil				
(1)	(2)	(3)	(4)	(5)	(6)	(7)	(8)	(9)	(10)	
16	1.50	1.21	201 (7)	148	100	171	157	193	± 4	
17		1.28	(9)				184	226	± 5	
18		1.34	(10)				200	246	±12	
19	1.00	1.19	280 (19)	204	126	235	257	316	± 5	Water separated out
20		(1.28)	(23)				275	338	±12	
21		1.29	(23)				300	370	±50	
22	0.75	1.28	363 (38)	258	154	300	425	523	±50	

[a] Anomalous systems.

Notes

Column 4 gives the diameter of spheres with the values of the gap in brackets. The two values should be added together to compare with column 9.

Column 6 gives the calculated spacings for lamellae swollen by water only.

Column 7 gives the calculated spacings for lamellae completely swollen by water and oil. 7 cc. oil has been used except for specimens 12 and 13, which contain more; the spacings for these two specimens are given in brackets.

V. GENERAL RESUMÉ OF X-RAY RESULTS

The specimens in general gave well defined low-angle X-ray bands of moderate breadth (Plate I), but both the diffuseness and the intensity of the bands varied between wide limits. The water-continuous systems gave markedly weaker diffraction effects than the oil-continuous, although the scattering from two "anomalous" oil-continuous systems (6 and 7) was so weak as to be hardly measurable. The highest Bragg

8.
108 A.
(133)

14.

16.
157 A.
(193)

11.
133 A.
(164)

19.
257 A.
(316)

12.
151 A.
(186)

13.
185 A.
(228)

(a)   (b)
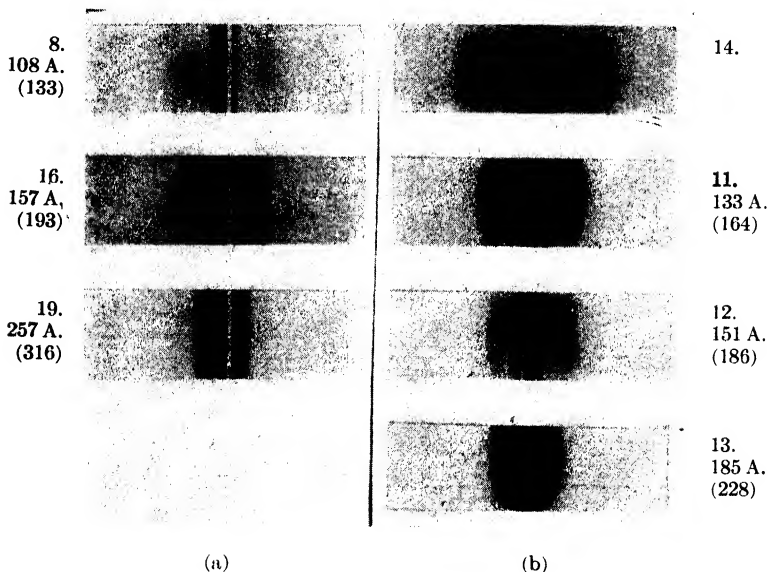
PLATE I.

X-ray photographs at 50 cm. of oil-continuous systems. Bragg spacings are given with corrected spacings in brackets. (a) Specimens 8, 16, 19 show increasing spacing with decreasing amount of soap. (b) Specimens 11, 12, 13 show increasing spacing with increasing amount of oil, while specimen 14 shows a very broad band due to anomalous "squashed" system.

spacing recorded was *ca.* 425 Å (specimen 22) corresponding to a diffraction angle (2θ) of only 12.5 minutes of arc.

Apart from the "reinforced" specimens, the best results were obtained with specimens 8, 16, and 19, which have the C_8 hydrocarbon as the continuous phase. In an attempt to increase the X-ray contrast, certain oil-continuous systems were made up with extra salts dissolved in the water phase. Cesium iodide (specimen 15) proved disappointing, but potassium sulphate (specimens 11, 13, 14) seemed quite efficacious as an enhancing agent.

It is obvious that, when dealing with such small angles of diffraction, it is impossible to achieve much accuracy in the measurement of the Bragg spacing, particularly in the case of broad bands. Estimated approximate limits of error are given in Tables II and III, and will be seen to be considerable for the highest spacings.

TABLE III
Water-Continuous Systems

Speci-men	Volume of oleic acid (cc.)	Phase ratio g	Calculated spacings (Å)				Observed X-ray spacings (Å)		Probable error in d (Corrected)
			Spheres (diam-eters and gap)	Cylinders (diam-eters)	Lamellae				
					Unswol-len by water	Com-pletely swollen by water	d (Bragg)	d (Cor-rected)	
(1)	(2)	(3)	(4)	(5)	(6)	(7)	(8)	(9)	(10)
23		0.64	142 (−7)	106	87	99	69	85	± 5
24		0.44	192 (−9)	140	103	115	70	86	± 4
25	3.16	0.58	160 (−7)	118	91	103		*a*	
26		1.03	158 (0)	118	91	112	115	141	± 6
27	1.97	0.67	206 (−4)	150	107	126	108	133	±12
28	1.50	0.70	252 (1)	180	122	147	154	190	± 7
29	1.00	0.78	332 (10)	234	149	187	255	314	±25
30	0.75	0.74	460 (18)	318	191	243	387	476	±50

a Very faint photograph.

Notes

Column 4 gives the diameter of spheres with value of gap in brackets. Add the two values of 28, 29, 30 to compare with column 9.

Column 6 gives the calculated spacings for lamellae swollen by oil only.

Column 7 refers to lamellae completely swollen by water and oil.

The diffuse nature of the bands suggests that we are dealing with a liquid-type of low-angle X-ray scattering (9). A rigorous interpretation of the effects can, therefore, only be achieved by a Fourier analysis which takes into account the whole course of the scattering curve over the appropriate region. This has not yet been attempted and, in any event, would require the use of crystal-reflected monochromatic radiation. For the purposes of this paper, it is probably sufficient to correct the mean

Bragg spacing of the bands by the factor suggested by Ehrenfest and Prins (10) in the case of close-packed liquids, which has reference to the first maximum in the $\frac{\sin x}{x}$ curve. All Bragg spacings $\left(d = \frac{\lambda}{2\sin\theta}\right)$ have, therefore, been multiplied by the factor 1.23, and the resulting spacing is considered to refer to the average center-to-center distance between neighboring diffracting units, e.g., spherical micelles. It is impossible to affirm at our present state of knowledge that this factor applies over the whole range of spacings and for all the systems studied, and this uncertainty should be borne in mind when discussing the results in detail. Nevertheless, as will be seen later, the general trend of results (see Fig. 2) provides convincing evidence for the existence of spherical micelles in many of the systems.

It is essential to the present theory that mixed monolayers can be formed of equimolecular mixtures of soap and alcohol and the following experiments were done in an attempt to throw light on this point. X-ray photographs were taken, under identical conditions, of

(a) a concentrated solution of potassium oleate (gel) (3.16 cc. oleic acid, 5 cc. 2 N KOH),

(b) a mixture of potassium oleate and p-methylcyclohexanol (gel) (3.16 cc. oleic acid, 5 cc. 2 N KOH, 3.32 cc. p-methylcyclohexanol),

(c) pure p-methylcyclohexanol (liquid),

and the following Bragg spacings were measured: (a) 4.6, (b) 4.8, (c) 5.1 and 11.1 Å (two bands).

The 11 Å band given by pure p-methylcyclohexanol is of about the same strength as the 5 Å band. The fact that it is not observed in (b) indicates that, in this mixture, the alcohol is not present in the normal liquid state. Further, the 4.8 Å band in (b) is not noticeably broader than the equivalent bands in (a) and (c), which suggests that it is not simply the result of their superposition.

The hypothesis that in (b) the soap and alcohol form a mixed monolayer is also supported by a comparison of the high spacing given by this mixture with that given by the soap solution alone. For (a) a value of 54 Å was measured, corresponding to a water-swollen lamellar micelle (see Fig. 1), whereas in (b) the spacing had diminished to 42.5 Å. It is clear that the alcohol cannot be present between the soap layers as in oil-swollen lamellar micelles (nonpolar oil), and it seems probable that a mixed crystallite has been formed with layers inclined as in the more normal soap crystallites. Drawings to illustrate this argument are given in Fig. 1.

It has been considered that the single side-spacing of 4.5 Å given by soap solutions of concentration greater than 5% could provide a value

for the area per molecule on the assumption that the molecules are arranged on a two-dimensional hexagonal lattice. The value thus derived is 26 Å². The sodium or potassium soaps are above the Krafft point at room temperatures and their concentrated solutions can be considered to be in a liquid crystal state which would support the concept of hexagonal packing in the soap layers. If the layers in the mixture of potassium oleate and p-methylcyclohexanol consist of a lattice of a 1 : 1 complex, the molecular arrangement in the monolayer can no longer have hexagonal symmetry but probably is two-dimensionally tetragonal in nature. The derivation of the area per soap molecule from the side-spacing of 4.8 Å is open to question, but a possible approach is as follows. The side-spacing may be corrected by the liquid factor 1.23 to give a value of 5.9 Å between neighboring molecules in a square array, which corresponds to an area of 70 Å² per soap molecule. In any event, it is certain that the area per molecule is greater than the $2 \times 26 = 52$ Å² for the soap alone, and the true value probably lies between the two figures. From monolayer experiments, the area per soap molecule is at least 30 Å².

VI. Predicted Spacings for Different Structural Models

Spherical Micelles

In the following calculations we shall assume that the soap-alcohol monolayer is impenetrable by either water or nonpolar oil, and that the spherical micelles can be considered as having a solid shell of thickness equal to the length of a soap molecule. This length, l, is taken to be 25 Å.

The total area of the soap-alcohol monolayer is

$$\sigma = \frac{N_o\, W\, S}{M},$$

where W = weight of oleic acid,
M = molecular weight of oleic acid,
S = area per molecule of oleic acid,
N_o = Avogadro's number.

This expression may be reduced to

$$\sigma = 0.137 \times 10^8\, v,$$

where v = volume of oleic acid, assuming that all the oleic acid is in the monolayer and taking $S = 70$ Å².

The case of the oleophilic hydromicelles (see Fig. 1) is the simpler of the two to treat, as this surface area can be taken as equal to that of the water spheres, the surface of contact C_1 (Fig. 3) obviously passing through the inward-pointing polar groups. If the system consists of
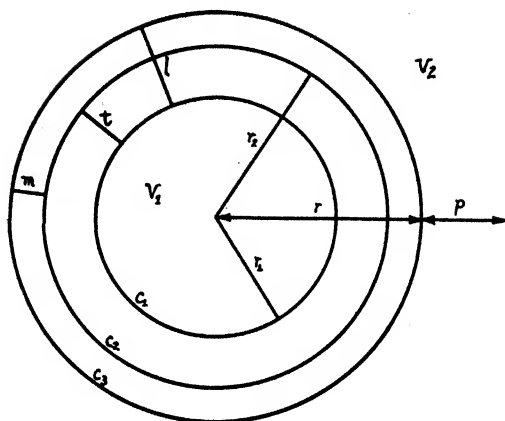
FIG. 3. Schematic picture of spherical or cylindrical micelle. l and m represent lengths of soap and alcohol molecules, respectively. v_1 = volume of intramicellar liquid; v_2 = volume of intermicellar liquid; p represents gap between spheres.

spherical micelles of equal size, the radius r_1 of the water spheres (Fig. 3) is obviously

$$r_1 = \frac{3\ V_w}{\sigma} = \frac{3\ V_w}{0.137\ v}\ \text{Å}, \tag{1}$$

where V_w = volume of water, and the overall radius of the micelle

$$r = r_1 + l. \tag{2}$$

For a given volume of water a straight line should, therefore, be obtained by plotting diameter against the reciprocal of the volume of oleic acid. This, however, assumes that the whole of the oleic acid is available for making the interface. It is more probable that there is an equilibrium between the soap molecules in the monolayer and those dissolved in the water phase and this involves a modification in Eq. (1) of the following type:

$$r_1 = \frac{3\ V_w}{0.137\ (v - v_o)}\ \text{Å.}, \tag{3}$$

where v_o represents the volume of oleic acid not in the surface layer.

This volume of oleic acid in these systems may be taken as 1%, being the concentration of soap at which a marked change in density of the solution is observed, and below which no characteristic X-ray side-spacings are observed. With V_w = 5 cc., (3) thus becomes

$$r_1 = \frac{109.5}{v - 0.05}\ \text{Å.} \tag{4}$$

and a plot of diameter against the reciprocal of the volume of soap will show an upward curve (Fig. 7) which is more pronounced at the lower concentrations of soap. The theoretical values for sphere diameters in Table II were calculated from Eqs. (4) and (2) and are shown as the top curve in Fig. 7.

The surface of contact in the hydrophilic oleomicelles is no longer over the inner circumference C_1 of the soap-alcohol shell, and is consequently related to the volume of oil, V_o, in a less simple fashion than in the previous case. The surface of contact is presumably defined by the nonpolar ends of the alcohol molecules and is marked C_2 in Fig. 3. The explicit equation for r_1 in this case is

$$r_1^3 - Rr_1^2 - 2Rtr_1 - Rt^2 = 0, \qquad (5)$$

where t = the difference in length of soap and alcohol molecules and

$$R = \frac{3\ V_o}{\sigma} \qquad (6)$$

and, a good approximation,

$$r_1 \approx R - \frac{t}{2}. \qquad (7)$$

The values given in Table III were computed from this expression and the corrected form of Eq. (6) analogous to Eq. (3). t was taken as 15 for p-methylcyclohexanol, 16 for 1-hexanol, and 17.5 for 1-pentanol.

Cylindrical Micelles

It is easily shown that all the foregoing expressions except Eq. (5), apply to systems containing cylindrical micelles of equal diameter and height, if Eqs. (1) and (6) are rewritten as

$$r_1 = \frac{2V_w}{\sigma},$$
$$R = \frac{2V_o}{\sigma}. \qquad (8)$$

The cubic equation (5) becomes the quadratic equation

$$r_1^2 - Rr_1 - Rt = 0$$

but, here again, the approximation (7) may be used.

The values for cylindrical micelles given in Tables II and III were derived from Eq. (8) using the same constants and correction terms as for the spherical micelles.

Lamellar Micelles

Fig. 1 shows a schematic picture of an oil-and-water-swollen lamellar micelle. The identity period is

$$d = x + y + 2l,$$

where x and y represent the thicknesses of the water and oil layers, respectively. Rewriting in the usual terms gives

$$d = \frac{2V_w}{\sigma} + \frac{2V_o}{\sigma} + 2l, \qquad (9)$$

where V_w and V_o refer here to the volumes of water and oil actually between the layers, $i.e.$, intra- as opposed to intermicellar liquid. This expression, appropriately corrected, was used to derive the listed calculated spacings for two extreme cases: (a) with no "continuous phase" liquid between the layers (b) with the whole of the "continuous phase" liquid between the layers.
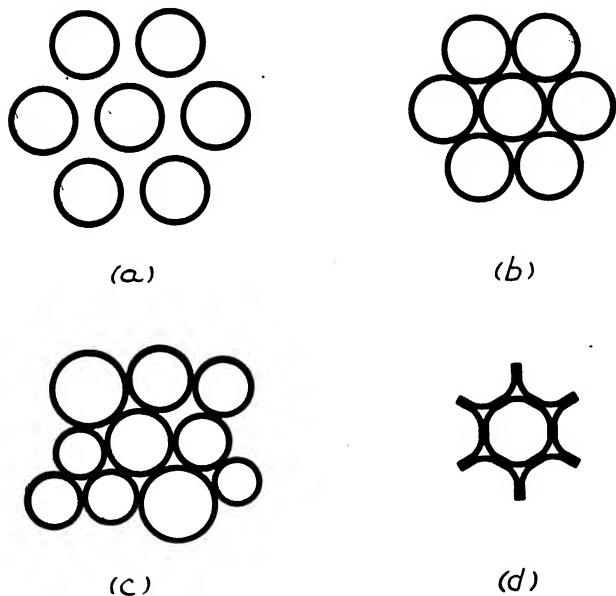
FIG. 4. Possible assemblies of spherical micelles. (a) separated; (b) in contact; (c) unequal spheres; (d) squashed.

Packing of Spherical Micelles and Phase Ratio

It is obvious that spheres of a given size will be more separated the greater the volume of the continuous intermicellar medium (Fig. 4). Similarly, for closest-packing of spheres, there will be a definite ratio between the volumes of intra- and intermicellar liquid. The phase ratio, g, is defined by

$$g = \frac{\text{volume of intermicellar liquid}}{\text{volume of intramicellar liquid}} = \frac{v_2}{v_1}. \qquad \text{(Fig. 3).}$$

The gap, p, between neighboring spheres depends both on this ratio and on the overall radius, r, of the spheres. If the spheres are assumed to be in regular 12-coordination, then the center-to-center distance, d, between neighboring micelles may be shown to be given by the expression

$$d^3 = \frac{4\sqrt{2}}{3}\,\pi\,\big[g(r-l)^3 + r^3\big], \tag{10}$$

where $d = 2r + p$. In Fig. 5 have been plotted curves relating the gap, p, to the diameter $2r$, for a series of values of the phase ratio, g. It will be noted that for any given value of g there is a critical diameter, $2r_o$, corresponding to closest-packing of spheres ($p = 0$). These critical diameters have been plotted as a function of g in Fig. 6, which corresponds to the critical contact line in Fig. 5. Negative values of p may either correspond to "squashing" of the spheres or to an impossible system.

It is easily shown that the constant term in front of the bracket in Eq. (10), which is 5.92 for 12-coordination, drops only slightly to 5.44 ($\sqrt{3}\pi$) for 8-coordination. The distance apart of spheres is thus not very sensitive to the exact nature of the coordination and the assumption of the equivalent of closest-packing will not lead to any serious error.

Values of g are given for all the systems studied in Tables II and III and the corresponding values of p are written after the spherical diameters in column 4. In computing g, the volume of the oil-phase has been corrected by the amount of surplus alcohol above that required to make
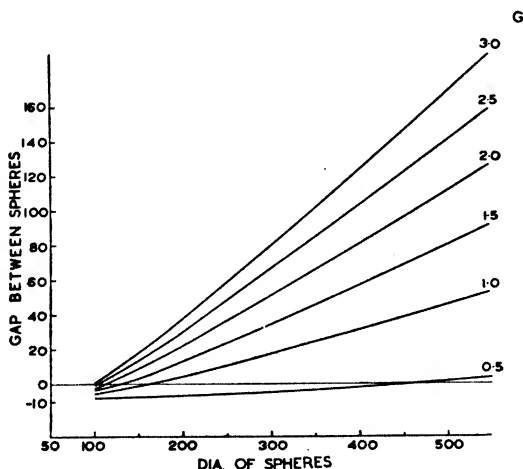
FIG. 5. Gap between spheres, p, plotted as function of diameter for different values of the phase ratio, g.
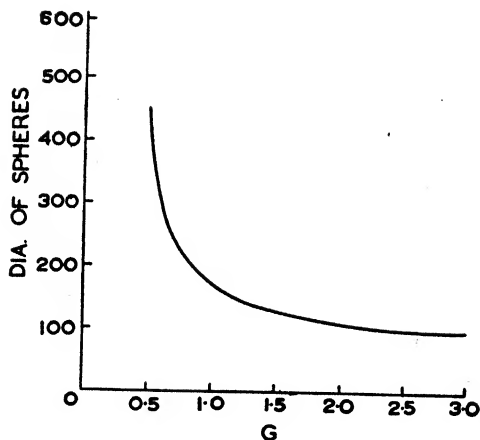
Fig. 6. Critical diameter of spherical micelles for
contact plotted as function of phase ratio, g.

an equimolecular layer with the soap. The oil-phase thus contains both
nonpolar oil and surplus polar oil (alcohol).

Similar calculations cannot be performed for cylinders unless some
assumption is made about their length. This has not been attempted.

Minimum Diameter for Hydrophilic Oleomicelles

Reference to Fig. 1 makes it clear that the structure of the monolayer-
shell in a hydrophilic oleomicelle will permit of only a limited amount of
curvature of the surface. Assuming the longer soap molecules to pivot
about the extremity of the shorter alcohol molecules, the limiting curva-
ture is reached when the nonpolar ends of neighboring soap molecules
come into contact. It is easily proved geometrically that the corresponding
limiting diameter is 80 Å if the following molecular dimensions are used:
length of soap molecule, $l = 25$ Å; length of alcohol molecule, $m = 10$ Å;
breadth of soap or alcohol molecule, $\simeq 5$ Å (the value is not critical in the
calculations). The data presented in Table III show that most of the
systems studied lie well above this critical region. It is interesting that
similar considerations do not apply in the case of the oleophilic hydro-
micelles.

VII. Discussion of Results

The first thing to consider is whether the general trend of the experi-
mental results is in harmony with the hypothesis of spherical micelles. In
order to do this for the oil-continuous systems, the corrected X-ray
spacings have been plotted against the reciprocal of the volume of oleic
acid in Fig. 7. A similar plot for the water-continuous systems would not

be as instructive, owing to the varying volume of the oil-phase (intra-micellar volume) in these systems, and the comparison between theory and experiment is here made in Table III.

It will be seen that the experimental points in Fig. 7 lie near or above the theoretical curve for spheres, except in the case of some of the more concentrated soap systems. The arrows indicate the spacings after sub-traction of the calculated gap, p, between spheres, and represent probable spherical diameters. Even so, certain spacings, notably that correspond-ing to specimen 22 (0.75 cc. oleic acid), still lie above the theoretical curve and the experimental error only partially explains the discrepancy. The fit would be better in this region if a smaller area per molecule and a
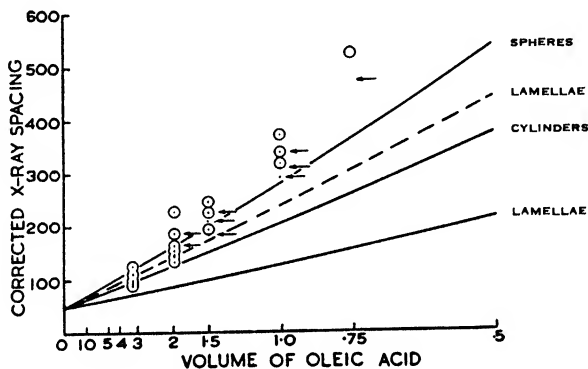
FIG. 7. Plot of corrected X-ray spacings against reciprocal of volume of oleic acid. Arrows indicate spacings after subtraction of estimated gap between spheres and cor-respond to diameters. Theoretical curves for spheres, cylinders and lamellae are given, the dashed curve representing lamellae swollen by 7 cc. oil in addition to all the water: the lowest curve refers to lamellae swollen by the water alone (5 cc.).

larger solubility factor were used. It should, however, be realized that the factor 1.23 used in the derivation of the spacings from the X-ray data may need adjustment, as was said in an earlier section.

The most striking feature of Fig. 7 is the way it shows the impossi-bility of reconciling the higher spacings with the hypothesis of cylindrical or lamellar micelles, even when the latter are swollen to an improbable extreme by both oil and water. It is of importance that the liquids which give spacings in the 400–500 Å region are commencing to give a strong Tyndall light scattering.

In the lower region of the curves, the spherical model seems less able to explain the results, particularly as regards the systems containing 3.16 cc. of oleic acid. The structure of these more concentrated systems is obscure, but they could consist of short cylindrical micelles or of small

lamellar micelles. Their relatively low viscosity and the absence of flow birefringence make it unlikely that the micelles are markedly aniso-dimensional.

Much the same considerations apply in the case of the water-continuous systems (Table III). Here the fit with the spherical hypothesis is good for the last two members of the series (29, 30), the results for which are quite inexplicable otherwise. Of the remaining members of the series, 26 is in better agreement with the spherical hypothesis than with the others. It is of interest to remark that this system is the only one with a higher soap concentration to have no "squashing" of postulated spherical micelles, extra water having been added to increase the phase ratio, g. The other 3 systems containing 3.16 cc. oleic acid (23, 24, 25), are all badly "squashed" on the spherical hypothesis and the observed results are difficult to explain simply. The agreement for 23 with the lamellar picture is good but is not so for 24 and 25, the latter of which gave an extremely weak and broad band. The results for 28 seem to favor the existence of cylindrical micelles in this system, which is also probably the case for 27. Both these systems are near the "squashing" limit on the spherical hypothesis.

It may be anticipated from the discussion in the previous sections that increasing the volume of intermicellar liquid, keeping other factors constant, should result in an increase in the X-ray spacings. This change would be due to the increased separation of the spheres and not to an alteration in size of the spheres themselves. Specimens 11, 12, and 13 were made up with an increasing volume of oil in the continuous phase but with the same volumes of oleic acid and dispersed water phase. The phase ratios, g, were determined and used in conjunction with Fig. 5 to predict the values of the gap, p, in each system. The diameter of the spherical hydromicelle should be 164 Å in each case. As will be seen by reference to Table II, the agreement between calculated and observed spacings is good—168, 184, 204 Å (predicted) as compared with 164, 186, 228 Å (observed). This quality of agreement would hardly be expected unless the general picture of the systems given in this paper were substantially correct. By analogy with the results on the scattering of X-rays by compressed gases, it would be expected that, at high enough dilutions of the spheres, the X-ray band would become less definite and finally give place to a "gas-type" diffuse central scattering. It is interesting to note that the band given by specimen 13 appears to exhibit a slight tendency of this sort (see Plate I).

The reverse procedure was carried out with specimen 14, in which a much smaller volume of oil was present. The value of p is thus made negative and if the system consists of equal "spherical" micelles, they must be squashed together and become roughly dodecahedral in shape

(see Fig. 4). This might account for the anomalous conduced. Conditions
specimen. Alternatively, the micelles may be unequal in size giving rise to
spherical, but still squashed, or the system may have a parti₊nductivity
structure. The complex nature of the structure of this liquid is₊ined very
the very broad X-ray band (Plate I) which it gives.   nents were

Similar considerations probably apply for the other at lamella₊s
oil-continuous systems (3–7) which all have p-methylcyclohexₐyers.   ne
polar oil. Specimen 4 gives a broad band with an outer band   ₊tly
superimposed on it; specimen 6 also gives a broad and faint   ₊oth
have negative p values. Specimen 7, somewhat inexplicably₆₅ ₍₁₉₊e no
measurable diffraction.

Specimens 1 and 2 gave quite sharp bands and might consi₊   ₊ short
cylindrical micelles. In both cases the nonpolar oil was 1-hexa₊hys.

Specimens 8, 16, and 19, which were made up with C_8 oct₊ ₊e as the
nonpolar oil, gave somewhat stronger photographs than those₊ given by
the benzene series. The spacing for 8 is in better agreement₊ with the
cylindrical than the spherical hypothesis.

To sum up, the X-ray evidence strongly supports the concept of
spherical micelles for systems containing less than 27.5% soap in water.
For the more concentrated soap systems, as for the "anoma₊ous" and
"squashed" systems, the evidence sometimes favors the e₊₊   ₊e of short
cylindrical micelles or small lamellar micelles. The T₊iol. 107, scattering
exhibited by the less concentrated soap systems, both   - and oil-
continuous, is in agreement with the spherical dimension₊   uced from
the low-angle X-ray bands. The relatively low viscosity and ₊ nsparency
of the liquids lend support to the general structural picture, as does the
absence of flow birefringence. The division of the systems into 2 groups,
electrically conducting and nonconducting, is particularly suggestive of
the concepts put forward. It is difficult to envisage a lamellar structure
which is swollen by several hundred Ångstroms as indicated by the
observed X-ray spacings.

VIII. STRUCTURE OF SOAP MICELLES

We consider it inadvisable to apply the conclusions reached in this
work on the structure of oil and water dispersions requiring 4 components
to the structure of the simple micelles in more dilute soap solutions,
originally investigated by Hartley and McBain. Whereas the soap mi-
celles swell with water within indefinite limits, and with oil only between
narrow limits, the soap-alcohol micelles investigated in the present work
can swell with either oil or water within extremely wide limits. It has been
shown that, at temperatures above 50°C., the soap micelle systems start
to behave in a similar fashion, which suggests an incipient breakdown of
their partially ordered structure. Further, at room temperatures, soap

lamellar micel'definitely sharper low-angle X-ray bands than those ob-
birefringence work. In addition, they show marked flow birefringence and
dimensionreases at soap concentrations where the soap-alcohol systems
    Much 'uid. This would suggest that the normal soap micelles are
ous syster stalline whereas the soap-alcohol systems are liquid.
for the la
quite inex,   IX. FUTURE WORK
is in better ents are in hand with new equipment to measure the X-ray
It is of inte ands for systems giving the golden coloring and opacity effects
soap conc, s of submicroscopic particle size. These dimensions will also
micelles, <d with the observed diameters of the droplets in the range
The other ite evidence for droplets in oil in the range 100–1000 Å, should
badly "sq e with light scattering equipment. Attempts in this direction
are difficu made.
picture is
extremely   ACKNOWLEDGMENTS

existence 'iled design of the low-angle X-ray camera used in this work was due to Mr.
case for 2 m. The instrument was constructed by Mr. W. Nunn and Mr. Lanham in
spherical p of the Department of Mineralogy and Petrology, and we should like to
    It may ppreciation of their skilled assistance. It is also a pleasure to thank Mr. K.
increasing the , his unfailing help in the experimental work and for preparing the drawings
stant, should res publication.
would be due to work on these systems as previously published (11) was carried out
alteration in si m Mr. T. S. McRoberts and we are most grateful to him for much
were made ur investigations. We should also like to thank Mr. B. Finean for
but with th ndon of our X-ray photographs with the 5 kw. X-ray tube at the Royal
phase rati ns paper. We are greatly indebted to Dr. H. Mark for his help in the pub-
predict th   SUMMARY
spherical ,acings of X-ray diffraction bands were studied for systems of
reference and soap which had been titrated to transparency and fluidity
spacings i dition of certain aliphatic or alicyclic alcohols. These systems
186, 228 pirefringent. Two systems were investigated in some detail; one,
expected t he oil was the continuous phase (electrically nonconducting),
substantia her, in which the aqueous solution was the continuous phase
X-rays by y strongly conducting). It was shown that, with soap solutions
dilutions (27% in the water phase, the spacings of the X-ray bands gave
finally giv port to the concept that the structure consisted of close-packed
to note th atr spheres in oil or close-packed uniform oil spheres in water.
tendency let is considered to be stabilized by a mixed monolayer of the
    The re ol molecules. By changing the soap-alcohol concentration, the
much sm of the spheres were varied from approximately 100 Å to 550 Å,
egative dimensions a strong Tyndall effect was observed. By changing
t be s ter ratio, the spacings of the X-ray bands suggested that the

distance between the spheres of oil or water was being varied. Conditions could be so chosen that the spheres were "squashed," this giving rise to broad diffuse X-ray bands and to an anomalous electrical conductivity of the oil-continuous systems. In those systems which contained very highly concentrated soap solutions (38%), the X-ray measurements were better interpreted as fitting a structure of short cylinders or short lamellae of the soap-alcohol molecules with oil and water between the layers.

REFERENCES

1. SCHULMAN, J. H., AND McROBERTS, T. S., *Trans. Faraday Soc.* **42B**, 165 (1946).
2. HESS, K., PHILIPPOFF, W., AND KIESSIG, H., *Kolloid-Z.* **88**, 46 (1939).
3. ROSS, S., AND McBAIN, J. W., *J. Am. Chem. Soc.* **68**, 547 (1946).
4. MATTOON, R. W., STEARNS, R. S., AND HARKINS, W. D., *J. Chem. Phys.* **15**, 209 (1947).
5. PINK, R. C., *Trans. Faraday Soc.* **42B**, 170 (1946).
6. HARKINS, W. D., MATTOON, R. W., AND CORRIN, M. L., *J. Colloid Sci.* **1**, 119 (1946).
7. HOAR, T. P., AND SCHULMAN, J. H., *Nature* **152**, 102 (1943).
8. HARKINS, W. D., *J. Chem. Phys.* **16**, 156 (1948).
9. RILEY, D. P., The Ultra-fine Structure of Coals and Cokes, p. 232. London (B.C.U.-R.A.), 1944.
10. EHRENFEST, P., *Amsterdam Akad.* **17**, 1184 (1915); PRINS. J. A., *Physica* **6**, 315 (1926).
11. SCHULMAN, J. H., McROBERTS, T. S., AND RILEY, D. P., *J. Physiol.* **107**, May (1948).

NOTE ON LIGHT SCATTERING IN SOAP SOLUTIONS

P. Debye

From the Dept. of Chemistry, Cornell University, Ithaca, N. Y.
Received May 3, 1948

The scattering of light by soap solutions has been measured in order to verify McBain's picture of their constitution, according to which, from a certain critical concentration on, conglomerates (micelles) are formed, and to measure the molecular weight of such micelles. The measurements were made by E. W. Anacker and R. M. Hagen in the Chemistry Department of Cornell University; the investigation was supported by the Office of Rubber Reserve.

Ordinary soaps, like K laurate, were the first to be investigated. However, they showed some secondary complications around the critical concentration, presumably due to hydrolysis. Acid soaps, like dodecylamine hydrochloride (DAH), were found to be free of these complications. The following report covers only DAH and some homologues with different lengths of the hydrocarbon tail.

The excess turbidity of DAH solutions over that of the water is negligibly small up to a concentration which is identical with the critical concentration as determined by the usual methods. From this point on, the turbidity increases rapidly and follows a curve similar to that which starts from zero concentration in the case of high polymer solutions. The discussion of this curve along familiar lines (P. Debye, *J. Phys. Colloid Chem.* **51**, 18 (1947)), combined with the observed diffraction difference between solution and solvent, leads to the molecular weight of the micelle. For DAH this was found to be 17,300, which corresponds to a conglomerate of 66 single DAH molecules. It is well known that the critical concentration as determined by the usual methods decreases if salts like NaCl, $BaCl_2$, or $LaCl_3$, are added. It was found that the same is true for the critical concentration determined by light scattering. Moreover, we found that the molecular weight is raised markedly by the addition of salt. In a 0.046 M solution of NaCl it is 37,200 instead of 17,300 (as in pure water). For the molecular weight, as well as for the critical concentration itself, only the concentration of the Cl ions is important, whereas the nature or the valency of the compensating ion (which has the same sign of charge as the micelle) generally is of only minor importance. At the same time, other negative univalent ions can be substituted for the Cl

ions without changing either the critical concentration or the molecular weight.

Comparing DAH with its homologues having varying lengths of their hydrocarbon tails, it was found that the decrease of the critical concentration with increasing number of CH_2 groups in the chain is coupled with an increase in the number of single molecules contained in the micelle.

A tentative theory of the micelles is proposed based on the double-layer, or sandwich, picture advocated by McBain and recently adopted by W. D. Harkins and co-workers (R. H. Mattoon, R. S. Stearns and W. D. Harkins, *J. Chem. Phys.* **15**, 209 (1947)). It is supposed that the micelle structure represents an equilibrium between the repulsive long-range Coulomb forces due to the charges concentrated in the "heads" of the soap molecules and the short range attractive van der Waals forces which come into play when the "tails" are brought from the surrounding water into the hydrocarbon part of the micelle structure. If N is the number of single molecules in the micelle, it can be shown that the work W_e done against the electrical Coulomb forces in assembling the micelle is proportional to $N^{\frac{4}{3}}$

$$W_e = {}^{\frac{4}{3}}N \ w_e.$$

In this relation w_e is a fundamental electrical energy which can be expressed in the ionic charge of the soap molecule and the distance of the heads in the layer. At the same time, molecular work is gained due to the short range forces and this work is proportional to N,

$$W_m = -N \ w_m,$$

in which w_m is a fundamental molecular energy. The curve for the total work $W = W_e + W_m$ has a minimum for a certain $N = N_o$ and this minimum is taken to represent the equilibrium structure. If W_o is the total work gained in assembling, it is found that

$$\frac{w_m}{w_e} = \frac{3}{2} \ N_o^{\frac{1}{3}} \text{ and } w_m = -3 \ \frac{W_o}{N_o}.$$

From our light scattering experiments we know N_o. The energy W_o can be calculated from the critical concentration according to classical thermodynamic principles. In the case of DAH with a critical concentration of 0.0131 molar, we have $N_o = 66$ and $W_o/N_o = 8.36 \ kT$. This leads (at 25°C.) to

$$w_m = 25 \ kT \text{ and } w_e = 2.1 \ kT.$$

The question is whether these values are reasonable.

According to the measurements of the National Bureau of Standards, in the American Petroleum Institute Research Project 44, the heat of vaporization, at 25°C., of nonane is 11.099 Kcal/mole and the increase

for one CH_2-group is 1.18 Kcal/mole. Extrapolating to dodecane, this corresponds to a heat of vaporization per dodecane molecule of 25 kT.

According to W. D. Harkins, the surface area occupied by one head is 27 Å². Taking for the charge the electronic charge and assuming for the effective dielectric constant the average of that of water and that of a hydrocarbon, leads to $w_e = 2.8 \, kT$.

From thermodynamic principles coupled with the assumption that w_m is a linear function of the number of CH_2 groups in the tail, it follows that the log of the critical concentration should be a linear function of the number of these groups. This checks with the experimental facts and the observed slope of this straight line corresponds, per CH_2 group, to $w_m = 2.14 \, kT$, whereas the increment in heat of vaporization of 1.18 Kcal./mole mentioned before corresponds to 2.0 kT.

If electrolyte is added to the soap solution we have to expect that, due to the same shielding effect which is of fundamental importance in the interionic attraction theory of strong electrolytes, the electrical work W_e will diminish. This means that the minimum in the curve for the total work W will be displaced to larger values of N. Hence the micelle will increase in size as observed. Thus far, however, the quantitative aspect of this question has not yet been worked out in detail.

The independence of the micelle structure on the kind or valency of added ions with the same sign of charge seems peculiar at first sight, especially if confronted with the principle of ionic strength. However it should not be forgotten that the formulation of this principle is linked essentially with the assumption that the electrical work performed by the charges in changing their position within the solution is always small as compared to kT. This assumption is certainly not valid for ions which approach the micelle. A calculation according to Gouy reveals that the potential at the micelle should be of the order of 200 millivolts, and this means that at this point the concentration of ions of equal sign will be at least 3×10^{-4} times smaller than in the bulk of the solution. Keeping this in mind, it seems probable that eventually also this point will fall in line.

STATISTICAL ANALYSIS OF THE SORPTION
OF VAPORS BY HIGH POLYMERS

In a recent publication[1] the following general equation for the total number of moles of vapor, N, immobilely sorbed or adsorbed on a number of localized sites, N_s,

$$\frac{N}{N_s} = a\,\frac{\theta'}{\theta}, \tag{1}$$

was given where

$$\theta = 1 + c_1 a + c_1 \cdot c_2 a^2 + \ldots \tag{2}$$

and θ' is the first derivative of θ with respect to a, the relative vapor pressure of the material being sorbed, or the activity if the vapor obeys the perfect gas law. The constants, c_1, c_2, etc., are the ratios of the internal partition functions of the sorbed molecules in the first, second, etc., layers with respect to the internal partition function of the molecules in their pure liquid phase.

For the case that c_2, c_3, etc., equal zero, the Langmuir sorption equation is obtained:

$$\frac{a}{N} = \frac{1}{c_1 N_s} + \frac{a}{N_s} \tag{3}$$

while for c_1, c_2, c_3, etc., all equal to unity, an equation results which can be considered as Raoult's law applied to the solution, vapor molecules N mixed with solid sorption sites, N_s,

$$\frac{a}{N} = \frac{1}{N_s} - \frac{a}{N_s}. \tag{4}$$

If c_1, c_2, c_3 are not unity but are all equal to a constant k, a modified form of Raoult's law is obtained:

$$\frac{a}{N} = \frac{1}{kN_s} - \frac{a}{N_s}. \tag{5}$$

To test these various equations we have plotted a/N against a for a number of sorption systems with rather striking results, particularly in

[1] M. Dole, J. Chem. Phys. **16**, 25 (1948). This treatment follows very closely that of T. L. Hill, J. Chem. Phys. **14**, 263 (1946).

the case of the sorption of organic vapors by rubber. Fig. 1 illustrates the application of Eq. (5) to the well-known data of Gee and Treloar[2] where the validity of this function up to a relative vapor pressure of 0.8 can be seen. For the system rubber-toluene,[3] the linearity of a/N as a function of a persists up to a relative vapor pressure of toluene equal to 0.95.
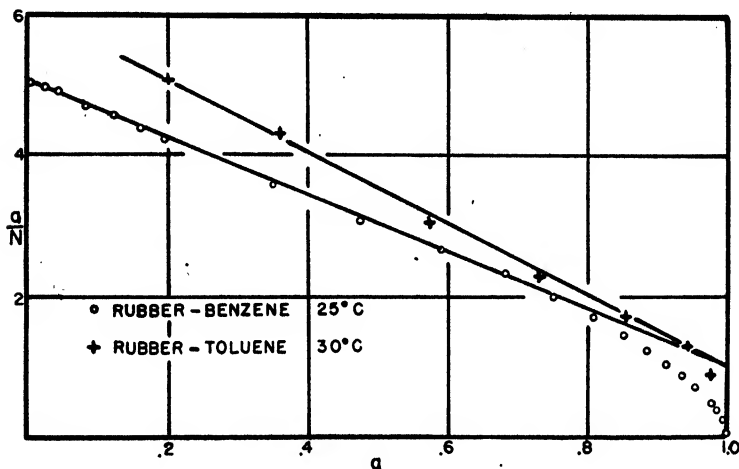
FIG. 1. The activity of benzene or toluene, a (actually the partial pressure p/p_0), divided by N, the number of moles of vapor sorbed/mole of isoprene units, plotted as a function of a.

The significance of these equations and their relation to the statistical equations of Flory, Huggins and others will be discussed in the complete publication of this work which will appear shortly in the *Ann. N. Y. Acad. Sci.*

Northwestern University,   MALCOLM DOLE
Evanston, Illinois.
    Received April 28, 1948

[2] G. Gee and L. R. G. Treloar, *Trans. Faraday Soc.* **38**, 147 (1942). See also Gee and W. J. C. Orr, *ibid.* **42**, 507 (1946).
[3] The rubber-toluene data are those of Meyer, Wolff and Boissonnas, *Helv. Chim. Acta* **23**, 430 (1940).

MIXED MONOLAYERS. I. ADSORBED FILMS AT AIR-WATER SURFACES

Eric Hutchinson [1]

From the Department of Chemistry, Stanford University, Calif.
Received June 8, 1948

INTRODUCTION

A considerable amount of information is available about mixed mono-layers of insoluble films placed on water surfaces (8), but very little is available for corresponding films *adsorbed* from solution.

Much attention has been focused recently (10,12,15) on the so-called type III surface tension curves which are frequently obtained with solutions of synthetic detergents and in which minima are often observed in the surface tension-concentration curves, although frequently there is no minimum but the surface tension after rapid lowering in very dilute solution remains nearly constant. In the case of at least one such detergent, sodium dodecyl sulfate, Miles and Shedlovsky (14) have clearly demonstrated that the minimum is absent provided the detergent is highly purified, and that the minimum is restored by the addition of very small amounts (*ca.* 0.1%) of "impurity" to the solution. These findings have been confirmed by Brady (4) using a different method of purifying the sample, and by Robinson[2] who added further amounts of lauryl alcohol to intensify such minima.

Further, with highly purified samples of sodium dodecyl sulfate time effects on surface tension are almost entirely absent, as found by Brady (4) and by the author. So much discussion has taken place about the surface aging of detergents of this kind (2,3,16), and so many theories have been proposed to account for the long time effects on surface tension, that it is of prime importance to study systems in which the materials are really pure, and then deliberately to add impurities and observe the effects.

While experiments of Miles and Shedlovsky (14) and Brady (4) demonstrate such effects qualitatively, it was thought desirable to make a quantitative study of the effects of a known impurity while applying the Gibbs adsorption theorem to such a system. The materials used were sodium dodecyl sulfate, with *n*-octyl alcohol as the impurity. Sodium dodecyl sulfate was chosen (a) because of the data available on the pure

[1] Bristol-Myers Company Postdoctorate Fellow and Research Associate in Chemistry.
[2] Unpublished results, Stanford University.

compound from the work of Miles and Shedlovsky, and (b) because a fairly large sample of the highly purified material, kindly supplied by E.I. du Pont de Nemours & Co., was available. Although the most likely source of impurity is dodecyl alcohol, octyl alcohol was used because of the greater ease in the preparation of the solutions, for which the low solubility of dodecyl alcohol would have proved troublesome.

EXPERIMENTAL

Measurements of the surface tension of the solutions of octyl alcohol and sodium dodecyl sulfate in distilled water and conductivity water were made by means of the ring method (9), and the Wilhelmy plate method (5,6,7) in its differential form. Usually 50 ml. of the solution was placed in a 10 cm. glass dish provided with a cover to prevent accidental contamination from the air. No attempt was made to thermostat the solutions, but the laboratory temperature during the experiments remained at 23°C. ± 1°. The Wilhelmy plate method showed that only very small time effects in surface tension occurred. After a preliminary drop of *ca*. 0.2 ~ 0.4 dynes/cm. during the first 2–3 mins., no further change in surface tension was observed, either in the solutions of octyl alcohol and sodium dodecyl sulfate alone, or in solutions containing both components during at least 3 hrs. The slide used in this method was a square microscope cover slip *ca*. 2.4 × 2 × 0.02 cm, and was hung from the arm of a torsion balance. Harkins (7) describes two alternative methods of using the Wilhelmy plate method in its differential form. Firstly, a constant upward pull may be exerted on the slide, and the surface pressure (*i.e.*, the decrease in surface tension) studied as a function of the depth of immersion of the slide. Secondly the slide may be maintained at a constant depth of immersion and the surface pressure studied as a function of the upward pull on the slide required to maintain this constant position. The second of these methods was adopted.

The ring used in the ring method was a Cenco platinum-iridium ring 4.0 cm. in circumference and had a $\frac{R}{r}$ factor (9) equal to 39.5.

Agreement between the two methods was generally within 0.2 dyne/cm., and in the worst cases was within 0.6 dyne/cm. This agreement is significant in itself, demonstrating that, in cases like the present, where aging is almost entirely absent, the ring method may be used with solutions as well as with pure liquids. Both methods are dependent, for simple use, on the maintenance of zero contact angle at the solid-liquid interface. With solutions there exists the possibility that this may be difficult to ensure but, since the solid was glass in the one case and platinum-iridium in the other, and agreement was obtained, the assumption may reasonably be made that zero contact angle was obtained in both cases.

No appreciable differences could be found for the surface tensions of solutions prepared in distilled water from those of solutions prepared in conductivity water.

RESULTS

Surface tensions for a number of solutions of octyl alcohol and sodium dodecyl sulfate in water are given in Tables I–VI.[3] In Fig. 1 are given curves for the surface tension as a function of the mole fraction N_2 of the octyl alcohol in water and in solutions of sodium dodecyl sulfate of various concentrations. Fig. 2 presents corresponding data for the variation of surface tension as a function of the mean mole fraction $N_{3\pm}$ of the sodium dodecyl sulfate in water and in various solutions of octyl alcohol.

TABLE I

Surface Tension of Mixed Solutions of Octyl Alcohol and Sodium Dodecyl Sulfate

Conc. of alcohol molality M_2	Conc. of NaLS[a] molality M_3	Surface excess			Area	Film pressure
		g./mole $\times 10^{10}$				
		Γ_2	Γ_3	Γ		
2.52×10^{-3}	—	5.57	—	5.57	29.6	36.9
2.016	—	5.17	—	5.17	32.0	33.8
1.512	—	5.22	—	5.22	31.6	29.3
1.008	—	5.22	—	5.22	31.6	24.6
0.504	—	5.30	—	5.30	31.2	14.8
0.252	—	3.00	—	3.00	52.0	6.6

[a] Sodium dodecyl sulfate.

TABLE II

Surface Tension of Mixed Solutions of Octyl Alcohol and Sodium Dodecyl Sulfate

Conc. of alcohol molality M_2	Conc. of NaLS[a] molality M_3	Surface excess			Area	Film pressure
		g./mole $\times 10^{10}$				
		Γ_2	Γ_3	Γ		
2.52×10^{-3}	0.5×10^{-3}	5.28	0.53	5.81	28.4	38.7
2.016	0.5×10^{-3}	5.08	.49	5.57	29.6	35.9
1.512	0.5×10^{-3}	4.57	.64	5.21	31.7	32.9
1.008	0.5×10^{-3}	4.16	.64	4.80	34.4	28.0
0.504	0.5×10^{-3}	3.23	.93	4.16	39.7	21.0
0.252	0.5×10^{-3}	2.21				13.9
0	0.5×10^{-3}	0	.90	.90	183.0	4.9

[a] Sodium dodecyl sulfate.

[3] In Tables I–VI, Γ_2 = surface excess of octyl alcohol; Γ_3 = surface excess of sodium dodecyl sulfate.

TABLE III

Surface Tension of Mixed Solutions of Octyl Alcohol and Sodium Dodecyl Sulfate

Conc. of alcohol molality M_2	Conc. of NaLS[a] molality M_1	Surface excess			Area	Film pressure
		g./mole $\times 10^{10}$				
		Γ_2	Γ_1	Γ		
2.53×10^{-3}	1.0×10^{-3}	4.37	0.78	5.15	32.0	40.3
2.016	1.0×10^{-3}	4.36	.86	5.22	31.6	39.0
1.512	1.0×10^{-3}	4.37	1.00	5.37	30.7	36.1
1.008	1.0×10^{-3}	4.25	0.95	5.20	31.6	32.0
0.504	1.0×10^{-3}	3.02	1.25	4.27	38.7	24.8
0	1.0×10^{-3}	0	1.80	1.80	91.7	9.5

[a] Sodium dodecyl sulfate.

TABLE IV

Surface Tension of Mixed Solutions of Octyl Alcohol and Sodium Dodecyl Sulfate

Conc. of alcohol molality M_2	Conc. of NaLS[a] molality M_1	Surface excess			Area	Film pressure
		g./mole $\times 10^{10}$				
		Γ_2	Γ_1	Γ		
2.56×10^{-3}	1.50×10^{-3}	4.47	1.03	5.50	30.0	42.5
2.016	1.50×10^{-3}	3.95	1.02	4.97	33.1	40.8
1.512	1.50×10^{-3}	4.15	1.11	5.26	31.4	37.7
1.008	1.50×10^{-3}	3.77	1.18	4.95	33.2	34.2
0.504	1.50×10^{-3}	2.85	1.69	4.54	36.3	28.3
0	1.50×10^{-3}	0	2.70	2.70	61.4	14.2

[a] Sodium dodecyl sulfate.

TABLE V

Surface Tension of Mixed Solutions of Octyl Alcohol and Sodium Dodecyl Sulfate

Conc. of alcohol molality M_2	Conc. of NaLS[a] molality M_1	Surface excess			Area	Film pressure
		g./mole $\times 10^{10}$				
		Γ_2	Γ_1	Γ		
2.56×10^{-3}	2.0×10^{-3}	4.04	1.08	5.12	32.2	43.8
2.016	2.0×10^{-3}	3.66	1.07	4.73	34.9	41.5
1.512	2.0×10^{-3}	3.48	1.18	4.66	35.9	39.6
1.008	2.0×10^{-3}	3.28	1.38	4.66	35.9	36.1
0.504	2.0×10^{-3}	2.62	1.90	4.52	36.5	30.5
0	2.0×10^{-3}	—	3.66	3.66	45.9	17.9

[a] Sodium dodecyl sulfate.

TABLE VI

Surface Tension of Mixed Solutions of Octyl Alcohol and Sodium Dodecyl Sulfate

Conc. of alcohol molality M_2	Conc. of NaLS^a molality M_3	Surface excess g./mole $\times 10^{10}$			Area	Film pressure
		Γ_2	Γ_3	Γ		
2.52×10^{-3}	2.50×10^{-3}	3.82	1.26	5.08	32.5	45.2
2.016	2.50×10^{-3}	3.05	1.25	4.25	(38.8)	42.5
1.512	2.50×10^{-3}	2.76	1.33	5.09	32.4	40.7
1.008	2.50×10^{-3}	3.05	1.66	4.68	35.3	37.9
0.504	2.50×10^{-3}	2.68	2.23	4.91	33.6	32.5
—	2.50×10^{-3}	—	4.50	4.50	36.7	22.1
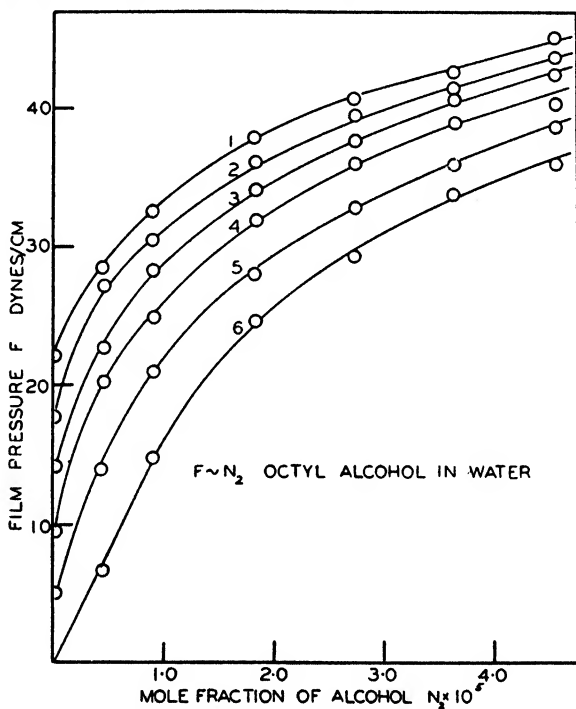
FIG. 1. Surface pressure as a function of octyl alcohol concentration. Curve 1, octyl alcohol in 2.5×10^{-3} M sodium dodecyl sulfate; Curve 2, octyl alcohol in 2.0×10^{-3} M sodium dodecyl sulfate; Curve 3, octyl alcohol in 1.5×10^{-3} M sodium dodecyl sulfate; Curve 4, octyl alcohol in 1.0×10^{-3} M sodium dodecyl sulfate; Curve 5, octyl alochol in 0.5×10^{-3} M sodium dodecyl sulfate; Curve 6, octyl alcohol in water.
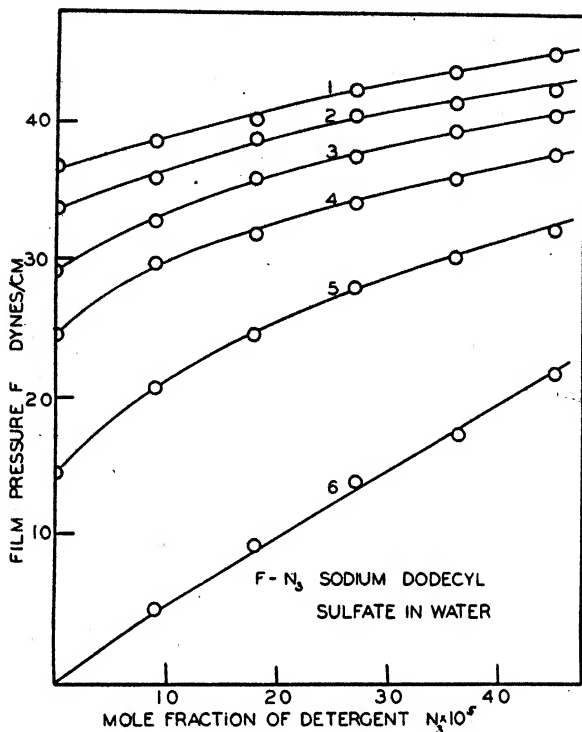
FIG. 2. Surface pressure as a function of sodium dodecyl sulfate concentration. Curve 1, sodium dodecyl sulfate in 2.52×10^{-3} M octyl alcohol; Curve 2, sodium dodecyl sulfate in 2.01×10^{-3} M octyl alcohol; Curve 3, sodium dodecyl sulfate in 1.51×10^{-3} M octyl alcohol; Curve 4, sodium dodecyl sulfate in 1.008 Æ 10^{-3} M octyl alcohol; Curve 5, sodium dodecyl sulfate in 0.504×10^{-3} M octyl alcohol; Curve 6, sodium dodecyl sulfate in water.

In Fig. 3 are given force-area curves for the adsorbed films of octyl alcohol, sodium dodecyl sulfate, and a mixed film containing both components. The areas per molecule in the film were obtained as described in following sections.

DISCUSSION

The generalized form of the Gibbs adsorption theorem may be written:

$$d\gamma = - \sum_1^k d\mu_i \Gamma_i, \qquad (1)$$
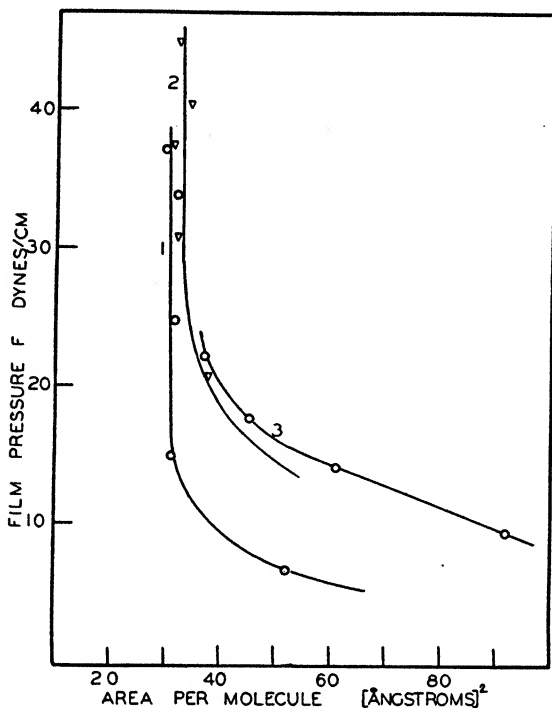
FIG. 3. (1) Force-area curve for film adsorbed from alcohol solutions; (2) Force-area curve for film adsorbed from solutions containing 1:1 proportions of alcohol and sodium dodecyl sulfate; (3) Force-area curve for film adsorbed from sodium dodecyl sulfate solutions.

where

$$\gamma = \text{surface tension} = \gamma(T, x_2, x_3 \cdots x_k),$$

μ_i = chemical potential of the ith component,

Γ_i = surface excess of the ith component,

$x_2, \cdots x_k$ = any independent intensive variables of the system,

k = number of components in the system.

Also:

$$\frac{\partial \gamma}{\partial x_j} = - \sum_{1}^{k} \frac{\partial \mu_i}{\partial x_j} \Gamma_i. \tag{2}$$

The difficulty in applying the Gibbs theorem lies in the calculation of the

various derivatives $\dfrac{\partial \mu_i}{\partial x_j}$. Koenig (11)[4] has calculated these derivatives for a number of systems.

According to the scheme set up by Koenig the present case may be considered as a two-phase system $(\alpha + \beta)$ containing 3 components all of which are present in at least one phase, α, the solution, and in which β is a dilute vapor.

Taking as the independent intensive variables, T, N_2^α, $N_{3\pm}^\alpha$,

$$\gamma = \gamma(T, N_2^\alpha, N_{3\pm}^\alpha),$$

where

N_1^α = mole fraction of water in phase α,

N_2^α = mole fraction of octyl alcohol in phase α,

$N_{3\pm}^\alpha$ = mean mole fraction of sodium dodecyl sulfate in phase α.

It may then be shown (11) that, generally, for such a system:

$$\sum_1^k \frac{\partial \mu_i^\alpha}{\partial N_j^\alpha} \Gamma_i^\alpha = - \frac{\partial \sigma}{\partial N_j^\alpha}, \qquad j = 2, 3, \cdots k. \tag{3}$$

For ideal solutions of non-electrolytes we may write:

$$\mu_1^\alpha = \mu_1^{\alpha_0} + RT \ln N_1^\alpha,$$

$$\left(\frac{\partial \mu_1}{\partial N_j} \right)_{T,P} = RT \left(\frac{\partial \ln N_1^\alpha}{\partial N_j^\alpha} \right)$$

$$= \frac{RT}{N_1^\alpha} \left(\frac{\partial}{\partial N_j^\alpha} \left(1 - \sum_2^k N_l \right) \right) \qquad l = 2, 3, \cdots k$$

$$= - \frac{RT}{N_1^\alpha}, \tag{4}$$

and

$$\mu_h^\alpha = \mu_h^{\alpha_0} + RT \ln N_h^\alpha;$$

$$\left. \begin{aligned} \therefore \quad \frac{\partial \mu_h^\alpha}{\partial N_j^\alpha} &= \frac{RT}{N_j} \\ &= 0 \end{aligned} \right\} \quad \begin{aligned} j &= h. \\ j &\neq h \end{aligned}$$

Hence

$$- \frac{RT}{N_1^\alpha} \Gamma_1^\alpha + \frac{RT}{N_j^\alpha} \Gamma_j^\alpha = - \frac{\partial \gamma}{\partial N_j^\alpha}. \tag{5}$$

The equation for $\dfrac{\partial \gamma}{\partial N_j^\alpha}$ thus contains only two unknowns Γ_1^α and Γ_j^α. In

the case that one of the components, *e.g.*, the lth is an ideal electrolyte, we have

$$\mu_l^\alpha = \mu_l^{\alpha 0} + \nu RT \ln N_{l\pm}^\alpha,$$

and

$$\frac{\partial \mu_1^\alpha}{\partial N_{l\pm}^\alpha} = -\frac{\nu RT}{N_1^\alpha},$$

and

$$\left. \begin{array}{ll} \dfrac{\partial \mu_h^\alpha}{\partial N_{l\pm}^\alpha} = \dfrac{\nu RT}{N_{l\pm}^\alpha} & \quad \text{for} \quad h = l, \\[2mm] \qquad\quad = 0 & \quad \text{for} \quad h \neq l. \end{array} \right.$$

Thus $-\dfrac{\nu RT}{N_1^\alpha} \Gamma_1^\alpha + \dfrac{\nu RT}{N_{3\pm}^\alpha} \Gamma_l^\alpha = -\dfrac{\partial \gamma}{\partial N_{l\pm}^\alpha}$ for l = ideal electrolyte. For the system water, octyl alcohol, sodium dodecyl sulfate/water vapor,

$$\text{Component } 1 = \text{water},$$
$$2 = \text{octyl alcohol},$$
$$3 = \text{sodium dodecyl sulfate}.$$

$$\therefore \quad -\frac{RT}{N_1^\alpha} \Gamma_1^\alpha + \frac{RT}{N_2^\alpha} \Gamma_2^\alpha = -\frac{\partial \gamma}{\partial N_2^\alpha} \tag{6}$$

and

$$-\frac{2RT}{N_2^\alpha} \Gamma_1^\alpha + \frac{2RT}{N_{3\pm}^\alpha} \Gamma_3^\alpha = -\frac{\partial \gamma}{\partial N_{3\pm}^\alpha}, \tag{7}$$

assuming the solutions to be ideal. These two equations contain three unknowns Γ_1, Γ_2, Γ_3 and to solve for these we require a third equation, *viz.*, a *normal convention* to define the position of the Gibbs surface.

In this particular case, where the solutions are dilute, a suitable convention is $\Gamma_1 = 0$: the so-called Gibbs' convention.

Then

$$\Gamma_2^\alpha = -\frac{N_2^\alpha}{RT} \frac{\partial \gamma}{\partial N_2^\alpha} = \frac{N_2^\alpha}{RT} \frac{\partial F}{\partial N_2^\alpha} \tag{8}$$

where

$$F = \text{the film pressure} = \gamma^0 - \gamma$$

and

$$\Gamma_3 = \frac{N_{3\pm}^\alpha}{2RT} \frac{\partial F}{\partial N_{3\pm}^\alpha}. \tag{9}$$

Values for Γ_2 and Γ_3 obtained by measuring the slopes of the F–N curves are given in Tables I–VI. Values of the total surface excess $\Gamma = \Gamma_2 + \Gamma_3$ and the corresponding areas per molecule in the films. $A = \dfrac{1}{N\Gamma}$ are given in Tables I–VI also.

Any study of adsorbed films, and particularly those involving detergents such as sodium dodecyl sulfate, is critically dependent on the purity of the materials used. The *n*-octyl alcohol used here was a pure sample and was well shaken up with "Florisil" prior to use. The sodium dodecyl sulfate showed practically no signs of aging and this may be taken as indicative of a high degree of purity. The surface tension curve of aqueous solutions of this material, however, was some 1–3 dynes/cm. lower than those of Brady (4) and of Miles and Shedlovsky (14), depending on the concentration. Hence, it is possible that very small traces (≪0.05%) of impurity still remained in the material. This does not invalidate some of the more important conclusions which may be drawn from the results.

By virtue of Eq. (8) the Γ_2 values quoted for the octyl alcohol are independent of any impurities in the sodium dodecyl sulfate (except in the event that the adventitious impurity is itself octyl alcohol). The values quoted for Γ_3 will, in general, be greater than the true values for Γ_3, in the absence of impurity, since the measured slope $\dfrac{\partial F}{\partial N_{3\pm}}$ ought strictly to be written $\dfrac{\partial F}{\partial (N_{3\pm} + N_{\text{impurity}})}$. Hence, the Γ_3 values quoted represent upper limits for this quantity. Even so, it is immediately apparent that the number of molecules of octyl alcohol in the film is at least equal to that of the sodium dodecyl sulfate, and is generally 2 or 3 times greater. Even when the bulk concentration of alcohol is only one-fifth that of the sodium dodecyl sulfate, there are rather more molecules of alcohol than of detergent in the film. Hence, the alcohol is relatively more surface active than the detergent containing 4 more carbon atoms, and it is, therefore, highly probable that, owing to the Traube rule effect, dodecyl alcohol would be very much more surface active than sodium dodecyl sulfate. Thus, even when present at only small concentration as impurity, the alcohol would form a significant portion of the surface film. Beyond the critical concentration of the sodium dodecyl sulfate, when micelles are present, the alcohol will be largely, if not entirely, removed from free solution by solubilization, and the film will now consist almost entirely of sodium dodecyl sulfate. Thus, in terms of the mixed film it becomes apparent why type III curves are obtained with impure materials. It is still a problem why type III curves without a minimum exhibit a constant low surface tension over a wide range of concentration.

Inasfar as the absolute magnitudes of the Γ values are concerned it must be borne in mind that these were calculated on the *assumption* that the solutions are ideal. From the work of McBain and Johnston (13) it is clear that, in dilute solutions, sodium dodecyl sulfate is almost ideal,

yielding solutions with an osmotic coefficient $g \sim 0.98-1.00$. No data are available to show how good an approximation holds in the case of octyl alcohol. However, the values of Γ_2 quoted for octyl alcohol represent a lower limit, for, if the solutions are non-ideal, the true values of Γ_2 must necessarily be greater than these since with non-ideal solutions the slopes of the $F \sim N_2$ curves will be greater than for ideal solutions.

The force-area curve for *n*-octyl alcohol alone shows the film to be a highly compressed gaseous film with large deviations from ideality above *ca.* 10 dynes/cm.: this is in agreement with the generally observed higher degree of condensation of alcohols as compared with corresponding acids in insoluble films (1).

The force-area curve for sodium dodecyl sulfate shows that this compound forms a "gaseous" type film with a roughly constant value for the product (Force $\times$ Area) $\sim 800-900$. A large number of force-area curves may be drawn for films adsorbed from solutions of the two solute components. Curve 2 in Fig. 3 shows that for the film adsorbed from approximately equimolar solutions, and it is seen that the film has properties intermediate between the condensed film of the alcohol and the gaseous film of the sodium dodecyl sulfate. Inspection shows that *all* of the mixed films have intermediate properties, approximating more or less closely to the behavior of the major component of the film. This is essentially the same as was found for a number of mixed *insoluble* films by Harkins and Florence (8). There is no obvious variation in the properties of the system, *e.g.*, rapid changes of slope in the $F \sim N$ curves, to suggest surface compound formation such as was suggested by Schulman (17) for insoluble films of cetyl alcohol penetrated by sodium cetyl sulfate; nor is there any evidence, except possibly in extreme dilution, that one component sensibly increases the adsorption of the other by any kind of "boosting" action.

The probable accuracy of the values of A, the area per molecule in the film is of course much lower than in the case of insoluble films. Not only are the measurements of the surface tension themselves relatively inaccurate ($\pm$ 0.2–0.3 dynes/cm.) but the determination of the Γ_s involve drawing tangents to curves which in some places have a small radius of curvature, and errors are easily introduced at this stage. Thus, since the areas are subject to a probable error of *ca.* 1–2 Å², it is felt that quantitative deductions from the $F - A$ curves might not be justifiable.

SUMMARY

Measurements have been made of the surface tensions of solutions containing octyl alcohol and sodium dodecyl sulfate. By the application

of the Gibbs adsorption theorem for 3-component systems, values have been determined for the surface concentration of alcohol and detergent. Even in solutions in which the alcohol concentration is low relative to that of the sodium dodecyl sulfate, the alcohol remains the main constituent in the mixed film. By analogy, reasons are adduced to explain "type III" surface tension curves for detergents of this kind. The properties of the mixed films are intermediate between those of the pure components, and there is no evidence for interaction in the mixed film. There is apparently mere competition for the available surface in the monolayer.

REFERENCES

1. Adam, The Physics and Chemistry of Surfaces. Oxford, 1944.
2. Adam and Shute, *Trans. Faraday Soc.* **34**, 1 (1938).
3. Alexander, *ibid.* **37**, 15 (1940).
4. Brady, Navy Report#4, N6ori—154—T.O., II.
5. Dervichian, *J. phys. radium* **6**, 221, 429 (1935).
6. Harkins, in J. Alexander's Colloid Chemistry. Reinhold, 1944.
7. Harkins and Anderson, *J. Am. Chem. Soc.* **59**, 2189 (1937).
8. Harkins and Florence, *J. Chem. Phys.* **6**, 847 (1938).
9. Harkins and Jordan, *J. Am. Chem. Soc.* **52**, 1751 (1930).
10. Hauser, Recent Advances in Colloid Science. Interscience, 1942.
11. Koenig, Private communication.
12. McBain, *Repts. Progress of Physics* **5**, 30 (1939).
13. McBain and Johnston, *Proc. Roy. Soc. London* **181A**, 119 (1942).
14. Miles and Shedlovsky, *J. Phys. Chem.* **48**, 57 (1944).
15. Powney and Addison, *Trans. Faraday Soc.* **33**, 1243 (1937).
16. Ross, *J. Phys. Chem.* **49**, 377 (1945).
17. Schulman and Stenhagen, *Proc. Roy. Soc. London* **126B**, 356 (1938).

THE OSMOTIC ACTIVITY AND CONDUCTIVITY OF AQUEOUS SOLUTIONS OF SOME TYPICAL COLLOIDAL ELECTROLYTES [1]

Ann Cushman, A. P. Brady and J. W. McBain

Stanford University, Palo Alto, California
Received April 23, 1948

INTRODUCTION

Much of our knowledge of the behavior of colloidal electrolytes in solution is a result of the measurement of colligative properties. The conductivity is a property that can be measured both conveniently and accurately. However, realizing the danger of drawing extensive conclusions from a single type of measurement, an effort has been made in the Stanford laboratories to measure both the freezing point lowering of these solutions and their conductivities whenever possible. Although the field is limited by the insolubility of many of these materials at 0°C., there nevertheless exist many gaps in the literature where such a measurement can be made. The present paper presents data for some typical colloidal electrolytes of widely different molecular structures.

EXPERIMENTAL METHOD

Freezing points were measured by a modified Beckmann method. The usual precautions were observed in keeping the thermometer always at 0°C. and avoiding large heat loss through the walls of the freezing compartment.

Conductivities were measured at 2000 cycles with a Dyke-Jones bridge and an oscilloscope detector. The cells were of Pyrex glass with platinized platinum electrodes, and were maintained at $25.000 \pm .005°C.$ in an oil thermostat. The conductivity water was distilled through a Barnstead conductivity water still with block tin condensers and stored in a Jena glass bottle. The specific conductivity of the water averaged about 7×10^{-7} ohm^{-1}cm^{-1}.

Since the salts of carboxylic acids hydrolyze, in studying these materials a small excess (usually about 4 mole %) of base was added to

suppress this hydrolysis. Osmotic coefficients and equivalent conductivities for the colloidal electrolytes were then calculated by subtracting the theoretical effect of the excess base on the assumption that the two electrolytes are without influence on each other. This will introduce no error in concentrated solutions (1, 2). The distortion at other concentrations is far less than that which would arise if the material were allowed to hydrolyze.

Materials

Sodium linoleate and linolenate: from Kahlbaum linoleic and linolenic acids, respectively.

Sodium ricinoleate: from Eimer and Amend ricinoleic acid. This material had polymerized, but after treatment with alcoholic potassium hydroxide it gave an equivalent weight of 300.6 (theory: 298.3).

Benzyl trimethylammonium laurate: from Triton B (Röhm and Haas) and Kahlbaum lauric acid. Electrometric titration of the Triton B gave no indication of unquarternized material.

Morpholine laurate: from Union Carbide and Carbon morpholine and Kahlbaum lauric acid.

Monobutyl biphenyl sodium monosulfonate and monobutyl phenylphenol sodium monosulfonate: the commercial wetting agents, Aresket and Areskap (Monsanto), were used without further purification.

Lauryl pyridinium chloride: Emulsol Corp.

Sodium abietate: E. I. du Pont de Nemours & Co.

Lauryl benzyl dimethylammonium chloride: a specially purified sample of Zephiran, furnished by Winthrop Chemical Co.

Myristyl trimethylammonium chloride: special sample from E. I. du Pont de Nemours & Co.

Cetyl benzyl dimethylammonium chloride: Wm. S. Merrell Co.

Cetyl trimethylammonium chloride: Wm. S. Merrell Co.

Anion-Active Colloidal Electrolytes

The osmotic coefficients, g, of 3 types of anion-active colloidal electrolytes as determined by freezing point lowering are given in Table I and Fig. 1; they are equal to the freezing point lowering divided by the lowering for ideal fully dissociated electrolyte; namely, 1.858 times twice the molality, m.

For comparison, already published curves for potassium oleate (3) and potassium laurate (4, 5), determined largely by a much more accurate freezing point method, are also shown in the Fig. 1. Results from the Beckmann method become undependable below about 0.05 N, which is still above the critical concentration for all these substances. Several conclusions may be drawn, however, from the data at high concentration.

Considering first the salts of the unsaturated acids, it may be noted that sodium linoleate, sodium linolenate, and potassium oleate, all have about the same osmotic coefficient throughout the concentration region where comparison is possible. On the other hand, sodium ricinoleate, where there is a hydroxyl group on the long chain, has a definitely higher osmotic coefficient, connoting less ready packing into micelles.

TABLE I

Osmotic Coefficients of Some Anion-Active Colloidal Electrolytes

A. Unsaturated

Sodium linoleate		Sodium linolenate		Sodium ricinoleate	
m	*g*	*m*	*g*	*m*	*g*
0.340	0.111	0.500	0.096	0.302	0.172
0.116	0.132	0.128	0.108	0.152	0.211
0.0622	0.143	0.0474	0.134	0.0604	0.331

B. Laurates

Benzyl trimethyl-ammonium laurate		Morpholine laurate	
m	*g*	*m*	*g*
0.389	0.288	0.592	0.203
0.181	0.300	0.379	0.215
0.0866	0.371	0.180	0.294
0.0424	0.556	0.0872	0.395
0.0177	0.99	0.0416	0.521

C. Polycyclics

Monobutyl biphenyl sodium monosulfonate		Monobutyl phenylphenol sodium monosulfonate		Sodium abietate	
m	*g*	*m*	*g*	*m*	*g*
0.566	0.600	0.568	0.580	0.0481	0.597
0.368	0.628	0.268	0.633	0.0239	0.615
0.178	0.687	0.105	0.745	0.0095	0.811
0.103	0.713	0.0500	0.840		
0.0501	0.784	0.0252	0.940		
0.0342	0.779				

Fig. 1 also permits a comparison of the 3 laurates: potassium, morpholine, and benzyl trimethyl ammonium. It may be seen that at concentrations where the colloid is fully formed, the salts with the large gegenions, morpholine and benzyl trimethylammonium laurate, have about the same osmotic coefficient. Both, however, have higher coefficients than the potassium salt. Although these data do not allow establishing the critical concentration with any exactness, it is evident that the

laurates with the large counter ions have a much lower critical concentration than potassium laurate. It would be desirable to investigate other positive ions, but it is difficult to find one that is reasonably pure, and forms both a strong base and a soluble soap. Morpholine ($K_b = 10^{-5}$) is about as weak a base as is practical, and even this is too weak to form isotropic solutions with lauric acid below approximately 0.05 N.

The third class of colloidal electrolytes shown in Fig. 1 includes the biphenyl derivatives, sodium salts of monosulfonated butyl biphenyl and butyl phenylphenol. They behave similarly to each other, but quite differently from the other compounds shown. The osmotic coefficient definitely shows aggregation in more concentrated solutions, but it occurs much more gradually and to a much lesser extent that in the straight
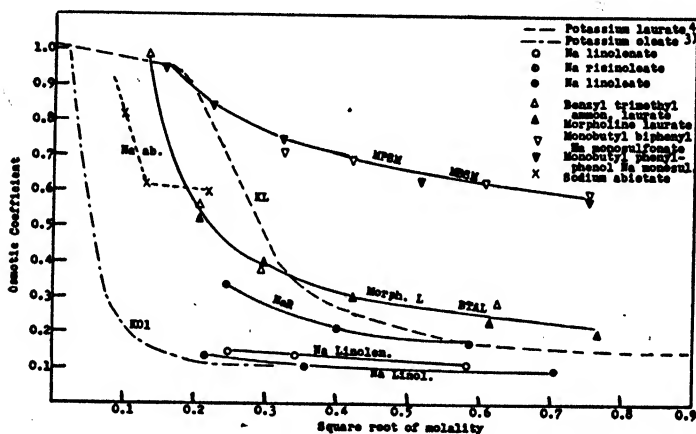
FIG. 1. Osmotic coefficient *vs.* square root of molality for some anion-active colloidal electrolytes.

chain compounds (6, 7). Sodium abietate, another type of polycyclic structure, appears to have an osmotic behavior intermediate between that of the long chain compounds and the biphenyl derivatives.

Fig. 2 and Table II present the equivalent conductivities of the same materials whose osmotic coefficients are given in Table I and Fig. 1. The trends are the same as those noted for the osmotic coefficients. The sodium salts of the 18 carbon unsaturated acids, linoleic, linolenic, and ricinoleic, have conductivities rising in that order in the flat portion of the curve, which is the same order observed for the osmotic coefficients. The biphenyl derivatives show only a gentle decrease in conductivity with increasing concentration, with no evidence of a "critical" concentration by this measurement. This conductometric behavior appears to be

TABLE II
Equivalent Conductivities of Some Anion-Active Colloidal Electrolytes
A. Unsaturates

Sodium linoleate		Sodium linolenate		Sodium ricinoleate	
c	Λ	c	Λ	c	Λ
0.305	25.8	0.440	30.8	0.152	36.4
0.112	23.2	0.123	27.4	0.0604	39.4
0.0608	23.5	0.0466	28.6	0.0304	44.0
0.0304	24.9	0.0174	35.9	0.00608	54.7
0.0111	31.4	0.00841	48.3		
0.00605	44.3	0.00438	59.4		
0.00380	44.7	0.00436	61.1		
0.00303	54.2				

B. Laurates

Benzyl trimethyl-ammonium laurate		Morpholine laurate	
c	Λ	c	Λ
0.339	21.3	0.502	20.6
0.169	25.2	0.340	21.6
0.0836	28.5	0.170	22.1
0.0415	34.2		
0.0175	46.5		
0.00838	56.8		
0.00431	59.9		
0.00175	64.9		

C. Polycyclics

Monobutyl biphenyl sodium monosulfonate		Monobutyl phenylphenol sodium monosulfonate	
c	Λ	c	Λ
0.501	56.1	0.499	52.4
0.339	61.2	0.251	61.6
0.170	68.4	0.101	70.6
0.101	73.4	0.0497	56.7
0.0499	79.4	0.0250	82.6
0.0338	82.5	0.0100	89.8
0.0170	89.3	0.00495	93.7
0.0101	93.5	0.000996	99.6
0.00497	99.0	0.000399	102.4
0.00135	104.6		
0.000401	108.6		

typical for polycyclic structures, which apparently form only small aggregates, judging from freezing point measurements. Similar conductivity curves without a break have been reported for sodium desoxycholate (3) and sodium abietate (6, 7), both of which are shown by freezing point data to be typical colloidal electrolytes with well marked critical concentration.

The conductance data afford a direct comparison between the critical concentrations of benzyl trimethylammonium laurate and potassium laurate. From the curves in Fig. 2 it can be seen that the critical concentration for the benzyl trimethyl derivative is about 0.01 N, less than half of that for the potassium salt (0.024 N).
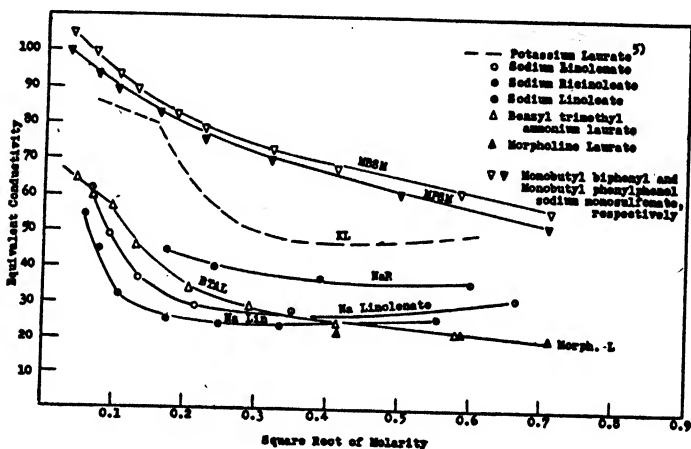
FIG. 2. Equivalent conductivity *vs.* square root of molarity for some anion-active colloidal electrolytes.

Cation-Active Colloidal Electrolytes

Freezing point results for 3 cation-active materials are given in Table III in terms of the molality, m, the freezing point depression, θ, and the osmotic coefficient, g.

The critical concentrations of all these salts are far too low to be investigated by the present freezing point method. However, the compounds do not hydrolyze, and thus are especially amenable to investigation by conductivity. The equivalent conductivities of the compounds listed in Table III are given in Table IV and plotted against the square root of the concentration in Fig. 3. Two additional cation-active agents, cetyl benzyl dimethylammonium chloride and cetyl trimethylammonium bromide, are also included in Fig. 3. These latter are too insoluble at 0°C.

TABLE III

Freezing Point Results for Some Cation-Active Detergents

Substance	m	θ	g
Lauryl pyridinium chloride	0.050	0.070	0.355
	0.100	0.115	0.311
	0.200	0.213	0.287
Lauryl benzyl dimethyl ammonium chloride	0.0316	0.033	0.28
	0.0638	0.049	0.204
	0.168	0.102	0.163
	0.358	0.200	0.150
Myristyl trimethylammonium chloride	0.050	0.033	0.181
	0.100	0.056	0.152
	0.200	0.102	0.137

for freezing point determination to be practical. The conductivity curves for the 3 chlorides for which freezing measurements are given in Table III fall in the same order as the osmotic coefficients.

It is evident from Fig. 3 that measurements have been made at a sufficient dilution to show the critical concentration in the cases of lauryl pyridinium chloride, lauryl benzyl dimethylammonium chloride, and myristyl trimethylammonium chloride. One point for cetyl trimethyl-ammonium bromide appears to be below the critical concentration, but
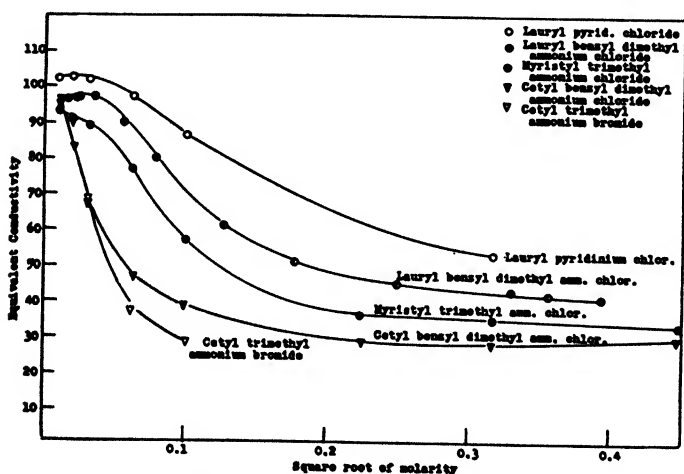
FIG. 3. Equivalent conductivity *vs.* square root of molarity for some cation-active colloidal electrolytes at 25°C.

this cannot be considered established from the present data. The critical concentration for cetyl benzyl dimethylammonium chloride is definitely at or below the most dilute solution measured (1×10^{-4} N). Because of

TABLE IV

Equivalent Conductivities of Some Cation-Active Colloidal Electrolytes

Lauryl benzyl dimethylammonium chloride			
c	Λ	c	Λ
0.317	38.8	0.00619	79.2
0.159	40.8	0.00315	89.6
0.126	41.6	0.00126	96.4
0.0948	42.5	0.000617	96.4
0.0622	44.5	0.000493	96.1
0.0316	50.3	0.000248	95.7
0.0158	60.4		

Lauryl pyridinium chloride		Myristyl trimethylammonium chloride	
c	Λ	c	Λ
0.10	52.2	0.20	32.3
0.010	86.0	0.10	34.7
0.004	96.4	0.050	35.8
0.0010	101.0	0.010	56.6
0.00040	101.8	0.0040	76.5
0.00010	101.9	0.0010	88.5
		0.00040	89.5
		0.00010	92.8

Cetyl benzyl dimethylammonium chloride		Cetyl trimethylammonium bromide	
c	Λ	c	Λ
0.20	28.1	0.01	28.5
0.10	27.7	0.0040	36.7
0.050	28.6	0.0010	67.4
0.010	38.1	0.00040	89.1
0.0040	46.1	0.00010	94.3
0.0010	67.0		
0.00040	84.3		
0.00010	95.0		

the spacing of the points in Fig. 3, the break in the conductivity curve can be fixed only within rather wide limits from this type of plot. A plot of specific conductivities against concentration of these materials, however, gives two intersecting straight lines (8). This intersection serves as

TABLE V

Critical Concentrations of Some Cation-Active Agents as Determined by Conductivity

Substance	Crit. conc.
Lauryl pyridinium chloride	0.0028
Lauryl benzyl dimethylammonium chloride	0.0023
Myristyl trimethylammonium chloride	0.0030
Cetyl benzyl dimethylammonium chloride	$<1 \times 10^{-4}$
Cetyl trimethylammonium chloride	$1-4 \times 10^{-4}$ (?)

a useful definition of the critical concentration as determined by conductivity. The concentrations so obtained are listed in Table V.

Potassium Laurate plus Sucrose

Previous workers have shown that, upon the addition of simple electrolytes to colloidal electrolytes with the same counter ions, the change in conductivity and freezing point is nearly the same as that occurring in pure water, if the colloidal electrolyte is at a concentration sufficient for colloid to have fully formed (1, 2). In dilute regions, the addition of such an electrolyte tends to decrease the critical concentration, probably through common ion effect (9, 10). No data are extant, however, on the influence of the addition of non-electrolytes, except in solvent quantities. Fig. 4 and Table VI give the results of freezing point measurements on solutions of sucrose, potassium laurate, and mixtures of the two solutes, in terms of the osmotic coefficient, *g*. The curves marked "ideal" in the figure are calculated on the basis that the freezing point depressions are
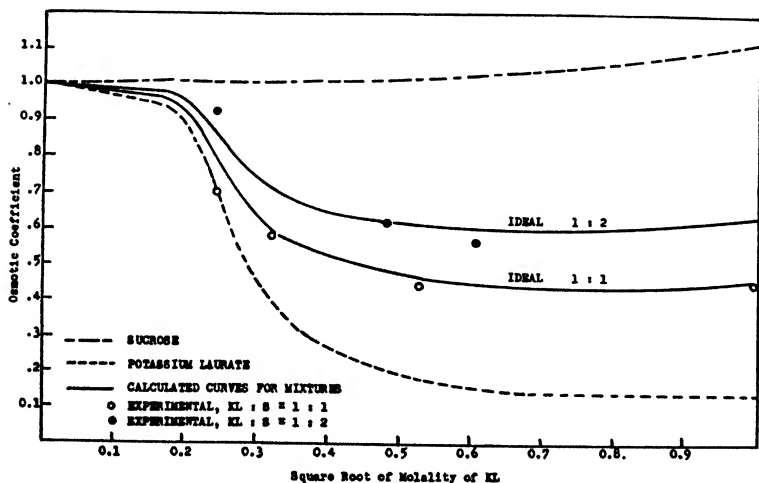
FIG. 4. Osmotic coefficients of mixtures of potassium laurate and sucrose.

merely additive, that is, that the two solutes are without influence upon each other. It may be seen that the observed osmotic curves are quite close to the ideal curves, indicating that there is but little interaction between the two solutes. The equivalent conductivities of potassium laurate plus sucrose are also given in Table VI, and in Fig. 5 these are compared with those for potassium laurate alone. Here the sucrose has a pronounced effect in lowering the equivalent conductivity, but it appears that the effect can be largely attributed to the increased viscosity of the solution, since the points obtained by multiplying the potassium laurate plus sucrose curve (mole ratio 1:1) by its viscosity relative to potassium laurate alone fall very nearly on the potassium laurate curve.

TABLE VI
*Osmotic Coefficients and Equivalent Conductivities of
Mixtures of Potassium Laurate and Sucrose*

A. Mole ratio KL:S = 1:1

Osmotic coefficient		Conductivity	
m_{KL}	g	c_{KL}	Λ
1.039	0.50	0.248	34.0
0.279	0.447	0.101	43.9
0.104	0.579	0.0497	54.3
0.0596	0.700	0.00998	89.2
0.0101	1.02		

B. Mole ratio KL:S = 1:2

Osmotic coefficient		Conductivity	
m_{KL}	g	c_{KL}	Λ
0.368	0.565	0.295	21.0
0.232	0.618	0.200	27.1
0.0961	0.677	0.0886	38.3
0.0413	0.887	0.0400	56.9

Potassium Laurate plus Dimethyl Phthalate

Dimethyl phthalate is an interesting substance in that, although it is virtually insoluble in both water and oil, it is appreciably solubilized by soap solutions (11). In Table VII the osmotic coefficients and equivalent conductivities of several solutions of potassium laurate are compared with those of the same solutions saturated with dimethyl phthalate. The osmotic coefficients with the phthalate present are similar to, but about 10% higher than, those in which it is absent. The phthalate has an even
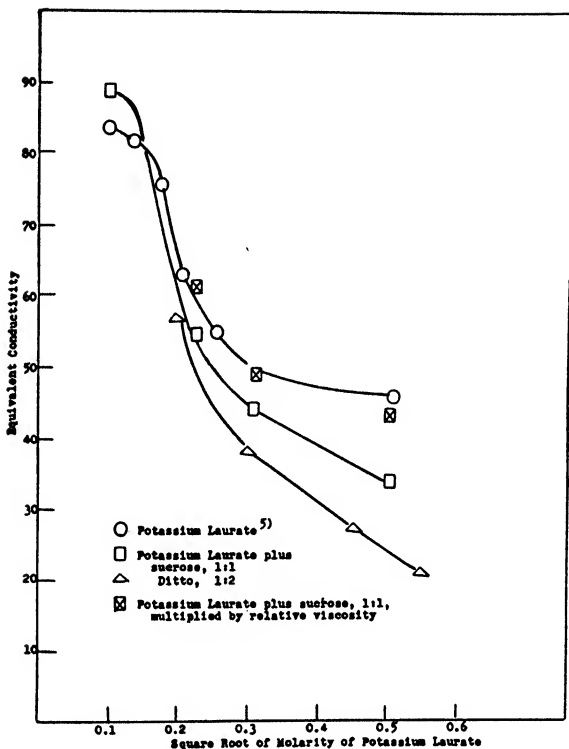
FIG. 5. Conductivity curves at 25°C.

more pronounced effect on the equivalent conductivity. In more dilute solutions the conductivity of the potassium laurate containing the solubilized oil has a considerably higher conductivity than the pure

TABLE VII

Comparison of Osmotic Coefficients and Equivalent Conductivity of Solution of Potassium Laurate with and without Solubilized Dimethyl Phthalate

Conc., molar	g		Λ	
	KL	KL + DMP	KL	KL + DMP
0.100	0.400	0.434	48.0	53.0
0.250	0.205	0.210	45.6	50.4
0.500	—	—	47.4	47.7
0.739	—	—	52.5	46.2
0.999	0.151	0.172	50	42.9

colloidal electrolyte; as the concentration is increased, the difference grows smaller, until at about 0.4 N it disappears. Thereafter the solution containing dimethyl phthalate is less conducting. This latter effect could, at least in part, arise from the greatly increased viscosity that accompanies the solubilization at higher concentrations.

SUMMARY

1. The osmotic coefficients of aqueous solutions of 10 different anionic and cationic colloidal electrolytes have been measured by freezing point depression, now bringing the total number of those investigated to 64. Conductivities were also measured for these and two other materials too insoluble at 0°C. for freezing point determinations.

2. The relative lowering of conductivity with increasing concentration is less than that of osmotic coefficient. In the case of polycyclic structures, such as a bile salt or sodium abietate, the latter measurement shows the presence of colloid with a critical concentration, whereas this does not appear in the conductivity curve.

3. Addition of dimethyl phthalate, a substance insoluble in oil and water but solubilized by soap solutions, appears slightly to decrease colloid formation as reflected in osmotic coefficient and equivalent conductivity.

4. The colloidal behavior of the laurate of several complex organic bases has been compared with that of potassium laurate.

5. An ordinary molecule, sucrose, lowers the freezing point of water to the same extent as it lowers the freezing point of a solution of the colloidal electrolyte, potassium laurate.

REFERENCES

1. QUICK, *J. Chem. Soc.* **127**, 1401 (1925).
2. MCBAIN AND SEARLES, *J. Phys. Chem.* **40**, 493 (1936).
3. MCBAIN AND JOHNSTON, *Proc. Roy. Soc. London* **181A**, 119 (1942).
4. MCBAIN AND BOLDUAN, *J. Phys. Chem.* **47**, 95 (1943).
5. BRADY, Ph.D. Thesis, Stanford University, 1944.
6. KOLTHOFF AND JOHNSON, *J. Phys. Chem.* **50**, 440 (1946).
7. CARR, JOHNSON AND KOLTHOFF, *J. Phys. Chem.* **51**, 636 (1947).
8. WRIGHT, ABBOTT, SIVERTZ AND TARTAR, *J. Am. Chem. Soc.* **61**, 549 (1933).
9. POWNEY AND ADDISON, *Trans. Faraday Soc.* **33**, 1243, 1253 (1937).
10. MCBAIN AND BRADY, *J. Am. Chem. Soc.* **65**, 2072 (1943).
11. MCBAIN AND MCHAN, *J. Am. Chem. Soc.* communicated.

LIBERATION OF H+, Al+++ AND Fe+++ IONS FROM PURE CLAY MINERALS ON REPEATED SALT TREATMENT AND DESATURATIONS [1]

J. N. Mukherjee, B. Chatterjee [2] and A. Ray

From the Physical Chemistry and Colloid Research Laboratories, University College of Science and Technology, Calcutta, India

Received May 5, 1948

The liberation of H+, Al+++, and Fe+++ ions from hydrogen clays prepared from Indian soils under repeated neutral salt treatment and desaturations has been dealt with in previous publications (1–3) from this laboratory. It has been observed that hydrogen clays prepared from soils containing different clay minerals show different behaviors under above treatments. The present investigation aims at studying the behaviors of pure minerals under repeated salt treatment and desaturations. For this purpose, estimations have been made of the amounts of (i) Al+++ and Fe+++ ions and (ii) the acid displaced from hydrogen systems, prepared from the clay fractions isolated from a kaolinite, a bentonite,[3] and a pyrophyllite, after successive leaching with normal solution of barium chloride till no H+, Al+++, or Fe+++ ions could be detected in the leachate. The Ba-system, *i.e.*, the residue obtained after continued leaching with N BaCl$_2$, was converted into H-clay by treating with 0.02 N HCl followed by washing with distilled water, repeatedly leached with N BaCl$_2$ and each leachate analyzed as in the previous case. The amount of dissolved silicic acid in the neutral salt extract has also been estimated. The sequence of operations described above has been repeated 8 times with the hydrogen kaolinite, 4 times with the hydrogen montmorillonite, and 5 times with the hydrogen pyrophyllite. The base exchange capacity, calculated at the final inflection point, in the titration curves of the hydrogen systems with NaOH has been determined before and after the whole series of treatments.

[2] Senior Assistant Soil Chemist under the Scheme.

[3] X-ray analysis (5) of the clay fraction from the bentonite shows that it is practically pure montmorillonite. The hydrogen system prepared from the subfraction of the entire clay fraction of this bentonite has, therefore, been referred to as hydrogen montmorillonite.

EXPERIMENTAL

Preparation of Subfraction. A fine subfraction ($<0.05\,\mu$) was prepared from the entire clay fraction isolated from a bentonite by controlled centrifugal subsidence following the method of Baver and Whitt (4) with the aid of a Sharples supercentrifuge. The depth of sampling and the rate of revolution were kept constant and only the quantity of effluent per min. was varied.

Preparation of Hydrogen Systems. The clay fractions isolated from the kaolinite and pyrophyllite, as also the subfraction of montmorillonite, were repeatedly leached with 0.02 N HCl to replace all the exchangeable cations by H$^+$ ions. The excess acid was removed by repeated washing with distilled water until the filtrate gave no test for chloride. The hydrogen system thus obtained was dispersed in redistilled water.

Estimation of Displaced (Exchange) Acidity. The acid in the neutral salt extract was estimated by potentiometric titration against 0.01 N Ba(OH)$_2$ using Tinsley Vernier Potentiometer (Type 3126) reading up to 0.01 mv. and a Hartman Braun galvanometer with a critical damping resistance of 22×10^4 ohms and having a current sensitivity of 4.2×10^{-11} amp. The hydrogen electrode was employed in conjunction with the saturated calomel half cell for the e.m.f. measurements.

Estimation of Aluminum in the Salt Extract. Berg's method (6) was used for this purpose. The clear neutral salt extract (10 cc.)[4] was treated with 12 cc. of 1 N H$_2$SO$_4$ and warmed. The precipitated BaSO$_4$ was filtered and washed with distilled water and then thrice with 10 cc. portions of 0.05 N NaOH. The filtrate, together with the washings, was concentrated by evaporation, 8 cc. of 2 N caustic soda solution added, and boiled. Aluminum remained in solution as sodium aluminate and iron was precipitated as hydroxide. The precipitated ferric hydroxide (only traces in the majority of cases) was filtered and washed with hot distilled water. The filtrate, together with the washings, was concentrated and made slightly acid with acetic acid. Three g. of sodium acetate were added, heated gently to 45°C., and the aluminum precipitated by adding a solution of 8-hydroxyquinoline weakly acidified with acetic acid. After standing overnight, the precipitate was washed free from excess reagent with hot water, using a micro filter stick. A sufficient quantity of 2 N HCl and a little ethyl alcohol were added to dissolve the precipitate. An excess of standard solution of potassium bromate-bromide was added and then back titrated with a standard sodium thiosulphate solution. The amount of Al was calculated from the number of cc's. of

---

[4] In the case of leachates containing small amount of Al^{+++} ions, larger volumes, varying from 20 to 50 cc., were taken. Further, the sulphuric acid and caustic soda treatments were omitted if the leachate did not contain Fe^{+++} ions.

$N/10$ bromate-bromide mixture used up according to the following equation:

$$1 \text{ cc. } N/10 \text{ (KBrO}_3 + \text{KBr)} \equiv 0.2248 \text{ mg. of Al.}$$

Control experiments with known amounts of aluminum indicate that (i) the data presented in this paper are accurate within 2%, and (ii) aluminum can be precipitated directly in the salt extract, *i.e.*, in presence of barium chloride, if the latter does not contain iron. The salt extract is neutralized with NH_4OH and then made slightly acid with acetic acid. The rest of the procedure is the same as described above.

Estimation of Iron. To 10 cc. of the clear salt extract, a few drops of nitric acid and 2 cc. of $2 N$ ammonium thiocyanate solution were added and shaken until the red color attained its maximum intensity. It was matched against that produced in 10 cc. of a standard iron solution containing the same amounts of nitric acid and ammonium thiocyanate as the unknown. The strength of the standard iron solution was varied until the intensity of the color developed in both the standard and the unknown solution was the same. A Lovibond tintometer was used for this purpose.

Estimation of Dissolved Silicic Acid in the Neutral Salt Extract. Two cc. of a 10% solution of ammonium molybdate and 8 drops of hydrochloric acid were added to 50 cc. of the clear $BaCl_2$ extract. The yellow color developed was matched after 10 mins. against that produced in 50 cc. of a standard sodium silicate solution containing the same amounts of ammonium molybdate and hydrochloric acid. A Hellige colorimeter was used for these measurements.

Particulars of the minerals used in this work are given below:

Description of sample	Mineral present[6]	Reference number of corresponding H-system	Average equivalent spherical diameter (μ)
Bentonite from Kashmir (India)	Montmorillonite	K-B₅	<0.05
Kaolin from Singbhum (India)	Kaolin	H-K	<2.0
Pyrophyllite (supplied by Ward's Natural Science Co. Ltd., U.S.A.)	Pyrophyllite	H-P	<2.0

[6] Judged by X-ray analysis (5).

RESULTS AND DISCUSSION

The Total Amount of Acid Displaced from Hydrogen Systems on Repeated Leaching with Salt Solutions

Definite weights (about 3 g.) of K-B₅, H-K, and H-P were repeatedly leached with 100 cc. portions of N $BaCl_2$ solution until the leachate gave

practically no acidity when titrated with Ba(OH)$_2$. The Ba-system thus obtained was reconverted into H-system (*vide* p. 1), then repeatedly leached with N BaCl$_2$, and the acidity of the clear salt extract estimated in each leachate. The whole sequence of operations was repeated 4 times with K-B$_5$, 8 times with H-K, and 5 times with H-P. The results have been shown in Table I.

TABLE I

The Amount of Acid Displaced from K-B$_5$, H-K, and H-P on Repeated Leaching with N BaCl$_2$ and Desaturations

System	Serial no. of desaturations	Acidity in the leachates, expressed in milliequivalents/100 g. of H-system								Total acid displaced
		Serial no. of leachings with N BaCl$_2$								
		1st	2nd	3rd	4th	5th	6th	7th	8th	
K-B$_5$	1st	104.0	29.0	6.5	2.1	1.1	1.0	0.5	nil	144.2
	2nd	61.0	7.0	2.0	1.7	nil	—	—	—	71.7
	3rd	52.5	10.5	2.5	1.2	0.9	nil	—	—	67.6
	4th	37.0	6.0	2.3	0.6	nil	—	—	—	45.9
H-K	1st	3.50	0.5	nil	—					4.00
	2nd	3.20	0.2	—	—					3.40
	3rd	2.35	nil	—	—					2.35
	4th	2.15	nil	—	—					2.15
	5th	2.15	nil	—	—					2.15
	6th	1.25	nil	—	—					1.25
	7th	1.20	nil	—	—					1.20
	8th	1.20	nil	—	—					1.20
H-P	1st	5.30	0.90	nil	—					6.20
	2nd	1.80	0.40	—						2.20
	3rd	1.25	nil	—						1.25
	4th	1.25	nil	—						1.25
	5th	1.25	nil	—						1.25

With successive desaturations the total amount of displaced acid decreases with the progress of leaching, regularly in the case of K-B$_5$, but attains a constant value with H-K and H-P. These results are in agreement with those previously reported (2–3) for hydrogen clays having, respectively, montmorillonite and kaolinite as their major clay mineral.

The Total Amounts of Al^{+++} and Fe^{+++} Ions Displaced from Hydrogen Clays on Repeated Leaching with Solutions of Neutral Salts

Al^{+++}, as also Fe^{+++}, ions are present on the surface of hydrogen clays. These are exchanged for the Ba^{++} ions of added BaCl$_2$ and contribute to the acidity of the supernatant liquid above the H-clay-BaCl$_2$ mixtures. Estimations were, therefore, made of the amounts of Al^{+++}

and Fe^{+++} ions displaced from K-B$_5$, H-K, and H-P in each of the successive leachings with N BaCl$_2$ until no Al^{+++} or Fe^{+++} ions could be detected in the leachate, and also after repeated reconversion of the Ba-system into H-system, each time followed by leaching with N BaCl$_2$ as in the previous case. The results have been reported in Table II.

The amounts of Al^{+++} ions displaced on the addition of BaCl$_2$ decreases with the progress of leaching until practically no Al^{+++} ions could be detected in the leachate, indicating that there is a limit to the amount of Al^{+++} ions which can be displaced by repeated leaching of

TABLE II

The Amounts of Al^{+++} and Fe^{+++} Ions Displaced from K-B$_5$, H-K, and H-P on Repeated Leaching with N BaCl$_2$ and Desaturations

System	Serial no. of desaturations	Displaced Al^{+++} in leachates, milliequivalents/100 g.					Displaced Fe^{+++} in leachates, milliequivalents/100 g.			Total amount of Al^{+++} plus Fe^{+++} displaced me./100 g.
		1st	2nd	3rd	4th	Total	1st	2nd	Total	
K-B$_5$	1st	39.8	14.3	2.0	nil	56.1	1.8	nil	1.8	57.9
	2nd	13.3	5.6	0.2	—	19.1	1.5	nil	1.5	20.6
	3rd	3.0	1.7	nil	—	4.7	nil	—	nil	4.7
	4th	1.5	nil	—	—	1.5	nil	—	nil	1.5
H-K	1st	2.6	nil	—	—	2.6	nil	—	nil	2.6
	2nd	2.0	nil	—	—	2.0	nil	—	nil	2.0
	3rd	2.0	nil	—	—	2.0	nil	—	nil	2.0
	4th	0.7	nil	—	—	0.7	nil	—	nil	0.7
	5th	0.8	nil	—	—	0.8	nil	—	nil	0.8
	6th	0.2	nil	—	—	0.2	nil	—	nil	0.2
	7th	0.02	nil	—	—	0.02	nil	—	nil	0.02
	8th	nil	—	—	—	nil	nil	—	nil	nil
H-P	1st	2.9	0.05	nil	—	2.95	nil	—	—	2.95
	2nd	0.08	nil	—	—	0.08	nil	—	—	0.08
	3rd	0.08	nil	—	—	0.08	nil	—	—	0.08
	4th	nil	—	—	—	nil	nil	—	—	nil
	5th	nil	—	—	—	nil	nil	—	—	nil

the hydrogen minerals with BaCl$_2$ solution. The amount of Al^{+++} ions thus liberated does not correspond with the total amount of exchangeable Al^{+++} ions present. Al^{+++} ions are again displaced when the Ba-minerals are rendered desaturated by repeated leaching with 0.02 N HCl, followed by washing with distilled water, and then treated with N BaCl$_2$. The total amount of Al^{+++} ions displaced by BaCl$_2$ greatly decreases after the first desaturation in the case of K-B$_5$ and H-P. This decrease is, however, not so pronounced with H-K. K-B$_5$, which is pure montmorillonite, judged from X-ray studies (5), shows a gradual decrease in

the total amount of Al^{+++} ions displaced within the range of desaturations studied. In the case of H-K this amount decreases tending to a constant value in the fifth desaturation, but on further desaturations, each time followed by repeated leaching with N $BaCl_2$, it decreases and assumes an almost negligible value in the eighth desaturation. With H-P the amount of displaced Al^{+++} ions decreases to an almost negligible value with progressive desaturations. The total amounts of Al^{+++} ions displaced from the above systems are in the order: $K-B_5 > H-K > H-P$.

Appreciable amounts of Fe^{+++} ions are displaced from H-montmorillonite, but its amount decreases with successive leaching, and the $BaCl_2$ extract in the third desaturation does not seem to contain any Fe^{+++} ions. Fe^{+++} ions could not be detected in the $BaCl_2$ leachate of H-K and H-P.

The results obtained with H-montmorillonite and H-kaolinite on the liberation of Al^{+++} and Fe^{+++} ions by $BaCl_2$ are in fair agreement with those previously obtained (2, 3) with montmorillonitic and kaolinitic hydrogen clays.

The Variations in the Ratio of Displaced H^+ Ions to Al^{+++} Plus Fe^{+++} Ions on Successive Desaturations

A comparison of the data reported in Tables I and II indicates that the total amount of neutralizable acids displaced from $K-B_5$, H-K and H-P cannot be wholly accounted for by the amounts of Al^{+++} plus Fe^{+++} ions liberated in the same treatment. It appears, therefore, that H^+ ions in addition to Al^{+++} and Fe^{+++} ions are exchanged for the added Ba^{++} ions. The relation between the amounts of H^+ ions and Al^{+++} plus Fe^{+++} ions displaced on the addition of N $BaCl_2$ to the H-minerals are shown in Table III.

The ratio of displaced H^+ ions to Al^{+++} plus Fe^{+++} ions regularly increases with successive desaturations in the case of H-montmorillonite and H-pyrophyllite. With H-K it shows an irregular variation, but on the whole increases with progressive desaturation. With H-K and H-P this ratio assumes infinite value in the eighth and fourth desaturations, respectively.

Displaced H^+ ions decrease with successive desaturations with H-montmorillonite. The amount of H^+ ions displaced in the second desaturation steps out of this regular variation. In the case of H-kaolinite displaced H^+ ions remain practically constant up to the fifth desaturation and then slightly decreases, tending to a constant value. An exception is observed in the third desaturation. With H-pyrophyllite it regularly decreases tending to a constant value.

Data cited in Table III show that H$^+$ ions constitute the major fraction of the exchangeable ions present in H-montmorillonite. With H-kaolinite, Al^{+++} ions form the major portion of the exchangeable ions up to the third desaturation, but thereafter H$^+$ ions constitute the main

TABLE III

Relation Between the Amounts of Displaced H$^+$ Ions and Al^{+++} Plus Fe^{+++} Ions

System	Serial no. of desaturations	Total amount of acid displaced[a]	Total amount of Al^{+++} plus Fe^{+++} displaced[a]	Total amount of H$^+$ displaced[a]	H$^+$/Al^{+++} plus Fe^{+++}
K-B$_5$	1st	144.2	57.9	86.3	1.5
	2nd	71.7	20.6	51.1	2.5
	3rd	67.6	4.7	62.9	13.4
	4th	45.9	1.5	44.4	29.6
H-K	1st	4.0	2.6	1.4	0.5
	2nd	3.4	2.0	1.4	0.7
	3rd	2.35	2.0	0.35	0.2
	4th	2.15	0.7	1.45	2.1
	5th	2.15	0.8	1.35	1.7
	6th	1.25	0.2	1.05	5.2
	7th	1.20	0.02	1.18	59.0
	8th	1.20	nil	1.20	
H-P	1st	6.2	2.95	3.25	1.1
	2nd	2.2	0.08	2.12	2.6
	3rd	1.25	0.08	1.17	14.6
	4th	1.25	nil	1.25	
	5th	1.25	nil	1.25	

[a] Expressed in milliequivalents/100 g. of H-system.

fraction. In the first desaturation Al^{+++} ions constitute about half of the exchangeable ions present in H-pyrophyllite, but from the second desaturation and thereafter H$^+$ ions form the major fraction.

The Effect of Repeated Treatment with Neutral Salts and Desaturations on the Base Exchange Capacity

The base exchange capacities (b.e.c.) of K-B$_5$, H-K, and H-P have been calculated from the final inflection point in the titration curves with NaOH before and after several desaturations. The data have been presented in Table IV.

The base exchange capacity of K-B$_5$ diminishes markedly on leaching with BaCl$_2$ solution and desaturations, indicating a decomposition of the bsorption complex. The b.e.c. of H-K remains practically unaltered 'er similar conditions. H-pyrophyllite also undergoes an appreciable

TABLE IV

Variations in the b.e.c. of H-Minerals on Repeated Neutral Salt Treatment and Desaturations

System	Base exchange capacity, milliequivalents/100 g.	Reduction in b.e.c. per cent
K-B$_5$ (original)	104.0	
K-B$_5$ (after one desaturation)	68.0	34.0
K-B$_5$ (after two desaturations)	56.0	45.6
K-B$_5$ (after four desaturations)	30.0	70.8
H-K (original)	8.0	
H-K (after eight desaturations)	8.1	nil
H-P (original)	10.6	
H-P (after five desaturations)	7.5	29.2

decomposition as shown by the reduction in its b.e.c. The results obtained with K-B$_5$ and H-K are thus in agreement with those previously obtained (1–3) with montmorillonitic and kaolinitic clays. X-ray studies with "original" as well as "salt treated and desaturated" K-B$_5$ and H-K lead to the same conclusion. X-ray diagram of the "treated" H-P also suggests a slight decomposition of the absorption complex.

It will appear, therefore, that neutral salt treatments and desaturations bring about a decomposition of the absorption complex in the case of H-montmorillonite and H-pyrophyllite, but H-kaolinite is quite stable under similar conditions. It now becomes important to see whether dissolved silicic acid is present in the neutral salt extract. The results obtained with K-B$_5$, H-P, and H-K are recorded in Table V.

In the case of K-B$_5$, the absorption complex of which suffers the greatest decomposition under neutral salt treatments and desaturations,

TABLE V

Estimation of Dissolved Silicic Acid in the Neutral Salt Extracts
(Data expressed in mg. of SiO_2/100 g. colloid)

System	First desaturation			Second desaturation			Third desaturation
	1st leach	2nd leach	3rd leach	1st leach	2nd leach	3rd leach	1st leach
K-B$_5$	47.5	22.2	nil	9.6	3.9	nil	nil
H-P	2.0	1.2	nil	nil	—	—	—
H-K	nil	—	—	nil	—	—	—

the leachates contain quite an appreciable amount of dissolved silicic acid. After the second desaturation and after the second leachate no silicic acid could be detected in the neutral salt extract. A small amount of silicic acid is obtained in the $BaCl_2$ leach of H-P in the first desaturation. The salt extracts of H-K, which suffers no decomposition under similar conditions, contain no dissolved silicic acid.

The differences in the behavior of H-montmorillonite, H-pyrophyllite, and H-kaolinite recorded in this paper may be attributed, at least in part, to the differences in lattice structure of these minerals. This point will be dealt with by Dr. S. N. Bagchi in another publication.

BIBLIOGRAPHY

1. MUKHERJEE, J. N., CHATTERJEE, B., AND GOSWAMI, P. C., *J. Indian Chem. Soc.* **19**, 405 (1942).
2. MUKHERJEE, J. N., AND CHATTERJEE, B., *Nature* **155**, 268 (1945).
3. MUKHERJEE, J. N., CHATTERJEE, B., AND BANERJEE, B. M., *J. Colloid Sci.* **2**, 247 (1947).
4. WHITT, D. M., AND BAVER, L. D., *J. Am. Soc. Agron.* **29**, 405 (1937).
5. BAGCHI, S. N., Unpublished work.
6. BERG, R., *Z. anal. Chem.* **71**, 369 (1927).

THE SITE OF REACTION IN DIRECT PHOTOGRAPHIC DEVELOPMENT. II.[1] KINETICS OF DEVELOPMENT INITIATED BY GOLD NUCLEI

T. H. James

A brief bathing treatment of certain exposed, positive-type photographic emulsions in an aurous thiocyanate solution will substantially increase the rate of subsequent direct development and the emulsion speed obtained for moderate development (1). The silver of the latent image probably is replaced, at least in part, by gold during the treatment. Such a replacement occurs rapidly when colloidal silver is added to the aurous thiocyanate solution. Moreover, the latent image of the gold-treated emulsion is much more resistant than the normal image to the action of certain oxidizing agents, indicating that the silver has been replaced by gold, or at least plated over by gold. However, the action of the gold definitely does not stop at a simple replacement. If the photographic material is allowed to remain in the gold solution for a prolonged period, a visible gold image appears. This image shows a progressive increase in optical density with increase in exposure and constitutes a "physical development" of the latent-image specks by the gold of the thiocyanate solution. Similar "development" was observed by Homolka (2), and subsequently by Sheppard and Mees (3), when they bathed exposed photographic plates in an auric chloride solution.

The image obtained by prolonged treatment of the exposed material in the aurous thiocyanate solution is composed of roughly spherical gold particles. This is shown by electron micrographs prepared by A. L. Schoen, of these Laboratories. Fig. 1a reproduces an electron micrograph of gold particles obtained by bathing an exposed emulsion for 64 hrs. at 20°C. in a solution prepared by heating to boiling 40 cc. of 0.1% potassium chloraurate with 0.50 g. of KCNS, adding 0.60 g. of KBr, and diluting the whole to 1 liter. The silver halide was removed before the electron micrograph was made. Fig. 1b shows an electron micrograph of an unfixed silver halide grain taken from the image area. A portion of the grain has been printed out by the action of the electron beam, but

[1] James, T. H., Part I, *J. Chem. Phys.* **14**, 536 (1946).

the presence of gold particles is readily seen, both in the area which has printed out and in that which has not.

The gold particles appear to have grown out from the grain surface and to be in contact with the grain surface at only a relatively small area. They differ from the protrusions of print-out silver often observed under the electron microscope in that the latter have thick bases at the grain surface and, indeed, have the general appearance of warts with a larger diameter at the base than at any other part. The prolonged gold treatment thus supplies a method whereby the latent-image nuclei can be built up to far larger than their normal size, but with most of the nuclei material situated well beyond the confines of the silver halide grain surface.
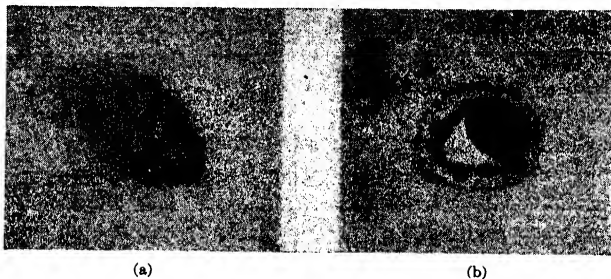
Fig. 1a. Electron micrograph of gold particles. 1b. Electron micrograph of gold particles associated with original silver halide grain. Magnification, $12,500\times$ (Schoen).

The electron micrographs of the gold particles which developed in 64 hrs. indicate a particle size of from 20 to 80 mμ radius. This corresponds to a range of from 1.95×10^6 to 1.25×10^8 gold atoms per particle and a range of 5 to 80×10^3 mμ^2 surface per particle. Direct analysis for gold in the area of highest exposure used in this investigation gave a value of 0.0023 g./100 cm.^{2} film, or approximately 2×10^8 atoms of gold per silver halide grain.[2] Accordingly, it appears that several gold particles on the average are associated with each grain.

Gold analyses were made on film which had remained 18 hrs. and 42 hrs. in the gold solution. The values obtained were 0.00012 and 0.00093 g./100 cm.^{2}, respectively. These figures suggest that the formation of the gold is autocatalytic in nature. However, speculation on the nature of the reaction by which the gold is formed will be reserved until more data are available.

[2] The analysis was carried out by A. Moyse and A. E. Ballard, using the colorimetric method of Sandell [*Anal. Chem.* **20**, 253 (1948)]. The film samples were washed in repeated changes of 10% $Na_2S_2O_3 \cdot 5H_2O$ solution at pH 5.2 to eliminate ionic gold.

The present interest lies in the effect of the gold particles upon the kinetics of development by the usual photographic developing agents. Results have been obtained which have a bearing on the mechanism of the development process, particularly in reference to the "electrode" and "triple-interface" mechanisms (4).

THE INDUCTION PERIOD

The effect of the gold treatment on the induction period of development was investigated, using a simple motion-picture positive-type film and developers which show normally a considerable induction period, *i.e.*, hydroquinone and *p*-hydroxyphenylglycine solutions. The gold solution was prepared as already described. The film was bathed in the solution for the desired time, then washed in running water, and dried before subsequent development. The hydroquinone developer used in the first series of experiments contained no sulfite and was prepared and used in the absence of oxygen (5). The pH was adjusted to 8.72 with a
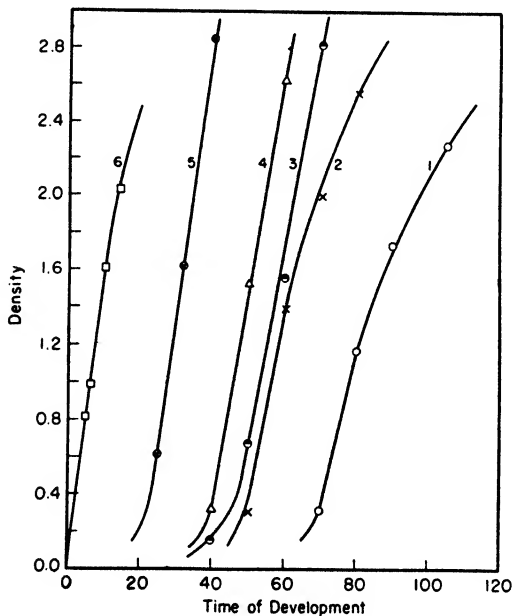
FIG. 2. Effect of duration of gold treatment on development in a sulfite-free hydroquinone solution at pH 8.72. Log E = 1.75; temperature = 20°C. Curve 1 = no gold treatment; Curve 2 = 10 mins'. treatment; Curve 3 = 4 hrs'. treatment; Curve 4 = 16 hrs'. treatment; Curve 5 = 64 hrs'. treatment; Curve 6 = no gold treatment, lauryl pyridinium *p*-toluenesulfonate added to developer.

borax-boric acid buffer, and the solution contained 0.60 g. of KBr/l.
All operations were carried out at 20°C.

Fig. 2 shows density-time of development curves for a constant exposure and different times of gold treatment. The exposure chosen was in the region where previous experiments had indicated that the majority of the exposed grains are following roughly the same course of development, and, hence, the induction period of the density-time of development curve for the entire grain ensemble can be taken as a fair measure of the

TABLE I

Effect of Time of Gold Treatment on the Rate of Development

Developer	Time of Au treatment	$1/t$ (t in min.)	R	$1/Rt$
I. Hydroquinone	0	0.015	0.087	0.171
(no sulfite)	10 min.	.021	.100	.208
	4 hr.	.024	.103	.241
	16 hr.	.026	.115	.229
	64 hr.	.050	.150	.333
Pyridinium compd. added	0	.667	.160	4.17
II. Hydroquinone with sulfite	0	0.50	0.80	0.625
	10 min.	.61	.94	.641
	16 hr.	1.49	1.06	.1.41
Pyridinium compd. added	0	5.88	1.34	4.35
III. *p*-Hydroxyphenylglycine	0	0.282	0.65	0.433
	10 min.	.392	.80	.490
	1 hr.	.476	.90	.529
	4 hr.	.645	1.06	.610
	16 hr.	.714	1.36	.526
	64 hr.	1.11	1.59	.699
Pyridinium compd. added	0	4.00	0.80	5.00

induction period of the typical individual grain (6). It is seen that the gold treatment decreases the induction period but does not eliminate it. This is in contrast to the action of the quaternary lauryl pyridinium salt. Lottermoser and Steudel (7) showed that the induction period in hydroquinone and *p*-hydroxyphenylglycine development was practically eliminated by bathing the exposed film in a solution of this compound before introducing the film into the developer. Under the conditions of the present experiments, addition of 0.3 g. of lauryl pyridinium *p*-toluenesulfonate to the developing solution eliminates the induction period

completely while producing only a relatively small increase in the rate of development beyond the induction period. Curve 6 of Fig. 2 illustrates the action of this agent.

Table I gives some data derived from the curves of Fig. 2, together with similar data for two other developers, a sulfite-free p-hydroxyphenylglycine solution of pH 10.45 containing 0.6 g. of KBr/l. and a sulfite-containing hydroquinone solution of pH 10.30 containing 1.2 g. of KBr/l. The reciprocal of the time, t, required to obtain a density of 0.20 is taken as a measure of the rate of development in the induction period region. The slope, R, of the density-time curve at a density of 0.80, which corresponds to the maximum slope in most cases, is taken as a measure of the rate of development beyond the induction period region. The rate of development, both in the induction period region and beyond, increases with increasing time of gold treatment. The relative increase of the rate in the induction period is larger than that beyond the induction period region, but not greatly so. This is shown by the increase in the reciprocal of the product, Rt, which, however, amounts to only about 2-fold for the maximum time of gold treatment. On the other hand, addition of the pyridinium compound to the developer produces an increase of 8-fold to 25-fold. The pyridinium compound (0.3 g./l.) completely eliminated the induction period for each developer.

DEPENDENCE OF RATE ON HYDROQUINONE CONCENTRATION

The rate of development by hydroquinone varies as a fractional power of the hydroquinone concentration (4). This dependence suggests that the reactive hydroquinone is adsorbed at the silver-silver halide interface. The gold treatment should form a gold-silver halide interface. Accordingly, it was of interest to determine the dependence upon hydroquinone concentration of the rate of development of the gold-treated material.

Table II gives some results obtained with film which had been bathed in the gold solution for 10 mins. or 64 hrs., then developed in a sulfite-free hydroquinone solution of pH 8.72. No bromide was added to the developer. A log-log plot of rate against concentration yields straight lines for both $1/t$ and R rates. The slope of the $1/t$ plot was 0.61–0.63 for the gold-treated film, as compared with 0.60 for untreated film. The slope of the R plot was 0.50 for the gold-treated film, as compared with 0.53 for the untreated film. These variations between treated and untreated film are not considered significant, so that the data give no evidence that the gold treatment affects the relative dependence of rate upon concentration of the hydroquinone.

TABLE II

Dependence of Rate of Development on Hydroquinone Concentration

Time of Au treatment	Hydroquinone concentration	Log E = 1.75		Log E = 0.85	
		$1/t$	R	$1/t$	R
None	0.0125	—	0.090	0.038	0.058
	.0250	—	.130	.055	.082
	.0500	—	.192	.089	.123
	.1000	—	.280	.122	..170
	.2000	—	.397	.156	.270
10 min.	.00625	0.054	.077	.044	.055
	.0125	.091	.101	.071	.087
	.0250	.128	.155	.105	.104
	.0500	.227	.201	.167	.167
	.1000	.323	.240	.238	.193
64 hr.[a]	.00625	.074	—	.068	—
	.0125	.117	—	.105	—
	.0245	.175	—	.159	—
	.0500	.278	—	.232	—
	.1000	.370	—	.323	—

[a] In this series, the image developed by the gold treatment alone had densities of 0.16 and 0.10, respectively, for the two exposures. The t values for the series were taken as 0.15 above the density of the gold image.

DISCUSSION

The developers used in this investigation yield predominantly direct development. Physical development can be of no consequence with the two developers which were free from silver halide solvent and can be of little consequence with the third developer. The experimental results show clearly that the gold treatment increases the rate at which the film will undergo direct development. The increase, however, is not large, and this fact has some implications for the theory of development.

There is no reason to believe at this stage that the gold particles formed by the gold treatment are not firmly attached to the latent-image centers of the grains. The formation of the particles is dependent upon exposure to light and, hence, upon the latent image. The gold particles; indeed, have grown as a "development" of the latent image (without, however, drawing upon the silver halide for development material). The electron micrographs show that the particles are situated at the grain surface. (The particles forming the halo around the grain, as shown in Fig. 1b, are not connected with the gold treatment and are often obtained

in electron micrographs of normal silver halide grains.) The rate of development of the gold-treated samples changes monotonically with changing time of gold treatment beyond the first few minutes, where replacement of silver by gold probably is occurring. Accordingly, the assumption that electrical contact is maintained between the bulk of the gold particle and the latent-image center (gold which has replaced silver plus any residual silver) appears justified.

The bond holding the gold particles to the grain surface may be further strengthened by adsorption forces. Biltz (8) has observed that gold particles from a highly purified sol are adsorbed by silver bromide grains, provided the gelatin has been sufficiently destroyed by enzyme action. However, the gold is not adsorbed by grains which have not been treated to remove gelatin, and purified gold sols added to a normal emulsion before coating do not induce fog on subsequent bathing in a developer, *i.e.*, do not induce development (8, 9).

The present results on the effect of gold particles on the development rate are not in accord with Bagdasar'yan's "electrode" mechanism of development (10), according to which the rate-determining process is the transfer of electrons from the developing agent to the latent-image centers. Bagdasar'yan deduces the rate equation:

$$d\text{Ag}/dt = k[Red][\text{Br}^-]^{-\alpha}S,$$

in which *Red* is the developing agent, α is a constant smaller than unity, and S is the extent of interface between the development center and the solution, *i.e.*, the effective area of latent image or developed silver accessible to the developer. The required dependence of rate upon S is in satisfactory agreement with published data (11) on the rate of development of individual grains. However, from Bagdasar'yan's derivation, it should not matter whether the latent-image speck grows by spread of the interface with the silver halide, as in development, or is built up in the manner accomplished by the gold treatment. The present results show that an increase in the duration of the gold treatment of from 10 mins. to 64 hrs. results in an increase of only 3- to 4-fold in the rate of reaction in the induction period region. The corresponding change in the surface of the gold particles cannot be computed from the data at hand but is obviously much greater than the change in rate. The gold particles were too small to be detected directly even for one hour's treatment in the gold solution.

The data presented in this paper likewise are not in accord with any electrode mechanism which seeks to explain the induction period solely on the basis of electrostatic capacity or mere size of the latent-image centers. Increase in size of the gold particles results in a decrease of the induction period, but a definite induction period remains even after the

64-hr. gold treatment. On the other hand, the induction period of un-treated film is completely eliminated by the addition to the developer of lauryl pyridinium *p*-toluenesulfonate, which depresses the surface charge of the silver halide (7, 12).

There is no disagreement between the present results and the charge-barrier explanation of the induction period (6). The magnitude of the barrier in the immediate vicinity of the metal-silver halide interface is the important factor in this explanation. It is likely that only a relatively small increase in the actual metal-silver halide interface occurs as the gold particles enlarge, and a change in the charge barrier produced by this increase may be very small. Whatever effect such a decrease in charge has on the development rate may be at least partially offset by the physical form of the gold particle which is not such as to make the interface more readily accessible to the developer but may actually exert some shielding action.

The influence of the gold particles on the rate of development prob-ably is exerted only at the start of development of each center. As soon as the center becomes appreciably enlarged, the catalytic action is exerted at the interface between silver halide and newly developed silver, and the nature of the initial center becomes unimportant. The fact that the gold treatment resulted in an increase in measured development rate throughout the entire course of development is not contrary to the pre-ceding statement. The average grain, under the exposure conditions used, contains several latent-image centers and sub-latent-image centers. The gold treatment, as shown previously (1), markedly increases the rate of development in the low-exposure regions and, hence, markedly increases the rate of initiation of development by the smallest latent-image centers. Possibly it causes initiation of development by some sub-latent-image centers. Hence, in the present case, the gold treatment may increase the number of centers from which development is proceeding in each grain. Such action would result in an overall increase in rate of development well beyond the point where the direct action of the gold has ceased.

The gold treatment has not changed the qualitative properties of the metal-silver halide interface so far as indicated by the concentration dependence of the development rate on the developing agent. This is readily understandable if adsorption of the hydroquinone to silver halide is a prerequisite to development, and is not surprising if the adsorption must occur at the interface itself. Accordingly, the data offer no decision between these two possibilities.

SUMMARY

A visible gold image, consisting of roughly spherical particles varying in size up to 80 mμ in radius for the longest times of treatment, was obtained by bathing exposed photographic film in an aurous gold solution. The particles are formed by a "physical development" of the latent-image specks. Electron micrographs show that they are situated at the surface of the silver halide grains.

The gold treatment increases the emulsion speed and the rate of direct development and decreases, but does not eliminate, the induction period in sulfite-free hydroquinone or p-hydroxyphenylglycine developers. The gold treatment does not change the relative dependence of the rate of development upon the hydroquinone concentration.

The relatively small decrease which the gold treatment effects in the induction period is not in accord with Bagdasar'yan's mechanism of development or with electrode mechanisms which seek to explain the induction period on the basis of size and capacity of the development centers.

REFERENCES

1. JAMES, T. H., VANSELOW, W., AND QUIRK, R. F., *PSA Journal* **14**, 349 (1948).
2. HOMOLKA, B., Eder's *Jahrbuch*, pp. 104–5 (1903).
3. SHEPPARD, S. E., AND MEES, C. E. K., Investigations on the Theory of the Photographic Process, p. 266–7. Longmans, Green and Co., London, 1907.
4. *Cf.* JAMES, T. H., *J. Chem. Phys.* **14**, 536 (1946).
5. JAMES, T. H., *J. Phys. Chem.* **43**, 701 (1939).
6. JAMES, T. H., *J. Franklin Inst.* **240**, 83 (1945).
7. LOTTERMOSER, A., AND STEUDEL, R., *Kolloid-Z.* **82**, 319 (1938).
8. BILTZ, M., private communication.
9. CARROLL, B. H., AND HUBBARD, D., *Bur. Standards J. Research* **1**, 565 (1928); CHARRIOU, A., AND VALETTE, S., *Sci. ind. phot.* **6**, 395 (1935).
10. BAGDASAR'YAN, K. S., *J. Phys. Chem. (U.S.S.R.)* **17**, 336 (1943); *Acta Physicochim. U.R.S.S.* **19**, 421 (1944).
11. RABINOVICH, A. J., BOGOYAVLENSKI, A. N., AND ZUEV, Y. S., *ibid.* **16**, 307 (1942).
12. LOTTERMOSER, A., AND STEUDEL, R., *Kolloid-Z.* **83**, 37 (1938).

PHYSICOCHEMICAL PROPERTIES OF KARAYA GUM
AND LOCUST BEAN MUCILAGE

J. V. Kubal[1] and Nils Gralén

From the Swedish Institute for Textile Research, Göteborg, Sweden

Received June 19, 1948

INTRODUCTION

Both substances studied in this work are complex polysaccharides. Karaya gum is the dried exudate from the stem of *Sterculia urens*, a native tree of India. It often has various other names (kadaya, indian, tragacanth, india gum, sterculia gum) and is an important raw material in the textile, cosmetic, food, and other industries.

Locust bean gum or mucilage (there exists no satisfactory classification of plant gums and mucilages and no clear distinction between the two groups of substances) is the dried extract from the seeds of the locust bean. The locust kernel gum is the same substance, but contains less starch and other impurities. It is often designated by other names (carob gum, St. John's bread gum, tragon, tragasol, *etc.*). The locust bean tree, *Ceratonea siliqua*, is cultivated in southern Europe and northern Africa. The pods of this tree are gathered and dried in the sun, and then the seeds are removed by hand or machine. The seeds are ground and the gum extracted by water. It generally comes to the textile industry in powdered form or as a thick solution.

From a physicochemical point of view karaya gum and locust bean mucilage are very similar to each other. Both are typical colloids, macromolecular compounds. They swell in water, form gels and slowly dissolve, giving viscous solutions. Their viscosity increases very rapidly with concentration. Solutions which contain more than 1% flow very slowly; if they contain more than 2% they form opaque pastes; 5% solutions are solid gels. The best way to prepare dilute solutions is as follows: to the solid powdered substance cold water is gradually added while vigorously stirring. After standing for several hours (for higher concentrations overnight) the solutions are heated to boiling. Karaya gum forms only seemingly homogeneous solutions. From each particle there remains an insoluble gelatinous residue, suspended in the solution. These residues can be removed by centrifugation or by filtration through a sintered glass filter. More concentrated solutions of karaya can be prepared in the

shortest time by means of autoclaving, as pressure increases its solubility in water.

Most water-soluble gums and mucilages are polyuronides and thus closely related to pectin, which contains uronic acids (primarily galacturonic acid). However, there are exceptions, and one of them is locust bean mucilage, which contains no acid. The composition of the gums is mostly studied by hydrolysis and identification of the hydrolytic products which are mono- or disaccharides or derivatives of these. Very little is known about the composition of karaya gum. Mantell (1947) noted the chief chemical constituent to be galactan gelose, without giving any closer information about this substance. The solution of karaya gum is acid. Thrun (1935) found that the pH of a 1% solution is 4.6, and remarks that this value becomes higher after 24 hr. and increases up to 5.1 after 76 hr., if determined electrometrically with quinhydrone; the colorimetric estimation with bromocresol shows no change. Thrun explains the divergency by assuming that the gum particles absorb the indicator and are themselves more acid than the solution in which they are suspended, that the quinhydrone value gives the pH of the solution, while the indicator after sufficient time gives the pH of the particles.

Research on the chemical composition of the locust bean gum has shown that it does not contain uronic acid. Gortner and Lew (1943) found that the gum consists of mannose and galactose in the molecular proportion 3:1 or 4:1. Knight and Dowsett (1936) and Williams (1928) give accurate analyses of the mucilage, which differ within a few per cent, and according to them the locust bean contains: galactan (27%), mannan (60%), pentosans (3%), proteins (4%), cellular tissue and small quantities of mineral matter (1–2%).

PREPARATION AND PROPERTIES OF MATERIALS

Karaya gum was obtained in small pieces, some of them quite colorless and clean. They were carefully chosen, ground to a fine powder and used directly for the preparation of solution.

Locust bean kernel gum, from a chemist's shop, was mixed with water (1:25) and left standing for 10 hr. The thick solution was centrifuged to separate insoluble particles and then precipitated with 2 volumes of 96% ethyl alcohol. The precipitated mucilage was dissolved in hot water and reprecipitated. The same procedure was repeated 3 times. The wet precipitate was washed with 96% alcohol, dried at 80°C., and ground to a powder. The pH for a sample of karaya gum in solution examined in the present work was found to be 4.5 (glass electrode). After preparation the solution has an inclination to change its pH to lower values; later (after two days) the pH increases to 4.5 again. Solutions to which traces of toluene have been added are quite stable. The acid reaction of karaya

gum shows that there are free acid groups contained in this substance. These may belong to an uronic acid residue. Further experiments regarding the composition were not made. The solution of locust bean mucilage was found to have a pH of 6.3.

To determine the molecular weights of these substances Svedberg's (1940) ultracentrifuge method has been used. It involves the determination of 3 physicochemical quantities: sedimentation and diffusion constants and partial specific volume.

SEDIMENTATION EXPERIMENTS

Solutions of the gums were subjected to sedimentation experiments in the ultracentrifuge. To reduce charge effects NaCl was added to $0.2N$. The measurements were made at a speed of 800 r.p.s. (corresponding to a centrifugal force of about 170,000 g) with karaya gum. Sedimentation runs with solutions of locust bean mucilage were performed at a speed of 1000 r.p.s. (about 260,000 g). Lamm's (1937) scale method was used for the observations. The scale photographs were taken with mercury light, filter Zeiss monochromat C (436 mμ Hg line) on Kodak Process Plates. The sedimentation constants are given in Svedberg units $(1S = 10^{-13}$ cm./sec. dyne), reduced to 20°C. and pure water by ordinary corrections for the viscosity and the density of the medium.

The sedimentation constants were extrapolated to zero concentration by means of the empirical formula

$$s = \frac{s_o}{1 + kc}$$

(Gralén, 1944), where s_o is the sedimentation constant at $c = 0$, and k is a constant for each substance. By plotting s as a function of the product $s \cdot c$ a straight line is obtained and the extrapolation is performed graphically.

Figs. 1 and 2 show the variation of s_{20} with concentration for both substances.

Investigations of Gralén (1944) on cellulose and other substances with filamentous molecules show that the width B of the sedimentation curve varies approximately linearly with x (distance from the center of rotation). (See also Kinell, 1947.) The derivative $\frac{dB}{dx}$ varies with the total concentration of the solution (cf. Gralén and Lagermalm, 1948). According to this the curve width for free sedimentation can be obtained by plotting $\frac{dB}{dx}$ as ordinate and c as abscissa in a diagram and extrapolating to $c = 0$. B is taken as the quotient between area (A) and height (H) of the sedimentation curve.
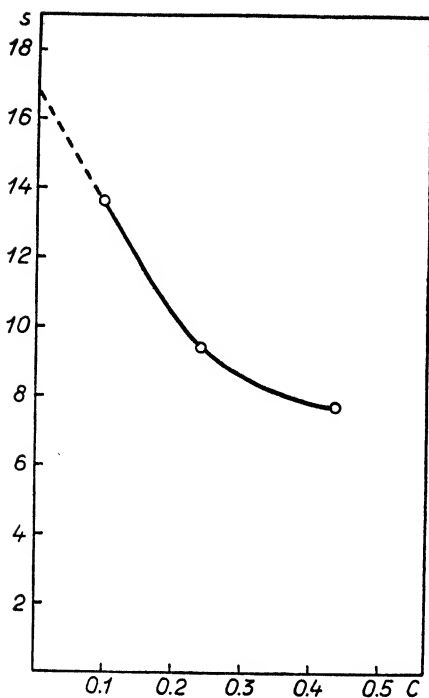
FIG. 1. Variation of s_{20} of karaya gum with concentration.
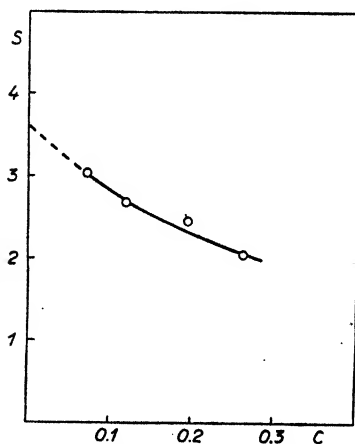
FIG. 2. Variation of s_{20} of locust bean mucilage with concentration.
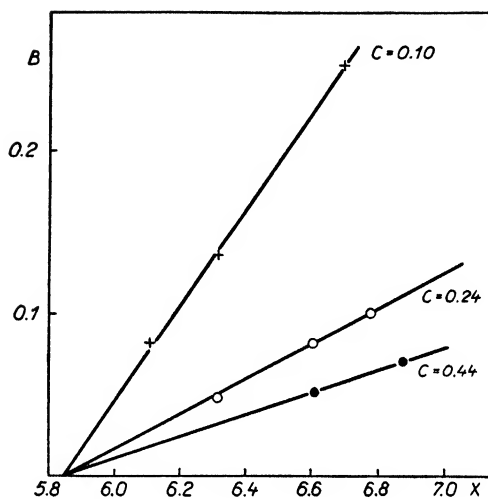
FIG. 3. *B* as a function of *x* for karaya gum.
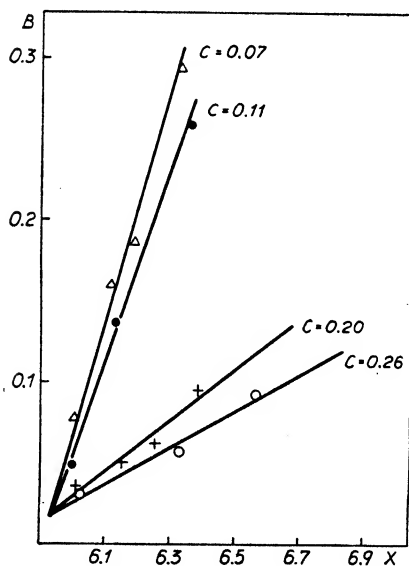
FIG. 4. *B* as a function of *x* for locust bean mucilage.

Figs. 3 and 4 show the linear dependence of B on x and Figs. 5 and 6 give $\dfrac{dB}{dx}$ as a function of c and the graphical extrapolation to $c = 0$. The value $\left(\dfrac{dB}{dx}\right)_{c=0}$ can be taken as a measure of the polydispersity with regard to sedimentation.
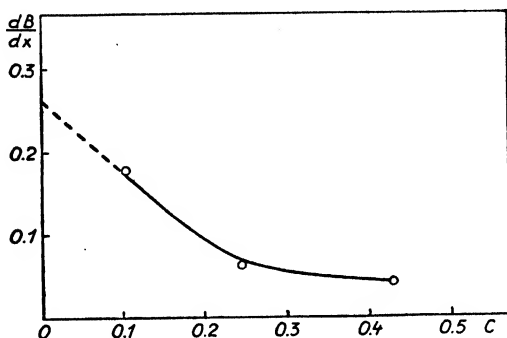
FIG. 5. $\dfrac{dB}{dx}$ as a function of c for karaya gum.
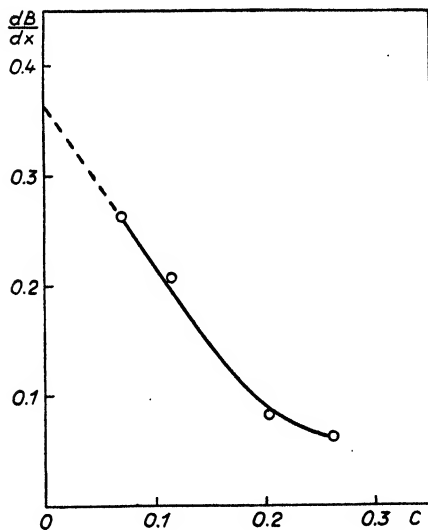
FIG. 6. $\dfrac{dB}{dx}$ as a function of c for locust bean mucilage.

Tables I and II give the results of the sedimentation experiments. From the values of $\left(\dfrac{dB}{dx}\right)_0$ are also calculated the values of the distribution coefficients γ_s, assuming a logarithmic distribution (Gralén, 1944, p. 19). The values of $\left(\dfrac{dB}{dx}\right)_0$ and γ_s indicate a rather small polydispersity. This seems to be a common feature of natural soluble high-molecular products; they have a lower polydispersity than synthetic substances, as pointed out in 1938 by Svedberg and Gralén (1938, *cf*. Gralén and Svedberg, 1940).

TABLE I

Karaya Gum

c (g./100 ml.)	s	$s.c$	$\dfrac{dB}{dx}$
0.44	8.7	3.8	0.05
0.24	10.4	2.5	0.08
0.10	14.6	1.5	0.18
0	17.5	—	0.25
		$k = 2.3$	$\gamma_s = 0.14$

TABLE II

Locust Bean Mucilage

c (g./100 ml.)	s	$s.c$	$\dfrac{dB}{dx}$
0.26	2.1	0.55	0.07
0.20	2.5	0.50	0.08
0.11	2.7	0.30	0.21
0.07	3.0	0.21	0.26
0	3.6	—	0.38
		$k = 2.8$	$\gamma_s = 0.21$

DIFFUSION MEASUREMENTS

The diffusion was studied by the method worked out by Lamm (1937). Lamm's slide cells of stainless steel were used, and two experiments were made simultaneously in one thermostat, the cells being introduced in the light path for observation by a simple arrangement for lateral displacement. The medium was 0.2 N NaCl. The course of the diffusion was followed optically by means of the scale method. The diffusion curves are obtained by plotting the scale line displacement against the scale line position x.

For the calculation of diffusion constants two different formulas were used. The first is Wiener's (1893) "area" method, which gives the value D_A:

$$D_A = \frac{A^2}{4\pi t H^2},$$

where A is the area between the diffusion curve and the x-axis, and H is the maximum ordinate (height) of the curve. The other method (the "moment" method) gives D_m:

$$D_m = \frac{m_2}{2tA},$$

where m_2 is the second moment of the curve around the vertical axis through the arithmetic medium of the curve (original boundary position). The values of D_A and D_m are obtained from several exposures (different times) by plotting of the values of A^2/H^2 and m_2/A in a diagram with t as abscissa. Straight lines through the origin are obtained and the diffusion constants are obtained from the slope of the lines:

$$D_A = \frac{1}{4\pi} \cdot \frac{d\left(\dfrac{A^2}{H^2}\right)}{dt}; \qquad D_m = \frac{1}{2} \cdot \frac{d\left(\dfrac{m_2}{A}\right)}{dt}.$$

The curves obtained are not ideal Gaussian frequency curves. The deviations from the ideal diffusion curve are best studied by plotting the experimental curves from different exposures together with an ideal curve in one diagram with normal coordinates (Lamm, 1937). The calculation of these coordinates are based on the area A and the standard deviation $\sigma = \sqrt{\dfrac{m_2}{A}}$ of each single curve. The experimental values of x and y of the curve are expressed in normal coordinates x_n and y_n by the equations

$$x_n = \frac{x}{\sigma} \qquad \text{and} \qquad y_n = y \cdot \frac{\sigma}{A}.$$

The advantage of this transformation is that the time is eliminated as a parameter. The diffusion curve of karaya gum in normal coordinates is illustrated in Fig. 7. It is seen that the curve is rather skewed, the apex being shifted from the original boundary position toward the solvent. Skew curves indicate dependence of the diffusion constant on concentration. From Boltzmann's (1894) equation

$$D = \frac{1}{2ty} \int_x^\infty xy\,dx$$
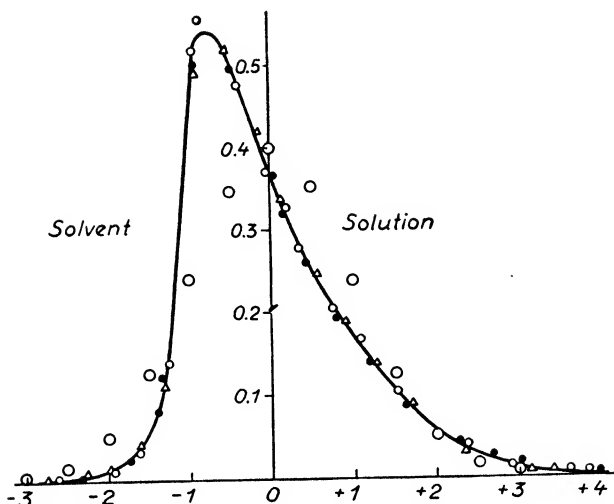
Fig. 7. Skew diffusion curve (in normal coordinates) of karaya gum in the solution of 0.2 N NaCl. The differently marked points are obtained from 3 different exposures, and the large circles indicate the corresponding normal curve.

the diffusion constant at each point of the curve can be derived, *i.e.*, at each concentration up to the total concentration in the experiment. It has been found that the dependence on concentration for high-molecular substances like this is generally linear. If so, the diffusion constant at zero concentration, D_o, can be calculated by the formula (Gralén, 1944, p. 63)

$$D_o = D_m + \frac{A \cdot M_o}{4Ht},$$

where M_o (mode) is the difference between the positions of the maximum ordinate and the original boundary. In general, as here, M_o is negative, and thus $D_o < D_m$.

The diffusion of locust bean mucilage gave symmetrical curves. For both substances, the heights of the experimental curves are higher than those of the corresponding normal curves. This means that D_m is greater than D_A. As D_m and D_A give different averages of the diffusion constants for polydisperse substances, this fact indicates polydispersity, and the ratio D_m/D_A can even be taken as a measure of the polydispersity (Gralén, 1941). The experimental accuracy is not sufficient, however, for any far-reaching conclusions.

The results of the diffusion measurements are given in the following table, where the diffusion constants are given in units of 10^{-7} cm.^{2}/sec.

TABLE III

Substance	D_m	D_A	D_m/D_A	$\dfrac{A\,M_o}{4\,Ht}$	D_o
Karaya gum	0.46	0.27	1.7	0.32	0.14
Locust bean mucilage	0.85	0.49	1.7	—	0.85

The Partial Specific Volume

This quantity was determined pycnometrically according to Kraemer's equation (1940) for binary solutions.

$$V = v\left(1 - \frac{100 - p}{m} \cdot \frac{dm}{dp}\right),$$

where v is the specific volume of the solution, m the weight of the pycnometer content, and p the concentration of the substance in weight per cent.

For both substances under investigation the values of v, p, and m were determined for 3 concentrations. The weights were corrected for buoyancy (Drucker, 1941). The results are contained in Table IV. The function $\Delta m = f(p)$ is linear for both substances. For karaya gum was found $\dfrac{dm}{dp} = 0.123$ and for locust bean mucilage $\dfrac{dm}{dp} = 0.133$. The partial specific volume for karaya gum is 0.68 and for locust bean mucilage 0.66 (see last column of Table IV).

TABLE IV

Substance	p	m	v	V
Karaya gum	0.000	38.7779	1.0017	0.684
	0.040	38.7809	1.0016	0.684
	0.077	38.7866	1.0015	0.684
	0.176	38.8015	1.0011	0.684
Locust bean mucilage	0.000	38.7779	1.0017	0.657
	0.086	38.7879	1.0015	0.661
	0.198	38.8039	1.0010	0.658
	0.467	38.8445	1.0000	0.659

Viscosity Measurements

The viscosities were measured in an Ostwald viscosimeter. The relative viscosities $\eta_r = \eta/\eta_o$ and the quotient $\eta_{sp}/c = \dfrac{\eta - \eta_o}{\eta_o \cdot c}$ are given in the

Tables V and VI and the dependence of η_{sp}/c on concentration is shown in Figs. 8 and 9. The addition of salt (0.2 N NaCl, Fig. 9) reduces the influence of the electrical charge of the molecules. It can certainly be assumed that 0.2 N NaCl is enough to eliminate most of the charge effects. It is striking that the viscosity of karaya gum in 0.2 N NaCl solution is about the same as that of locust bean mucilage, but in pure water

TABLE V

Viscosity of Karaya Gum at 20°C.

	H₂O			0.2 N NaCl	
c (g./100 ml.)	η_r	η_{sp}/c	c (g./100 ml.)	η_r	η_{sp}/c
0.704	37.48	51.8	0.563	12.4	20.2
0.410	16.24	37.2	0.328	4.82	11.7
0.235	7.76	28.8	0.236	3.12	9.0
0.226	6.75	25.5	0.164	2.08	6.6
0.108	3.40	22.2	0.112	1.72	6.5
0.091	2.89	20.8	0.102	1.64	6.2
0.074	2.46	19.8	0.086	1.52	6.1
0.033	1.63	19.1	0.059	1.34	5.7
0.000	1.00	———	0.026	1.14	5.5
			0.000	1.00	5.5

TABLE VI

Viscosity of Locust Bean Mucilage at 20°C.

	H₂O			0.2 N NaCl	
c (g./100 ml.)	η_r	η_{sp}/c	c (g./100 ml.)	η_r	η_{sp}/c
0.467	16.44	33.1	0.390	10.56	24.5
0.300	6.88	19.6	0.373	9.46	22.7
0.220	4.18	14.5	0.312	6.65	18.1
0.198	3.51	12.7	0.240	4.84	16.0
0.132	2.43	10.8	0.176	3.35	13.3
0.086	1.70	8.2	0.158	2.68	10.6
0.042	1.29	7.0	0.107	2.00	9.3
0.000	1.00	—	0.069	1.52	7.5
			0.034	1.24	7.1
			0.000	1.00	5.0

much greater. On the other hand, the sedimentation constant and the molecular weight (see below) of karaya are much greater than those of locust bean.

It is not possible to use Staudinger's equation

$$[\eta] = K_m \cdot D.P.$$

for calculation of degrees of polymerization $(D.P.)$, as the constant K_m is unknown. $[\eta]$ is the intrinsic viscosity, $\lim \left(\dfrac{\ln \eta/\eta_0}{c} \right) = \lim (\eta_{sp}/c)$. By extrapolation from Fig. 9 we get for karaya gum $[\eta] = 5.5$ and for locust bean mucilage $[\eta] = 5.0$.
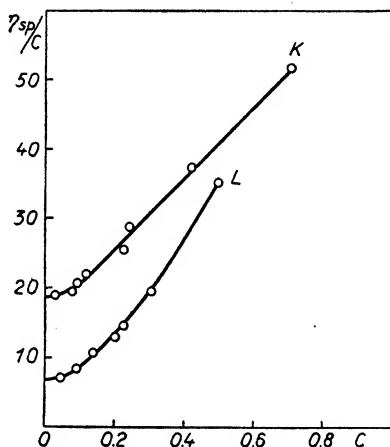
FIG. 8. η_{sp}/c for karaya gum (K) and locust bean mucilage (L) in pure water as a function of concentration.
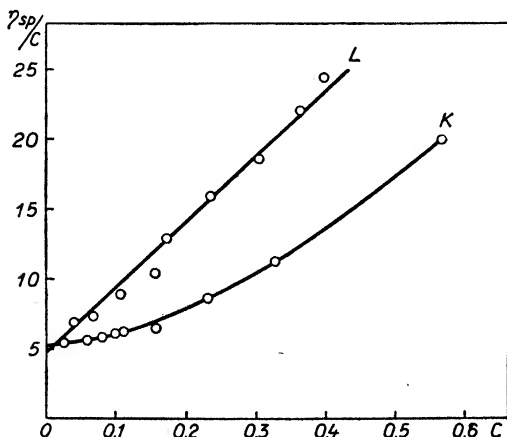
FIG. 9. η_{sp}/c for karaya gum (K) and locust bean mucilage (L) in 0.2 N NaCl as a function of concentration.

Molecular Weights

The molecular weights for macromolecular substances are calculated by introducing the values for s, D, and V into Svedberg's formula

$$M = \frac{\cdot RTs}{D(1 - V\rho)},$$

where R is the gas constant, T the absolute temperature, and ρ the density of the solution. As all measurements refer to the concentration zero and are corrected to pure water at 20°C., the value for ρ was taken as the density of water at 20°C., $\rho = 0.9982$.

The calculation gives:

	M
karaya gum	9,500,000
locust bean mucilage	310,000

The molecular weights calculated from Svedberg's equation can represent different averages, which depend on the way of calculating s and D (Jullander, 1945). The diffusion constant D_o is a weight average (Gralén, 1944), and also the sedimentation constants obtained for karaya gum and locust bean mucilage can be considered as weight averages, because they are calculated from the peak of symmetrical curves. The weight averages are designated as s_w and D_w. The molecular weight obtained is a weight-weight average

$$M_{w,w} = \frac{RT}{1 - V\rho} \cdot \frac{s_w}{D_w}.$$

In general, this is not equal to the weight average (Jullander, 1945)

$$M_w = \frac{\sum c_i \cdot M_i}{\sum c_i}.$$

The Shape of the Molecules

To get an indication of the shape of the molecules the frictional coefficients have been calculated. For spherical, unsolvated particles, the value of the frictional coefficients is, according to Stokes' law,

$$f_o = 6\pi N \left(\frac{3MV}{4\pi N} \right)^{\frac{1}{3}}.$$

The sedimentation and diffusion measurements give the frictional coefficient

$$f = \frac{RT}{D} = \frac{M(1 - V\rho)}{s}.$$

If the ratio f/f_o is greater than unity, it can be concluded that the particles in solution are hydrated or that the particle shape deviates from spherical; both factors naturally may be of influence.

For unhydrated molecules having the shape of oblong ellipsoids with the axial ratio l/d (l = length, d = diameter) Herzog, Illig and Kudar (1933) have derived an equation giving the relation between f/f_o and l/d. From this equation and from the values of the molecular weight and the partial specific volume, it is possible to calculate l and d. Cf. Svedberg and Pedersen (1940) and Gralén (1944).

Table VII gives the results of this calculation for both substances under investigation.

TABLE VII

Substance	f/f_o	l/d	d	l
			(Ångstrom units)	
Karaya gum	2.4	32	86	2750
Locust bean gum	1.24	5	51	255

SUMMARY AND DISCUSSION

Two plant gums, karaya gum and locust bean mucilage, have been the objects of a physicochemical investigation regarding their molecular properties. The following table contains the results obtained.

TABLE VIII

	Karaya gum	Locust bean mucilage
Sedimentation constant at zero concentration, s_o	17.5 S	3.6
Concentration dependence of sed. constant, k_s (c in g./100 cm.³)	2.3	2.8
$(dB/dx)_o$	0.25	0.38
Diffusion constant at zero concentration, D_o	0.14 × 10⁻⁷ cm.²/sec.	0.85
D_m/D_A	1.7	1.7
Partial specific volume	0.68	0.66
Molecular weight from s_o and D_o	9,500,000	310,000
Intrinsic viscosity (c in g./100 cm.³)	5.5	5.0
Frictional ratio f/f_o	2.4	1.24
l/d	32	5
l = length of molecule	2750 Å	255
d = width of molecule	86 Å	51

It is remarkable that the molecular weight of karaya gum is about 30 times greater than that of locust bean mucilage, but the viscosity is about the same for both substances. The high viscosity of locust bean probably also accounts for most of the high dependence of the sedimentation on concentration. Obviously there are big differences in molecular shape and behavior. The frictional ratio assumes a great asymmetry in shape for karaya. However, the frictional ratio may also indicate a higher solvation for karaya than for locust bean. This explanation seems

rather probable, because karaya contains many acid groups, which attract and immobilize large amounts of water, whereas locust bean is neutral. We are, therefore, inclined to lay not too much emphasis on the figures of length and width of the molecules given in the table, but to attribute the difference in the frictional ratios partly to differences in solvation.

Kuhn and Kuhn (1943) have presumed that filamentous molecules can behave as "free-draining molecules," which are completely bathed by the solvent, or as "matted coils," where the solvent is immobilized within the coilings of the molecules. Of course all intermediates are possible. If this theory is applied, the locust bean mucilage is close to free-draining, whereas karaya behaves more as matted coils.

ACKNOWLEDGMENT

REFERENCES

BOLTZMANN, L., *Ann. Physik Chem.* **53**, 959 (1894).

DRUCKER, C., *Arkiv Kemi, Mineral., Geol.* **14A**, No. 15 (1941).

GORTNER, R. A., AND LEW, B. W., *Arch. Biochem.* **1**, 325 (1943).

GRALÉN, N., AND SVEDBERG, T., *Biochem. J.* **34**, 234 (1940).

GRALÉN, N., *Kolloid-Z.* **95**, 188 (1941).

GRALÉN, N., Dissertation, Uppsala, 1944.

GRALÉN, N., AND LAGERMALM, G., Polydispersity of Polystyrene. Festskrift tillägnad J. Arvid Hedvall, p. 215. Göteborg, 1948.

HERZOG, R. O., ILLIG, R., AND KUDAR, H., *Z. physik. Chem.* **167**, A, 329 (1933).

JULLANDER I., *Arkiv Kemi, Mineral. Geol.* **21A**, No. 8 (1945).

KINELL, P. O., *Acta Chem. Scand.* **1**, 355 (1947).

KNIGHT, N. A., AND DOWSETT, M. M., *Pharm. J.* **136**, 35 (1936).

KRAEMER, E. O., The Partial Specific Volume Factor, in Svedberg and Pedersen, The Ultracentrifuge, p. 57. Oxford, 1940.

KUHN, W., AND KUHN, H., *Helv. Chim. Acta* **26**, 1394 (1943).

LAMM, O., Dissertation, Uppsala, 1937.

MANTELL, C. L., The Water Soluble Gums. New York, 1947.

SVEDBERG, T., AND GRALÉN, N., *Nature* **142**, 261 (1938).

SVEDBERG, T., AND PEDERSEN, K. O., The Ultracentrifuge. Oxford, 1940.

THRUN, W. E., *Ind. Eng. Chem.* **27**, 1218 (1935).

WIENER, O., *Ann. Physik Chem.* **49**, 105 (1893).

WILLIAMS, A. L., *Analyst* **53**, 411 (1928).

ON THE COLLOIDAL BEHAVIOR OF SOME
COMPLEX-FORMING SYSTEMS

Arun K. Dey

From the Department of Chemistry, The University, Allahabad, India
Received January 17, 1947

There are many heterogeneous systems, claimed by the colloid chemists as within their jurisdiction, whereas the formation of complex compounds in such cases cannot be denied. The problems of complex and colloid formation have not been fully studied, and in one of the publications from this laboratory, Ghosh and Dhar (1) discussed this problem and tabulated a long list of such systems which show both colloid and complex behavior. They ascribe the colloidal behavior of these systems to the adsorption of ions, which imparts the necessary charge.

During the study of the formation of some complex compounds, I came across certain systems which display colloidal behavior as well. In some publications (2), I have described the studies on the formation of cuprammonium compounds. As early as 1884, Grimaux (3) pointed out the colloidal behavior of a cuprammonia solution. Dhar and coworkers (4) studied the adsorption of alkalis and ammonia by hydrated cupric oxide, and concluded that a part consists of colloidal cupric hydroxide. Similarly Bhatnagar and collaborators (5) have emphasized the role of colloid formation in cuprammonia solutions. They compared the absorption spectra of colloidal cupric hydroxide and that of a cuprammonia solution and found them to be similar. They further support their idea by the absence of any molecularly dispersed cuprammonium ions in the outer liquid when a cuprammonia solution is dialyzed. It has been observed by me (6) that the cuprammonium compounds on dilution undergo hydrolysis, with evolution of ammonia, according to the equation:

$$Cu(NH_3)^{++} + (n + 2)H_2O \rightleftharpoons Cu(OH)_2 + nNH_3 + 2H°.$$
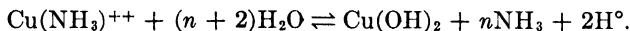
It is thus obvious that hydrolysis of the cuprammonium complex is liable to precipitate cupric hydroxide in the parchment, and thus no cuprammonium ions can pass out of the parchment. Further, I have studied the light absorption of these solutions, and from shifts in the absorption maxima deduce the presence of definite ammino compounds

in the solution. Electrical conductivity results also support complex formation.

During the conductometric study of the formation of cuprammonium complexes, I have observed that, with lower concentrations of ammonia, the electrical conductivity of mixtures with cupric salts remarkably decreases; when further quantities of ammonia are added, the conductivity values increase, and exceed the sum of the conductivities of the constituents. The following tables will make this clear.

TABLE I

Cupric Chloride-Ammonia System

Ratio Cu:NH₃	Percentage difference in conductivity
1:1.00	−16.84
1:1.25	−11.81
1:1.67	+ 0.30
1:2.00	+ 2.53
1:2.38	+ 5.95
1:2.94	+12.51

TABLE II

Cupric Nitrate-Ammonia System

Ratio Cu:NH₃	Percentage difference in conductivity
1:1.00	−11.94
1:1.25	−11.60
1:1.67	−10.57
1:2.00	+ 0.75
1:2.38	+ 8.95
1:2.94	+12.10

A perusal of the above tables shows that with ratios of $Cu:NH_3$ below $1:2$, the conductivities are lower than those of the sums of the conductivities of the constituents. It might be suggested that below this ratio copper is mostly precipitated as hydroxide and is removed from the field of the reaction and hence does not contribute to the conductivity of the mixture. The reaction between a cupric salt and ammonia in solution proceeds according to the equations:

$$CuCl_2 + 2NH_4OH \rightleftharpoons Cu(OH)_2 + 2NH_4Cl,$$
$$Cu(NO_3)_2 + 2NH_4OH \rightleftharpoons Cu(OH)_2 + 2NH_4NO_3.$$
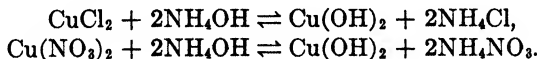
Now, as cupric hydroxide continues precipitating, an equivalent quantity of ammonium chloride or nitrate continues to form. The electrical conductivity of ammonia is very low, and the conductivity of the ammonium salt (chloride or nitrate) is definitely greater than that of the cupric salt (choride or nitrate). Hence, even after precipitation of cupric hydroxide, the conductivity of the mixture should not decrease if the

reaction proceeds only in accordance with the above reactions. It is evident, therefore, that the mechanism of the reaction is not as simple as that suggested by the above equations. It appears that, with the precipitation of cupric hydroxide, ammonium ions are adsorbed by the active surface of freshly precipitated cupric hydroxide and thus the electrical conductivity of the system is diminished. Thus, the particles acquire the necessary charge and display Brownian movement. This occurs in the cases cited in Tables I and II. The conductivity of the mixture is less than that of the sum of the conductivities of the constituents, when the ratio of $Cu:NH_3$ is below 1:2. When this ratio is reached, the conductivity increases and this indicates the beginning of the formation of complex ions. Hence, we can conclude that below this point the system is in the form of a colloid, and further increase in ammonia concentration leads to the formation of complex ammino compounds of different compositions.

Another interesting case is that of the so-called Fehling's solution. A solution of cupric sulphate in tartrate solutions is known to show colloidal behavior, and many metallic salts dissolved in organic acids have been found to exhibit a colloidal nature. Almost no conclusive proof was available to identify complex ions in such solutions. Thus Dumanski and Chalisew (7), Britton and coworkers (8), and Morton (9), regard the phenomenon of dissolution of organic salts of metals in organic acids as that of peptization resulting in the formation of a colloidal solution. But very recently, Bobtelsky and Jordan (10), by an extensive study of cupric and nickel citrates and tartrates, have inferred the formation of complex ions in solution. The method adopted by these workers was physicochemical, and hence is more reliable. I have studied the complex formation between silver citrate and sodium citrate (11) by the solubility method and have obtained similar results.

Stannic hydroxide is known to adsorb many ions, and yield colloidal solutions. Ghosh and coworkers (12), while studying the peptization of stannic hydroxide, observed the formation of complex stannates with ammonia. Also, complex formation has been reported as taking place between stannic tin compounds and carboxylic acids in recent publications (13) from this laboratory. When, however, stannic hydroxide is employed, with the formation of complex ions adsorption also plays a predominant part. The quantitative study of the adsorption has also been made, and it has been noted that, with lower dilutions of oxalic acid, Freundlich's isotherm is obeyed, but increase in the concentration of oxalic acid gives results which are anomalous from this viewpoint. Further, during the electrical conductivity studies of the stannic hydroxide-oxalic acid system, we found that, as in the case of the cuprammines, the electrical conductivity of the mixture was lower than that of the sum of the constituents by as much as 72% with lower concentrations of oxalic

acid, even though the stannic hydroxide dissolves (or disperses) in the oxalic acid. These results naturally show the predominance of adsorption. When the amount of oxalic acid is further increased, the conductivity values increase also. This occurs when the ratio $Sn^{IV}:C_2O_4^-$ has reached the value $1:2.6$. In this case, too, the formation of a colloid is evident prior to the formation of complexes.

The dimension of a precipitate is usually greater than 10^{-5} cm., and that of a colloid particle lies between 10^{-5} and 10^{-7} cm. Now, in the case of an insoluble precipitate, a suitable solvent (solution of a compound forming a complex with the precipitated compound) is added, and solvent action commences, naturally, on the surface of the precipitate. When dissolution has proceeded to such an extent that the size of the precipitate particle has attained the dimensions of a colloid particle, just before undergoing total dissolution the particles will begin to display Brownian movement like the colloid particles. The preferential adsorption on the active surface of the precipitate imparts the necessary charge, and the precipitate passes to the colloidal state. At this stage, the solution is saturated with respect to the precipitate, and the contention of Ghosh (14) regarding the colloidal nature of saturated solutions is justified. All studies of the system, while in this condition, will indicate colloidal nature and the tests for a colloid will be positive. Further addition of the solvent, however, will bring about complete dissolution of the precipitate, and complex ions will form in solution. But it must be pointed out that any generalization is impossible regarding the colloidal behavior of complex compounds in solution. It has been observed that the colloidal behavior is pronounced only in the case of reversible reactions, for example, in those of the copper ammines, copper cyanides, *etc.* It is also essential that the product should be easily hydrolyzed with water; otherwise, formation of the hydroxide sol will not be possible.

Thus, it is evident that the isolation of complex compounds and direct analysis thereof, are liable to include adsorption complexes (in addition to double salts also), and hence cannot be relied upon for the study of complex compounds. It should, therefore, be emphasized that physicochemical methods seem to furnish us with exact information regarding the composition of complex compounds, rather than direct quantitative methods.

It is a pleasure to express my indebtedness to Dr. S. Ghosh for his helpful discussions and advice.

REFERENCES

1. GHOSH AND DHAR, *Z. anorg. Chem.* **152**, 405 (1926).
2. DEY AND BHATTACHARYA, *Current Sci. (India)* **14**, 69, 201 (1945).
   DEY, *Nature* **158**, 95 (1946).

3. GRIMAUX, *Compt. rend.* **87**, 1434 (1884).

4. DHAR and coworkers, *Trans. Faraday Soc.* October, 1920. *J. Phys. Chem.* **27**, 376 (1920); **29**, 1394 (1928); **33**, 316 (1929).

5. BHATNAGAR and coworkers, *Kolloid-Z.* **44**, 79 (1928); *Current Sci. (India)* **14**, 263 (1945).

   BHATNAGAR, Private communication, Sept. 1945.

6. DEY AND BHATTACHARYA, *Proc. Indian Acad. Sci.* **23A**, 259 (1946).

7. DUMANSKI AND CHALISEW, *Kolloid-Z.* **47**, 121 (1929).

8. BRITTON and coworkers, *J. Chem. Soc.* **1926**, 269; **1932**, 96; **1933**, 5.

9. MORTON, *Trans. Faraday Soc.* **28**, 84 (1932).

10. BOBTELSKY AND JORDAN, *J. Am. Chem. Soc.* **67**, 1824 (1945).

11. DEY, Doctoral Thesis, Allahabad, 1946.

12. GHOSH AND SINGH, *Proc. Natl. Acad. Sci. India, Abstracts,* 1943.

13. GHOSH AND JHA, *J. Indian Chem. Soc.* **22**, 270 (1945).

13. DEY AND BHATTACHARYA, *Current Sci. (India)* **14**, 70 (1945).

    DEY, *Univ. Allahabad Studies,* 1946. *Proc. Natl. Acad. Sci. India,* in press.

14. GHOSH, Private communication.

NOTE ON ANION EXCHANGE RESINS. "ACID ADSORPTION" OR "ANION EXCHANGE"?

E. Heymann and I. J. O'Donnell

From the Chemistry Department, University of Melbourne, Melbourne, Australia
Received April 26, 1948

There has been a good deal of discussion (1) as to whether the reactions of anion exchange resins with acids involve an exchange of anions or an "adsorption" of acids. Kunin and R. J. Myers (1) have stated recently that the mechanism is "essentially an exchange of anions." On closer scrutiny, it appears, however, that, as far as aqueous systems are concerned, there is at present no experimental means of distinguishing between the two possibilities, and that, therefore, the discussion is somewhat unprofitable.

Exchange resins of the polyamine type, *e.g.*, Amberlite IR4, may contain primary and secondary amino groups. For the sake of simplicity, we shall consider groups of one type which form part of the permutoid structure of the resin which is swollen when in contact with water. These groups are very weakly basic. In analogy to aniline, we may assume their ionization constant to be no greater than 10^{-9} to 10^{-10}. Thus the equilibrium

$$RNH_2 + H_2O \rightleftarrows RNH_3^+ + OH^- \tag{1}$$
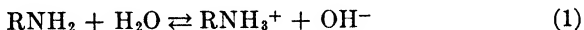
is very much to the left;[1] only one in about 10^5 amino groups will be present as NH_3^+.

When a strong acid, such as hydrochloric acid, is added, we may have

$$\boxed{RNH_3^+ + OH^-} + H_3O^+ + Cl^- \rightleftarrows \boxed{RNH_3^+ + Cl^-} + 2H_2O \tag{2}$$

and

$$RNH_2 + H_3O^+ + Cl^- \rightleftarrows \boxed{RNH_3^+ + Cl^-} + H_2O. \tag{3}$$
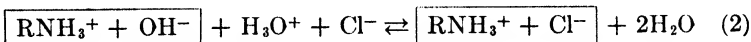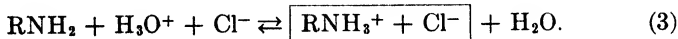
Both equilibria are appreciably to the right because H_3O^+ is a strong acid. Reaction 2 is an anion exchange. Reaction 3 corresponds to what

---

[1] It is because of this very weak dissociation that anion exchange resins—unlike cation exchange resins containing sulfonic acid groups—react with neutral salts only to a slight extent. What has been described as a fundamental difference between the reactions of cation and anion exchangers of the Amberlite type (2) is the difference in behavior between strong acids and weak bases.

some authors call "acid adsorption." This term is unfortunate, since, in the case of strong acids, the reaction merely consists of a proton transfer from H_3O^+ (or a higher hydrate of the proton) to $-NH_2$, the anion being retained in the resin essentially by electrostatic attraction (Bishop, 3). It is highly improbable that "molecular adsorption" of HCl on the resin occurs to an appreciable extent, in view of the fact that aqueous hydrochloric acid is virtually completely dissociated.[2]

When the resin reacts with hydrochloric acid, the equilibrium according to Eq. 1 may be displaced to the right through removal of OH^- and the reaction may proceed as indicated by Eq. 2 through proton transfer from H_3O^+ to OH^-; or else proton transfer may occur directly from H_3O^+ to $-NH_2$ according to Eq. 3. In view of the small initial number of $-NH_3^+$ ions present, it would appear that reaction according to Eq. 3 is very appreciable, unless the rate constant of reaction 3 is much smaller than those of reactions 1 and 2.

We are not aware of any experimental results which allow of an unambiguous distinction between the two possibilities of reaction between a resin and an aqueous solution of a strong acid, just as a similar distinction in the reaction between aniline and aqueous hydrochloric acid is not possible.

Jenny (4) found that, in a suspension of fine resin particles, the pH was higher before than after settling of the particles, and the particles proved to be positively charged in an electrophoresis experiment; moreover, the resin catalyzed the mutarotation of glucose. These observations prove that hydroxyl ions are present in a small concentration, and that, therefore, reactions 1 and 2 occur to some extent, but they do not exclude reaction 3. The observation of Jenny that heat is evolved when the dry resin is brought in contact with water merely shows that the hydration of the hydrophilic groups of the resin is exothermic. Similar effects are found on hydration of macromolecular compounds, the process in many cases not involving ionization.

A distinction between the two possibilities should be easier in systems involving organic solvents. Aniline dissolved in dry ether is reported to react with dry HCl gas. This reaction must be essentially one of direct proton transfer, *viz.*

$$C_6H_5NH_2 + HCl = C_6H_5NH_3Cl,$$
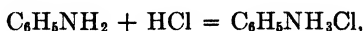
even if traces of water are present, since the amount of reaction 1 would be extremely small in these circumstances. The experimental material on

[2] van der Waals adsorption, in addition to chemical reaction, may be appreciable with weak organic acids.

reactions of polyamine resins with acids dissolved in organic solvents is scarce and admits of various interpretations (5).

We are indebted to A. N. Hambly for stimulating discussions.

REFERENCES

1. KUNIN, R., AND MYERS, R. J., *J. Am. Chem. Soc.* **69**, 2874 (1947); many references to the earlier literature.
2. MYERS, F. J., Colloid Chemistry, ed. Alexander, **6**, 1109 (1946).
3. BISHOP, J. A., *J. Phys. Chem.* **50**, 6 (1946).
4. JENNY, H. J., *J. Colloid Sci.* **1**, 33 (1946).
5. MYERS, F. J., *Ind. Eng. Chem.* **35**, 863 (1943).

Erratum

On page 529, Volume 2, No. 5, Equation (10) should read

$$g_2 = \tfrac{3}{2}\, \frac{na^2}{\langle r^2 \rangle}$$

instead of

$$g_2 = \tfrac{3}{2}\, \frac{'\langle r^2 \rangle}{na^2}$$

THE USE OF METAL MEMBRANES FOR FRACTIONATING HIGH POLYMERS

Jerome L. Rosenberg and Charles O. Beckmann

From the Department of Chemistry, Columbia University, New York, N. Y.
Received June 28, 1948

INTRODUCTION

The use of a diffusion method for the separation of solute molecules in a mixture was suggested by the successful separation of isotopes by gaseous diffusion (1,2). The glass membrane diffusion cell, developed by Northrop and Anson for analytical purposes (3), could, in principle, be used for quantity separations as well. Signer and coworkers (4,5) have recently described the construction of a cascade of such diffusion cells for the efficient separation of solute components by a counter-current process. The diffusion membranes for the cascade were apparently made of a cellulose-type dialysis membrane, and the solute mixture separated consisted of sodium chloride and sodium sulfate.

These methods should be applicable also to large solute molecules. The sensitivity of diffusion coefficient to molecular size was one of the earliest known properties of macromolecules. The combined Einstein-Stokes equation for the diffusion of hard spheres through a viscous medium is:

$$D = \frac{RT}{6\pi\eta r N}. \tag{1}$$

D is the diffusion coefficient;
η is the viscosity of the solvent;
r is the radius of the sphere;
N is Avogadro's number.

In a polymer homologous series, the dependence of the diffusion coefficient on molecular weight may be represented by the equation

$$D = b/M^a. \tag{2}$$

The magnitude of the exponent a is crucial for diffusion fractionation. Hydrodynamic treatments of the behavior of long-chain molecles in solution have been carried out by Simha (6), Kuhn and Kuhn (7), J. J. Hermans (8), Debye and Bueche (9), and Kirkwood and Riseman (9a). These theoretical treatments place upper and lower limits of 1.0 and 0.5

on the value of a. In general, values close to 1.0 are predicted for stiff or stretched out molecules, and values close to 0.5 for flexible or compact molecules. The value of a may vary with the molecular weight within a polymer homologous series, from 1.0 for low molecular weight members to 0.5 for high members.

Table I is a tabulation of a values from data reported in the literature. The values reported in the table are within the predicted range of 0.5 to 1.0. It is therefore reasonable to expect molecular weight fractionation to take place in a diffusion cell.

TABLE I

Experimental Values of a

Polymer system	Reference	a
Cellulose in cuprammonium	Gralén (10)	.55
Cellulose acetate in acetone	Singer (11)	.62
Cellulose acetate in acetone	Polson (12)	.80
Methyl cellulose in water	Polson (12)	.58
Nitrocellulose in acetone	Mosimann (13)	.55
Nitrocellulose in acetone	Gralén (10)	.69
Nitrocellulose in amyl acetate (low M)	Jullander (14)	.77
Nitrocellulose in amyl acetate (high M)	Jullander (14)	.55
Sodium cellulose xanthate	Gralén (10)	.52
Amylose acetate in methyl acetate	Dombrow-Beckmann (15)	.57
Buna-S in carbon tetrachloride	Bevilacqua (16)	.68

EXPERIMENTAL METHODS

The choice of membrane material is of prime importance. Dialysis membranes, such as Signer used (4), have pores which are too small for high polymers. Sintered glass membranes have suitable pore diameters, $5–15\mu$, but are too slow for the fractionation of large molecules. Glass membranes have been used for measuring the diffusion coefficients of large molecules, but the time required for such an experiment is much smaller than the time required for the fractionation of large amounts of material. Metal membranes, which have become increasingly important in chemical technology in recent years, are now manufactured with a wide variety of pore characteristics. Stainless steel membranes, made by the sintering of metal powder, were found to be suitable for diffusion experiments. Thin sheets were made to specifications in thicknesses as low as 0.020 in.[1]

The membrane cell is shown in Fig. 1. It was made of two pieces of brass round stock, fastened together with 5 flange nuts E. The inner diam-

[1] All experiments on membrane diffusion in this research were carried out with the stainless steel material manufactured by the Micro Metallic Corporation, 193 Bradford St., Brooklyn 7, N. Y.

These membranes are available in different grades, with average diameters of 5, 10, 15, or 25 μ. The manufacturer claims for any given grade that the ratio of the largest pore diameter to the smallest is no greater than 4.

eter of the cell was 2″ and the outer diameter was 3″ at the body and 4″ at the flanges. The 2½″ membrane, F, was placed on a ¼″ shelf machined into the cell case. A ¼″ gum rubber gasket, G, provided the seal between the upper compartment, R, and the lower compartment, S, and between the inside of the cell and the thermostat. Nozzles A, B, C, D were soft soldered into the cell. A threaded brass needle valve was attached by a nut to the end of each nozzle. These valves were provided with threaded connections on the outside so that various types of adapters could be fitted to the cell for filling, emptying, evacuating, etc.
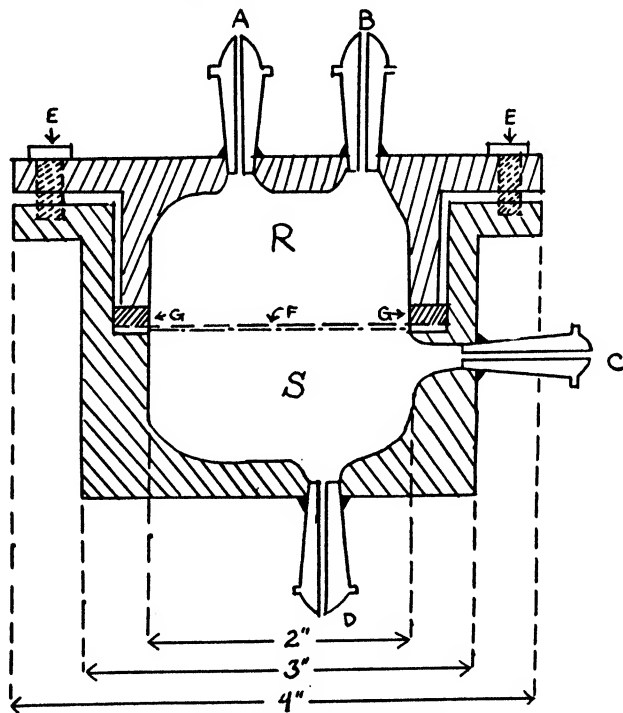
FIG. 1. Metal membrane cell.

The cell had to be tight for several reasons: (1) to prevent inleaking air from forming bubbles at the membrane surface; (2) to prevent diffusion of the thermostat water into the cell; (3) to keep the partial pressure of oxygen and carbon dioxide low and prevent corrosion at the soldered joints; (4) to maintain a sterile atmosphere and prevent the growth of molds in the carbohydrate solutions used in this research. The cell was therefore tested for leaks after each assembly by filling it with 2½ atm. of hydrogen and immersing it in water.

Pore sizes were measured by two methods, the capillary flow method and the surface tension method.

1. Capillary Flow Method

For this method the membrane was assumed to be a bundle of n independent capillaries of uniform radius r and effective length L. According to Poiseuille's Law, a liquid of viscosity η will flow through such a medium under a pressure P with a velocity v cc./sec., where

$$v = \frac{Pr^4\pi n}{8L\eta}.$$

The following substitution was used to eliminate n:

$$\theta = \pi n r^2 L. \tag{3}$$

θ is the free volume of the membrane; and it is calculated from the weight of the membrane, the overall dimensions of the membrane, and the known density of solid stainless steel. Since the capillaries are tortuous and thus longer than the measured thickness of the membrane (l), the effective length (L) is assumed to equal $l\pi/2$, according to Hitchcock (17). Then the equation for calculating the pore size is

$$r = \frac{\pi}{2} l \sqrt{\frac{8\eta v}{P\theta}}. \tag{4}$$

v is the velocity of flow of a liquid, in cc./sec.;
η is the viscosity of the liquid;
P is the driving pressure.

Measurements of the flow rate were made by attaching a long tube of known cross section to valve B (actually to the valve attached to nozzle B in Fig. 1). The tube, which was mounted on a millimeter scale and filled with liquid, was used as the hydrostatic head for forcing liquid through the membrane and out of the cell at valve C. The millimeter scale measured both the driving pressure and the rate of efflux. Water was used as the flow liquid for measuring small porosities and glycerine-water mixtures for large porosities. The viscosities of the glycerine-water mixtures were measured in a Bingham viscometer.

2. Surface Tension Method

This method is based on the well-known relationship between P, the pressure required to force a bubble of gas through a wet capillary, and r, the radius of the capillary (18):

$$P = \frac{2\gamma \cos \phi}{r}, \tag{5}$$

where γ is the surface tension of the liquid in the capillary. Because the contact angle, ϕ, could not be measured, a maximum value of the radius was calculated from the equation:

$$r = \frac{2\gamma}{P}. \qquad (6)$$

The bubble pressure was measured in the diffusion cell as follows. The cell was completely filled with liquid. Valve B (Fig. 1) was connected to a hydrogen tank with an open-end mercury manometer in the line, and valve C was opened to the air. Valves A and D were kept closed. Any positive pressure applied at B would force liquid down from the top compartment of the cell to the exit at C. The bottom compartment, however, remained completely filled with liquid until the pressure was sufficient to force a bubble through the membrane. The bubble pressure (at which a steady emptying of the bottom section began) was measured to 1 mm. of mercury.

Table II lists the pore sizes of a number of membranes determined by one or both of these methods. Discrepancies between the values listed are

TABLE II

Pore Sizes of Steel Membranes

Membrane type	Membrane number	r Capillary flow	r Bubble pressure
G	2	3μ	27μ
G	3		31
FMG	4	4	13
H	6	3	16
G	13		12

due to the fact that the capillary flow measures an average pore size, and the bubble pressure measures the largest pore size. The membranes prepared by sintering have a range of pore sizes, in accordance with the manufacturer's description.

The pore size value was the first criterion of the suitability of a new membrane. Small pores, which might restrict diffusion, were avoided. The minimum requirement for unrestricted diffusion was estimated to be a ratio of 30 between the pore diameter and the maximum molecular dimension. The largest molecular dimension of the solute materials used in this work was estimated by a viscosity method (19) to be 800 Å. Therefore, it was desirable to have a membrane without pores of diameters less than 2 or 3 μ.

To avoid entrapment of air bubbles and prevent mixing of the top and bottom compartments, the following procedure was adopted for filling the

cell. The diffusion cell was filled with an atmosphere of hydrogen. The solvent was placed in a two-necked flask. One neck led to a pressure-vacuum manifold; the other neck led to the diffusion cell through a copper tube attached by means of a rubber ring seal. The solvent was degassed by successively evacuating and flushing with hydrogen. Then a positive hydrogen pressure of 2 or 3 cm. of mercury was applied to force the solvent into the diffusion cell at B (Fig. 1). Valve D was opened to the atmosphere to let the hydrogen escape as the cell filled. The S part of the cell filled completely but a large gas pocket remained in the R compartment. The R compartment was drained at B by a positive hydrogen pressure of 2 cm. applied at A. Solution was then forced into the R compartment at A from another two-necked flask. Either compartment of the cell could be drained without disturbing the other as long as the positive pressure applied was less than the bubble pressure for the largest pore (Eq. 5). Hydrogen was used for these operations because it is the least water-soluble of the common gases, and is chemically inert with respect to the solutes used in these experiments. The amount of mixing across the membrane during the filling operation was found to be insignificant.

The membranes were calibrated by diffusing sucrose solutions of less than 3 g./l. In Gordon's notation (20), the fundamental equation for membrane diffusion is

$$\frac{\Delta c_f}{\Delta c_o} = e^{-\beta D t}. \tag{7}$$

Δc_f is the difference in concentration of the two solutions (above and below the membrane) at time t;

Δc_o is the difference in concentration at the beginning of the experiment ($t = 0$);

β is a geometrical constant of the cell.

$$\beta = \frac{A}{L} \left(\frac{1}{V'} + \frac{1}{V''} \right). \tag{8}$$

V' is the volume of the R compartment;

V'' is the volume of the S compartment;

A is the effective cross sectional area of the pores;

L is the effective average length of a pore.

The diffusion coefficient of the sucrose in water was 53×10^{-7} cm.^{2}/sec. at 25°.[2] Duplicate determinations of β were carried out with an average deviation of 2%, the limit of the analytical method.

[2] McBain and Liu (21) found that the diffusion coefficient of sucrose was 53.5×10^{-7}, using a sintered glass cell calibrated with KCl. The recalculated value, in terms of the accepted D for KCl (20), is 51.6×10^{-7}. A value of 55×10^{-7} was determined in the present research by free diffusion.

Values of β, the cell constant, are listed in Table III. The cell constants for some typical glass cells reported in the literature are also listed for purposes of comparison. The A/L values are also tabulated for each membrane, so that the contributions to β of the membrane and of the cell geometry may be separated. The various membranes have different cross sectional areas. Hence, a specific membrane constant, F/L, is defined as

$$F/L = \frac{A/L}{\pi r^2}, \qquad (9)$$

where r is the gross radius of the membrane. F can be defined as the effective cross sectional area of pores per unit area of membrane. It is apparent from Eq. 7 that large β values are desired to shorten the time of an experiment. The membrane material that makes the greatest contribution to β is the one with the largest value of F/L. The data in Table III show that

TABLE III
Some Membrane Cell Constants

Membrane material	Reference	β cm.$^{-2}$	A/L cm.	F/L cm.$^{-1}$	V' cc.
Metal	This work	2.1	66	2.6	67
Metal	This work	1.4	44	2.0	60
Glass	Northrop and Anson (3)	1	10	.6	20
Glass	Northrop and Anson (3)	1	12	.8	20
Glass	Anson and Northrop (22)	.4	10	.8	50
Glass	McBain and Liu (21)	.2	7	.4	91
Glass	Gordon (20)	.2	10	.5	100
Glass	Scherp (23)	7	32	2	5

the metal membranes are much faster than all but one of the glass membranes. The glass membrane used by Scherp is the one exception. Scherp's cell was so small ($V' = 5$cc.) that it could not be used for quantity separations. The metal cells used in the present work were approximately the same size as the average glass cells reported in the literature. It would be easier to increase the area of a metal membrane than of a glass membrane and still maintain mechanical strength. This could be done by constructing an open metal grill support for the membrane.

Type G discs were selected as the most desirable of the various grades available. The manufacturer rated the average pore diameter as 10μ. The pores of the F discs, rated at 20 μ, were too large and allowed liquid streaming. The H discs available for this work had desirable pore sizes, 5 μ, but the discs were thick and their fractional free volumes small. Both of these facts contributed to a low β, which made the H discs too slow for use.

Standard water-soluble materials of widely different diffusion coefficients were not available to check the calibration of the cells. Neither electrolytes nor buffered protein solutions could be used because they might corrode the cell. A low molecular weight amylopectin, prepared in this laboratory by the acid degradation of starch (25), was used to check all cell calibrations. The sample, LS648-A2, appeared fairly homogeneous in a diffusion experiment carried out in a Tiselius electrophoresis cell (26). Its free diffusion coefficient was 14.4, with no measurable concentration dependence. (All diffusion measurements reported in this paper were made at 25°C. The values are reported in units of 10^{-7} cm.^{2}/sec.) The diffusion coefficient, $D_{2,0}$, was calculated from the experimental data by Eq. 10. The membrane diffusion coefficient was measured by allowing 10–15% of the solute to diffuse into the bottom (S) compartment; and it was found to be 17.9 ± 3%. The results of the separate experiments are tabulated in Table IV.

TABLE IV

Diffusion Coefficient of LS648-A2

Cell	Membrane	$D \times 10^7$
1	G 4	17.9
1	G 11	18.6
2	G 13	18.3
2	G 13	17.3
2	G 13	17.5

The close agreement among the membrane determinations indicates that the measured value is a real one. The discrepancy between this value and the free diffusion value may be ascribed to the presence of some material in the sample which diffuses faster than the average. A fractionation during the diffusion experiment was proved by a molecular weight analysis of the solute remaining on either side of the membrane after the experiment. The molecular weights of the diffused and undiffused fractions were calculated from measurements of the reducing value, R_{Cu}. R_{Cu} is a quantitative measure of the number of reducing end groups in the sample, and is inversely proportional to the number average molecular weight.[3] The results of a typical experiment, in which 15% of the LS648-A2 was transported across the membrane, are listed in Table V. Although the heterogeneity of the working sample is not great enough to show up in the Tiselius cell, it could cause the increased value of the diffusion coefficient in the fractionating cell.

The discrepancy between the diffusion values may also be caused by leaks in the membrane through which bulk liquid could be transferred.

[3] These molecular weight values are usually less, by a factor of 2–4, than the value determined by sedimentation and diffusion because of the heterogeneity of most amylopectin preparations (24). They are useful, however, as relative values of molecular size.

Such a transfer of material by viscous flow, often labeled as streaming in the literature, would be superimposed upon the normal diffusive flow of the molecules. Streaming would be expected from ordinary convection principles in a cell like this, where the denser solution is on top, if the pores were too big or if there were some mechanical shock to permit passage of bulk liquid through the pores. Several precautions were taken to avoid leaks. Rotation of the cell, which increased β (Eq. 8) (27), also introduced streaming. It was found necessary to use a stationary cell mounted firmly in the thermostat. The width of the shelf supporting the membrane within the cell was found to be crucial. Streaming was observed when a $\frac{1}{8}''$ shelf was used. The difficulty was corrected when a $\frac{1}{4}''$ shelf was substituted. A flat grill support of the entire area of the membrane might be desirable for membranes larger than those used in this research.

A solute with an extremely low diffusion coefficient was used to make a sensitive test for streaming. This sample, DDF-3, was obtained by the

TABLE V

Fractionation of LS648-A2

Fraction	Per cent of total	R_{Cu}	M
Original	100	224	3080
Diffusate	15	238	3280
Residue	85	216	2970

alcoholic fractionation of corn amylopectin. Its free diffusion coefficient was 0.65×10^{-7}, as measured in the Tiselius cell. In such a sample, the contribution of streaming to the apparent diffusion coefficient would be large compared with the real diffusion coefficient.[4] Diffusion experiments with this material in the metal cell were used to determine an upper limit to the influence of leakage in all membranes. A limit in K of 1×10^{-7} was considered tolerable for this work. Many steel discs supplied by the manufacturer were discarded because they did not meet this requirement.

RESULTS

A mixture of two homologous amylopectin samples, LS648A-2 and DDF-5, was used to test the experimental procedures of diffusion fractionation. The diffusion coefficients of these samples measured separately in aqueous solution on the membrane cell were 17.9 and 3.1, respectively.

[4] It can be shown that the fundamental flow equation (Eq. 7) still obtains for combined diffusion and streaming, except that the D in that equation becomes an apparent diffusion coefficient. It is equal to the real D plus K, where K is the contribution of the streaming. K is proportional to the velocity of streaming, if this velocity is assumed to be constant, but is independent of the substance diffusing. This treatment is similar to that of Hartley and Runnicles (28).

The total concentration of solute was determined interferometrically since both samples had identical refractive indices. The relative amounts of the two in the mixture were determined by measuring the reducing values, R_{Cu}, of their solutions. In the experiments, summarized in Table VI, the "original" mixture was charged into the top (R) compartment of the membrane cell. After a prediffusion period, during which a steady state was established in the membrane, the bottom solution was replaced with fresh solvent. The material which diffused into the bottom compartment was the "fraction." After a fraction of sufficient size was collected, the bottom solution was again replaced with fresh solvent. The prediffusion stage was omitted and the next stage of fractionation was begun immediately. A small error existed in applying the equations to this procedure,

TABLE VI

Diffusion Fractionation of Mixtures of Amylopectins LS648A-2 and DDF-5
Compositions of the fractions are given in per cent LS648A-2 (based on total solute).
Amounts of the fractions are given in mg. of total solute.

	Fraction	Composition	Amount	*D* of LS648A-2	*D* of DDF-5
		per cent	*mg.*		
	Original	19.5	364	17.9	3.1
Series I	A	46.8	25.7	17.4	4.1
	B	66.9	20.5	24.2	1.9
	C	14.2	317.5		
	Original	54.4	372	17.9	3.1
	A	88.5	31.2	18.4	1.9
	B	79.4	25.7	18.9	3.4
Series II	C	78.9	29.4	18.0	2.8
	D	73.4	35.0	17.2	2.8
	E	31.7	248		

because the boundary condition for the lower surface of the membrane changed suddenly from a finite to zero concentration of solute. As a result, some finite time was again required to reestablish a steady state in the membrane. If the concentrations in the bottom compartment remained close to zero throughout the experiment, the discontinuity could be kept small and the error negligible. This could be done by having a large volume of the lower compartment and by taking fractions that were small compared with the amount of material in the top compartment.

The last fraction tabulated for each series of experiments was the material remaining in the top compartment after all the diffusate fractions were collected. The last two columns list the diffusion coefficients of the separate components calculated from the analysis of each stage of fractionation. The calculations were made for each component by the use of

Eq. 7 on the assumption that each component diffused independently of the other. Except for Fraction B in Series I, these D values agree very well with the measurements on the separate components (tabulated on the "original" lines), despite the accumulated errors in this type of calculation. In this instance, the experiments are satisfactory proof of the independence of the diffusion coefficient of a given substance on the presence of homologous substances. This result, however, cannot lead to a generalization about the behavior of chain-like polymers in solution, because the amylopectin molecules are branched.

In the previous experiments, the distribution function of the working mixture was known and the diffusion experiments were consistent with the known distribution function. These results suggest that diffusion measurements on an unknown sample might yield information about the distribution function, even when sharp fractionation is not possible. For this purpose, it is necessary to combine several kinds of experiments. The first restrictions on the distribution function are set by the average diffusion coefficient measured in the fractionating cell. A measurement of some physical property of each diffusion fraction further restricts the number of possible distributions. In the previous experiments the measured property was the reducing value, or the number average molecular weight. The average diffusion coefficient is another measurable property of the fractions. The advantage of a diffusion measurement is that it avoids the correlation of diffusion coefficient with another property.

A scale method diffusion measurement (29) yields not only the average diffusion coefficient but also a measure of the heterogeneity of the sample. The experimental measurement is the displacement, Z, of a scale line on a photographic plate. The displacement is proportional to the refractive index gradient (and the concentration gradient) in the diffusion cell. When Z is observed as a function of the position x in the diffusion cell, the average diffusion coefficient, $D_{2,0}$, can be evaluated from the second and zero moments of the Z-x curve and the equation,

$$\frac{\int_{-\infty}^{+\infty} x^2 Z \, dx}{\int_{-\infty}^{+\infty} Z \, dx} = 2D_{2,0}t = \sigma^2. \tag{10}$$

t is the elapsed time from the beginning of the diffusion experiment to the time at which the scale lines are observed.

Gralén (30) has shown that $D_{2,0}$ is a weight average diffusion coefficient for systems that are polydisperse.

$$D_{2,0} = \frac{\Sigma c_i D_i}{\Sigma c_i}, \tag{11}$$

where c_i and D_i are the weights and diffusion coefficients of the individual components in a polydisperse sample.

It is advantageous to transform the experimental Z-x data obtained at various times of diffusion to Lamm's normal coordinates. This eliminates time, diffusion coefficient, concentration, and the geometry of the optical system as variables (29). These coordinates are defined as

$$X = \frac{x}{2\sigma} \quad \text{and} \quad Y = \frac{5\sigma\,Z}{\displaystyle\int_{-\infty}^{+\infty} Z\,dx} . \tag{12}$$

The maximum value of Y, denoted by $Y_{max.}$, is a measure of the polydispersity of a solute. By a method similar to that of Gralén (30), it can be shown that $Y_{max.}$ depends on the distribution thusly:

$$Y_{max.} = 2.00\,\frac{\sqrt{\Sigma c_i D_i}\,\Sigma\dfrac{c_i}{\sqrt{D_i}}}{(\Sigma c_i)^{\frac{3}{2}}} \tag{13}$$

$$= 2.00\,\frac{\sqrt{D_{2,0}}\,\Sigma\dfrac{c_i}{\sqrt{D_i}}}{\Sigma c_i} . \tag{14}$$

If the solute is homogeneous, this reduces to

$$Y_{max.} = 2.00. \tag{15}$$

These equations were derived with the assumption that each component in a mixture diffuses independently. An infinite number of distribution functions (set of c_i, D_i values) can be constructed that fit the given experimental values $D_{2,0}$ and $Y_{max.}$. The number of distribution functions can be limited by assembling diffusion data for several samples prepared from a single starting material by fractionation.

A sample of an unknown distribution function was chosen to illustrate these methods. The sample, AD 6.0 168, was prepared by Willis by treating corn amylopectin with 6.0 N sodium hydroxide for 168 hr. at 25°C. (24). Willis showed that alkali causes a degradation of the amylopectin molecule. She observed some material that was smaller in molecular size than the bulk of the sample in those preparations that were most degraded. The sedimentation constant of the small fraction of AD 6.0 168 was 6×10^{-13} and that for the major portion of the sample was 24×10^{-13}. These two peaks in the sedimentation diagram showed up sharply against a very heterogeneous background.

The sample was charged into the diffusion cell and fractions were collected. The results are summarized in Table VII. Fraction I is the residue in the top compartment after all other fractions were collected.

The third column lists the free diffusion coefficent, $D_{2,0}$. The fourth column lists the parameter k_1 which describes the concentration dependence of $D(c)$ according to:

$$D(c) = D(0) [1 + k_1 c]. \tag{16}$$

Reducing values, R_{Cu}, were measured for two of the fractions, but could not be used for an accurate characterization because of their low order of magnitude.

The Y_{max}. values in Table VII are exceptional. They are larger than any previously measured in this laboratory, and show extreme heterogeneity. The range of $D_{2,0}$ values of Fractions B and I is additional evidence for the heterogeneity of AD 6.0 168. It is certain that the original sample contained some material with a D less than 1.56 (Fraction I) and some with a

TABLE VII

Diffusion Fractionation of Amylopectin AD 6.0 168

Fraction	Relative amount	$D(0) \times 10^7$	k_1 (g./100 cc.)$^{-1}$	Y_{max}.	R_{Cu}
	per cent				
Original	100.0	2.4	0.8	3.32	12
A	1.5				
B	9.0	4.7	1.7	3.44	
C	10.5				
D	14.3				
E	6.2				
F	6.2				
G	5.7				
H	4.2				
I	42.2	1.56	1.2	2.94	3

D greater than 4.7 (Fraction B). It is known from the previous history of the sample that all species in the sample have D values between 0.30 and 20. It can be shown that at least 30% of the original has a diffusion coefficient of less than 1.56 by the D and Y_{max}. values of the original material, the known overall limits of D, and the requirements of Eqs. 11 and 14. It can also be shown that at least 7% of the original must have a diffusion coefficient greater than 4.7 from the D of Fraction B, the relative amount of B with respect to the total material, and the requirement of Eq. 7. These minimum percentages were calculated independently of each other. When the two results are combined, at least 50% of the original is found to have a diffusion coefficient less than 1.56 and at least 15% greater than 4.7. The combined calculations further show that the original sample contains some material with a diffusion coefficient less than 0.90 and some greater than 5.7.

TABLE VIII

Calculated Distribution Functions for AD 6.0 168

	D_a	D_b	c_a	c_b
			per cent	*per cent*
Distribution 1	6.81	0.55	26	74
Distribution 2	8.14	0.59	21	79

The original sample was represented by a distribution function containing two sharp peaks. The c_i's and D_i's of the function were selected that best fit the experimental data. Two such distribution functions are listed in Table VIII. In each distribution, the sample is assumed to be composed of just two components, a and b. A comparison is made in Table IX between the experimental data and the results calculated on the basis of the distribution functions of Table VIII. Neither of the calculated functions agrees exactly with experiment, but the discrepancies are not large. No improvement was observed when a third or fourth peak was added to the distribution function.

The following assumptions were made in these calculations. (1) The component species were assumed to diffuse independently of each other. This assumption was probably not too poor for this solvent-solute system. (2) The use of a constant average diffusion coefficient was assumed to be a fair substitute for a detailed treatment of the concentration dependence. This assumption should not lead to serious difficulty since the K_1 values of Eq. 16 were small for the 3 solutions measured. (3) The effect of leakage across the membrane was assumed to be calculable by the method described in footnote 4. Although leakage is small in a single membrane experiment, its effect is multiplied in successive experiments. This error would be small in systems whose D's are well above the leakage limit of the membrane.

In spite of these limitations, the calculated distributions in Table VIII are fair approximations of the true distribution. (The two calculated

TABLE IX

Test of Calculated Distribution Functions

	Original		Fraction B		Fraction I	
	$D(0)_{2,9}$	$Y_{max.}$	$D(0)_{2,9}$	$Y_{max.}$	$D(0)_{2,9}$	$Y_{max.}$
Experimental	2.4	3.32	4.7	3.44	1.56	2.94
Calculated for Distribution 1	2.4	3.32	4.2	3.28	1.23	2.78
Calculated for Distribution 2	2.4	3.32	4.6	3.46	1.13	2.62

distributions do not differ much from each other.) The results agree with the observation of two peaks for this material in the ultracentrifuge. Each of the two components in the calculated function is really polydisperse, but the variation of D within each peak is small compared with the difference between the D's of the two peaks.

APPLICATION TO COMPLETE FRACTIONATION

The goal in the previous experiments was the isolation of two components. The goal in a complete fractionation is the separation of a sample into a larger number of fractions of graded physical properties. The starting point of the calculation is Eq. 7. This equation is assumed to be valid for each solute component. If a stage of the diffusion fractionation begins with zero concentration in the dilute compartment and steady state concentrations in the membrane, Eq. 7 reduces to:

$$c'' = \frac{c_o r}{1 + r}\left(1 - e^{-\beta D t}\right) \tag{17}$$

and

$$c' = \frac{c_o}{1 + r}\left(r + e^{-\beta D t}\right). \tag{18}$$

c'' is the concentration in the bottom solution at time t;
c' is the concentration in the top solution at time t;
c_o is the concentration in the top solution at zero time;

$$r = \frac{V' + V'''/2}{V'' + V'''/2}; \tag{19}$$

V' is the volume of the top solution;
V'' is the volume of the bottom solution;
V''' is the free volume of the membrane pores.

These equations show that a small value of r is required for efficient, as well as fast fractionation. V' is determined by the volume of solution to be fractionated. If V'' is chosen to be 3–10 times V', a reasonable value of r will be obtained, between 0.3 and 0.1. The fractionation efficiencies for a polymer of a known distribution function can be calculated from Eqs. 17 and 18. The known quantities are the β and r of the cell, and the c_o's and D's of the various components. The quantities c' and c'' can be calculated for the separate components from a given value of βt. The correct value of βt for a desired sum of the c'' values (a desired percentage cut in the fraction) can be calculated by successive approximations. The calculation can be applied to a given molecular weight distribution if the dependence of D on M is known.

Calculations were made for a GR–S sample whose distribution function was studied by Scott (31). This sample is a typical flexible chain polymer,

for which the thermodynamic treatment of Scott (32) and of Flory (33) is valid. The function, illustrated in Fig. 2, has a sharp maximum in the low molecular range of the distribution curve and a long flat tail that extends into the large molecular weight range. The efficiency of fractionating the same sample by the thermodynamic precipitation method was also calculated. Ten fractions, equal in weight, were calculated for both methods of fractionation. (In some cases, the last two fractions could not be separated by the diffusion method because of the geometry of the diffusion cell.) In the thermodynamic calculations, the volume of polymer precipitated in a fraction was 0.001 times the total volume in the two phase (Scott's $c = 10^{-3}$). This corresponds to an original solution concentration of about 1% of polymer.
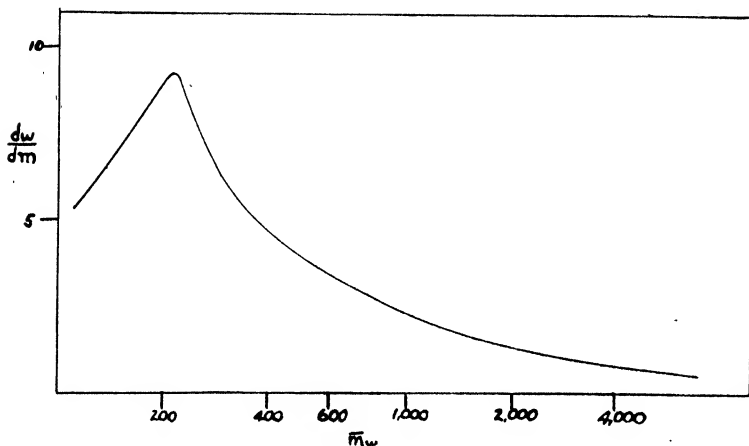
FIG. 2.   Molecular size distribution function of a GR-S.

The calculated fractionations are summarized in Table X. $\overline{m}_w$ is the weight average molecular weight expressed as the number of chain segments.[5] The spread of the $\overline{m}_w$ values in succeeding fractions is a measure of the efficiency of fractionation. The diffusion calculations were carried out for several assumed values of a (Eq. 2) and r (Eq. 19).

The table indicates that the thermodynamic precipitation method is superior, except in the preparation of the highest molecular weight fraction. In the precipitation method, the highest molecular weight fractions are removed first and are the most poorly defined fractions. The thermodynamic extraction method corresponds to the diffusion method in that the lowest molecular weight fractions are removed first and are the most poorly defined. The thermodynamic extraction method is rarely used

[5] The molecular weight is about 100 times the m value in flexible organic polymers.

because of experimental difficulties (31). Hence, thermodynamic calculations were carried out only for the precipitation method. The diffusion method has some of the advantages of the extraction method, *i.e.*, the preparation of well-defined large molecular weight fractions, without some of the experimental disadvantages.

The precipitation method of fractionation becomes less useful for higher molecular weight materials. Scott (32) and Flory (33) have both spoken of the "tail-effect," the contamination of large molecular weight fractions with low molecular weight material. Flory indicated that the "tail-effect" becomes most extreme when the precipitation is carried out at

TABLE X

Calculated Fractionations of a GR-S Sample

Thermodynamic			Diffusion			
Fraction	μ	$10^{-3}m_w$	$a=1$ $r=0.1$	$a=1$ $r=1$	$a=0.5$ $r=1$	Fraction
			$\overline{m}_w$	$\overline{m}_w$	$\overline{m}_w$	
1	.5202	42.9	48.9			10
2	.5215	42.0	39.8	41.4	35.4	9
3	.5237	40.0	33.3	33.8	29.1	8
4	.5271	34.6	27.5	29.2	25.2	7
5	.5330	27.6	22.3	22.9	22.1	6
6	.5434	18.6	17.6	18.4	19.7	5
7	.5632	11.4	13.7	14.6	17.7	4
8	.5864	6.4	10.7	11.6	16.1	3
9	.6252	3.6	8.4	9.2	14.7	2
10	———	1.7	6.9	7.5	13.6	1
Original		22.9	22.9	22.9	22.9	Original

the critical point.[6] This means that extreme dilution is necessary for efficient fractionation of very high molecular weight materials. Detailed calculations showing the effect of increasing molecular weight on the efficiency of fractionation by the precipitation method will be described in a forthcoming publication. The efficiency of fractionation by the diffusion method is practically insensitive to changes in the molecular weight scale, since fractionation by this method depends on the ratio of diffusion coefficients and not on the absolute magnitudes. Diffusion fractionation becomes slightly less efficient with increasing molecular weights because of

[6] The critical point is determined in terms of the concentration of the solution and the μ value (Huggins' μ) (34) of the solvent. In general, μ increases as a precipitating agent is added. The critical μ value is that value below which phase separation cannot take place, however high the concentration of solute. The critical concentration is the concentration necessary for phase separation at the critical value of μ.

the decrease of the exponent value a (Eq. 2). Although the efficiency of fractionation by the diffusion method does not change much with increasing molecular weight, the time required for the experiments will increase. Improvements in the methods of manufacturing metal membranes can be expected to shorten the time for diffusion experiments and compensate for the effect of increasing molecular weights.

To summarize the comparison of the two methods, the thermodynamic precipitation method is superior to the diffusion method for molecular weights to about a million. The diffusion method may have special applications for preparing high molecular weight fractions free of low molecular weight material. Its fractionation efficiency can be extended by the use of continuous flow multiple-unit cells.

The calculations of diffusion fractionation efficiencies were made on the assumption that each component in a solute mixture diffuses independently of the other components. The validity of this assumption can be examined in terms of the general behavior of high polymer mixtures. Onsager and Fuoss (35), in a strictly formal treatment of the diffusion of polycomponent systems, have expressed the diffusive flow of any component as a linear function of the chemical potential gradients of all components:

$$J_i = -\sum_j \Omega_{ij} \frac{d\bar{F}_j}{dx}. \tag{20}$$

$\Omega_{ii} = c_i/f_i$ = concentration divided by frictional coefficient. If $i \neq j$, Ω_{ij} is a generalized coefficient of which a simple physical picture cannot be drawn;

$\bar{F}_j$ is the partial molal free energy;

x is the distance along the concentration gradient;

J_i is flow of material per unit area cross section per unit time.

The number of independent matrix elements, Ω_{ij}, is reduced by certain symmetry conditions. If these matrix elements were all known, the equations for a polycomponent system could be solved. Even in a two-component system, however, there is uncertainty about the term $\Omega_{1,2}$. The experimental tests to secure exact information about the cross terms must be postponed until more precise methods of measurement are developed.

Meanwhile, Onsager's convenient assumption for dilute solutions may be adopted; namely, that only the Ω_{ii} terms need be considered (36). The thermodynamic treatment of high polymer solutions yields information about the free energy gradients, the second factor in Eq. 20. Flory (33) and Scott and Magat (37) have established that the partial molal free energy of one member of a polymer homologous series depends on both the concentration of that particular member and also on the total polymer concentration. They express the partial molal free energies of solution of

the solvent (component $_1$) and of polymer of length m:

$$\Delta \bar{F}_1 = RT \left[\ln v_1 + \left(1 - \frac{1}{\bar{m}_n} \right) (1 - v_1) + \mu (1 - v_1)^2 \right]. \qquad (21)$$

$$\Delta \bar{F}_m = RT \left[\ln v_m + \left(1 - \frac{1}{\bar{m}_n} \right) (1 - v_1) m + \mu m v_1^2 \right]. \qquad (22)$$

$\bar{m}_n$ is the number average chain length.

v is the concentration expressed as a volume fraction.

v_m and v_1 can be chosen as independent variables. Then,

$$\frac{d\bar{F}_m}{dx} = \frac{d\Delta \bar{F}_m}{dx} = \frac{\partial \bar{F}_m}{\partial v_1} \frac{dv_1}{dx} + \frac{\partial \bar{F}_m}{\partial v_m} \frac{dv_m}{dx}$$

$$= RT \left\{ \left[- m \left(1 - \frac{1}{\bar{m}_n} \right) + 2\mu \, mv \right] \frac{dv_1}{dx} + \frac{1}{v_m} \frac{dv_m}{dv_x} \right\}. \qquad (23)$$

If $\left(1 - \frac{1}{\bar{m}_n} \right) \sim 1$; and $v_1 \sim 1$; and since $\frac{dv_1}{dx} = - \frac{dv_2}{dx}$; then

$$\frac{d\bar{F}_m}{dx} = \frac{RT}{v_m} \frac{dv_m}{dx} \left[1 + 2mv_m \left(\tfrac{1}{2} - \mu \right) \frac{\frac{dv_2}{dx}}{\frac{dv_m}{dx}} \right]. \qquad (24)$$

In this equation, v_2 is the total solute concentration. If

$$J_m = - \Omega_m \frac{d\bar{F}_m}{dx} = - \frac{v_m}{f_m} \frac{RT}{v_m} \frac{dv_m}{dx} \left[1 + 2mv_m \left(\tfrac{1}{2} - \mu \right) \frac{\frac{dv_2}{dx}}{\frac{dv_m}{dx}} \right], \qquad (25)$$

then, by reference to Fick's first law of diffusion which defines the diffusion coefficient:

$$J = - D \frac{dc}{dx}; \qquad (26)$$

the diffusion coefficient may be written:

$$D_m = \frac{RT}{f_m} \left[1 + 2mv_m \left(\tfrac{1}{2} - \mu \right) \frac{\frac{dv_2}{dx}}{\frac{dv_m}{dx}} \right]. \qquad (27)$$

The ratio of the coefficient at a finite concentration to its value at infinite

dilution may then be written as:

$$\frac{D_m(c)}{D_m(0)} = \frac{f_m(0)}{f_m(c)}\left[1 + 2mv_m\left(\tfrac{1}{2} - \mu\right)\frac{\dfrac{dv_2}{dx}}{\dfrac{dv_m}{dx}}\right]. \tag{28}$$

For a two-component system this reduces to

$$D_m = \frac{RT}{f_m}\left[1 + 2mv_m\left(\tfrac{1}{2} - \mu\right)\right]. \tag{29}$$

In a previous publication (38), Eq. 29 was the basis for discussing the concentration dependence of D for sharp fractions. The concentration dependence of D was measured directly by free diffusion experiments. The thermodynamic term was evaluated from osmotic pressure data. Thus, f_m could be calculated as a function of concentration by elimination. f_m was shown to increase with increasing concentration for several samples studied in this manner. The assumption that f_m is proportional to the relative viscosity of the solution was found to be valid only to a first approximation. The available data were neither sufficiently exact nor sufficiently comprehensive to formulate an exact law for dependence on viscosity. The conclusion that f_m increases with increasing concentration agrees with the fact that the diffusion coefficients of polymers of low molecular weight do not depend greatly on concentration. This also explains the discrepancy between the experimental and calculated concentration dependence of Jullander's nitrocellulose samples (14). He calculated the concentration dependence from the osmotic term alone, without allowing for the increase of f_m with concentration. His calculated k_1 value (Eq. 16) was in every case greater than his observed value. No quantitative test could be made from his data for the variation of f_m with viscosity because he did not include viscosity values for the same solvent in his paper.

There is no solution for the set of Eq. 28 in the general case of a multicomponent system because of the uncertainty of the concentration dependence of the f_m terms. Two general conclusions can be drawn. (1) The molecular weight sensitivity of D is lowered at increasing concentration, provided that μ is less than 0.5, because the second term in the brackets of Eq. 28 is greater for materials with low values of $D(0)$ and high m. (2) A solvent with a μ value close to 0.5 will avoid the disadvantages of increased concentrations. The only disadvantage of changing the solvent is the accompanied change in a of Eq. 2. For very large molecular weights, however, a is close to its lower limit of 0.5, regardless of the nature of the solvent.

If a solvent cannot be chosen with a μ value of 0.5, the fractionation efficiency may be considerably less than that estimated for infinite dilution, as in the calculations for Table X. When the second term in the brackets in Eq. 28 is large compared with unity, a reversal of the direction of variation of D with M may take place. If the change in frictional coefficient with concentration depends only on the viscosity of the solution, then the hydrodynamic contribution to the concentration dependence of D is the same for all components. The concentration at which the reversal of the D vs. M relationship occurs can be estimated from the thermodynamic term alone. The ratio $\dfrac{dv_2}{dx} \Big/ \dfrac{dv_m}{dx}$ is of the order $\dfrac{v_2}{v_m}$. Then, if a is 0.5, the reversal will take place for $\mu = 0.48$, $m = 10^3$, at $v_2 = 0.025$ (concentration of 2.5%). If a and μ are the same and $m = 10^4$, the point will be at $v_2 = 0.0025$. If each f_m depends on the contribution of just the m-mer to the viscosity of the solution, most of these difficulties will disappear. Each component's hydrodynamic contribution to the concentration dependence will tend to counterbalance the thermodynamic contribution. In this case, the fractionation efficiency at a finite concentration will not differ much from that at infinite dilution. Careful experiments will decide which of these two cases more closely represents the hydrodynamic behavior of polymer mixtures. Neither the high precision diffusion methods nor the sharp fractions, which are necessary for a crucial test, were available in the present research.

SUMMARY

A diffusion cell has been constructed with highly permeable stainless steel membranes. The cell allows more rapid diffusion than previously described glass membrane cells. It is, therfore, suitable for quantity diffusion experiments on large molecules. The method of gaseous diffusion separation has been modified for use in the fractionation of high polymers in solution. Experiments have been performed to demonstrate the partial fractionation of mixtures. A method has been proposed for the construction of size distribution curves by combining data from free diffusion measurements on the fractions obtained by membrane diffusion. Advantages of the diffusion method over the fractional precipitation method are predicted for cases where very large molecular weight fractions free of low molecular weight material are desired.

REFERENCES

1. SMYTH, H. D., Atomic Energy for Military Purposes, **173**. Princeton University Press, 1945.
2. UREY, H. C., *J. Applied Phys.* **12**, 270 (1941).
3. NORTHROP, J. H., AND ANSON, M. L., *J. Gen. Physiol.* **12**, 543 (1928).
4. SIGNER, R., HANNI, H., KOESTLER, W., ROTTENBERG, W., AND VON TAVEL, P., *Helv. Chim. Acta* **29**, 1984 (1946).
5. VON TAVEL, P., *ibid.* **30**, 334 (1947).
6. SIMHA, R., *J. Chem. Phys.* **13**, 188 (1945).
7. KUHN, W., AND KUHN, H., *Helv. Chim. Acta* **26**, 1394 (1943); **30**, 1233 (1947).
8. HERMANS, J. J., *Rec. trav. chim.* **63**, 219 (1944).
9. DEBYE, P., AND BUECHE, A. M., *J. Chem. Phys.* **16**, 573 (1948).
9a. KIRKWOOD, J. G., AND RISEMAN, J., *ibid.* **16**, 565 (1948).
10. GRALÉN, N., Dissertation, Uppsala, 1944.
11. SINGER, S. J., *J. Chem. Phys.* **15**, 341 (1947).
12. POLSON, A., *Kolloid-Z.* **83**, 173 (1938).
13. MOSIMANN, H., *Helv. Chim. Acta* **26**, 61 (1943).
14. JULLANDER, I., *Arkiv Kemi Mineral. Geol.* **21A**, No. 8 (1945).
15. DOMBROW, B. A., AND BECKMANN, C. O., *J. Phys. Colloid Chem.* **51**, 107 (1947).
16. BEVILACQUA, E. M., Dissertation, Univ. Wisconsin, 1944.
17. HITCHCOCK, D. I., *J. Gen. Physiol.* **9**, 755 (1926).
18. BARTELL, F. E., AND OSTERHOF, H. J., *J. Phys. Chem.* **32**, 1553 (1928).
19. FLORY, P. J., *J. Chem. Phys.* **13**, 453 (1945).
20. GORDON, A. R., *Ann. N. Y. Acad. Sci.* **46**, 285 (1945).
21. MCBAIN, J. W., AND LIU, T. H., *J. Am. Chem. Soc.* **53**, 59 (1931).
22. ANSON, M. L., AND NORTHROP, J. H., *J. Gen. Physiol.* **20**, 575 (1937).
23. SCHERP, H. W., *ibid.* **16**, 795 (1933).
24. WILLIS, P. M., Dissertation, Columbia Univ., 1946.
25. HORAN, F. E., Dissertation, Columbia Univ., 1944.
26. TISELIUS, A., *Trans. Faraday Soc.* **33**, 524 (1937).
27. MOUQUIN, H., AND CATHCART, W. H., *J. Am. Chem. Soc.* **57**, 1791 (1935).
28. HARTLEY, G. S., AND RUNNICLES, D. F., *Proc. Roy. Soc. London* **168A**, 401 (1938).
29. LAMM, O., *Nova Acta Regiae Soc. Sci. Upsaliensis IV*, **10**, No. 6 (1937).
30. GRALÉN, N., *Kolloid-Z.* **95**, 188 (1941).
31. SCOTT, R. L., Dissertation, Princeton Univ., 1945.
32. SCOTT, R. L., *J. Chem. Phys.* **13**, 178 (1945).
33. FLORY, P. J., *ibid.* **12**, 425 (1944).
34. HUGGINS, M. L., *Ann. N. Y. Acad. Sci.* **43**, 1 (1942).
35. ONSAGER, L., AND FUOSS, R. M., *J. Phys. Chem.* **51**, 158 (1938).
36. ONSAGER, L., *Ann. N. Y. Acad. Sci.* **46**, 241 (1945).
37. SCOTT, R. L., AND MAGAT, M., *J. Chem. Phys.* **13**, 172 (1945).
38. BECKMANN, C. O., AND ROSENBERG, J. L., *Ann. N. Y. Acad. Sci.* **46**, 329 (1945).

THE ADSORPTION OF HYDROGEN ON NICKEL CATALYSTS.
I. THE EFFECT OF SINTERING

O. Beeck, A. W. Ritchie and A. Wheeler [1]

From the Shell Development Company, Emeryville, Calif.

Received June 30, 1948

INTRODUCTION

Adsorption isobars of hydrogen on nickel have been studied by Benton and White (1), Maxted and Hassid (2), and Iizima (3). In all cases the catalysts were prepared from nickel oxide by reduction with hydrogen, and isobars typical of "activated adsorption" were found. Maximum adsorption was observed in the room temperature region, the slow temperature-dependent adsorption being 2–4 times higher than the initial fast adsorption at liquid air temperature. On supported nickel catalysts Griffin (4) found a somewhat smaller increase. Beeck, Smith and Wheeler (5), in their work on the influence of crystal structure on the rate of ethylene hydrogenation over evaporated metal films, did not observe a large difference in the amount of adsorption of hydrogen on nickel at liquid air and at room temperatures on films which had been deposited at room temperature. Moreover, they found, in contrast to previous studies on reduced oxide catalyst, that the hydrogen adsorption on nickel films was practically instantaneous, both at room and at liquid air temperatures, indicating a very low activation energy. The upper limit of the activation energy was given by the time required to make the first measurement after admitting the gas, and was estimated to be not more than a few hundred cal./mole.

The striking discrepancy between the behavior of reduced nickel oxide and evaporated nickel films has found a ready explanation through more recent experiments[2] which are presented in this paper. Briefly, hydrogen adsorption isobars at 0.1 mm. Hg pressure were measured on evaporated nickel films over the temperature range of $-196°C.$ to $400°C.$ with the main result that the shape of the isobar can be controlled at will by controlling the degree of sintering of the film. Films produced at 23°C. give flat isobars with little increased adsorption between $-196°$ and 23°C., while films sintered at 200–400°C. give isobars similar to those found on

---

[1] Now with E. I. du Pont and Company, Experiment Station, Wilmington, Delaware.
[2] Briefly reported before the Am. Assoc. Advancement Sci. Catalysis Conference at Gibson Island, June, 1946.

nickel catalysts obtained by reduction of the oxide. The results suggest that recent experiments by Taylor and Shou-Chu Liang (6, 7) on the adsorption of hydrogen on zinc oxide may deserve reexamination in the light of these findings.

EXPERIMENTAL

The experimental technique for producing the evaporated metal films has previously been described in detail (5). The films used in these experiments were evaporated onto a glass surface at room temperature and were subsequently heated to the desired sintering temperature. The isobars reported here were measured on films evaporated in high vacuum. A few experiments were also made with oriented films produced in 1 mm. pressure of nitrogen. For details see reference (5).

RESULTS

In Fig. 1 are shown isobars at 0.1 mm. pressure for hydrogen on high vacuum-evaporated nickel films for films presintered in vacuum at room temperature, 200°C, and 400°C. Measurements were started at liquid nitrogen temperature ascending to the temperature of sintering and then
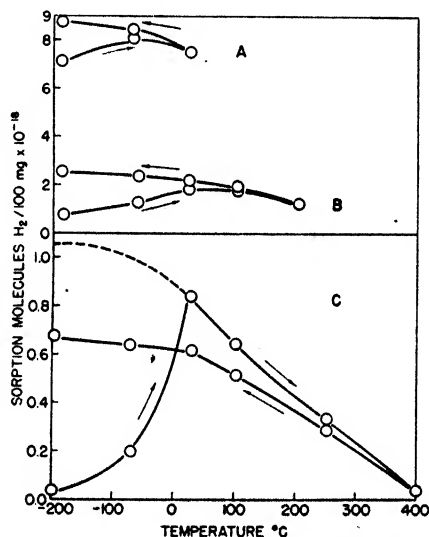
FIG. 1. Sorption isobars of hydrogen at 0.1 mm. Hg pressure on evaporated nickel films presintered at various temperatures. A: Presintered at 23°C.; B: Presintered at 200°C.; C: Presintered at 400°C. (Although this film was presintered in high vacuum at 400°C. for ½ hr., additional sintering apparently occurred on reheating in the presence of hydrogen. The dotted line indicates the curve to be expected with decreasing temperature if no additional sintering had occurred.)

again descending to liquid nitrogen temperature. Curve A shows the hydrogen isobar for a film sintered at 23°C. Starting at −196°C. the adsorption increases as the temperature is raised, and decreases slightly again at room temperature. When the film is cooled back to −196°C., the adsorption increases again slightly. The effect is much more pronounced in films sintered at 200°C., as shown in Curve B. Increasing the temperature from −196° to 200° and decreasing it again to −196°C. shows a final adsorption which is larger by a factor of 3 over the initial adsorption, which was decreased by a factor of 10. The ascending branch of the curve shows a pronounced maximum near 23°C. The points on the ascending branch of the curve are not true equilibrium points. It is, therefore, believed that with longer waiting time this maximum would have occurred at somewhat lower temperature. While, for instance, at −78°C., enough time was allotted to obtain most of the slow adsorption which took place at this temperature, the rate of adsorption became ultimately so slow that it did not seem justifiable to jeopardize the experiment by lengthy waiting. At −196°C. the adsorption is practically instantaneous. On the descending branch of curves, adsorption was found to be fast at all temperatures, and equilibrium was obtained within a few minutes.

It is obvious that we are dealing here with two distinctively different types of "sorption." The word sorption is used advisedly, because we shall show in the following that the slow type of sorption is not "adsorption" in the customary sense of the word. There are several compelling reasons why this slow sorption must be regarded as *ab*sorption or solution into the interior of the structure.

1. It is seen in Fig. 1 that the difference between the adsorption at −196°C., as obtained initially, and the sorption found at −196°C. after obtaining the isobars decreases little with temperature of sintering, while the initial adsorption at −196° decreases rapidly with temperature of sintering, films sintered at 23°C. having about 10 times the adsorption of films sintered at 200°C. and about 175 times the adsorption of films sintered at 400°C. Since the sorption is given in molecules per weight of film, the slow sorption appears to be dependent on the weight of the film rather than on the surface available for fast adsorption. This was also borne out by comparing isobars for metal films evaporated in vacuum and in 1mm. of nitrogen. As was reported previously (5), the films produced in 1 mm. of nitrogen were oriented and had a surface for fast adsorption twice as large as the nonoriented high vacuum films for the same film weight. The small slow adsorption, however, was found to be equal for both films, indicating a weight effect rather than a relation to the fast adsorption.

2. It was already shown previuosly (5) that for oriented and unoriented films sintered at higher temperatures the CO adsorption at room

temperature decreased proportionally to the activity for hydrogenation of ethylene. More recent experiments in these laboratories have shown that the surfaces of films sintered at various temperatures and measured by the Brunauer-Emmett-Teller method using van der Waals' adsorption of krypton at $-196°C$. decrease also proportionally to the decrease in activity for hydrogenation of ethylene at room temperature. Thus, both the relative chemisorption of CO at room temperature and the van der Waals adsorption of krypton are measures for the surface available for hydrogenation of ethylene. The same is true for the fast adsorption of hydrogen at $-196°C$., so that also the relative hydrogen adsorption at $-196°C$. is a direct measure of the surface available for the activity of sintered films. In Fig. 2 data for catalytic activity, CO adsorption at
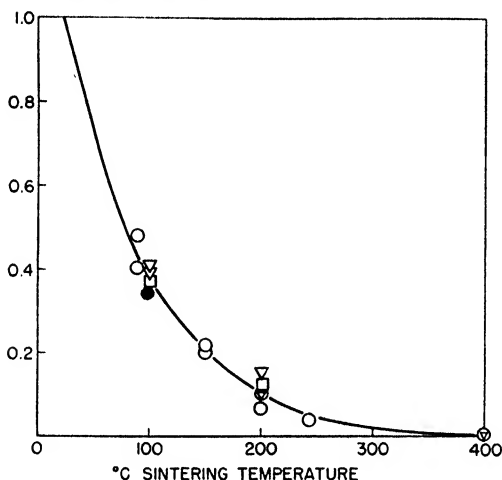
FIG. 2. Correlation of catalytic activity with adsorption and the surface area. (The ordinate represents fraction of respective values obtained for films sintered at 23°C.) ○ Catalytic activity for hydrogenation of ethylene □ Fast CO adsorption at 23°C. ▽ Fast H₂ adsorption at $-196°C$. ● Surface by B.E.T. method using krypton at $-196°C$.

23°C., surface area by the B.E.T. method using krypton at $-196°C$., and the fast hydrogen adsorption at $-196°C$. are plotted against the temperature at which the various films were sintered. All quantities are. taken as unity for films sintered at 23°C.

DISCUSSION

The experiments reported indicate that the previously observed slow "adsorption" of hydrogen on nickel is not adsorption but is "sorption"

of hydrogen into positions inaccessible to CO, Kr, and the fast hydrogen adsorption at −196°C. and also inaccessible to ethylene. While the slow sorption of hydrogen may be due to solution in the crystal lattice, the process is probably more complex since the effect is about 1000 times larger than the reported solution of hydrogen in bulk nickel (8). One may speculate that the effect is due to sorption of hydrogen into the interfaces between the crystallites which form the larger particles of the sintered structure. The hydrogen atoms may be small enough to penetrate into these interfaces, whereas molecules such as ethylene and carbon monoxide are unable to assume these positions. If this latter explanation were right, it would remain to be explained why the interfaces in the agglomerate of crystallites do not increase more rapidly with sintering than the experiments indicate. It is also possible that the reported solubility data may
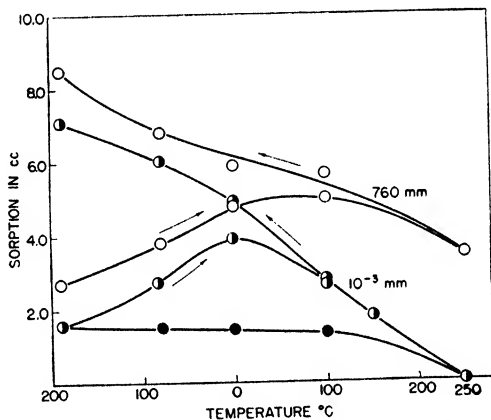
FIG. 3. Sorption isotherms on reduced nickel catalyst plotted from the data of Maxted and Hassid (2). (Catalyst was degassed at 250°C before making measurements). ● H₂ adsorption at 10⁻³ mm. when catalyst was contacted with H₂ at −190°C. and then evacuated prior to raising the temperature.

have been vitiated by sorption of the type reported in these experiments, and it is therefore of little value to speculate further whether the phenomenon is one of true solution or of a pseudo-solution into regions of crystal imperfection.

The hitherto unexplained discrepancy between the behavior of evaporated metal films and nickel catalysts prepared by reduction from the oxide are satisfactorily explained by the present experiments. The earlier work of Maxted and Hassid (2) had as its main objective the measurement of the slow adsorption of hydrogen. Had Maxted and Hassid plotted their data in the form in which we have plotted them in Fig. 3, it

may have become evident much earlier that the "activated adsorption" of hydrogen on nickel is actually a sorption of hydrogen into the interior of the structure. It is seen from Fig. 3 that their results show great similarity to those obtained with sintered evaporated nickel films.

SUMMARY

1. Measurements of isobars for the adsorption of hydrogen at 0.1 mm. pressure on evaporated nickel films sintered at various temperatures show that the ratio of slowly *sorbed* hydrogen to rapidly *ads*orbed hydrogen increases with the sintering temperature of the film.

2. It has been shown that the slow "activated adsorption" of hydrogen on nickel, which has been previously observed by several investigators, is not *adsorption* but is slow *sorption* of hydrogen into the interior of the metal structure.

3. Sites which are occupied by hydrogen which is slowly sorbed into the interior of the metal structure are not accessible to chemisorption of carbon monoxide or van der Waals' adsorption of krypton, nor are they accessible to ethylene.

4. The very fast adsorption (chemisorption) of hydrogen at liquid nitrogen temperature is a true measure of the surface available for chemisorption of CO and for van der Waals' adsorption of krypton and for surface reactions such as the hydrogenation of ethylene.

5. The experiments and conclusions by Taylor and Shou-Chu Liang (6, 7) regarding "The Heterogeneity of Catalytic Surfaces for Chemisorption," parts I and II, may deserve reexamination in the light of the present experiments because of the possibility that their observed slow adsorption is also not *ads*orption but sorption into the crystal structure and thus noncontributing to catalysis.

REFERENCES

1. BENTON, A. F., AND WHITE, T. A., *J. Am. Chem. Soc.* **52**, 2325 (1930).
2. MAXTED, E. B., AND HASSID, N. J., *J. Chem. Soc.* **1932**, 1532.
3. IIZIMA, S., *Rev. Phys. Chem. Japan* **12**, 83 (1938).
4. GRIFFIN, C. W., *J. Am. Chem. Soc.* **61**, 270 (1939).
5. BEECK, O., SMITH, A. E., AND WHEELER, A., *Proc. Roy. Soc. London* **177**, 62 (1940).
6. TAYLOR, H. S., AND SHOU-CHU LIANG, *J. Am. Chem. Soc.* **69**, 1306 (1947).
7. TAYLOR, H. S., AND SHOU-CHU LIANG, *ibid.* **69**, 2989 (1947).
8. ARMBRUSTER, M. H., *ibid.* **65**, 1043 (1943).

THE TEMPERATURE DEPENDENCE OF CONDUCTIVITY AND CRITICAL CONCENTRATION OF TWO TYPICAL COLLOIDAL ELECTROLYTES [1]

A. P. Brady and Harriette Huff

From the Stanford Research Institute, Stanford, Calif.

Received July 12, 1948

INTRODUCTION

The data on a number of physical properties of aqueous solutions of colloidal electrolytes have accumulated during the past few years. Too often, however, these data are obtained at a temperature which happens to be convenient for the particular measurement involved, *e.g.*, osmotic coefficients at 0°C., surface tensions at room temperature and conductivity measurements at room and higher temperatures. It therefore appeared worth while to select two typical but quite different colloidal electrolytes for which a number of types of data are extant, and to study the variation of one property over the complete temperature range of interest. To this end potassium laurate and lauryl sulfonic acid were chosen for study by conductivity measurements from 0°C. to 90°C.

EXPERIMENTAL METHOD

Conductivities were measured at 1000 or 2000 cycles with a Dyke-Jones bridge and an oscilloscope detector. The cells were of Pyrex glass at 0°C. and 25°C.; measurements at higher temperatures were made in Jena glass cells. Platinized platinum electrodes were used throughout. In the experiments at 0°C. and 25°C. the cell constant was determined at both temperatures, and the concentrations of the solutions, which were made up by weight, were calculated from experimentally measured densities. From experience at these temperatures, it was felt to be sufficiently accurate at higher temperatures to neglect any change in cell constant with temperature and to assume the solution densities to be the same as those of water at the same temperatures. Measurements were carried out at 0.00 ± 0.01°C., 25.000 ± 0.005°C., 50.00 ± 0.02°C., 70.00 ± 0.02°C., and 90.0 ± 0.1°C. An oil thermostat was used for all measure-

ments except those at 0°C., in which case crushed ice in a large Dewar flask was found to be satisfactory.

MATERIALS

The lauryl sulfonic acid was from a sample prepared by M. Synerholm. Since this material picks up water very rapidly, the concentration of the stock solution was determined by titration. The potassium laurate solutions, which were from a Kahlbaum preparation of potassium laurate made especially for Professor McBain, were overneutralized with about 4 Eq.-% excess KOH to suppress hydrolysis. In calculating results, the theoretical conductivity of the excess base was subtracted from that observed on the assumption that the two electrolytes are without influence on each other. This introduces no error at concentrations where colloid is fully formed, as shown by McBain and collaborators (1,2,3,). The distortion at intermediate concentrations is much less than that which would result from hydrolysis. It is well known that the presence of added electrolytes will tend to lower the critical concentration for micelles, but if the potassium hydroxide acts as other potassium salts, it can be calculated from the results of Corrin and Harkins (4) that the error so introduced in the critical concentration is only about 1%, which is within experimental error.

The conductivity water was distilled from a Barnstead conductivity still through block tin condensers and had a specific conductivity of less than 10^{-6} mho/cm. at 25°C. In the most dilute solution tested, the water correction was 0.2%, but in other solutions it was negligible.

RESULTS AND DISCUSSION

The conductivity results for lauryl sulfonic acid are given in Table I, and those for potassium laurate in Table II.

Figs. 1 and 2 show a plot of the specific conductivity *vs.* the concentration for lauryl sulfonic acid and for potassium laurate, respectively. As Wright *et al.* (5) have already pointed out, such a plot gives two nearly straight lines of different slope whose intersection may be defined as the critical concentration by conductivity. Similar lines result if the refractive index (6), density (7), and osmotic concentration (8) are plotted against the concentration and serve to define the critical concentrations as determined by these methods. In theory there cannot be a true discontinuity in the slopes since there is no phase change, but in practice enough molecules seem to be involved in the aggregation to make the concept of a critical concentration as a point, rather than a range, a useful one for straight chain colloidal electrolytes of moderately high molecular weight.

TABLE I

Conductivity of Lauryl Sulfonic Acid Solutions at Several Temperatures

Temp.	Conc.	Specific cond.[a] $\times 10^3$	Equiv. cond.
°C.	moles/l.		
0	0.0915	8.22	89.8
	0.0522	5.07	96.9
	0.03673	3.96	107.7
	0.02513	3.19	126.8
	0.01651	2.68	162.0
	0.01191	2.40	201.2
	0.00781	1.745	223.0
	0.00517	1.172	225.9
	0.003383	0.767	226.
25	0.0915	14.00	153.1
	0.0522	8.09	155.1
	0.03673	6.17	168.0
	0.02513	4.83	192.5
	0.01651	3.91	237.
	0.01191	3.43	288.
	0.00781	2.745	351.
	0.00517	1.845	354.
	0.003383	1.210	358.
50	0.0899	19.39	215.7
	0.0470	10.92	232.2
	0.02526	7.14	282.6
	0.01363	5.29	388.
	0.00632	3.11	492.
	0.003100	1.538	496.5
70	0.0595	16.91	284.1
	0.02975	10.34	347.2
	0.01487	7.33	493.
	0.00892	5.09	570.5
	0.00594	3.41	573.
	0.002975	1.728	580.8
90	0.0886	29.53	333.4
	0.0465	18.03	387.9
	0.0458	18.00	393.
	0.02988	13.89	465.
	0.01788	10.79	603.
	0.01422	9.24	649.
	0.00576	3.79	659.
	0.002109	1.414	670.
	0.000705	0.462	678.

[a] Corrected for conductivity of the water.

The critical concentrations by conductivities, which can be read from these Figs. 1 and 2 to about 5%, are given in the second column of Table III and are plotted in Fig. 3. The Table also compares the critical concen-

TABLE II

Conductivity of Potassium Laurate Solutions at Several Temperatures

Temp.	Conc.	Specific cond.[a] $\times 10^3$	Equiv. cond.[b]
°C.	moles/l.		
0	0.3817	9.7	25.4
	0.2014	4.92	24.5
	0.1369	3.46	25.3
	0.0957	2.595	27.1
	0.0894	2.52	28.1
	0.0638	2.030	31.9
	0.0423	1.624	38.3
	0.03925	1.576	40.1
	0.02875	1.224	42.7
	0.01777	0.780	43.9
	0.0113	0.497	44.6
25	0.3817	19.1	50.0
	0.2014	9.67	48.1
	0.1369	6.56	48.0
	0.0957	4.73	49.6
	0.0894	4.54	50.8
	0.0638	3.50	55.0
	0.0423	2.67	63.3
	0.03925	2.62	66.9
	0.02875	2.16	75.7
	0.01777	1.455	82.0
	0.0113	0.932	83.8
50	0.2546	23.22	79.6
	0.1165	10.67	79.9
	0.0697	6.87	87.1
	0.0552	5.78	93.1
	0.03560	4.231	107.3
	0.02416	3.263	123.3
	0.01192	1.735	133.9
	0.00585	0.866	136.8
70	0.1233	15.17	108.8
	0.0617	8.55	124.6
	0.03701	5.98	147.3
	0.02470	4.47	166.8
	0.01233	2.343	175.8
	0.00493	0.958	180.0
90	0.0978	16.34	150.0
	0.0489	9.68	181.2
	0.03914	8.18	192.1
	0.02642	6.02	210.9
	0.01957	4.66	221.3
	0.00978	2.234	211.5

[a] Corrected for conductivity of the water.
[b] Further corrected for conductivity of excess KOH.

trations obtained here with those obtained from dye spectra (9,10), refractive index (6), osmotic coefficient (11,12,13,14), and surface tension (15). It may be seen that, on the whole, the different methods agree approximately within their respective limits of experimental error. The notable exception to this is the refractive index results for potassium
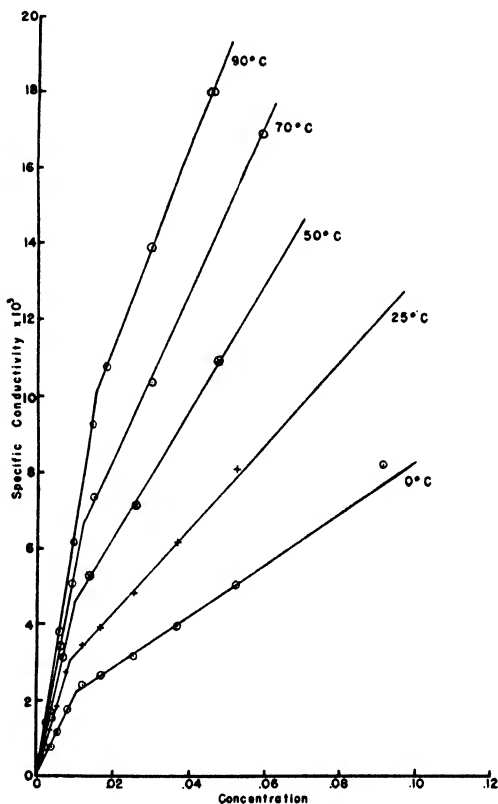
FIG. 1. Specific conductivity *vs.* concentration of lauryl sulfonic acid.

laurate above room temperature (6), from which a much higher critical concentration is reported than that obtained by the other methods. Kolthoff and Stricks (20) have determined the critical concentration of potassium laurate from dye solubilization at 30°C. and 50°C., and find little change with temperature in this region.

The unexpected aspect of the conductivity results is the decrease in critical concentration as the temperature is raised from 0°C. to room temperature—this decrease is slight for lauryl sulfonic acid, but quite
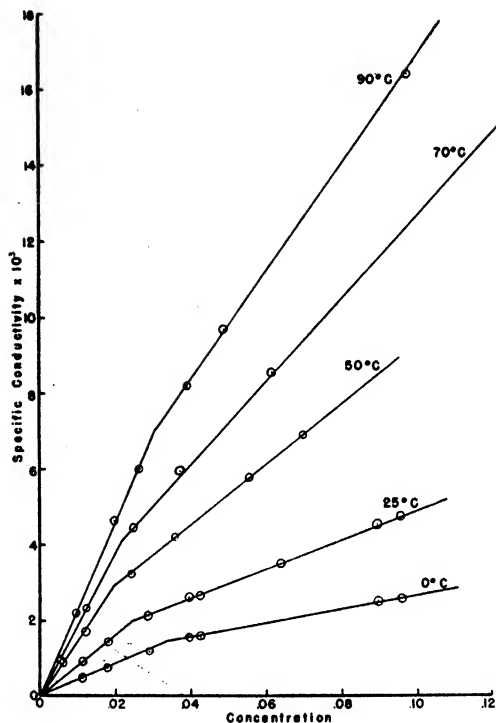
FIG. 2. Specific conductivity *vs.* contentration of potassium laurate.

FIG. 3. Critical concentration *vs.* temperature for lauryl sulfonic acid and
potassium laurate.

TABLE III

Potassium Laurate—Critical Concentration $\times 10^2$

Temp.	Conductivity	Dye spectra	Refractive index	Osmotic coefficient
°C.				
0	3.5	——	——	3.5
25	2.4	2.15–2.35	2.55	2.0–2.7
50	2.0	2.07[a]	3.27	2.0–2.5
70	2.2	——	>4.20	——
90	3.1	——	——	——

[a] Interpolated.

Lauryl Sulfonic Acid—Critical Concentration $\times 10^2$

Temp.	Conductivity	Dye spectra	Surface tension	Osmotic coefficient
°C.				
0	1.00	0.95	——	1.05
25	0.85	0.75	0.79	——
50	0.95	——	——	——
70	1.20	——	——	——
90	1.55	——	——	——
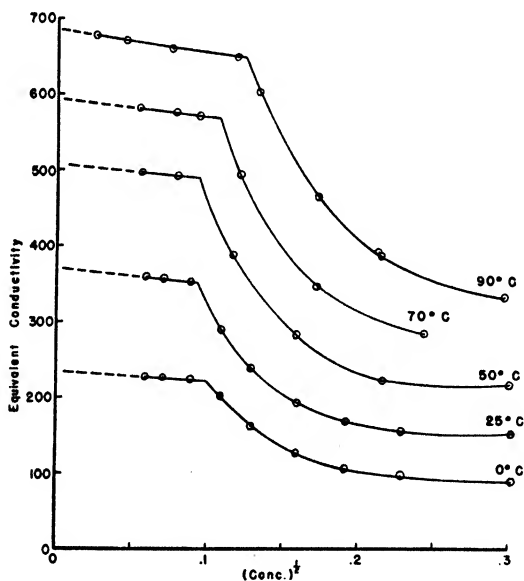
Fig. 4. Equivalent conductivity *vs.* the square root of the concentration for lauryl sulfonic acid.

pronounced for potassium laurate. Above 50°C. the critical concentration of both colloidal electrolytes increases with temperature in a manner to be expected from results with other similar compounds in the same temperature region (5,17,18).

Figs. 4 and 5 give the conductivity results for lauryl sulfonic acid and potassium laurate in terms of the usual plot of equivalent conductivity against the square root of the concentration. At all temperatures the curves are typical for straight chain salts of moderate molecular weight in that the equivalent conductivity in dilute solutions approximates that of an ordinary uni-univalent electrolyte until the critical concentration is reached, whereupon the equivalent conductivity falls rapidly with increasing concentration. The actual locations of the breaks were taken from Figs. 1 and 2. The data permit reasonable estimates of the conduc-
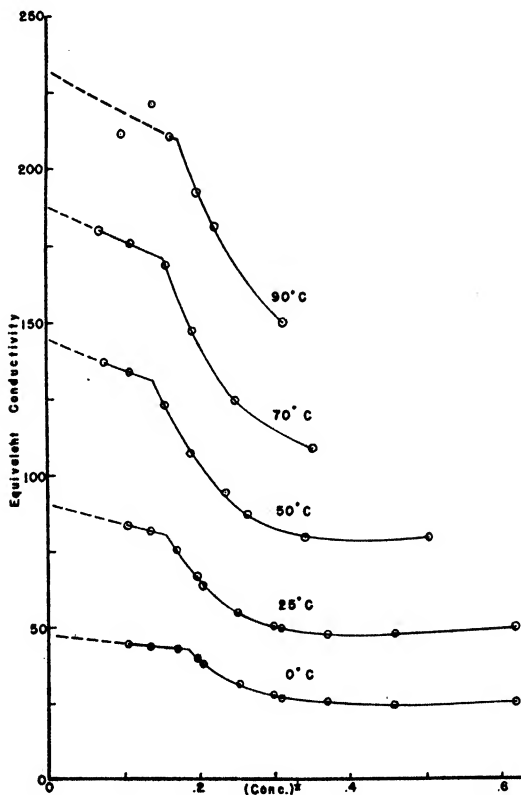
FIG. 5. Equivalent conductivity vs. the square root of the concentration for potassium laurate.
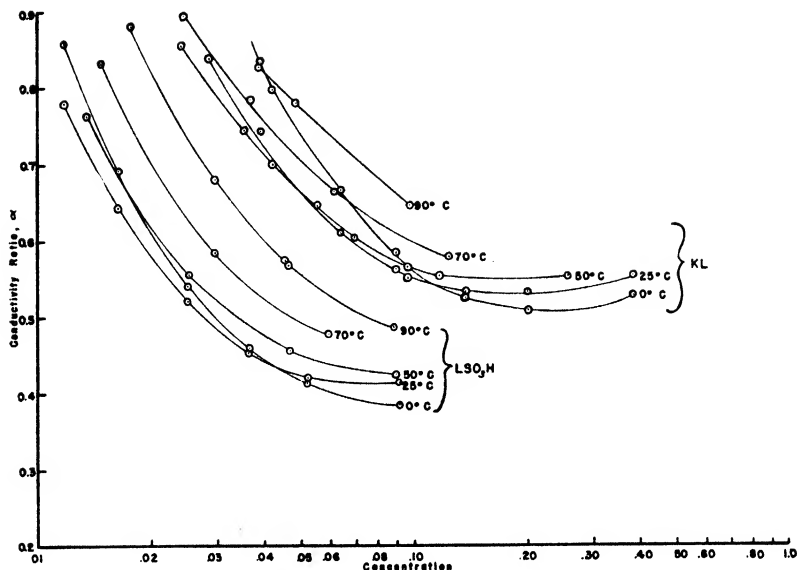
FIG. 6. Conductivity ratio, α, vs. log concentration for lauryl sulfonic acid and potassium laurate.

tivity at infinite dilution, except in the case of potassium laurate at 90°C., where, because of scattering of the points, the line below the critical concentration was simply drawn with the theoretical slope. Taking the mobility of potassium ion at infinite dilution as 40.4, 73.6, 114.8, 150 and 186.4 at 0°, 25°, 50°, 70°, and 90°C., respectively; that of the laurate ion is 8 at 0°, 19 at 25°, 30 at 50°, 39 at 70° and 46 at 90°.

It is instructive to examine the variation of α, the ratio of the equivalent conductivity at a given concentration to that at infinite dilution, with concentration and with temperature. Below the critical concentration, α shows only the minor variations to be expected from the influence of temperature on Debye-Hückel-Onsager effects. A plot of α vs. the logarithm of the concentration is given in Fig. 6 for concentrations above the critical. The logarithmic type of plot was chosen because, at a given value of α, the slope is a rough measure of the rate of agglomeration with increase of concentration as may be seen from the equation:

$$\frac{d\,\alpha}{d\ln c} = \frac{d\,L}{\Lambda_0 dc} - \alpha,$$

where L denotes the specific conductivity at concentration c, and Λ_0 is the equivalent conductivity at infinite dilution. From Fig. 6 the following general trends may be noted: (a) the relative decrease in conductivity is

greater for lauryl sulfonic acid than for potassium laurate. (b) Despite the previously noted complicated dependence of the critical concentration on temperature, at concentrations where colloid is fully formed (approximately 10 times the critical) the value of α increases in a regular manner with temperature. This is in accord with the results from vapor pressure measurements of potassium laurate solutions from 35 to 105°C., made by O'Connor (19) at the Stanford laboratories. (c) As reflected in the initial slopes of the curves, the rate of colloid formation with increase in concentration does not change rapidly with temperature, but there appears to be a slight decrease in the absolute value of the slope as the temperature is increased.

SUMMARY

1. Conductivity curves for aqueous solutions of two colloidal electrolytes, lauryl sulfonic acid and potassium laurate, were determined at 0°, 25°, 50°, 70°, and 90°C.

2. The critical concentrations, as determined by conductivity, pass through a minimum in the neighborhood of room temperature. A comparison of the critical concentrations determined here with those determined by other methods shows approximate agreement with all except those reported for refractive index of potassium laurate at elevated temperatures.

3. The variation of the conductivity ratio, α, with temperature is briefly discussed.

REFERENCES

1. McBAIN, J. W., AND SEARLES, J., *J. Phys. Chem.* **40**, 493 (1936).
2. QUICK, W. C., *J. Chem. Soc.* **127**, 1401 (1925).
3. McBAIN, J. W., AND BETZ, M., *J. Am. Chem. Soc.* **57**, 1909 (1935).
4. CORRIN, M. L., AND HARKINS, W. D., *ibid.* **69**, 683 (1947).
5. WRIGHT, K. A., ABBOTT, A. D., SIVERTZ, V., AND TARTAR, H. V., *ibid.* **61**, 549 (1939).
6. KLEVENS, H. B., *J. Colloid Sci.* **2**, 301 (1946).
7. WRIGHT, K. A., AND TARTAR, H. V., *J. Am. Chem. Soc.* **61**, 544 (1939).
8. BRADY, A. P., AND SALLEY, D. J., *ibid.* **70**, 914 (1948).
9. KLEVENS, H. B., *J. Phys. Colloid Chem.* **51**, 480 (1946).
10. WALTON, H. F., *J. Am. Chem. Soc.* **69**, 469 (1947).
11. BRADY, A. P., Thesis, Stanford University, 1944.
12. McBAIN, J. W., AND BOLDUAN, O. E. A., *J. Phys. Chem.* **47**, 94 (1943).
13. McBAIN, J. W., DYE, W. B., AND JOHNSTON, S. A., *J. Am. Chem. Soc.* **61**, 3210 (1939).
14. FINEMAN, M. N., AND McBAIN, J. W., *J. Phys. Colloid Chem.* **52**, 881 (1948).
15. BRADY, A. P., presented at Colloid Symposium, Cambridge, Mass. (1948).
16. McBAIN, J. W., *Advances in Colloid Sci.* **1**, 132 (1942).
17. LOTTERMOSER, A., AND PÜSCHEL, F., *Kolloid-Z.* **63**, 175 (1933).
18. RALSTON, A. W., HOERR, C. W., AND HOFFMAN, E. J., *J. Am. Chem. Soc.* **63**, 2576 (1941).
19. O'CONNOR, J. J., Thesis, Stanford University, 1948.
20. KOLTHOFF, I. M., AND STRICKS, W., *J. Phys. Colloid Chem.* **52**, 915 (1948).

MIXED ADSORBED FILMS AT OIL-WATER INTERFACES

Eric Hutchinson[1]

From the Department of Chemistry, Stanford University, Calif.
Received July 21, 1948

INTRODUCTION

In a recent paper on the effects of interfacial adsorbed films on the rate of diffusion of molecules across an oil-water interface (6) it was postulated that the role of the film was not merely that of a sieve, but rather that it imposed an energy barrier on the diffusing molecule due to the interaction of the diffusing molecule with the film molecules. This appeared to be borne out by the observed large effect of the shape and nature of the diffusing molecule on the rate of diffusion through the film. At that time no information was available as to the number of molecules, either of the film material or of the diffusing molecules in the film at any time.

Previous work (7,8) has shown that the number of molecules in the film may be calculated in the case of only one solute in the solution. The present paper describes the determination of the number of molecules in the interfacial film composed of more than one solute component, *i.e.,* a case essentially similar to that encountered in the diffusion experiments.

The experiments described here consisted of placing a solution of *n*-octyl alcohol in benzene in contact with a solution of sodium dodecyl sulfate in water and studying the interfacial tension of the system as a function of the concentrations of the two solutes. In the previous work (6) sodium cetyl sulfate was used to form the interfacial film, but there were some doubts as to its purity. For quantitative investigation, it was clearly desirable to use a sample of sodium dodecyl sulfate, the high purity of which was fairly well established by experiment. *n*-Octyl alcohol was used since its behavior at a benzene-water interface, in the absence of a solute in the aqueous phase, was known, and freezing point data of its solutions in benzene were available (7).

EXPERIMENTAL

Measurements of the interfacial tensions were made by means of the sessile "bubble" method (2,3,7) described in earlier papers and no further

description will be given here. The apparatus was not thermostated, but the laboratory temperature during the experiments remained in the region of $23° \pm 1°C$. The densities of the solutions of alcohol in benzene were known from earlier unpublished work, and the densities of the dilute solutions of sodium dodecyl sulfate were taken as being the same as that of pure water. Experiments were carried out using both distilled water and conductivity water to prepare the aqueous solutions, and no significant difference could be observed. Attempts to check the results by means of the drop-volume method (5) failed, owing to the poor reproducibility of the method for this system. This may be ascribed to the aging which occurs during the first 20–30 min. from the beginning of the experiment.

RESULTS

Interfacial tensions are recorded in Table I for solutions of n-octyl alcohol in benzene against a number of aqueous solutions of sodium dodecyl sulfate. In Fig. 1 the interfacial tension is shown as a function of the freezing point depression θ of the benzene solutions, and in Fig. 2 as a function of the mean mole fraction of the sodium dodecyl sulfate.
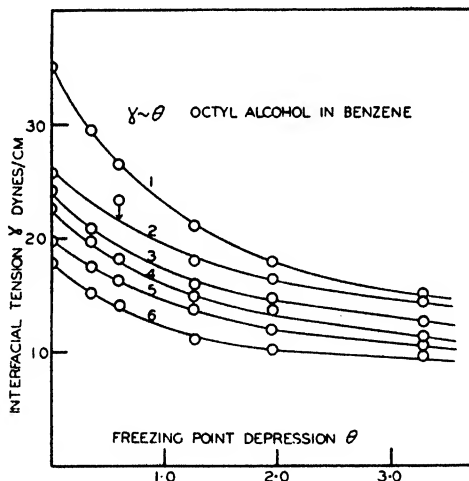
FIG. 1. Interfacial tension of solutions of octyl alcohol in benzene against aqueous solutions of sodium dodecyl sulfate as a function of the freezing point depression of the solution. Curve 1. Octyl alcohol vs. water. Curve 2. Octyl alcohol vs. $1.0 \times 10^{-4} M$ sodium dodecyl sulfate. Curve 3. Octyl alcohol vs. $2.5 \times 10^{-4} M$ sodium dodecyl sulfate. Curve 3. Octyl alcohol vs. water $5.0 \times 10^{-4} M$ sodium dodecyl sulfate. Curve 5. Octyl alcohol vs. $7.5 \times 10^{-4} M$ sodium dodecyl sulfate. Curve 6. Octyl alcohol vs. $10.0 \times 10^{-4} M$ sodium dodecyl sulfate.
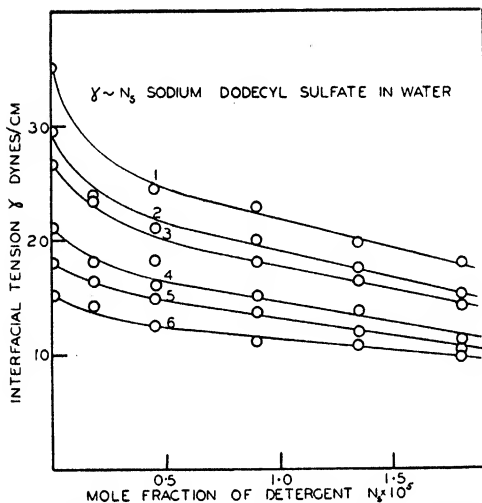
FIG. 2. Interfacial tension of solutions of sodium dodecyl sulfate against solutions of octyl alcohol in benzene as a function of the mean mole fraction of the detergent N_s. Curve 1. Sodium dodecyl sulfate *vs.* benzene. Curve 2. Sodium dodecyl sulfate *vs.* 0.075 M octyl alcohol solution. Curve 3. Sodium dodecyl sulfate *vs.* 0.142 M octyl alcohol solution. Curve 4. Sodium dodecyl sulfate *vs.* 0.315 M octyl alcohol solution. Curve 5. Sodium dodecyl sulfate *vs.* 0.63 M octyl alcohol solution. Curve 6. Sodium dodecyl sulfate *vs.* 1.26 M octyl alcohol solution.
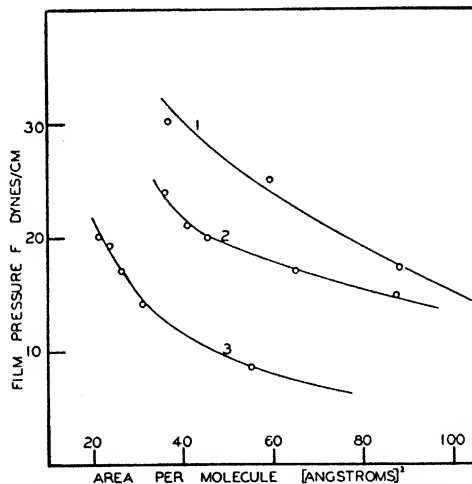
FIG. 3. Force-area curves of films adsorbed at a benzene water interface. Curve 1. Sodium dodecyl sulfate alone. Curve 2. A mixed film containing both octyl alcohol and sodium dodecyl sulfate. Data taken from section D of Table I. Curve 3. Octyl alcohol alone.

Included in Table I are the respective surface excesses of the alcohol and the detergent calculated as described below.

DISCUSSION

The surface excesses of the various components of the system may be calculated as follows.[2] The system benzene + octyl alcohol || water + sodium dodecyl sulfate may be regarded as approximating to a particular example of the generalized system.

Phase$^\alpha$ (κ^α components) || Phase$^\beta$ (κ^β components), in which α and β are mutually insoluble phases, and all the κ^α, κ^β are volume components, there being no components which are purely surface components. (In

TABLE I

Interfacial Tension of Solutions of Octyl Alcohol in Benzene against Aqueous Solutions of Sodium Dodecyl Sulfate

	Moles alc./ liter	Moles NaLS^a/ liter	Dynes/cm.		G.-mol. $\times 10^{-10}$/cm^2.			Å^2 Area
			γ	F	$\Gamma_2{}^{\alpha b}$	$\Gamma_2{}^{\beta c}$	Γ	
A	1.26	—	15.1	20.0	0	7.52	7.52	21.5
	0.63	—	18.0	17.1	0	6.24	6.24	26.4
	0.315	—	21.1	14.0	0	5.30	5.30	31.1
	0.142	—	26.5	8.6	0	3.04	3.04	55.0
	0.073	—	29.5	5.6	0	2.12	2.12	78.0
	0	—	35.1	—	0	0	—	—
B	1.26	1×10^{-4}	14.4	20.7	0.23	4.58	4.81	34.2
	0.63		16.4	18.7	0.27	4.71	4.98	33.2
	0.315		18.0	17.1	0.35	3.28	3.63	45.5
	0.142		23.4	11.7	0.47	1.80	2.27	72.8
	0.073		23.5	11.6	0.53	1.15	1.68	98.5
	0		25.1	10.0	0.66	0	0.66	250.0
C	1.26	2.5×10^{-4}	12.5	22.6	0.32	4.35	4.67	35.3
	0.63		14.9	20.2	0.32	3.91	4.23	39.0
	0.315		15.9	19.2	0.45	3.02	3.47	47.6
	0.142		18.1	17.0	0.65	1.38	2.03	81.2
	0.073		20.9	14.2	0.67	1.13	1.80	91.8
	0		24.4	10.7	0.75	0	0.75	220.0
D	1.26	5.0×10^{-4}	11.1	24.0	0.37	4.19	4.56	36.0
	0.63		13.8	21.3	0.56	3.49	4.05	40.8
	0.315		15.1	20.0	0.66	2.99	3.65	45.3
	0.142		18.1	17.0	0.77	1.75	2.52	65.5
	0.073		20.1	15.0	0.87	1.08	1.95	84.5
	0		23.0	12.1	0.99	0	0.99	167.0

[2] The author is greatly indebted to Dr. F. O. Koenig for this theoretical analysis.

TABLE I—*Continued*

	Moles alc./liter	Moles NaLS[a]/liter	Dynes/cm.		G.-mol. ×10⁻¹⁰/cm.²			Å² Area
			γ	F	$\Gamma_2^{\alpha b}$	$\Gamma_2^{\beta c}$	Γ	
E	1.26	7.5×10^{-4}	10.8	24.3	0.55	4.13	4.68	35.2
	0.63		11.9	23.2	0.84	3.26	4.10	40.2
	0.315		13.8	21.3	0.99	2.70	3.69	44.8
	0.142		16.4	18.7	1.15	1.43	2.58	63.8
	0.073		17.5	17.6	1.30	0.94	2.24	73.8
	0		19.4	15.7	1.49	0	1.49	111.0
F	1.26	1.0×10^{-3}	9.65	25.4	0.74	3.46	4.14	39.9
	0.63		10.1	25.0	1.11	2.89	4.00	41.2
	0.315		11.0	24.1	1.32	2.37	3.69	44.8
	0.142		14.1	21.0	1.53	1.38	2.91	56.9
	0.073		15.2	19.9	1.73	1.00	2.73	60.5
	0		17.9	17.2	1.98	0	1.98	83.2
G	0	5.0×10^{-3}	5.00	30.4	4.50	——	4.50	36.5
	0	2.5×10^{-3}	9.98	25.1	2.78	——	2.78	59.5
	0	1.5×10^{-3}	16.20	18.9	(3.18)	——	3.18	(57.5)
	0	1.0×10^{-3}	17.9	17.2	1.98	——	1.98	83.3
	0	7.5×10^{-4}	19.7	15.4	1.49	——	1.49	111
	0	5.0×10^{-4}	23.0	12.1	0.99	——	0.99	166
	0	2.5×10^{-4}	24.4	10.7	0.75	——	0.75	219
	0	1.0×10^{-4}	25.7	9.4	0.66	——	0.66	249

[a] NaLS = sodium dodecyl sulfate.
[b] = surface excess of sodium dodecyl sulfate.
[c] = surface excess of octyl alcohol.

the particular system under investigation the two phases are not strictly mutually insoluble, but the approximation is good.)

$$\frac{\partial \mu_1^\alpha}{\partial N_{2\pm}^\alpha} \Gamma_1^\alpha + \frac{\partial \mu_2^\alpha}{\partial N_{2\pm}^\alpha} \Gamma_2^\alpha = -\left(\frac{\partial \gamma}{\partial N_{2\pm}^\alpha}\right)_{T.P.}, \tag{1}$$

$$\frac{\partial \mu_1^\beta}{\partial N_2^\beta} \Gamma_1^\beta + \frac{\partial \mu_2^\beta}{\partial N_2^\beta} \Gamma_2^\beta = -\left(\frac{\partial \gamma}{\partial N_2^\beta}\right)_{T.P.}, \tag{2}$$

where component 1^α = water,
where component 2^α = sodium dodecyl sulfate,
where component 1^β = benzene,
where component 2^β = n-octyl alcohol.

Γ_1^α, Γ_2^α, Γ_1^β, Γ_2^β are the surface excesses (g./mole cm.²) of components 1^α, 2_κ, 1^β, 2^β, respectively. N_1^α, $N_{2\pm}^\alpha$, N_1^β, N_2^β are the mole fractions of components 1^α, 2^α, 1^β, 2^β, respectively, ($N_{2\pm}^\alpha$ being the *mean mole fraction*

of the sodium dodecyl sulfate), μ_1^α, μ_2^α, μ_1^β, μ_2^β are the chemical potentials of components 1^α, 2^α, 1^β, 2^β, respectively, and γ = interfacial tension. The complete solution for all 4 unknowns requires a *normal convention*, to fix the position of Gibbs' surface. The equation used in this case is

$$A_2^\alpha \Gamma_2^{\alpha(u)} + A_1^\beta \Gamma_1^{\beta(u)} + A_2^\beta \Gamma_2^{\beta(u)} = 1, \tag{3}$$

where A_2^α = area/g. mol. of component 2^α,

A_1^β = area/g. mol. of component 1^β,

A_2^β = area/g. mol. of component 2^β.

This equation, which is closely analogous to that of Guggenheim and Adam (4), is the expression of a hypothesis as to the physical nature of the adsorbed film. It implies that the film is monomolecular and contains no water molecules. This latter condition is speculative, while the assumption that the film is monomolecular seems justified by previous work (7).

The choice of an equation such as the above is arbitrary, and, provided the equations are dimensionally correct and contain only observable intensive variables, an infinite variety of such equations may be written to determine uniquely the position of the Gibbs surface. However, while such a *convention* is arbitrary, it may embody a hypothesis as to the physical nature of the film. The value of the results arising from the use of such a convention must be judged entirely from the reasonableness of the derived data and the correspondence with data obtained by other methods. For example, the close agreement between the force-area curves for fatty acids obtained from a study of insoluble films and from soluble adsorbed films lends sound physical support to the reasonableness of the common "Gibbs" convention of writing $\Gamma_{\text{water}} = 0$ in dilute solutions of fatty acids.

Previous work (7) led to the conclusion that the hydrocarbon chains of the film molecules are entirely in the benzene so that the values to be assigned to the areas A_2^α, A_1^β, A_2^β, are unambiguous, *viz.*, the areas obtained from close packed insoluble films. Since the convention defines $\Gamma_1^{\alpha(u)} = 0$ we have

$$\frac{\partial \mu_2^\alpha}{\partial N_2^\alpha{}_\pm} \Gamma_2^{\alpha(u)} = - \left(\frac{\partial \gamma}{\partial N_2^\alpha{}_\pm} \right)_{\text{T.P.}} \tag{4}$$

and, since the work of McBain and Johnston (10) shows that, at the concentrations used, the sodium dodecyl sulfate behaves approximately as an ideal uni-univalent electrolyte, we may write

$$\frac{2RT}{N_2^\alpha{}_\pm} \Gamma_2^{\alpha(u)} = - \left(\frac{\partial \gamma}{\partial N_2^\alpha{}_\pm} \right)_{\text{T.P.}}, \tag{5}$$

where $N_2^\alpha{}_\pm$ = *mean mole fraction* of the sodium dodecyl sulfate. $\Gamma_2^{\alpha(u)}$ is readily calculated from the slopes of the $\gamma \sim N_2^\alpha{}_\pm$ curve. To be quite

exact, since the convention places the Gibbs surface in the physical boundary layer the value of $\Gamma_2^{\alpha(u)}$ calculated in this way should be corrected by a small factor

$$\Delta \Gamma_2^{\alpha(u)} = \Delta x \cdot C_2^{\alpha} \pm,$$

where $C_2^{\alpha} \pm$ = concentration of the detergent in moles/ml. $\sim 10^{-6}$ moles/ml. and Δx = length of the detergent molecule ~ 30Å. Hence $\Delta \Gamma_2^{\alpha(u)} \sim 3 \times 10^{-13}$ g.-mol./cm.^{2} which is negligible.

With the known values of $\Gamma_2^{\alpha(u)}$, and employing Eqs. 2 and 3, values for $\Gamma_1^{\beta(u)}$ and $\Gamma_2^{\beta(u)}$ may be obtained, but the following *approximation* was made to facilitate the calculations. Inspection showed that $\Gamma_2^{\alpha(u)}$ is relatively small, being of the order $0.3 \sim 1.5 \times 10^{-10}$ g.-mol./cm^2. Hence we may write approximately

$$A_1^{\beta} \Gamma_1^{\beta(u)} + A_2^{\beta} \Gamma_2^{\beta(u)} = 1, \tag{6}$$

instead of

$$A_1^{\beta} \Gamma_1^{\beta(u)} + A_2^{\beta} \Gamma_2^{\beta(u)} = 1 - A_2^{\alpha} \Gamma_2^{\alpha(u)}. \tag{7}$$

Since $A_2^{\alpha} \sim 0.12 \times 10^{10}$ cm.^{2}/g.-mol. the right hand side of Eq. 7 will have values ranging from 0.96 to 0.82 instead of unity, and the error involved will vary from 4% to 18%. Large errors are only involved in the case of very dilute solutions of octyl alcohol, in which case $\Gamma_2^{\alpha(u)} \sim 1.5 \times 10^{-10}$ g.-mol./cm.^{2}

Using the approximate solution, the calculation of Γ_1^{β} and Γ_2^{β} follows exactly the methods described in the earlier paper (7,8), *viz.*,

$$\Gamma_2^{\beta(1)} = \frac{N_2^{\beta}}{N_1^{\beta}} \cdot \frac{T_0^2}{L \cdot T} \cdot \frac{\partial \gamma}{\partial \theta},$$

$$\Gamma_2^{\beta(N)} = \frac{\Gamma_2^{\beta(1)}}{1 + N_2^{\beta}/N_1^{\beta}},$$

where $L^{\cdot}$ = latent heat of fusion of benzene-ergs/mole,

$\quad T_0$ = freezing point of benzene,

$\quad \theta$ = freezing point depression of the solution,

$\quad T$ = temperature of experiment.

$$\Gamma_2^{\beta(u)} = \frac{A_1^{\beta} \Gamma_2^{\beta(N)} + N_2^{\beta}}{A_1^{\beta} N_1^{\beta} + A_2^{\beta} N_2^{\beta}}. \tag{8}$$

Values obtained in this way are given in Table I, and in most cases the error introduced by approximation is less than 10%.

An exact solution to the problem involves the knowledge of the differential $\left(\frac{\partial \gamma}{\partial P} \right)_{\text{T.N.}}$ (9). While this information is at present lacking, it seems reasonable to assume that it would be small, and as this present work is primarily exploratory only the simplest approximation has been used

throughout. The area per molecule in the mixed film is given by

$$A = \frac{1}{\Gamma} = \frac{1}{\Gamma_2{}^\alpha + \Gamma_2{}^\beta}.$$

As in the case of mixed adsorbed films at an air-water surface, the purity of materials is a critical factor in these experiments. The sodium dodecyl sulfate used is known to be of a high degree of purity. Aging at an air-water surface was almost entirely absent, and the results were in fairly good agreement with those of Miles and Shedlowsky (11). At oil-water interfaces against pure oils no aging beyond the first 2 or 3 min. was ever observed. In contact with solutions of octyl alcohol in benzene, which themselves showed no signs of aging against pure water, solutions of sodium dodecyl sulfate aged slightly, *ca.* 1–2 dynes/cm. during the first 20–30 min., and thereafter remained at constant interfacial tension for periods up to 2 days. It therefore seems probable that orientation and rearrangement at a benzene-water interface takes appreciably longer than at an air-water surface.

Examination of Table I shows that, as in the case at an air-water surface, the octyl alcohol generally forms the major portion of the interfacial film, but that, in order to achieve this, the concentration of alcohol in the benzene phase must be very much higher $\left(\dfrac{N_2{}^\beta}{N_2{}^\alpha{}_\pm} \sim 50\text{–}1000 \right)$ than that of the detergent in the water. Hence, it should follow that, if the probable impurity in sodium dodecyl sulfate is dodecyl alcohol, the effect of the impurity, in the *equilibrium* interfacial film, should be very much less than is the case at air-water surfaces, since experiment has shown that the chain length of the solute in the benzene has practically no effect on adsorption (7). However, it is very doubtful whether true equilibrium is attained in normal practice with impure solutions of sodium dodecyl sulfate. Since minima are reported for interfacial tension, as well as for surface tension (12), it seems probable that the free alcohol goes to the interface along with the sodium dodecyl sulfate, but that it interacts strongly with the detergent molecules in the film and does not pass through the interface to its equilibrium position in the bulk benzene phase at any measurable rate.

Experiments were carried out in which 40 ml. benzene were shaken vigorously with 40 ml. of sodium dodecyl sulfate solution containing an added 0.1% of dodecyl alcohol. The initial interfacial tension was compared with that obtained after the system had been shaken, and the resultant emulsion broken in a centrifuge. Even for periods of shaking extended to 24 hr., there was no such increase in interfacial tension as should have resulted if the free alcohol had attained equilibrium distribution between the benzene and water.

As in the case of mixed films at an air-water surface, the mixed films at the benzene-water interface appear to have properties intermediate between those of the two pure solute components. In all cases, the area at high compression is between those for the pure materials and neither in the force-area curves nor in the slopes of the respective interfacial tension-concentration curves is there any evidence indicative of compound or complex formation.

ACKNOWLEDGMENT

SUMMARY

Measurements have been made of the interfacial tensions of aqueous solutions of sodium dodecyl sulfate against solutions of octyl alcohol in benzene. By the application of the Gibbs adsorption theorem approximate calculations have been made of the surface excess of alcohol molecules and detergent molecules in the mixed adsorbed interfacial film on the assumption that this film contains no water molecules. The suggestion is made that, for systems in true equilibrium, the effect of oil-soluble impurities in the sodium dodecyl sulfate should be less than in corresponding experiments at air-water surfaces.

The properties of the mixed adsorbed films are intermediate between those of the two pure components.

REFERENCES

1. ADAM, N. K., AND SHUTE, H. L., *Trans. Faraday Soc.* **34**, 758 (1938).
2. BURDON, R. S., *ibid.* **35**, 727 (1939).
3. GOUY, G. *Ann. phys.* **6**, 5 (1916).
4. GUGGENHEIM, E. A., AND ADAM, N. K., *Proc. Roy. Soc. London* **139A**, 218 (1933).
5. HARKINS, W. D., AND BROWN, F. E., *J. Am. Chem. Soc.* **41**, 499 (1919).
6. HUTCHINSON, E., *J. Phys. Colloid Chem.* **52**, 897 (1948).
7. HUTCHINSON, E., *J. Colloid Sci.* **3**, 219 (1948).
8. HUTCHINSON, E., *ibid.* **3**, 235 (1948).
9. KOENIG, F. O., to be published.
10. McBAIN, J. W., AND JOHNSTON, S. A., *Proc. Roy. Soc. London* **181A**, 119 (1942).
11. MILES, G. D., AND SHEDLOWSKY, L., *J. Phys. Colloid Chem.* **48**, 67 (1944); **49**, 71 (1945).
12. POWNEY, J., AND ADDISON, C. C., *Trans. Faraday Soc.* **33**, 1246 (1937).

FILMS AT OIL-WATER INTERFACES. III

Eric Hutchinson[1]

From the Department of Chemistry, Stanford University, Calif.
Received July 21, 1948

INTRODUCTION

In previous papers (7,8) data were presented for the force-area curves of fatty acids and alcohols in films adsorbed at a number of oil-water interfaces; the data were obtained by the application of the Gibbs Adsorption Theorem to the interfacial tensions of solutions of the acids and alcohols in the oil phase. In this paper similar data are presented for films adsorbed from aqueous solutions of sodium dodecyl sulfate in contact with a number of oils.

EXPERIMENTAL

The interfacial tensions were measured by means of the sessile bubble method (2,4,5,7) and no further description will be given here except that, in the case of two of the oils which had a density greater than that of water, the sessile bubble was formed in an inverted cup instead of the hanging tube used for liquids less dense than water. Measurements were carried out at 23° ± 1°C.

Values of the freezing point depression of the solutions necessary for a solution of the Gibbs equation were taken from the paper of McBain and Johnston (11).

RESULTS

Data for the interfacial tensions of aqueous solutions of sodium dodecyl sulfate against benzene, cyclohexane, chlorobenzene, and nitrobenzene are given in Table I. Graphs of the interfacial tension as a function of the freezing point depression of the aqueous solution, for the same systems are given in Figs. 1–4, and in Fig. 5 calculated force-area curves for the adsorbed films are given.

The surface excess of sodium dodecyl sulfate Γ was calculated as in previous papers (7,8) from the equation,

$$\Gamma = \frac{N_{\bullet\pm}}{N_0} \cdot \frac{T_0{}^2}{L \cdot T} \frac{\partial \gamma}{\partial \theta}, \tag{1}$$

[1] Bristol Myers Postdoctorate Fellow and Research Associate in Chemistry. Present address: Chemistry Department, Fordham University, New York 58, N. Y.

where

$N_{s\pm}$ = mean mole fraction of the sodium dodecyl sulfate,
N_0 = mole fraction of water,
T_0 = freezing point of water,
T = temperature of experiment,
L = latent heat of fusion of water, ergs/mole,
γ = interfacial tension, dynes/cm,
θ = freezing point depression of the aqueous solution.

The calculations involve the *assumption* that the bulk solute is soluble only in one phase, the aqueous phase, and that the two liquid phases are immiscible. It is not known whether the detergent is appreciably soluble in the benzene relative to the low concentration in the aqueous phase. The benzene and water only approximate to the condition of immiscibility. The solutions used were dilute, the maximum concentration being 7.0×10^{-3} M, so that the values of Γ given by the various *normal con-*

TABLE I

Interfacial Tension of Sodium Dodecyl Sulfate Solutions

Molality NaLS[a]	F.P. depn. $\theta \times 10^{-3}$	$N_{s\pm} \times 10^{-5}$	γ dynes/cm.	$\partial\gamma/\partial\theta \times 10^4$	Γ g.-mol./ cm². $\times 10^{-10}$	Å² Area	F dynes/cm.	Product FA.
				Against benzene				
1.0×10^{-2}		18.0	4.7				30.4	
5.0×10^{-3}	17.0	9.02	5.0	6.0	4.50	36.5	30.1	1110
4.0×10^{-3}	14.15	7.20	6.7				28.4	
2.5×10^{-3}	9.0	4.51	9.9	7.4	2.78	59.5	25.1	1490
1.5×10^{-3}	5.55	2.70	16.2	9.9	3.18	57.5	18.9	1080
1.0×10^{-3}	3.75	1.80	17.9	14.2	1.86	88.5	17.2	1520
5.0×10^{-4}	1.85	0.902	23.0	18.5	1.38	114	12.1	1380
2.5×10^{-4}	0.95	0.451	24.4	24.6	0.92	129	10.7	1380
1.0×10^{-4}	0.30	0.18	25.7	39.0	0.58	283	9.4	2670
0	0	0	35.1	0	—	—	—	
				Against cyclohexane				
7.0×10^{-3}	20.0	12.6	5.3	11.6	12.2	13.6	45.9	625
5.0×10^{-3}	17.0	9.02	9.0	11.6	8.68	19.0	42.3	800
3.3×10^{-3}	11.8	6.00	15.1	11.6	5.78	28.7	36.2	1040
2.5×10^{-3}	9.0	4.51	17.9	12.5	4.68	35.2	33.4	1180
1.5×10^{-3}	5.55	2.70	24.2	14.7	3.30	50.0	27.1	1320
1.0×10^{-3}	3.75	1.80	25.0	18.5	2.78	59.5	26.3	1560
5.0×10^{-4}	1.85	0.902	27.9	35.8	2.68	62.0	23.4	1450
2.5×10^{-4}	0.95	0.451	35.9	70.2	2.62	63.0	15.4	970
0	—	—	51.3	—	—	—		

TABLE I—*Continued*

Molality NaLS[a]	F.P. depn. $\theta \times 10^{-3}$	$N_{s\pm} \times 10^{-6}$	γ dynes/cm.	$\partial\gamma/\partial\theta \times 10^4$	Γ g.-mol./cm.^{2} $\times 10^{-10}$	Å^2 Area	F dynes/cm.	Product FA.
Against chlorobenzene								
7.0×10^{-3}	20.0	12.6	4.3	5.3	5.54	29.8	31.9	950
5.0×10^{-3}	17.0	9.02	5.6	6.2	4.64	35.6	30.7	1090
3.3×10^{-3}	11.8	6.00	9.4	9.0	4.48	36.8	26.9	990
2.5×10^{-3}	9.0	4.51	12.5	11.8	4.52	36.5	23.8	870
1.5×10^{-3}	5.55	2.70	17.7	13.7	3.08	54.0	18.6	1000
1.0×10^{-3}	3.75	1.80	19.8	16.0	2.38	69.0	16.5	1140
5.0×10^{-4}	1.85	0.902	24.1	35.0	2.62	63.0	12.2	770
0	—	—	36.3	—	—	—	—	—
Against nitrobenzene								
7.0×10^{-3}	20.0	12.6	5.8	6.3	6.58	25.0	19.1	480
5.0×10^{-3}	17.0	9.02	5.4	6.3	4.70	35.0	18.9	660
3.3×10^{-3}	11.8	6.00	10.3	6.3	3.08	54.0	14.7	850
2.5×10^{-3}	9.0	4.51	12.2	6.7	2.46	67.0	12.9	865
1.5×10^{-3}	5.55	2.70	15.2	8.6	1.92	85.5	9.9	840
1.0×10^{-3}	3.75	1.80	16.3	10.0	1.68	98.0	8.8	865
5.0×10^{-4}	1.85	0.902	20.6	23.9	1.85	(85.0)	(4.5)	(385)
..	—	—	25.7					

[a] NaLS = sodium dodecyl sulfate.

ventions $\Gamma^{(1)}$, $\Gamma^{(N)}$, $\Gamma^{(o)}$, of Guggenheim and Adam (6) are practically identical.

DISCUSSION

In previous papers (8,9,10) the purity of the sodium dodecyl sulfate has been discussed and it was concluded that the specimen probably contained less than 0.05% of impurity. At an air-water surface, aging was practically absent, and the same was true in the present case, except in the experiments with nitrobenzene where the interfacial tension decreased by about 1–3 dynes/cm. in the first two hr. or so, after which no appreciable decrease occurred. It therefore appears likely that the nitrobenzene contributed some impurity.

The interfacial tensions quoted in the tables are equilibrium values obtained after a minimum time of two hr.

From Fig. 5 it will be seen that, over the small range investigated, the adsorbed films of the detergent appear to be of the "gaseous" type, as would be expected for a strong electrolyte such as sodium dodecyl sulfate. However, the large variations in the (force × area) product show that deviations from true gaseous behavior are quite large. The values of the
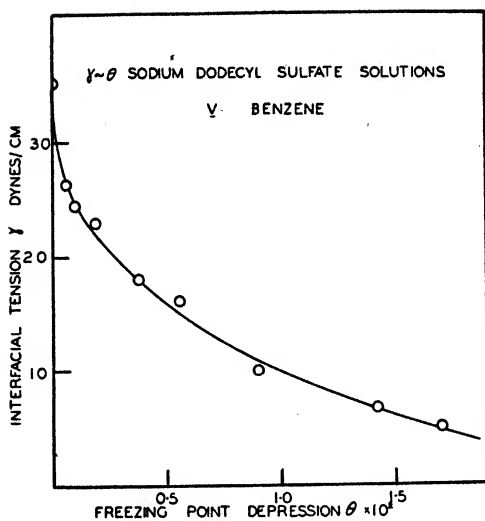
FIG. 1. Interfacial tension for benzene-aqueous solutions of sodium dodecyl sulfate as a function of the freezing point depression of the solution.
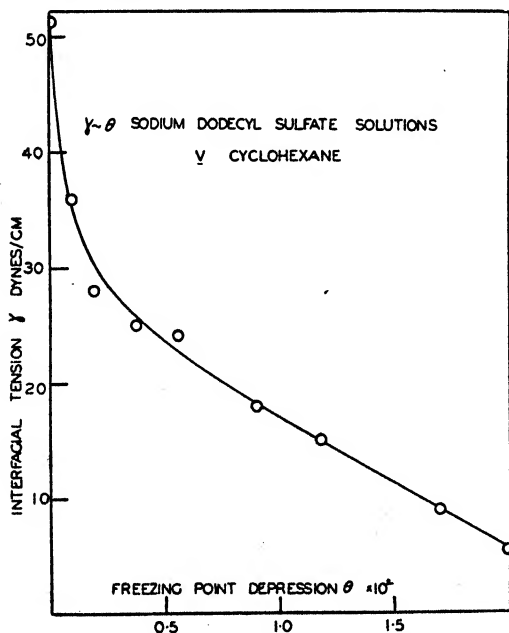
FIG. 2. Interfacial tension for cyclohexane-aqueous solutions of sodium dodecy sulfate as a function of the freezing point depression of the solution.
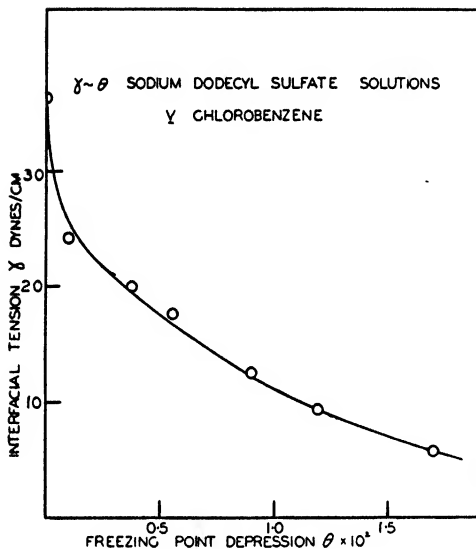
FIG. 3. Interfacial tension for chlorobenzene-aqueous solutions of sodium dodecyl sulfate as a function of the freezing point depression of the solution.
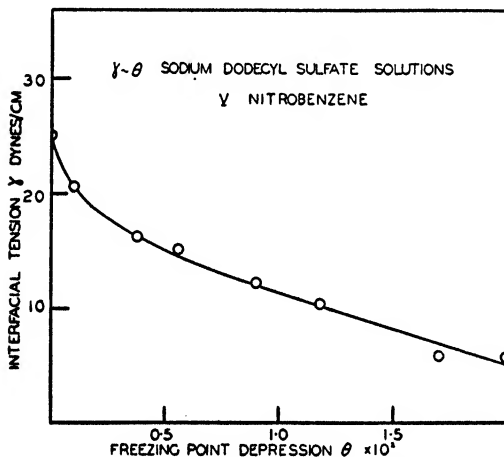
FIG. 4. Interfacial tension for nitrobenzene-aqueous solutions of sodium dodecyl sulfate as a function of the freezing point depression of the solution.
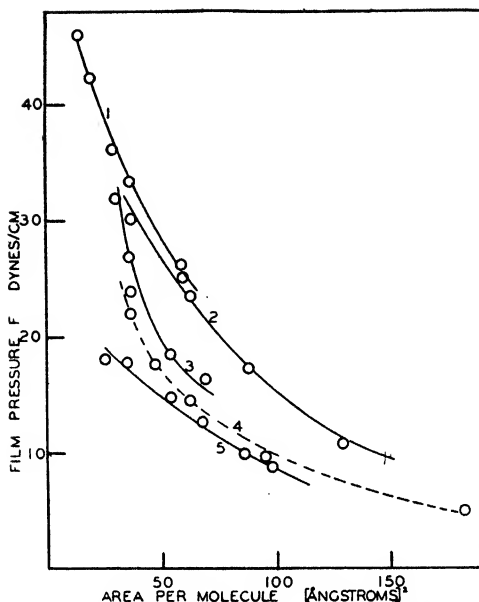
Fig. 5. Force-area curves for adsorbed films of sodium dodecyl sulfate. 1. Cyclohexane-water interface, 2. Benzene-water interface, 3. Chlorobenzene-water interface, 4. Air-water surface, 5. Nitrobenzene-water interface.

product range between 500 and 2000 for the various interfaces; these are much larger than the usual value of about 400 observed for nonionized "gaseous" films on water (1). Alexander and Teorell (3) find a value of the force-area product of about 720 for sodium cetyl sulfate *spread* at a benzene water interface.

The effects of the type of solvent on the properties of the interfacial film are large and appear to be in the same order as for adsorbed films of fatty acids and alcohols, *viz.*, the films are more condensed at nitrobenzene interfaces than at chlorobenzene, cyclohexane, or benzene interfaces against water, indicating that the polar group of the oil molecule contributes to the lateral adhesion in the film.

In earlier papers the suggestion was put forward that lateral adhesion in films at oil-water interfaces is likely to be greater, rather than less, than is the case at air-water surfaces, since the hydrocarbon chains of the surface active molecules are entirely in the oil phase. A higher degree of lateral adhesion in the film would render the film more condensed at oil-water interfaces than at air-water surfaces. This appeared to be the case for the fatty acids, which at 25° and 40°C. gave curves of the expanded type even for homologues as low as butyric acid, whereas, at air-water surfaces at 15°C., the films are approximately "gaseous" up to the C_{10} homologue.

No corresponding data were available for alcohol films adsorbed on water; Traube's investigation of the alcohols were carried out only as far as amyl alcohol, so that no direct comparison of behavior at air-water and oil-water surfaces was possible. The force-area curve of octyl alcohol adsorbed on water has recently been obtained (9), and it is found that octyl alcohol is considerably more condensed at an air-water surface than at a benzene-water interface. Only in the case of nitrobenzene-water interfaces is the alcohol more condensed than on water.

Similar results are here obtained for adsorbed films of sodium dodecyl sulfate. At benzene-water and cyclohexane-water interfaces the detergent film is considerably more expanded than on water. For chlorobenzene-water the film properties are closely similar to those on water, and at a nitrobenzene-water interface the film is more condensed than on water.

Hence, it would seem that the author's earlier generalization is invalid, and that the question of whether condensation or expansion of a film occurs in changing from an air-water to an oil-water interface depends both on the nature of the oil and of the film material.

SUMMARY

Measurements have been made of the interfacial tensions of aqueous solutions of sodium dodecyl sulfate against benzene, cyclohexane, chlorobenzene, and nitrobenzene by the sessile bubble method.

Calculations have been made of the number of molecules of solute adsorbed in the interface on the basis of a monomolecular film, and force-area curves for the adsorbed films of detergent are given. It is shown that, at a nitrobenzene-water interface, the detergent film is more condensed than on a water surface, but that at benzene-water and cyclohexane-water interfaces the film is more expanded. At a chlorobenzene-water interface the film properties are similar to those on water. The films appear to be imperfect "gaseous" type films over the range investigated.

REFERENCES

1. ADAM, N. K., The Physics and Chemistry of Surfaces. Oxford, 1944.
2. ADAM, N. K., AND SHUTE, H. L., *Trans. Faraday Soc.* **34**, 758 (1938).
3. ALEXANDER, A. E., AND TEORELL, T., *ibid.* **35**, 727 (1939).
4. BURDON, R. S., *ibid.* **28**, 866 (1932).
5. GOUY, G., *Ann. phys.* **6**, 5 (1916).
6. GUGGENHEIM, E. A., AND ADAM, N. K., *Proc. Roy. Soc. London* **139A**, 218 (1933).
7. HUTCHINSON, E., *J. Colloid Sci.* **3**, 219 (1948).
8. HUTCHINSON, E., *ibid.* **3**, 235 (1948).
9. HUTCHINSON, E., *ibid.* in press.
10. HUTCHINSON, E., in press.
11. McBAIN, J. W., AND JOHNSTON, S. A., *Proc. Roy. Soc. London* **181A**, 119 (1942).

SOME OF THE FACTORS INVOLVED IN THE USE OF THE TISELIUS ELECTROPHORESIS APPARATUS AT 20°C

P. Johnson and E. M. Shooter

From the Davy-Faraday Research Laboratory of the Royal Institution, London

Received August 2, 1948

One of the important contributions of Tiselius (1) to electrophoretic technique was his suggestion to use 4°C. as a working temperature. While this enabled higher potential gradients than had been previously permissible to be applied across the protein boundary it imposed some restrictions on the materials which could thus be analyzed—the chief restriction being that of solubility. Some proteins, notably of globulin type, have a very low solubility (<0.5 g. in 100 cc.) at or below 4°C., especially near their isoelectric points, in the usual buffers employed in electrophoretic work of ionic strength between 0.02 and 0.40. Since, for accurate electrophoretic analysis, concentrations should preferably be of the order of 1.0 g. protein in 100 cc. buffer, the examination of such proteins at 4°C. offers difficulty. In certain cases, for example, the proteins of the ground nut, the solubility is increased when the temperature is raised to 20°C., and it becomes possible at this temperature to prepare solutions for accurate analysis over wider ranges of pH and at pH's closer to their isoelectric point. For this reason, we have reverted to the older idea of electrophoresis at or about 20°C.

Experimentally electrophoresis at 20°C. offers considerable advantages. No refrigeration is required, condensation of water vapor on the thermostat windows is avoided, and thermostatic control can be accurately achieved with standard technique. On the other hand, much biological material is not stable at 20°C. for the period of time required for the initial dialysis—a minimum of 30–40 hr.—and solutions of stable proteins (*e.g.*, serum proteins) are more prone to bacterial action. However as will be shown, materials which are stable in solution for several days at 20°C. can be successfully analyzed electrophoretically at this temperature (see Fig. 2). An outline will be given of the factors involved by this change from 4° to 20°C. and a detailed comparison will be made of analyses at the two temperatures.

Thermal Convection. Its Detection and Effects

The separation of protein components of differing mobilities by migration in an electric field is hindered by the normal process of diffusion

which gradually broadens the initially sharp boundaries. It is advantageous, therefore, to use strong electrical fields and permit the boundaries to migrate over considerable path lengths and at high velocities so that the effect of diffusion on each boundary is kept small. The field strengths permissible are limited, however, by the unavoidable Joule heating effect which gives rise to a temperature gradient across the channel of the tube, the temperature reaching a maximum along its axis.

For a given liquid under a standard set of conditions the temperature and its gradient will increase as the field strength is raised. For temperatures above that of maximum density the density of the liquid will thus be lower at the axis than at the periphery, and a vertical circulation of the liquid within the channels of the U tube will tend to occur. If the density differences between axis and periphery are large, the convection currents will be sufficient to disturb, or even completely break up the boundary. Boundaries between solvent and solution owe their stability to the change of density across them and it follows that larger applied potentials are possible for the higher solute (*i.e.*, protein) concentrations.

Detection of Convection

Convection effects are first noticed at the edges of the schlieren peaks, either as a sharpening of the smooth Guassian curves or by the appearance of very sharp, small subsidiary peaks. This effect may be obtained at both

(a)   (b)
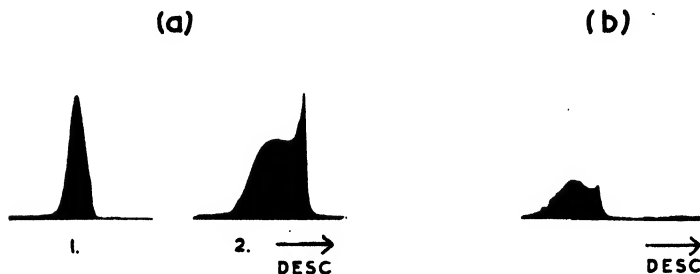
FIG. 1. Figure illustrating the effect of convection. (a) 1.3% Bovine serum albumin in phosphate buffer, pH 7.82, ionic strength 0.10. Migrated for (i) 176 min.; (ii) 482 min. at 3.0 volts/cm. at 20°C. (b) 0.58% Bovine serum albumin in phosphate buffer, pH 7.96, ionic strength 0.10. Migrated at 4°C. for 12 hr. at 3.75 volts/cm. giving a symmetrical peak. Further migrated for 2 hr. at 7.75 volts/cm. to obtain the above photograph. *Note:* All photographs are (except where stated) direct prints from the original photographic plate.

4° and 20°C. as indicated in Fig. 1, a higher potential being required at 4°C. The ultimate effect is to destroy the boundary, but under certain conditions (*e.g.*, 1% gum arabic in phosphate buffer, pH 7.98, ionic

strength 0.10, potential 5.0 volts/cm. at 20°C.) an apparent stabilizing action may be observed and the boundary migrates unchanged, with little diffusion, throughout.

Electrophoresis at Low Temperatures

To enable relatively high potential gradients to be used without convection, Tiselius, in 1937, introduced the rectangular section U tube to allow more efficient removal of heat, and conducted his experiments near 4°C. to minimize the density changes arising from unavoidable temperature differences. He found that a field strength of 7 volts/cm. could be conveniently used in experiments with serum while Alvarez-Tostado (2), using 0.5% sucrose to give a standard boundary, stated that no convection occurred in experiments lasting 10 hr. if the total wattage (Ei) in the apparatus did not exceed the value 6.0.

The calculations of Longsworth and MacInnes (3), based on the equations of Mooney for cylindrical tubes, show that differences of temperature between axis and periphery in normal electrophoretic experiments at 25°C. may amount to 0.65°C. with a corresponding density change of 1.8×10^{-4}. At the temperature of the maximum density of the buffer solution, this density change would become zero and no boundary disturbance could occur. However, under conditions such that the temperature change, as calculated from the above equations, was 0.66°C. (conductivity of buffer 0.01 mhos., current density 1.6×10^{-2} amps. cm.$^{-2}$) with a density change at 20°C. of 1.4×10^{-4}, the boundaries formed with 0.6–0.8% protein solution moved at 20°C. for 10 hr. without convectional disturbance. If, therefore, these temperature differences do arise, the resulting density changes are too low to produce convection.

Electrophoresis at 20°C.

For reasons previously stated, the thermostat temperature was maintained at 20°C. and controlled to ±0.003°C. This latter condition is dictated again by the finite value of $\dfrac{d\rho}{dt}$ (where $\rho =$ density of solvent) at 20°C. and prevents appreciable fluctuations of density within the U tube due to thermostating. Anticipating the results of this section, it was found experimentally that the field strength at 20°C. had, in general, to be lower by a factor of 3 from that at 4°C. Thus, for specific conductivities between 0.0020 and 0.0150 mhos., the maximum potential which could be applied across the boundary was 2.5 volts/cm. for a 1% protein solution and 2 volts/cm. for a 0.5% solution. Under these conditions boundaries migrated successfully for long periods as illustrated in Fig. 2 and in the experiments contained in the following sections.
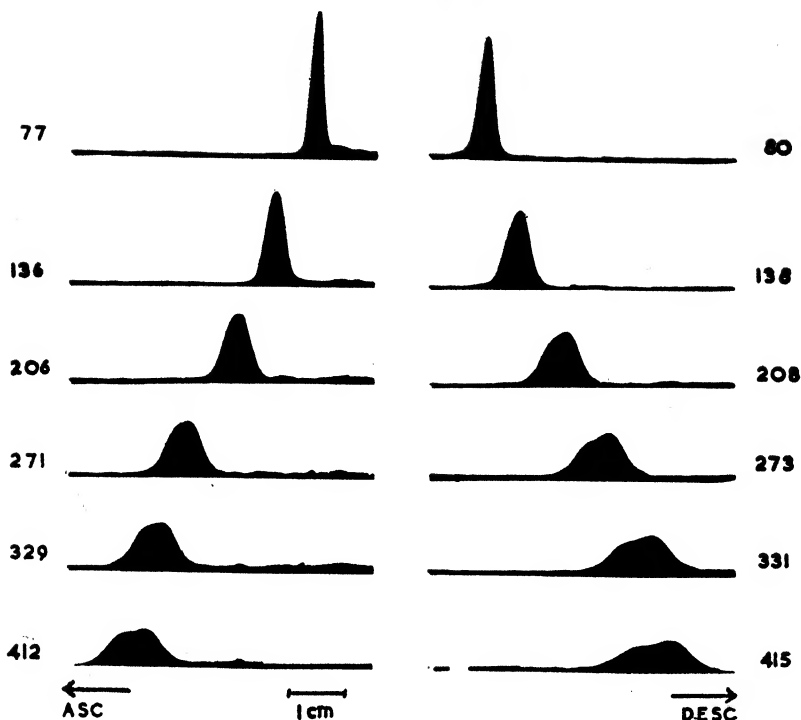
FIG. 2. Solution of ground nut globulins precipitated at pH 5.0 from 6% NaCl extraction. Phosphate/NaCl buffer, pH 6.90, ionic strength 0.10. Protein concentration ≈ 0.65%. Potential 1.8 volts/cm. Figures alongside each photograph denote the time (in min.) from the start of the migration. The "centimeter" length refers to the actual path length traversed in the cell.

Mobilities of Proteins

The mobility of a protein molecule has, in general, been observed to be independent of the field strength under which it is migrating (4) (within the defined limits) if the working temperature is between 0° and 4°C. This criterion should hold also at 20°C., and Table I indicates the mobilities of the substance gum arabic at 20°C. under the various applied potentials. Gum arabic appears essentially homogeneous under the conditions given and has been used previously in this type of investigation (5). Table II contains data on fractions of the ground nut globulins under two potentials only. The constancy of the gum arabic mobility under field strengths up to 4.85 volts/cm. is evident. It must be noted, however, that migration under field strengths greater than 2.70 volts/cm. was not free from convectional disturbance.

TABLE I

Gum arabic migrating in phosphate—NaCl buffer, pH 7.80, ionic strength 0.10

Conc. of solute	Field strength	Mobility $\times 10^4$ cm.^{2} volt^{-1} sec^{-1}	
		Desc.	Asc. (apparent)
	volts/cm.		
1%	1.10	(1.06) ±0.03	1.29 ±0.03
	1.55	1.39	1.39
	2.00	1.15	1.30
	2.70	1.16	1.31
	3.60	1.24	1.35
	4.85	1.20	1.33
0.5%	2.00	1.18	1.27
	2.70	1.22	1.29

The limitation of field strength at 20°C. would alone involve, for a given protein, a longer time of migration over a particular path length at 20°C. than at 4°C. approximately by the factor 3, which limits the applied potential. Fortunately, there occurs an increase of mobility with increase of temperature. The mobility of a protein molecule under ordinary conditions of electrophoretic analysis is inversely proportional to the viscosity of the solvent (buffer) in which it is migrating. Thus,

TABLE II(a)

Solution of ground nut globulin, precipitated by 40% $(NH_4)_2SO_4$ from 6% NaCl extract, migrating in NH_3/HCl buffer, pH 9.56 (18°C.), ionic strength 0.10

Conc. of protein	Field strength	Mobility $\times 10^4$ cm.^{2} volt^{-1} sec^{-1}	
		Desc.	Asc. (apparent)
	volts/cm.		
0.8%	1.35	0.89	1.03
1.0%	2.10	0.87	0.99

TABLE II(b)

Solution of ground nut globulin, precipitated at isoelectric point from 6% NaCl extract, migrating in NH_2/HCl buffer, pH 9.56 (18°C.), ionic strength 0.10

Conc. of protein	Field strength	Mobility $\times 10^4$ cm.^{2} volt^{-1} sec^{-1}	
		Desc.	Asc. (Apparent)
	volts/cm.		
0.4 %	1.20	0.93	1.03
0.66%	1.80	0.94	1.04

the mobilities of proteins at 4° and 20°C. should differ only by a factor which is the ratio of the viscosities at 4° and 20°C. Table III gives a comparison of mobilities at these two temperatures for 3 different proteins. Since the exact temperatures within the U tube are not known, the agree-

TABLE III

Mobilities of proteins at 4° and 20°C.

Protein	Buffer	pH	Ratio $\left\{ \dfrac{\text{Mobility at 4°C.}}{\text{Mobility at 20°C.}} \right.$		Viscosity H_2O, 20°C.
					Viscosity H_2O, 4°C.
			Desc.	Asc. (apparent)	
Human serum albumin	Phosphate, ionic strength 0.20	7.15	0.61	0.63	
Human fibrinogen	Phosphate, ionic strength 0.20	7.15	0.64	0.62	0.64
Ground nut globulin ppt'd at isoelectric point	Borate—NaCl, ionic strength 0.10	8.99	0.70	0.69	

ment may be considered satisfactory—viscosities of water used in the table vary little from those of dilute salt solutions. Thus, the limitation of applied potential is partly compensated by the increase in mobility (by the factor $\dfrac{1}{0.645} = 1.55$) at higher temperatures. The time of migration over a particular path length at 20°C. is, therefore, now reduced from 3 times to $\dfrac{3.0}{1.55}$ or approximately twice the time required at 4°C. This added time of migration directs attention to the diffusion of protein boundaries.

Diffusion of Protein Boundaries

The diffusion coefficients of macromolecules are proportional to the absolute temperature and inversely proportional to the relative viscosity, both factors leading to an increase of diffusion at 20° as compared with 4°C. Fig. 3 gives a series of calculated schlieren curves of a diffusing boundary 1.5, 3, 6, 12, and 24 hr. after formation at the two temperatures 4° and 20°C. A high diffusion coefficient (low molecular weight globular protein) has been chosen as a basis for calculation; in practice the change in diffuseness at corresponding times will probably be less for most proteins. Thus, the relative diffuseness of this protein boundary after migration over the same path length at the two temperatures may be judged from the horizontal lines of the figure. The additional spread of a bound-
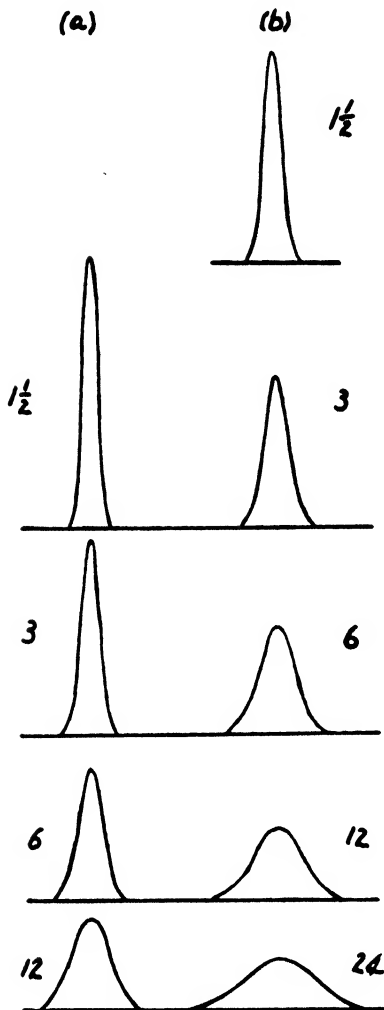
Fig. 3. Calculated schlieren curves for a diffusing protein boundary. (a) At 4°C. $D_0{}^4 = 6.1 \times 10^{-7}$ cm²./sec. (b) At 20°C. $D_0{}^{20} = 10 \times 10^{-7}$ cm.²/sec. Figures by each curve denote the time (in hr.) from formation of boundary.

ary migrating at 20°C. (assuming electrical homogeneity) causes difficulty only when individual components have like mobilities and the maxima of the schlieren peaks remain close. In Fig. 4 a comparison is made of the separation of protein components at the two temperatures. It has been assumed that the two components of slightly different mobilities have

equal concentrations and diffusion coefficients ($D_0{}^{20} = 10 \times 10^{-7}$ cm.^{2}/sec.). In Fig. 4(a) it has been further assumed that these two components after migration for 6 hr. at 4°C., achieve a separation of the peak maxima of 0.54 cm. This separation is just adequate to construct the Gaussian curves of the individual boundaries and determine their relative concentrations accurately. At 20°C. the boundaries will have migrated exactly the same distances in approximately 12 hr. and Fig. 4(b) illustrates how

(a)

0.54 cm.

(b)   *(c)*

0.54 cm.   0.91 cm.
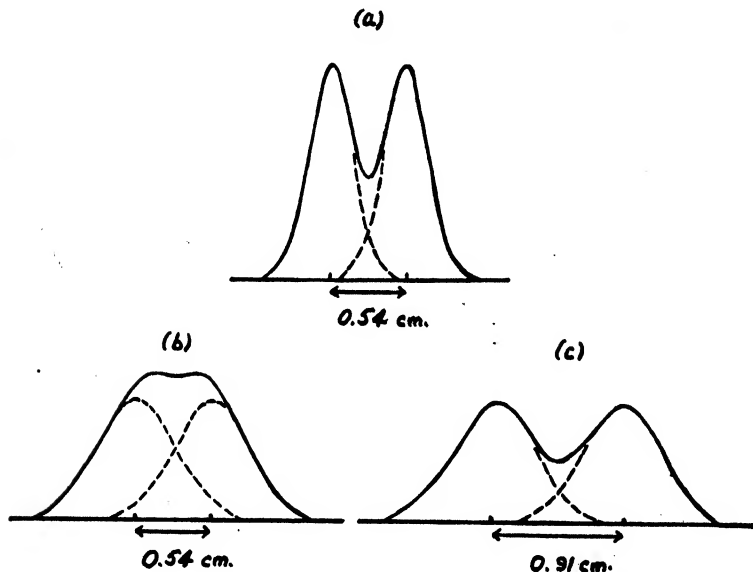
Fig. 4. Equal concentrations of similar protein components migrating (a) at 4°C. and (b) and (c) at 20°C. In (a) and (b) migration has occurred over the same path length, occupying approximately 6 hr. at 4°C. and 12 hr. at 20°C. (c) shows larger distance required for the separation of the two components when diffusion is more rapid. $D_0{}^{20} = 10 \times 10^{-7}$; $D_0{}^4 = 6.1 \times 10^{-7}$ cm.^{2}/sec.

little apparent separation has occurred and the greater difficulty in assigning the correct areas to each boundary.

A protein whose mobility at 20°C. is 1.0×10^{-4} cm.^{2} volt^{-1} sec^{-1} will, under normal electrophoretic conditions at this temperature (*i.e.*, potential gradient 2.0 volts/cm.), migrate 8.60 cm. in the 12 hr. If this represents the faster component, then the slower will have migrated 8.06 cm. and will indeed have a mobility at 20°C. of $\dfrac{8.06}{8.60} \times 10^{-4} = 0.94 \times 10^{-4}$ cm.^{2} volt^{-1} sec.$^{-1}$. This component is well differentiated from the faster at 4° but not at 20°C. To enable an accurate estimate of the relative areas
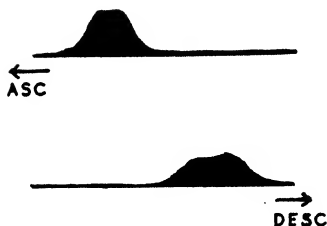
FIG. 5. Solution of ground nut globulins precipitated at pH 5.0 from a 6% NaCl extract in phosphate buffer, pH 7.15, ionic strength 0.04. Protein conc. ≈ 0.65%. Time of migration 284 min. Potential 1.8 volts/cm.

to be made at 20°C. the peak maxima of the two components have to be separated by 0.90 cm. as in Fig. 4(c). In this case the mobility of the slower component becomes $\dfrac{7.70}{8.60} = 0.90 \times 10^{-4}$ cm.² volt⁻¹ sec⁻¹. Thus, electrophoresis at 20°C. is not particularly suited to the analysis of mixtures of proteins of like mobility since here (e.g., as in Fig. 5) no attempt

A — ALBUMIN
ϕ — FIBRINOGEN
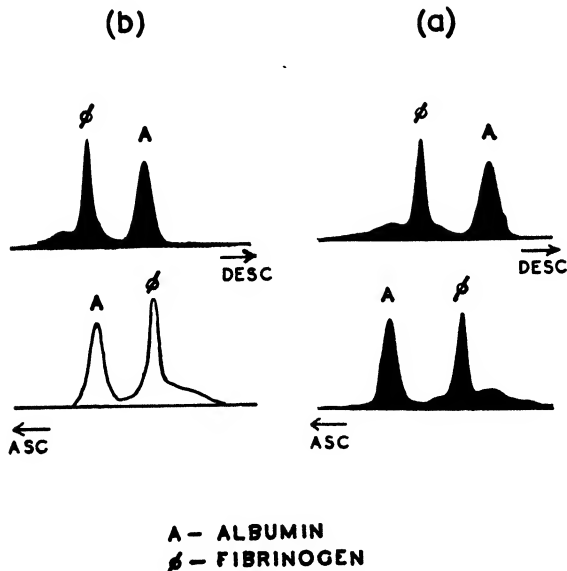
FIG. 6. Migration of a mixture of human serum albumin and fibrinogen, approximately 0.60% each. Fibrinogen contaminated with β- and γ-globulins. Phosphate buffer (pH 7.7, cf. gal. ionic strength 0.20), plus citrate to prevent clotting. (a) Migration at 20°C. for 183 min. Potential 1.55 volts/cm. (b) Migration at 4°C. for 154 min. Potential 3.2 volts/cm. Note: Photograph of ascending boundary at 4°C. was not suitable for a direct print.

can be made to assign relative concentrations to the components. This short discussion has been restricted to conditions where it can be assumed that boundary anomaly effects are small.

Analysis of Mixtures at 4° and 20°C.

A sensitive comparison of electrophoresis at 4° and 20°C. is provided by an analysis of a particular mixture of proteins at the two temperatures. The mixtures used comprised approximately equal concentrations of human serum albumin and fibrinogen (0.6% each), the latter being contaminated with small quantities of β- and γ-globulins. All conditions of the two experiments, except temperature, were identical. The resolution of the 4 components took place at 20°C. exactly as at 4°C. (except that, in both cases, the γ-globulin did not completely separate from the small δ- and ϵ-anomalies), see Fig. 6. In addition, the relative concentrations (as determined by relative areas and assuming an identical specific refractive increment for all components) of the two components (fibrinogen, β- and γ-globulin considered as one component) showed satisfactory agreement at the two temperatures (Table IV). The scatter indicated in

TABLE IV

Ratios of the components (fibrinogen + β- + γ-globulin to albumin) at 4° and 20°C

Plate	4.0°C.		20.0°C.	
	Desc.	Asc.	Desc.	Asc.
1	1.17	1.29	1.25	1.20
2	1.05	1.17	1.08	1.08
3	1.07	1.11	1.01	1.24
Mean value	1.14±0.03		1.14±0.04	

the ratios of the 2 components, a maximum of 8% about the mean, falls within the experimental error, since individual areas can usually only be determined to within 5–10%.

SUMMARY

1. While, in general, electrophoresis at or below 4°C., involving rapid, and hence highly effective, separation of protein components, is to be

preferred, insolubility of some proteins at these temperatures necessitates an increase in the working temperature to 20°C.

2. It has been found experimentally that the field strengths permissible at 20°C. are smaller by a factor of 3 than those possible at 4°C.

3. The corresponding increase in time of migration over a particular path length is partly offset by the decrease in viscosity and subsequent increase in mobility. Diffusion is greater at 20°C. than at 4°C. but becomes important only when components have like mobilities.

4. Analysis of a known mixture of proteins gave identical results for their distributions at the two temperatures 4° and 20°C.

REFERENCES

1. TISELIUS, *Trans. Faraday Soc.* **33**, 524 (1937).
2. ALVAREZ-TOSTADO, *J. Biol. Chem.* **135**, 799 (1940).
3. LONGSWORTH AND MACINNES, *Chem. Revs.* **24**, 271 (1939).
4. SVENSSON, *Arkiv Kemi Mineral. Geol.* **22**A, No. 10, 117 (1946).
5. SCHWERT, PUTNAM AND BRIGGS, *Arch. Biochem.* **4**, 371 (1944).

THE EFFECT OF SURFACE ON MELTING POINT *

Howard Reiss

Columbia University, N. Y.

and

Irwin B. Wilson

College of the City of New York
Received August 16, 1948

Very few quantitative investigations of the effect of surface upon fusion have been carried out. This is not surprising, because it has been difficult to prepare a system having a large surface, and, at the same time, enough simplicity to be amenable to mathematical treatment. Furthermore, theoretical treatments of specific fusion processes in which surface is an important factor have been confused and incomplete. The purpose of the present paper is to clarify the nature of two such fusion processes, namely, the fusion of small spheres and thin films.

The internal equilibrium of a one-component system is characterized by the equality of the chemical potentials, μ, of its phases. To symbolize the continuance of equilibrium as the constraints are altered, the increments of the chemical potentials of all phases are equated:

$$d\mu_1 = d\mu_2 = \cdots = d\mu_n. \qquad (1)$$

When the ratio of surface to mass is large, the system may be regarded as containing surface phases in addition to the usual volume phases (1). By an obvious extension it can be shown that the above equilibrium condition applies to these phases also. When the surface of a body is increased, the increase of Thermodynamic Potential is given by

$$\Delta G = \sigma \Delta A, \qquad (2)$$

where σ is the surface tension, and ΔA is the reversible increment in surface area.

Now, the chemical potentials of the volume and surface phases must remain equal if the body is to persist in a state of equilibrium. Therefore, an increase in surface area represents a simultaneous, equal increase in the chemical potentials of the volume and surface phases. Consequently,

for an isothermal process, an increase in the pressure of the volume phase is demanded as the only mechanism for increasing its chemical potential;

$$\Delta\mu = v\Delta p, \tag{3}$$

where v is the molar volume, considered to be invariant for a condensed phase and Δp is the pressure increment. Since

$$\Delta\mu = \frac{\partial(\Delta G)}{\partial n}, \tag{4}$$

where n is the number of moles comprising the body, it follows from Eqs. (2) and (3) that

$$\Delta p = \frac{\sigma}{v}\frac{\partial(\Delta A)}{\partial n}. \tag{5}[1]$$

If the external pressure is constant, this increase in internal pressure will be obtained by an increase in the curvature of the surface. The difference of pressure across a curved boundary is given by Kelvin's formula (2)

$$p - p^0 = \sigma\left(\frac{1}{r_1} + \frac{1}{r_2}\right), \tag{6}$$

where p is the internal pressure, p^0 is the external pressure, and r_1 and r_2 are the principal radii of curvature. If the surface remains flat, as in the

---

[1] As an example of the use of equation (5) let us derive equation (6), specialized to the case of a sphere, i.e., $r_1 = r_2 = r$.

Consider a sample of material in bulk. If we divide this sample, uniformly, into spheres, all of which have the radius, r, we can disregard the initial surface area, and employ the total area of the spheres as the numerical value of ΔA. Thus, if N represents the number of drops which are formed

$$\frac{\partial(\Delta A)}{\partial n} = \frac{\partial A}{\partial n} = N\frac{\partial}{\partial n}(4\pi r^2) = 8\pi Nr\frac{\partial r}{\partial n}.$$

But,

$$nv = \tfrac{4}{3}\pi r^3 N,$$

from which it follows that

$$\frac{\partial r}{\partial n} = \frac{v}{4\pi r^2 N},$$

which when substituted in the first equation of this note yields

$$\frac{\partial(\Delta A)}{\partial n} = \frac{2v}{r},$$

and when this is substituted into equation (5) we obtain

$$\Delta p = \frac{2\sigma}{r}.$$

Now, Δp refers to the difference between the internal pressures of the material in bulk and in droplet form. But, when the material is in bulk, its internal pressure is identical with the external pressure, and, therefore, the last equation is identical with (6) for $r_1 = r_2 = r$.

case of films, then the increase of internal pressure must arise by an increase in external pressure calculable by Eq. (5).

The application of this additional external pressure will necessarily involve the use of walls which maintain the deformation of the body. Consequently, we will have to consider, σ_{bw}, wall-body interfacial tensions in place of the air-body tensions. Furthermore, an extension of the wall-body interface decreases the wall-air interface so that an amount of free energy, $\sigma_w \Delta A$, where σ_w is the wall-air interfacial tension, will be lost by this effect. This quantity may be regarded as reversible work performed on the body during the process of deformation, so that the thermodynamic potential change, for the body, is given by

$$\Delta G = \sigma_{bw}\Delta A - \sigma_w \Delta A = (\sigma_{bw} - \sigma_w)\Delta A. \tag{7}$$

For cases including walls, Eq. (7) then replaces Eq. (2), and all the equations following (2) retain their form, but σ is replaced by $(\sigma_{bw} - \sigma_w)$.

In considering an equilibrium between liquid and solid, in which surface phases are important, Eq. (1) is to be utilized where

$$d\mu_i = -s_i dT + \text{a term due to surface}, \tag{8}$$

and s_i is the molar entropy. Where the curvature is obvious, it is often convenient to use $v_i dp_i$ for the value of the surface term, formally ignoring the existence of the surface, and computing dp_i from Kelvin's formula. In other cases, the surface term may be evaluated directly as $\dfrac{\sigma_i \partial A i}{\partial n_i}$.

It is now possible to develop a general relation between extent of surface and melting point. According to Eq. (1)

$$d\mu_s = d\mu_l, \tag{9}$$

where μ_s and μ_l are, respectively, the chemical potentials of the solid and liquid volume phases. Eq. (9) must be integrated over any path extending from the normal melting point, T_o, at which the extent of surface is negligible to the temperature, T, the melting point of the extended system. By Eq. (8)

$$d\mu_s = -s_s dT + \begin{cases} v_s dp_s \\ \dfrac{\sigma_s \partial A_s}{\partial n_s}, \end{cases}$$

$$\tag{10}$$

$$d\mu_l = -s_l dT + \begin{cases} v_l dp_l \\ \dfrac{\sigma_l \partial A_l}{\partial n_l}. \end{cases}$$

Integration with respect to temperature, between T_o and T, at constant pressure (constant surface), followed by integration with respect to pressure (surface) at the constant temperature, T, represents a convenient path. If we make the approximation that s, v, and σ are independent of temperature, over the small range involved, and that v is, in addition, independent of pressure, then Eq. (10) integrates to yield

$$\Delta\mu_s = -s_s(T - T_o) + \begin{cases} v_s\Delta p_s \\ \dfrac{\sigma_o\partial A_s}{\partial n_s} \end{cases},$$

$$\Delta\mu_l = -s_l(T - T_o) + \begin{cases} v_l\Delta p_l \\ \dfrac{\sigma_l\partial A_l}{\partial n_l} \end{cases}. \tag{11}$$

Consequently, we obtain for the integrated form of Eq. (9)

$$(s_l - s_s)(T - T_o) = \begin{cases} v_l\Delta p_l - v_s\Delta p_s \\ \dfrac{\sigma_l\partial A_l}{\partial n_l} - \dfrac{\sigma_s\partial A_s}{\partial n_s} \end{cases}. \tag{12}$$

However

$$s_l - s_s = \frac{\lambda_o}{T_o}, \tag{13}$$

where λ_o is the heat of fusion for bulk matter at the normal melting point. Eq. (12) becomes

$$\frac{\lambda_o}{T_o}(T - T_o) = \begin{cases} v_l\Delta p_l - v_s\Delta p_s \\ \dfrac{\sigma_l\partial A_l}{\partial n_l} - \dfrac{\sigma_s\partial A_s}{\partial n_s} \end{cases}. \tag{14}$$

The terms on the right of (14) must be evaluated subject to the geometrical demands of any special problem. In addition, if walls are involved, the σ may be replaced by wall-dependent terms, as in Eq. (7).

Pavlov, in 1909, considered the effect of surface upon the melting point and heat of fusion of a solid material $(3,4)$. His experiments have now been discredited (5), but his theoretical treatment of what he called the melting point was correct, although vague and incomplete. Pavlov computed the temperature for which a solid and liquid sphere, having identical masses, and consisting of the same material, would be in equilibrium. He defined this temperature as the melting point. By equating the vapor pressures of both liquid and solid spheres, as they appear in Kelvin's equation (6), he obtained the formula

$$T\ln\frac{\pi_1}{\pi} = \left(\frac{k}{rd} - \frac{k_1}{r_1d_1}\right)\frac{2}{R\sigma}, \tag{15}$$

where T is the melting temperature, $R\sigma$ (Pavlov's notation) is the gas constant, d is the density of the solid, d_1 is the density of the liquid, r is the radius of the solid, r_1 is the radius of the liquid, k is the surface tension of the solid, k_1 is the surface tension of the liquid, π is the pressure, at T, over the solid in bulk, and π_1 is the pressure, at T, over the liquid in bulk. This equation contains a larger number of parameters than is necessary to characterize the equilibrium temperature, and, in addition, requires the value of the difficultly measurable vapor pressure, π_1, of a supercooled liquid. It represents the correct solution of the problem which Pavlov considered, but the T which appears *is not a melting* point. It is an *equilibrium* point which might be determined by mixing spheres of solid and liquid having the same mass, and consequently different radii, and observing the temperature for which no net transfer of material from solid to liquid, or *vice versa*, occurs. Ordinarily, a melting point is recognized as that temperature, during the heating of a solid, at which fusion occurs. It will be shown, later, that the calculation of the melting point of a sphere requires the consideration of an equilibrium involving liquid and solid spheres having the *same* radius.

As a matter of fact, the determination of the melting point of small spheres (melting point in the usual sense) is now feasible. Recently, V. K. LaMer and his coworkers have prepared monodispersed aerosols whose size they have measured by an optical means (7,8,9). The matter contained in such aerosols is in an extremely fine and yet uniformly spherical state of subdivision. It is suggested that the melting point of these aerosols be determined by an optical method sensitive to the change of refractive index which occurs upon fusion.

The correct thermodynamic treatment of the fusion of small spherical particles requires a careful examination of several fine points.

When a solid, in bulk, melts, each step of the process may be regarded as a reversible transfer of material from one phase to another, while the intensive properties of the individual phases remain unchanged. The situation is not so simple for the case of a small particle, since the intensive properties depend upon the radius, which varies upon the transfer of material.

On the basis of considerations of thermal conductivity it is the outer layer of a particle which first reaches the fusion temperature and melts. Therefore, the initial step is equivalent to the reversible transfer of material from a solid to a liquid sphere having the same radius. The particle, then, consists of a solid core surrounded by a liquid shell, and the second step in the fusion process involves the transfer of material from a solid core having smaller dimensions than the initial sphere.

The pressure exerted on the solid by the surface films is responsible for the change of the melting point. After the first portion of the solid is

melted, the remaining core is subject to pressure arising from the liquid-gas interface and the solid-liquid interface. This pressure, p, is given, by application of Kelvin's formula, by

$$p = p^0 + \frac{2\sigma_l}{r} + \frac{2\sigma_{ls}}{r_c}, \qquad (16)$$

where r is the radius of the drop, r_c is the radius of the solid core, σ_l is the surface tension of the liquid-gas interface, and σ_{ls} is the surface tension of the liquid-solid interface. The surface tensions, σ_s, σ_l, and σ_{ls}, where σ_s is the surface tension of the solid-gas interface, are related for $\theta > 0$ by Young's equation (10).

$$\sigma_s = \sigma_{ls} + \sigma_l \cos \theta, \qquad (17)$$

where θ is the angle of contact of liquid on solid. For $\theta = 0$, the relation

$$\sigma_s \geqslant \sigma_{ls} + \sigma_l \qquad (17a)$$

holds.

We shall prove that the equality $\sigma_s = \sigma_{ls} + \sigma_l$ in $(17a)$ holds exactly, when the liquid and solid are the same material and are in equilibrium. Consider the change in thermodynamic potential attending the isothermal transfer of an infinitesimal quantity of liquid from a bulk supply to the surface of a small, spherical solid of the same material. The change of area of the bulk liquid is negligible. On the small sphere the solid-gas interface is replaced by the solid-liquid interface, and, in addition, a liquid-gas interface is formed. The change of thermodynamic potential is thus given by

$$4\pi r^2 (\sigma_{sl} + \sigma_l - \sigma_s).$$

If the temperature is the melting point of the outer layer of the solid sphere, then the same process can be carried out by melting the outer layer, but this process involves zero change in thermodynamic potential. Hence, we may conclude that

$$4\pi r^2 (\sigma_{sl} + \sigma_l - \sigma_s) = 0$$

or

$$\sigma_s = \sigma_{sl} + \sigma_l,$$

the equality in $(17a)$.

The melting point of the sphere depends upon r, and, therefore, the equality in $(17a)$ holds for all temperatures and pressures corresponding to equilibrium between solid and melt.

If the contact angle were not zero $(17a)$ could not hold. Since $(17a)$ does hold for the case in question, it follows that the contact angle is zero.

Since $r_c < r$, and because of the equality in $(17a)$, the pressure on the solid core of the melting particle must be greater than in the original

particle. The core must, therefore, be superheated at the temperature corresponding to the inception of the melting process, and so the process must continue. The transition temperature, experimentally, is then that temperature at which liquid and solid drops having the same radius are in equilibrium, despite the fact that the melting process brings about an alteration of radius.

The correction involved is obviously small. However, it is worth while pointing it out, as an example of how the sharp dependence of intensive properties upon mass, characteristic of extended systems, influences a theoretical treatment.

Eq. (14) can now be applied to the case of spheres. Since the curvature is, in this case, obvious, the right hand member can be evaluated, utilizing the first of the two alternate expressions which it contains. Δp can be computed, employing Kelvin's formula, specialized to the case of a sphere, $i.e.$, $r_1 = r_2$, so that

$$\Delta p_s = p_s - p_o = \frac{2\sigma_s}{r},$$

$$\Delta p_l = p_l - p_o = \frac{2\sigma_l}{r}.$$

(18)

Eq. (14) then becomes

$$\frac{\lambda_o}{T_o}(T - T_o) = \frac{2}{r}(\sigma_l v_l - \sigma_s v_s)$$

or

$$T_o - T = \frac{2T_o}{r\lambda_o}(\sigma_s v_s - \sigma_l v_l),$$

(19)

where T_o is the normal melting point $(r = \infty)$, and T, the melting point of a particle of radius r. It is interesting to compare Eq. (19) with Eq. (8).

If we substitute the identity, $v_l = v_s - (v_s - v_l)$, in (19) we obtain

$$T_o - T = \frac{2T_o}{r\lambda_o}v_s(\sigma_s - \sigma_l) + \frac{2T_o}{r\lambda_o}(v_s - v_l)\sigma_l.$$

(20)

The form of this equation makes it easy to distinguish the individual pressure effects which influence the melting point. If $\sigma_s = \sigma_l$, then

$$T_o - T = \frac{2T_o}{r\lambda_o}\sigma(v_s - v_l) = \frac{T_o}{\lambda_o}\Delta p(v_s - v_l).$$

(21)

This is the ordinary Clapeyron equation, applicable to equilibrium in a system throughout which the pressure is uniformly p.

On the other hand, the first term measures the effect the non-uniformity in pressure, $i.e.$, the difference between the pressures of the solid and liquid phases, has upon the melting point.

It is important to understand that both of these effects are operative in altering the melting point. In this sense, the present phenomenon must be distinguished from the more familiar situation in which there may be an increment of pressure which is the same in both liquid and solid. Since σ_s always exceeds σ_l, the first term in (20) is positive and tends to depress the melting point. The second term can be either positive or negative.

For a depression of melting point to occur, the second term must be positive or the absolute value of the first term must exceed that of the second, i.e.,

$$\frac{\sigma_s}{\sigma_l} > \frac{v_l}{v_s}.$$

It is probable that this inequality is generally valid, and that a depression of melting point is to be anticipated.

In any event Eq. (19) applies.

The search for simple systems in which the thermal effect of surface is pronounced, led Tammann and Meissner $(11,5)$ to consider the melting point of thin flat films. They contended that films melt at lower-than-normal temperatures, and derived a relation which represented the dependence of melting point upon film thickness. Meissner obtained experimental data with films several microns thick which supported this relation. This relation is not complete, in that the surface work terms are not evaluated in detail and, consequently, the influence of the wall material (Eq. 7) is not emphasized. In addition, the relation can be expressed in terms of an alternate set of variables which are more commonly measured. Because of these insufficiencies, a more thorough presentation is given below.

It is to be assumed that the solid and liquid films are constrained by walls. Consequently, we must, in Eq. (2), employ

$$\sigma_{lw} - \sigma_{w},$$
$$\sigma_{sw} - \sigma_{s}. \tag{22}$$

Furthermore, the surface terms in Eq. (14) are to be evaluated, using the following relations

$$\frac{\partial A_s}{\partial n_s} = \frac{v_s}{t},$$
$$\frac{\partial A_l}{\partial n_l} = \frac{v_l}{t}, \tag{23}$$

where t is the film thickness, and where it has been assumed that the original surface, in bulk, was negligible and equivalent to zero. In this light Eq. (14) reduces to

$$\frac{\lambda_o}{T}(T - T_o) = \frac{1}{t}\left[v_l(\sigma_{lw} - \sigma_w) - v_s(\sigma_{sw} - \sigma_w)\right]. \qquad \centerdot \tag{24}$$

In Meissner's experiment, the melting point was determined by maintaining a temperature gradient parallel to the extent of the film. At that point in the gradient corresponding to the melting point of the film, a liquid-solid interface could be discerned and, from the relation between position and temperature, one could estimate the melting point.

Because the pressures are different in liquid and solid, the profile of this interface must necessarily be that of a cylindrical surface, having the two principal radii, ∞ and $\dfrac{2 \cos \theta}{t}$ (see below). It is instructive to develop the melting point Eq. (24) in terms of the geometrical parameters associated with this interface.

Using the equations

$$\sigma_{lw} - \sigma_w = - \sigma_l \cos \theta_l,$$
$$\sigma_{sw} - \sigma_w = - \sigma_s \cos \theta_s, \tag{25}$$

where θ_l and θ_s are the equilibrium contact angles of liquid and solid, respectively, upon the wall material, in the presence of air, we obtain

$$T_o - T = \frac{2T_o}{\lambda_o t} (v_l \sigma_l \cos \theta_l - v_s \sigma_s \cos \theta_s). \tag{26}$$

This equation can be transformed to include the interfacial tension between solid and melt, σ_{ls}, by the use of Equations (25) and

$$\sigma_{sw} - \sigma_{lw} = \sigma_{ls} \cos \theta, \tag{27}$$

where θ is the equilibrium contact angle of liquid on wall in the presence of solid (see Fig. 1).
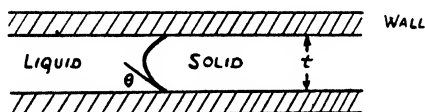
FIG. 1.

It follows that

$$\sigma_l \cos \theta_l - \sigma_s \cos \theta_s = \sigma_{ls} \cos \theta, \tag{28}$$

which, when substituted into Eq. (26) with the aid of the identity $v_l = v_s - (v_s - v_l)$, yields

$$T_o - T = \frac{2T_o}{\lambda_o t} v_s \sigma_{ls} \cos \theta + \frac{2T_o}{\lambda_o t} (v_l - v_s)\sigma_l \cos \theta_l. \tag{29}[2]$$

[2] Eqs. (24), (26), and (29) may be altered to apply to matter in the form of fine threads (constrained within capillary tubes) by substituting the diameter of the thread, d, for $\dfrac{t}{2}$.

Just as in the case of spheres, the melting point change is given by the sum of two terms, the first of which arises from a difference in pressure between liquid and solid, $\frac{2\sigma_{ls} \cos \theta}{t}$, and the second is related to the usual Clapeyron equation, since $\frac{2\sigma_l \cos \theta_l}{t}$ is the difference in the internal pressures of the liquid in film and in bulk, at constant external pressure.

Examination of Eq. (19) indicated that the melting point of spherical particles will usually be lower than normal, since σ_s exceeds σ_l, while the molar volumes do not differ greatly. With films, the complications introduced by the walls make predictions more difficult. Neglecting the difference in molar volume, Eq. (26) shows that the melting point will be raised or depressed, depending upon whether $(\sigma_s \cos \theta_s - \sigma_l \cos \theta_l)$ is positive or negative. The chemical nature of the wall and the substance being investigated determine the contact angles, and therefore the wall affects not only the magnitude of the change, but also its sense.

Eq. (19) and (29) both might be used as bases for measuring solid surface tensions since all of the other quantities appearing in these equations are comparatively easy to measure. It should be indicated that these surface tensions are mean quantities, since the different crystal faces may have different surface tensions. In this connection, the fusion of spheres offers a simpler tool, because the melting of films involves additional parameters characteristic of the wall.

Meissner found that a film of azobenzene, 1μ thick (glass walls) melted at about 0.35°C. below normal. Since t and $2r$ are comparable quantities, the depression should be at least twice as great for azobenzene spheres 1μ in diameter, if we suppose the molar volumes of liquid and solid to be equal. Experimentally, it is a simple matter to make aerosol particles as small as 0.2μ in diameter, and so a depression of at least 3.5°C. should be observable.

SUMMARY

The macroscopic nature of fusion in extended systems is discussed in detail. In this connection, the experimental significance of the term "melting point" is examined.

A relation between the extent of surface and internal pressure is derived. The new relation is to be distinguished from Kelvin's formula which relates the pressures on either side of a curved surface, although,

in special cases, the two formulas may coincide. A relation between the solid-melt interfacial tension, the solid-gas interfacial tension, and the liquid-gas interfacial tension is derived for the case of equilibrium between solid and melt. Finally, a general relation between melting point and extent of surface is derived, and applied to the case of spheres, films, and threads.

REFERENCES

1. GUGGENHEIM, Modern Thermodynamics after the Methods of Willard Gibbs. Methuen & Co. Ltd., London, 1933, pp. 160–181.
2. EPSTEIN, Textbook of Thermodynamics. Wiley, New York, 1945, p. 214.
3. PAVLOV, Z. physik. Chem. **65**, 1 (1909).
4. PAVLOV, Kolloid-Z. **7**, 37 (1910).
5. MEISSNER, Z. anorg. Chem. **110**, 169 (1920).
6. LEWIS AND RANDALL, Thermodynamics. McGraw-Hill, New York, 1923, p. 252.
7. LaMER AND SINCLAIR, O.S.R.D. Rep. 1668, P.B. 32200 B.S. 1R2662 (1941); O.S.R.D. Rep. 1837 (1943), Dept. of Commerce Off. of Pub. Rep. 944. Chem. Revs. in press. WILSON AND LaMER, J. Ind. Hyg. Toxicol. in press.
8. SINCLAIR, J. Optical Soc. Am. **37**, 475 (1947).
9. JOHNSON AND LaMER, J. Am. Chem. Soc. **69**, 1184 (1947).
10. WEISER, Colloid Chemistry. Wiley, New York, 1939, p. 62.
11. TAMMANN, Z. anorg. Chem. **110**, 166 (1920).

VARIATION WITH TEMPERATURE OF THE NUCLEATION RATE
OF SUPERCOOLED LIQUID TIN AND WATER DROPS

Bernard Vonnegut

From the General Electric Research Laboratory, Schenectady, N. Y.

Introduction

In investigations of the kinetics of the formation of a new phase, it is important to learn at what rate nuclei, or centers of formation for the new phase, make their appearance. It is possible to investigate the rate of nucleation by observing single masses of material during and after a phase transformation. However, in many cases it is difficult to separate the kinetics of nucleation from the kinetics of the growth of the new phase after nuclei have made their appearance. The nucleation of a substance can often be more easily studied by dividing it into a large number of small mutually independent particles and observing as a function of time the number of particles which have undergone transformation. The time required for a particle to change from one phase to another once a nucleus has formed will, in general, be proportional to the first power of the particle radius. The chance that a nucleus will form will generally be proportional to the second or third power of its radius. Therefore, by making the particle sufficiently small, the time required for the occurrence of a nucleus can be made large in relation to the time required for the particle to transform once a nucleus has appeared. It is advantageous to make nucleation measurements on systems containing a sufficiently large number of particles to be easily treated statistically.

Preliminary investigations have been on the nucleation of supercooled tin and supercooled water. Observations were made at constant temperatures on the freezing rate of systems composed of large numbers of supercooled drops.

Experimental Methods and Results

Nucleation of Supercooled Liquid Tin

In the experiments on tin, the samples were prepared from a fine tin powder (obtained from Eimer and Amend) consisting of small spheres of tin ranging in diameter from approximately 1 to 10 μ.

The first determinations of the rate of nucleation of supercooled tin drops were made using X-ray diffraction measurements. The sample of

tin powder was mixed with a Bakelite varnish and spread as a film on a
glass slide. The slide was mounted in a small electric furnace built to fit on
a Philips X-ray diffraction apparatus. The apparatus was adjusted to
give a strong diffraction line of the crystalline tin powder. The sample
was then heated above its melting point (231.89°C.) to 240°C. At the
melting point, the diffraction line of the solid tin disappeared. Hydrogen
gas was run through the furnace to prevent oxidation of the sample. After
having been heated above the melting point, the sample was cooled and
held at some temperature below its freezing point. The rate at which the
supercooled particles crystallized was determined by measuring the rate
at which the intensity of the diffraction line of solid tin returned to its
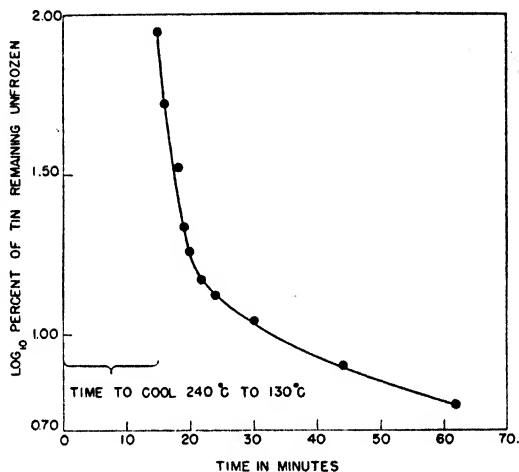
FIG. 1. Fraction of tin drops remaining unfrozen as function of time at 130°C., from
X-ray data.

former value. The results of a typical experiment are shown in Fig. 1. It
was soon found that the rate of nucleus formation was greatly increased
by a small decrease in temperature and that the temperature control was
not sufficiently sensitive to permit measurements with any accuracy.

A different apparatus was then set up in which the rate at which the
tin particles solidified could be measured by the rate at which their
volume changed. When liquid tin crystallizes, its volume decreases by
about 5%. The tin powder was first heated in air for about 0.5 hr. at
150°C. to give it a thin coating of oxide to separate the particles. It was
sealed into a bulb of a dilatometer (see Fig. 2). The dilatometer was then
pumped out and baked at a pressure of less than 1 μ to remove any gas.
"Octoil S" was then distilled into the dilatometer under vacuum. A

measurement of the rate of nucleation was made by first heating the bulb to a temperature above the melting point of tin (265°C.), and then placing it in a silicone oil constant temperature bath. The rate of nucleation was determined by observing the rate of volume decrease as measured by the motion of the "Octoil S" along a graduated capillary tube. A long capillary tube was used in the first experiments, but it was found that appreciable error was caused by the slow drainage of the liquid from the walls of the tube. This difficulty was minimized by using the oil reservoir shown in Fig. 2. During the melting of the sample, the tube was held at an angle so that the liquid covered the end of the capillary tube. When the sample had been cooled to almost the desired temperature, the tube was tipped so that the excess liquid ran away from the end of the capillary tube, thus forming the meniscus in a convenient position.
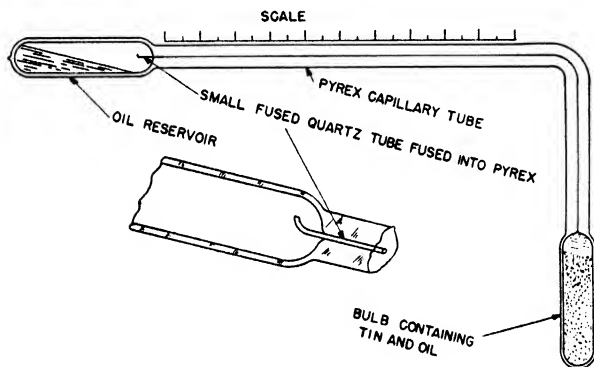
Fig. 2. Dilatometer.

The results of the experiments are shown in Fig. 3. The time has been plotted on a log scale to condense the curves for runs made over a long time interval. If the chances of a nucleus occurring in each tin particle were exactly the same and were independent of the length of time it had been supercooled, one would expect the rate of nucleation to decrease exponentially with time. The curves show clearly that in these experiments this is not the case. The fraction of the unfrozen portion of the sample crystallizing per unit time steadily decreases with time. Some drops nucleate more rapidly than others, probably because they are either larger than the others or because they contain certain impurities which increase the probability of nucleus formation. The data obtained should be interpreted as the behavior of supercooled tin with whatever impurities were present. It is probable that tin, free of impurities, if it could be obtained, might behave very differently.
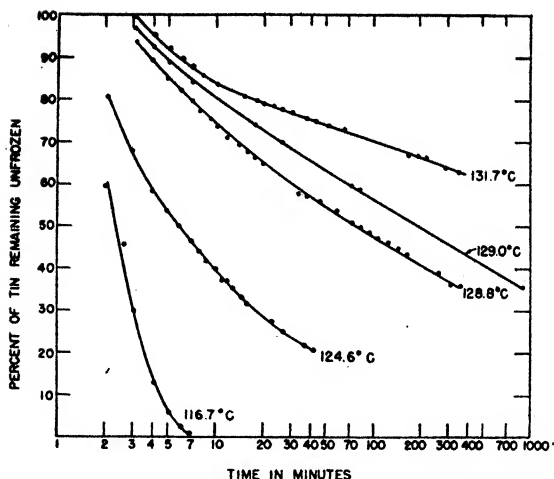
FIG. 3. Fraction of tin drops remaining unfrozen as a function
of time from dilatometer data.

One of the most striking features of the data is the very great effect
of temperature on the rate of nucleation. A decrease in temperature of 7°
causes a 60-fold increase in the nucleation rate. In observations on the
rate of nucleation of supercooled water clouds in the presence of silver
iodide smoke, the author has observed a similar large negative tempera-
ture coefficient (1). For a given smoke the rate of ice crystal formation was
approximately 30 times greater at $-13°C$. than at $-10°C$.
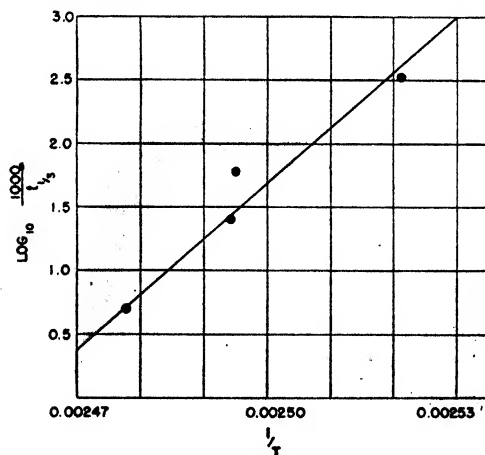
FIG. 4. Nucleation rate of tin drops as a function of temperature.

An approximate value for the activation energy of the nucleation reaction can be computed from the data in Fig. 3. The log of the reciprocal of the time required for $\frac{1}{3}$ of the sample to freeze was plotted against the reciprocal of the absolute temperature to give the curve in Fig. 4. This corresponds to an activation energy of -2×10^5 calories. The data taken at 116.7°C. have not been used because nucleation at that temperature proceeds so rapidly that most of the sample is frozen by the time its temperature has come to equilibrium with the constant temperature bath.

The fact that the tin particles had widely differing diameters greatly limits the deductions which can be obtained from these experimental results. Not only is the probability of nucleus formation far larger in a large drop than in a small one, but the freezing of a large drop would produce a far greater effect on the diffraction of the X-rays or the volume of the system than would the freezing of a small drop. The data, therefore, probably reflect primarily the behavior of the larger drops.

It is highly desirable that future experiments be conducted on samples containing drops that are as nearly identical as possible.

Nucleation of Supercooled Water

The author first attempted to measure the nucleation of supercooled water in experiments conducted while at the De-icing Research Laboratory at M.I.T. An emulsion of water drops suspended in lubricating oil was cooled to −29°C. with the expectation of measuring the nucleation rate by the rate of volume increase. This method was not successful, because the solubility of water in the oil was sufficiently large that diffusion rapidly took place from the unfrozen to the frozen drops.

Some preliminary studies on water have been made in this laboratory using a variation of the above method. In these experiments, 64 drops of distilled water, weighing approximately 3 mg. each, were placed in a square pattern on a polished chromium plated metal plate.

On the recommendation of V. J. Schaefer of this laboratory, the chromium surface of the metal plate was covered with a thin film of polystyrene by dipping it into a solution. This had been found by Schaefer to lower the temperature to which the water could be supercooled. The plate with the drops on its surface was then placed on a thermostated copper block at some temperature below freezing. To prevent impurities in the air from settling on the water drops, the plate was covered with a piece of plate glass which rested on a raised rim on the copper block. The heat transfer between the block and plate was sufficient to bring the drops on the plate to the temperature of the block in less than 1 min. The number of unfrozen water drops was measured as a function of time
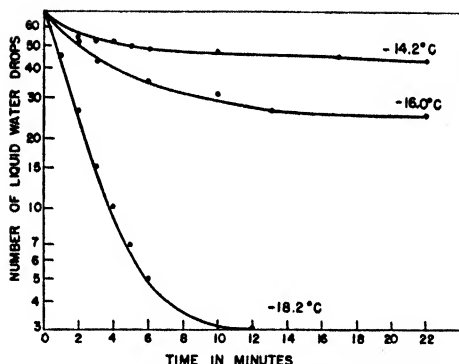
FIG. 5. Fraction of water drops remaining unfrozen as a function of time.

by visual observation. Fig. 5 is a curve showing the nucleation of the drops at various temperatures.

Despite precautions to keep the water drops free of impurities, it is certain that they were contaminated by foreign material from the atmosphere and by the surface of the plate which increased the rate of nucleation. Here again the data would probably be far different for completely pure water. The striking feature of the data is again the large negative
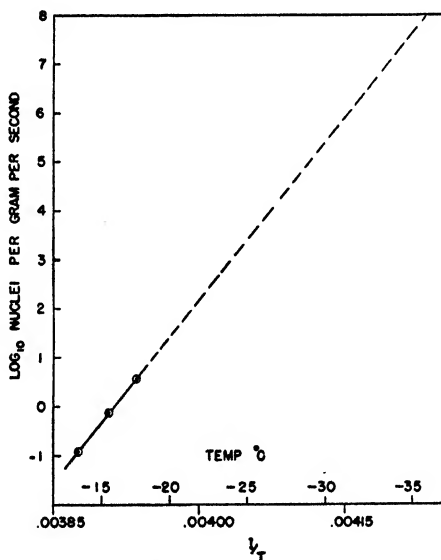
FIG. 6. Nucleation rate of water drops as a function of temperature.

temperature coefficient which characterized the results of the experiments on supercooled tin and on a supercooled cloud seeded with silver iodide.

The data for the freezing of water drops given in Fig. 5 can be interpreted in terms of the rate of nucleus formation per gram of water. Fig. 6 relates the rate of nucleus formation per gram to the reciprocal of the absolute temperatures. The rate of nucleation was calculated from the times required for the first 22 drops to freeze at the various temperatures. The energy of activation computed from the slope of the curve in Fig. 6 is $- 1.6 \times 10^5$ cal. It is interesting to extrapolate these data for comparison with observations made by Schaefer (2, 3) in his experiments on supercooled clouds. If it is assumed that the liquid water content in the cloud in the cold box is of the order of 1 g./m.^{3}, at a temperature of $-25°$C., according to these data ice crystals should be appearing at the rate of about 10^4/sec. Actually, with clean air at this temperature, no crystals are observed. It is not until the temperature falls below $- 39.0 \pm 0.1°$C. that many crystals begin to form. The rate of nucleation in the water drops on the metal plate is much larger than that in the water drops in a cloud, probably because of the nucleating effect of the surface of the plate and chance impurities.

The sudden appearance of large numbers of ice crystals when the temperature is $-39°$C., or lower, indicates that in Schaefer's experiments the increase in nucleation rate with decreasing temperature must be even greater than that found in this work.

SUMMARY

X-ray diffraction, dilatometric, and visual techniques are described for measuring the extent of crystallization of systems composed of many small mutually independent volumes of supercooled liquid. Preliminary measurements on supercooled liquid tin and supercooled water show their rate of nucleation has a very large negative temperature coefficient corresponding to an activation energy of the order of $- 2 \times 10^5$ calories.

REFERENCES

1. VONNEGUT, B., To be published in *Chem. Revs.*
2. SCHAEFER, V. J., *Science* **104**, 457–459 (1946).
3. SCHAEFER, V. J., *Bull. Am. Meteorological Soc.* **29**, 175–182 (1948).

THE KINETICS OF THE FORMATION AND GROWTH OF MONODISPERSED SULFUR HYDROSOLS

Ethel M. Zaiser and Victor K. La Mer

Contribution from the Department of Chemistry, Columbia University, New York 27, N. Y.

Received January 8, 1948 [1]

INTRODUCTION

Colloidal dispersions which are formed by condensation from an initially homogeneous phase pass very rapidly through an early stage of growth and coagulation. The processes that occur in this stage cannot be studied satisfactorily by present techniques until the rate decreases. By that time a polydispersed colloid has formed. If, however, the substance which is to constitute the dispersed phase is slowly and continuously produced in the system, for example by a chemical reaction, repetitive nucleation is obviated and the growth on the first nuclei proceeds uniformly. The product is a monodispersed colloid which can be characterized precisely as to particle size and number by optical methods.

Aerosols which were so monodispersed in respect to particle size that they exhibited higher order Tyndall spectra were prepared for the first time by La Mer and Sinclair by regulating the cooling of vapors in the presence of controlled numbers of nuclei. These monodispersed preparations were used in the experimental verification of the Mie theory for the scattering of light (1,2). These findings were extended by La Mer and Barnes to monodispersed sulfur hydrosols (3,4). When the homogeneous solution of sulfur produced by the reaction of very dilute thiosulfate and acid becomes sufficiently supersaturated, droplets of supercooled liquid sulfur suddenly appear (5). These droplets grow slowly and so uniformly that monodispersed systems of different particle sizes are readily obtainable for study, after stabilization by the addition of iodine. The sphericity of the micelles and their monodispersed character simplifies the application of the Mie theory as a means of determining the size and number of particles (4,6,7,8).

It is the purpose of this paper to investigate the factors which influence the formation and growth of the particles in these sols, which are easy to reproduce and measure quantitatively. This study may be divided into 3 stages.

---

[1] This paper was presented at the Conference on "Molecular Interaction" held under the auspices of the New York Academy of Sciences on April 8, 1948.

I. The homogeneous reaction. The reaction begins as soon as the acid and thiosulfate are mixed, and produces molecularly dispersed sulfur. This stage is terminated when the sulfur solution becomes sufficiently supersaturated for stable nuclei to form.

II. The condensation stage. Here the rapid condensation of molecularly dispersed sulfur upon the nuclei relieves the supersaturation with the result that the rate of subsequent nucleation is greatly decreased.

III. The heterogeneous stage. The sulfur droplets slowly increase in size by diffusion of dissolved sulfur to the particle surfaces. The preservation of a high degree of monodispersity in this stage depends upon a low rate of formation of dissolved sulfur and the absence of repetitive nucleation and of secondary coagulation.

I. The Homogeneous Reaction

A. Historical Summary

Landolt (9) reported that an acidified solution of sodium thiosulfate remains clear for a time interval which depends on temperature and concentration, following which colloidal sulfur appears. This "induction period" was investigated by Foussereau (10). He reported a steady decrease in conductivity from the time the reactants were mixed. Biltz and Gahl (11) improved Landolt's method for detecting the Tyndall beam by using an ultramicroscope. A comprehensive review is given by Sheffer and Böhm (12). Ostwald (13) expressed the view that the sudden appearance of colloidal sulfur marks the end, not of an induction period, but of a state of supersaturation with respect to dissolved sulfur. In the absence of foreign nuclei a high degree of supersaturation would be expected. Since the reaction does not go to completion the removal of sulfur by the formation of a second phase should favor the forward progress of the reaction. Jablczynski and Warszawska-Rytel (14) reported transmission curves in the visible range using a Koenig-Martens spectrophotometer for $0.025 \ M \ Na_2S_2O_3$ and $0.125-1.25 \ M \ HCl$. At these high concentrations stage I is complete in less than 1 min. and a polydispersed colloidal system is formed. They interpreted their results as revealing an autocatalytic effect attributable to the formation of colloidal sulfur.

The products of the reaction have been studied extensively (12,14,15, 16,17). It has been shown that near pH = 3 about 80% of the reaction yields sulfur and sulfite, while side reactions produce polythionates. The results of different kinetic investigations (12,14,16,18) are not in harmony as to the mechanism of the reaction or even the identity of the reacting species, although it now seems certain that $HS_2O_3^-$ is involved (18,19).

La Mer and Kenyon (5) demonstrated experimentally the formation of dissolved sulfur by transmittance studies in the ultraviolet region, where sulfur absorbs. Their results indicate that, under ordinary condi-

tions, a definite concentration of molecularly dispersed (*i.e.*, dissolved) sulfur must be produced before sulfur micelles appear. Experiments designed to test the order of the reaction and the effects of added salts should yield information about the nature of the homogeneous reaction and the identity of the reacting species.

B. Experimental

Materials. Sodium thiosulfate, C. P., was recrystallized according to the method of La Mer and Tomlinson (20). The wet crystals were dissolved immediately in water and the solutions were standardized against $K_2Cr_2O_7$, then diluted and restandardized to give stock solutions whose concentration was $1.000 \pm .001$ M. Stock solutions of 1.5 M H_2SO_4 and 3 M HCl were made from reagent grade acids and standardized against Bureau of Standards potassium acid phthalate. Lanthanum sulfate was made from the nitrate by the action of sulfuric acid. The other salts used were C. P. grade and were not purified further.
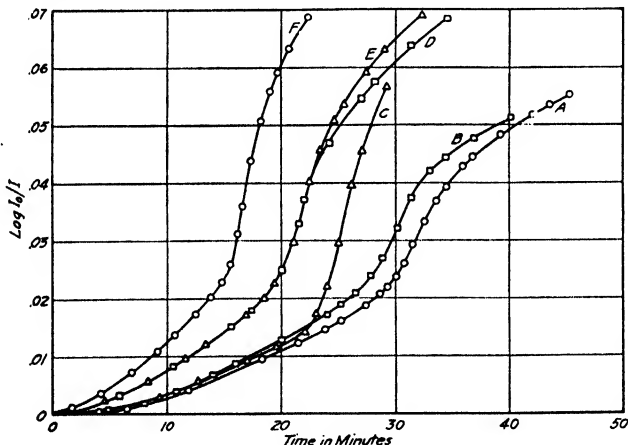
Fig. 1. Effect of salts on optical density as a function of time after mixing at $\lambda = 3000$ Å. $Na_2S_2O_3 = 0.002$ M, HCl $= 0.002$ M. A. No added salt, B. 0.0118 M NaNO₃, C. 0.2 M KCl, D. 0.0014 M La₂(SO₄)₃, E. 0.0005 M La(NO₃)₃, F. 0.0028 M La(NO₃)₃.

Method. Suitable aliquots of thiosulfate stock solution were delivered from a 2 ml. hypodermic syringe and mixed in nearly 1 l. of distilled water or a specified salt solution. The addition of acid from a syringe, mixing, and making up to volume occupied 20 ± 3 sec. The temperature was maintained at $25 \pm 0.05°$C. The ranges covered were from 0.001 to 0.003 M in thiosulfate, from 0.001 to 0.006 M in H⁺, and from 0.007 to 0.03 in ionic strength.

The formation of molecularly dispersed sulfur (5) can be followed by transmittance measurements at $\lambda = 3000$ Å. The increase in optical density as a function of time was accordingly measured at this wavelength in 10 cm. quartz cells with a Beckman quartz spectrophotometer (model DU), using a solution of appropriate thiosulfate concentration as the blank. The absorption cells were refilled every few minutes from the reaction mixture which was kept at 25°C. The optical density readings were reproducible to within ± 0.0005. Typical curves for log (I_0/I) vs. time are shown in Fig 1.

The time at which a sharp break occurs in the log (I_0/I) curve, marking the beginning of light scattering by colloidal sulfur, is desig-
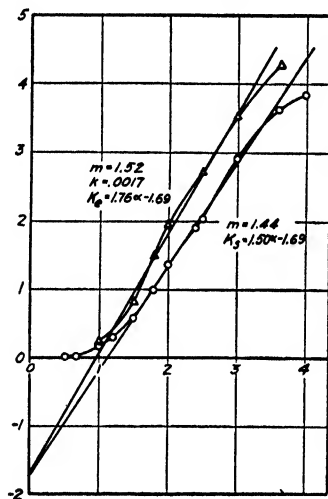
Fig. 2. Theoretical scattering area coefficient K_s as a function of $\alpha = 2\pi r/\lambda'$.

nated as "t_B." The uncertainty in the estimation of t_B is decreased to $\pm \frac{1}{2}$ min. if the slope of the log (I_0/I) vs. time curve for $\lambda = 3000$ Å is examined and t_B taken as the point at which the slope increases rapidly. The application of this criterion to the data of La Mer and Kenyon (5) gives t_B values of 61 min. for 0.0010 M thiosulfate and 0.0015 M H_2SO_4, and 30 min. for 0.0015 M thiosulfate and 0.003 M HCl, instead of their values of 70 and 35 min., respectively. It also changes their estimate of the sulfur concentration at t_B from 5.5×10^{-6} to between 3 and 4×10^{-6} g.-atom/l.

C. Results

Constancy of Log (I_0/I) at t_B. Table I shows some results of experiments designed to test the reproducibility of t_B data. The average devia-

tion is ± 1 min. In Table II are indicated the values of $\log (I_0/I)$ observed at t_B for sols representing the entire range of reactant concentrations and ionic strengths studied. The constancy of $\log (I_0/I)$ at t_B $(0.020 \pm 5\%)$ makes it possible to use t_B as a measure of the rate of the formation of dissolved sulfur. The value 0.020 could be used to determine the sulfur concentration in the supersaturated solution just before condensation occurs if the extinction coefficient of sulfur in water were known. Using La Mer and Kenyon's (5) averaged value of 1460 cm²./g.-atom for the extinction coefficient of sulfur in organic solvents, the sulfur concentration at t_B is 3.2×10^{-6} g.-atom/l. The order of magnitude of this figure is correct and is a qualitative indication of how very small the solubility of sulfur in water must be.

TABLE I

Reproducibility of t_B at $\lambda = 3000$ Å

Thiosulfate	H⁺	t_B, min.	Average t_B
0.002 M	0.002 M	31, 29, 27.5, 30.5, 29, 28, 28, 28, 30	29 ± 1
0.002	0.003	25, 21, 24, 25, 22, 24	23.5 ± 1

Dependence of Rate on Reactant Concentrations. Since the amount of sulfur formed at t_B is constant, and the extent of reaction is very small, the following relationship is valid:

$$(S)_B/t_B = k(T)^a (H)^b,$$

where $(S)_B$ = sulfur concentration at t_B, and (T) and (H) = concentrations of total thiosulfate and acid, respectively. A comparison of the reaction rates at constant ionic strength for different thiosulfate and acid concentrations shows that $a = \frac{3}{2}$ and $b = \frac{1}{2}$. Table II shows the results of the calculation of a constant $k_S = k/(S)_B = [t_B(T)^{\frac{3}{2}}(H)^{\frac{1}{2}}]^{-1}$, from which it is seen that $k_S = 8700 \pm 5\%$ liter² mol⁻² min.⁻¹.

Salt Effect. From an examination of the data in Table II it is evident that the effect on t_B of small amounts of univalent salt such as were used to adjust the ionic strength of some reaction mixtures is hardly differentiated from the usual variations in t_B that are due to failure of exact reproduction of a given set of condensation conditions, or merely to uncertainties in estimating t_B. The slight trend toward a positive salt effect indicated that further experimentation designed to prove or disprove the existence of such an effect might prove fruitful. The effect of adding a larger amount of KCl (0.2 M) is shown in Fig. 1, curve C. Here the rate of sulfur formation increases only slightly, but condensation begins at a

TABLE II

Constancy of log (I_0/I) at t_B and Dependence of Homogeneous Reaction Rate on Molar Concentrations of Reactants

10^3 (T)	10^3 (H)	10^3 KCl	μ	log (I_0/I) at t_B	t_B min.	10^{-3} k_S
1	3 x	—	0.0075	0.0200, 0.0190	66	8.8
	x	6.0	.0135	.0205	66	8.8
	x	9.9	.0174	.0185, .0195	63	9.2
	x	10.4	.0179	.0200, .0195	61	9.5
1	4	0.4	.0074	.0205	62	8.1
1	6 x	6.0	.0180	.0200	46	8.9
2	1	—	.0070	.0190, .0215	43	8.2
		0.3	.0073	.0225, .0205	45	7.9
		3.2	.0102	.0195	43	8.2
2	2	—	.0080	.0185, .0200	29	8.6
		5.4	.0134	.0190, .0185	29	8.6
		10.0	.0180	.0190, .0205	26	9.6
2	3 x	—	.0105	.0205, .0225	24	8.5
	x	—	.0105	.0195, .0210	25	8.2
	x	3.0	.0135	.0210, .0215	24	8.5
	x	7.5	.0180	.0180, .0190	22	9.3
	x	20.0	.0305	.0195, .0180	21	9.7
3	1	8.0	.0180	.0185	24	8.0
3	1.5	7.5	.0180	.0185	17	9.2
3	2	7.0	.0180	.0185	15	9.1

x = H_2SO_4 was used; HCl used in all other runs.

Average log (I_0/I) at t_B = 0.020 ± .001.

Average 10^{-3} k_S = 8.7 ± 0.4 liter^4 mol^{-2} min.$^{-1}$.

TABLE III

Effect of Salts on the Rate of the Homogeneous Reaction of 0.002 M $Na_2S_2O_3$ and HCl

Salt	Log (I_0/I) at t_B	t_B	10^{-3} k_S
None	0.0210	28.5	8.8
0.0118 M $NaNO_3$	.0205	28.5	9.4
.0028 M $La(NO_3)_3$	.0205	14	17.8
.0010 M $La(NO_3)_3$	.0215	16	15.6
.0005 M $La(NO_3)_3$	.0210	19	13.2
.0014 M $La_2(SO_4)_3$	.0195	18.5	13.5

value of optical density lower than usual, indicating that salting out or perhaps some effect on nucleus formation may have occurred. The positive catalytic salt effect is demonstrated more clearly by the experiments with La^{+++} salts (Table III and Fig. 1), in which increasing quantities of $La(NO_3)_3$ produce correspondingly increasing catalytic effects. The nitrate ion has no specific effect on the reaction, as shown by the very small catalysis by 0.01 M $NaNO_3$. When $La_2(SO_4)_3$ is used, however, the catalysis is much less efficient, 0.0028 M La^{+++} in that form being only as effective as 0.0005 M La^{+++} in the form of the nitrate. This can be explained in the same manner as was Tomlinson's kinetic data on the bromacetate-thiosulfate reaction (21). The La^{+++} ions set up very large local deviations from the average bulk concentration of reactant ions, thus making it easier for the negative ions which are attracted to their vicinity to react. This interpretation is further supported by the opposing effect of sulfate ion to the La^{+++} catalysis, since these doubly charged anions offer the reacting species serious competition for places near La^{+++} ions.

II. The Condensation Stage

A. Theory

The onset of the condensation stage under constant conditions of medium and temperature has been used in the preceding section as a criterion of the rate of the homogeneous reaction. We now examine some of the factors other than the rate of formation of dissolved sulfur that affect the beginning of the phase transition and the early stages of growth of the particles (22,23).

Thermodynamic Equilibrium between Phases. It was first shown by J. Willard Gibbs (24) that a spherical mass of phase II of radius r^* can remain in equilibrium with a surrounding mass of phase I which is supersaturated with respect to a droplet of II having an infinite radius. When the influence of the surface of contact between the two phases is taken into account, the equality $P_I = P_{II}$ is replaced by

$$P_{II} - P_I = 2\sigma/r^*,$$

where σ = surface tension, P_{II} = the pressure of the interior mass of the droplet of phase II, and P_I = the pressure of the exterior mass, phase I. The reversible work required to form such a mass in the interior of an infinite mass of the other phase is given by the general equation

$$W = \sigma s - V_{II}(P_{II} - P_I), \tag{1}$$

where σs = the work spent in forming the surface s, and $V_{II}(P_{II} - P_I)$ = the work gained in forming the interior mass of volume V_{II}. Gibbs further pointed out that W is always positive and equal to $\sigma s/3$—*i.e.*, the second term in Eq. 1 is $\frac{2}{3}$ of the first for a spherical droplet.

J. J. Thomson arrived at an equivalent and more often quoted expression for r^* in terms of

$$(\mu_r^* - \mu_\infty) = 2\sigma v_{II}/r^*,$$

where μ_r^* and μ_∞ = chemical potentials of the molecules in droplets of phase II of radius r^* and of infinite radius, respectively, and v_{II} = molecular volume in the droplet. For the case of equilibrium in a supersaturated vapor the J. J. Thomson equation takes on the familiar form

$$\ln (p_r^*/p_\infty) = 2\sigma v_{II}/kTr^*,$$

where k = Boltzmann gas constant, T = absolute temperature, p_r^* = vapor pressure of a liquid droplet of radius r^*, and p_∞ = vapor pressure over a flat surface of the liquid. Droplets smaller than the critical size are unstable because phase I is unsaturated with respect to them, while for $r > r^*$ phase I is supersaturated and again instability results. For $r = r^*$, a metastable equilibrium exists. Since the work required to form the surface of a droplet is of considerable magnitude, a comparable degree of supersaturation is necessary before the formation of droplets of the critical size can proceed at a measurable rate (22).

Nucleus Formation. The probability of the formation of the smallest mass of a new phase which can grow in the mother phase through further acquisition of molecules depends on $e^{\Delta S/k}$, where ΔS is the increase in entropy associated with a variation from the normal state of the system large enough to produce a nucleus. If the minimum work required to bring about such a change by an isothermal reversible process is $W = \sigma s/3$, the probability of forming Z droplets of phase II of the critical size in a large mass of phase I is

$$w = Ze^{-W/kT}.$$

If τ = the average lifetime and J' = the frequency of formation of the droplets,

$$J' = w/\tau = (Z/\tau)e^{-W/kT}.$$

In reality, a nucleus once formed has an equal chance of decreasing in size or of growing. However, only the latter course produces a change of state of the original phase I. If we imagine a process by which each nucleus on which any additional growth has taken place is removed from the system, so that the state of phase I remains substantially unchanged, the frequency J of formation of nuclei effective in the phase transition will be $J = J'/2 = (Z/2\tau)e^{-W/kT}.$

The factor Z/τ can be evaluated for some special cases by a kinetic treatment (22). The order of magnitude of the exponent W/kT, however, is all that is really important in determining the sharp limit of supersaturation at which J becomes so large that a spontaneous phase transition occurs. For water vapor at 300°C. in the absence of foreign nuclei

this limit lies between $p_r/p_\infty = 4.1$ and 4.2. The very rapid increase of J with supersaturation is shown by the fact that for $p_r/p_\infty = 3$ it would take 1000 years to form a droplet in 1 cm.³ of vapor, while the process would require only 10^{-8} seconds if $p_r/p_\infty = 5$.

The work W required for nucleus formation is the analog of the free energy of activation for a chemical process, and the path followed has been assumed to be the one of lowest activation energy or highest probability. The theory as sketched here does not assume any mechanism for the nucleus formation, although it is believed that the fluctuations in the density of the molecular population of a phase produce "embryos" of a new phase. The fluctuations required are of the heterophase type, $i.e.$, they exceed the limits of the normal homophase fluctuations which are insufficient to lead to a macroscopic change of state.

Growth of Particles. After nucleus formation, growth proceeds by the diffusion of molecules from the original phase to the nucleus. This can be expressed in a simple mathematical form by making the following assumptions (25): (a) the particle is spherically symmetrical, and (b) a stationary state is reached soon. In terms of the number of molecules dn diffusing in time dt through each spherical surface about the particle one gets:

$$dn/dt = 4\pi R^2 D(dc/dR), \tag{2}$$

where c = molecular concentration at the distance R from the nucleus, and D = diffusion coefficient. The following expression can be differentiated to find dc/dR:

$$(c - c_s)/(c_o - c_s) = 1 - r/R,$$

where c_s = concentration of the saturated solution at the particle surface where $R = r$, and c_o = original concentration at the distance $R = \infty$. Substitution for dc/dR in Eq. 2 and expression of n in terms of the particle radius r and the molecular volume v_{II} in the new phase, followed by integration, yields the final equation:

$$r^2 = r_o^2 + kt,$$

where $k = 2Dv_{II}(c_o - c_s)$, and r_o = radius of particle when growth begins (at $t = 0$). Consequently, when a stationary state is set up, a spherical particle of phase II should exhibit a constant rate of increase of the area of the surface it presents to the surrounding phase I, provided the rate is diffusion controlled.

B. Some Qualitative Observations

Any change in the medium that affects the solubility of sulfur will produce a corresponding change in the concentration of sulfur that can exist before condensation starts. Examples are furnished by the salting-

out effect of 0.2 M KCl (see Fig. 1), and reports by earlier workers (26) of the greater "stability" of thiosulfuric acid in alcoholic solution. The addition of small amounts of alcohol, dioxane, or similar solvents to the reaction mixture increases the concentration of sulfur (or the optical density) that is reached before condensation sets in. An extreme example is the solvent 50% dioxane-water, in which colloidal sulfur does not appear after 2 days. The addition of water brings about an immediate precipitation of sulfur.

Since neither the solubility nor the extinction coefficient of sulfur in water is known, it is impossible at present to determine the degree of supersaturation at the phase transition. "Self-nucleation" of the sort described above would be indicated if the limiting degree of supersaturation were consistent with that predicted from theory. If the degree of supersaturation at t_B were much less than the theoretical, the presence of foreign nuclei favoring condensation at a lower degree of supersaturation would be suspected. There are several ways in which this could occur: a charged nucleus decreases the critical radius r^*, a surface-active substance would lower the energy required for the formation of the surface of the nucleus, or minute particles of another phase might provide small surfaces on which condensation could proceed. If the phase transition is not initiated by self-nucleation, the foreign nuclei must be present in ordinary distilled water in fairly constant amounts, and must be unaffected by ordinary methods of purification. Attempts to modify the behavior of the usual solvent, distilled water, by redistillation or treatment with nitrogen to remove dissolved oxygen produced no noticeable effects. The "artificial" nuclei tried thus far have not proven attractive to the dissolved sulfur, e.g., sulfur particles from an older sol of the same type, polysulfides, and sulfur precipitated from acetone by water were tried. The nucleation process is currently under investigation by Mr. James Yates of this laboratory (27).

C. Particle Size and Growth Rate Immediately after the Phase Transition

Method. La Mer and Kenyon (5) noted that, when condensation begins, scattering of light without the added complication of absorption can be detected at wavelengths to which sulfur is transparent. It was hoped that the growth rate of particles in this stage could be determined by measuring the time of initiation of scattering (t_B) at different wavelengths. When such measurements were made, however, no simple dependence of wavelength on time was found. An attempt was then made to calculate particle sizes from optical density *vs.* time curves obtained at different wavelengths. When Rayleigh's law was applied to such data the radii corresponding to the smallest increase in optical density that is

detectable as scattering starts were calculated to be of the order of $\frac{1}{4}$ to $\frac{1}{3}$ the wavelength of the light used, *i.e.*, above the range of sizes for which Rayleigh's law is valid. The more general Mie theory for the scattering of light must be used.

An examination of the theoretical scattering area (2,28,29) coefficient K_s as a function of $\alpha = 2\pi r/\lambda'$ (Fig. 2) shows that, for α values between 1.2 and 3.0, K can be expressed approximately by the empirical linear relations

$K_s = 1.50\alpha - 1.69$ for $m = 1.44$,
$K_e = 1.76\alpha - 1.69$ for $m = 1.52$ and $k = 0.0017$,

where m = relative refractive index of sulfur and water,
    λ = wavelength in air,
    λ' = wavelength in water,
    k = extinction coefficient of sulfur,
    K_e = extinction area coefficient (for scattering plus absorption).

Since $K = 2.3 \log (I_0/I)/\pi r^2 nl$ and $\alpha = 2\pi r/\lambda'$, the above equations will give relations of the form

$$A \log (I_0/I)/n = Br^3/\lambda' - r^2, \qquad (3)$$

where A and B are constants depending on m, the absorption path length l, *etc.* For optical density measurements at $\lambda = 8000$ Å (for which $m = 1.44$), $A = 4.34 \times 10^6$ and $B/\lambda' = 9.24$, while at 4000 Å (for which $m = 1.52$ and $k = 0.0017$) A is unchanged and $B/\lambda' = 21.9$. If it is assumed that the particle number n is nearly constant during the short period of rapid condensation and is approximately equal to the number found to be present shortly after the initial condensation rate has fallen off somewhat, r can be calculated from optical density data. It can be understood from inspection of Eq. 3 why no simple relationship was found for the time of appearance of scattering (*i.e.*, the time when $\log (I_0/I)$ reaches the just measurable magnitude of 0.0005 corresponding to a decrease in transmittance of 0.1%) and the wavelength used for its detection.

Experimental. In order to utilize linear relationships between K and α it was necessary to work at wavelengths for whose m values computations of K were available, *i.e.*, at 4000 Å and 8000 Å. The procedure followed in the preparation of the sols, and the measurement of their optical density as a function of time, was the same as that used in the study of the homogeneous reaction. The most convenient procedure was to prepare tables of optical densities calculated for arbitrary values of radii, of λ', and values of n corresponding to the condensation stage. The times corresponding to the given sizes were then read off the experimental curves for $\log (I_0/I)$ as a function of time. The method for finding n will

be described later when the heterogeneous stage is discussed. The values of the radius determined by these experiments are in error by not more than $\pm.01\mu$.

Results. The smallest particle radius found was 0.07μ, calculated from optical density data at $\lambda = 4000$ Å just after scattering was perceptible in a sol which had 2.7×10^6 particles/cm.³ This particle number is larger than that of most of the monodispersed sols studied previously in this laboratory. In more dilute sols the particle size would have to be larger than 0.07μ before a decrease in transmittance could be observed. Since
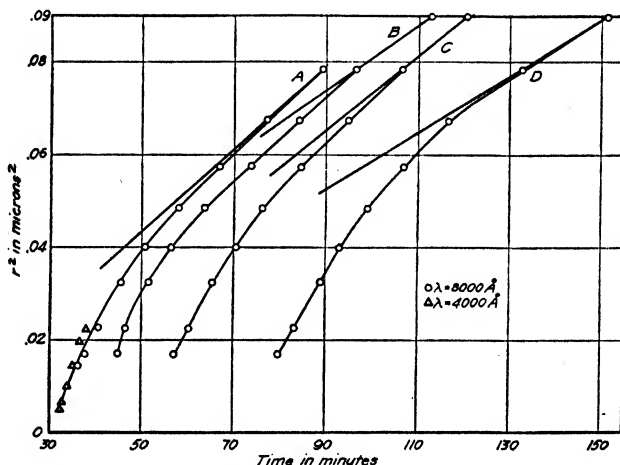
Fig. 3. Variation of r^2 with time in the condensation stage.

	Thiosulfate	HCl	$10^{-6}n/$cm.³
A.	0.002 M	0.002 M	2.7
B.	.002	.0015	2.1
C.	.001	.006	1.8
D.	.001	.003	1.0

a Tyndall beam usually cannot be detected visually until 2 or 3 min. after the scattering of light of wavelength 4000 Å is detected spectrophotometrically, it is safe to say that true Rayleigh scattering (proportional to r^6/λ^4) has never been observed in any of the monodispersed sulfur sols because the number of particles (10^6/cm.³) is too small. The particle number which is necessary to give perceptible scattering in the Rayleigh region ($r < \lambda/10$) is so large that rapid coagulation would occur according to Smoluchowski's theory (as will be discussed later). These sulfur sols are quite different from dispersions of high polymers where stability is possible with particle numbers of the order of 10^{15}/cm.³ No

data have been obtained, therefore, to describe the growth of particles from the time of nucleation until the time when $r = 0.07\mu$. This time interval is no greater than 2 min., and it seems fairly certain that, at its conclusion, the supersaturation of sulfur has been sufficiently relieved that further nucleus formation occurs only slowly.

By assuming that the particle number is constant for about an hour (*i.e.*, that formation of nuclei has virtually ceased) the growth of particles between $r = 0.07\mu$ and 0.30μ can be followed. Fig. 3 shows the variation of r^2 with time for 4 different sols in the early stage of growth. It would be expected that these systems should reach a steady state in which the generation of sulfur by the chemical reaction balances the loss of sulfur from solution by deposition on the colloidal particles. It will be noted, however, that dr^2/dt is not constant, indicating that a steady state has not been reached. The decrease in dr^2/dt could be interpreted as a lowering of the concentration gradient about each particle. This may be due to the gradual relief of the initial supersaturation, or to a decrease in the rate of formation of dissolved sulfur, or to both. The relief of supersaturation is the dominant factor here, since the system eventually reaches a steady state in which the variation of r^2 with time is linear (*cf.* Fig. 6). This will be shown when the heterogeneous stage of the reaction is discussed.

III. The Heterogeneous Stage

A. Discussion of Methods to Be Applied

Chemical Analyses. The sols exhibit an increase in iodine titer and a decrease in NaOH titer with time, caused by the following stoichiometric reactions (17):

$$H^+ + S_2O_3^- = S + HSO_3^-,$$
$$6H^+ + 5S_2O_3^- = 2S_5O_6^- + 3H_2O.$$
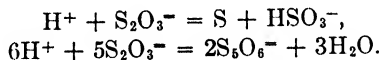
Thus, titrations should reveal the total extent of reaction, and through that, the total amount of sulfur formed. Iodine can be consumed in these systems only by thiosulfate and sulfite, and one mol of iodine is equivalent to two mols of thiosulfate or one mol of sulfite. Polythionates are not affected by iodine in neutral or acid solutions (30), and influence the iodine titer only because they require thiosulfate for their formation. If $\Delta(I_2)$ denotes the increase in iodine titer (in mols iodine/liter of sol), $\Delta(I_2)$ = mols sulfite formed

$$-\tfrac{1}{2} \text{ mols thiosulfate consumed in sulfite formation}$$
$$-\tfrac{1}{2} \text{ mols thiosulfate used to form polythionate.} \qquad (4)$$

The decrease in NaOH titer will depend on the extent of polythionate formation and on the amount of sulfite present. One may choose as the endpoint in the titration a pH at which the first dissociation of H_2SO_3

is complete, *e.g.*, at pH = 5.8, since $K_1 = 1.7 \times 10^{-2}$, $(HSO_3^-)/(H_2SO_3)$ $\sim 10^4$. Since $K_2 = 5 \times 10^{-6}$, $(SO_3^-)/(HSO_3^-) = 3.1$, so that the total sulfite concentration is given by

$$(SO_3^-) + (HSO_3^-) = 4.1(HSO_3^-).$$

If $-\Delta(H^+)$ denotes the decrease in hydrogen ion concentration,

$-\Delta(H^+) = $ mols H^+ bound as HSO_3^-
   + mols H^+ used in polythionate formation,

or $-\Delta(H^+) = (1/4.1)$ mols total sulfite
   + 6/5 mols thiosulfate used in polythionate formation. (5)

Eqs. 4 and 5 can be solved simultaneously to give Eqs. 6 and 7, by means of which the extent of sulfite and polythionate formation can be calculated from experimentally determinable quantities:

$$\text{Total sulfite } = [2\Delta(I_2) - (5/6)\Delta(H^+)]/1.20. \quad (6)$$

$$\text{Polythionate} = (2/5)[\text{total sulfite} - 2\Delta(I_2)]. \quad (7)$$

Optical Measurements. By methods developed in this laboratory (4,7,8), the radius and number of particles can be calculated from transmittance data on a monodispersed colloid. In practice, it is necessary only to find the wavelength and optical density corresponding to the principal maximum in the curve for transmittance *vs.* wavelength of a sol. Values of the scattering coefficient K_s as a function of α as calculated from the Mie theory can be used to relate transmittance data to the radius and number of particles, since $\alpha = 2\pi r/\lambda'$ and $K_s = 2.3 \log (I_0/I)/\pi r^2 nl$. At wavelengths at which sulfur absorbs, the calculations of the extinction area coefficient K_e, based on the complex index of refraction, must be used (8). The number of mols of sulfur in colloidal suspension at any time can be calculated as $1000 \times 4\pi r^3 n\rho/3M = 261.8nr^3$ mols/l., where $n = $ number of particles/cm.^{3}, $r = $ radius in cm., $\rho = $ density of sulfur, and $M = 32 = $ atomic weight of sulfur.

Coagulation and Settling Corrections. Only the colloidal sulfur in suspension is measured by this optical method. To find the total amount of colloidal sulfur formed, the number of particles settling out and/or coagulating must be considered. The following equation gives the fractional decrease in number per unit time due to coagulation (first term) and stirred settling (second term) (6):

$$- dn/n = \kappa n + v/h,$$

where $\kappa = 4kT/3\eta$ as in the Smoluchowski coagulation theory, and v/h comes from $n = n_0 e^{-vt/h}$, in which $v = $ velocity of fall as predicted from Stokes' law, $h = $ height of the system, and $t = $ time. The coagulation term is independent of the radius of the particles, while the settling term

depends upon $v = 2r^2g(\rho - \rho_0)/9\eta$, where r = radius of particle, g = acceleration due to gravity, $(\rho - \rho_0)$ = effective density of the particle, and η = viscosity. The proposed corrections are, of course, only approximate, since stirring is certainly not complete and no account is taken of the effect of micellar electric charges on the coagulation rate (31). It should be of interest, nevertheless, to obtain an estimate of the extent of decrease in number and of the relative importance of coagulation and settling in that decrease.

B. Experimental

The technique for preparation of the sols was the same as that described in Section I on the homogeneous reaction. The sols were prepared in 2-liter quantities and held at 25°C. Two separate aliquots of each solution were prepared, one of which was studied from time = 0 to 12 hr. and the other from time = 12 to 24 hr. after mixing. The concentrations ranged from 0.0005 to 0.003 M in thiosulfate and 0.00075 to 0.006 M in HCl. Preliminary experiments showed that small amounts of added KCl made no perceptible difference in any of the quantities measured, and the use of KCl in adjusting the ionic strength of the reaction mixtures to equality was omitted. In the experiments reported here, the only case in which a salt was added was in the demonstration of a positive kinetic salt effect by La^{+++} ion.

Titration Experiments. At approximately 2-hr. intervals, 25 ml. aliquots were removed from the reaction mixture for titration with iodine and NaOH. The iodine solution for each run was made by diluting a stock solution of 0.1 M I_2 in 0.25 M KI so that its molarity was half that of the thiosulfate in the sol. The iodine was standardized against a $Na_2S_2O_3$ solution for which $K_2Cr_2O_7$ had been used as the primary standard. In each titration 1 ml. of 1% starch solution served as an indicator, and a blank was run on 1 ml. of indicator in a volume of distilled water equal to the total volume present at the endpoint of the titration of the sample. The NaOH reagent was carbonate-free. The molarity of the NaOH used in each run was approximately equal to that of the HCl in the sol. Methyl red was the indicator, and the titration was concluded at pH = 5.8. When the endpoint was very near, the volume of the solution was adjusted to 60 ml. and the titration was completed by further addition of NaOH and comparison with Clark and Lubs buffers of pH values 5.6, 5.7, 5.8, and 5.9 to which indicator had been added. The blanks consisted of indicator and distilled water.

Optical Density Measurements. Measurements of transmittance were made on aliquots of sol, in which the progress of the reaction was arrested by the addition of 50% of the stoichiometrically equivalent amount of 0.1 M I_2, in quartz cells, 10 cm. length, in a Beckman spectrophotometer

(model DU). In most cases the minimum in the curve for optical density as a function of wavelength could be located in 15 min. The particle radius was calculated from the wavelength of this minimum transmittance from the relation $\alpha_{min.} = 2\pi r/\lambda'_{min.} = 6.8$ for $\lambda' > 3200$ Å. For lower wavelengths, where absorption occurs, Kenyon's (8) values for $\alpha_{min.}$ were used. The particle number was calculated from the optical density (7,8):

$$(K_s)_{min.} = 2.3 \log (I_0/I)_{min.}/\pi r^2 n l = 2.08.$$

Errors. The accuracy and reproducibility of the quantities of reactants delivered by the hypodermic syringes used in the preparation of the sols was within 1%, as determined by titration. The pH (5.8) at the endpoint of the NaOH titrations was estimated to within 0.05 pH unit. An error of 0.05 pH unit causes a 1.5% error in the calculated amount of total sulfite. The latter quantity exhibits an average total error of ±3%, since it also depends on the iodine titration.

The optical method used has been shown (7) to yield values of the radius that are accurate to within ±0.01μ, while the numbers of particles are correct to within 5%. A total error as large as 10% in the quantity nr^3, from which the number of mols of colloidal sulfur in suspension is calculated, is small in comparison with the change in that quantity produced by varying the concentration of one of the reactants.

C. Results

Chemical Analyses. To obtain values of $-\Delta(H^+)$ and $\Delta(I_2)$ for the same time, the experimentally determined curves for $-\Delta(H^+)$ and $\Delta(I_2)$ as a function of time were plotted. Values at arbitrarily chosen time intervals were read from them and used, as shown in Table IV, to calculate the concentrations of sulfite and polythionate. The concentrations of sulfite and polythionate as a function of time from Table IV are plotted in Fig. 4. Both runs shown are 0.002 M in $Na_2S_2O_3$ and HCl. In run 83, 0.0005 M La(NO$_3$)$_3$ was added. As in the homogeneous reaction, a positive salt effect indicates that the rate-controlling step in the formation of sulfite is a reaction between ions of like (and therefore negative) charge. The rate of formation of sulfite in the heterogeneous stage of the reaction is expressed by:

$$d(\text{sulfite})/dt = k(T)^2(H).$$

Table V shows the effect of the concentrations of the reactants on the rate of sulfite formation. The k values are calculated for times at which 10% of the original thiosulfate had decomposed. In most cases, formation of polythionate accounts for $\frac{1}{4}$ to $\frac{1}{3}$ of the consumption of thiosulfate. This means that polythionate determined by the decrease in H$^+$ concentration represents only about 8 mol-% of the sulfur-containing products of the reaction.

TABLE IV

Sulfite and Polythionate Calculated from Titration Data for 0.002 M $Na_2S_2O_3$ and HCl
(Units of concentration $= 10^{-5}$ mols/l.)

Run	Time	$-\Delta(H^+)$	$\Delta(I_2)$	Sulfite	Polythionate	Thiosulfate decomposed
	hrs.					
83[a]	4	6.5	3.8	10.6	1.2	13.6
	8	11.9	6.1	18.6	2.5	24.8
	12	17.3	7.5	24.5	3.8	34.0
	16	21.3	8.6	29.2	4.8	41.1
	20	24.0	9.7	32.8	5.4	46.2
	24	25.6	10.7	35.6	5.7	49.8
84	4	5.8	2.8	8.7	1.2	11.8
	8	10.8	4.8	15.6	2.4	21.5
	12	14.8	6.1	20.4	3.3	28.6
	16	18.4	7.1	24.6	4.2	35.0
	20	21.0	8.2	28.2	4.7	40.0
	24	23.2	9.2	31.4	5.2	44.8

[a] La(NO$_3$)$_3$ added $= 0.0005$ M.

Variation in Number of Suspended Particles. Table VI shows data obtained from optical measurements in a typical run, the calculated particle radii and numbers, and the corresponding molar concentrations
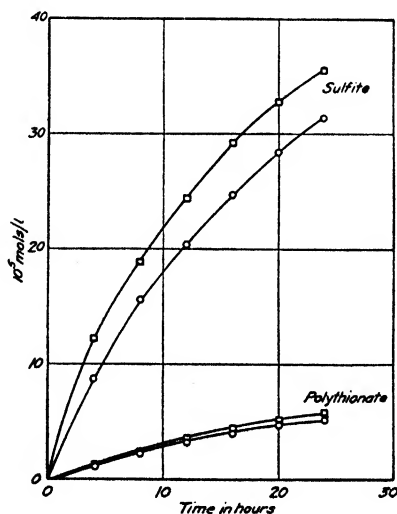
FIG. 4. Formation of sulfite and polythionate as a function of time from 0.002 M Na$_2$S$_2$O$_3$ and 0.002 M HCl. ○ no added salt. □ 0.0005 M La(NO$_3$)$_3$ added.

TABLE V

Dependence of Rate of Sulfite Formation on Reactant Concentrations

$(T)_0$, $(H)_0$ = initial conc. of $Na_2S_2O_3$ and HCl in mols/l.

$(H)_t$ = conc. of HCl at time t when 10% of thiosulfate has decomposed.

10^5 $(T)_0$	10^3 $(H)_0$	t	10^3 $(H)_t$	10^6 (sulfite)	$\dfrac{10^6 \text{ (sulfite)}}{t(H)}$	10^{-3} k
		hr.				
0.5	3	14.4	2.98	3.16	73.2	3.2
	6	7.1	5.98	3.09	72.8	3.2
1	1.5	15.3	1.47	7.20	308	3.4
	3	10.2	2.97	7.34	241	2.7
	4.5	6.8	4.47	7.08	232	2.6
	6	4.0	5.97	7.30	304	3.4
2	0.75	18.0	0.69	15.3	1180	3.3
	1.5	9.0	1.42	14.9	1130	3.1
	2	7.4	1.90	14.5	1010	2.8
	3	4.5	2.92	13.4	1010	2.8
	4.5	2.8	4.43	14.4	1150	3.2
3	0.75	18.0	0.66	22.4	1770	2.2
	1.5	6.6	1.40	21.5	2250	2.8
	3	3.5	2.89	21.0	2040	2.5
2^a	2	6.3	1.90	15.2	1240	(3.4)

[a] $La(NO_3)_3$ added = 0.0005 M.

Average 10^{-3} k = 2.9 ± 0.3.

of the sulfur in colloidal suspension—*i.e.*, the sulfur capable of scattering light. When the variation of particle number with time was examined, it was noted that in every sol studied the particle number increased in

TABLE VI

Typical Transmittance Data and Results for 0.001 M $Na_2S_2O_3$ and 0.0015 M HCl

Time	λ' min. Å	Log (I_0/I) min.	τ, μ	10^{-8} n/cm.³	$10^5(S)^a$ mols/l.
hr.					
2.5	2750	0.0093	0.26	0.47	0.22
4.8	3510	.0222	.38	.54	.78
6.7	3670	.0263	.40	.59	.96
11.6	3900	.0300	.42	.59	1.17
14.0	4700	.0370	.51	.50	1.74
15.8	4810	.0347	.52	.45	1.66
19.2	5130	.0314	.56	.36	1.61
24.1	5650	.0272	.61	.26	1.53

[a] (S) = colloidal sulfur *in suspension* in the solution.

the early stages of growth, then decreased later. This is illustrated by the uncorrected curves for number *vs.* time in Fig. 5. It was also observed (see Table VII) that the maximum reached by the number of suspended particles in a sol was dependent on $(T)^2(H)$, or the rate of the chemical reaction, and that n began to fall off when r was approximately 0.4μ, a size at which the rate of settling of the particles becomes appreciable (32). These facts can be explained if it is assumed that increases in particle
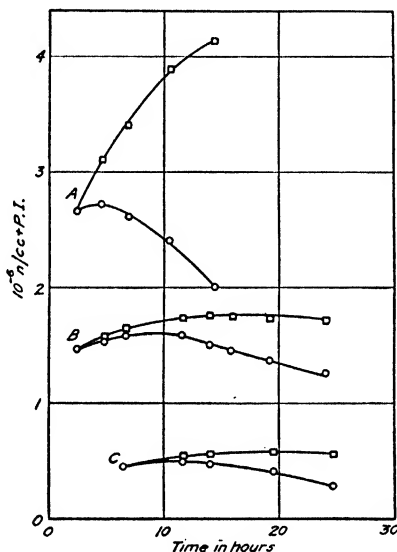
Fig. 5. Particle number *vs.* time, ○ uncorrected and □ corrected for losses due to coagulation and settling.

	Thiosulfate	HCl	P.I.
A.	0.002 M	0.002 M	0
B.	.001	.0015	1
C.	.0005	.006	0

number are caused by the generation of sulfur at a greater rate than it can be deposited on the growing particles already available. If N = total number of sulfur droplets, and n = number in suspension,

$$dn/dt = dN/dt - \kappa n^2 - vn/h.$$

When $n = n_{\text{maximum}}$, $dn/dt = 0$, and $dN/dt = \kappa n^2_{\text{max.}} + vn_{\text{max.}}/h$. In the sols with which we are dealing, appropriate values for the quantities in the above equation are $n_{\text{max.}} = 10^6/\text{cm}.^3$, $\kappa = 6 \times 10^{-12}$ cm.^{3}/sec., $v = 4 \times 10^{-5}$ cm./sec. (for $r = 0.4\mu$), and $h = 10$ cm. Thus, the coagulation term is only 6×10^{-24} cm.$^{-3}$ sec.$^{-1}$, while the settling term is 4×10^{-12}

cm.$^{-3}$ sec.$^{-1}$ Since r, when $n = n_{max.}$, is nearly constant (as shown in Table VII), v is nearly constant also. Therefore, $n_{max.}$ is proportional to dN/dt. If dN/dt is proportional to the rate of the sulfur-producing reaction, $n_{max.}$ becomes proportional to $(T)^2(H)$. This confirms the experimental results in Table VII.

Growth of Particles in the Heterogeneous Stage. The curves in Fig. 6 show the variation of r^2 with time. After an initial rapid rise, r^2 becomes linear in time, showing that a steady state has been reached in the diffusion process that is responsible for particle growth. This steady state

TABLE VII

Particle Radii when $n = n_{maximum}$ and Effect of Reactant Concentrations on $n_{maximum}$
$$k_n = n_{max.}/(H)_0(T)_0{}^2$$

10^3 $(T)_0$	10^3 $(H)_0$	Time when $n = n_{max.}$	r when $n = n_{max.}$	10^{-6} $n_{max.}/cm.^3$	10^{-9} $n_{max.}/(H)_0$	10^{-14} k_n
0.5	3	12.0 hr.	0.44 μ	0.26	0.087	3.5
	4.5	12.0	.45	.38	.084	3.4
	6	11.5	.45	.50	.083	3.3
1	1.5	9.5	.41	.62	.413	4.1
	3	4.5	.38	1.19	.397	4.0
	4.5	12.0	.44	1.52	.338	3.4
	6	6.5	.38	2.06	.343	3.4
2	0.75	11.0	.46	1.24	1.65	4.1
	1.5	11.0	.44	2.45	1.63	4.1
	3	8.0	.38	5.44	1.81	4.5
	4.5	4.0	.35	7.84	1.74	4.3
3	0.75	6.0	.36	3.04	4.05	4.5
	1.5	5.0	.35	5.84	3.89	4.3
	3	<0.2	—	11.3	3.76	4.2

Average r when $n = n_{max.}$ is 0.41 $\pm$ .04μ.
Average $10^{-14} k_n = 3.9 \pm 0.4$.

is reached when r is between 0.35 and 0.40μ. The data for $r \leq 0.3\mu$ agrees with that obtained in the study of the condensation stage. The slopes of the r^2 vs. time curves in all the cases studied were between 0.007 and 0.012μ^2/hr. The average slope for 15 sols, all having different concentrations of reactants, was 0.010μ^2/hr. $\pm$ 20%. It has been shown that the rate of sulfur formation has a very marked effect on the number of particles formed. This seems to be the chief effect produced, since the rate of increase of r^2 with time is relatively constant. It is this constancy that accounts for the ease of reproduction of the sols when particle radius is the sole criterion, since a 20% variation in r^2 causes only a 10% vari-

ation in r. This is the basis for the hitherto unexplained fact that the radius vs. time data of both Johnson (6) and Barnes (4) (see Fig. 6) fall on the same curve, although each experimenter used different concentrations of thiosulfate and acid.
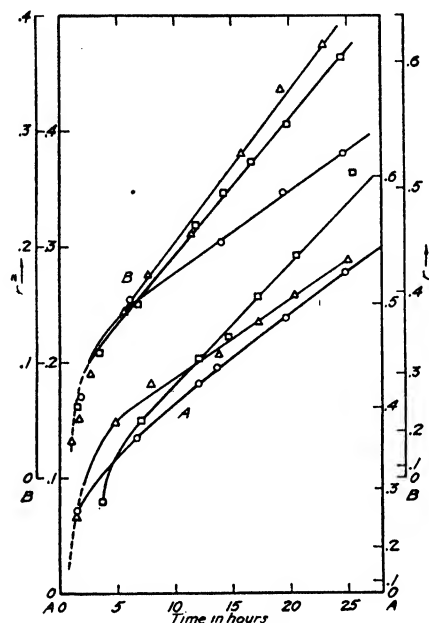
FIG. 6. Growth of droplets by diffusion process (r^2 and r in μ vs. time). Dotted lines represent data obtained during the condensation stage (cf. Fig. 3). Points were obtained as described under the heterogeneous stage.

		Thiosulfate	HCl	Slope (μ^2/hr.)
A.	○	0.003 M	0.0015 M	0.0076
	□	.0005	.0045	.0104
	△	.002	.00075	.0070
B.	○	.001	.0045	.0070
	□	.001	.006	.0119
	△	.001[a]	.002	.0130
		.0015[b]	.003	.0130

[a] Johnson and La Mer.
[b] Barnes and La Mer.

Correction of n for Coagulation and Settling. Fig. 5 shows some results of correcting n for decreases due to coagulation and settling. Since κ for water at 25°C. = 6.08×10^{-12} cm.³/sec., the percentage decrease in particle number/hr. is equal to $(6.08 \times 10^{-12} n + v/h) \times 3.6 \times 10^5$ or

$(2.19 \times 10^{-6}n + 3.6 \times 10^5 v/h)$. Corrections were made on each n value observed by adding the number of particles that had disappeared due to coagulation and settling. The calculation of each correction was based on the average number and radius of the suspended particles during the time interval between the measurement to be corrected and the one before it. At any time, then, the total number of particles that had been formed was taken to be the measured number plus the sum of all the corrections calculated for each measurement up to that time. This method is illustrated in Table VIII which shows some typical corrections applied to n. It should be noted that in Table VIII the particle number is fairly large for this type of sol, so that, until the particles reach a size of about 0.5μ, the hourly decrease in number due to coagulation far exceeds the decrease due to settling. In more dilute sols this is not the case—e.g., when $Na_2S_2O_3 = 0.0005\ M$ and $HCl = 0.003, 0.0045$, or $0.006\ M$, the

TABLE VIII

Correction of n for Coagulation and Settling, 0.002 M Na$_2$S$_2$O$_3$, 0.002 M HCl

$-\Delta n' =$ decrease in n between a given measurement and the one immediately preceding it.

Time, hr.	2.5	4.6	6.9	10.5	14.4
r, μ	0.31	0.36	0.40	0.46	0.50
$10^5 v$, cm./sec.	2.29	3.19	3.99	5.13	6.08
h, cm.	11.8	10.2	9.1	7.7	6.7
$10^{-6}n/\text{cm}^3$.	2.65	2.73	2.59	2.40	2.01
$\%(-\Delta n)/\text{hr. due to settling}$	0.70	1.12	1.58	2.40	3.27
$\%(-\Delta n)/\text{hr. due to coagulation}$	5.80	5.98	5.67	5.26	4.40
$10^{-6}(-\Delta n)/\text{cm}^3./\text{hr.}$	0.17	0.19	0.19	0.18	0.15
$10^{-6}(-\Delta n')/\text{cm}^3$.	—	0.38	0.44	0.67	0.66
Corrected $10^{-6}n/\text{cm}^3$.	(2.65)	3.11	3.41	3.89	4.16

particle number is in the range 0.2–$0.5 \times 10^6/\text{cm}^3$. This means that the rate of disappearance of particles due to settling will be from 2 to 4 times greater than that attributable to coagulation. Such sols are more nearly monodispersed than the ones in which the coagulation rate is greater. Polydispersity caused by coagulation increases rapidly with increasing concentrations of thiosulfate and acid. If both reagents are $0.004\ M$, the n_{max} predicted by using the average k_n from Table VII is $2.5 \times 10^7/\text{cm}^3$, and such a number will have an initial rate of decrease of $55\%/\text{hr.}$ due to coagulation.

These corrections are only approximate because of the following sources of error: incomplete stirring (settling correction should be larger), electric charge on micelles (coagulation correction should be smaller), and decrease in monodispersed character as the sol ages (coagulation correction assumes a monodispersed system exists). A further error may

be present in the case where La^{+++} is added, since coagulation there is probably faster than in other sols. The corrections serve, however, to give a better estimate of the total amount of colloidal sulfur formed in these sols than can be obtained from the uncorrected data. A comparison of the relative importance of coagulation and settling in sols of different particle size and number also furnishes an explanation for the dependence of monodispersed character on low reactant concentrations (as already shown), and for the instability of the sols as they "age." From a comparison of the corrected and uncorrected curves for n vs. time, it will be noted that a few new particles are continually being formed. As the sol ages, the original monodispersed set of particles first formed when
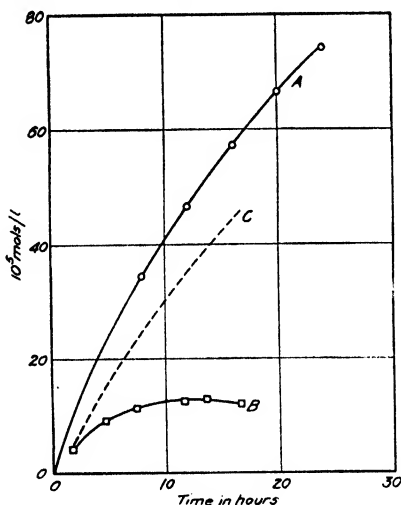
Fig. 7. Sulfite (A), suspended colloidal sulfur (B), and estimated total colloidal sulfur (C) as a function of time for 0.002 M Na$_2$S$_2$O$_3$ and 0.0045 M HCl.

the supersaturation built up in the homogeneous stage was relieved, and which comprised the majority of the suspended particle population, gradually settles out. Both these factors, in addition to coagulation, make for polydispersity when the sol ages. At higher dilutions, where the rate of generation of sulfur has decreased after 15–20 hr., the formation of new particles at that time is slow and settling has taken such a toll that the solutions are almost clear.

Particles which have settled out or which have coagulated and then settled out are still in contact with the solution in which they grew. It is, therefore, not unreasonable to suppose that further growth will take place on them. If it is assumed that growth occurs on all particles, whether

still in suspension or not, curves for total colloidal sulfur such as the one in Fig. 7 are obtained. Such curves parallel the formation of sulfite as measured in titration experiments somewhat better than would curves based on the assumption that growth ceases after settling. The total colloidal sulfur which is calculated if the growth of the particles is assumed to continue, even after settling occurs, is certainly an overestimate of the total colloidal sulfur in the system, not only because of this latest assumption but because of the assumptions made in correcting n for settling and coagulation. Despite this, the difference between the number of mols of sulfite and the estimated number of mols of colloidal sulfur is too large to be interpreted as the number of mols of dissolved sulfur present. The application of such an interpretation to the data on the heterogeneous stage would lead to the conclusion that the concentration of dissolved sulfur increases very greatly with time. This is not the case, as was seen above when the growth rate of particles in this stage was discussed. It is well known, however, that polythionates in acid solution form higher polythionates by reacting with free sulfur or by taking up sulfur directly from thiosulfate (33,34):

$$S_5O_6^- + S \rightleftarrows S_6O_6^-$$

or

$$H^+ + S_5O_6^- + S_2O_3^- \rightleftarrows S_6O_6^- + HSO_3^-.$$
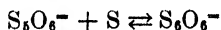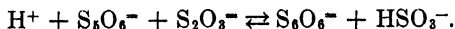
Either reaction would account for the fact that the quantity of sulfur is less than that of the sulfite found in the heterogeneous stage. The number of mols of sulfite and polythionate computed from titration data are correct since the reactions above do not alter the stoichiometric relations used in the calculation of those quantities.

IV. Summary

An investigation has been made of the kinetics of the formation and growth of monodispersed sulfur sols prepared by the action of dilute HCl (0.00075–0.006 M) on Na$_2$S$_2$O$_3$ (0.0005–0.003 M). The study has been divided into three parts.

I. The Homogeneous Reaction. The formation of molecularly dispersed sulfur begins as soon as the reactants are mixed. Ultraviolet absorption measurements with a Beckman quartz spectrophotometer at $\lambda = 3000$ Å show that the concentration of dissolved sulfur reaches a constant value representing a limiting state of supersaturation, after which further formation of sulfur leads to condensation. Within the limits of experimental error the concentration of sulfur at the time, t_B, when the phase change occurs is unaffected by changing the concentrations of

the reactants or by adding small amounts of salts. Furthermore, this time is reproducible and varies with the rate of formation of sulfur. It depends also upon the degree of supersaturation of sulfur, the solubility of sulfur in the medium, the nature of the nucleation process that occurs at the phase transition, and the wavelength of light used to detect the initiation of scattering. Since these variables were eliminated by using the same solvent and wavelength for all experiments, t_B is a valid measure of the rate of the homogeneous reaction.

The effect of changing the concentrations of the reactants showed that the rate of formation of sulfur is proportional to $(T)^{\frac{1}{2}}(H)^{\frac{1}{2}}$, where (T) and (H) are the total molar concentrations of thiosulfate and hydrogen ion. The fractional order and the shape of the curves for optical density as a function of time indicate an autocatalytic reaction, probably of the chain type. The reaction exhibits a positive Brønsted primary salt effect —e.g., the addition of lanthanum salts produces a marked acceleration. The rate-controlling step is, therefore, a reaction between negatively charged ionic species, either $(S_2O_3^- + HS_2O_3^-)$ or $(2HS_2O_3^-)$.

II. The Condensation Stage. This stage begins with the formation of nuclei capable of further growth, less than 2 min. before the appearance of colloidal sulfur is detected experimentally. The existence of a limiting state of supersaturation is in accord with the accepted theory for phase transitions. The degree of supersaturation that must be reached before condensation occurs is dependent to a critical extent on the rate of nucleus formation.

Although, when the Tyndall beam first appears, the scattered light is bluish, its intensity is not proportional to r^6/λ^4 and Rayleigh's limiting law (for $r < \lambda/10$) cannot be applied to the determination of the sizes of particles because their radii are already $\frac{1}{3}$ the wavelength of light. Attempts to detect the scattering at smaller radii failed because the number of particles is so small ($10^6/cm.^3$). The particle number which is necessary to give perceptible scattering in this region is so large that rapid coagulation would occur according to Smoluchowski's law. Values of the radius were determined by applying the Mie theory to measurements of optical density as a function of time at $\lambda = 4000$ and 8000 Å. At these wavelengths sulfur is transparent and has refractive indices for which calculated values of the scattering area coefficient $K_s = 2.3 \log (I_0/I)/\pi r^2 n l$ as a function of $\alpha = 2\pi r/\lambda'$ are available. In the range $\alpha = 1.2$–3.0 the variation of K_s with α can be expressed by empirical linear relationships, thus permitting the determination of radii from 0.07 to 0.30μ. Since the variation of r^2 with time is non-linear, a steady state in the diffusion process by which dissolved sulfur is deposited on the surfaces of the particles is not set up in the early stage of growth.

III. The Heterogeneous Stage. The overall rate of the chemical changes that occur during the growth of a sol has been found by titrations with iodine and alkali to be proportional to $(T)^2(H)$. The variation with time of the number and radii of the particles in suspension was determined by an application of the Mie theory to transmittance measurements. The occurrence of a maximum in the number *vs.* time curves is explained by ascribing increases in number to the formation of molecularly dispersed sulfur at a greater rate than it can diffuse to the growing particles already present. Decreases in number result from coagulation and settling. From the asymptotic linear variation of r^2 with time it is suggested that a steady state has been reached in which the rate of diffusion of dissolved sulfur to the particle surfaces remains constant.

The monodispersity of a sol is strongly influenced by the rate of sulfur formation. Polydispersity in the early stages of particle growth is caused by the continued formation of new particles while older ones are growing, and by coagulation, and is, therefore, favored by high reactant concentrations. The deterioration of a monodispersed sol on aging is largely due to the settling out of the particles.

An overestimate of the total amount of colloidal sulfur in these systems has been made by correcting the particle number for decreases due to coagulation and settling, and by assuming that growth continues on all particles whether they are in suspension or not. In spite of this, the difference between the amount of sulfite found and the estimated total colloidal sulfur is too great to be interpreted as the quantity of dissolved sulfur present. This indicates that the pentathionate which is the product of a side reaction takes up sulfur to give higher polythionates.

V. Conclusions

1. The homogeneous reaction proceeds in an autocatalytic manner with a rate dependence on $(T)^{\frac{1}{2}}(H)^{\frac{1}{2}}$ to a constant concentration of dissolved sulfur at which condensation occurs.

2. Positive salt catalysis by La^{+++} ion shows that the rate controlling step in the homogeneous reaction and in the overall chemical reaction that continues as the colloidal particles grow is a reaction between negatively charged ionic species, either $(2HS_2O_3^-)$ or $(S_2O_3^- + HS_2O_3^-)$.

3. An empirical linear relationship expressing the variation of the scattering area coefficient K_s with $\alpha = 2\pi r/\lambda'$ as calculated from the Mie theory has been used to determine particle sizes in the range $r = 0.07\div 0.30\mu$.

4. Studies of the growth rate of particles show that growth proceeds by a diffusion process in which a steady state is reached after a pre-

liminary stage in which rapid condensation partially relieves the super-saturation existing at the time of nucleation.

5. The rate of sulfite formation is proportional to the rate of the overall chemical reaction which titration measurements show depends on $(T)^2(H)$ in the heterogeneous stage. Optical measurements show that this rate determines the number of colloidal particles that form.

6. Increases in the number of particles in suspension with time are due to the production of dissolved sulfur more rapidly than it can diffuse to the growing particles, while decreases in number are caused by coagulation and settling. The characteristics of sols on aging are ascribable to these effects.

REFERENCES

1. LA MER, V. K., *J. Phys. Colloid Chem.* **52**, 65 (1948).
2. LA MER, V. K., AND SINCLAIR, D., Verification of Mie Theory, *O. S. R. D. No.* **1857** (1943); Dept. Commerce, Office of Publ. Board, Report No. 944.
3. LA MER, V. K., AND BARNES, M. D., *J. Colloid Sci.* **1**, 71 (1946).
4. LA MER, V. K., AND BARNES, M. D., *ibid.* **1**, 79 (1946).
5. LA MER, V. K., AND KENYON, A. S., *ibid.* **2**, 257 (1947).
6. JOHNSON, I., AND LA MER, V. K., *J. Am. Chem. Soc.* **69**, 1184 (1947).
7. BARNES, KENYON, ZAISER AND LA MER, *J. Colloid Sci.* **2**, 349 (1947).
8. KENYON, A. S., AND LA MER, V. K., in press.
9. LANDOLT, H., *Ber.* **16B**, 2958 (1883).
10. FOUSSEREAU, G., *Ann. chim. phys.* [6] **15**, 533 (1888).
11. BILTZ, W., AND GAHL, W., *Nachr. Ges. Wiss. Göttingen, Math.-physik. Klasse,* 300 (1904).
12. SHEFFER, J., AND BÖHM, F., *Z. anorg. allgem. Chem.* **183**, 151 (1929).
13. OSTWALD, W., Lehrbuch der allgemeine Chemie, 2d ed., pp. 291–294. 1902.
14. JABLCZYNSKI, C. K., AND WARSZAWSKA-RYTEL, Z., *Bull. soc. chim. France* **39**, 409 (1926). For similar data at concentrations of 0.01–0.04 M Na$_2$S$_2$O$_3$ and 0.005–0.02 M H$_2$SO$_4$ see G. OSTER, *J. Colloid Sci.* **2**, 291 (1947). He considers the rate of coagulation.
15. HOLLEMAN, A. F., *Rec. trav. chim.* **14**, 71 (1895).
16. BASSETT, H., AND DURRANT, R. G., *J. Chem. Soc.* **1927**, 1401.
17. PRAKKE, F., AND STIASNY, E., *Rec. trav. chim.* **52**, 615 (1933).
18. TAUBE, H., *J. Am. Chem. Soc.* **65**, 526 (1943).
19. FOSS, O., *Tids. Kjemi, Bergvesen Met.* **1**, 3 (1946).
20. LA MER, V. K., AND TOMLINSON, H., *Ind. Eng. Chem., Anal. Ed.* **9**, 588 (1937).
21. LA MER, V. K., *J. Franklin Inst.* **225**, 709 (1938). See p. 726.
22. VOLMER, M., Kinetik der Phasenbildung. Edwards Bros., Ann Arbor, Michigan, 1945.
23. FRENKEL, J. J., Kinetic Theory of Liquids, Chap. VII. Oxford Univ. Press, 1946.
24. GIBBS, J. W., *Trans. Conn. Acad.* **III**, 1875–1878. Reprinted in The Collected Works of J. Willard Gibbs, Vol. I (Thermodynamics), pp. 242, 252–258. Longmans, Green and Co., New York, N. Y., 1928.
25. Problems similar to this have been treated by M. VON SMOLUCHOWSKI, *Z. physik. Chem.* **92**, 129 (1917); I. LANGMUIR, *Phys. Rev.* **12**, 368 (1918); K. NEUMANN, see VOLMER (ref. 22), p. 209.

26. GIL, J. C., AND BEATO, J., *Ber.* **56B**, 2451 (1923).

27. LA MER, V. K., AND YATES, J., *Science* **106**, 508 (1947).

28. BARNES, M. D., AND LA MER, V. K., *J. Colloid Sci.* **2**, 361 (1947).

29. SINCLAIR, D., *J. Optical Soc. Am.* **37**, 475 (1947).

30. KURTENACKER, A., Analytische Chemie der Sauerstoffsäuren des Schwefels, p. 137. Stuttgart, 1938.

31. DEBYE, P., *Trans. Am. Electrochem. Soc.* **82**, 265 (1942).

32. JOHNSON AND LA MER (ref. 6) were able to utilize the rate of deposition for radius measurements on 0.38μ and larger particles.

33. FOERSTER, F., AND CENTNER, K., *Z. anorg. allgem. Chem.* **157**, 45 (1926).

34. KURTENACKER, A., MUTSCHIN, A., AND STASTNY, F., *ibid.* **224**, 399 (1935).

Erratum

On page 334 of this volume, the sentence ending on the last line should read ".... is here invalid," instead of " .... is herein valid."

BOOK REVIEWS

Advances in Carbohydrate Chemistry, Vol. 3, edited by W. W. PIGMAN AND M. L. WOLFROM. Academic Press, Inc., New York, 1948, xvii + 748 pp., $10.80.

The many fields of investigation legitimately falling under the heading of carbohydrate chemistry are represented in this, the third volume of the series. The first article of this volume is by Professor C. S. Hudson who also was the author of the first articles in the earlier volumes. Thus, a precedent is being established which, one hopes, will be followed through many future volumes. Professor Hudson presents in his paper the historical aspects of conventions for writing stereo-formulae with a thoroughness and clarity which reflects his love for his subject.

A series of articles review the chemistry of certain sugar derivatives. Thus E. G. V. Percival discusses hydrazone and osazone derivatives of sugars; Hewitt G. Fletcher, Jr., the cyclitols; Burckhardt Helferich, the trityl ethers and John W. Green, the oxidation of simple sugars. The question of glutose in cane molasses is analyzed interestingly by Louis Sattler. The article by Jack Compton on the molecular constitution of cellulose includes much material that has been reviewed in other places. It should, however, serve the purpose of calling to the attention of carbohydrate chemists the possibility of applying physical methods to polysaccharides other than cellulose with the promise of great success.

Karl Myrbäck's article on starch and glycogen will be welcomed by the starch chemist since it brings into the compass of fifty-eight pages a discussion of the results of approximately seventy published papers from Professor Myrbäck's laboratory.

Modern techniques are represented by a review of "Isotopic Tracers in the Study of Carbohydrate Metabolism" by Samuel Gurin. The subjects of bacterial polysaccharides and of carbohydrate antibiotics are being pursued at a fast pace at the present time; the article on the polysaccharides of mycobacterium tuberculosis by M. Stacey and P. W. Kent could well serve as an introduction to the one subject, while the article by R. U. Lemieux and M. L. Wolfrom on streptomycin as a complete story on the other.

With few exceptions the articles in this volume attempt a complete review of the subject and are not limited to a discussion of recent advances. The volume should, therefore, find an audience outside of the group of carbohydrate chemists.

CHARLES O. BECKMANN, New York, N. Y.

Organic Chlorine Compounds. By ERNEST HAMLIN HUNTRESS. John Wiley & Sons, Inc., New York, 1948. 1443 pp. *Price $27.50.*

This book is the second in a series of tables of data on organic compounds by the present author. It presents a compilation of material on a selected list of compounds of carbon, hydrogen, oxygen and chlorine. The compounds are arranged as before in order of increasing melting or boiling points and the literature has been covered through 1945. According to the author 47% of the references are of a vintage later than 1929.

Certain novel features of the book deserve special comment. All reported values of each physical constant are listed separately. For example, 9 melting points, all uncorrected and all lying between 65° and 68°C. (inclusive), are listed for desyl chloride. Since these differ from each other by less than the experimental error it is difficult to see the value of the 8 repetitions of the original melting point. A second innovation is

the inclusion of what Professor Huntress calls "negative entries." When common derivatives of a compound have not been reported in the abstract journals up to 1945 they are often listed with the notation "unreported." As the author points out this should save considerable effort which might otherwise be wasted in a futile literature search.

The work differs from the previous volume, which concerned itself largely with the problem of identification, in that it has been expanded to include methods of synthesis, uses, and general chemical properties of the compounds described. It has, therefore, been necessary to omit a number of fairly common chlorine-containing compounds in the category under consideration. For example, although 22 pages and over 600 references are devoted to chloroacetic acid, γ-chloropropyl methyl ether is not listed, although it appears in both the main work and the first supplement of Beilstein's *Organic Chemistry*. It occurs to the reviewer that a work which had a more comprehensive list of compounds and less detailed information of the sort that can be found in Beilstein would be of somewhat more general use.

The present compilation has been made with the same care as the previous volume and is relatively free from typographical errors. It should be of considerable value as a reference work to anyone doing research in organic chemistry. In view of the limited scope of the work and its high price, however, it is unlikely that many organic chemists will feel able to afford a personal copy.

DAVID Y. CURTIN, New York, N. Y.

AUTHOR INDEX

A

AOTO, K. See Matuhasi, T.,   63

ATEN, A. H. W., DIPPEL, C. J., KEUNING, K. J., AND VAN DREVEN, J. Denaturation and optical rotation of proteins,   65

B

BECKMANN, C. O. See Rosenberg, J. L., 483

BEECK, O., RITCHIE, A. W., AND WHEELER, A. Adsorption of hydrogen on nickel catalysts. I. Effect of sintering,   505

BENSON, G. C., AND MCINTOSH, R. L. Surface pressure-area measurements for films of polyvinyl acetate polymers spread on water,   323

BIKERMAN, J. J. A penetroviscometer for very viscous liquids,   75

BRADY, A. P. See Cushman, A.,   425

BRADY, A. P., AND HUFF, H. Temperature dependence of conductivity and critical concentration of two typical colloidal electrolytes,   511

BUCHDAHL, R. Rheology of thermoplastic materials. I. Polystyrene,   87

C

CAMPBELL, D. H. See Lanni, F.,   273

CHATTERJEE, B. See Mukherjee, J. N., 437

COE, R. H., MYSELS, K. J., AND SMITH, G. H. Bound and free acid in aluminum soap prepared by precipitation,   293

CORRIN, M. L. The effect of salts and chain length on the critical concentrations of colloidal electrolytes,   333

CUSHMAN, A., BRADY, A. P., AND MCBAIN, J. W. The osmotic activity and conductivity of aqueous solutions of some typical colloidal electrolytes,   425

D

DAVIES, J. T., AND RIDEAL, E. K. The distribution of ions at interfaces,   313

DEXTER, F. D. See Dienes, G. J.,   181

DEY, A. K. On the colloidal behavior of some complex-forming systems,   473

DIENES, G. J., AND DEXTER, F. D. Notes on "Viscous flow of molten polystyrene,"   181

DILLON, R. E. See Spencer, R. S.   163

DIPPEL, C. J. See Aten, A. H. W.,   65

DOW, R. B. The Cragoe L function for the viscosity of oils under pressure at certain temperatures,   99

DREVEN, J. VAN. See Aten, A. H. W.,   65

DUNN, R. C. See McBain, J. W.,   303

F

FISCHER, E. K. Note on the origin of the term "rheology,"   73

FISCHER, E. K., AND LINDSLEY, C. H. Pseudoplastic flow properties of lyophilic colloids,   111

G

GINELL, R. Association phenomena. II. Theories of chain molecules and their application to hydrogen bonding in gaseous hydrogen fluoride,   1

GRALÉN, N. See Kubal, J. V.,   457

GRANDINE, J. D., 2nd. See Vold, R. D., 339

GREEN, H. The effect the consistency curve has had on the development of modern viscometers,   129

H

HATTIANGDI, G. S. The effect of concentration and temperature on gelation time,   207

HELLER, W., AND OPPENHEIMER, H. Comparative studies of photoelasticity of elastomers and plastomers,   33

HERNANDEZ, L., AND NORD, F. F. Interpretation of the mechanism of catalytic reductions with colloidal rhodium in the liquid phase,   363

The influence of sulfur on catalytic dehydrogenations with rhodium,   377

HEYMANN, E., AND O'DONNELL, I. J. Note on anion exchange resins. "Acid absorption" or "anion exchange,"   479

601

SUBJECT INDEX

INDEX OF BOOK REVIEWS